

City Research Online

City St George's, University of London

Citation: Friis, J. (2003). Structural performance of confined high strength concrete columns. (Unpublished Doctoral thesis, City, University of London)

This is the accepted version of the paper.

This version of the publication may differ from the final published version. To cite this item please consult the publisher's version.

Permanent repository link: https://openaccess.city.ac.uk/id/eprint/30429/

Copyright and Reuse: Copyright and Moral Rights remain with the author(s) and/or copyright holders. Copies of full items can be used for personal research or study, educational, or not-for-profit purposes without prior permission or charge, unless otherwise indicated, provided that the authors, title and full bibliographic details are credited, a hyperlink and/or URL is given for the original metadata page and the content is not changed in any way. For full details of reuse please refer to City Research Online policy.

City Research Online: http://openaccess.city.ac.uk/ publications@citystgeorges.ac.uk

Structural Performance of Confined High Strength Concrete Columns

by

Jesper Friis

A thesis submitted for the partial requirements for the degree of Doctor of Philosophy

School of Engineering and Mathematical Sciences

City University London

May 2003

To Janice

The Lamb who was slain is worthy to receive strength and divinity, wisdom and power and honour: to him be glory and power forever.

Contents

	Page
List of Figures	0.7
List of Tables	0.18
Abstract	0.20
Acknowledgements	0.21
List of Symbols	0.22
Chapter 1: Introduction	1.1
1.1 Background	1.1
1.2 Objectives of the Present Project	1.4
1.3 Organisation of the Thesis	1.5
Chapter 2: High Strength Concrete Materials	2.1
2.1 High Strength Concrete	2.1
2.1.1 Mix Design	2.1
2.1.2 Workability of Fresh Concrete	2.5
2.1.3 Casting and Curing Procedure	2.5
2.1.4 Compressive Strength	2.7
2.1.5 Stress-Strain Characteristics	2.14
2.1.6 Split Cylinder Strength	2.17
2.2 Reinforcement Properties	2.19
Chapter 3: Mechanical Properties of High Strength Concrete	3.1
3.1 Behaviour in Uniaxial Compression	3.1
3.1.1 Fracture Phenomenon	3.1
3.1.2 Size and Shape Effects	3.4

3.1.3 Modulus of Elasticity 3.6

3.1.4 Strain at Peak Stress 3.9

3.1.5 Poisson's Ratio 3.12

3.1.6 Analytical Expression for Stress-Strain Curve 3.13

3.2 Behaviour in Uniaxial Tension 3.20

3.3 Behaviour of Actively Confined Concrete 3.22

3.3.1 Confined Strength 3.22

3.3.2 Strain at Confined Peak Stress 3.30

3.3.3 Analytical Expression for the Confined Stress-Strain Curve 3.32

3.4 Behaviour of Passively Confined Concrete 3.38

3.4.1 General 3.38

3.4.2 Effective Confining Stress 3.43

3.4.3 Computational Model for the Stress-Strain Behaviour 3.54

3.4.4 Existing Confinement Models 3.62

3.5 Behaviour of Concrete in Flexure 3.75

3.6 Summary 3.80

Chapter 4: Structural Behaviour of Concrete Columns 4.1

4.1 General 4.1

4.1.1 Failure of Concrete Columns 4.1

4.1.2 Methods for Numerical Analysis of Concrete Columns 4.3

4.2 Numerical Analysis of Concrete Columns 4.6

4.2.1 Model for Generating Interaction Diagrams 4.6

4.2.2 Model for Analysing Slender Columns 4.15

4.3 Validation of Numerical Models 4.30

4.3.1 Concrete Columns Failing in Uniaxial Bending 4.30

4.3.2 Concrete Columns Failing in Biaxial Bending 4.60

4.3.3 Summary 4.67

Chapter 5: Full-Scale Tests of High Strength Concrete Columns 5.1

5.1 Experimental Programme 5.1

5.1.1 Test Columns 5.1

5.1.2 Testing Rig 5.8

5.1.3 Instrumentation and Testing Procedure 5.13

5.2 Test Observations 5.20

5.2.1 Test Loads and Failure Modes 5.20

5.2.2 Load-Strain Behaviour 5.30

5.2.3 Load-Deflection Behaviour 5.48

5.3 Analysis of Test Results 5.58

5.3.1 Expected Behaviour of Test Columns 5.58

5.3.2 Supplementary Investigation 5.64

5.4 Summary 5.71

Chapter 6: Parametric Study of the Behaviour of Confined Concrete Columns 6.1

6.1 Parametric Study 6.1

6.1.1 Influence of Concrete Strength 6.1

6.1.2 Influence of Confinement 6.5

6.1.3 Influence of Longitudinal Reinforcement 6.17

6.1.4 Influence of Concrete Cover 6.25

6.1.5 Summary 6.31

Chapter 7: Conclusion and Future Research 7.1

7.1 General Comments 7.1

7.2 Mechanical Behaviour of High Strength Concrete 7.1

7.3 Slender High Strength Concrete Columns 7.4

7.3.1 Experimental Investigation 7.4

7.3.2 Numerical Investigation 7.6

7.2 Suggestions for Future Research 7.8

References 8.1

Appendix A: Test Results on Passively Confined Concrete Columns 9.1

Appendix B: Computer Programs for Numerical Analysis of Concrete Columns 10.1

B.1 MNCALC - Program for Generating Interaction Diagrams 10.1

B.2 COLS - Program for Analysing Slender Columns 10.18

List of Figures

Figure		Page
2.1	Particle size distribution of fine aggregates	2.4
2.2	Particle size distribution of coarse aggregates	2.5
2.3	Typical failure mode for small-sized concrete specimens	2.12
2.4	Fracture along diagonal plane in test series LH15U	2.13
2.5	Splitting type failure of wood packed cylinder	2.13
2.6	Stress-strain behaviour of grade C100 concrete	2.16
2.7	Stress-strain behaviour of grade C12 concrete	2.16
2.8	Fracture of cylinder tested for splitting strength	2.17
2.9	Typical stress-strain curves for reinforcement bars	2.20
3.1	Modulus of elasticity versus compressive strength	3.8
3.2	Strain at peak stress versus compressive strength	3.11
3.3	Poisson's ratio versus normalised stress	3.13
3.4	Comparison of proposed stress-strain model with experimental data reported by Hsu and Hsu	3.16
3.5	Comparison of proposed stress-strain model with experimental data reported by Dahl	3.17
3.6	Comparison of proposed stress-strain model with CEB model	3.18
3.7	Modelling of the complete stress-strain behaviour of the grade C100 and C120 concretes	3.19
3.8	Tensile strength versus compressive strength	3.21
3.9	Normalised relationship between octahedral shear strength and normal stress	3.28

3.10	Normalised relationship between compressive strength and confining pressure	3.28
3.11	Strength enhancement as a function of confining pressure	3.29
3.12	Normalised relationship between peak strain and strength of confined concrete	3.30
3.13	Peak strain ratio versus confining pressure	3.31
3.14	Residual strength of confined concrete	3.34
3.15	Comparison of proposed confinement model with experimental data reported by Attard and Setunge	3.35
3.16	Comparison of proposed confinement model with experimental data reported by Xie *et al*	3.36
3.17	Comparison of proposed confinement model with experimental data reported by Xie *et al*	3.36
3.18	Comparison of proposed confinement model with experimental data reported by Richart *et al*	3.37
3.19	Schematic illustration of load-strain behaviour of transversely reinforced concrete columns	3.40
3.20	Concentric load capacities of transversely reinforced concrete columns	3.42
3.21	Illustration of arching action for two typical tie configurations	3.46
3.22	Strength of uniformly confined concrete	3.49
3.23	Strength of concrete confined by means of circular hoops	3.52
3.24	Strength of concrete confined by means of square hoops	3.52
3.25	Effect of passive confinement on peak strain of concrete	3.53
3.26	Comparison of computed and experimental stress-strain curves for a	3.57

70 MPa concrete confined by type A ties

3.27 Comparison of computed and experimental stress-strain curves for a 101 MPa concrete confined by type A ties 3.58

3.28 Comparison of computed and experimental stress-strain curves for a 82 MPa concrete confined by type B ties 3.58

3.29 Comparison of computed and experimental stress-strain curves for a 82 MPa concrete confined by type C ties 3.59

3.30 Comparison of computed and experimental stress-strain curves for a 82 MPa concrete confined by type D ties 3.59

3.31 Comparison of computed and experimental stress-strain curves for a 78 MPa concrete confined by type D ties 3.60

3.32 Comparison of computed and experimental stress-strain curves for a 92 MPa concrete confined by type D ties 3.60

3.33 Comparison of computed and experimental stress-strain curves for a 88 MPa concrete confined by type D ties 3.61

3.34 Predicted stress-strain behaviour of the passively confined concrete in test columns SL05U and LH05U 3.62

3.35 Stress-strain behaviour of core concrete according to CEB model 3.66

3.36 Stress-strain behaviour according to Saatcioglu and Razvi's model 3.68

3.37 Stress-strain behaviour according to Bjerkeli *et al's* model 3.70

3.38 Stress-strain behaviour according to El-Dash and Ahmad's model 3.72

3.38 Stress-strain behaviour according to Cusson and Paultre's model 3.74

4.1 Numerical representation of cross-section 4.7

4.2 Transformation of coordinates for a quadrilateral element 4.8

4.3 Sign convention and action points for forces 4.9

4.4	Modelling of slender column	4.17
4.5	Sign convention and action points for external forces	4.18
4.6	Modelling of cross-sections of uniaxially bent columns	4.32
4.7	Cross-sections of columns tested by Saatcioglu *et al*	4.35
4.8	Assumed stress-strain behaviour of concretes	4.36
4.9	Computed influence of confinement on load-deflection diagrams	4.37
4.10	Computed influence of confinement on interaction diagrams	4.38
4.11	Cross-sections of columns tested by Lloyd and Rangan	4.39
4.12	Assumed stress-strain behaviour of concretes	4.40
4.13	Observed effect of eccentricity on ultimate load capacity of columns in test series I, III, IX and XI	4.42
4.14a	Load-deflection curves for columns in test series I	4.42
4.14b	Load-deflection curves for columns in test series XI	4.43
4.15	Cross-sections of columns tested by Foster and Attard	4.45
4.16	Assumed stress-strain behaviour of concretes	4.46
4.17	Computed influence of confinement on interaction diagrams	4.50
4.18	Computed increase in axial load capacity due to confinement	4.51
4.19	Computed increase in axial load capacity due to confinement when ignoring the presence of the concrete cover	4.51
4.20	Cross-sections of columns tested by Claeson and Gylltoft	4.53
4.21	Assumed stress-strain behaviour of concretes	4.53
4.22	Observed load-deflection curves for columns with type 2 cross-section	4.54
4.23	Influence of slenderness on ultimate load	4.55
4.24	Cross-sections of columns tested by Kim and Yang	4.57
4.25	Assumed stress-strain behaviour of concretes	4.57

4.26	Influence of slenderness ratio on ultimate load	4.59
4.27	Computed interaction diagrams and failure combinations	4.59
4.28	Modelling of cross-sections of biaxially bent columns	4.60
4.29	Cross-sections of columns tested by Cranston and Sturrock	4.62
4.30	Assumed stress-strain behaviour of concretes	4.62
4.31	Load-deflection curves for test column 3	4.63
4.32	Cross-sections of columns tested by Hsu	4.64
4.33	Assumed stress-strain behaviour of concrete	4.64
4.34a	Biaxial moment curvature relations for column U-5	4.66
4.34b	Biaxial moment curvature relations for column U-5	4.66
5.1	Test columns SH20U, SL15U, SH10U and SL05U	5.5
5.2	Test columns SH20B and SL15B	5.6
5.3	Test columns LL20U, LH15U, LL10U, LH05U, LH10B and LL05B	5.7
5.4	Loading rig for the testing of the 4 m long columns	5.10
5.5	Suspension rig for the testing of the 4 m long columns	5.11
5.6	Experimental setup for the testing of the 8 m long columns	5.12
5.7	Positioning of displacement transducers	5.16
5.8	Positioning of external strain gauges	5.17
5.9	Positioning of internal strain gauges	5.18
5.10	Failed section of column SH20U	5.26
5.11	Failed section of column SH10U	5.26
5.12	Failed section of column SH10U	5.26
5.13	Failed section of column SH20B	5.27
5.14	Failed section of column SL15B	5.27
5.15	Failed section of column LL20U	5.28

5.16	Failed section of column LH15U	5.28
5.17	Failed section of column LL10U	5.28
5.18	Failed section of column LH05U	5.29
5.19	Failed section of column LH10B	5.29
5.20	Failed section of column LL05B	5.29
5.21	Strain profiles for test column SH20U	5.31
5.22	Strain profiles for test column SH10U	5.32
5.23	Strain profiles for test column SL05U	5.32
5.24	Strain profiles for test column SH20B	5.32
5.25	Strain profiles for test column SL15B	5.33
5.26	Strain profiles for test column LL20U	5.33
5.27	Strain profiles for test column LH15U	5.33
5.28	Strain profiles for test column LL10U	5.34
5.29	Strain profiles for test column LH05U	5.34
5.30	Strain profiles for test column LH10B	5.34
5.31	Strain profiles for test column LL05B	5.35
5.32	Extreme fibre strains for column SH20U	5.39
5.33	Extreme fibre strains for column SH10U	5.39
5.34	Extreme fibre strains for column SL05U	5.40
5.35	Extreme fibre strains for column SH20B	5.40
5.36	Extreme fibre strains for column SL15B	5.40
5.37	Extreme fibre strains for column LL20U	5.41
5.38	Extreme fibre strains for column LH15U	5.41
5.39	Extreme fibre strains for column LL10U	5.41
5.40	Extreme fibre strains for column LH05U	5.42

5.41	Extreme fibre strains for column LH10B	5.42
5.42	Extreme fibre strains for column LL05B	5.42
5.43	Straining of main reinforcement bars	5.45
5.44	Typical straining of transverse reinforcement	5.46
5.45	Mid-height deflections of shorter columns	5.48
5.46	Mid-height deflections of longer columns	5.48
5.47	Mid-height curvatures of shorter columns	5.50
5.48	Mid-height curvatures of longer columns	5.51
5.49	Defected shape of column SH20U	5.52
5.50	Deflected shape of column SH10U	5.52
5.51	Deflected shape of column SL05U	5.52
5.52	Deflected shape of column SH20B	5.53
5.53	Deflected shape of column SL15B	5.53
5.54	Deflected shape of column LL20U	5.53
5.55	Deflected shape of column LH15U	5.54
5.56	Deflected shape of column LL10U	5.54
5.57	Deflected shape of column LH05U	5.54
5.58	Deflected shape of column LH10B	5.55
5.59	Deflected shape of column LL05B	5.55
5.60	Modified mid-height deflections of shorter columns	5.56
5.61	Modified mid-height deflections of longer columns	5.57
5.62	Modelling of cross-sections	5.58
5.63	Computed mid-height deflections for shorter columns	5.62
5.64	Computed mid-height deflections for longer columns	5.62
5.65	Computed extreme fibre strains for shorter columns	5.63

5.66	Computed extreme fibre strains for longer columns	5.63
5.67	Assumed stress-strain behaviour of concretes	5.66
5.68	Computed effect of non-zero tensile concrete strength on extreme strains	5.66
5.69	Computed effect of friction forces on extreme strains	5.68
5.70	Assumed stress-strain behaviour of concretes	5.69
5.71	Computed effect of underestimated concrete strength on extreme strains	5.69
5.72	Computed effect of load eccentricity on extreme strains	5.70
6.1	Cross-sections of analysed columns	6.1
6.2	Stress-strain behaviour of unconfined concretes	6.2
6.3	Eccentric load capacities for unconfined C20 columns	6.4
6.4	Eccentric load capacities for unconfined C60 and C100 columns	6.5
6.5	Stress-strain behaviour of confined concretes	6.6
6.6	Effect of confinement on the squash loads	6.7
6.7a	Effect of confinement on eccentric load capacity of the C20 column having a slenderness ratio of 8	6.9
6.7b	Effect of confinement on eccentric load capacity of the C20 column having a slenderness ratio of 16	6.9
6.7c	Effect of confinement on eccentric load capacity of the C20 column having a slenderness ratio of 32	6.10
6.8a	Effect of confinement on eccentric load capacity of the C60 column having a slenderness ratio of 8	6.10
6.8b	Effect of confinement on eccentric load capacity of the C60 column having a slenderness ratio of 16	6.11
6.8c	Effect of confinement on eccentric load capacity of the C60 column	6.11

having a slenderness ratio of 32

6.9a Effect of confinement on eccentric load capacity of the C100 column having a slenderness ratio of 8 6.12

6.9b Effect of confinement on eccentric load capacity of the C100 column having a slenderness ratio of 16 6.12

6.9c Effect of confinement on eccentric load capacity of the C100 column having a slenderness ratio of 32 6.13

6.10a Effect of confinement on load-deflection diagrams for the C20 column having a slenderness ratio of 8 6.14

6.10b Effect of confinement on load-deflection diagrams for the C20 column having a slenderness ratio of 16 6.14

6.10c Effect of confinement on load-deflection diagrams for the C20 column having a slenderness ratio of 32 6.15

6.11a Effect of confinement on load-deflection diagrams for the C100 column having a slenderness ratio of 8 6.15

6.11b Effect of confinement on load-deflection diagrams for the C100 column having a slenderness ratio of 16 6.16

6.11c Effect of confinement on load-deflection diagrams for the C100 column having a slenderness ratio of 32 6.16

6.12a Effect of increased bar size on eccentric load capacity of the C20 column having a slenderness ratio of 8 6.19

6.12b Effect of increased bar size on eccentric load capacity of the C20 column having a slenderness ratio of 16 6.19

6.12c Effect of increased bar size on eccentric load capacity of the C20 column 6.20

having a slenderness ratio of 32

6.13a Effect of increased bar size on eccentric load capacity of the C100 column having a slenderness ratio of 8 6.20

6.13b Effect of increased bar size on eccentric load capacity of the C100 column having a slenderness ratio of 16 6.21

6.13c Effect of increased bar size on eccentric load capacity of the C100 column having a slenderness ratio of 32 6.21

6.14a Effect of increased bar size on load-deflection diagrams for the C20 column having a slenderness ratio of 8 6.22

6.14b Effect of increased bar size on load-deflection diagrams for the C20 column having a slenderness ratio of 16 6.23

6.14c Effect of increased bar size on load-deflection diagrams for the C20 column having a slenderness ratio of 32 6.23

6.15a Effect of increased bar size on load-deflection diagrams for the C100 column having a slenderness ratio of 8 6.24

6.15b Effect of increased bar size on load-deflection diagrams for the C100 column having a slenderness ratio of 16 6.24

6.15c Effect of increased bar size on load-deflection diagrams for the C100 column having a slenderness ratio of 32 6.25

6.16a Influence of concrete cover on eccentric load capacity of confined C20 columns having a slenderness ratio of 8 6.27

6.16b Influence of concrete cover on eccentric load capacity of confined C20 columns having a slenderness ratio of 16 6.28

6.17a Influence of concrete cover on eccentric load capacity of confined C100 6.28

columns having a slenderness ratio of 8

6.17b Influence of concrete cover on eccentric load capacity of confined C100 columns having a slenderness ratio of 16 6.29

6.18a Load-deflection diagrams for externally confined C20 columns having a slenderness ratio of 8 6.29

6.18b Load-deflection diagrams for externally confined C20 columns having a slenderness ratio of 16 6.30

6.19a Load-deflection diagrams for externally confined C100 columns having a slenderness ratio of 8 6.30

6.19b Load-deflection diagrams for externally confined C100 columns having a slenderness ratio of 16 6.31

List of Tables

Table		Page
2.1	Mix proportions for concretes	2.2
2.2	28 days cube strength of C100 concrete	2.9
2.3	28 days cube strength of C120 concrete	2.9
2.4	Field cube strength of C100 concrete	2.9
2.5	Field cube strength of C120 concrete	2.10
2.6	Field cylinder strength of C100 concrete	2.11
2.7	Field cylinder strength of C120 concrete	2.11
2.8	Key results from strain-gauged cylinder tests	2.15
2.9	Results from split cylinder tests	2.18
2.10	Average material properties for reinforcement bars	2.20
3.1	Nominal confining stress for standard tie configurations	3.45
3.2	Reduction coefficients according to the 45°arching action method	3.47
3.3	Reduction coefficients according to the modified arching action method	3.50
3.4	Predicted property enhancements for core concrete of column SL05U	3.63
3.5	Predicted property enhancements for core concrete of column LH05U	3.64
4.1a	Details of columns tested by Saatcioglu *et al*	4.36
4.1b	Comparison of experimental and analytical results	4.37
4.2a	Details of columns tested by Lloyd and Rangan	4.40
4.2b	Comparison of experimental and analytical results	4.41
4.3a	Details of columns tested by Foster and Attard	4.46
4.3b	Comparison of experimental and analytical results	4.48
4.4a	Details of columns tested by Claeson and Gylltoft	4.53

4.4b	Comparison of experimental and analytical results	4.54
4.5a	Details of columns tested by Kim and Yang	4.57
4.5b	Comparison of experimental and analytical results	4.58
4.6a	Details of columns tested by Cranston and Sturrock	4.62
4.6b	Comparison of experimental and analytical results	4.63
4.7a	Details of column tested by Hsu	4.65
4.6b	Comparison of experimental and analytical results	4.65
5.1	Details of columns included in the experimental investigation	5.3
5.2	Normalised position, z/L, of gauges and transducers	5.19
5.3	Failure loads for columns tested	5.21
5.4	Summary of extreme fibre strains at column failure	5.44
5.5	Maximum tensile strain in links	5.47
5.6	Mid-height deflections at column failure - measured and modified	5.57
5.7	Material properties of concrete components	5.59
5.8	Comparison of experimental and computed results - failure loads and corresponding vertical mid-height deflections	5.60
5.9	Comparison of experimental and computed results - extreme fibre strains at column failure	5.64
5.10	Computed effect of non-zero tensile concrete strength on failure loads and deflections	5.66
5.11	Computed effect of friction forces on failure loads and deflections	5.66
5.12	Computed effect of underestimated concrete strength on failure loads and deflections	5.69
6.1	Material properties of concretes	6.3

Abstract

The mechanical and physical properties of high strength concrete make it an attractive building material, especially for components resisting high compressive loads such as the lower columns in high-rise buildings. However, due to the brittle nature of this material, concern exists about the ductility of high strength concrete columns. This thesis investigates the possibility of improving the ductility of slender high strength concrete columns by means of hoop reinforcement.

A total of twelve full-scale columns with 250 mm square cross-sections was experimentally tested under either uniaxially or biaxially eccentric compression. The columns had effective lengths of either 4 m or 8 m, and were transversely reinforced by hoops with spacings ranging from 200 mm to 50 mm. Observations were made on failure mode, axial loads, deflections and strains. The tests indicated that a dense reinforcement cage had some effect of enhancing both the strength and the pre-peak ductility of the columns. The maximum compressive concrete strains at failure were significantly less than the 3.5 mm/m used in traditional stress block design of normal strength concrete sections. For none of the columns was the hoop reinforcement found to yield at the time of strength failure.

A new confinement model, which is equally valid for normal and high strength concrete, was developed. According to this model the effect of confinement on the complete stress-strain behaviour of concrete can be expressed directly through its influence on the strength and corresponding strain. Empirical equations for estimating both of these quantities are presented. By modifying a well-known method for calculating the effective confining pressure the stress-strain model is shown to be equally capable of describing test results obtained under passive and active confinement conditions.

A computer program, which incorporated the findings from the investigation into the modelling of confinement effects, was developed for the analysis of slender high strength concrete columns. From a parametric study, backed up by a survey of published information on eccentrically loaded reinforced concrete columns, it was demonstrated that the unconfined concrete cover plays a major role in negating the structural benefits of confinement, and that this is especially the case for high strength concrete columns. For a given column slenderness and load eccentricity the deflections at strength failure were found to be largely independent of the concrete strength. However, in terms of load capacity high strength concrete was shown to be most effective in short columns subjected to nearly concentric compression.

Acknowledgements

The investigation reported in this thesis was carried out under the supervision of Professor K.S. Virdi, to whom the author is deeply grateful. Throughout the investigation and its reporting Professor K.S. Virdi provided encouragement and valuable guidance to the author.

The author is indebted to the Danish Research Council for the generous financial support given by them to cover expenses incurred by the author during the first part of his stay at City University, London. Likewise, the funding provided towards the project by The Engineering and Physical Sciences Research Council is deeply acknowledged.

The deepest debts of gratitude are owed to my wife Janice, who has shown extraordinary patience and support, not least during the darker patches of the tale. Finally, the author would like to thank his family for their support.

List of Symbols

A	Area
$A_{cc,eff}$	Cross-sectional area of effectively confined concrete core
A_{cc}	Cross-sectional area of nominal concrete core
A_g	Cross-sectional area of all longitudinal reinforcement bars within cross-section
A_s	Cross-sectional area of tie bar
A_{tot}	Gross area of cross-section
α_n , α_s	Efficiency factors associated with given tie configuration and distribution
β	Parameter governing the softening behaviour of concrete
d	Dimension of cross-section
d_c	Nominal dimension of concrete core
d_g	Spacing between laterally supported longitudinal reinforcement bars
d_x, d_y	Dimension of cross-section after x- and y-axis respectively
detJ	Determinant of Jacobian matrix
E_c	Modulus of elasticity for concrete
E_{ccs}	Secant modulus at peak stress for confined concrete, $E_{ccs} = f_{cc}/\varepsilon_{cc}$
E_{cs}	Secant modulus at peak stress for concrete, $E_{cs} = f_c/\varepsilon_c$
E_s	Modulus of elasticity for steel reinforcement
e_x, e_y	Eccentricity of applied axial load after x- and y-axis respectively
ε_c	Compressive strain at peak stress for concrete
ε_{c50}	Compressive post peak strain at $\sigma_3 = -0.50 f_c$ for concrete
ε_{c85}	Compressive post peak strain at $\sigma_3 = -0.85 f_c$ for concrete
ε_{cc}	Compressive strain at peak stress for confined concrete
ε_{cc50}	Compressive post peak strain at $\sigma_3 = -0.50 f_{cc}$ for confined concrete

ε_{cc85}	Compressive post peak strain at $\sigma_3 = -0.85 f_{cc}$ for confined concrete
$\varepsilon_{cc85'}$	Compressive post peak strain at $\sigma_3 = -0.85 f_c$ for confined concrete
ε_o	Longitudinal strain at centroid of cross-section
$\varepsilon_1, \varepsilon_2$	Transverse strains
ε , ε_3	Longitudinal strain
ε_s	Tensile strain
ε_{sf}	Strain at peak stress for steel reinforcement
ε_{su}	Nominal breaking strain for steel reinforcement
ε_{sy}	Yield strain for steel reinforcement
ε_v	Volumetric strain, $\varepsilon_v = \varepsilon_1 + \varepsilon_2 + \varepsilon_3$
f_c	Compressive strength of concrete
f_{cc}	Compressive strength of confined concrete
$f_{c,cub}$	Compressive cube strength
$f_{c,cyl}$	Compressive cylinder strength
f_{2c}	Equibiaxial compressive strength of concrete
f_s	Tensile strength of steel reinforcement
f_{sp}	Split cylinder strength
f_{sy}	Yield strength of steel reinforcement
f_t	Direct tensile strength of concrete
γ_{ssd}	Water absorption ratio
h	Length of column segments
k_x, k_y	Spring constants for rotations about x- and y-axis respectively
κ_x, κ_y	Curvatures resolved after x- and y-axis respectively
L	Length of column or cylinder
M_x, M_y	Bending moments about x- and y-axis respectively

M_x^f, M_y^f	Free bending moments about x- and y-axis respectively
N_i	Shape functions, $i = 1, 2, 3, 4$
ν	Poisson's ratio
ν_0	Initial Poisson's ratio
ν_c	Poisson's ratio at peak stress
P	Axial load
P_c	Axial load capacity of column
p_x, p_y	Uniformly distributed loads after x- and y-axis respectively
P_x, P_y	Point loads after x- and y-axis respectively
φ	Angle defining axis for biaxial bending moment
ρ	Bulk density
ρ_a	Particle density
ρ_g	Volumetric ratio of longitudinal steel reinforcement, $\rho_g = A_g / A_{tot}$
ρ_s	Volumetric ratio of confining steel reinforcement within nominal core
ρ_s^*	Total transverse steel area in two orthogonal directions divided by the corresponding concrete area
s	Pitch of transverse reinforcement
$\sigma_{l,eff}$	Effective confining stress
$\sigma_{l,nom}$	Nominal confining stress
σ_{cr}	Critical stress
σ_1, σ_2	Transverse stresses
σ , σ_3	Longitudinal stress
σ_{oct}	Octahedral normal stress
σ_s	Tensile stress
τ_{oct}	Octahedral shear stress

θ	Angle of similarity (defines orientation of shear stresses)
θ_x, θ_y	Rotations about y- and x-axis respectively
u, v, w	Deflections after Cartesian axes
x, y, z	Cartesian coordinates
x_{imp}, y_{imp}	Imperfections for centroidal axis
x_o, y_o	Centroid of cross-section
ξ, η	Natural coordinates

Chapter 1: Introduction

1.1 Background

Due to the continuing advances in concrete technology normal weight concrete with compressive strengths in excess of 100 MPa can nowadays easily be obtained by using carefully selected, but readily available, materials and conventional methods for mixing, placing and curing. In particular the development of high range water reducing admixtures, which ensure workability of the fresh concrete at very low water-cement ratios, has played an essential role in the quest for concrete of ever higher strength. In some cases, silica fume is used to enhance the strength of the concrete mix.

High strength concrete has a greater stiffness, a higher strength at early age, a lesser amount of shrinkage and creep, and a greater resistance against physical and chemical deterioration than normal strength concrete. For these reasons it has been the preferred building material in a small, but increasing, number of very different onshore and offshore projects (CEB, 1994). However, the major application of high strength concrete has been in the lower columns of high-rise buildings, where smaller cross-sectional dimensions can have significant economical benefits by increasing the rentable floor space and speeding up the construction process.

Since the recommendations in existing Codes of Practice, such as BS 8110 (1997), are based on tests on concrete with strengths up to about 50 MPa, these recommendations are not directly applicable to members made from high strength concrete. Thus, there appears to be a need to test the applicability of the existing Codes for structural design using high strength concrete.

An increase in concrete strength is accompanied by a change in mechanical behaviour. The ascending branch of the stress-strain curve becomes increasingly linear, and material failure increasingly brittle. The latter reflected by a steep descending branch. In this study concrete having compressive strengths below 40 MPa is referred to as being of normal strength, and concrete having compressive strengths in excess of 80 MPa as being of high strength. This appears to be the currently accepted definition of high strength concrete.

In order to satisfy the design requirements concrete members are, implicitly if not explicitly, required to be ductile, i.e. the members need to be capable of responding inelastically without losing their load carrying capacity. Ductility is necessary for many reasons. It ensures warning in the form of large deflections prior to failure, and facilitates the redistribution of forces, for example in continuous construction. In earthquake scenarios ductility is important because lateral inertia forces prevail, and because energy dissipation dampens the oscillations caused by the loading. Because of the brittle material behaviour of high strength concrete, concern exists whether structural components made from this material have sufficient ductility.

It is well known that the strength and deformation properties of compressed concrete can be enhanced by confinement through suitably arranged transverse reinforcement. Indeed, the effects of spiral reinforcement on the behaviour of plain concrete was investigated as early as in 1929 by Richart *et al.* Almost all of the available experimental work carried out on confined high strength concrete has focussed on the behaviour under concentric compression. Thus, it is not surprising that the modelling of confinement effects is still a controversial issue, and no widely used model applies to members made from high strength concrete.

Some experimental results on the structural response of full-scale, or near full-scale, high strength concrete columns subjected to eccentric compression have also been reported. In the case of short columns, investigations have been carried out by Limsuwan (1993), Bjerkeli *et al* (1993), Ibrahim and MacGregor (1996a), Lloyd and Rangan (1996) and Foster and Attard (1997), and in the case of slender columns only by Chuang and Kong (1997) and Claeson and Gylltoft (1998).

The objectives of the thesis were determined in the context of the above background.

1.2 Objectives of the Present Project

The objectives of the work described in this thesis may be outlined as follows:

- To test means of modifying the behaviour of columns of high strength concrete so as to obtain a ductile failure mode. The method chosen was to use hoop reinforcement, in the manner of shear reinforcement, to confine the concrete through the passive straining of the hoop reinforcement

- To quantify the effect of confinement on the stress-strain characteristics of high strength concrete.

- To extend a previously developed method of stability and ultimate load analysis of reinforced concrete columns, incorporating the interaction between the transverse reinforcement and the longitudinal stress-strain characteristics of confined concrete, making it particularly applicable to high strength concrete columns.

- To conduct uniaxial and biaxial eccentric compression tests on a total of 12 full-scale high strength concrete slender length columns. Test parameters to be varied included the spacings between the reinforcement hoops. The test were to be used to measure the effectiveness of the hoop reinforcement on enhancing the ductility of columns made of high strength concrete.

1.3 Organisation of the Thesis

The following outlines how the sections of the thesis are put together.

The next chapter gives a detailed description of the production and material characteristics of the two high strength concrete mixes employed in the experimental investigation.

Chapter 3 provides a general description of the material characteristics of high strength concrete made from normal weight aggregates, using traditional methods for mixing, curing and placing. Aspects of existing empirical expressions used to predict the modulus of elasticity, the strain at peak stress, the apparent Poisson's ratio and the tensile strength are assessed when applied to high strength concrete.

An incremental model is developed for calculating the relationship between the average longitudinal stress and strain for the concrete core in transversely reinforced stub columns subjected to concentric compression. The model, which is equally applicable to normal and high strength concrete, is validated against a large set of experimental results. Stress-strain curves generated by the new confinement model are compared to the curves generated by some of the existing models.

In chapter 4 the investigation is widened to include reinforced concrete columns failing due to a combination of flexural and axial loading effects. A versatile numerical method for calculating the biaxial load-deformation response of slender high strength concrete columns is described. Available test data on columns, covering a wide range of geometric and physical properties, are used to validate a computer implementation of the numerical method. The effects on the structural response of slenderness, load eccentricity, concrete grade, confinement and cover concrete are addressed.

Although this investigation is limited to pinned columns subjected to uniaxial and biaxial eccentric compression, the computer program is capable of analysing braced columns with non-constant cross-sections of arbitrary shape supporting flexible beam members. The columns can be analysed for increasing eccentric compression under a condition of constant lateral loading, and vice versa. In both cases the analysis terminates as soon as further incrementation in the principal loading variables cannot be sustained by the column.

Chapter 5 gives a detailed description of the experimental programme, in which a total of 12 columns was tested in a rig specially built for the purpose.

With the principal test parameters being the column slenderness, the concrete strength, the load eccentricity and the distribution of the transverse reinforcement ties, observations on failure mode, ultimate load capacity, deflections and strains are discussed. The test results are compared to their analytical counterparts, and the likely impact on the results of some of the uncertainties associated with the experimental tests are assessed.

A numerical investigation into the effect of confinement on the load-deflection response of eccentrically loaded columns is presented in chapter 6. The analysed columns all have cross-sectional dimensions identical to the columns tested in the experimental investigation, but slenderness, concrete strength, load eccentricity and effective confining pressure all vary within significantly larger bounds than was the case for the experimentally tested columns. In addition, the effect of increasing the size of the longitudinal reinforcement bars as an alternative to confinement is investigated. Special attention is given to the effect that the concrete cover has on the behaviour of the confined concrete columns.

Conclusions from the present investigation are described in chapter 7, which also includes some suggestions for extending the investigation reported in this thesis.

Chapter 2: High Strength Concrete Materials

2.1 High Strength Concrete

The principal part of this thesis relates to the behaviour of slender columns made from high strength concrete. A total of 12 columns with 250 mm square cross-sections, and lengths of either 3.3 m or 7.3 m (nominal length of either 4.0 m or 8.0 m) were fabricated and tested in the laboratories of the Civil Engineering Department at City University. The two mix designs employed in the production of the test columns had target cube strengths of 100 MPa and 120 MPa respectively. The basis for the high strength of the mixes was a high content of binder material, high quality aggregates, a low water to binder ratio and the use of superplasticiser for workability.

Usually the quality assessment of hardened concrete is based on strength tests only. However, in order to facilitate a rigorous analysis of the behaviour of the test columns, supplementary information on the stress-strain characteristic of the two grades of high strength concrete was required. In this chapter, the materials employed in fabricating the high strength concrete columns are described.

2.1.1 Mix Design

Table 2.1 lists the mix proportions used in the experimental investigation for producing concrete with a target cube strength of 100 MPa and 120 MPa respectively. The mix designs, which were the result of several trials, differed primarily by the grade C120 mix containing more binder material and less water than the grade C100 mix. Furthermore, the grade C120 mix contained microsilica in addition to cement as a binder material. The

tabulated aggregate contents refer in accordance with common practice to aggregates in a saturated and surface dry state.

Table 2.1
Mix proportions for concretes

	Concrete grade	
Material	C100	C120
Cement, (kg/m^3)	541	512
Microsilica, (kg/m^3)	0	51
Water, (kg/m^3)	142	119
Fine aggregates, (kg/m^3)	899	874
Coarse aggregates, (kg/m^3)	830	874
Superplasticiser, (kg/m^3)	16.2	20.7
Water/binder ratio (%)	28.0	23.3
Plasticiser/binder ratio (%)	3.0	3.7
Aggregates/binder ratio (-)	3.1	3.1

The origin and essential characteristics of the constituent materials were as follows:

Cement: "*Ordinary Portland Cement, class 42.5*".

Supplied by "Blue Circle Industries, Northfleet Works".

Particle density, $\rho_a = 3140\ kg/m^3$.

Microsilica: "*EMSAC 500S*" (microsilica slurry).

Supplied by "Elkem Materials".

Bulk density, $\rho = 1410\ kg/m^3$.

50% free water by weight.

Superplasticiser: "*Cormix SP6*".

Supplied by "W.R. Grace Ltd, Cormix Division".

Bulk density, $\rho = 1200\ kg/m^3$.

59% free water by weight.

Fine aggregates: "*Thames Valley, zone 2*".

Particle density, $\rho_a = 2550\ kg/m^3$.

Water absorption ratio, $\gamma_{ssd} = 0.0178$.

Coarse aggregates: "*Crushed Carboniferous limestone, screened 6-10 mm*".

Supplied by "ARC Southern, Chipping Sodbury Quarry".

Particle density, $\rho_a = 2720\ kg/m^3$.

Water absorption ratio, $\gamma_{ssd} = 0.0032$.

Water: *"Ordinary tap water"*

The particle densities and water absorption ratios of the aggregates were determined following the procedures specified in BS 812: Part 2 (1995). The water absorption ratio is defined as the weight of moisture contained in the saturated and surface dry aggregates divided by their oven dry weight.

The particle size distributions of the aggregates, shown in figures 2.1 and 2.2, were determined by the sieving method described in BS 812: Section 103.1 (1985). Interestingly, the coarse aggregates were found to contain a significant proportion of crusher dust. Approximately 1.7% of the total weight of these aggregates passed through a sieve having a nominal aperture size of 65 μm.

Prior to commencing the column production, an accidental leakage caused a significant amount of water to seep into the hopper containing the mixing sand. Besides dramatically rising the average moisture content of the sand, the leakage resulted in unacceptable large variations in the moisture content of tested samples. A much lower and almost uniformly distributed moisture content was achieved by air drying the required amount of mixing sand for about a week prior to it being used. The sand was turned over several times throughout

the drying period. As a result of the drying procedure the average moisture content of the mixing sand on the days of column casting ranged from 1.21% to 2.41%, but the maximum difference between the moisture content of two samples taken on any given casting day was reduced to below 0.30%. The hopper containing the coarse aggregates was not affected by the water leakage, and the moisture content of the coarse aggregates was determined to reduce from 0.61% to 0.46% during the four-month period of column production.

Based on the actual moisture content of the aggregates, and when ignoring the temporal aspects of water transport, the ratio of effective water content to cement content in the grade C100 concrete mix was calculated to vary between 27.3% and 29.5% during the column production period. Likewise, the effective water to binder ratio of the grade C120 concrete mix was calculated to vary between 22.7% and 24.8%.

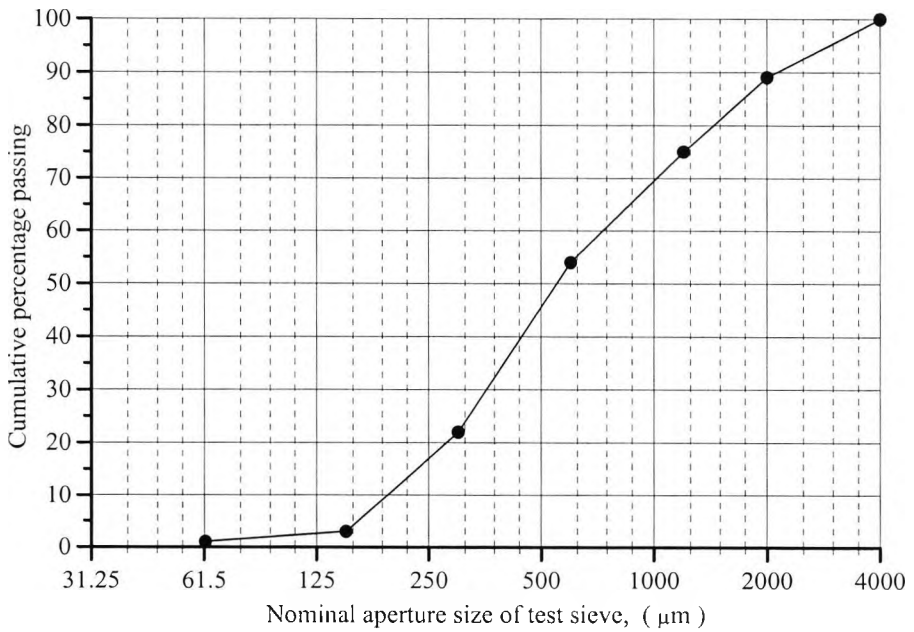

Figure 2.1
Particle size distribution of fine aggregates

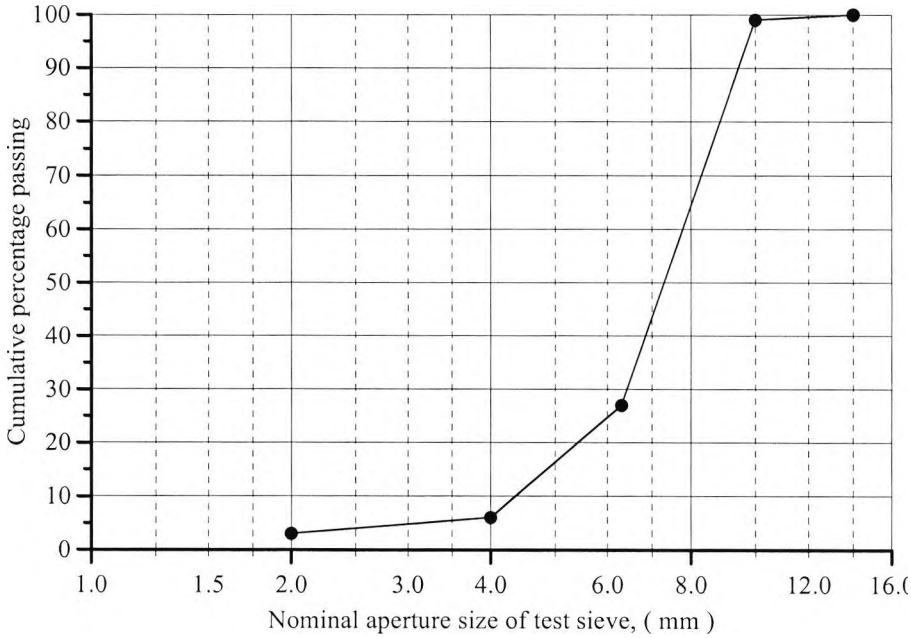

Figure 2.2
Particle size distribution of coarse aggregates

2.1.2 Workability of Fresh Concrete

The workability of the fresh concrete was measured both by means of the slump test described in BS 1881: Part 102 (1983), and the flow test described in BS 1881: Part 105 (1984). The slump measure always exceeded 175 mm, which is considered to be the limit for which this test is suitable for describing the workability of fresh concrete. The flow measures varied from 390 mm to 490 mm for the grade C100 mix, and from 390 mm to 430 mm for the grade C120 mix. Thus, the workability of the employed concrete mixes are classified as high to very high. However, their cohesive consistency made them very heavy to shovel compared to the much leaner mixes normally used.

2.1.3 Casting and Curing Procedure

The concrete was mixed in a paddle mixer having a maximum capacity of 0.09 m^3. Because of the mixer's limited capacity it was necessary to mix three batches of concrete for casting a 3.3 m long column, and six batches for casting an 7.3 m long column. Nevertheless, a

consistent and uniform concrete quality could be guaranteed by adhering to the following mixing procedure:

1/ Fine and coarse aggregates are mixed for 2 minutes to give a uniform mixture.

2/ The slurrified microsilica is added, and mixing continues for a further 3 minutes to ensure a uniform coating of the aggregates by silica fume.

3/ The cement is added, and mixing continues for a further 3 minutes.

4/ A mixture consisting of 50% of the superplasticiser dissolved in the mixing water is added, and mixing continues for a further 3 minutes.

5/ The remaining superplasticiser is added, and mixing continues for a further 2 minutes before discharging the concrete.

The full-scale columns were cast in a horizontal position in moulds fabricated from "Douglas fir" plywood, and were compacted by means of an internal vibrator. From each batch of concrete mix at least two 100 mm cubes and one 100×200 mm cylinder were cast so as to facilitate an assessment of the concrete quality. The small-sized control specimens were compacted on a vibrating table.

In an attempt to reduce the moisture loss from the newly cast columns to a minimum, the columns were covered by impervious sheeting immediately after casting, and by wet hessian 24 hours later. The hessian was sprinkled regularly so as to remain moist for 6 days. The columns were demoulded after about 10 days, after which they were stored in ambient laboratory conditions until the time of testing. The concrete cubes to be tested after the standard 28 days were demoulded after 2 days, and then water-cured until the time of testing. It is interesting that the cubes had not hardened sufficiently to allow demoulding and submersion within the recommended period of 16 hours to 28 hours of casting (BS1881: Part 111, 1983). This indicates that the large quantity of superplasticiser used in

the mix had a retarding effect on the rate of hydration of the cement paste. The control specimens to be tested on the same days as the full-scale columns were cured under conditions closely resembling those of their parent columns.

Despite the meticulous curing procedure, the development of plastic shrinkage cracks on the exposed surface of the columns could not be entirely avoided. A few very fine surface cracks developed at positions and in directions which appeared to closely follow the shrinkage obstructions originating from the hoop reinforcement.

The trowelled ends of the hardened test cylinders were in accordance with BS 1881: Part 110 (1983) smoothened by means of mortar-capping. Before applying the 1 - 2 mm thick mortar caps, the trowelled ends of the cylinders were roughened by hacking and wire-brushing. The capping materials were mixed in the following weight ratios: high alumina cement: microsilica: water: silicious sand (screened 150 - 300 μm): superplasticiser, 100: 10: 30: 33: 4.

2.1.4 Compressive Strength

In the present investigation, the uniaxial compressive strength of concrete was assessed from tests on 100 mm cubes and 100×200 mm cylinders. The choice of specimen sizes was dictated by the 200 tons loading capacity of the in-house Avery-Denison testing machine. The specimens were in accordance with BS 1881: Part 116 (1983) and BS 1881: Part 120 (1983), tested directly between steel loading platens at a constant stress rate of 0.25 MPa/s. The stress rate was maintained constant by manually operating the controls on the testing machine.

All the tested specimens failed explosively, and had smooth failure surfaces passing indiscriminately through mortar and coarse aggregates. When testing the cubes, a relatively

large-pyramid shaped fragment containing the face in contact with the stationary loading platen of the testing machine usually remained after failure (see figure 2.3). In contrast, the face of the cube in contact with the tilt cap always disintegrated into a number of smaller fragments. In the cylinder tests failure appeared to initiate at mid-height, and then propagate towards the ends so as to produce the well-known conical shape (see figure 2.3). In general, the ends of the cylinders remained uncracked after failure, which indicates that the adopted capping procedure did not adversely affect the load-carrying capacity of the cylinders. Thus, the confining effect of the friction forces developing at the interface between the specimen and the loading platen more than compensated for the lesser strength of the capping material. The compressive strength of the capping component was 59 MPa when determined from tests on 50 mm cubes at 7 days of age. This incidentally was the minimum time passing between capping and testing the cylinders.

Tables 2.2 and 2.3 summarise the results from the standard 28 days cube tests. It can be noted that both of the targeted concrete grades were obtained with a good degree of consistency throughout the duration of the experimental programme.

Tables 2.4 and 2.5 summarise the strength data for the cubes tested on the same days as the columns to which they were related. In the case of test series LH10B, only four of the six specimens cast were included in the statistics. This was because two of the specimens belonging to this test series failed in an asymmetric mode with the failure plane localised to a single face, which according to BS1881: Part 116 (1983) makes them unacceptable for strength assessment. Both of the discarded specimens had a compressive strength equal to approximately 83% of the mean strength of the remaining specimens in the series.

When comparing the 28-days strengths to the field strengths, it can be seen that the grade C100 concrete in general gained somewhat more strength with age than the grade C120 concrete. The gain in average strength of the cubes made from grade C100 concrete ranged

from 10.1 MPa to 21.4 MPa, and for the cubes made from grade C120 concrete from 10.2 MPa to 16.1 MPa. The tables also show that the field strength of the cubes was little, if at all, affected by the variations in testing age.

Table 2.2
28 days cube strength of C100 concrete

Parent column	SL05U SL15U	LL20U	LL10U	LL05B	SL15B	All
Casting date	13/6/96	16/9/96	19/9/96	10/10/96	18/10/96	-
Sample size	6	6	6	6	6	30
Mean strength, (MPa)	95.4	101.6	97.0	103.7	106.0	100.7
Coefficient of variation, (%)	3.8	2.8	6.9	3.5	2.5	5.5

Table 2.3
28 days cube strength of C120 concrete

Parent column	SH20U SH10U	LH15U	LH05U	LH10B	SH20B	All
Casting date	14/8/96	26/9/96	3/10/96	15/10/96	18/10/96	-
Sample size	6	6	6	6	6	30
Mean strength, (MPa)	124.0	121.8	124.7	121.4	122.0	122.7
Coefficient of variation, (%)	6.9	4.1	4.3	4.2	4.2	4.7

Table 2.4
Field cube strength of C100 concrete

Parent column	SL05U SL15U	LL20U	LL10U	LL05B	SL15B	All
Casting date	13/6/96	16/9/96	19/9/96	10/10/96	18/10/96	-
Age at testing, (days)	208	304	307	316	195	-
Sample size	6	6	6	6	3	27
Mean strength, (MPa)	116.8	119.3	115.9	113.8	116.9	116.5
Coefficient of variation, (%)	4.1	4.2	6.8	3.6	6.0	4.8
Mean strength gain, (MPa)	21.4	20.0	18.9	10.1	10.9	16.2

Table 2.5
Field cube strength of C120 concrete

Parent column	SH20U SH10U	LH15U	LH05U	LH10B	SH20B	All
Casting date	14/8/96	26/9/96	3/10/96	15/10/96	18/10/96	-
Age at testing, (days)	176	328	321	315	182	-
Sample size	6	6	6	4	3	25
Mean strength, (MPa)	137.6	137.3	134.9	133.0	138.1	136.2
Coefficient of variation, (%)	5.6	2.6	5.4	3.6	0.9	4.2
Mean strength gain, (MPa)	14.3	15.5	10.2	11.6	16.1	13.5

Tables 2.6 and 2.7 summarise the results from the cylinder tests. Due to various technical problems, the statistics for these tests often had to be based on reduced sample sizes. In the case of test series LL05B, the compressive strength of 75.9 MPa determined for one of the cylinders was significantly lower than the strengths determined for the other cylinders in the series. Since the failure plane in the weaker cylinder included the capped end-zone, it was concluded that the end preparation had been responsible for the weakening. During test series LL10U, problems developed with the testing machine, and the testing of the last specimen in the series had to be prematurely abandoned. In the case of test series LH15U, the cylinder strengths ranged from 37 MPa to 117 MPa. Furthermore, as illustrated by figure 2.4, failure in four of the six specimens developed along a single diagonal crack. It was later realised that the erratic results were caused by a machine fault. In view of the cube strength data, there is no reason to believe that the quality of test column LH15U was impaired in any way . For each of the test series LH 05U and SH20B, a single specimen had lost its mortar cap and as such could not be tested using the standard method. In an attempt to overcome this problem, the two specimens were tested using soft wood packing. However, the lateral expansion of the packing material initiated splitting failure at the top

of the specimens (see figure 2.5), and caused a strength reduction of approximately 20% when compared to the strengths of the similar specimens tested directly between the steel loading-platens.

Table 2.6
Field cylinder strength of C100 concrete

Parent column	SL05U SL15U	LL20U	LL10U	LL05B	SL15B	All
Casting date	13/6/96	16/9/96	19/9/96	10/10/96	18/10/96	-
Age at testing, (days)	216	304	307	316	195	-
Sample size	6	6	5	5	6	28
Mean strength, (MPa)	95.2	101.3	101.8	98.2	110.4	101.5
Coefficient of variation, (%)	7.3	4.9	5.6	1.3	1.3	6.8
Cylinder/cube strength ratio, (-)	0.82	0.85	0.88	0.86	0.94	0.87

Table 2.7
Field cylinder strength of C120 concrete

Parent column	SH20U SH10U	LH15U	LH05U	LH10B	SH20B	All
Casting date	14/8/96	26/9/96	3/10/96	15/10/96	18/10/96	-
Age at testing, (days)	176	328	321	316	196	-
Sample size	6	-	5	6	5	22
Mean strength, (MPa)	128.8	-	123.0	120.4	128.2	125.0
Coefficient of variation, (%)	4.1	-	5.1	5.4	4.5	5.3
Cylinder/cube strength ratio, (-)	0.94	-	0.91	0.91	0.93	0.92

It can be seen from tables 2.2 - 2.7 that the coefficients of variation evaluated for the individual test series ranged from 0.9% to 7.3%, whereas the six overall coefficients lay within the rather narrow band of 4.2% to 6.8%. This suggests that the coefficient of variation was largely independent of the quality of concrete, time of testing, and the shape of the specimen. According to guidelines for quality control of normal strength concrete, a coefficient of variation between 5% and 10% can be classified as "approaching laboratory

conditions" (Neville, 1959). Considering the strength data obtained in the investigation described in this thesis, and in the investigations carried out by Dahl (1992a), Lessard *et al* (1993) and Larrard *et al* (1994), this classification appears also to be applicable to the quality control of high strength concrete. In this context, it should be mentioned that the experimental work carried out by Lessard *et al* (1993) showed that end preparation of 100×200 mm cylinders by grinding rather than by capping had the effect of reducing the coefficient of variation by 1 - 2%.

In the present investigation, the average ratio of the 100×200 mm cylinder strength to the 100 mm cube strength was determined to be 0.87 and 0.92 for the grade C100 and C120 concrete respectively.

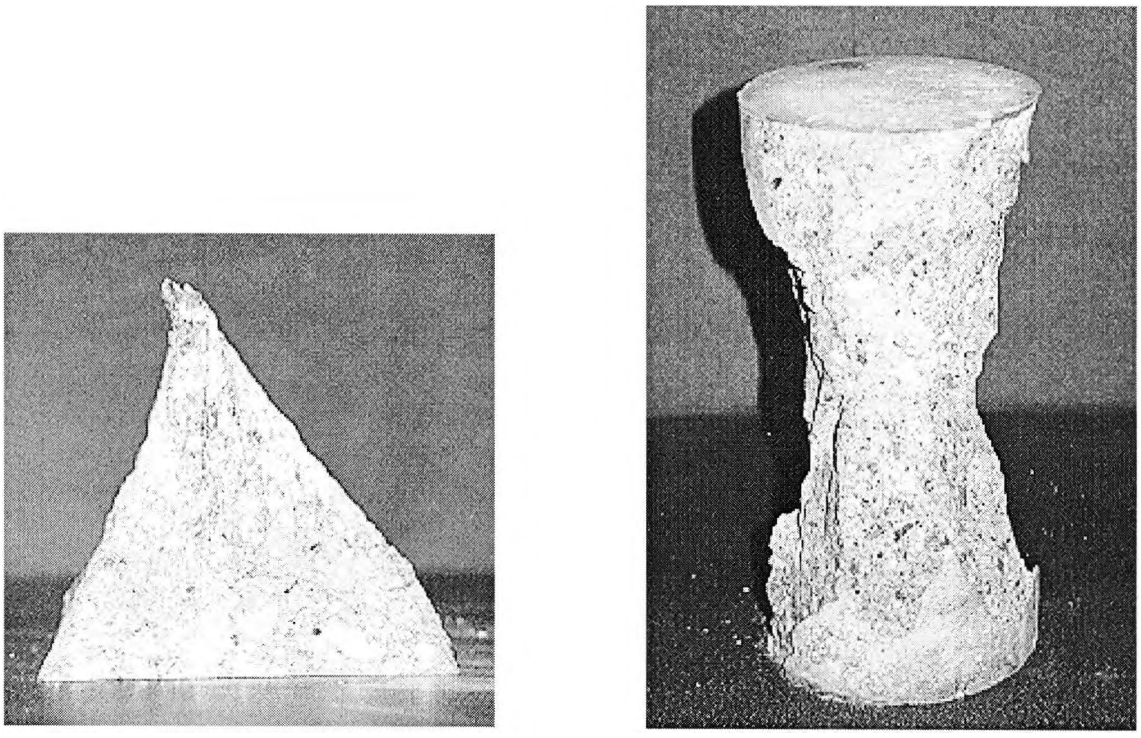

Figure 2.3
Typical failure modes for small-sized concrete specimens

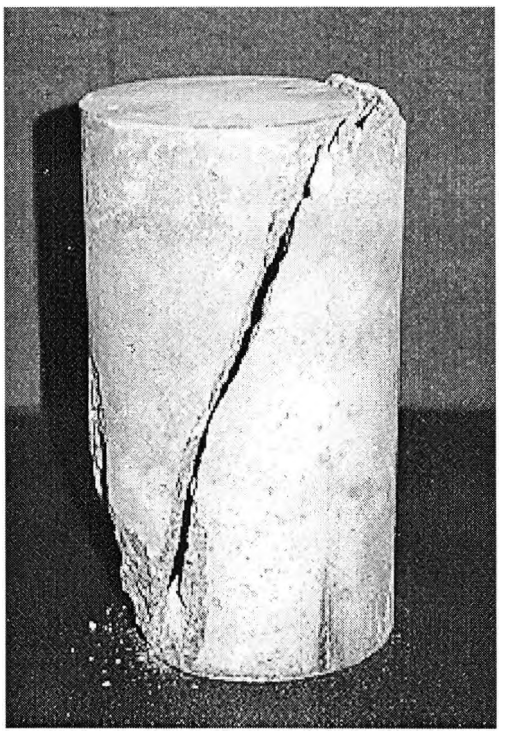

Figure 2.4
Fracture along diagonal plane in test series LH15U

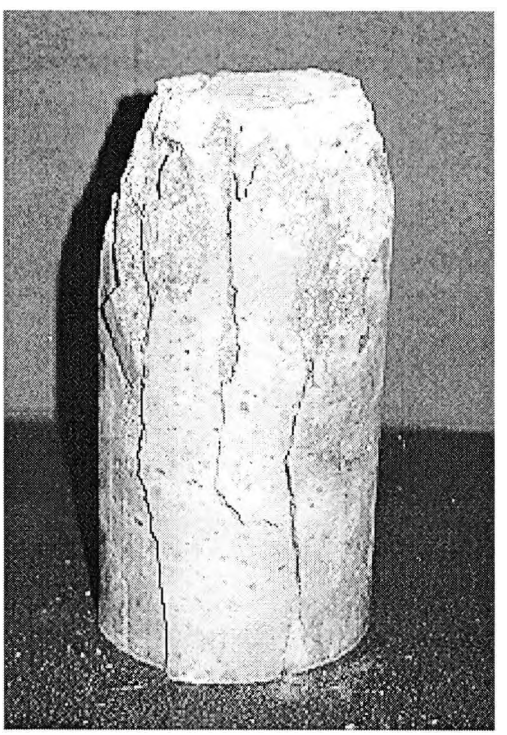

Figure 2.5
Splitting type failure of wood packed cylinder

2.1.5 Stress-Strain Characteristics

The uniaxial stress-strain characteristic of the high strength concretes used for fabricating the test columns were investigated by strain gauging three of the cylinders in each of the test series SL15B and SH20B. The strains were monitored by means of electrical resistance gauges of type PL-60-11, and the applied load by means of a 300 tons load cell. The load cell had been calibrated with respect to the built-in load cell of the Avery-Dension testing machine. The stress-strain data were logged at intervals of approximately 6.3 MPa until reaching a load corresponding to 85 - 90% of the expected failure load. Hereafter, the stress-strain data were logged at shorter intervals of about 1.3 MPa. Since the testing machine operated in a load-controlled mode, the specimens failed immediately after having reached their peak stress, and no data points were recorded on the descending part of the stress strain curves.

According to BS 1881: Part 121 (1983) the static modulus of elasticity, E_c , should be determined as the secant modulus for the third or higher reloading cycle between 33% of the full compressive strength and a small basic stress of 0.5 MPa. Both at the peak and floor stress in each cycle, a waiting period of 60 seconds is prescribed. The load cycling is performed in order to eliminate the effects of primary creep, i.e. initial plastic deformations. The strain-gauged specimens were subjected to three such load cycles before being loaded to failure, and primary creep strains between 0.02 - 0.04 mm/m were recorded.

Figures 2.6 and 2.7 show the stress-strain curves determined from testing the grade C100 and C120 concrete specimens respectively. The longitudinal strain, ε_3 , and transverse strain, ε_2 , both represent the average of two measurements taken at diametrically opposite locations at mid-height of the specimens. The volumetric strain, ε_v , was calculated from

the following small strain formulae:

$$\varepsilon_v = \varepsilon_1 + \varepsilon_2 + \varepsilon_3 \tag{2.1}$$

which for axisymmetric conditions simplifies to:

$$\varepsilon_v = \varepsilon_3 + 2\varepsilon_2 \tag{2.2}$$

It can be noted that the high strength concrete specimens exhibited a nearly linear stress-strain response up to a high fraction of their peak stress. The degree of non-linear behaviour can be quantified by the critical stress, σ_{cr} , which is defined as the stress at which the volume of concrete begins to dilate rather than continue to contract. The critical stress is of much structural importance as it is believed to reflect the strength of concrete when subjected to long-term loading (Shah, 1968; Smadi, 1985; Loo, 1995).

Table 2.8 lists the experimental results for the critical stress, σ_{cr} , the uniaxial compressive strength, f_c , the modulus of elasticity, E_c , the initial Poisson's ratio, ν_0, and the strain at peak stress, ε_c. Apart from the compressive strength, the main difference between the material properties of the two grades of concrete is the somewhat larger critical stress ratio of the grade C120 concrete.

Table 2.8
Key results from strain-gauged cylinder tests

Concrete grade	f_c (MPa)	E_c (GPa)	ν_0 (-)	σ_{cr}/f_c (-)	ε_c (mm/m)
C100	110.8	48.1	0.20	0.83	2.7
	112.2	45.0	0.23	0.80	3.0
	110.1	48.5	0.23	0.82	2.8
C120	132.2	48.1	0.22	0.82	3.0
	119.9	48.1	0.22	0.90	2.8
	131.9	50.2	0.22	0.90	2.9

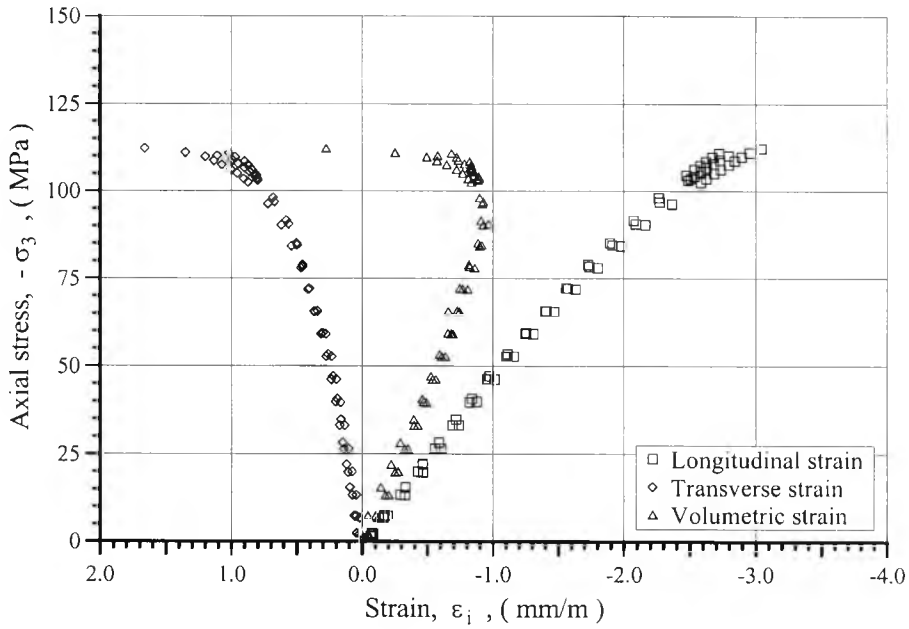

Figure 2.6
Stress-strain behaviour of grade C100 concrete

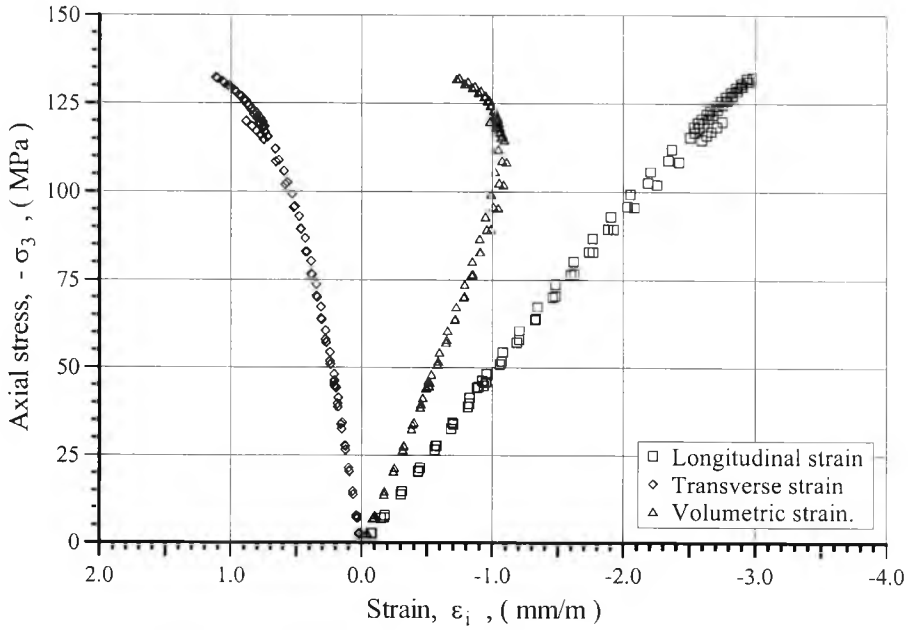

Figure 2.7
Stress-strain behaviour of grade C120 concrete

2.1.6 Split Cylinder Strength

A few of the 100×200 mm cylinders were tested for tensile splitting strength, f_{sp} , in accordance with the procedure outlined in BS 1881: Part 117 (1983). The tensile splitting strength was calculated from the following formulae derived from the theory of elasticity:

$$f_{sp} = - \frac{2 P_{max}}{\pi L d} \tag{2.3}$$

where:

f_{sp} is the tensile splitting strength

P_{max} is the maximum applied load

L is the length of the specimen (here 200 mm)

d is the cross-sectional dimension of the specimen (here 100 mm)

As shown in figure 2.8, the cylinders fractured by a single crack passing through mortar and coarse aggregates without bias, so as to link the two diametrically opposite loading strips

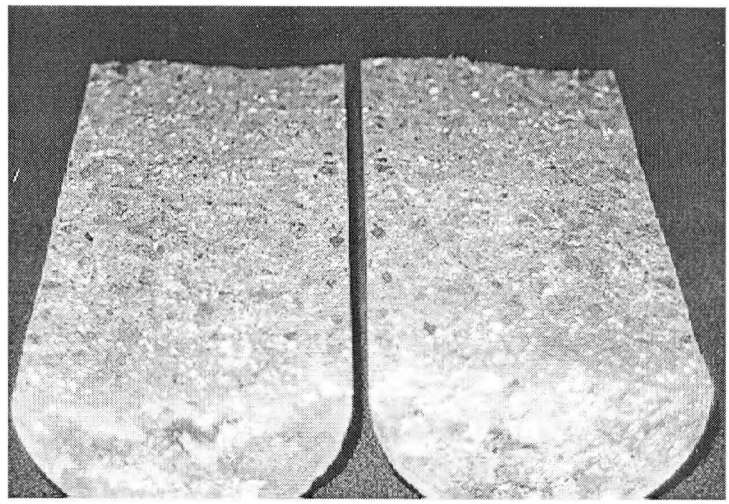

Figure 2.8
Fracture of cylinder tested for splitting strength

The results from the split cylinder tests are given in table 2.9, and are compared to the compressive mean strengths of the cylinders cast and tested on the same days as the cylinders used in the split tests. The average ratio of split cylinder strength to compressive mean strength was determined to be 5.9%.

Table 2.9
Results from split cylinder tests

Concrete grade	Parent column	Age (days)	f_c (MPa)	f_{sp} (MPa)	f_{sp}/f_c (%)
C100	SL05U	216	95.2	5.0	5.3
	LL05B	316	98.2	7.4	7.5
				6.0	6.1
	SL15B	195	110.4	6.0	5.4
				6.1	5.5
C120	SH20U	176	128.8	7.8	6.1
				7.5	5.8
				8.0	6.2
	LH05U	321	123.0	7.8	6.3
				5.8	4.7
	LH10B	316	120.4	7.2	6.0
				Mean	5.9

2.2 Reinforcement Properties

Tensile tests were carried out on samples of the four different types of reinforcement bars employed in the experimental programme. The reinforcement bars included ribbed cold worked steel bars of grade 460 with a nominal diameter of 10 mm and 12 mm respectively, and plain hot-rolled steel bars of grade 250 with a nominal diameter of 8 mm and 10 mm respectively.

The tests were carried out in a Dartec 2500 kN tensile testing machine. Operating in a displacement controlled mode, the testing machine was adjusted to automatically strain the test piece at a constant strain rate of about $5.0 \cdot 10^{-5}$ s^{-1}, which incidentally is the strain rate recommended in BS 4449 (1988). After the occurrence of yielding the testing machine was switched to a manual control mode, and the test was continued at a much higher rate until the test piece failed. The maximum strain rate during the second phase of testing was approximately $1.0 \cdot 10^{-3}$ s^{-1}, which according to the research on the effect of elevated strain rates carried out by Ammann *et al* (1982), can be estimated to have raised the tensile strength of the test pieces by a maximum of 3%.

Figure 2.9 illustrates a typical stress-strain curve for each of the four types of reinforcement bars. Prior to yielding, the strain was determined as the average of the recordings from two FLA-6-11 electrical resistance gauges mounted diametrically opposite at mid-height of the 600 mm long test piece. Thus, the initial straightening of the bar, as well as the slip between the test piece and the jaws of the testing machine, was eliminated from the strain data. However, soon after the occurrence of yielding, the strain gauges began to give erratic readings, and from this point onwards the stress-strain curve was established using the overall extension of the test piece.

Table 2.10 lists the mean values of the essential material properties as determined from testing three bars of each type. The material properties listed are: the modulus of elasticity, E_s , the yield stress, f_{sy} , the tensile strength, f_s , and the corresponding peak strain, ε_{sf} .

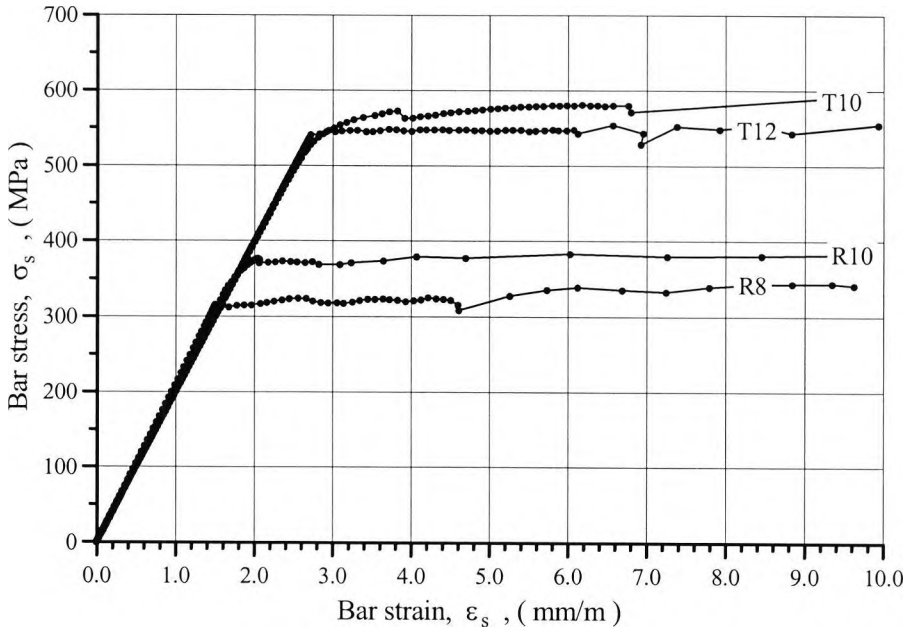

Figure 2.9
Typical stress-strain curves for reinforcement bars

Table 2.10
Average material properties for reinforcement bars

	Bar type			
	R8	R10	T10	T12
E_s , (Gpa)	209.9	206.4	196.8	198.9
f_{sy} , (MPa)	316.3	369.3	535.2	538.6
f_s , (MPa)	437.9	488.1	649.3	618.9
ε_{sf} , (%)	15.6	11.8	4.5	6.6

Chapter 3: Mechanical Properties of High Strength Concrete

3.1 Behaviour in Uniaxial Compression

This section describes the stress-strain behaviour of high strength concrete tested in uniaxial compression. Existing empirical expressions for estimating the modulus of elasticity, strain at peak stress and Poisson's ratio, are evaluated against experimental results obtained in the present and similar investigations on high strength concrete. A new analytical formulation for the complete stress-strain curve of concrete in uniaxial compression is presented. The formulation, which is equally applicable to normal and high strength concrete, serves as the basis for the more complex formulation proposed to describe the stress-strain behaviour of confined concrete.

Since high strength concrete is brittle when compared to normal strength concrete, the modulus of elasticity and the strain at peak stress are of increased engineering importance. Errors in these two material properties will, in general, have relatively more effect on the calculated load capacity of a high strength concrete member than of a similar normal strength concrete member.

3.1.1 Fracture Phenomenon

On the micro-mechanical level, concrete can be described as a heterogeneous system composed of different sized coarse aggregates, i.e. aggregates with a nominal size larger than about 2 mm, embedded in a matrix of mortar. When a concrete specimen is subjected to uniaxial compression, it is the inclusion of coarse aggregates and flaws in the matrix that give rise to the local tensile stress concentrations which are responsible for the progressive

formation and propagation of micro-cracks in the specimen. The micro-cracks can conveniently be classified into the following three types: bond cracks at the interface between the coarse aggregates and the mortar; cracks through the mortar; and cracks through the coarse aggregates. On the basis of the experimental research reported by Hsu *et al* (1963), Shah and Chandra (1968), Ngab *et al* (1981), Carrasquillo *et al* (1981a) and Smadi and Slate (1989), a description is given of how the formation and propagation of each type of crack is closely related to distinct features in the macro-mechanical behaviour of concrete.

A hardened concrete specimen will, even before it is being subjected to loading, contain a considerable number of randomly orientated micro-cracks. These cracks, which are mainly caused by the early volume changes of the cement paste, are almost exclusively bond cracks. When subjecting the specimen to increasing uniaxial compression, the increase in the number and length of the bond cracks will initially remain small, and the stress-strain response of the specimen will be nearly linear.

Later in the loading process, the stress-strain curve deviates increasingly from the straight line to horizontal, and the apparent Poisson's ratio begins to increase continuously. The beginning of this part of the stress-strain behaviour is associated with a significant growth in the formation and propagation of bond cracks. Smadi and Slate (1989) reported that significant bond cracking typically commenced at a stress to strength ratio of 30 - 50% for normal strength concrete, and at 60 - 70% for high strength concrete. In the investigation carried out by Smadi and Slate, concrete with a compressive strength of 21 - 24 MPa was classified as normal strength, and concrete with a compressive strength of 59 - 69 MPa as high strength.

The second stage of the stress-strain behaviour ends when the volume of the concrete begins to dilate rather than continue to contract. The stress at minimum volume is termed the critical stress, and is on the micro-mechanical level related to a significant increase in the formation of mortar cracks bridging between neighbouring bond cracks. In the investigation carried out by Smadi and Slate (1989) a noticeable increase in mortar cracking was observed at a stress to strength ratio of 70 - 75% for normal strength concrete, and at 85 - 90% for high strength concrete. The high strength concrete specimens tested in the present investigation were observed to have minimum volume at stress-to-strength ratios of 80 - 90%.

When further increasing the load, the combined bond and mortar cracking will form with an increasing rate until the continuous crack-pattern is so extensively developed that the load-carrying capacity of the concrete is exhausted. Within this range, the process of micro-cracking is unstable and with time will eventually lead to failure.

At all stress-to-strength ratios, the amount of micro-cracking observed in a high strength concrete specimen is smaller than that observed in a similar normal strength concrete specimen. Furthermore, the failure surface in a high strength concrete specimen typically develops explosively along a smooth plane which passes through aggregates and mortar without bias. In contrast, the typical failure surface in a normal strength concrete specimen develops gradually along a tortuous plane which seldom involves aggregate failures. The reduction in micro-cracking explains why the stress-strain diagram for high strength concrete is more pointed and has a steeper descending branch than that for normal strength concrete. Neville (1997) ascribed the reduced micro-cracking observed in high strength concrete to the improved mechanical compatibility between the mortar and the aggregates.

3.1.2 Size and Shape Effects

The mechanical properties of concrete are determined from tests on small-sized specimens, and it is necessary to adjust these for the influence of the testing conditions before they can be applied on a structural level.

It is well known that the compressive strength of a concrete specimen, which is tested directly between dry steel platens in general, is reduced when either increasing its slenderness ratio or cross-sectional dimensions. In this context, DS 411 (1984) provides a comprehensive table over recommended reduction coefficients when assessing the strength of normal strength concrete from tests on specimens of a smaller size than the standard 150×300 mm cylinder.

The larger strength observed for a short specimen, such as a cube, can be explained by the favourable multiaxial stress state induced by the frictional restraint forces developing between the dry steel platens of the testing machine and the contact faces of the specimen. Experimental studies have indicated that the common practice of employing a slenderness ratio of 2 is sufficient to eliminate the effect of the frictional end restraints on the ascending part of the stress-strain curve measured at mid-height of the specimen (Sangha, 1972; Kotsovos, 1983).

The ratio of the compressive strengths of 150×300 mm to 100×200 mm cylinders has been experimentally investigated for a wide range of concrete qualities. The tests carried out by Lessard *et al* (1993) on concretes with compressive cylinder strengths ranging from 72 MPa to 126 MPa produced strength ratios between 0.91 and 1.00 with a mean value of 0.95. For a similar range of concrete qualities, Iravani (1996) found the average strength ratio to be 0.94 with a sample standard deviation of 0.035. By testing concretes with cylinder strengths

of 20 - 70 MPa, Carrasquillo *et al* (1981b) found that the somewhat smaller conversion coefficient of 0.90 was applicable regardless of the strength and age of the specimens.

In the experimental investigation reported herein, the average ratio of the 100×200 mm cylinder strength to the 100 mm cube strength was determined to be 0.87 for the grade C100 concrete, and 0.92 for the grade C120 concrete. Both of these ratios are significantly larger than the conversion factor of 0.75 recommended for normal strength concrete in DS 411 (1984).

Imam *et al* (1995) reported the ratio of the compressive strengths of 100 mm cubes to 150×300 mm cylinders to lie between 0.86 and 0.92 with an average value of 0.90. The cylinder strengths of the specimens tested by Imam *et al* ranged from 82 MPa to 117 MPa. When combining these results with those reported by Lessard *et al* (1993) it follows that a conversion coefficient of 0.95 can be employed to relate the strength of a 100 mm cube to that of a 100×200 mm cylinder. This ratio compares to the smaller ratios of 0.87 and 0.92 determined for the two grades of high strength concrete employed in the present investigation. In this context, it should be mentioned that Larrard *et al* (1994) observed the strength ratio to be significantly influenced by the selected mix constituents. By altering the mix constituents, it was possible to produce concretes with a constant cube strength of about105 MPa and yet to have cylinder conversion coefficients ranging from 0.71 to 1.02. As was the case for the concrete mixes employed in the present investigation, the use of microsilica was observed to result in a larger cube to cylinder conversion coefficient. The results of Larrard *et al* raise some concern regarding the suitability of the cube tests for assessing the strength of high strength concrete.

When calculating the load capacity of a full scale concrete column, the unconfined compressive strength of concrete is usually taken to be 0.85 times the concrete strength as determined from standard tests on 150×300 mm cylinders. This reduction factor accounts for behavioural differences caused by the compaction of the concrete being less complete, the rate of loading being much slower, and the curing conditions being less favourable in actual columns than in small-sized control specimens. The review given by Razvi and Saatcioglu (1994) indicates that, provided the cover concrete does not fail prematurely due to instability of the shell under high compressive stresses, the strength reduction factors for high strength concrete members lie within similar bounds as those for normal strength concrete members, i.e. from about 0.85 to 1.00. However, the average value of the strength reduction factor appears to increase with the concrete strength.

Throughout this thesis, the unconfined compressive strength of full-scale columns was assumed equal to 0.85 times the mean strength of the 150×300 mm control cylinders, and equal to 0.81 times the mean strength of the 100×200 mm control cylinders. The latter reduction factors are obtained by assuming that the 150×300 mm cylinder strength equals 0.95 times the 100×200 mm cylinder strength.

3.1.3 Modulus of Elasticity

Figure 3.1 shows experimental data for the modulus of elasticity as a function of the compressive strength. The experimental data were obtained from tests on 100×200 mm cylinders, and the measured strengths were converted to the plotted 150×300 mm cylinder strengths by multiplying them with a reduction factor of 0.95. The plotted data supports the generally accepted trend of the modulus of elasticity to increase with the compressive strength.

The figure also shows the curves for three of the better known empirical expressions for predicting the modulus of elasticity. Equation 3.1 is the expression given in BS 8110: Part 2 (1985) when assuming that the 150×300 mm cylinder strength can be set equal to 0.95 times the 150 mm cube strength. The utilised conversion coefficient was drawn from the experimental studies on high strength concrete specimens carried out by Imam *et al* (1995). It compares to the conversion coefficient of 0.85 recommended for normal strength concrete by CEB (1990).

$$E_c = 20 + 0.21 f_c \tag{3.1}$$

Carrasquillo *et al* (1981b) proposed equation 3.2 as an alternative to the expression given in ACI 318-77, which was observed to overestimate the modulus of elasticity when applied to concrete with a compressive strength in excess of about 41 MPa.

$$E_c = 3.32 \sqrt{f_c} + 6.90 \tag{3.2}$$

The expression recommended in the CEB Model Code 90 (1990) is valid for concrete with a compressive strength of up to about 60 MPa. This expression has later been replaced by equation 3.3 so as to include concrete with a compressive strength of up to about 110 MPa (CEB, 1995).

$$E_c = 22.0 \, (f_c / 10)^{0.3} \tag{3.3}$$

In the foregoing relationships the modulus of elasticity, E_c , is expressed in GPa, and the compressive strength, f_c , in MPa.

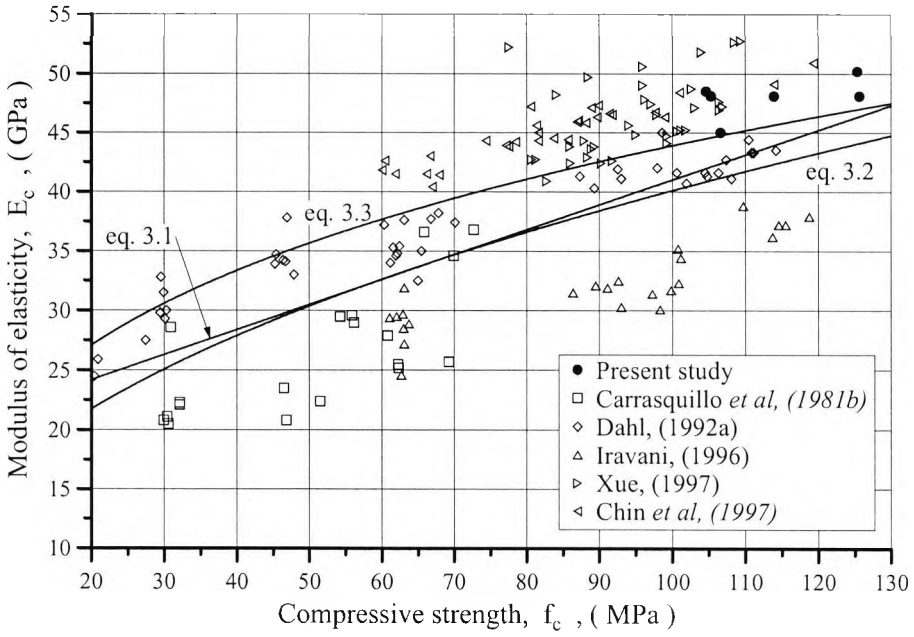

Figure 3.1
Modulus of elasticity versus compressive strength

It is likely that at least part of the scattering in the experimental data can be explained by differences in the proportions and properties of the utilised coarse aggregates. Carrasquillo *et al* (1981b) observed that for concretes of comparable strength those based on crushed limestone aggregates had a higher modulus of elasticity than those based on gravel aggregates. Likewise, Hsu and Hsu (1994) found that the use of basalt instead of crushed stone as coarse aggregates improved the modulus of elasticity by approximately 29% without having much effect on the strength of the concrete. An even more noticeable influence of the coarse aggregates was observed in the investigation by Baalbaki *et al* (1992). For a given mix design, the replacement of quartzitic aggregates with sandstone aggregates produced a concrete with an 11% higher strength and a 44% lower modulus of elasticity than the original mix. The quartzitic concrete had a compressive strength of 90 MPa and a modulus of elasticity of 42 GPa.

The dependency of the modulus of elasticity on the type of coarse aggregates is incorporated into the recommendations given in the CEB Model Code 90 (1990). According to the Model Code, the modulus of elasticity for a concrete based on non-quartzitic aggregates can be estimated by factorising the modulus of elasticity for a quartzitic concrete of similar strength. A multiplication factor of 1.2 is given for basalt and dense limestone aggregates, a multiplication factor of 0.9 is given for limestone aggregates, and a multiplication factor of 0.7 is given for sandstone aggregates. However, the revised formula recommended for high strength concrete is not associated with such multiplication factors accounting for the type of coarse aggregates (CEB, 1995).

It was stated in the references (Baalbaki, 1991) and (Baalbaki, 1992) that, due to an increased effect of the mineralogical characteristics of the coarse aggregates, the modulus of elasticity of high strength concrete cannot be expressed as a function of the compressive strength only. However, in view of the experimental data collected in the present study, it appears that an extrapolation of the empirical expressions beyond their intended use does not further impair their often rather poor capability in estimating the modulus of elasticity.

When compared to the experimental results for the C100 and C120 concretes, the reviewed empirical expressions all somewhat underestimate the modulus of elasticity. The most accurate of the expressions is the one recommended by CEB (1995), which on average predicts the modulus to within 5% of the experimental results.

3.1.4 Strain at Peak Stress

It is generally agreed that the strain at peak stress, or peak strain, has a tendency to increase with increasing compressive strength, but it is debatable whether it is feasible to express the peak strain as a function of the compressive strength only.

Figure 3.2 shows experimental data for peak strain together with the curves for three expressions proposed for predicting it. The experimental data were obtained from tests on 100×200 mm cylinders, and the recorded strengths were converted to the equivalent 150×300 mm cylinder strengths using a conversion factor of 0.95.

Equation 3.4, which was proposed by Saenz (1964) for normal strength concrete, approximately defines a lower bound to the experimental data. Equation 3.5, given in (CEB, 1995), predicts the peak strain to be constant 2.2 mm/m for concrete with a compressive strength less than 40 MPa, and to increase with a decreasing rate for concrete with a higher strength than 40 MPa. In this context, it should be recalled that according to BS 8110: Part 2 (1985) the peak strain can be assumed to be 2.2 mm/m irrespective of the grade of concrete. Equation 3.6, proposed by Hsu and Hsu (1994), was derived entirely on the basis of their test results on high strength concrete.

$$\varepsilon_c = 0.12 \sqrt[4]{f_c} \left(9.10 - \sqrt[4]{f_c} \right) \tag{3.4}$$

$$\varepsilon_c = \max \begin{cases} 2.2 \\ 0.7 f_c^{0.31} \end{cases} \tag{3.5}$$

$$\varepsilon_c = 0.013 f_c + 2.11 \tag{3.6}$$

In the above equations the strain at peak stress, ε_c , is expressed in mm/m, and the compressive strength, f_c , in MPa.

It can be seen from the figure that none of the empirical models is capable of providing a convincing fit to the test results. It is likely that this, at least partly, can be explained by the

fact that none of the models account for the influence of the type of coarse aggregates.

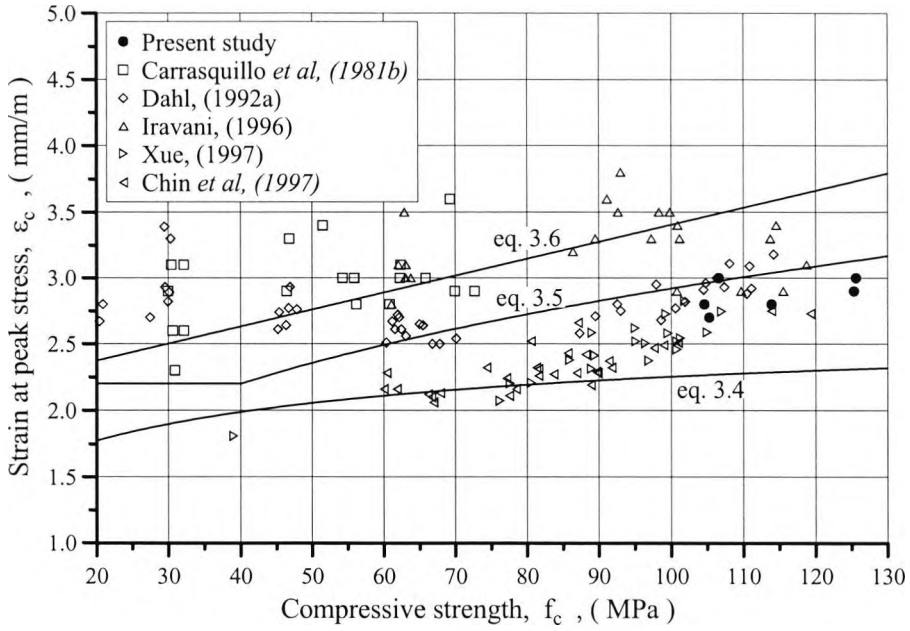

Figure 3.2
Strain at peak stress versus compressive strength

In the tests carried out by Dahl (1992a) the strain at peak stress was little affected by the concrete strength. An increase in the concrete strength from 20 MPa to 114 MPa resulted in an increase in the peak strain by a modest 0.2 mm/m. Likewise, the data recorded by Iravani (1996) indicate that the strength of the concrete has little, if any, influence on the peak strain. In contrast to this, Ahmad and Shah (1982) observed the peak strain to increase from 2.1 mm/m for a 26 MPa concrete to 3.0 mm/m for a 65 MPa concrete.

Of the reviewed expressions, the one recommended by CEB (1995) agree the best with the results for the two high strength concrete qualities employed in the present investigation. The peak strains predicted by the CEB expression are, on average, a modest 6% higher than the experimental results.

3.1.5 Poisson's Ratio

Figure 3.3 shows experimental data for Poisson's ratio versus normalised stress. It can be noted that, in the immediate vicinity of the peak stress, due to the proliferation of the ongoing fracture processes, Poisson's ratio will often exceed 0.5, which is the theoretical maximum value of Poisson's ratio for a continuum. Since the increase in Poisson's ratio primarily is caused by the formation and propagation of micro-cracks, it is sometimes referred to as an apparent ratio.

It is commonly accepted that the initial Poisson's ratio is independent of the concrete strength (ACI, 1984; Ibrahim, 1994; Iravani, 1996). Furthermore, the test observations by Dahl (1992b) on concrete with compressive strengths ranging from 20 MPa to 110 MPa show that Poisson's ratio at higher levels of stress is largely independent of the grade of concrete when expressed in terms of normalised stress.

Equations 3.7a-b were proposed by Ottosen (1979) for calculating Poisson's ratio, ν, as a function of the normalised stress, σ_3 / f_c.

$$\nu = \nu_0 \qquad \text{for } 0 \le -\sigma_3 / f_c \le \alpha_p \qquad (3.7a)$$

$$\nu = \nu_c - (\nu_c - \nu_0)\sqrt{1 - \left(\frac{-\sigma_3 / f_c - \alpha_p}{1 - \alpha_p}\right)^2} \qquad \text{for } \alpha_p \le -\sigma_3 / f_c \le 1 \qquad (3.7b)$$

The above expressions were incorporated into the CEB Model Code 90 (1990) with the initial Poisson's ratio, $\nu_0 = 0.20$, the normalised initiation stress, $\alpha_p = 0.80$, and Poisson's ratio at peak stress, $\nu_c = 0.36$.

Figure 3.3 shows that the model recommended by CEB (1990) is in reasonable agreement with the experimental data taken from the references (Dahl, 1992b; Kupfer, 1973).

However, the two concrete grades employed in the present study exhibited significantly more lateral expansion at small to medium range loads than predicted by the CEB model. An improved fit to the test data was obtained by adjusting the model parameters as follows: $\nu_0 = 0.22$, $\alpha_p = 0.40$, and $\nu_c = 0.40$.

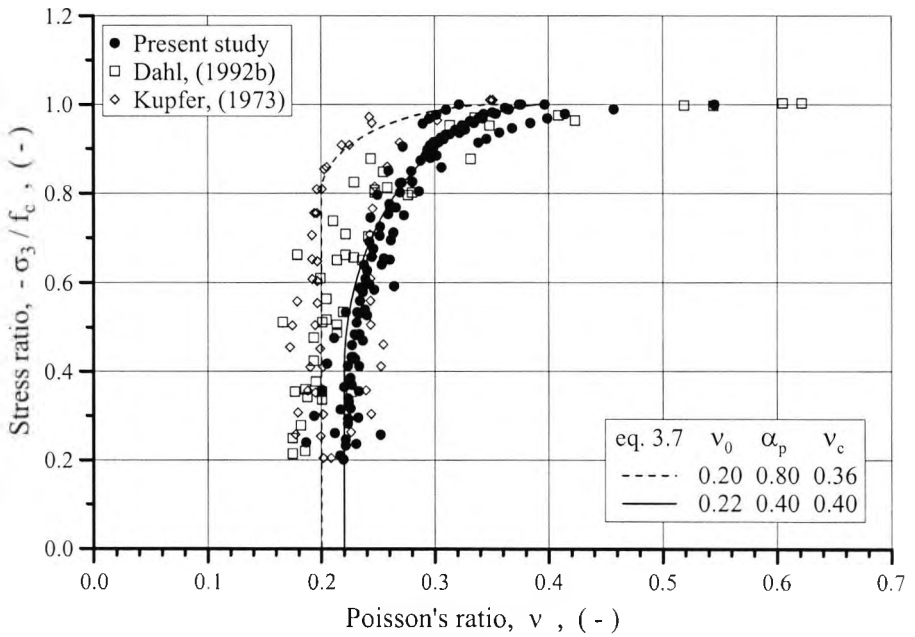

Figure 3.3
Poisson's ratio versus normalised stress

3.1.6 Analytical Expression for Stress-Strain Curve

With the further goal of facilitating a rigorous analysis of concrete structures, many researchers have developed analytical expressions for the stress-strain curves recorded in uniaxial compression tests.

A general analytical expression should preferably only require knowledge of parameters of physical significance such as: the compressive strength, the modulus of elasticity, and the strain at peak stress. Furthermore, since it is not possible to establish a convincing functional relationship between these material properties, they should all be included as

independent variables. However, many of the stress-strain models proposed in the literature attain their mathematical simplicity by assuming some kind of functional relationship between them. Examples of such models are those given in BS 8110: Part 1 and 2 (1985).

The behaviour of a concrete specimen in the post-peak region is characterised by a continuing strain localisation in a narrow failure zone, which is accompanied by strain recovery in portions outside the failure zone (Van Mier, 1986; Torrenti, 1993; Choi, 1996). As a consequence, when calculating the strains from the overall displacements of a specimen, the steepness of the descending branch of the stress-strain curve will increase with an increase in the height of the specimen. The steepness of the descending branch of the stress-strain curve is also known to increase when reducing the frictional restraints at the ends of the specimen (Kotsovos, 1983; Choi, 1996). Thus, a constitutive model based on data recorded from standard tests will not represent a state of uniaxial stress in the post-peak region. However, due to the restraints originating from reinforcement, boundary conditions and even the surrounding concrete, actual concrete structures never fail under true axial stress conditions. This explains why it is accepted to assume that the softening stress-strain characteristics as determined from standard tests on cylinders with a slenderness ratio of 2 can be applied on a structural level.

The ascending branch of the uniaxial stress-strain curve for normal as well as high strength concrete can be accurately represented by equation 3.8 given in the CEB Model Code 90 (1990). However, the strain at peak stress should be allowed to vary, and not, as assumed in the Model Code, to be a constant of 2.2 mm/m.

$$\sigma_3 = f_c \frac{\frac{E_c}{E_{cs}}\frac{\varepsilon_3}{\varepsilon_c} + \left(\frac{\varepsilon_3}{\varepsilon_c}\right)^2}{1 - \left(\frac{E_c}{E_{cs}} - 2\right)\frac{\varepsilon_3}{\varepsilon_c}} \qquad \text{for } |\varepsilon_3| \le \varepsilon_c \tag{3.8}$$

where: $E_{cs} = f_c / \varepsilon_c$ is the secant modulus at peak stress.

Equation 3.8 can be seen to satisfy the following boundary conditions:

$$\sigma_3 = 0 \qquad \text{for } \varepsilon_3 = 0 \tag{3.9a}$$

$$d\sigma_3/d\varepsilon_3 = E_c \qquad \text{for } \varepsilon_3 = 0 \tag{3.9b}$$

$$\sigma_3 = -f_c \qquad \text{for } \varepsilon_3 = -\varepsilon_c \tag{3.9c}$$

$$d\sigma_3/d\varepsilon_3 = 0 \qquad \text{for } \varepsilon_3 = -\varepsilon_c \tag{3.9d}$$

Equation 3.10 was developed during the present study to describe the descending branch of the stress-strain curve of unconfined concrete. The equation also serves as the basis for the more complex formulation proposed to describe the post-peak behaviour of confined concrete. The proposed expression incorporates a positive material parameter β, which controls the steepness of the descending branch. The larger the value of β the steeper is the descending branch.

$$\sigma_3 = f_c \frac{\frac{\varepsilon_3}{\varepsilon_c}}{\beta\left(-\frac{\varepsilon_3}{\varepsilon_c} - 1\right)^3 - \frac{\varepsilon_3}{\varepsilon_c}} \qquad \text{for } |\varepsilon_3| \ge \varepsilon_c \tag{3.10}$$

Equation 3.10 can be seen to satisfy the following boundary conditions:

$$\sigma_3 = -f_c \qquad \text{for } \varepsilon_3 = -\varepsilon_c \tag{3.11a}$$

$$d\sigma_3/d\varepsilon_3 = 0 \qquad \text{for } \varepsilon_3 = -\varepsilon_c \tag{3.11b}$$

$$\sigma_3 \to 0 \qquad \text{for } \varepsilon_3 \to -\infty \tag{3.11c}$$

$$d\sigma_3/d\varepsilon_3 \to 0 \qquad \text{for } \varepsilon_3 \to -\infty \tag{3.11d}$$

A very satisfactory fit to the available experimental data was achieved by choosing the parameter β so as to force the stress-strain curve to pass through the data point $(\varepsilon_{c50}, 0.50 f_c)$ on the descending branch. Thus, the parameter β can be determined from the strains ε_c and ε_{c50} as follows:

$$\beta = \frac{\dfrac{\varepsilon_{c50}}{\varepsilon_c}}{\left(\dfrac{\varepsilon_{c50}}{\varepsilon_c} - 1\right)^3} \tag{3.12}$$

Figures 3.4 and 3.5 compare the proposed formulation for the complete stress-strain relationship with experimental results reported by Hsu and Hsu (1994) and Dahl (1992a) respectively. The experimental results were made available to this investigation by digitizing, and for reasons of clarity are shown as discrete data points in the figures.

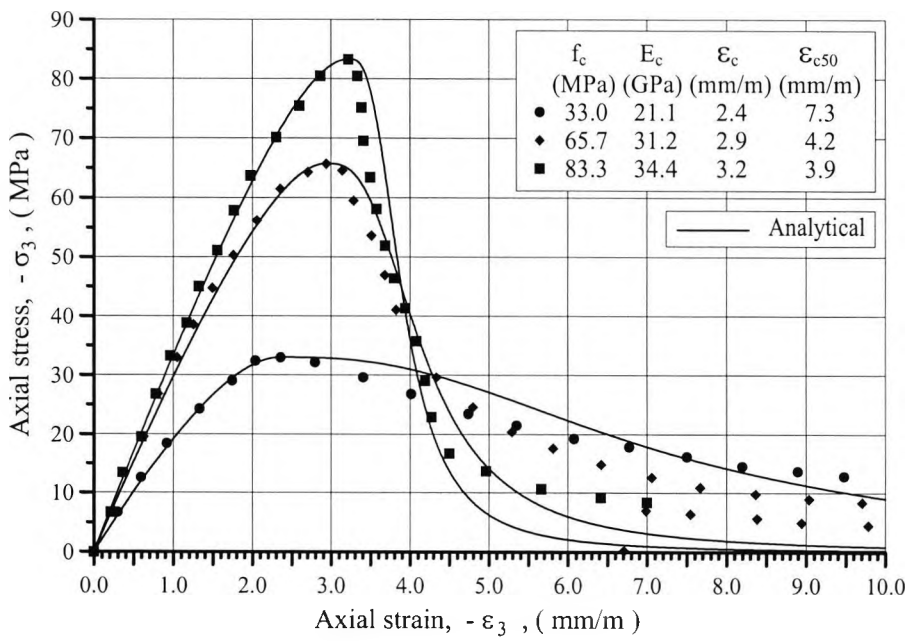

Figure 3.4
Comparison of proposed stress-strain model with experimental data reported by Hsu and Hsu, (1994)

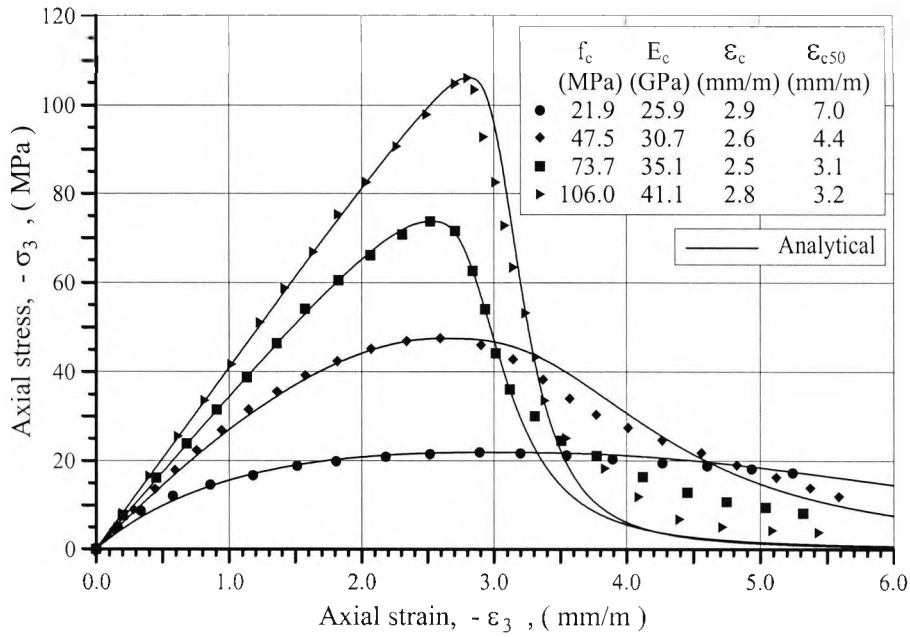

Figure 3.5
Comparison of proposed stress-strain model with experimental data reported by Dahl, (1992a)

In many practical situations the data point $(\varepsilon_{c50}, 0.50 f_c)$ is not available. Under these circumstances, it is recommended to calculate the material parameter β from the compressive strength, f_c, using the following equation:

$$\beta = 0.7\, e^{0.05 f_c} \tag{3.13}$$

Equation 3.13 was derived by regression analysis using numerical data generated by the model given in the CEB Model Code 90 (1990). For an assumed compressive strength, f_c, the modulus of elasticity, E_c, and the strain at peak stress, ε_c, was calculated from equation 3.3 and 3.5 respectively. These material properties were substituted into the stress-strain relations given in the CEB Model Code 90, where after the strain ε_{c50} and the material parameter β corresponding to this strain was calculated. The above described process was repeated until a sufficient number of data points had been established for the regression analysis to be performed.

Figure 3.6 compares stress-strain curves generated by the expressions given in the CEB Model Code 90 (1990) with those generated by the model proposed herein. For each concrete strength, the modulus of elasticity and the peak strain was calculated from equation 3.3 and 3.5 respectively. The material parameter β , which in the proposed model governs the steepness of the descending branch of the stress-strain curve, was determined from equation 3.13.

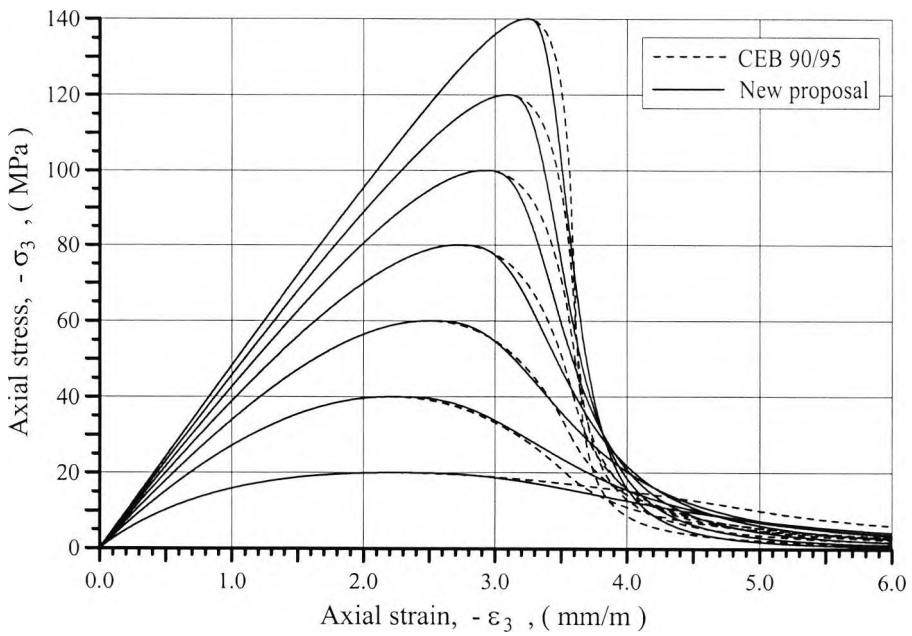

Figure 3.6
Comparison of proposed stress-strain model with CEB model

Figure 3.7 shows the proposed stress-strain model when applied to the 100×200 mm concrete cylinders tested in the present investigation. The compressive strength, the modulus of elasticity and the peak strain were taken as the averages of the experimental data given in table 2.8. The transverse strains were calculated from equation 3.7a-b with the initial Poisson's ratio, the normalised initiation stress, and Poisson's ratio at peak stress being set to 0.22, 0.40 and 0.40 respectively. In the post-peak region, Poisson's ratio was assumed to be constant at 0.40.

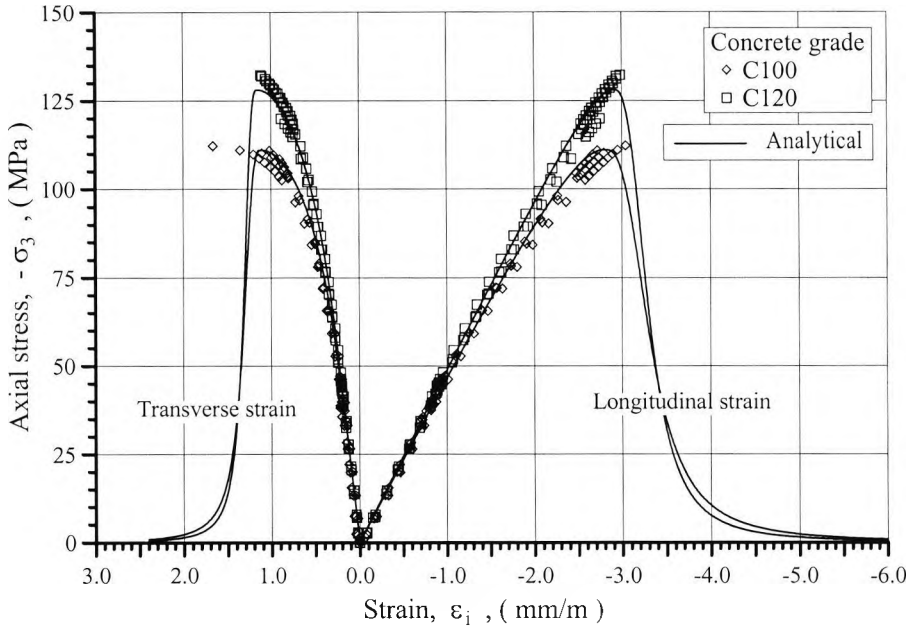

Figure 3.7
Modelling the complete stress-strain behaviour of the grade C100 and C120 concretes

3.2 Behaviour in Uniaxial Tension

It is a general consensus that the uniaxial tensile strength of concrete will increase, albeit with a decreasing rate, with the compressive strength. The direct tensile strength, f_t, according to CEB (1995) can be estimated from the compressive strength, f_c, by equation 3.14, where both the tensile and the compressive strength are measured in MPa.

$$f_t = 1.80\left(\frac{f_c}{18}\right)^{0.6} \tag{3.14}$$

Figure 3.8 shows available experimental results for the tensile strength versus the compressive strength. Since the compressive strengths were determined from tests on 100×200 mm cylinders, they were converted to the equivalent 150×300 mm cylinder strengths by being multiplied with a conversion factor of 0.95. Also, with the exception of the investigation conducted by Dahl (1992c), the split cylinder strength rather than the direct tensile strength was tested. Because of a more favourable stress distribution, the split cylinder test tends to somewhat overestimate the tensile strength. According to the CEB Model Code 90 (1990) the ratio of the split cylinder strength to the tensile strength can be assumed to be 0.90. This was the ratio used for converting the data plotted in the figure.

The large scatter of the data can be explained by the tensile strength of concrete being much influenced by the shape and texture of the aggregates as well as by the environmental conditions. Furthermore, since the tensile strength is governed by the propagation of a single crack rather than multiple cracks, a large statistical variability is naturally to be expected.

Equation 3.14 underestimates the tensile strength of the specimens tested in the present

investigation by an average of 11%, which in view of the variability of the test data is quite acceptable.

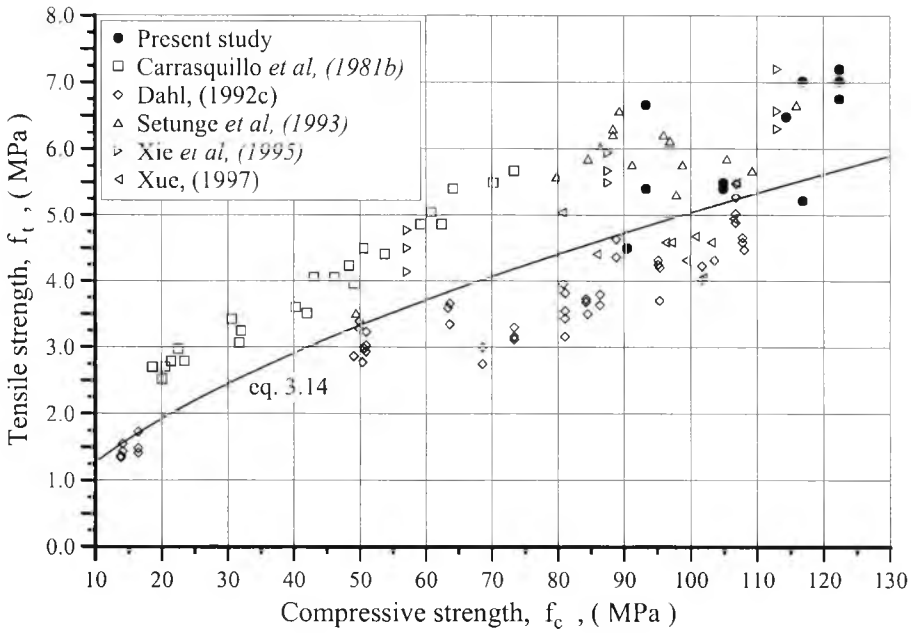

Figure 3.8
Tensile strength versus compressive strength

3.3 Behaviour of Actively Confined Concrete

This section describes the stress-strain behaviour of concrete under a condition of triaxial axisymmetric compression. Published results from triaxial load cell tests were used to establish expressions for the effect of confinement on both the compressive strength and the peak strain of high strength concrete. Furthermore, the stress-strain model described in section 3.1 was generalised so as to include confined concrete.

The advantage of triaxial load cell results is that they represent uniform confinement conditions. In contrast, when confinement is provided by means of transverse reinforcement bars, the confining pressure is not uniformly distributed, but varies from point to point within the specimen. Thus, in order to assess the effect of confinement on the behaviour of concrete from tests on passively confined specimens, not only the size but also the distribution of the confining pressure needs to be taken into account.

3.3.1 Confined Strength

Since the behaviour of concrete can be approximated with that of an homogeneous and isotropic material, its strength under general multiaxial stress conditions can be represented by a unique surface in the principal stress space. A much acclaimed failure criterion for normal strength concrete under general multiaxial states of stress is the four parameter model proposed by Ottosen (1977); see equations 3.15a-b. Ottosen's failure criterion is defined in terms of the following three octahedral stresses: the octahedral normal stress, σ_{oct}, the octahedral shear stress, τ_{oct}, and the angle of similarity, θ.

$$a\frac{\tau_{oct}^2}{f_c^2} + \lambda\frac{\tau_{oct}}{f_c} + b\frac{\sigma_{oct}}{f_c} - 1 = 0 \qquad (3.15a)$$

where:

$$\lambda = \begin{cases} k_1 \cos\left(\frac{1}{3}\cos^{-1}(k_2 \cos(3\theta)) \right) & \text{for} \quad \cos(3\theta) \geq 0 \\ k_1 \cos\left(\frac{\pi}{3} - \frac{1}{3}\cos^{-1}(-k_2 \cos(3\theta)) \right) & \text{for} \quad \cos(3\theta) \leq 0 \end{cases} \tag{3.15b}$$

The octahedral stresses are again defined in terms of the principal stresses by equations 3.16 - 3.18. In practice, the octahedral stresses are determined directly from the stress tensor without the need to solve an eigenvalue problem, see (Chen, 1982).

$$\sigma_{oct} = \frac{1}{3}(\sigma_1 + \sigma_2 + \sigma_3) \tag{3.16}$$

$$\tau_{oct} = \frac{1}{3}\sqrt{(\sigma_1 - \sigma_2)^2 + (\sigma_1 - \sigma_3)^2 + (\sigma_2 - \sigma_3)^2} \tag{3.17}$$

$$\theta = \frac{1}{3}\cos^{-1}\left(\frac{\sqrt{2}(\sigma_1 - \sigma_{oct})(\sigma_2 - \sigma_{oct})(\sigma_3 - \sigma_{oct})}{\tau_{oct}^3} \right) \tag{3.18}$$

Furthermore, the principal stresses can be calculated in descending order, $\sigma_1 \geq \sigma_2 \geq \sigma_3$, from the octahedral stresses as follows:

$$\sigma_1 = \sqrt{2}\,\tau_{oct}\cos(\theta) + \sigma_{oct} \tag{3.19}$$

$$\sigma_2 = \sqrt{2}\,\tau_{oct}\cos(\theta + 4\pi/3) + \sigma_{oct} \tag{3.20}$$

$$\sigma_3 = \sqrt{2}\,\tau_{oct}\cos(\theta + 2\pi/3) + \sigma_{oct} \tag{3.21}$$

It can be seen from equations 3.19 - 3.21 that an angle $\theta = 0$ corresponds to the stress state $\sigma_1 \geq \sigma_2 = \sigma_3$, and an angle $\theta = \pi/3$ to the stress state $\sigma_1 = \sigma_2 \geq \sigma_3$. The meridian on the failure surface corresponding to $\theta = 0$ is named the tensile meridian and represents the

minimum octahedral shear stress for all permissible values of the octahedral normal stress. Likewise, the meridian corresponding to $\theta = \pi/3$ is named the compressive meridian and represents the maximum octahedral shear stress. The compressive meridian includes all combinations of compressive failure under conditions of axisymmetric confinement. From solving equation 3.15a with respect to τ_{oct}/f_c, it follows that the compressive meridian can be expressed by equation 3.22. Alternatively, the normalised confined strength, f_{cc}/f_c, can be expressed as a function of the confinement ratio, $-\sigma_1/f_c$, by equation 3.23. Equation 3.23 can be derived by setting $\sigma_1 = \sigma_2$ and $\sigma_3 = -f_{cc}$ in equations 3.16 - 3.18 before substitution into equation 3.15a.

$$\frac{\tau_{oct}}{f_c} = \frac{1}{2a}\left(-\lambda_c + \sqrt{\lambda_c^2 - 4a\left(b\frac{\sigma_{oct}}{f_c} - 1\right)} \right) \tag{3.22}$$

$$\frac{f_{cc}}{f_c} = \frac{3b - 3\lambda_c\sqrt{2}}{4a} - \frac{\sigma_1}{f_c} + \frac{3}{4a}\sqrt{8a + (b - \sqrt{2}\lambda_c)^2 - 8ab\frac{\sigma_1}{f_c}} \tag{3.23}$$

where: λ_c denotes the value of the function λ for $\theta = \pi/3$.

Ottosen proposed calibrating the failure criterion using the following four combinations of failure stress:

- The uniaxial tensile strength: $\sigma_1 = f_t$, $\sigma_2 = \sigma_3 = 0$
- The equibiaxial compressive strength: $\sigma_1 = 0$, $\sigma_2 = \sigma_3 = -f_{2c}$
- The uniaxial compressive strength: $\sigma_1 = \sigma_2 = 0$, $\sigma_3 = -f_c$
- A point on the compressive meridian: $\sigma_{oct} = \sigma_{oct,f}$, $\tau_{oct} = \tau_{oct,f}$

Employing the above boundary conditions, and after some algebraic calculations assisted by the Maple computer system for advanced mathematics, equations 3.24a-h were derived

for the calculation of the four model parameters: a , b , k_1 and k_2.

$$c_1 = \frac{1}{\sqrt{2}} \frac{\tau_{oct,f}}{f_c} \left(\frac{3}{\sqrt{2}} \frac{\tau_{oct,f}}{f_c} - 1 \right) \tag{3.24a}$$

$$c_2 = \frac{1}{3} \frac{f_{2c}}{f_c} \left(\frac{f_{2c}}{f_c} - \frac{f_t}{f_c} \right) \tag{3.24b}$$

$$b = \frac{\frac{1}{c_2} \left(\frac{f_{2c}}{f_c} \frac{f_c}{f_t} - 1 \right) - \sqrt{2} \frac{f_c}{\tau_{oct,f}}}{\frac{1}{c_1} \left(\frac{1}{\sqrt{2}} \frac{\tau_{oct,f}}{f_c} + \frac{\sigma_{oct,f}}{f_c} \right) + \frac{1}{c_2} \frac{f_{2c}}{f_c}} \tag{3.24c}$$

$$a = \frac{9}{2} \frac{\frac{f_c}{f_{2c}} - \frac{f_c}{f_t} + b}{\frac{f_{2c}}{f_c} - \frac{f_t}{f_c}} \tag{3.24d}$$

$$\lambda_c = \frac{a \left(3 \frac{\tau_{oct,f}^2}{f_c^2} - \frac{2}{3} \right) + b \left(3 \frac{\sigma_{oct,f}}{f_c} + 1 \right)}{\sqrt{2} - 3 \frac{\tau_{oct,f}}{f_c}} \tag{3.24e}$$

$$\lambda_t = \frac{2a \left(\frac{f_t^2}{f_c^2} - \frac{f_{2c}^2}{f_c^2} \right) + 3b \left(\frac{f_t}{f_c} + 2 \frac{f_{2c}}{f_c} \right)}{3\sqrt{2} \left(\frac{f_{2c}}{f_c} - \frac{f_t}{f_c} \right)} \tag{3.24f}$$

$$k_2 = \cos\left(3\tan^{-1}\left(\frac{2}{\sqrt{3}}\left(\frac{\lambda_c}{\lambda_t} - \frac{1}{2}\right)\right)\right) \tag{3.24g}$$

$$k_1 = \frac{\lambda_c}{\cos\left(\frac{\pi}{3} - \frac{1}{3}\cos^{-1}(k_2)\right)} = \frac{\lambda_t}{\cos\left(\frac{1}{3}\cos^{-1}(k_2)\right)} \tag{3.24h}$$

Ottosen's failure criterion was numerically calibrated using the tensile strength ratio $f_t/f_c = 0.08$, the equibiaxial strength ratio $f_{2c}/f_c = 1.16$, and the data point on the compressive meridian $(\sigma_{oct}/f_c\ ,\tau_{oct}/f_c) = (-1.54\ ,1.32)$. Using these data points the model parameters, $a = 5.40$, $b = 12.93$, $k_1 = 1.00$ and $k_2 = 17.17$, are calculated from equations 3.24a-h. When inserting the model parameters into equations 3.22 and 3.23 the following expressions are found for estimating the strength of confined concrete:

$$\tau_{oct}/f_c = -0.808 + \sqrt{0.838 - 2.396(\sigma_{oct}/f_c)} \tag{3.25}$$

$$f_{cc}/f_c = 0.219 - \sigma_1/f_c + \sqrt{0.610 - 9.976(\sigma_1/f_c)} \tag{3.26}$$

Since a tensile strength ratio below 0.074 leads to a breakdown in the mathematical formulation of Ottosen's failure criterion, the tensile strength ratio used for the calibration was larger than the ratio of about 0.06 determined for the high strength concretes employed in the present investigation. However, with respect to the prediction of confined strengths, the tensile strength ratio used for the calibration of Ottosen's failure criterion has virtually no effect. The equibiaxial compressive strength ratio of 1.16 was reported by Kupfer (1973) from biaxial tests on concretes with compressive strengths up to 57 MPa. No information regarding the equibiaxial compressive strength of concrete of higher strength could be

found in the literature. The arbitrary calibration point on the compressive meridian was chosen using the comprehensive triaxial strength data for high strength concrete obtained by Dahl (1992c). The calibration point represents the average normalised confined strength at a confinement ratio of 0.6.

Figures 3.9 and 3.10 show test results on the compressive meridian when expressed in terms of octahedral and principal stress variables respectively. Both equation 3.25 and 3.26 can be seen to provide a good fit to the experimental data obtained from tests on normal weight concretes with strengths ranging from 20 MPa to 132 MPa. It can also be noted that the effect of employing octahedral stress variables is to reduce the data scatter somewhat.

Except for the data taken after Schickert and Winkler (1977) the experimental data shown in the figures were produced by employing a normal stress path. For a normal stress path, a predefined hydrostatic pressure is reached by increasing the applied stress so that $\Delta\sigma_1 = \Delta\sigma_2 = \Delta\sigma_3$, after which the axial stress is increased under a condition of constant lateral pressure, i.e. $\Delta\sigma_1 = \Delta\sigma_2 = 0$. In Schickert and Winkler's investigation a deviatoric stress path was followed. For a deviatoric stress path, the lateral pressure is reduced simultaneously with an increase in the axial pressure so as to maintain a constant hydrostatic pressure, i.e. $\Delta\sigma_1 = \Delta\sigma_2 = -1/2\,\Delta\sigma_3$. However, in most practical situations the confining pressure is generated by the lateral dilatation of the concrete core, and the stress path is essentially proportional, i.e. $\Delta\sigma_1 = \Delta\sigma_2 = k\Delta\sigma_3$. Kotsovos and Pavlovic (1995) reported that for a hydrostatic pressure less than about $0.8\,f_c$ the failure stresses are virtually independent of the followed stress path, and they can therefore be represented by a single envelope.

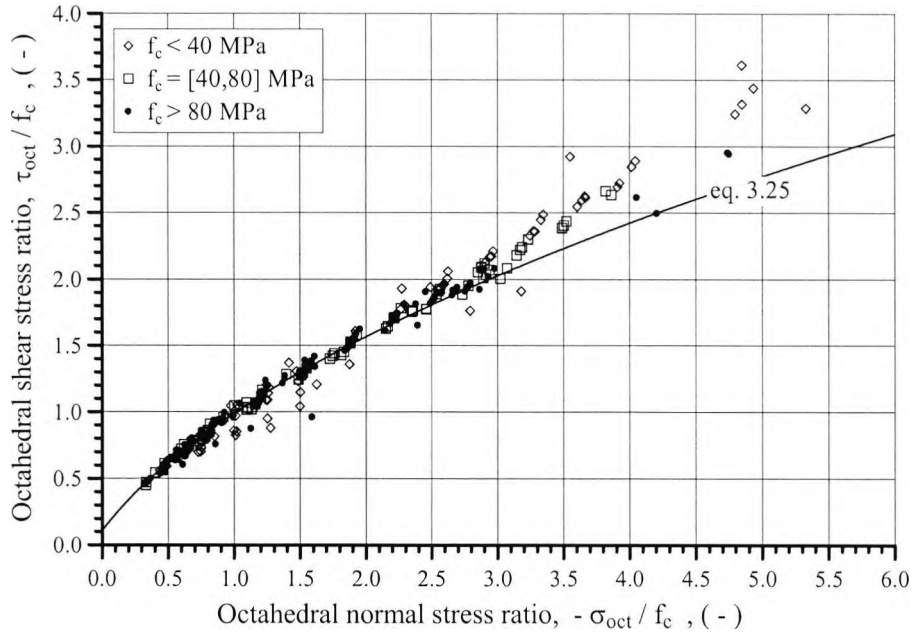

Figure 3.9
Normalised relationship between octahedral shear strength and normal stress, test data after (Richart, 1928; Newman, 1973; Kotsovos, 1974; Schickert, 1977; Dahl, 1992c; Setunge, 1993; Xie, 1995; Sfer, 2002)

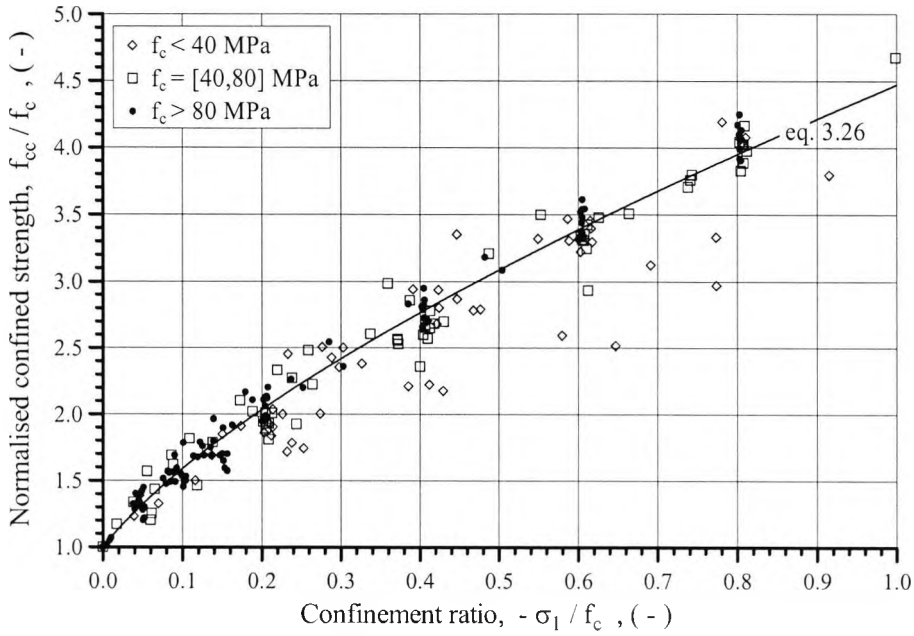

Figure 3.10
Normalised relationship between compressive strength and confining pressure, test data after (Richart, 1928; Newman, 1973; Kotsovos, 1974; Schickert, 1977; Dahl, 1992c; Setunge, 1993; Xie, 1995; Sfer, 2002)

According to the proposed confinement model, see equation 3.26, the absolute gain in compressive strength, $f_{cc} - f_c$, will, for a fixed value of confining pressure, $-\sigma_1$, increase with increasing uniaxial strength, f_c. This aspect of the model is visualised in figure 3.11, and is in agreement with the experimental results which, though being scattered, show clear signs of being grouped according to the grade of concrete.

In summary, the comparative study showed:

- The confined strength is increased, albeit at a decreasing rate, with increasing confinement.
- A unique nonlinear relationship can be formulated between the normalised confined strength and the confinement ratio.

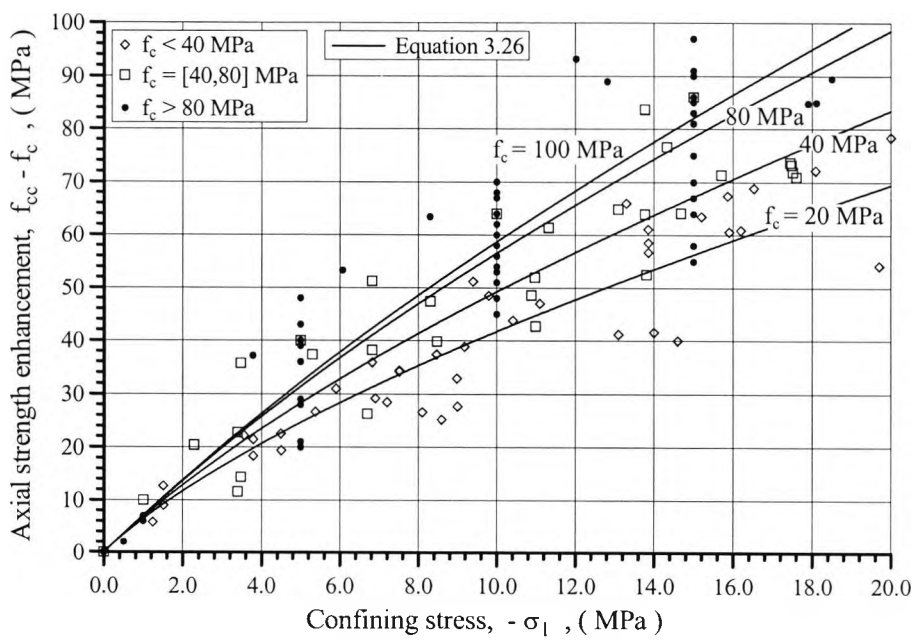

Figure 3.11
Strength enhancement as a function of confining pressure, test data after (Richart, 1928; Newman, 1973; Kotsovos, 1974; Schickert, 1977; Dahl, 1992c; Setunge, 1993; Xie, 1995; Sfer, 2002)

3.3.2 Strain at Confined Peak Stress

Figures 3.12 and 3.13 show experimental results for the influence of confinement on the peak strain of concrete. The ratio between the peak strain of confined and unconfined concrete, $\varepsilon_{cc}/\varepsilon_c$, is plotted as a function of the normalised confined strength, f_{cc}/f_c , in figure 3.12, and as a function of the confining stress, $-\sigma_1$, in figure 3.13.

From examining the test data, the following characteristics could be identified:

- The peak strain ratio is increased, and at a continuously higher rate, with an increase in the normalised confined strength.
- Confinement always enhances the peak strain relatively more than the strength, i.e. the data points shown in figure 3.12 lie above the line of equality.
- The sensitivity of the peak strain ratio to confinement is much less for high strength concrete than for normal strength concrete.

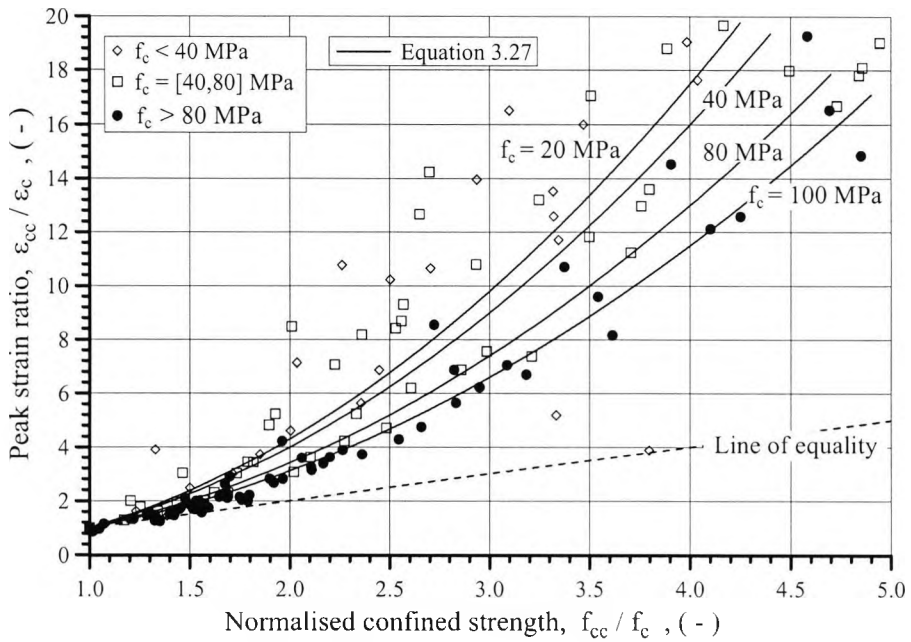

Figure 3.12
Normalised relationship between peak strain and strength of confined concrete, test data after (Richart, 1928; Newman, 1973; Kotsovos, 1974; Dahl, 1992b; Xie, 1995; Attard, 1996; Sfer, 2002)

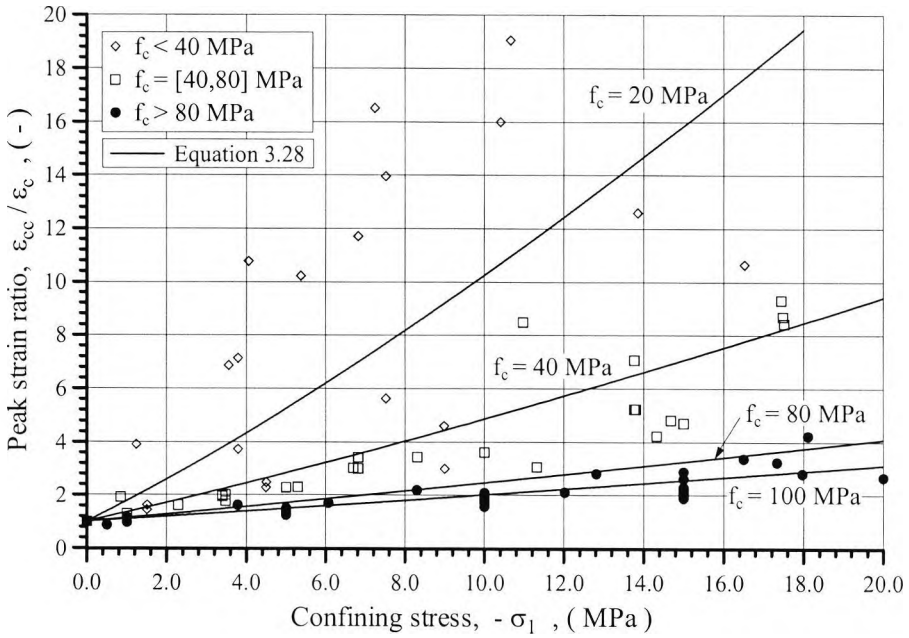

Figure 3.13
Peak strain ratio versus confining pressure, test data after (Richart, 1928; Newman,1973; Kotsovos, 1974; Dahl, 1992b; Xie, 1995; Attard, 1996; Sfer, 2002)

It can be seen from figure 3.13 that the variability in the test data is increased with an increase in the confining stress as well as with a lowering of the concrete grade. Such an increase in the variability is to be expected since both an increase in the confining stress and a lowering of the concrete grade have the effect of flattening the peak of the stress-strain curve. The flatter the stress-strain curve the more sensitive the recorded peak strain is to small variations in the testing procedure and to statistical variations in the material itself.

A suitable empirical model for the relationship between the peak strain and the strength of confined concrete was developed on the basis of the available experimental data. The proposed model, equation 3.27, was calibrated by means of the general least square method. The model is illustrated in figure 3.12 for four selected concrete grades.

$$\frac{\varepsilon_{cc}}{\varepsilon_c} = (1.2 - 0.005 f_c)\left(\left(\frac{f_{cc}}{f_c}\right)^2 - 1\right) + 1 \qquad (3.27)$$

When further estimating the confined strength by equation 3.26, the relationship between the confining pressure and the peak strain can be expressed as follows:

$$\frac{\varepsilon_{cc}}{\varepsilon_c} = (1.2 - 0.005 f_c)\left(\left(0.083 - \sigma_1/f_c + \sqrt{0.841 - 10.784(\sigma_1/f_c)}\right)^2 - 1\right) + 1 \qquad (3.28)$$

where: f_c is given in MPa

As illustrated in figure 3.13, the model captures the important characteristic of high strength concrete requiring substantially more confinement than normal strength concrete in order to produce a given increase in the peak strain. Considering that the mean strength of the concrete specimens tested in the group labelled $f_c > 80$ MPa was 101 MPa, the peak strain predictions are very accurate for high strength concrete. Because of the increased data scatter, the predictions are naturally associated with less certainty for reduced concrete strengths.

3.3.3 Analytical Expression for Confined Stress-Strain curve

The ascending part of the stress-strain curve can be represented by equation 3.29, which is obtained by replacing the material properties f_c and ε_c in equation 3.8 with the similar properties for confined concrete, i.e. f_{cc} and ε_{cc} .

$$\sigma_3 = f_{cc} \frac{\frac{E_c}{E_{ccs}}\frac{\varepsilon_3}{\varepsilon_{cc}} + \left(\frac{\varepsilon_3}{\varepsilon_{cc}}\right)^2}{1 - \left(\frac{E_c}{E_{ccs}} - 2\right)\frac{\varepsilon_3}{\varepsilon_{cc}}} \qquad \text{for } |\varepsilon_3| \le \varepsilon_{cc} \qquad (3.29)$$

where: $E_{ccs} = f_{cc}/\varepsilon_{cc}$ is the secant modulus at peak stress for confined concrete.

Equation 3.29 can be seen to satisfy the following boundary conditions:

$$\sigma_3 = 0 \qquad \text{for} \quad \varepsilon_3 = 0 \tag{3.30a}$$

$$d\sigma_3/d\varepsilon_3 = E_c \qquad \text{for} \quad \varepsilon_3 = 0 \tag{3.30b}$$

$$\sigma_3 = -f_{cc} \qquad \text{for} \quad \varepsilon_3 = -\varepsilon_{cc} \tag{3.30c}$$

$$d\sigma_3/d\varepsilon_3 = 0 \qquad \text{for} \quad \varepsilon_3 = -\varepsilon_{cc} \tag{3.30d}$$

In view of available test results for concrete confined by fluid pressure (Xie, 1995; Attard, 1996) and by closely spaced steel spirals (Ahmad, 1982; Martinez, 1984; Sudo, 1993; Issa, 1994) the characteristics of the post-peak behaviour of confined concrete can be summarised as follows:

- The slope of the descending branch of the stress-strain curve is reduced with an increase in the confining pressure.
- For a given level of confining pressure an increase in the grade of concrete is associated with a more rapid lowering in the post peak stress.
- Confined concrete exhibits a non-zero residual strength, which is raised with increasing confinement.

The outlined characteristics are all reflected in equation 3.31, which is proposed for modelling the descending part of the stress-strain curve of confined concrete. The equation is a generalisation of the similar equation proposed for unconfined concrete.

$$\sigma_3 = -(f_{cc} - f_c) + f_c \frac{\dfrac{\varepsilon_3}{\varepsilon_{cc}}}{\dfrac{\beta}{1 + (f_{cc} - f_c)}\left(-\dfrac{\varepsilon_3}{\varepsilon_{cc}} - 1\right)^3 - \dfrac{\varepsilon_3}{\varepsilon_{cc}}} \qquad \text{for} \quad |\varepsilon_3| \geq \varepsilon_{cc} \tag{3.31}$$

Equation 3.31 can be seen to satisfy the following boundary conditions:

$$\sigma_3 = -f_{cc} \qquad \text{for} \quad \varepsilon_3 = -\varepsilon_{cc} \tag{3.32a}$$

$$d\sigma_3/d\varepsilon_3 = 0 \qquad \text{for} \quad \varepsilon_3 = -\varepsilon_{cc} \tag{3.32b}$$

$$\sigma_3 \rightarrow -(f_{cc} - f_c) \qquad \text{for} \quad \varepsilon_3 \rightarrow -\infty \tag{3.32c}$$

$$d\sigma_3/d\varepsilon_3 \rightarrow 0 \qquad \text{for} \quad \varepsilon_3 \rightarrow -\infty \tag{3.32d}$$

According to equation 3.31, the residual strength equals the strength enhancement due to confinement, i.e. $f_{cc} - f_c$. However, when compared to the experimental results reported by Xie *et al* (1995) and Attard and Setunge (1996), this appears to be a rather conservative prediction of the residual strength, see figure 3.14. It was decided against improving this aspect of the model as it called for a more complex mathematical formulation in order to ensure that the initial and most important part of the descending branch of the stress-strain curve continued to compare favourably with the experimental results.

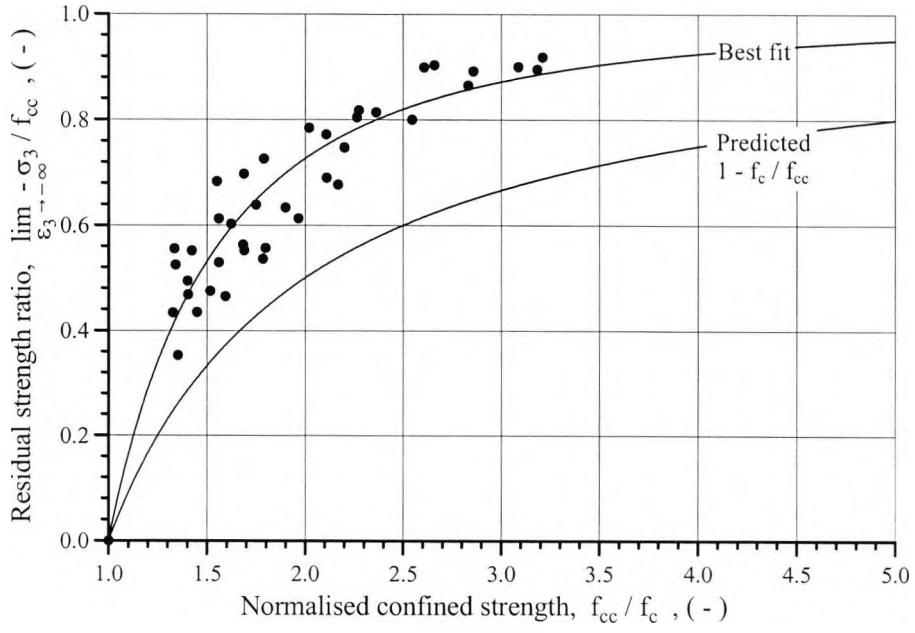

Figure 3.14
Residual strength of confined concrete, test data after (Xie, 1995; Attard, 1996)

Computed stress-strain curves in figures 3.15 - 3.18 are compared to experimental curves for a range of concrete qualities tested under various confining pressures. For reasons of clarity, the experimental results are graphically represented as discrete data points. The uniaxial material properties required for the numerical modelling were, in the case of f_c , ε_c and E_c , extracted from the experimental stress-strain data, and in the case of β, estimated using equation 3.13. It should be mentioned that the modulus of elasticity due to the applied loading conditions strictly speaking did not represent a uniaxial property but rather the bulk modulus associated with hydrostatic loading. For a given confining stress, σ_l , the confined strength, f_{cc} , and corresponding strain, ε_{cc} , were determined from equations 3.26 and 3.28 respectively. The figures demonstrate that the proposed stress-strain model is in agreement with the experimental data for confined concrete of both normal and high strength.

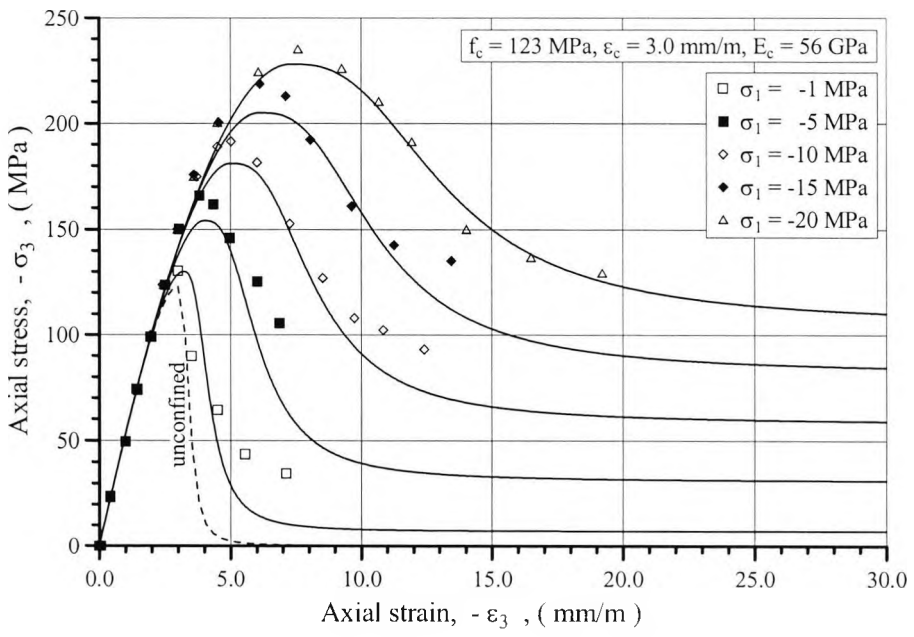

Figure 3.15
Comparison of proposed confinement model with experimental data reported by Attard and Setunge, (1996)

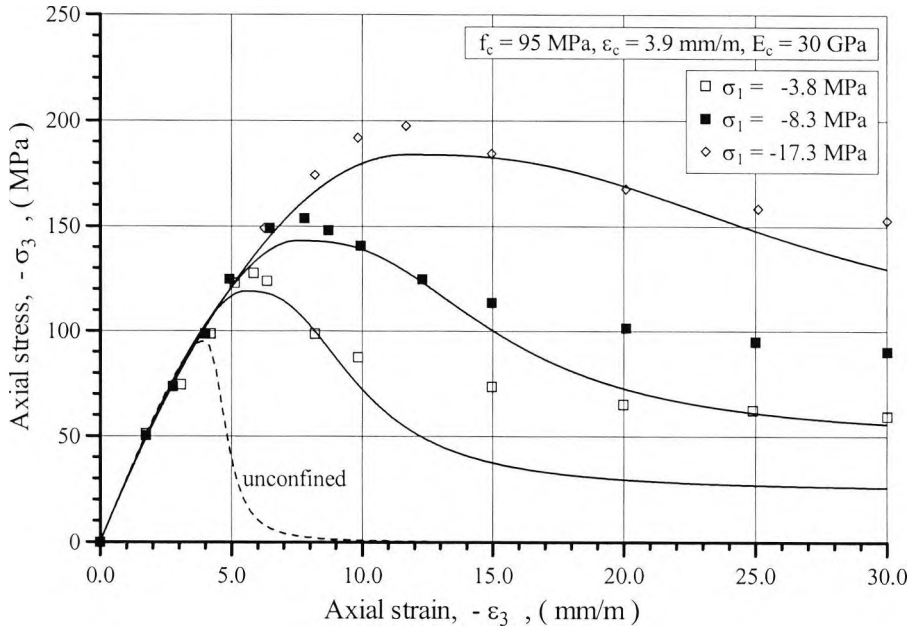

Figure 3.16
Comparison of proposed confinement model with experimental data reported by Xie *et al,* (1995)

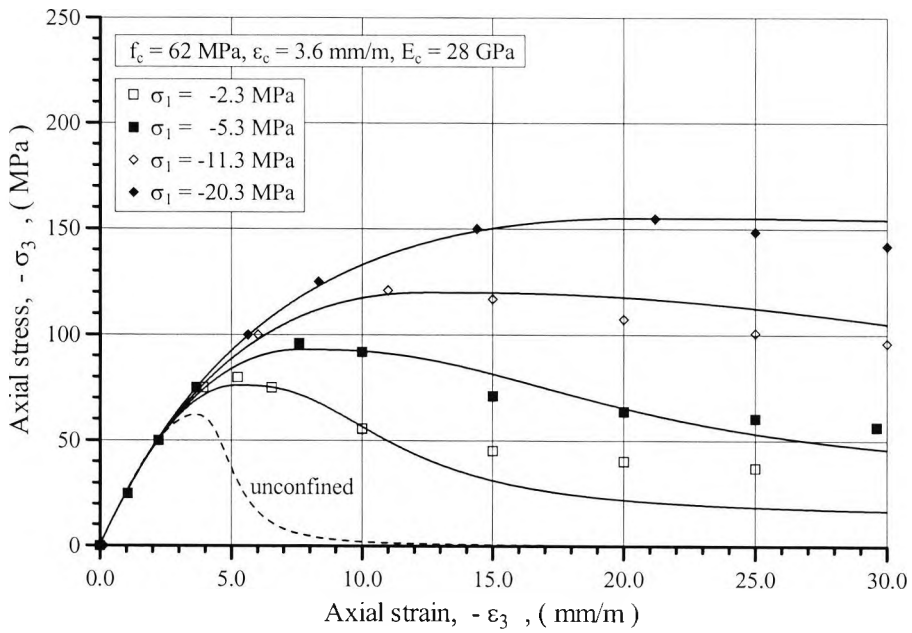

Figure 3.17
Comparison of proposed confinement model with experimental data reported by Xie *et al,* (1995)

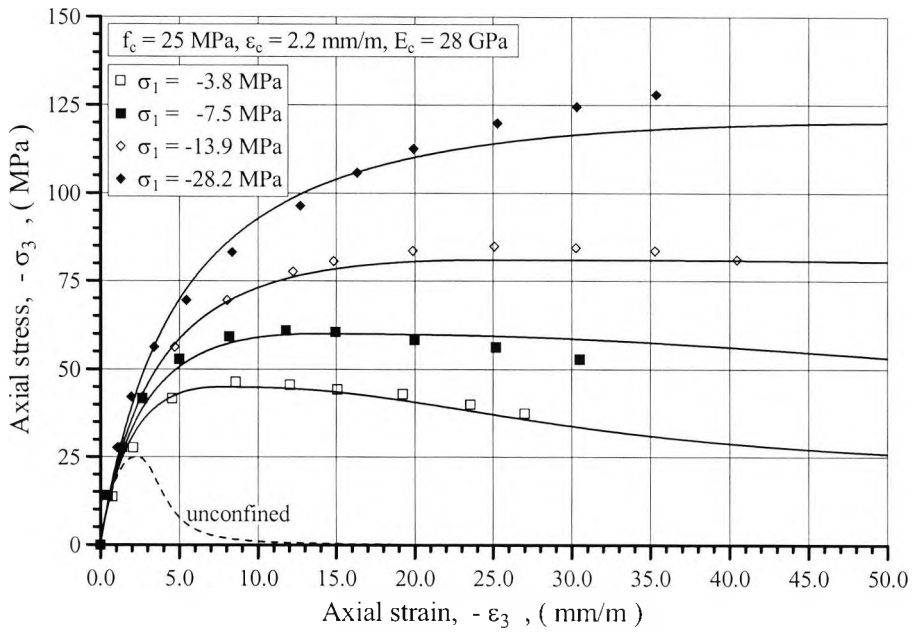

Figure 3.18
Comparison of proposed confinement model with experimental data reported by Richart *et al,* (1928)

3.4 Behaviour of Passively Confined Concrete

This section describes the stress-strain behaviour of concrete confined by means of lateral steel reinforcement. An existing method for assessing the efficiency of various tie arrangements is modified so as to establish a link between the results for transversely reinforced concrete columns and the results for plain concrete specimens tested under a condition of uniform confinement.

A computational model for automatically generating the nominal stress-strain curve for confined concrete was programmed. The computational model accounts for the effects of the material properties of the unconfined concrete, and for the configuration, distribution and stress-strain behaviour of the transverse reinforcement steel. Existing confinement models are discussed, and compared to the proposed model when applied to the concrete core of two of the high strength concrete columns tested in the present investigation.

3.4.1 General

When a transversely reinforced concrete column is subjected to axial compression, the lateral expansion due to Poisson's effect cannot take place freely, but must be associated with a compatible straining of the reinforcing steel. This in turn will cause the reinforcement to exert a confining pressure on the concrete core, which have the effect of improving the strength and ductility characteristics of the concrete in a manner similar to that described in section 3.3. Concrete is said to be passively confined when the confining pressure is a consequence of the dilatation of the concrete itself.

The effect that the transverse reinforcement has on the structural behaviour of a column can, as it was done in the research reported in the references (Xie, 1996), (Xie, 1997),

(Foster, 1998), (Liu, 1998) and (Liu, 2000), be predicted by carrying out a true three-dimensional finite element analysis. Throughout the analysis the interaction between the reinforcement and the concrete is monitored in order to evaluate the multiaxial stress state and instantaneous material behaviour at each of the integration points within the body of concrete. Alternatively, the nominal stress-strain characteristics for the confined concrete core can be given directly as input in the column analysis. It is the latter approach which was adopted in the present investigation by evaluating past experimental work on passive confinement in short concrete columns subjected to concentric compression.

The structural response of confined high strength concrete columns is contrary to normal strength concrete columns characterised by sudden spalling of the concrete cover. Furthermore, spalling is often initiated well before the stress in the cover reaches the level corresponding to the strength of the unconfined concrete. As a consequence of these failure characteristics, the load-displacement diagrams recorded for transversely reinforced high strength concrete columns (Martinez, 1984; Nishiyama, 1993; Held, 1993; Cusson, 1994; Pessiki, 1997; Saatcioglu, 1998), and incidentally also those for high strength concrete beams (Hansen, 1993), often display two distinct peaks. The first peak coincides with the onset of cover spalling, and the second with the exhaustion of the load carrying capacity of the confined concrete core. Whether or not the value of load at the second peak exceeds the value at the first depends on the efficiency of the ties in confining the concrete core, the level of stress at which cover spalling occurs and the dimensions of the core relative to those of the cover. Figure 3.19 schematically illustrates the load-strain behaviour recorded in two column tests carried out by Cusson and Paultre (1994). The two columns were identical except that they were manufactured from concrete with a 150×300 mm cylinder strength of 114 MPa and 56 MPa respectively. Because of the overall less brittle response

of the concrete cover, the column manufactured from the lower grade concrete exhibited a much less pronounced drop in the axial load after the onset of cover failure than the column manufactured from the higher grade concrete.

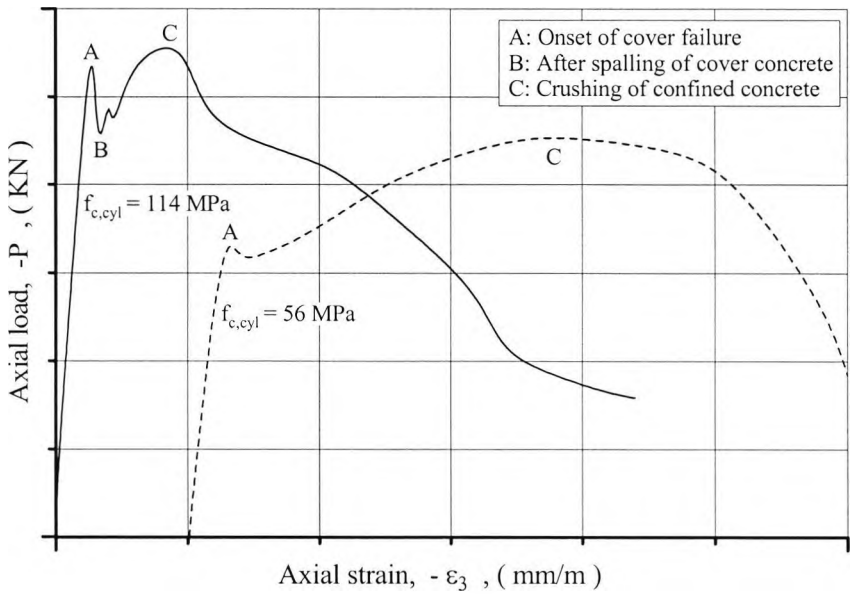

Figure 3.19
Schematic illustration of load-strain behaviour of transversely reinforced concrete columns, (Cusson, 1994)

Collins *et al* (1993) explained the occurrence of premature cover spalling by differential drying shrinkage causing extensive micro-cracking along the reinforcement bars. This creates a weak plane along which the cover can separate from the core. A three-dimensional finite element analysis carried out by Foster *et al* (1998) produced another explanation for the occurrence of premature cover spalling. According to Foster *et al*, the incompatibility between the lateral expansion characteristics of the confined core and the unconfined cover leads to the development of small tensile stresses across the interface between the core and the cover. The effect of the tensile stresses is to significantly reduce the compressive strength in the longitudinal direction. Although the precise circumstances required to trigger premature spalling yet are to be fully established, it is likely that an increase in the density

of the reinforcement cage and in the concrete grade both have an adverse effect on the stability of the cover shell (Cusson, 1994; Razvi, 1994; Saatcioglu, 1998). In this context, it should be recalled from section 3.2 that the tensile strength of concrete in general increases at a deceasing rate with the compressive strength.

Razvi and Saatcioglu (1994) reported that cover spalling in high strength concrete columns sometimes occurred at a stress level as low as that corresponding to 70% of the unconfined concrete strength. They investigated the structural consequences of premature cover spalling by applying equation 3.33, recommended for predicting the concentric load capacities of high strength concrete columns in the ACI state-of-the-art report (1984), to available test results. The findings from their study are summarised in figure 3.20.

$$P_c = 0.85 f_{c,cyl} (A_{tot} - A_g) + f_{sy} A_g \tag{3.33}$$

where:

P_c is the axial load capacity of the column

$f_{c,cyl}$ is the 150×300 mm cylinder strength of concrete

A_{tot} is the gross cross-sectional area of column

A_g is the area of longitudinal steel

f_{sy} is the yield strength of longitudinal steel

The figure shows that, although the strength of the unconfined high strength concrete columns safely could be calculated to 0.85 times the 150×300 mm cylinder strength, equation 3.33 often overestimated the load carrying capacity of the confined concrete columns. Thus, the strength of the confined concrete core was in many of the tested columns insufficient to compensate for the early loss of the concrete cover. It can be noted that Razvi and Saatcioglu (1994) employed a confinement index which increased with an

increase in the volumetric ratio of transverse reinforcement, ρ_s , an increase in the yield strength of the transverse reinforcement, f_{sy} , and a decrease in the cylinder strength of concrete, $f_{c,cyl}$.

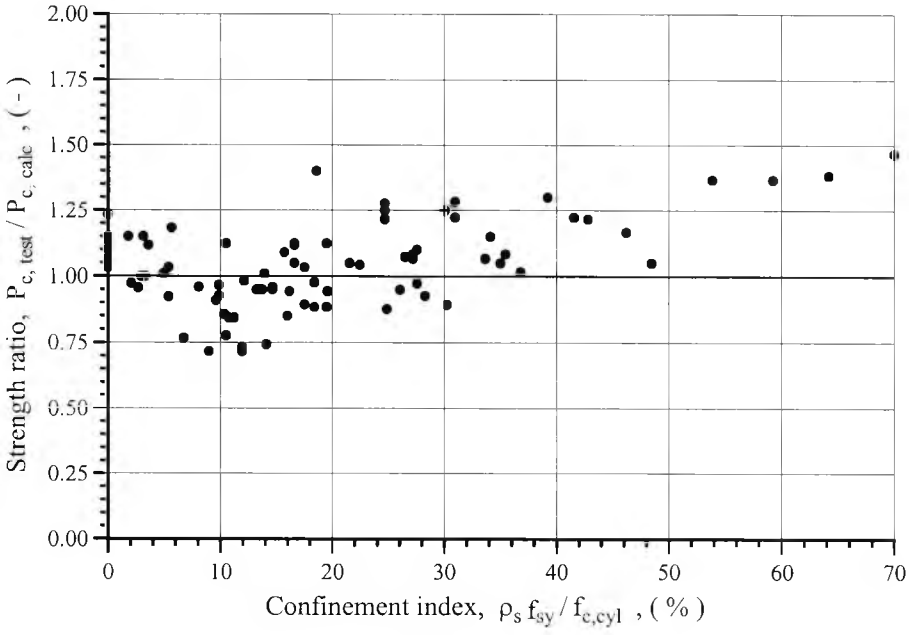

Figure 3.20
Concentric load capacities of transversely reinforced concrete columns, (Razvi, 1994)

Very little experimental information exists regarding the effect that the longitudinal reinforcement has on the confinement conditions in transversely reinforced concrete columns. However, the available information unequivocally suggests that an increase in the volumetric ratio of longitudinal reinforcement has a beneficial, though in general probably very limited, influence on the confinement conditions. The test results reported by Bjerkeli *et al* (1993) show that an increase in the size of the longitudinal reinforcement bars increased the strength of the concrete core by about 12% in the columns which had a volumetric ratio of transverse reinforcement of 1.1%, and by about 2% in the columns which had a volumetric ratio of transverse reinforcement of 3.1%. The columns tested by Bjerkeli *et al* had an unconfined concrete strength of 66 MPa, were transversely reinforced

by means of square hoops and had a volumetric ratio of longitudinal reinforcement of either 1.4% or 3.6%. In contrast, the results from tests carried out by Cusson and Paultre (1994) show that only for very efficient tie configurations will the strength and ductility characteristics of the core concrete benefit from an increase in the size of the longitudinal reinforcement bars. The stress-strain behaviour determined for the concrete cores which were transversely reinforced by either square hoops or square hoops overlayed by diamond shaped inner hoops, i.e. the tie configuration typically used for columns with eight longitudinal reinforcement bars, was only marginally improved when increasing the volumetric ratio of longitudinal reinforcement from 2.2% to 3.6%. However, in the case of the columns which were transversely reinforced by square hoops overlayed by either octagonal inner hoops or pairs of rectangular inner hoops, i.e. the tie configurations typically used for columns with 12 longitudinal reinforcement bars, the use of larger longitudinal bars resulted in a 7% increase in the strength of the concrete core. The columns tested by Cusson and Paultre had an unconfined concrete strength of about 81 MPa and a volumetric ratio of transverse reinforcement between 2.8% and 4.9%.

Mander *et al* (1988b) investigated the effect that the number of longitudinal reinforcement bars had on the confinement conditions in spirally reinforced normal strength concrete columns. They reported that for a given volumetric ratio of longitudinal reinforcement a change in the number of bars had virtually no effect.

3.4.2 Effective Confining Stress

In order to assess the effectiveness of various tie arrangements in confining the concrete core of a column, it is helpful to introduce the concept of effective confining stress. The effective confining stress, $\sigma_{l,eff}$, is in this thesis defined as the confining stress, which

would be required under triaxial axisymmetric loading conditions in order to obtain the exact same concrete strength, f_{cc}, as the mean strength of the passively confined concrete core.

The effective confining stress can conveniently be expressed in terms of the nominal confining stress, $\sigma_{l,nom}$, and two reduction coefficients, α_n and α_s, as follows:

$$\sigma_{l,eff} = \alpha_n \alpha_s \sigma_{l,nom} \tag{3.34}$$

The nominal confining stress is defined as the uniform stress over the surface of the concrete core which is in equilibrium with the tensile forces in the transverse reinforcement bars, and the reduction coefficients quantify the ability of the transverse reinforcement in providing such a state of uniform confinement. The first reduction coefficient accounts for the efficiency of the tie configuration, and the second for the efficiency of the tie distribution.

Expressions for calculating the volumetric ratio of transverse reinforcement and the nominal confining stress for some standard tie configurations are given in table 3.1. The bracketed superscripts in the expressions for tie configurations C, D and E indicate that the perimeter tie and supplementary ties are not necessarily of the same diameter or indeed identically stressed.

If it is assumed that all tie legs are equally stressed, the nominal confining stress for the standard tie configurations given in table 3.1 can be calculated, albeit only approximately in the case of tie configurations D and E, from the following formula:

$$\sigma_{l,nom} = -\frac{\rho_s}{2}\sigma_s \tag{3.35}$$

Table 3.1
Nominal confining stress for standard tie configurations

Tie arrangement		Volumetric ratio, ρ_s	Nominal confining stress, $\sigma_{l,nom}$
A)		$\rho_s = \frac{4A_s}{sd_c}$	$\sigma_{l,nom} = -\frac{2A_s}{sd_c}\sigma_s$
B)		$\rho_s = \frac{4A_s}{sd_c}$	$\sigma_{l,nom} = -\frac{2A_s}{sd_c}\sigma_s$
C)		$\rho_s = \frac{4A_s^{(1)} + 2\sqrt{2}A_s^{(2)}}{sd_c}$	$\sigma_{l,nom} = -\frac{2A_s^{(1)}\sigma_s^{(1)} + \sqrt{2}A_s^{(2)}\sigma_s^{(2)}}{sd_c}$
D)	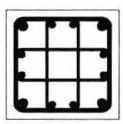	$\rho_s = \frac{4A_s^{(1)} + 5A_s^{(2)}}{sd_c}$	$\sigma_{l,nom} = -\frac{2A_s^{(1)}\sigma_s^{(1)} + 2A_s^{(2)}\sigma_s^{(2)}}{sd_c}$
E)		$\rho_s = \frac{4A_s^{(1)} + 4/3(1+\sqrt{2})A_s^{(2)}}{sd_c}$	$\sigma_{l,nom} = -\frac{2A_s^{(1)}\sigma_s^{(1)} + \sqrt{2}A_s^{(2)}\sigma_s^{(2)}}{sd_c}$

d_c : dimension of nominal concrete core as defined by the perimeter tie
A_s: cross sectional area of tie bars
σ_s : tensile stress in ties
s : pitch of ties

Mander *et al* (1988a) utilised a concept, similar to the one used by Sheikh and Uzumeri (1982), to develop a geometric method for calculating the effective confining stress for general tie configurations and distributions. The geometric method is based on the assumption that an effectively confined concrete core, where the confining stress has fully developed, can be determined from the principle of stress arching, and that the effective confining stress is directly proportional to the ratio between the minimum area of the effectively confined concrete core, $A_{cc,eff}$, and the area of the nominal concrete core, A_{cc}. Thus, according to Mander *et al's*, method the effective confining stress can be calculated as follows:

$$\sigma_{l,eff} = \frac{A_{cc,eff}}{A_{cc}}\sigma_{l,nom} \tag{3.36}$$

Because of the arching action, the area of the effectively confined concrete core will always be at a minimum midway between adjacent ties. At tie level, a circular tie configuration will apply a uniform pressure along its perimeter, whereas a non-circular tie configuration will experience stress arching between the points at which the tie is effectively restrained against lateral deformations. The mechanism of the arching action is in figure 3.21 illustrated for tie configurations B and C.

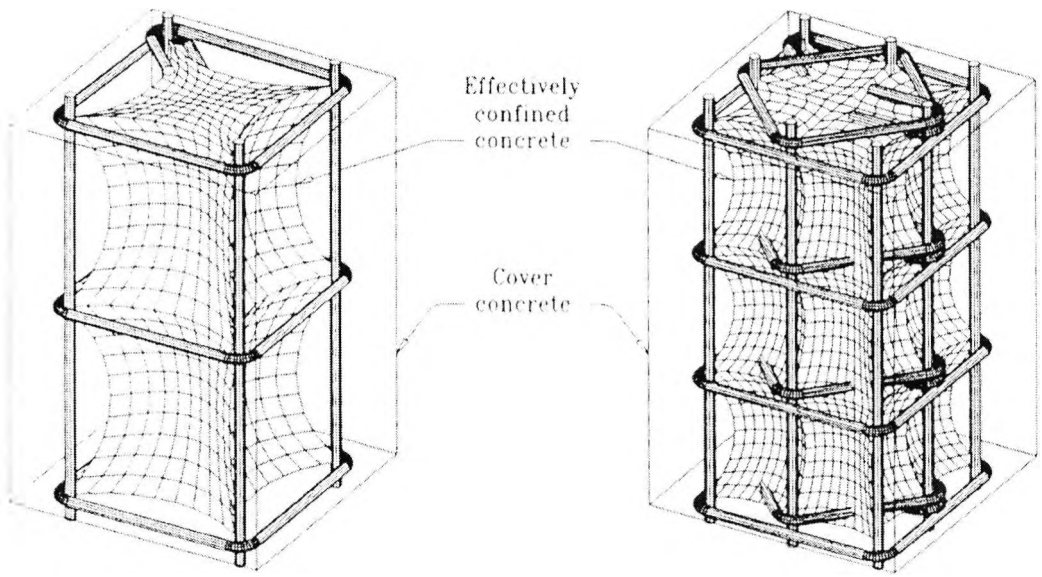

Figure 3.21
Illustration of arching action for two typical tie configurations, taken after (Cusson, 1994)

Mander *et al* (1988a) assumed the arching action in both the longitudinal and the transverse direction to occur in the form of a second degree parabola with an initial tangent slope of 45°. Table 3.2 lists the reduction coefficients determined for the standard tie configurations when applying the 45° arching action method. In the case of circular hoops, the arching action reduces the diameter of the effectively confined concrete core to $d_c - s/2$ midway between these. For quadratic hoops the arching action reduces the area of the effectively confined concrete core at tie level to $1/3\,d_c^2$, $2/3\,d_c^2$, $7/9\,d_c^2$ and $7/9\,d_c^2$ for tie

configurations B, C, D and E respectively. The area midway between the ties can be approximated using the scaling law applicable to circular hoops. For spiral reinforcement the cross-section of the effective confined concrete core can be shown to be an ellipse with a major axis diameter of d_c and a minor axis diameter of $d_c - s/2$.

Table 3.2
Reduction coefficients according to the 45° arching action method

Tie arrangement		Reduction coefficients, α_n and α_s	
A)		$\alpha_n = 1$	$\alpha_s = 1 - \frac{s}{2d_c}$, Spiral
		$\alpha_n = 1$	$\alpha_s = \left(1 - \frac{s}{2d_c}\right)^2$, Circular
B)		$\alpha_n = \frac{1}{3}$	$\alpha_s = \left(1 - \frac{s}{2d_c}\right)^2$
C)		$\alpha_n = \frac{2}{3}$	$\alpha_s = \left(1 - \frac{s}{2d_c}\right)^2$
D)	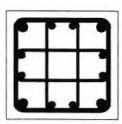	$\alpha_n = \frac{7}{9}$	$\alpha_s = \left(1 - \frac{s}{2d_c}\right)^2$
E)		$\alpha_n = \frac{7}{9}$	$\alpha_s = \left(1 - \frac{s}{2d_c}\right)^2$

According to the 45° arching action method, the confining effect of the ties vanishes when their pitch exceeds twice the dimension of the nominal concrete core. In the special case where the pitch is equal to the dimension of the concrete core, the effective confinement is reduced to 50% of the nominal confinement for spiral reinforcement, and to 25% of the nominal confinement for the other tie configurations. However, a number of tests have demonstrated that the transverse reinforcement has a negligible influence on the concrete

strength if the pitch of the ties is equal to the dimension of the concrete core (Iyengar, 1970; Ahmad, 1982; Martinez, 1984; Yong, 1988; Issa, 1994). These observations indicate that the 45° arching action method overestimates the effective confining stress, and as such will require a compensation for this by being used in conjunction with constitutive equations which in general underestimate the effect of confinement.

The stress-strain models for passively confined concrete recommended by CEB (1990), Cusson and Paultre (1995) and Mander *et al* (1988a) all utilise the 45° arching action method to calculate the effective confining pressure. According to the CEB model, the strength enhancement associated with the effective confining pressure can be determined from the bilinear expression given in equation 3.37. Cusson and Paultre (1995) proposed equation 3.38, and Mander *et al* (1988a) equation 3.39, for calculating the strength enhancement. Incidentally equation 3.39 is consistent with William Warnke's five parameter failure criterion (William, 1974).

$$\frac{f_{cc}}{f_c} = \begin{cases} 1.000 - 5.0\dfrac{\sigma_{1,eff}}{f_c} & \text{for } \dfrac{-\sigma_{1,eff}}{f_c} \le 0.05 \\ 1.125 - 2.5\dfrac{\sigma_{1,eff}}{f_c} & \text{for } \dfrac{-\sigma_{1,eff}}{f_c} \ge 0.05 \end{cases} \tag{3.37}$$

$$\frac{f_{cc}}{f_c} = 1.0 + 2.1\left(\frac{-\sigma_{1,eff}}{f_c}\right)^{0.7} \tag{3.38}$$

$$\frac{f_{cc}}{f_c} = -1.254 + 2.254\sqrt{1 - 7.94\frac{\sigma_{1,eff}}{f_c}} + 2.0\frac{\sigma_{1,eff}}{f_c} \tag{3.39}$$

Figure 3.22 illustrates the ability of the proposed equations to predict the strength of concrete when tested under triaxial axisymmetric loading conditions. It can be seen from the figure that the equations proposed by CEB (1990) and Cusson and Paultre (1995), i.e.

equations 3.37 and 3.38, in general underestimate the strength of the confined concrete. Thus, both of these equations, which were derived from regression analysis of test data on passively confined concrete columns, do not extend well to situations where the confining pressure is uniformly distributed. In contrast, equation 3.39 proposed by Mander *et al* (1988a) was calibrated using the results from the triaxial load cell tests carried out by Schickert and Winkler (1977), and is in excellent agreement with the experimental data plotted in figure 3.22. However, Mander *et al* (1988b) validated their model against experimental results for concrete columns with closely spaced ties, $s/d_c < 0.23$, and as such, they did not reveal the shortcomings of the 45° arching action method.

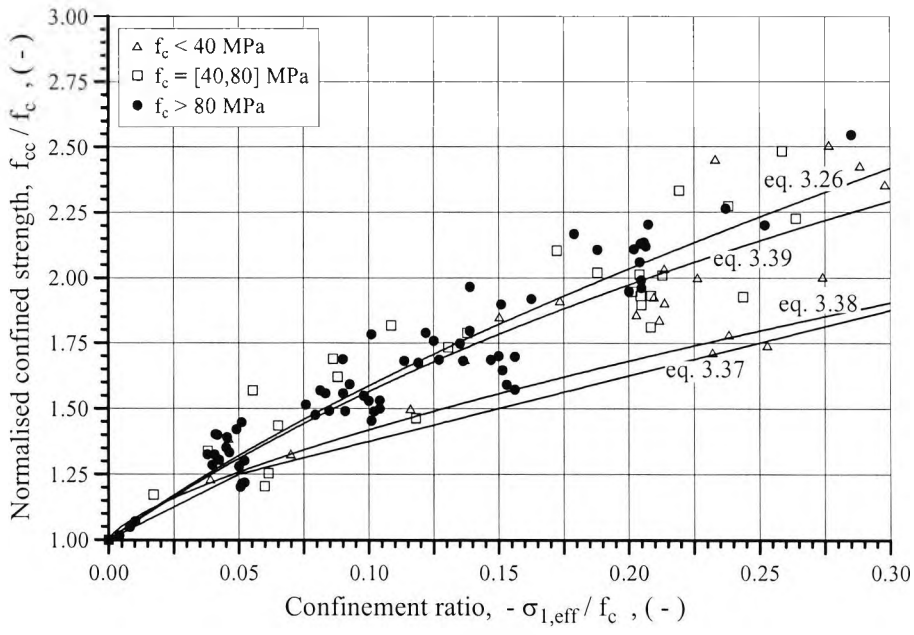

Figure 3.22
Strength of uniformly confined concrete, triaxial load cell data after (Richart, 1928; Newman, 1973; Kotsovos, 1974; Schickert, 1977; Dahl, 1992c; Setunge, 1993; Xie, 1995; Sfer, 2002)

A stress-strain model for confined concrete, which is equally capable of representing the experimental results for concrete specimens tested under triaxial axisymmetric loading conditions and the results for transversely reinforced concrete columns tested under

concentric compression, was established by introducing a new method for calculating the reduction coefficients. According to the new method, the effectiveness of the ties in confining the concrete core is reduced linearly with the pitch of the ties so as to have no effect when the pitch equals the dimension of the concrete core, i.e. $\alpha_s = 0$ for $s = d_c$. However, the reduction coefficient α_n , which accounts for the efficiency of a given tie configuration in providing a state of uniform confining pressure along its perimeter, continues to be found using the 45° arching action method. Table 3.3 lists the reduction coefficients for the standard tie configurations when calculated according to the proposed method.

Table 3.3
Reduction coefficients according to the modified arching action method

Tie arrangement		Reduction factors, α_n and α_s
A)		$\alpha_n = 1$ $\quad \alpha_s = 1 - \frac{s}{d_c}$, Spiral
		$\alpha_n = 1$ $\quad \alpha_s = 1 - \frac{s}{d_c}$, Circular
B)		$\alpha_n = \frac{1}{3}$ $\quad \alpha_s = 1 - \frac{s}{d_c}$
C)		$\alpha_n = \frac{2}{3}$ $\quad \alpha_s = 1 - \frac{s}{d_c}$
D)	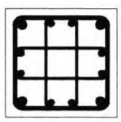	$\alpha_n = \frac{7}{9}$ $\quad \alpha_s = 1 - \frac{s}{d_c}$
E)		$\alpha_n = \frac{7}{9}$ $\quad \alpha_s = 1 - \frac{s}{d_c}$

Figures 3.23 and 3.24 show experimental data for the normalised strength of passively confined concrete as a function of the confinement ratio for a large number of concrete

columns. Since equation 3.26 approximately defines the running average of the experimental data, it can be concluded that the method proposed herein for calculating the reduction coefficients leads to a good estimate of the effective confining pressure applied to the concrete core by the various tie configurations and distributions. Full details of the test parameters and test results for the individual columns are given in Appendix A.

When plotting the experimental data, in accordance with standard practice, it was assumed that the confining steel reinforcement was yielding at the time the confined concrete core achieved its maximum resistance. However, a few researchers have pointed out that the ties, especially in high strength concrete columns, sometimes do not yield before the confined concrete core is strained into the post-peak region (Ahmad, 1982; Martinez, 1984; Yong, 1988; Cusson, 1995). The reason why a normal strength concrete column in general is better suited than a high strength concrete column to develop the full confining potential of a particular tie arrangement can be explained by the differences in their dilatation characteristics. Furthermore, the yield assumption can naturally be expected to become increasingly inaccurate with an increase in the yield strength of the transverse reinforcement. In order to avoid overestimating the confinement, it is recommended by CEB (1995) that a maximum yield strength of 500 MPa should be used when evaluating the effective confining pressure for high strength concrete columns. Alternatively, the actual straining of the ties, and hence also the confining pressure, at peak stress of the confined concrete core can be predicted by using the computational model described in the following. With the assistance of the computational model, the yield assumption was judged to have little overall impact on the data plotted in figure 3.23 and 3.24.

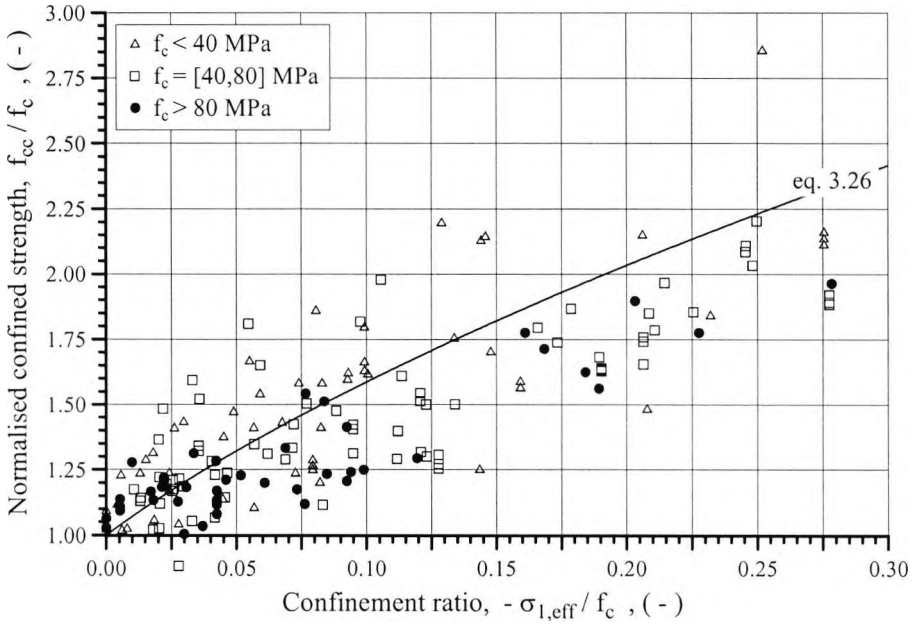

Figure 3.23
Strength of concrete confined by means of circular hoops, test data after (Ieyengar, 1970; Ahmad, 1982; Martinez, 1984; Mander, 1988b; Bjerkeli, 1993; Sudo, 1993; Hsu, 1994; Issa, 1994; Cusson, 1996; Hoshikuma, 1997; Razvi, 1999; Assa, 2001)

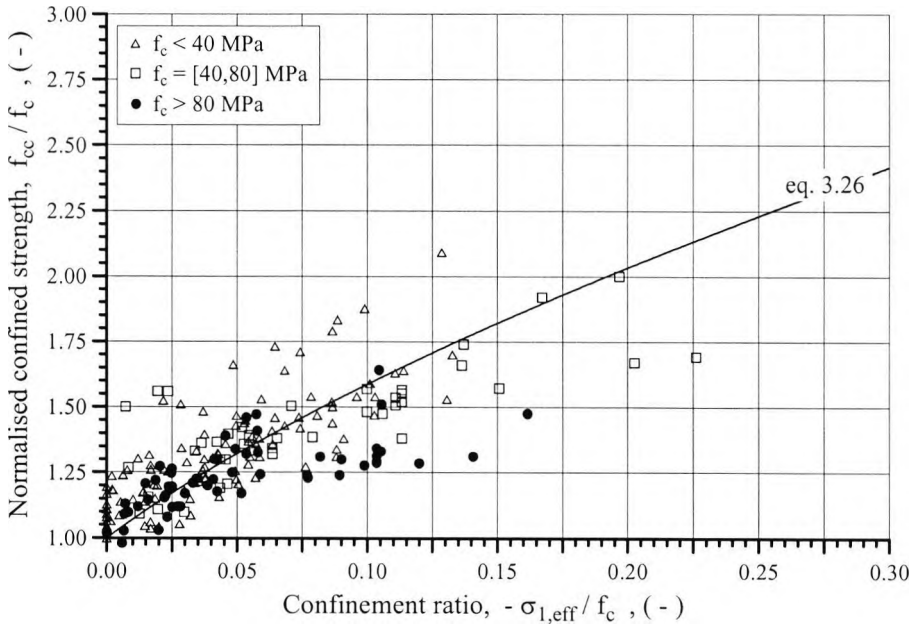

Figure 3.24
Strength of concrete confined by means of square hoops, test data after (Ieyengar, 1970; Somes, 1970; Scott, 1982; Yong, 1988; Razvi, 1989; Bjerkeli, 1993; Nishiyama, 1993; Cusson, 1994; Issa, 1994; Hoshikuma, 1997; Razvi, 1998; Razvi, 1999)

Test results for the peak strain of transversely reinforced concrete columns are plotted in figure 3.25. The results resemble those for actively confined concrete. For a given relative enhancement in strength, the relative enhancement in peak strain is in general less for high strength concrete than for normal strength concrete. It can also be seen from the figure that equation 3.27, which expresses the relationship between the strength and the peak strain of confined concrete, is much more reliable when applied to high strength concrete than when applied to normal strength concrete. In this context, it should be mentioned that for the purpose of a structural analysis, the need to accurately predict the peak strain diminishes with a decrease in the concrete strength since that also has the effect of increasing the post-peak ductility of concrete.

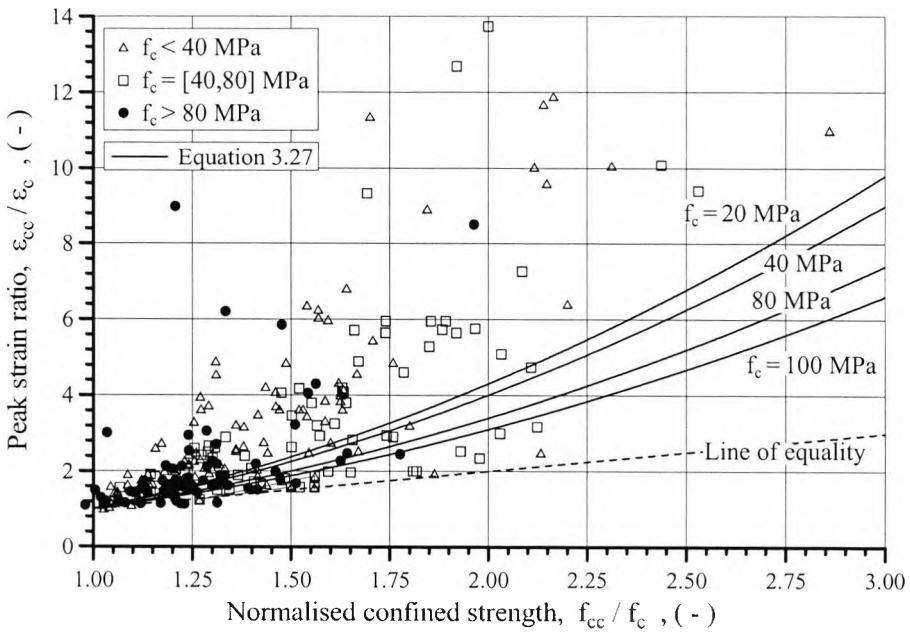

Figure 3.25
Effect of passive confinement on peak strain of concrete, test data after (Ieyengar, 1970; Ahmad, 1982; Martinez, 1984; Mander, 1988b; Yong, 1988; Nishiyama, 1993; Sudo, 1993; Cusson, 1994; Hsu, 1994; Issa, 1994; Hoshikuma, 1997; Razvi, 1999; Assa, 2001)

3.4.3 Computational Model for the Stress-Strain Behaviour

The following describes a computational model for generating the complete stress-strain curve for passively confined concrete. The model is based on the assumption that the effective confining stress, $\sigma_{l,eff}$, is increased proportionally with the transverse straining of the confined concrete core, and that it reaches its maximum when the transverse strains are equal to the yield strain of the hoop reinforcement. When the hoop reinforcement is strained beyond its yield strain, i.e. $\varepsilon_l \geq \varepsilon_{sy}$, the confining stress is assumed to remain constant. It should be emphasised that the transverse reinforcement does not necessarily yield at the time of strength failure of the confined concrete core. In the special case of $\sigma_{l,eff} = 0$, the computational model generates the uniaxial stress-strain curve described in section 3.2, and in the special case of $\varepsilon_{sy} = 0$ the stress-strain curve for actively confined concrete described in section 3.3. The algorithm for the computational model is outlined as follows:

0) INPUT: Material properties for the unconfined concrete, i.e. the compressive strength, f_c, the peak strain, ε_c, the modulus of elasticity, E_c, and the softening parameter, β. Yield strain of the transverse reinforcement steel, ε_{sy}, and the maximum effective confining pressure the transverse reinforcement is capable of applying to the concrete core, $\max \sigma_{l,eff}$.

1) Use the effective confining stress, $\sigma_{l,eff}$, to evaluate the instantaneous material properties of the confined concrete.

$$f_{cc} = f_c(0.219 - \sigma_{l,eff}/f_c + \sqrt{0.610 - 9.976(\sigma_{l,eff}/f_c)}) \tag{3.40}$$

$$\varepsilon_{cc} = \varepsilon_c((1.2 - 0.005 f_c)((f_{cc}/f_c)^2 - 1) + 1) \tag{3.41}$$

$$E_{ccs} = f_{cc}/\varepsilon_{cc} \tag{3.42}$$

2) Use the current longitudinal strain, ε_3 , to evaluate the corresponding stress, σ_3.

If $|\varepsilon_3| \le \varepsilon_{cc}$ then:

$$\sigma_3 = f_{cc} \frac{\frac{E_c}{E_{ccs}} \frac{\varepsilon_3}{\varepsilon_{cc}} + \left(\frac{\varepsilon_3}{\varepsilon_{cc}} \right)^2}{1 - \left(\frac{E_c}{E_{ccs}} - 2 \right) \frac{\varepsilon_3}{\varepsilon_{cc}}} \tag{3.43a}$$

If $|\varepsilon_3| \ge \varepsilon_{cc}$ then:

$$\sigma_3 = -(f_{cc} - f_c) + f_c \frac{\frac{\varepsilon_3}{\varepsilon_{cc}}}{\frac{\beta}{1 + (f_{cc} - f_c)} \left(-\frac{\varepsilon_3}{\varepsilon_{cc}} - 1 \right)^3 - \frac{\varepsilon_3}{\varepsilon_{cc}}} \tag{3.43b}$$

3) Use the longitudinal strain and stress, ε_3 and σ_3 , to determine the corresponding transverse strain, ε_1.

If $|\varepsilon_3| \le \varepsilon_{cc}$ and $(-\sigma_3 / f_{cc}) \le 0.6$ then:

$$\varepsilon_1 = -0.15 \varepsilon_3 \tag{3.44a}$$

If $|\varepsilon_3| \le \varepsilon_{cc}$ and $(-\sigma_3 / f_{cc}) \ge 0.6$ then:

$$\varepsilon_1 = -\varepsilon_3 (0.50 - 0.35 \sqrt{-1.25 + 7.50(-\sigma_3 / f_{cc}) - 6.25(-\sigma_3 / f_{cc})^2}) \tag{3.44b}$$

If $|\varepsilon_3| \ge \varepsilon_{cc}$ then:

$$\varepsilon_1 = -0.50 \varepsilon_3 \tag{3.44c}$$

4) Use the transverse strain, ε_1 , to update the effective confining stress, $\sigma_{1,eff}$.

If $|\varepsilon_1| \le \varepsilon_{sy}$ then:

$$\sigma_{1,eff} = \varepsilon_1 / \varepsilon_{sy} \max \sigma_{1,eff} \tag{3.45a}$$

If $|\varepsilon_1| \geq \varepsilon_{sy}$ then:

$$\sigma_{1,eff} = \max \sigma_{1,eff} \tag{3.45b}$$

5) Increment the longitudinal strain, $\varepsilon_3 = \varepsilon_3 + d\varepsilon_3$, and repeat step 1 to 5 until the strain reaches a user specified cut off value.

The expression for the apparent Poisson's ratio was taken as that given for confined concrete in (Dahl, 1992b). The expression, which was reported to be equally applicable to normal and high strength concrete, can be obtained by setting $\nu_0 = 0.15$, $\nu_c = 0.50$ and $\alpha_p = 0.60$ in equation 3.7a-b.

The computational model is, with emphasis on high strength concrete, validated against experimental stress-strain curves for passively confined concrete in figures 3.26 - 3.32. In the case of the tests carried out by Cusson and Paultre (1994) and Nishiyama *et al* (1993), the stress-strain behaviour of the unconfined concrete specimens was estimated using the material properties obtained from tests on 150×300 mm and 100×200 mm cylinders respectively. Whereas the modulus of elasticity and the peak strain were assumed to be independent of the specimen size, the unconfined compressive concrete strength was assumed equal to 85% of the150×300 mm cylinder strength or to 81% of the 100×200 mm cylinder strength. In order to highlight the above assumptions, the computed stress-strain curves for unconfined concrete are in figures 3.28 - 3.33 shown by a fine line type. The softening parameter, β, was always estimated from the compressive strength using equation 3.13.

A comparison of figure 3.26 with figure 3.27 illustrates the reduction in ductility associated with an increase in the grade of concrete. The figures 3.28 - 3.30 show the efficiency of the

various quadratic tie configurations. Clearly the type D configuration is the most efficient and the type B configuration the least efficient in enhancing the strength and ductility characteristics of the concrete core. It is interesting that the observed strength of the concrete core in the column with a volumetric ratio of 1.45% of type B hoops failed to exceed 85% of the mean strength of the 150×300 mm control cylinders. The figures 3.31 to 3.33 illustrate the beneficial effect an increase in the yield strength of the hoop reinforcement can have on the stress-strain response of the concrete core.

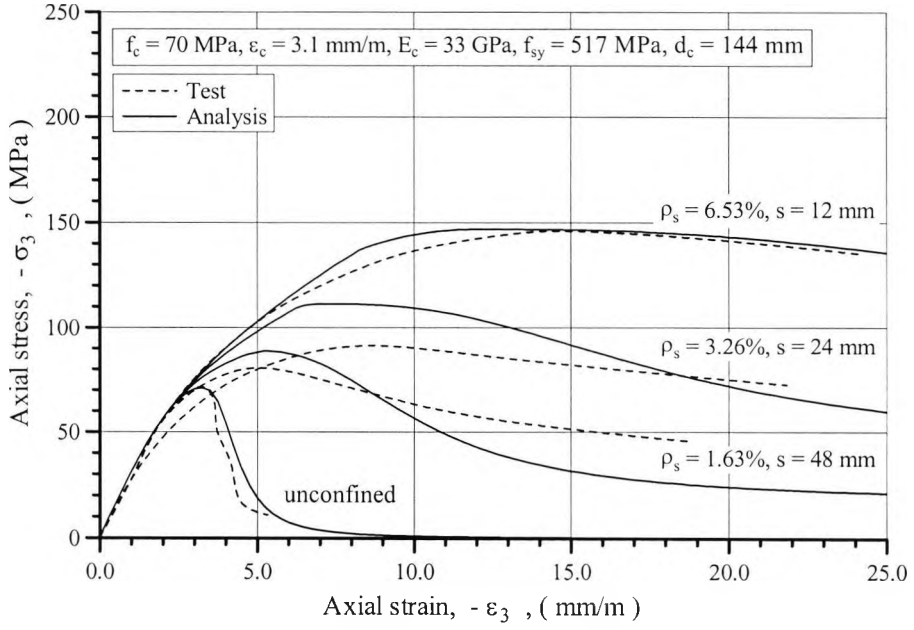

Figure 3.26
Comparison of computed and experimental stress-strain curves for a 70 MPa concrete confined by type A ties, test data after (Sudo, 1993)

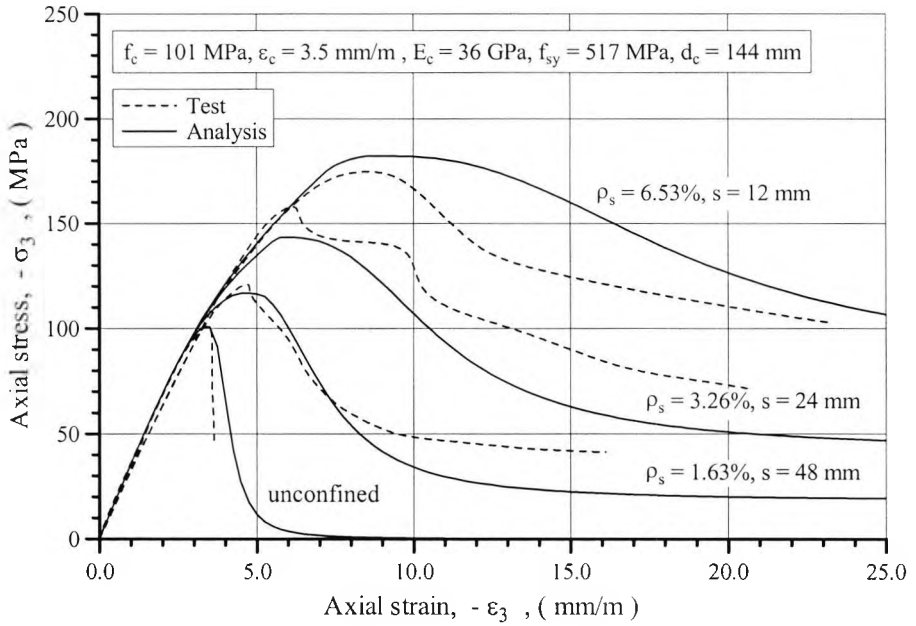

Figure 3.27
Comparison of computed and experimental stress-strain curves for a 101 MPa concrete confined by type A ties, test data after (Sudo, 1993)

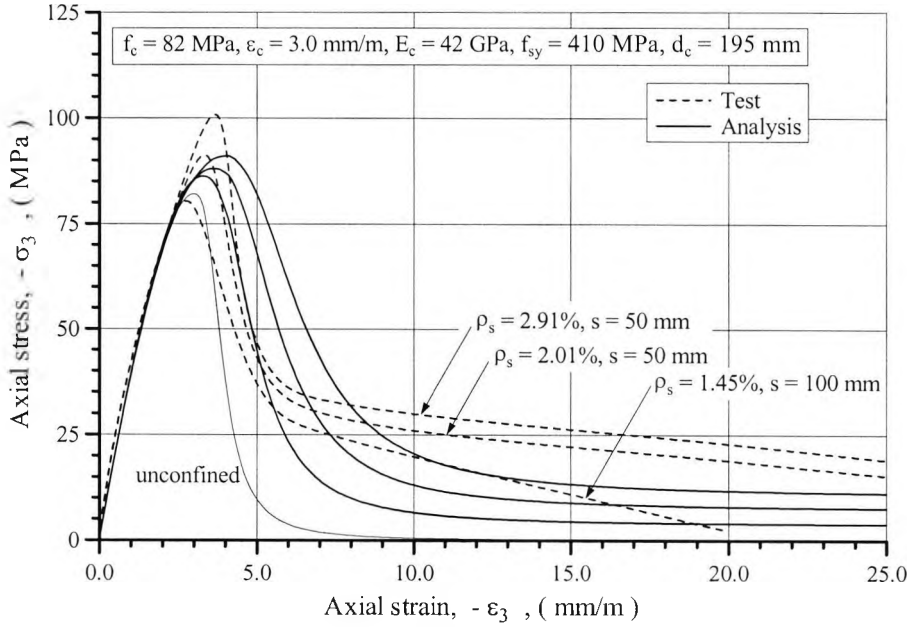

Figure 3.28
Comparison of computed and experimental stress-strain curves for a 82 MPa concrete confined by type B ties, test data after (Cusson, 1994)

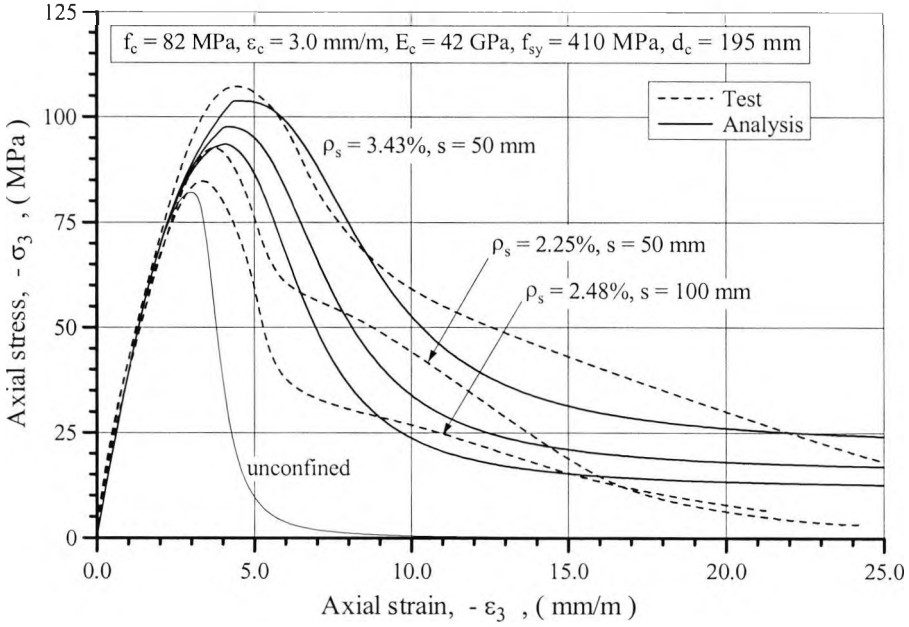

Figure 3.29
Comparison of computed and experimental stress-strain curves for a 82 MPa concrete confined by type C ties, test data after (Cusson, 1994)

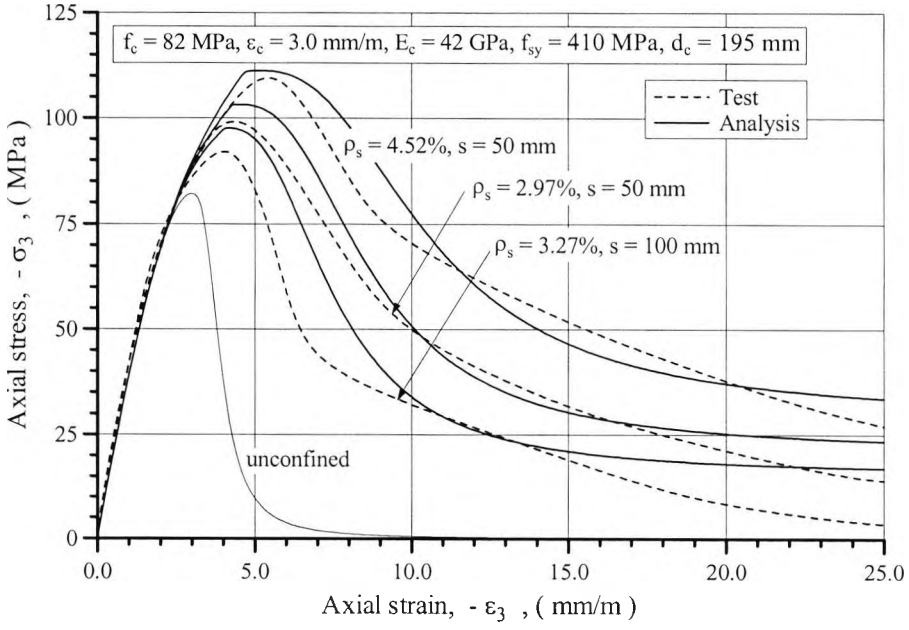

Figure 3.30
Comparison of computed and experimental stress-strain curves for a 82 MPa concrete confined by type D ties, test data after (Cusson, 1994)

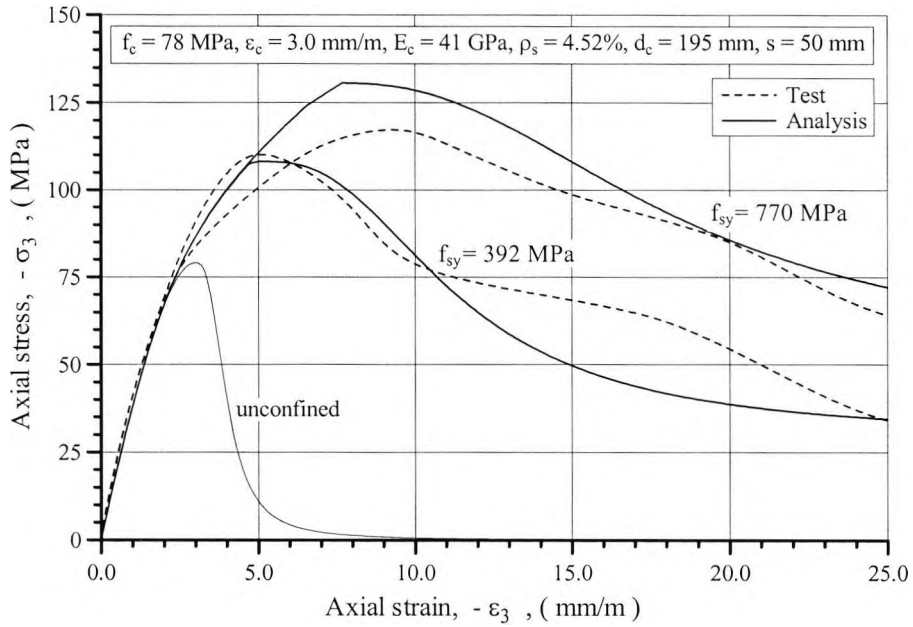

Figure 3.31
Comparison of computed and experimental stress-strain curves for a 78 MPa concrete confined by type D ties, test data after (Cusson, 1994)

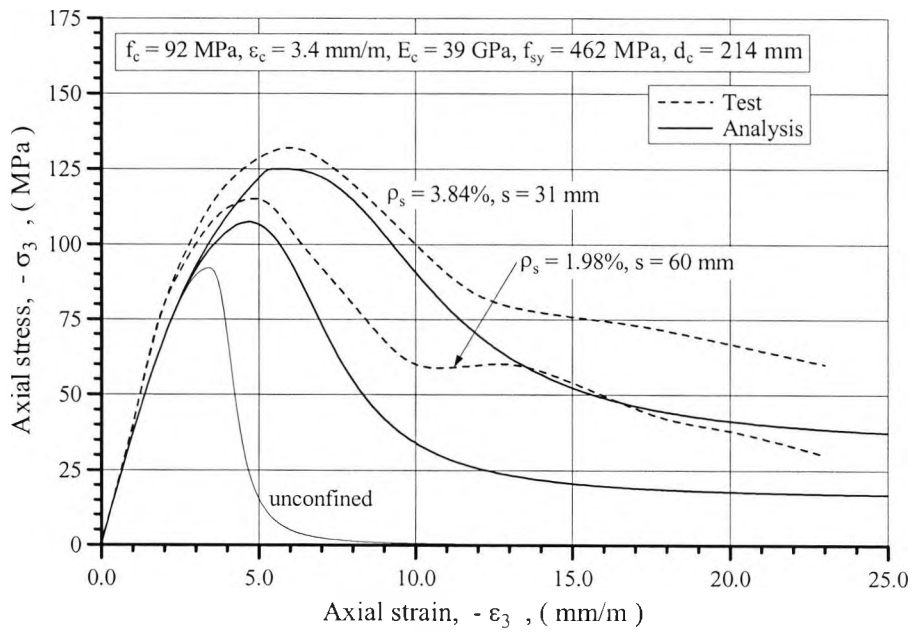

Figure 3.32
Comparison of computed and experimental stress-strain curves for a 92 MPa concrete confined by type D ties, test data after (Nishiyama, 1993)

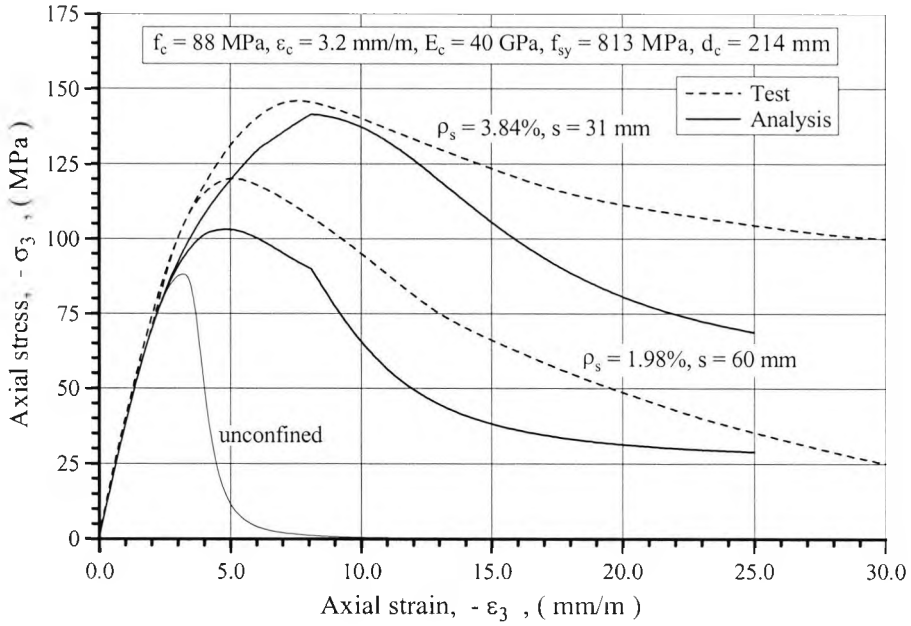

Figure 3.33
Comparison of computed and experimental stress-strain curves for a 88 MPa concrete confined by type D ties, test data after (Nishiyama, 1993)

Figure 3.34 illustrates the predicted stress-strain behaviour under concentric loading conditions of the concrete core of two of the full scale columns fabricated and tested as part of the present investigation. The columns, named SL05U and LH05U, had a 250×250 mm cross-section, and were transversely reinforced using type B ties with a pitch of 50 mm. The ties for column SL05U were manufactured from R10 bars, and the ties for column LH05U from R8 bars. The unconfined strength of concrete was, as discussed in section 3.1.2, estimated to be 81% of the mean strength of the 100×200 mm cylinders. The modulus of elasticity and the strain at peak stress of the unconfined concrete were estimated by equation 3.3 and 3.5 respectively, and the softening parameter, β , by equation 3.13. In the case of the column SL05U, the provided confinement was predicted to enhance the strength of the concrete core by 13% and the corresponding peak strain by 35%. For column LH05U, the enhancements in the same material properties were reduced to 6% and 9% respectively.

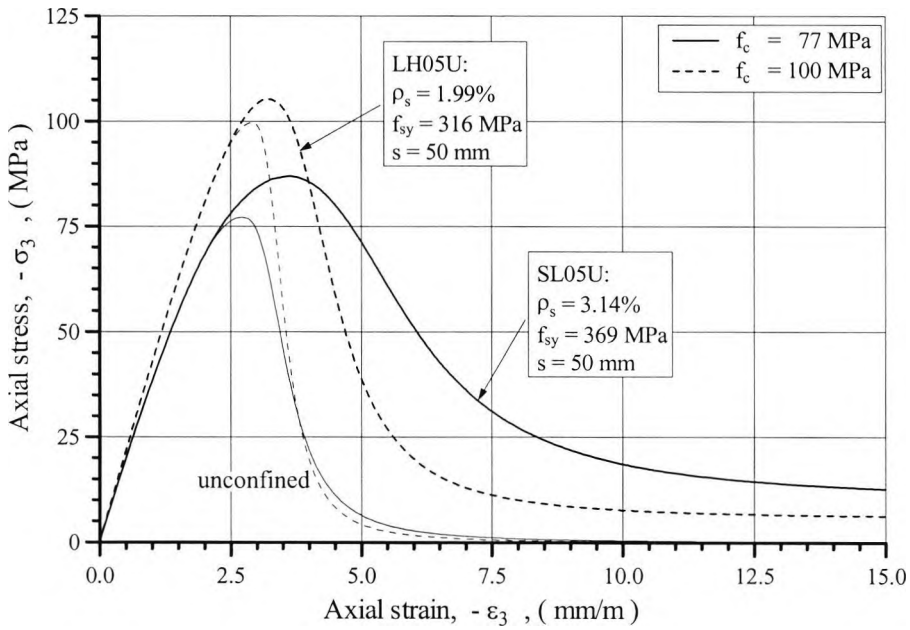

Figure 3.34
Predicted stress-strain behaviour of the passively confined concrete in test columns SL05U and LH05U

3.4.4 Existing Confinement Models

Some of the more recent of the confinement models proposed for predicting the complete stress-strain curve for passively confined concrete are described in the following. The reviewed models are the ones suggested by CEB (1990/1995), Saatcioglu and Razvi (1992), Bjerkeli *et al* (1993), El-Dash and Ahmad (1994) and Cusson and Paultre (1995). Although most of these models facilitate the analysis of columns with a rectangular cross-section, they have in the following been rewritten in a format applicable to the analysis of columns with a square cross-section.

Each confinement model was used to generate the stress-strain curve for the core concrete of the test columns SL05U and LH05U. The findings from the comparative study are summarised in table 3.4 and 3.5 by listing the effect that the provided confinement is

calculated to have on the peak stress, f_c , the peak strain, ε_c , as well as on two selected strains on the descending branch of the stress-strain curve, ε_{c85} and ε_{c50}. The variables ε_{c85} and ε_{c50} represent the post-peak strain where the stress has dropped to 85% and 50% of the peak stress respectively.

It can be seen from the tables that the reviewed confinement models are quite similar in terms of predicting the strengths and the peak strains, but much less so in terms of predicting the post-peak strains. In the case of column SL05U, the average of the core strengths predicted by the reviewed models is 11% above the strength of the unconfined concrete. In the case of column LH05U, the similar average is reduced to 5%. Likewise, the average peak strain enhancement predicted by the reviewed models is 37% for column SL05U and 22% for column LH05U. When excluding the model by Saatcioglu and Razvi, which was not calibrated against test results on high strength concrete columns, the mean values of the ratios $\varepsilon_{cc85} / \varepsilon_{c85}$ and $\varepsilon_{cc50} / \varepsilon_{c50}$ are 1.57 and 2.39 in the case of column SL05U, and 1.36 and 1.73 in the case of column LH05U. Thus, it can be concluded that the model developed as part of the present investigation predicts very much average results for $\varepsilon_{cc85} / \varepsilon_{c85}$ when compared to the existing confinement models.

Table 3.4
Predicted property enhancements for core concrete of column SL05U

Model	f_{cc} / f_c	$\varepsilon_{cc} / \varepsilon_c$	$\varepsilon_{cc85} / \varepsilon_{c85}$	$\varepsilon_{cc50} / \varepsilon_{c50}$
Proposed model	1.13	1.35	1.52	1.78
CEB (1990/1995)	1.06	1.12	1.44	2.31
Saatcioglu and Razvi (1992)*	1.11	1.55	6.31	15.85
Bjerkeli *et al* (1993)	1.09	1.57	2.08	3.51
El-Dash and Ahmad (1994)	1.16	1.53	1.87	2.19
Cusson and Paultre (1995)	1.13	1.07	0.99	1.53

Unconfined concrete: f_c = 77 MPa , E_c = 41 GPa , ε_c = 2.7 mm/m ,
ε_{c85} = 3.2 mm/m , ε_{c50} = 3.6 mm/m

* Model not calibrated against test results for high strength concrete.

Table 3.5
Predicted property enhancements for core concrete of column LH05U

Model	f_{cc} / f_c	$\varepsilon_{cc} / \varepsilon_c$	$\varepsilon_{cc85} / \varepsilon_{c85}$	$\varepsilon_{cc50} / \varepsilon_{c50}$
Proposed model	1.06	1.09	1.20	1.30
CEB (1990; 1995)	1.02	1.05	1.22	1.69
Saatcioglu and Razvi (1992)*	1.06	1.33	4.07	9.03
Bjerkeli *et al* (1993)	1.04	1.22	1.41	1.94
El-Dash and Ahmad (1994)	1.08	1.49	1.85	2.09
Cusson and Paultre (1995)	1.07	1.03	0.96	1.19

Unconfined concrete: f_c = 100 MPa , E_c = 44 GPa , ε_c = 2.9 mm/m ,
ε_{c85} = 3.3 mm/m , ε_{c50} = 3.6 mm/m

* Model not calibrated against test results for high strength concrete.

CEB 90 (1990) with modifications given in (CEB, 1995)

In the CEB model, which was originally described in the CEB Model Code 90 and later modified so as to include high strength concrete (CEB, 1995), the effective confining stress is evaluated in accordance with the 45° arching action method.

The strength and the peak strain of passively confined concrete is evaluated from equation 3.46 and 3.47 respectively. According to equation 3.46, high strength concrete gains relatively less strength than normal strength concrete for confinement ratios less than 0.25, and relatively more strength for confinement ratios larger than 0.25. No evidence supporting such behaviour was found during the course of the present investigation.

$$f_{cc} = \begin{cases} f_c - 5.0\sigma_{1,eff} & \text{for } |\sigma_{1,eff}| < 0.05 f_c \text{ , } f_c < 60 \text{ MPa} \\ 1.125 f_c - 2.5\sigma_{1,eff} & \text{for } |\sigma_{1,eff}| > 0.05 f_c \text{ , } f_c < 60 \text{ MPa} \\ f_c - 3.0\sigma_{1,eff} & \text{for } f_c > 60 \text{ MPa} \end{cases} \quad (3.46)$$

$$\varepsilon_{cc} = \varepsilon_c \left(\frac{f_{cc}}{f_c} \right)^2 \quad (3.47)$$

It is implicitly understood in the above, and indeed in all the following equations, that stress is expressed in MPa and strain in mm/m.

The ascending branch of the stress-strain curve for the confined concrete is represented by equation 3.48, and the descending branch by equation 3.49. The slope of the linear descending branch is governed by equation 3.50, which predicts the post-peak strain $\varepsilon_{cc85'}$ where the stress in the confined concrete has reduced to 85% of the unconfined concrete strength.

$$\sigma_3 = f_{cc} \frac{\frac{E_c}{E_{ccs}} \frac{\varepsilon_3}{\varepsilon_{cc}} + \left(\frac{\varepsilon_3}{\varepsilon_{cc}} \right)^2}{1 - \left(\frac{E_c}{E_{ccs}} - 2 \right) \frac{\varepsilon_3}{\varepsilon_{cc}}} \qquad \text{for } |\varepsilon_3| < \varepsilon_{cc} \tag{3.48}$$

$$\sigma_3 = -f_{cc} + \frac{f_{cc} - 0.85 f_c}{\varepsilon_{cc85'} - \varepsilon_{cc}} (-\varepsilon_3 - \varepsilon_{cc}) \qquad \text{for } |\varepsilon_3| > \varepsilon_{cc} \tag{3.49}$$

where:

$$\varepsilon_{cc85'} = \begin{cases} \varepsilon_{c85} - 200 \frac{\sigma_{1,eff}}{f_c} & \text{for } f_c < 60 \text{ MPa} \\ \varepsilon_{c85} - 100 \frac{\sigma_{1,eff}}{f_c} & \text{for } f_c > 60 \text{ MPa} \end{cases} \tag{3.50}$$

For test columns SL05U and LH05U, the CEB model predicts strengths and peak strains which are somewhat smaller than those predicted by the model proposed in this thesis, see figure 3.35. However, since the CEB model in general predicts the confined concrete to display a more ductile post-peak behaviour, the stress-strain curves generated by the two models intersect at a strain of 5.3 mm/m in the case of column SL05U, and at a strain of 4.1 mm/m in the case of column LH05U.

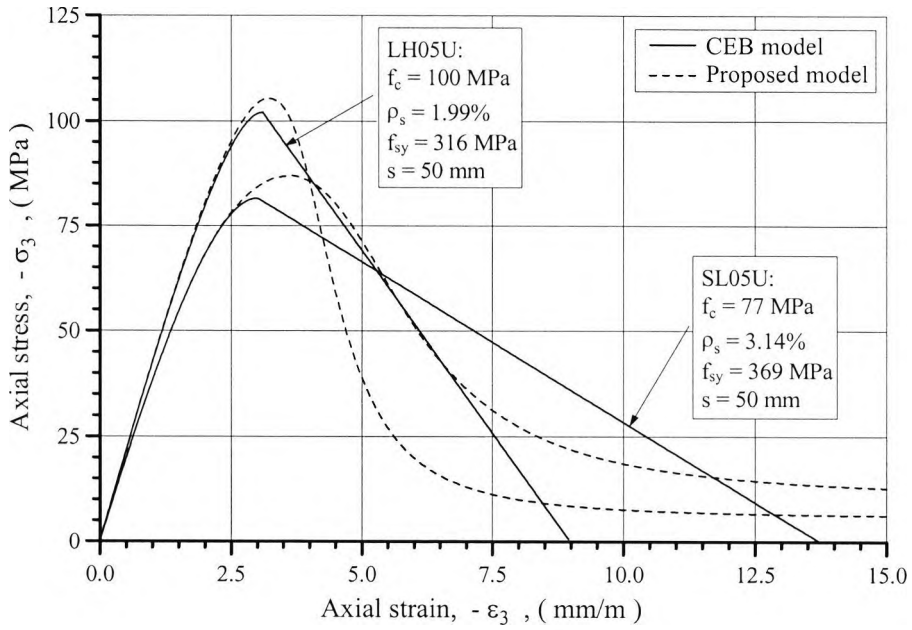

Figure 3.35
Stress-strain behaviour of core concrete according to CEB model

Saatcioglu and Razvi (1992)

The expression for the effective confining pressure in Saatcioglu and Razvi's model, see equation 3.51, involves a reduction coefficient which is a function of the dimension of the nominal concrete core, d_c , the spacing of the ties, s , the spacing of the longitudinal reinforcement bars, d_g , and the nominal confining stress itself, $\sigma_{1,nom}$. For a given tie configuration and distribution, an increase in the size or yield strength of the tie bars will according to this model produce less than a proportional increase in the effective confining pressure.

$$-\sigma_{1,eff} = \min \begin{cases} 0.26 \sqrt{\frac{d_c}{s}\frac{d_c}{d_g}\frac{1}{-\sigma_{1,nom}}}\,|\sigma_{1,nom}| \\ |\sigma_{1,nom}| \end{cases} \qquad (3.51)$$

The peak stress and the corresponding peak strain of the confined concrete is evaluated from the following expressions:

$$f_{cc} = f_c + 6.7(-\sigma_{1,eff})^{0.83} \tag{3.52}$$

$$\varepsilon_{cc} = \varepsilon_c \left(1 + 33.5 \frac{(-\sigma_{1,eff})^{0.83}}{f_c}\right) \tag{3.53}$$

The complete stress-strain behaviour of the confined concrete core is described by equations 3.54a-b and 3.55. A linear descending branch is followed until reaching a residual strength equal to 20% of the confined strength. The slope of the linear descending branch is governed by equation 3.56, which predicts the strain ε_{cc85} where the stress in the confined concrete has reduced to 85% of the confined concrete strength. It should be noted that Saatcioglu and Razvi defined the confinement ratio, ρ_s^*, as the total transverse steel area in two orthogonal directions divided by the corresponding concrete area. Thus, for the tie configurations illustrated in table 3.1, ρ_s^* is either equal to or approximately equal to the volumetric ratio of transverse reinforcement divided by 2, i.e. $\rho_s/2$.

$$\sigma_3 = -f_{cc}\left(-2\frac{\varepsilon_3}{\varepsilon_{cc}} - \left(\frac{\varepsilon_3}{\varepsilon_{cc}}\right)^2\right)^{1/(1+2k)} \qquad \text{for } |\varepsilon_3| < \varepsilon_{cc} \tag{3.54a}$$

where:

$$k = \frac{f_{cc}}{f_c} - 1 \tag{3.54b}$$

$$\sigma_3 = \min\begin{cases} -f_{cc} + \dfrac{0.15 f_{cc}}{\varepsilon_{cc85} - \varepsilon_{cc}}(-\varepsilon_3 - \varepsilon_{cc}) \\ -0.2 f_{cc} \end{cases} \qquad \text{for } |\varepsilon_3| > \varepsilon_{cc} \tag{3.55}$$

where:

$$\varepsilon_{cc85} = \varepsilon_{c85} + 260\,\rho_s^*\,\varepsilon_{cc} \tag{3.56}$$

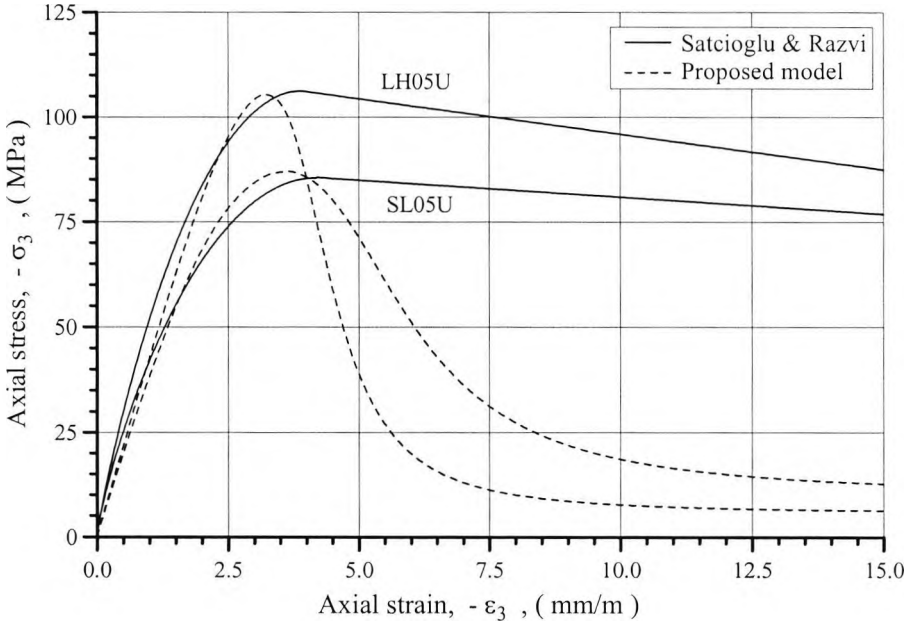

Figure 3.36
Stress-strain behaviour according to Saatcioglu and Razvi's model

It can be seen from figure 3.36 that the major difference between Saatcioglu and Razvi's model and the model proposed in this thesis is that the former predicts a much more ductile post- peak behaviour than the latter. This reflects the fact that Saatcioglu and Razvi calibrated their model against test results on columns with a maximum unconfined concrete strength of about 40 MPa. For their model to be valid for confined high strength concrete, it will require a modification of equation 3.56 so as to directly incorporate the effect that the grade of concrete has on ε_{cc85}.

Bjerkeli, Tomaszewics and Jensen (1993)

According to the confinement model by Bjerkeli *et al*, the effective confining pressure should be taken as the least of the values evaluated from equation 3.57. Thus, it is assumed that either the tie configuration or the tie distribution, and not a combination of these, dictates the effective confining pressure applied to the concrete core.

$$-\sigma_{1,eff} = \min \begin{cases} \left(1 - \frac{n d_g^2}{5.5 A_{cc}}\right) |\sigma_{1,nom}| \\ \left(1 - \frac{s}{d_c}\right) |\sigma_{1,nom}| \end{cases} \tag{3.57}$$

The strength and the peak strain of the confined concrete are determined from equation 3.58 and 3.59 respectively. It can be seen that the model predicts concrete with an unconfined strength above 70 MPa to benefit less from confinement than concrete with an unconfined strength below 70 MPa.

$$f_{cc} = \begin{cases} f_c - 4.0\sigma_{1,eff} & \text{for} \quad 40\ \text{MPa} < f_c < 70\ \text{MPa} \\ f_c - 3.0\sigma_{1,eff} & \text{for} \quad 70\ \text{MPa} < f_c < 80\ \text{MPa} \end{cases} \tag{3.58}$$

$$\varepsilon_{cc} = \varepsilon_c - 50 \frac{\sigma_{1,eff}}{f_c} \tag{3.59}$$

Equation 3.60 together with equation 3.61 describe the stress-strain curve for the confined concrete. In the post-peak region, the stress is assumed to decay linearly with increasing strain until it stabilises at a residual strength, the level of which being proportional to the nominal confining pressure. The slope of the descending branch is obtained from equation 3.62, which predicts the post-peak strain corresponding to 85% of the peak stress.

$$\sigma_3 = \frac{-E_c \varepsilon_3}{1 - \left(\frac{E_c}{E_{ccs}} - 2\right)\frac{\varepsilon_3}{\varepsilon_{cc}} + \left(\frac{\varepsilon_3}{\varepsilon_{cc}}\right)^2} \qquad \text{for} \quad |\varepsilon_3| < \varepsilon_{cc} \tag{3.60}$$

$$\sigma_3 = \min \begin{cases} -f_{cc} + \frac{0.15 f_{cc}}{\varepsilon_{cc85} - \varepsilon_{cc}} (-\varepsilon_3 - \varepsilon_{cc}) \\ -4.87\sigma_{1,nom} \end{cases} \qquad \text{for} \quad |\varepsilon_3| > \varepsilon_{cc} \tag{3.61}$$

where:

$$\varepsilon_{cc85} = \varepsilon_{c85} - 50 \frac{\sigma_{1,eff}}{f_c}(1 + (-\sigma_{1,eff})^{0.25}) \tag{3.62}$$

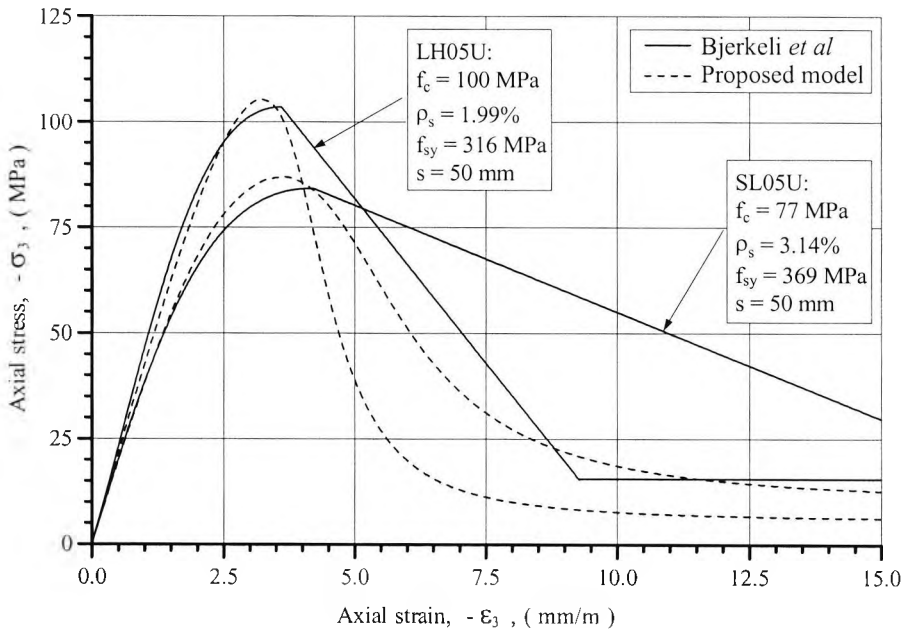

Figure 3.37
Stress-strain behaviour according to Bjerkeli *et al's* model

Figure 3.37 shows that, when compared to the model proposed in this thesis, the confinement model by Bjerkeli *et al* predicts the test columns to have significantly more post-peak resistance, this being more so for column SL05U than for column LH05U.

El-Dash and Ahmad (1994)

The confinement model proposed by El-Dash and Ahmad, contrary to the other models reviewed, does not employ an explicit expression for the effective confining pressure.

According to El-Dash and Ahmad's model, the strength and peak strain of passively confined concrete can be evaluated from equations 3.63a-c and 3.64a-c respectively.

$$f_{cc} = f_c - k_1 \sigma_{1,nom} \tag{3.63a}$$

where:

$$k_1 = 0.7\left(\frac{f_c}{f_{sy}}\frac{m}{\rho_s^*}\right)^{0.2} \tag{3.63b}$$

$$m = \left(\frac{d_c^2}{d_g s}\right)^2 \tag{3.63c}$$

$$\varepsilon_{cc} = \varepsilon_c - k_2\frac{\sigma_{1,nom}}{f_c} \tag{3.64a}$$

where:

$$k_2 = 55\cdot 10^6\,(m\rho_s^*)^{0.2}\left(\frac{f_c^a}{f_{sy}}\right) \tag{3.64b}$$

$$a = \frac{f_c}{78} - 3 \tag{3.64c}$$

The stress-strain curve for the confined concrete is given by equation 3.65a-b, in which the parameter B primarily dictates the shape of the post-peak portion of the curve. An increase in the value of B has the effect of flattening the descending branch of the stress-strain curve.

$$\sigma_3 = f_{cc}\frac{\frac{E_c}{E_{ccs}}\frac{\varepsilon_3}{\varepsilon_{cc}} - (B-1)\left(\frac{\varepsilon_3}{\varepsilon_{cc}}\right)^2}{1 - \left(\frac{E_c}{E_{ccs}} - 2\right)\frac{\varepsilon_3}{\varepsilon_{cc}} + B\left(\frac{\varepsilon_3}{\varepsilon_{cc}}\right)^2} \tag{3.65a}$$

where:

$$B = 130.9\,(\rho_s^*)^{0.3}\frac{f_{sy}}{f_c^{2.5}} \tag{3.65b}$$

Figure 3.38 shows that the model by El-Dash and Ahmad predicts significantly larger peak strains for both of the test columns than the new model. It can also be noted that the two different models overall predict quite similar rates of reduction in the post-peak stress.

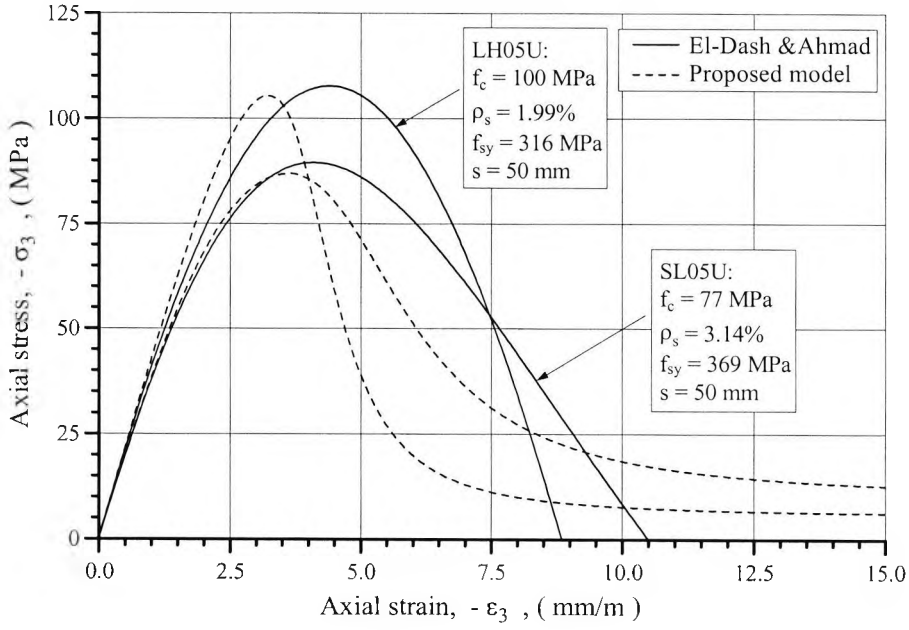

Figure 3.38
Stress-strain behaviour according to El-Dash and Ahmad's model

Cusson and Paultre (1995)

The model proposed by Cusson and Paultre (1995) employs the 45° arching action method for evaluating the effective confining pressure. The stress and peak strain corresponding to the effective confining pressure is determined from equation 3.66 and 3.67 respectively.

$$f_{cc} = f_c\left(1 + 2.1\left(\frac{-\sigma_{1,eff}}{f_c}\right)^{0.7}\right) \tag{3.66}$$

$$\varepsilon_{cc} = \varepsilon_c + 210\left(\frac{-\sigma_{1,eff}}{f_c}\right)^{1.7} \tag{3.67}$$

Furthermore, the post-peak strain at which the stress has dropped to 50% of the peak stress is predicted as follows:

$$\varepsilon_{cc50} = \varepsilon_{c50} + 150\left(\frac{-\sigma_{1,eff}}{f_c}\right)^{1.1} \tag{3.68}$$

The ascending part of the stress strain curve is represented by equation 3.69a-b, and the descending part by equations 3.70a-c. The coefficient c_1 was adjusted so as to force the stress-strain curve to pass through the point $(\varepsilon_{cc50}, 0.50 f_{cc})$. For well-confined concrete c_1 is large and produces a smooth falling branch, while for lightly confined concrete c_1 is small and produces a steep falling branch. The coefficient c_2 controls the curvature of the descending branch. For well-confined concrete, c_2 is large and produces a convex falling branch, while for lightly confined concrete, c_2 is small and produces a concave falling branch.

$$\sigma_3 = -f_{cc}\frac{k\frac{\varepsilon_3}{\varepsilon_{cc}}}{k-1+\left(\frac{-\varepsilon_3}{\varepsilon_{cc}}\right)^k} \qquad \text{for } |\varepsilon_3| \le \varepsilon_{cc} \tag{3.69a}$$

where:

$$k = \frac{E_c}{E_c - E_{ccs}} \tag{3.69b}$$

$$\sigma_3 = -f_{cc}\exp\left(c_1(-\varepsilon_3 - \varepsilon_{cc})^{c_2}\right) \qquad \text{for } |\varepsilon_3| \ge \varepsilon_{cc} \tag{3.70a}$$

where:

$$c_1 = -0.69(\varepsilon_{cc50} - \varepsilon_{cc})^{-c_2} \tag{3.70b}$$

$$c_2 = 0.58 + 16\left(\frac{-\sigma_{1,eff}}{f_c}\right)^{1.4} \tag{3.70c}$$

Compared to the model proposed in this thesis the model by Cusson and Paultre predicts significantly lower peak strains. Figure 3.38 also shows that the model by Cusson and Paultre predicts the descending part of the stress-strain curves to have a much steeper initial phase.

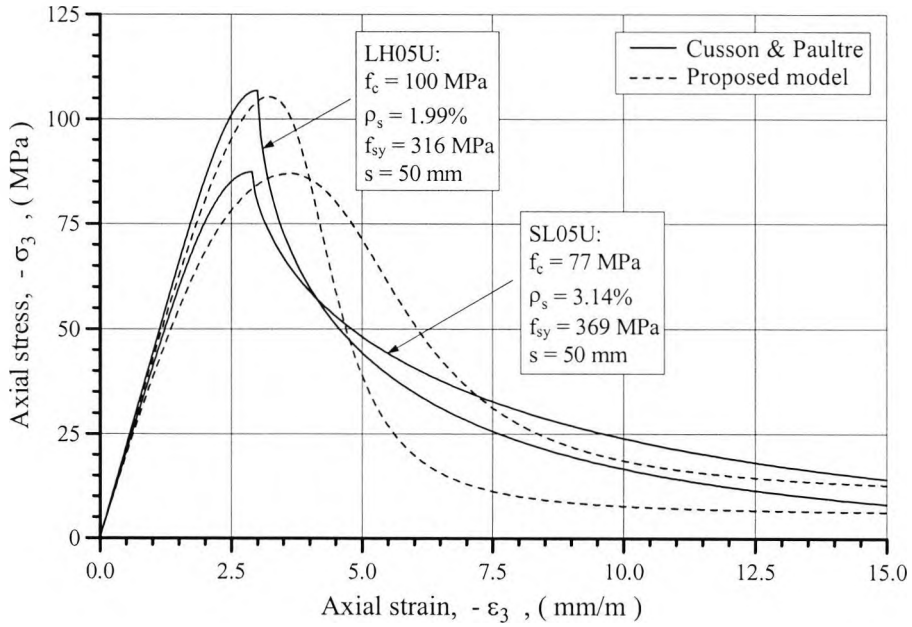

Figure 3.38
Stress-strain behaviour according to Cusson and Paultre's model

3.5 Behaviour of Concrete in Flexure

Reinforced concrete columns are usually designed for eccentric compression, yet most of the experimental research carried out to date has focussed on columns subjected to concentric compression. This section comments on the influence of strain gradients on the material behaviour of concrete.

Hognestad *et al* (1955) developed a novel testing method for determining the flexural stress-strain relationship of concrete. The method does not require the introduction of any assumptions regarding the mathematical formulation of the stress-strain relationship, but relies on the axial load being applied so as to maintain zero strain at one face of the test specimen while monotonically increasing the strain at the opposite face. They tested plain concrete specimens with compressive strengths of up to about 50 MPa, and concluded, from comparing the flexural stress-strain curves to those obtained from concentric compression tests, that the strain gradient did not influence the behaviour of plain concrete.

Ibrahim and McGregor (1996a, 1996b) extended this investigation to include concrete with compressive strength in excess of 100 MPa, and once again the strain gradient was observed to have negligible effect on the stress-strain diagram.

However, other researchers have reported strain gradients to enhance the material characteristics of plain concrete. The experimental investigation carried out by Karsan and Jirsa (1970) showed that strain gradients reduced the steepness of the descending part of the stress-strain curve, but had no effect on the strength or the peak strain. In the investigations by Sturman *et al* (1965) and by Sargin (1971), eccentric loading was observed to raise the peak strain by 50% and by 30% respectively. Sturman *et al* also reported that the strain gradient resulted in a 20% increase in the peak stress. Sargin employed an experimental method similar to the method used earlier by Hognestad *et al*

whereas both Karsan and Jirsa and Sturman *et al* employed methods, which relied on particular assumptions regarding the mathematical formulation of the stress-strain relationship.

In view of the experimental evidence, it appears that a structural analysis of an unconfined reinforced concrete column under eccentric compression, which is based on the stress-strain curve obtained from concentric load tests, can be expected to lead to either accurate or somewhat conservative results.

Whether or not it is reasonable to extend the above assumption to the analysis of passively confined concrete columns has not yet been fully established. In this context, it should be remembered that the stress-strain relationship for confined concrete is based on the average stress in the nominal concrete core of a concentrically loaded column.

The experimental investigation carried out by Scott *et al* (1982) showed that using the stress-strain curve derived from a concentric load test to calculate the stress resultants for a similar column under eccentric loading conditions lead to conservative results. Whereas the axial force was predicted reasonably well, the bending moment, especially in the post-peak region, was significantly underestimated. As a consequence, they proposed that a stress-strain curve with a less steep falling branch would be more appropriate for analysing eccentrically loaded columns. The columns tested in the investigation by Scott *et al* had a volumetric ratio of transverse reinforcement of 1.8%, and were manufactured from normal strength concrete with a cylinder strength of about 25 MPa. At strength failure the depth of the neutral axis was approximately equal to the depth of the cross-section.

Ibrahim and McGregor (1996a) employed the technique developed by Hognestad *et al* (1955) to study the response of confined high strength concrete columns. The tested

columns had cylinder strengths ranging from 60 MPa to 118 MPa, and volumetric ratios of transverse reinforcement ranging from 0.0% to 3.9%. As a result of the test programme a new confinement model, which was based on the model originally developed by Bjerkeli *et al* (1993) and described in detail in section 3.4.4, was proposed to describe the material behaviour of confined high strength concrete (Ibrahim, 1996b). Compared to Bjerkeli *et al's* model, the model proposed by Ibrahim and McGregor predicts confinement to have a somewhat reduced effect on the peak stress, the peak strain and the post-peak ductility of concrete.

The influence of strain gradients is incorporated in the confinement model proposed by Sheikh and Yeh (1986). According to this model, the peak strain is at minimum under concentric loading conditions, and increases with an increase in the ratio of the section depth to the depth of the neutral axis. This model, an extension to an earlier model proposed for describing the stress-strain curve under conditions of concentric compression (Sheikh, 1982), was shown to accurately reproduce the experimental results published by Scott *et al* (1982). More recently, Sheikh and Yeh (1990) conducted an experimental investigation into the behaviour of transversely reinforced normal strength concrete columns under increasing lateral loads. The columns were tested at constant axial loads corresponding to 0.60 and 0.75 times the squash load of the unreinforced concrete section. It was reported that the strength of the confined concrete reduced with the increase in the axial load, and a modified stress-strain model, which included both the influence of strain gradients on the peak strain and the influence of the level of axial load on the flexural strength, was developed to describe the test results (Sheikh, 1992).

Saatcioglu *et al* (1995) tested a number of confined concrete columns, and found that both their pre-peak and post-peak behaviour under eccentric loading could be computed with

reasonable accuracy by employing a confinement model developed for concentric loading conditions. The tested columns had volumetric ratios of transverse reinforcement ranging from 1.8% to 2.7%, and cylinder strengths ranging from 26 MPa to 34 MPa. The neutral axis was, in contrast to the investigation by Scott *et al* (1982), located well within the cross-section at the time the columns reached their peak load. The confinement model employed by Saatcioglu and Razvi (Saatcioglu, 1992) is described in detail in section 3.4.4.

In view of the limited experimental evidence, it appears that the efficiency of confinement under flexural loading conditions is comparable to that under concentric loading conditions, but attempting to quantify the effect of strain gradients seems to be somewhat futile. In this context it should be emphasised that only in the tests by Scott *et al* (1982) was the stress-strain relationship of the confined concrete derived directly from concentric load tests on specimens identical to those tested under flexural loading conditions. In the other investigations, the strength of unconfined concrete was determined on the basis of standard tests on small scale specimens, and the stress-strain behaviour of the confined concrete core under concentric compression was assumed to be accurately described by existing confinement models.

Another complication associated with increasing flexure is that the shift of the neutral axis towards the compressed face of the column may cause zones within the cross-section to undergo strain reversal. The concrete stress in such zones will decrease in accordance with the modulus of elasticity, or more accurately in accordance with the unloading portion of a hysteresis loop similar to those recorded in cyclic loading tests (Karsan, 1970; Priestley, 1981, Shah, 1983; Cheong, 1993; Thomsen, 1994; Sheikh, 1994; Legeron, 1997). Nevertheless, in the analysis of reinforced concrete columns under monotonic loading conditions, it is generally assumed that the relationship between stress and strain at each

material point can be represented by the virgin curve, i.e. non-linear elastic material modelling. A numerical study by Bazant *et al* (1991) of hinged columns subjected to eccentric loading convincingly demonstrated the occurrence of strain reversal to have a negligible influence on the predicted column behaviour. This was explained by the loading unloading reversal occurring at low strain levels for which the stress-strain diagram for loading is close to that for unloading.

3.6 Summary

Various empirical expressions for predicting the modulus of elasticity, the peak strain, the tensile strength and the apparent Poisson's ratio of high strength concrete were examined. With the exception of the apparent Poisson's ratio, which in general was underestimated significantly, the material properties predicted by the expressions recommended in the CEB publications (CEB, 1990) and (CEB, 1995) were in agreement with the test results for the two high strength concrete grades employed in the present investigation.

A new model for computing the complete stress-strain behaviour of concrete under uniaxial compression was proposed. Besides the standard parameters of modulus of elasticity, compressive strength, and peak strain, the calibration of the stress-strain model requires an additional parameter β, which is defined as function of the strain on the descending branch at which the stress has reduced to 50% of the compressive strength. Like the other material properties, β can be estimated directly from the compressive strength, and an equation for such was presented.

It was demonstrated that the strength of confined concrete increases, albeit at a decreasing rate, with increasing confinement, and that it is feasible to express the ratio of the confined to the unconfined strength as a non-linear function of the confinement ratio. Ottosen's failure criteria, which was originally developed to describe failure combinations for normal strength concrete, constituted the mathematical formulation for the proposed relationship between the concrete strength and the confining pressure.

The available test results show that the peak strain is enhanced relatively more by confinement than the strength, and that this is more so for normal strength than high strength concrete. An empirical relationship between the peak strain ratio, the confinement ratio and the unconfined strength was derived. Furthermore, increasing confinement has the

effect of reducing the slope of the descending branch of the stress-strain curve of concrete, but for a given level of confinement, the post-peak behaviour of high strength concrete is always less ductile than that of normal strength concrete.

In a passively confined concrete column, the confining pressure originates from the resistance of the steel reinforcement cage to the expansion of the enclosed concrete, and is as such non-uniformly distributed within the interior of the column. The concept of effective confining pressure was employed to assess the efficiency of various standard tie configurations for columns with circular or square cross-sections. The 45° arching action method, recommended in the CEB Model Code 90 for calculating the efficiency of a given tie arrangement, was modified so as to obtain a high degree of agreement with the running average of the experimental strength results for passively confined concrete columns tested under concentric compression.

The uniaxial stress-strain model was generalised to confined concrete by letting the effect of confinement on the post-peak behaviour be expressed in terms of the difference between the confined and the unconfined concrete strength. The stress-strain model was programmed, and then successfully validated against a number of published stress-strain curves for both actively and passively confined concrete specimens.

The proposed confinement model was compared with existing models when applied to the concrete core of two of the columns fabricated and tested as part of the present investigation. In general, the confinement models produced stress-strain curves with similar ascending branches, but with vastly different descending branches. In general, the proposed model predicted a less ductile post-peak response than most of the existing models.

Chapter 4: Structural Behaviour of Concrete Columns

4.1 General

The investigation, which so far has focussed on the stress-strain characteristics of confined high strength concrete, is in this chapter broadened to include the structural behaviour of slender reinforced concrete columns. A numerical method for calculating the load-deformation response of slender columns under monotonically increasing eccentric compression is presented and validated.

4.1.1 Failure of Concrete Columns

When describing the structural behaviour of slender columns, it is helpful to decompose the bending moments into primary and secondary moments. The primary moments are those originating from lateral loading, applied end-moments, the axial load acting at an eccentricity and imperfections in the straightness of the column axis. With the aim of safeguarding against unforeseen bending moments, BS 8110 recommends that a column always should be capable of withstanding a design moment equal to the maximum axial load acting at an eccentricity equal to 0.05 times the column's overall dimension in the plane of bending. However, if the dimension of the cross-section exceeds 400 mm, an eccentricity of 20 mm will suffice when determining the minimum design moment according to this standard (BS 8110, 1985).

The secondary bending moments are the additional moments induced by the axial load as the column axis deflects laterally. In contrast to the primary bending moments, which can be calculated on the basis of the initial geometry, the secondary moments need to be calculated on the basis of the displaced equilibrium configuration of the column, and are

as such also referred to as second order effects. Since a column's resistance against lateral deflections can be quantified by its slenderness or flexural stiffness, the reduction in its axial load capacity caused by second order effects can also be related to these measures. A column is referred to as being "slender" if the second order effects significantly influence its load-carrying characteristics, and as "short" if this is not the case. According to BS 8110, a braced column, i.e. a column restrained against side-sway at both ends, having a geometric slenderness ratio in excess of 15 should be designed as slender. The geometric slenderness ratio is defined as the ratio of the effective column length to the cross-sectional dimension in the plane of bending.

While the collapse of a short column coincides with the exhaustion of the material strength at its critical cross-section, this is not necessarily the case for a slender column. A column can, provided it is sufficiently slender, reach its maximum axial load prior to the exhaustion of the material strength. This type of failure is usually referred to as stability failure. Cranston (1972) concluded from an extensive numerical research on reinforced concrete columns that a geometric slenderness ratio in excess of about 30 was required for stability failure to occur. Thus, reinforced concrete columns used in practical structures are seldom sufficiently slender for stability failure to occur, though they are often slender enough for second order effects to considerably reduce their axial load capacity. In this context it is noticeable that the design method given in the BS 8110 is based on the assumption of material failure, which in the code is defined in terms of a limiting compressive concrete strain of 3.5 mm/m.

When plotting the maximum bending moments that can be sustained for the different axial loads one obtains a so-called column interaction diagram. A point inside the diagram represents a supportable combination of axial load and bending moment, and a point outside the diagram an unsupportable combination. A large number of column interaction diagrams are given in BS 8110: Part 3 (1985) for columns having rectangular cross-

sections. The diagrams are based on simplified design stress-strain curves, and apply to columns made from concrete with a 150 mm cube strength less than 50 MPa, and a volumetric ratio of longitudinal steel reinforcement less than 8%. In the case of a slender column, the bending moment consists of a primary and a secondary moment, and the diagram describing the critical combinations of axial load and primary moment is referred to as a reduced column interaction diagram (Bazant, 1991). This diagram can be constructed directly from the corresponding column interaction diagram provided a closed form expression for the secondary moment at failure can be formulated. Indeed, BS 8110: Part 1 contains a semi-empirical expression for estimating the secondary moment associated with a given axial load, and thus significantly simplifies the design process for slender columns. In the recommended expression, the secondary moment is a function of the column's cross-sectional dimensions, its slenderness, the applied axial load and a reduction factor, defined as the ratio of the difference between the squash load and the applied axial load to the difference between the squash load and the axial load corresponding to a balanced condition. A balanced condition exists when the compressive concrete strain reaches a maximum of 3.5 mm/m simultaneously with yielding occurring in the tensile steel reinforcement.

4.1.2 Methods for Numerical Analysis of Concrete Columns

A minimum requirement for any numerical method for the analysis of concrete columns is that it must take appropriate account of both material and geometric non-linearities, so as to accurately predict the load-deformation behaviour up to failure. In this context, it should be emphasised that the design method recommended in BS 8110, and similar standards, does not provide means for assessing the ductility of a particular column design. Furthermore, the design method recommended in BS 8110 is not directly applicable to high strength concrete columns.

The simplest of the available numerical methods are those developed for the analysis of pin-ended columns under uniaxial bending, in which the deflection curve of the column is assumed to be a sine wave (Bazant, 1991; Lloyd, 1996; Chuang, 1995; Chuang, 1998; Hong, 2001). Because the displaced configuration is described by a single displacement variable, the force and moment equilibriums can only be satisfied exactly at the critical section at mid-height of the column. When further introducing the standard assumption of plane sections remaining plane, the strain distribution at the critical section is uniquely represented by two variables, which conveniently can be chosen as the curvature and the height of the neutral axis. Thus, as the curvature again is directly expressed by the displacement variable, only two variables need to be iterated in order to find the equilibrium configuration of the column. A major advantage of these methods is that they are computationally efficient, and easily converted into displacement control so as to obtain information about the post-peak behaviour of the column. However, as the load is increased beyond the elastic limit the real deflection curve tends to be more pointed at mid-height than a sine wave.

A variant of this method is proposed by Diniz and Frangopol (1997) where the deflections are assumed to be described by a fourth order polynomial. The polynomial coefficients are given in terms of the curvatures at the two ends and at mid-height of the column, and the calculation of the displaced equilibrium configuration requires two successive iterations. In the first iteration the curvatures at the pinned ends of the column are determined, and in the second the deflection at mid-height of the column is determined.

In the more accurate methods, the column's deflection curve is represented by discrete displacements at a number of stations along its length, and the relationship between the curvatures and the displacements are given by finite difference expressions (Virdi, 1980; Metwally, 1990; Wang, 1992). Thus, in order to calculate the displaced equilibrium

configuration of the column, the generalised strains at all the stations need to be iterated simultaneously. As these methods do not restrict the deflection curve to a particular functional format, they are flexible in terms of both loading and boundary conditions.

The finite element method, as employed for the analysis of concrete columns by Kim and Yang (1995) and Claeson and Gylltoft (1998), is essentially a hybrid of the above described methods. In the finite element method, the deformation of each segment is restricted to adhere to a predefined functional format, but as the column is represented by many such segments, the overall deflected shape of the column is not similarly restricted.

Irrespective of the adopted numerical method, it is necessary to determine the stress-resultants by integrating over the cross-section. Typically the numerical integration is performed by dividing the cross-section into a number of smaller regions, such as narrow strips (Bazant, 1991; Kim, 1995; Diniz, 1997) or quadrilateral regions (Virdi, 1980; Metwally, 1990; Wang, 1992; Rodriguez, 1999), and then summing up the contribution from each region. In the special case of columns with rectangular cross-sections subjected to uniaxial bending, the numerical integration can be further simplified by directly integrating the stress-strain (Chuang, 1995; Chuang, 1998; Lloyd, 1996).

Finally, as an alternative to a series of interconnected cross-sections, the column can be modelled in a true three-dimensional manner as an assemblage of solid elements. This type of finite element modelling, which automatically tracks the interaction between the transverse reinforcement and the concrete, has a major disadvantage in requiring a high degree of detailing as well as being computationally heavy. Furthermore, to choose and calibrate an appropriate triaxial constitutive concrete model is a rather complicated task. Nevertheless, Xie *et al* (1996) demonstrated the ability of solid finite element modelling to simulate the behaviour of confined concrete columns under eccentric compression.

4.2 Numerical Analysis of Concrete Columns

This section describes the theory behind the two computer programs developed in order to investigate the influence of passive confinement on the structural behaviour of slender high strength concrete columns. The first program generates a column interaction diagram, and the second performs a load-deflection analysis.

4.2.1 Model for Generating Interaction Diagrams

The numerical model for generating interaction diagrams is based on the usual assumption of a loading history in which the axial load is applied prior to the bending moment. Initially, the squash load of the cross-section is calculated, then the applied axial load is reduced in equal steps to zero, and the biaxial moment capacity corresponding to each level of axial load is determined. The moment is applied in small increments and the section's load carrying capacity is assumed exhausted when static equilibrium can no longer be obtained.

Representation of cross-section

The cross-section is idealised as an assemblage of quadrilateral elements into each of which one or more point elements can be embedded (see figure 4.1). Since each quadrilateral element, defined by the Cartesian x- and y-coordinates of its four vertices, can be ascribed individual stress-strain characteristics, the numerical model does not only facilitate the description of complex cross-sectional shapes, but also that of varying material behaviour within the section. A condition of varying material behaviour exists within a cross-section of a passively confined concrete column. The point elements represent the longitudinal reinforcement bars, and cannot, unlike the quadrilateral elements, capture stress variations within their interior, i.e. all of the geometric and physical properties of a point element are assumed to be lumped at the point.

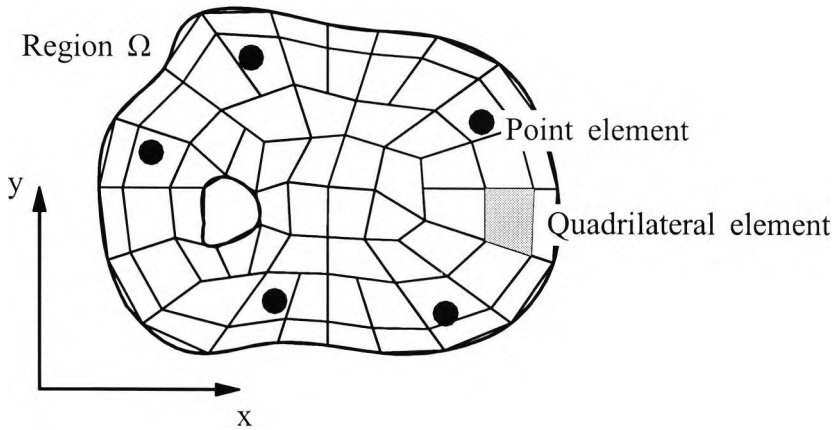

Figure 4.1
Numerical representation of cross-section

The integration of a function, $f(x,y)$, over a trapezoidal region, Ω_i , is facilitated by introducing the coordinate transformation given by equation 4.1a-e, and illustrated in figure 4.2. It should be noted that the coordinate transformation satisfies the required one-to-one correspondence between the Cartesian coordinates, (x,y) , and the natural coordinates, (ξ,η) , and that the region of integration is limited by -1 and 1 in the two natural coordinate directions.

$$\begin{Bmatrix} x \\ y \end{Bmatrix} = N_1 \begin{Bmatrix} x_1 \\ y_1 \end{Bmatrix} + N_2 \begin{Bmatrix} x_2 \\ y_2 \end{Bmatrix} + N_3 \begin{Bmatrix} x_3 \\ y_3 \end{Bmatrix} + N_4 \begin{Bmatrix} x_4 \\ y_4 \end{Bmatrix} \tag{4.1a}$$

where:

$$N_1 = 0.25(1-\xi)(1-\eta) \tag{4.1b}$$

$$N_2 = 0.25(1+\xi)(1-\eta) \tag{4.1c}$$

$$N_3 = 0.25(1+\xi)(1+\eta) \tag{4.1d}$$

$$N_4 = 0.25(1-\xi)(1+\eta) \tag{4.1e}$$

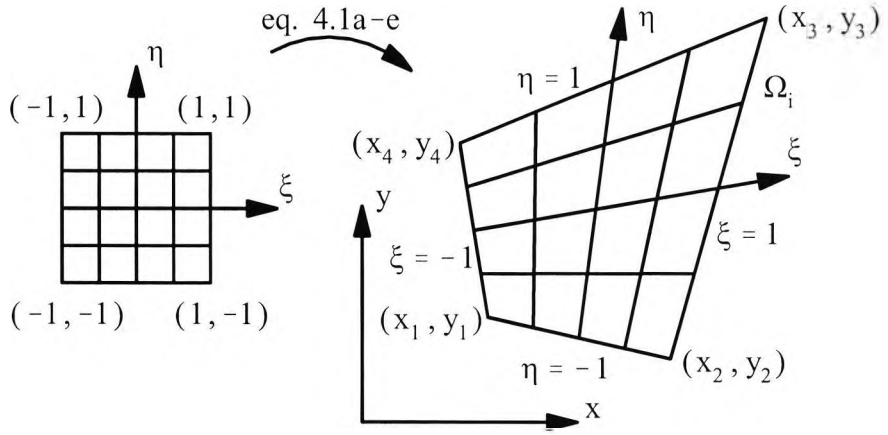

Figure 4.2
Transformation of coordinates for a quadrilateral element

The integral of $f(x,y)$ is given by equation 4.2a-b, in which the determinant of the Jacobian matrix, detJ , reflects that an area element $d\xi\, d\eta$ in the natural coordinate plane is mapped into an area element $\det J\, d\xi\, d\eta$ in the Cartesian coordinate plane.

$$\int_{\Omega_i} f(x,y)\, dA = \int_{-1}^{1}\int_{-1}^{1} f(\xi,\eta)\, \det J\, d\xi\, d\eta = \int_{-1}^{1}\int_{-1}^{1} g(\xi,\eta)\, d\xi\, d\eta \qquad (4.2a)$$

where:

$$\det J = \det\begin{bmatrix} \dfrac{\partial x}{\partial \xi} & \dfrac{\partial y}{\partial \xi} \\ \dfrac{\partial x}{\partial \eta} & \dfrac{\partial y}{\partial \eta} \end{bmatrix} = \det\begin{bmatrix} \displaystyle\sum_{i=1}^{4} \frac{\partial N_i}{\partial \xi} x_i & \displaystyle\sum_{i=1}^{4} \frac{\partial N_i}{\partial \xi} y_i \\ \displaystyle\sum_{i=1}^{4} \frac{\partial N_i}{\partial \eta} x_i & \displaystyle\sum_{i=1}^{4} \frac{\partial N_i}{\partial \eta} y_i \end{bmatrix} \qquad (4.2b)$$

The numerical value of the above integral is calculated using the Gauss-Legendre quadrature method given by equation 4.3. According to this method the integral is replaced by a weighted summation of the values of the integrand at a number, say $ng \times ng$, of *a priori* known sampling points, (ξ_i, η_j).

$$\int_{-1}^{1}\int_{-1}^{1} g(\xi,\eta)\, d\xi\, d\eta \approx \sum_{i=1}^{ng}\sum_{j=1}^{ng} g(\xi_i,\eta_j)\, W_i\, W_j \qquad (4.3)$$

Since ng sampling points are sufficient for the exact integration of a polynomial of order $2ng-1$ in one variable, a grid of $ng \times ng$ sampling points will be sufficient for the exact integration of a polynomial of the same order in two variables. The exact integration of a polynomial of order $2ng-1$ in two variables can in general be achieved using less than $ng \times ng$ sampling points. However, for integrands which are not polynomials, the accuracy of the numerical integration will in general improve with an increased number of sampling points. Printed tables of sampling points and weights are readily available for various integration orders (Zienkiewicz 1989).

Internal forces

Figure 4.3 illustrates the sign-convention adopted in the numerical model. It can be noted that the generalised forces, the axial force, P, and the bending moments, M_x and M_y, all act at the section's geometric centroid, (x_o, y_o). The bending moments M_x and M_y are taken about local axes which are parallel with the global x- and y-axis respectively. Since only stresses normal to the cross-section are included in the model, the analysis is only applicable to situations where shear stresses have negligible or no influence on the cross-section's ultimate load capacity.

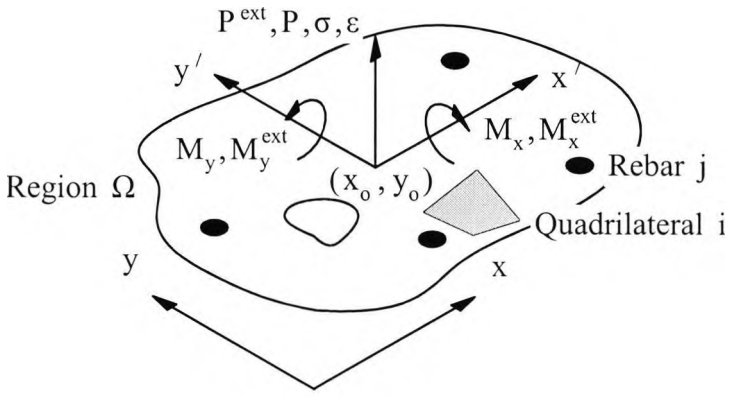

Figure 4.3
Sign convention and action points for forces

It follows from the assumption of plane sections remaining plane that the strain distribution over the cross-section is a function of three variables only. Thus, the strain distribution can be represented by equation 4.4, in which ε_o is the strain at the geometric centroid, and κ_x and κ_y are the curvatures for bending about the y- and x-axis respectively. The assumption of plane sections remaining plane also implies the existence of a perfect bond between the concrete and the reinforcement bars.

$$\varepsilon = \varepsilon_o + \kappa_x(x - x_o) + \kappa_y(y - y_o) \tag{4.4}$$

Since the materials are assumed to have non-linear elastic stress-strain characteristics, i.e. the unloading curve coincides with the loading curve, equation 4.4 provides all the necessary strain information for calculating the stress distribution, $\sigma(x,y)$, and hence also for calculating the internal forces:

$$P = \int_{\Omega} \sigma \, dA \tag{4.5}$$

$$M_y = \int_{\Omega} \sigma(x - x_o) \, dA \tag{4.6}$$

$$M_x = \int_{\Omega} \sigma(y - y_o) \, dA \tag{4.7}$$

Furthermore, as the cross-section is idealised as an assemblage of nq quadrilateral elements and np point elements, the internal forces can be evaluated by summing up the contributions from the individual elements as follows:

$$P = \sum_{i=1}^{nq} \int_{\Omega_i} \sigma \, dA + \sum_{j=1}^{np} \Delta\sigma_j A_j \tag{4.8}$$

$$M_y = \sum_{i=1}^{nq} \int_{\Omega_i} \sigma (x - x_o) \, dA + \sum_{j=1}^{np} \Delta\sigma_j (x_j - x_o) A_j \tag{4.9}$$

$$M_x = \sum_{i=1}^{nq} \int_{\Omega_i} \sigma\,(y - y_o)\,dA + \sum_{j=1}^{np} \Delta\sigma_j\,(y_j - y_o)\,A_j \qquad (4.10)$$

The differentials $\Delta\sigma_j$ in the above equations reflect that a point element numerically is treated as overlayed rather than embedded. Thus, a point element's contribution to the stress resultants should be modified for the contribution already included by integrating over its quadrilateral parent element, Ω_j.

By introducing the previously described coordinate transformation, the expressions for the internal forces, equations 4.8 - 4.10, can be rewritten to the following format suitable for Gauss-Legendre integration:

$$P = \sum_{i=1}^{nq} \int_{-1}^{1}\int_{-1}^{1} \sigma\,\det J\,d\xi\,d\eta + \sum_{j=1}^{np} \Delta\sigma_j A_j \qquad (4.11)$$

$$M_y = \sum_{j=1}^{nq} \int_{-1}^{1}\int_{-1}^{1} \sigma\,(x - x_o)\,\det J\,d\xi\,d\eta + \sum_{j=1}^{np} \Delta\sigma_j\,(x_j - x_o)\,A_j \qquad (4.12)$$

$$M_x = \sum_{i=1}^{nq} \int_{-1}^{1}\int_{-1}^{1} \sigma\,(y - y_o)\,\det J\,d\xi\,d\eta + \sum_{j=1}^{np} \Delta\sigma_j\,(y_j - y_o)\,A_j \qquad (4.13)$$

Computation procedure

The first step in the computational procedure is the calculation of the cross-section's squash load. This is achieved by incrementing the external axial load, P^{ext}, from zero until the axial force equilibrium, as given by equation 4.14, can no longer be established.

$$P^{res} = P^{ext} - P = 0 \qquad (4.14)$$

At the end of each load increment the uniform strain, ε_o, which minimises the absolute value of the force residual, $|P^{ext} - P|$, is determined by iteration. The advantage of

employing an optimisation method, in this case the "Golden Section Search" method (Press, 1989), is that it is robust in the sense that a non-existent solution to equation 4.14 does not result in numerical overflow. If the residual $|P^{ext} - P|$ converges towards a non-zero value, the applied load is reduced by an amount equal to half the current load increment, and the iteration is restarted from the last known equilibrium state. This process of cutting back and reiterating is repeated until the squash load has been determined to within a user-defined accuracy.

The biaxial bending moment capacity for axial loads less than the squash load is determined by following a load path in which the full axial load is applied prior to, and maintained constant during, the application of the moment. The direction of the plane in which the biaxial moment is acting is defined by an angle φ. The geometric angle φ relates the biaxial moment, M^{ext}, to its two Cartesian components, M_y^{ext} and M_x^{ext}, through equations 4.15 and 4.16.

$$M_y^{ext} = \sin(\varphi)\, M^{ext} \tag{4.15}$$

$$M_x^{ext} = \cos(\varphi)\, M^{ext} \tag{4.16}$$

The bending moment is applied in increments, and the strain distribution which satisfies the axial force equilibrium, i.e. equation 4.14, and the moment equilibrium, i.e. equations 4.17 and 4.18, is evaluated at the end of each increment.

$$M_y^{res} = M_y^{ext} - M_y = 0 \tag{4.17}$$

$$M_x^{res} = M_x^{ext} - M_x = 0 \tag{4.18}$$

The equilibrium equations are solved numerically by employing a mixed iteration procedure, in which an outer routine performs an iteration on the curvatures, κ_x and κ_y,

so as to establish the moment equilibrium, while an inner routine continuously adjusts the centroidal strain, ε_o , so as to maintain the axial force equilibrium. The inner routine is based on the "Golden Section Search" method, which is the method recommended by Press *et al* (1989) for calculating the minimum of a general one-dimensional function for which the derivatives cannot easily be computed. The outer routine is based on the well-known Newton Raphson method. According to the Newton Raphson method, the next guess of a solution, $(\kappa_x + d\kappa_x, \kappa_y + d\kappa_y)$, is taken as the roots of the first order Taylor series developed about the previous guess, (κ_x, κ_y) , i.e. the roots of equations 4.19 and 4.20.

$$M_y^{res}(\kappa_x + d\kappa_x, \kappa_y + d\kappa_y) \approx M_y^{res}(\kappa_x, \kappa_y) + \frac{\partial M_y^{res}}{\partial \kappa_x} d\kappa_x + \frac{\partial M_y^{res}}{\partial \kappa_y} d\kappa_y \tag{4.19}$$

$$M_x^{res}(\kappa_x + d\kappa_x, \kappa_y + d\kappa_y) \approx M_x^{res}(\kappa_x, \kappa_y) + \frac{\partial M_x^{res}}{\partial \kappa_x} d\kappa_x + \frac{\partial M_x^{res}}{\partial \kappa_y} d\kappa_y \tag{4.20}$$

Thus, the curvature corrections, $(d\kappa_y, d\kappa_x)$, in each iterative step are found by solving the following set of linear equations:

$$\begin{Bmatrix} M_y^{res} \\ M_x^{res} \end{Bmatrix} = \begin{bmatrix} \frac{\partial M_y}{\partial \kappa_x} & \frac{\partial M_y}{\partial \kappa_y} \\ \frac{\partial M_x}{\partial \kappa_x} & \frac{\partial M_x}{\partial \kappa_y} \end{bmatrix} \begin{Bmatrix} d\kappa_y \\ d\kappa_x \end{Bmatrix} \tag{4.21}$$

The partial derivatives of the bending moments in equation 4.21 are approximated using the finite difference expressions given by equations 4.22 - 4.25, in which $(\delta\kappa_y, \delta\kappa_x)$ represent some suitably small curvature increments.

$$\frac{\partial M_y}{\partial \kappa_x} \approx \frac{M_y(\kappa_x + \delta\kappa_x, \kappa_y) - M_y(\kappa_x - \delta\kappa_x, \kappa_y)}{2\delta\kappa_x} \tag{4.22}$$

$$\frac{\partial M_y}{\partial \kappa_y} \approx \frac{M_y(\kappa_x, \kappa_y + \delta\kappa_y) - M_y(\kappa_x, \kappa_y - \delta\kappa_y)}{2\delta\kappa_y} \tag{4.23}$$

$$\frac{\partial M_x}{\partial \kappa_x} \approx \frac{M_x(\kappa_x + \delta\kappa_x, \kappa_y) - M_x(\kappa_x - \delta\kappa_x, \kappa_y)}{2\delta\kappa_x} \tag{4.24}$$

$$\frac{\partial M_x}{\partial \kappa_y} \approx \frac{M_x(\kappa_x, \kappa_y + \delta\kappa_y) - M_x(\kappa_x, \kappa_y - \delta\kappa_y)}{2\delta\kappa_y} \tag{4.25}$$

After updating the curvatures, the axial force equilibrium is reestablished by iterating on the centroidal strain. The moment residuals and their derivatives corresponding to the new strain distribution are determined, after which a new pair of curvature corrections is calculated. This iteration continues until the moment residuals are reduced to a sufficiently small value, i.e an equilibrium between the internal and the external forces has been established.

The external moment is incremented, and the above described iteration is repeated. When an equilibrium state can no longer be established, the increment in the external moment is halved, and the iteration is restarted from the last known equilibrium state. The maximum sustainable moment corresponding to the given axial load is obtained when the increment in the external moment falls within a small user defined tolerance.

4.2.2 Model for Analysing Slender Columns

The computer program developed for the analysis of slender columns is based on the influence coefficient method (Chen, 1977). This method has a long history at City University, where it has formed the basis for the analysis of a large number of structural problems, such as steel columns with residual stress patterns (Virdi, 1981); concrete columns with non-uniform cross-section (Virdi, 1980; Brant, 1984); beam columns with semi-rigid end-restraints (Ragupathy, 1994); and latest of concrete and steel beams and columns exposed to fire (Jeyarupalingam, 1996).

Although the present investigation is limited to the behaviour of eccentrically loaded pinned columns with constant cross-section, a more general approach was adopted in the numerical modelling. As a consequence, the ensuing computer program reflects the true versatility of the method, and is readily available for future expanded investigations into the behaviour of reinforced high strength concrete columns.

Basic approach

The program allows for two types of load-controlled column analysis, namely a calculation of the ultimate axial load capacity and a calculation of the ultimate lateral load factor. In both types of analysis the structural response is monitored when incrementing the principal loading variable from zero up to the occurrence of failure. The external loads which are not specified as being principal loading variables are assumed to be applied at the onset of, and remain constant throughout, the analysis.

Lateral loads can be specified as a combination of uniformly distributed loads and point loads. End-moments and axial load eccentricities can be specified at both ends of the column. Imperfections in the straightness of the column axis can be included either by assuming them to follow a sinusoidal distribution, or by specifying them at discrete points

along the length of the column. The restraint conditions at the ends of the column can be specified as either pinned, fixed or flexible, and may vary in two orthogonal bending planes. The non-linear stress-strain curves for the materials are provided in a discrete format compatible with the output from the computational model described in section 3.4.3.

The numerical analysis is subjected to the following assumptions:

- Plane sections remain plane.
- Small deformations.
- Torsional effects are negligible.
- Shear deformations can be ignored.
- The member is free to shorten axially.
- No sway.
- Time-dependent effects of creep and shrinkage of concrete can be ignored.

Although the time-dependent effects of creep and shrinkage of concrete are not directly incorporated in the numerical model, the initial stress distribution caused by these effects could in principle be accounted for through the material stress-strain relations.

Figure 4.4 shows the displaced configuration of a pinned slender column when subjected to a combination of biaxial end-moments and axial compression. The column is divided into n segments of equal length, h, and the deflections in the x- and y-directions at the $n+1$ endpoints of these segments, also referred to as stations, are denoted u_i and v_i respectively. The deflections at the bottom and the top of the column are in accordance with the no-sway condition constant zero, i.e. $u_1 = v_1 = 0$ and $u_{n+1} = v_{n+1} = 0$. The cross-section of the column is defined at each station using the modelling technique described in section 4.2.1. Hence the numerical model applies to columns with irregular and/or variable cross-section.

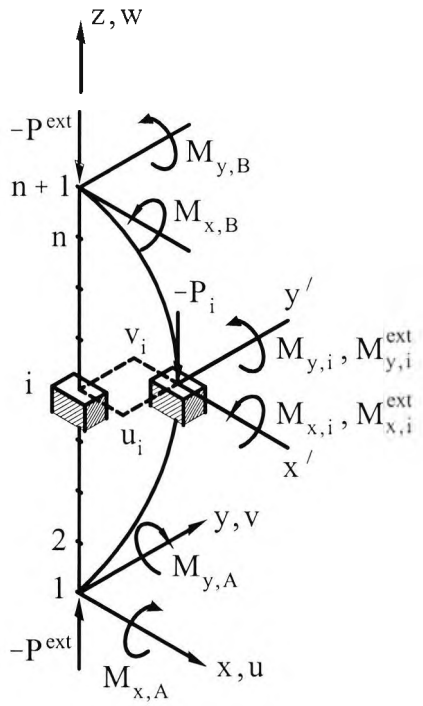

Figure 4.4
Modelling of slender column

The axial load, or alternatively the lateral load factor, is applied in increments, and the equilibrium configuration is determined at the end of each increment. A static equilibrium configuration is assumed when the residuals given by the equations 4.26 - 4.28 vanish, i.e. when the external forces, P^{ext}, $M^{ext}_{y,i}$ and $M^{ext}_{x,i}$, become equal to the internal forces, P_i, $M_{y,i}$ and $M_{x,i}$, at all of the $n+1$ stations.

$$P^{res}_i = P^{ext} - P_i = 0 \tag{4.26}$$

$$M^{res}_{y,i} = M^{ext}_{y,i} - M_{y,i} = 0 \tag{4.27}$$

$$M^{res}_{x,i} = M^{ext}_{x,i} - M_{x,i} = 0 \tag{4.28}$$

The internal forces are numerically calculated by employing the previously described Gauss-Legendre integration method. In this context, it should be mentioned that it follows

from the assumptions of negligible twist of the longitudinal axis and the displacements being small, i.e. du/dz and dv/dz being much smaller than unity, that a cross-section in the deformed column configuration is mapped by a pure translation in the xy-plane of the same cross-section in the undeformed column configuration.

The load-carrying capacity of the column is assumed to be exhausted as soon as a static equilibrium configuration can no longer be established. The numerical analysis terminates at this point, and is as such not designed to investigate the column response beyond the peak value of the equilibrium load.

External forces

Figure 4.5 shows a pinned column subjected to a combination of lateral loads, end-moments and axial load. The lateral loading consists of a uniformly distributed load, p_x, and a number of point loads, $P_{x,j}$, acting at various positions, z_j, along the column length, L. The applied loads are defined in the global coordinate system, and will not follow the column during deformation.

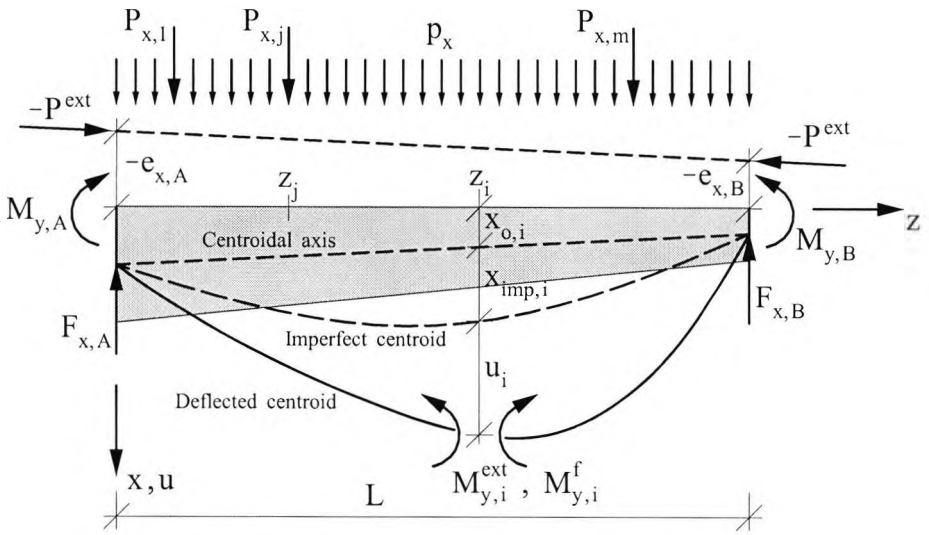

Figure 4.5
Sign convention and action points for external forces

The contribution to the external bending moment at station, i, from the lateral loads can be calculated from the following expressions:

$$M_{y,i}^{f} = F_{x,A} z_i - \frac{1}{2} p_x z_i^2 - \sum_{z_j < z_i} P_{x,j} (z_i - z_j) \tag{4.29a}$$

where:

$$F_{x,A} = \frac{1}{2} p_x L + \sum_{j=1}^{m} P_{x,j} (1 - \frac{z_j}{L}) \tag{4.29b}$$

The contribution to the external bending moment originating from the applied axial load, P^{ext}, depends on the lateral deflection, u_i, the eccentricities at the ends of the column, $e_{x,A}$ and $e_{x,B}$, the initial position of the centroidal axis, $x_{o,i}$, and the imperfection, $x_{imp,i}$. When further including the contribution originating from the applied end-moments, $M_{y,A}$ and $M_{y,B}$, the expression for the external bending moment acting at the deflected centroid about an axis parallel with the y-axis, $M_{y,i}^{ext}$, becomes:

$$\begin{aligned} M_{y,i}^{ext} = {} & (M_{y,A} + P^{ext} e_{x,A})(1 - \frac{i-1}{n}) + (M_{y,B} + P^{ext} e_{x,B})(\frac{i-1}{n}) \\ & - P^{ext}(x_{imp,i} + x_{o,i} + u_i) + M_{y,i}^{f} \end{aligned} \tag{4.30}$$

In a similar manner, the external bending moment acting at the deflected centroid about an axis parallel with the x-axis, $M_{x,i}^{ext}$, is given by:

$$\begin{aligned} M_{x,i}^{ext} = {} & (M_{x,A} + P^{ext} e_{y,A})(1 - \frac{i-1}{n}) + (M_{x,B} + P^{ext} e_{y,B})(\frac{i-1}{n}) \\ & - P^{ext}(y_{imp,i} + y_{o,i} + v_i) + M_{x,i}^{f} \end{aligned} \tag{4.31}$$

Solution procedure

The calculation of the equilibrium configuration consists of two nested procedures. In the first procedure, the axial force equilibrium is established at each of the $n + 1$ stations along the length of the column under a condition of the transverse displacements, u_i and v_i, and

hence also the curvatures, $\kappa_{x,i}$ and $\kappa_{y,i}$, being constant. Since plane sections remain plane, the strain distributions, ε_i, will under these circumstances only depend on the centroidal strains, $\varepsilon_{o,i}$ (see equation 4.32). Thus, the centroidal strains producing axial force equilibrium are found as the roots of $n+1$ uncoupled equations of the form $P_i^{res} = f(\varepsilon_{o,i})$. The roots of the non-linear equations are numerically calculated by employing the iterative procedure described in section 4.2.1.

$$\varepsilon_i = \varepsilon_{o,i} + \kappa_{x,i}(x_{,i} - x_{o,i}) + \kappa_{y,i}(y_{,i} - y_{o,i}) \tag{4.32}$$

In the second procedure, the axial force equilibrium is maintained, while the lateral displacements are iterated until the moment equilibrium has been established at all of the $n+1$ stations. The iteration is based on the Newton Raphson method for multidimensional problems. Thus, within each iterative step the residual moments, $(M_{y,i}^{res}, M_{x,i}^{res})$, and their partial derivatives corresponding to the approximate solution, (u_i, v_i), are calculated, whereafter the corrections, (du_i, dv_i), in the improved solution, $(u_i + du_i, v_i + dv_i)$, are obtained by solving equation 4.33.

$$\begin{Bmatrix} M_{y,1}^{res} \\ M_{y,2}^{res} \\ \vdots \\ M_{y,n}^{res} \\ M_{y,n+1}^{res} \\ M_{x,1}^{res} \\ M_{x,2}^{res} \\ \vdots \\ M_{x,n}^{res} \\ M_{x,n+1}^{res} \end{Bmatrix} = - \begin{bmatrix} \frac{\partial M_{y,1}^{res}}{\partial u_0} & \frac{\partial M_{y,1}^{res}}{\partial u_2} & \cdots & \frac{\partial M_{y,1}^{res}}{\partial u_n} & \frac{\partial M_{y,1}^{res}}{\partial u_{n+2}} & \frac{\partial M_{y,1}^{res}}{\partial v_0} & \frac{\partial M_{y,1}^{res}}{\partial v_2} & \cdots & \frac{\partial M_{y,1}^{res}}{\partial v_n} & \frac{\partial M_{y,1}^{res}}{\partial v_{n+2}} \\ \frac{\partial M_{y,2}^{res}}{\partial u_0} & \frac{\partial M_{y,2}^{res}}{\partial u_2} & \cdots & \frac{\partial M_{y,2}^{res}}{\partial u_n} & \frac{\partial M_{y,2}^{res}}{\partial u_{n+2}} & \frac{\partial M_{y,2}^{res}}{\partial v_0} & \frac{\partial M_{y,2}^{res}}{\partial v_2} & \cdots & \frac{\partial M_{y,2}^{res}}{\partial v_n} & \frac{\partial M_{y,2}^{res}}{\partial v_{n+2}} \\ \vdots & \vdots & & \vdots & \vdots & \vdots & \vdots & & \vdots & \vdots \\ \frac{\partial M_{y,n}^{res}}{\partial u_0} & \frac{\partial M_{y,n}^{res}}{\partial u_2} & \cdots & \frac{\partial M_{y,n}^{res}}{\partial u_n} & \frac{\partial M_{y,n}^{res}}{\partial u_{n+2}} & \frac{\partial M_{y,n}^{res}}{\partial v_0} & \frac{\partial M_{y,n}^{res}}{\partial v_2} & \cdots & \frac{\partial M_{y,n}^{res}}{\partial v_n} & \frac{\partial M_{y,n}^{res}}{\partial v_{n+2}} \\ \frac{\partial M_{y,n+1}^{res}}{\partial u_0} & \frac{\partial M_{y,n+1}^{res}}{\partial u_2} & \cdots & \frac{\partial M_{y,n+1}^{res}}{\partial u_n} & \frac{\partial M_{y,n+1}^{res}}{\partial u_{n+2}} & \frac{\partial M_{y,n+1}^{res}}{\partial v_0} & \frac{\partial M_{y,n+1}^{res}}{\partial v_2} & \cdots & \frac{\partial M_{y,n+1}^{res}}{\partial v_n} & \frac{\partial M_{y,n+1}^{res}}{\partial v_{n+2}} \\ \frac{\partial M_{x,1}^{res}}{\partial u_0} & \frac{\partial M_{x,1}^{res}}{\partial u_2} & \cdots & \frac{\partial M_{x,1}^{res}}{\partial u_n} & \frac{\partial M_{x,1}^{res}}{\partial u_{n+2}} & \frac{\partial M_{x,1}^{res}}{\partial v_0} & \frac{\partial M_{x,1}^{res}}{\partial v_2} & \cdots & \frac{\partial M_{x,1}^{res}}{\partial v_n} & \frac{\partial M_{x,1}^{res}}{\partial v_{n+2}} \\ \frac{\partial M_{x,2}^{res}}{\partial u_0} & \frac{\partial M_{x,2}^{res}}{\partial u_2} & \cdots & \frac{\partial M_{x,2}^{res}}{\partial u_n} & \frac{\partial M_{x,2}^{res}}{\partial u_{n+2}} & \frac{\partial M_{x,2}^{res}}{\partial v_0} & \frac{\partial M_{x,2}^{res}}{\partial v_2} & \cdots & \frac{\partial M_{x,2}^{res}}{\partial v_n} & \frac{\partial M_{x,2}^{res}}{\partial v_{n+2}} \\ \vdots & \vdots & & \vdots & \vdots & \vdots & \vdots & & \vdots & \vdots \\ \frac{\partial M_{x,n}^{res}}{\partial u_0} & \frac{\partial M_{x,n}^{res}}{\partial u_2} & \cdots & \frac{\partial M_{x,n}^{res}}{\partial u_n} & \frac{\partial M_{x,n}^{res}}{\partial u_{n+2}} & \frac{\partial M_{x,n}^{res}}{\partial v_0} & \frac{\partial M_{x,n}^{res}}{\partial v_2} & \cdots & \frac{\partial M_{x,n}^{res}}{\partial v_n} & \frac{\partial M_{x,n}^{res}}{\partial v_{n+2}} \\ \frac{\partial M_{x,n+1}^{res}}{\partial u_0} & \frac{\partial M_{x,n+1}^{res}}{\partial u_2} & \cdots & \frac{\partial M_{x,n+1}^{res}}{\partial u_n} & \frac{\partial M_{x,n+1}^{res}}{\partial u_{n+2}} & \frac{\partial M_{x,n+1}^{res}}{\partial v_0} & \frac{\partial M_{x,n+1}^{res}}{\partial v_2} & \cdots & \frac{\partial M_{x,n+1}^{res}}{\partial v_n} & \frac{\partial M_{x,n+1}^{res}}{\partial v_{n+2}} \end{bmatrix} \begin{Bmatrix} du_0 \\ du_2 \\ \vdots \\ du_n \\ du_{n+2} \\ dv_0 \\ dv_2 \\ \vdots \\ dv_n \\ dv_{n+2} \end{Bmatrix} \tag{4.33}$$

It can be noted that the system of linear equations include four auxiliary displacements, u_0 , v_0 , u_{n+2} and v_{n+2} , outside the length of the column as unknowns. The auxiliary displacements were primarily introduced as a matter of computational convenience, and are strictly only required when analysing columns with flexible end-supports.

The partial derivatives of the residual moments, also referred to as the influence coefficients, can be expressed in terms of the applied axial force and the partial derivatives of the internal moments as follows:

$$\frac{\partial M_{y,i}^{res}}{\partial u_j} = -P^{ext}\frac{du_i}{du_j} - \frac{\partial M_{y,i}}{\partial u_j} \tag{4.34}$$

$$\frac{\partial M_{y,i}^{res}}{\partial v_j} = -\frac{\partial M_{y,i}}{\partial v_j} \tag{4.35}$$

$$\frac{\partial M_{x,i}^{res}}{\partial u_j} = -\frac{\partial M_{x,i}}{\partial u_j} \tag{4.36}$$

$$\frac{\partial M_{x,i}^{res}}{\partial v_j} = -P^{ext}\frac{dv_i}{dv_j} - \frac{\partial M_{x,i}}{\partial v_j} \tag{4.37}$$

where: $i = 1,2,\ldots,n,n+1$ and $j = 0,2,3,\ldots,n-1,n,n+2$

Since the deformations are assumed to be small the curvatures $\kappa_{x,i}$ and $\kappa_{y,i}$ can be approximated by $-d^2u/dz^2|_i$ and $-d^2v/dz^2|_i$ respectively. These derivatives can again be related to the discrete displacements through the following finite difference approximations:

$$\kappa_{x,i} = -\left.\frac{d^2u}{dz^2}\right|_i \approx \frac{-u_{i-1}+2u_i-u_{i+1}}{h^2} \qquad \text{for } i = 1,2,\ldots,n+1 \tag{4.38}$$

$$\kappa_{y,i} = -\left.\frac{d^2v}{dz^2}\right|_i \approx \frac{-v_{i-1} + 2v_i - v_{i+1}}{h^2} \qquad \text{for } i = 1,2,\ldots,n+1 \tag{4.39}$$

Since the internal moments can be expressed as compound functions of the type $M_{y,i}(\kappa_{x,i}(u_{i-1},u_i,u_{i+1}),\kappa_{y,i}(v_{i-1},v_i,v_{i+1}))$, it follows from the chain rule of differentiation that the influence coefficients can be calculated from the equations 4.40 - 4.43. It should be emphasised that the influence coefficients have a value of zero for all combinations of the indices i and j not covered by these equations.

$$\frac{\partial M_{y,i}^{res}}{\partial u_j} = \begin{cases} \dfrac{1}{h^2}\dfrac{\partial M_{y,i}}{\partial \kappa_{x,i}} & \text{for } j = i-1 \\ -P^{ext} - \dfrac{2}{h^2}\dfrac{\partial M_{y,i}}{\partial \kappa_{x,i}} & \text{for } j = i \\ \dfrac{1}{h^2}\dfrac{\partial M_{y,i}}{\partial \kappa_{x,i}} & \text{for } j = i+1 \end{cases} \tag{4.40}$$

$$\frac{\partial M_{y,i}^{res}}{\partial v_j} = \begin{cases} \dfrac{1}{h^2}\dfrac{\partial M_{y,i}}{\partial \kappa_{y,i}} & \text{for } j = i-1 \\ -\dfrac{2}{h^2}\dfrac{\partial M_{y,i}}{\partial \kappa_{y,i}} & \text{for } j = i \\ \dfrac{1}{h^2}\dfrac{\partial M_{y,i}}{\partial \kappa_{y,i}} & \text{for } j = i+1 \end{cases} \tag{4.41}$$

$$\frac{\partial M_{x,i}^{res}}{\partial u_j} = \begin{cases} \dfrac{1}{h^2}\dfrac{\partial M_{x,i}}{\partial \kappa_{x,i}} & \text{for } j = i-1 \\ -\dfrac{2}{h^2}\dfrac{\partial M_{x,i}}{\partial \kappa_{x,i}} & \text{for } j = i \\ \dfrac{1}{h^2}\dfrac{\partial M_{x,i}}{\partial \kappa_{x,i}} & \text{for } j = i+1 \end{cases} \tag{4.42}$$

$$\frac{\partial M_{x,i}^{res}}{\partial v_j} = \begin{cases} \dfrac{1}{h^2}\dfrac{\partial M_{x,i}}{\partial \kappa_{y,i}} & \text{for} \quad j = i-1 \\ -P^{ext} - \dfrac{2}{h^2}\dfrac{\partial M_{x,i}}{\partial \kappa_{y,i}} & \text{for} \quad j = i \\ \dfrac{1}{h^2}\dfrac{\partial M_{x,i}}{\partial \kappa_{y,i}} & \text{for} \quad j = i+1 \end{cases} \tag{4.43}$$

where: $i = 1,2,\ldots,n,n+1$ and $j = 0,2,3,\ldots,n-1,n,n+2$

In the above equations the partial derivatives of the internal moments, $\partial M_{y,i}/\partial \kappa_{x,i}$, $\partial M_{y,i}/\partial \kappa_{y,i}$, $\partial M_{x,i}/\partial \kappa_{x,i}$ and $\partial M_{x,i}/\partial \kappa_{y,i}$, are approximated using the equations 4.44 - 4.47, where $\delta\kappa_y$ and $\delta\kappa_x$ represent some suitably small curvature increments.

$$\frac{\partial M_{y,i}}{\partial \kappa_{x,i}} \approx \frac{M_{y,i}(\kappa_{x,i}+\delta\kappa_x,\kappa_{y,i}) - M_{y,i}(\kappa_{x,i}-\delta\kappa_x,\kappa_{y,i})}{2\delta\kappa_x} \tag{4.44}$$

$$\frac{\partial M_{y,i}}{\partial \kappa_{y,i}} \approx \frac{M_{y,i}(\kappa_{x,i},\kappa_{y,i}+\delta\kappa_y) - M_{y,i}(\kappa_{x,i},\kappa_{y,i}-\delta\kappa_y)}{2\delta\kappa_y} \tag{4.45}$$

$$\frac{\partial M_{x,i}}{\partial \kappa_{x,i}} \approx \frac{M_{x,i}(\kappa_{x,i}+\delta\kappa_x,\kappa_{y,i}) - M_{x,i}(\kappa_{x,i}-\delta\kappa_x,\kappa_{y,i})}{2\delta\kappa_x} \tag{4.46}$$

$$\frac{\partial M_{x,i}}{\partial \kappa_{y,i}} \approx \frac{M_{x,i}(\kappa_{x,i},\kappa_{y,i}+\delta\kappa_y) - M_{x,i}(\kappa_{x,i},\kappa_{y,i}-\delta\kappa_y)}{2\delta\kappa_y} \tag{4.47}$$

After having updated the displacements, the new curvatures are determined and the axial force equilibrium is reestablished by iterating on the centroidal strains. The new residual moments and influence coefficients are calculated, after which the next displacement corrections can be calculated. This procedure is repeated until the displacements have converged to the equilibrium configuration. Convergence is assumed when the maximum absolute correction to any displacement variable becomes less than a user defined tolerance.

When an equilibrium configuration can no longer be established, the analysis is restarted at the last known equilibrium state using a reduced load increment. The analysis terminates when the absolute value of the load increment is reduced below a user defined tolerance.

Modification for fixed boundaries

If the column has fixed boundaries, it is necessary to impose constraints on the discrete displacements so as to ensure that the slopes at the ends remain zero. According to the central difference approximation, the zero slope condition can be expressed in terms of the equalities: $u_0 = u_2$, $u_{n+2} = u_n$, $v_0 = v_2$ and $v_{n+2} = v_n$. Hence the curvatures at the ends of the column are given as follows:

$$\kappa_{x,1} = -2u_2/h^2 \tag{4.48}$$

$$\kappa_{x,n+1} = -2u_n/h^2 \tag{4.49}$$

$$\kappa_{y,1} = -2v_2/h^2 \tag{4.50}$$

$$\kappa_{y,n+1} = -2v_n/h^2 \tag{4.51}$$

The reaction moments at the fixed ends are expressed by the equations 4.52 to 4.55. It should be noted that the reaction moments are taken about the x- and y-axis, which do not necessarily pass through the centroid of the cross-section. As the axial load eccentricities do not have a physical meaning for columns with fixed boundary conditions, they are included as a matter of computational convenience.

$$M_{y,A} = M_{y,1} - P^{ext}(e_{x,A} - x_{o,1}) \tag{4.52}$$

$$M_{y,B} = M_{y,n+1} - P^{ext}(e_{x,B} - x_{o,n+1}) \tag{4.53}$$

$$M_{x,A} = M_{x,1} - P^{ext}(e_{y,A} - y_{o,1}) \tag{4.54}$$

$$M_{x,B} = M_{x,n+1} - P^{ext}(e_{y,A} - y_{o,n+1}) \tag{4.55}$$

The expressions for the moment residuals, equations 4.56 and 4.57, can be obtained by substituting the above equations into the expressions for the external moments, i.e. into equations 4.30 and 4.31.

$$M_{y,i}^{res} = (M_{y,1} + P^{ext} x_{o,1})(1 - \frac{i-1}{n}) + (M_{y,n+1} + P^{ext} x_{o,n+1})(\frac{i-1}{n}) - P^{ext}(x_{imp,i} + x_{o,i} + u_i) + M_{y,i}^{f} - M_{y,i} \tag{4.56}$$

$$M_{x,i}^{res} = (M_{x,1} + P^{ext} y_{o,1})(1 - \frac{i-1}{n}) + (M_{x,n+1} + P^{ext} y_{o,n+1})(\frac{i-1}{n}) - P^{ext}(y_{imp,i} + y_{o,i} + v_i) + M_{x,i}^{f} - M_{x,i} \tag{4.57}$$

From differentiation, it follows that the influence coefficients for a column with fixed boundary conditions can be written as follows:

$$\frac{\partial M_{y,i}^{res}}{\partial u_j} = \frac{\partial M_{y,1}}{\partial \kappa_{x,1}}(\frac{-2}{h^2})(1-\frac{i-1}{n})\frac{du_2}{du_j} + \frac{\partial M_{y,n+1}}{\partial \kappa_{x,n+1}}(\frac{-2}{h^2})(\frac{i-1}{n})\frac{du_n}{du_j} - P^{ext}\frac{du_i}{du_j} - \frac{\partial M_{y,i}}{\partial u_j} \tag{4.58}$$

$$\frac{\partial M_{y,i}^{res}}{\partial v_j} = \frac{\partial M_{y,1}}{\partial \kappa_{y,1}}(\frac{-2}{h^2})(1-\frac{i-1}{n})\frac{dv_2}{dv_j} + \frac{\partial M_{y,n+1}}{\partial \kappa_{y,n+1}}(\frac{-2}{h^2})(\frac{i-1}{n})\frac{dv_n}{dv_j} - \frac{\partial M_{y,i}}{\partial v_j} \tag{4.59}$$

$$\frac{\partial M_{x,i}^{res}}{\partial u_j} = \frac{\partial M_{x,1}}{\partial \kappa_{x,1}}(\frac{-2}{h^2})(1-\frac{i-1}{n})\frac{du_2}{du_j} + \frac{\partial M_{x,n+1}}{\partial \kappa_{x,n+1}}(\frac{-2}{h^2})(\frac{i-1}{n})\frac{du_n}{du_j} - \frac{\partial M_{x,i}}{\partial u_j} \tag{4.60}$$

$$\frac{\partial M_{x,i}^{res}}{\partial v_j} = \frac{\partial M_{x,1}}{\partial \kappa_{y,1}}(\frac{-2}{h^2})(1-\frac{i-1}{n})\frac{dv_2}{dv_j} + \frac{\partial M_{x,n+1}}{\partial \kappa_{y,n+1}}(\frac{-2}{h^2})(\frac{i-1}{n})\frac{dv_n}{dv_j} - P^{ext}\frac{dv_i}{dv_j} - \frac{\partial M_{x,i}}{\partial v_j} \tag{4.61}$$

where: $i = 2,3,\ldots,n-1,n$ and $j = 2,3,\ldots,n-1,n$

When compared to a pinned column (see equations 4.34 - 4.37), the matrix of influence coefficients for a column with fixed boundaries will contain additional terms in the columns corresponding to the unknowns du_2 , du_n , dv_2 and dv_n. Furthermore, the fictitious displacements outside the length of the column are decoupled from the interior displacements.

Modification for flexible end-supports

In the case of a column with flexible end-supports the end-moments are decomposed into restoring and applied moments. As seen from equations 4.62 - 4.65, the restoring moments are assumed to be proportional to the end-rotations, $\theta_{x,1}$, $\theta_{x,n+1}$, $\theta_{y,1}$ and $\theta_{y,n+1}$, which again are approximated from the discrete displacements.

$$M_{y,A} = k_{y,A}\theta_{x,1} + \hat{M}_{y,A} = k_{y,A}\frac{u_2 - u_0}{2h} + \hat{M}_{y,A} \tag{4.62}$$

$$M_{y,B} = k_{y,B}\theta_{x,n+1} + \hat{M}_{y,B} = k_{y,B}\frac{u_n - u_{n+2}}{2h} + \hat{M}_{y,B} \tag{4.63}$$

$$M_{x,A} = k_{x,A}\theta_{y,1} + \hat{M}_{x,A} = k_{x,A}\frac{v_2 - v_0}{2h} + \hat{M}_{x,A} \tag{4.64}$$

$$M_{x,B} = k_{x,B}\theta_{y,n+1} + \hat{M}_{x,B} = k_{x,B}\frac{v_n - v_{n+2}}{2h} + \hat{M}_{x,B} \tag{4.65}$$

The residual moments are given by equations 4.66 and 4.67, which were obtained by substituting equations 4.62 - 4.65 into equations 4.30 and 4.31, i.e. by substituting the expressions for the end-moments into the expressions for the external moments.

$$M^{res}_{y,i} = (k_{y,A}\frac{u_2 - u_0}{2h} + \hat{M}_{y,A} + P^{ext} e_{x,A})(1 - \frac{i-1}{n}) + (k_{y,B}\frac{u_n - u_{n+2}}{2h} + \hat{M}_{y,B} + P^{ext} e_{x,B})(\frac{i-1}{n}) - P^{ext}(x_{imp,i} + x_{o,i} + u_i) + M^{f}_{y,i} - M_{y,i} \quad (4.66)$$

$$M^{res}_{x,i} = (k_{x,A}\frac{v_2 - v_0}{2h} + \hat{M}_{x,A} + P^{ext} e_{y,A})(1 - \frac{i-1}{n}) + (k_{x,B}\frac{v_n - v_{n+2}}{2h} + \hat{M}_{x,B} + P^{ext} e_{y,B})(\frac{i-1}{n}) - P^{ext}(y_{imp,i} + y_{o,i} + v_i) + M^{f}_{x,i} - M_{x,i} \quad (4.67)$$

The influence coefficients, given by equations 4.68 - 4.71, were simply obtained by differentiating the above equations.

$$\frac{\partial M^{res}_{y,i}}{\partial u_j} = \frac{k_{y,A}}{2h}(1 - \frac{i-1}{n})\frac{\partial(u_2 - u_0)}{\partial u_j} + \frac{k_{y,B}}{2h}(\frac{i-1}{n})\frac{\partial(u_n - u_{n+2})}{\partial u_j} - P^{ext}\frac{du_i}{du_j} - \frac{\partial M_{y,i}}{\partial u_j} \quad (4.68)$$

$$\frac{\partial M^{res}_{y,i}}{\partial v_j} = -\frac{\partial M_{y,i}}{\partial v_j} \quad (4.69)$$

$$\frac{\partial M^{res}_{x,i}}{\partial u_j} = -\frac{\partial M_{x,i}}{\partial u_j} \quad (4.70)$$

$$\frac{\partial M^{res}_{x,i}}{\partial v_j} = \frac{k_{x,A}}{2h}(1 - \frac{i-1}{n})\frac{\partial(v_2 - v_0)}{\partial v_j} + \frac{k_{x,B}}{2h}(\frac{i-1}{n})\frac{\partial(v_n - v_{n+2})}{\partial v_j} - P^{ext}\frac{dv_i}{dv_j} - \frac{\partial M_{x,i}}{\partial v_j} \quad (4.71)$$

where: $i = 1,2,\ldots,n,n+1$ and $j = 0,2,3,\ldots,n-1,n,n+2$

When compared to a pinned column, the matrix of influence coefficients for a column with flexible end-supports will contain additional entries corresponding to the displacements at either side of the supports, i.e. du_0 , du_2 , du_n , du_{n+2} , dv_0 , dv_2 , dv_n and dv_{n+2}. In the special case of all spring constants being zero, the ensuing system of equations is identical to that for a pinned column. In a similar manner, large spring constants will approximate the behaviour of a fixed column, but the solution path will be different as the fictitious displacements are not explicitly decoupled from the equations. The use of large spring constants to model fully restrained end-conditions is not recommended as it renders the system of equations to be ill-conditioned.

Modification for mixed boundary conditions

When establishing the influence coefficients for a column having mixed boundary conditions, it is constructive to write out the full differentials of the moment residuals. The differentials for bending about the y-axis, $dM_{y,i}^{res}$, are given by equations 4.72 to 4.74, and the influence coefficients are readily obtained from these by inserting the expressions for the end-moments and end-curvatures associated with the given boundary conditions.

for i = 1

$$\begin{aligned} dM_{y,1}^{res} = {} & \frac{\partial M_{y,A}}{\partial u_0} du_0 + \frac{\partial M_{y,A}}{\partial u_2} du_2 + \frac{\partial M_{y,A}}{\partial v_0} dv_0 + \frac{\partial M_{y,A}}{\partial v_2} dv_2 \\ & - \frac{\partial M_{y,1}}{\partial \kappa_{x,1}} \frac{\partial \kappa_{x,1}}{\partial u_0} du_0 - \frac{\partial M_{y,1}}{\partial \kappa_{x,1}} \frac{\partial \kappa_{x,1}}{\partial u_2} du_2 \\ & - \frac{\partial M_{y,1}}{\partial \kappa_{y,1}} \frac{\partial \kappa_{y,1}}{\partial v_0} dv_0 - \frac{\partial M_{y,1}}{\partial \kappa_{y,1}} \frac{\partial \kappa_{y,1}}{\partial v_2} dv_2 \end{aligned} \qquad (4.72)$$

for $i = 2, 3, \ldots, n-1, n$

$$
\begin{aligned}
dM_{y,i}^{res} = & \left(\frac{\partial M_{y,A}}{\partial u_0} du_0 + \frac{\partial M_{y,A}}{\partial u_2} du_2 \right) (1 - \frac{i-1}{n}) + \left(\frac{\partial M_{y,B}}{\partial u_n} du_n + \frac{\partial M_{y,B}}{\partial u_{n+2}} du_{n+2} \right) (\frac{i-1}{n}) \\
& + \left(\frac{\partial M_{y,A}}{\partial v_0} dv_0 + \frac{\partial M_{y,A}}{\partial v_2} dv_2 \right) (1 - \frac{i-1}{n}) + \left(\frac{\partial M_{y,B}}{\partial v_n} dv_n + \frac{\partial M_{y,B}}{\partial v_{n+2}} dv_{n+2} \right) (\frac{i-1}{n}) \\
& - P^{ext} du_i - \frac{\partial M_{y,i}}{\partial \kappa_{x,i}} \left(\frac{\partial \kappa_{x,i}}{\partial u_{i-1}} du_{i-1} + \frac{\partial \kappa_{x,i}}{\partial u_i} du_i + \frac{\partial \kappa_{x,i}}{\partial u_{i+1}} du_{i-1} \right) \\
& - \frac{\partial M_{y,i}}{\partial \kappa_{y,i}} \left(\frac{\partial \kappa_{y,i}}{\partial v_{i-1}} dv_{i-1} + \frac{\partial \kappa_{y,i}}{\partial v_i} dv_i + \frac{\partial \kappa_{y,i}}{\partial v_{i+1}} dv_{i+1} \right)
\end{aligned}
\tag{4.73}
$$

for $i = n + 1$

$$
\begin{aligned}
dM_{y,n+1}^{res} = & \frac{\partial M_{y,B}}{\partial u_n} du_n + \frac{\partial M_{y,B}}{\partial u_{n+2}} du_{n+2} + \frac{\partial M_{y,B}}{\partial v_n} dv_n + \frac{\partial M_{y,B}}{\partial v_{n+2}} dv_{n+2} \\
& - \frac{\partial M_{y,n+1}}{\partial \kappa_{x,n+1}} \frac{\partial \kappa_{x,n+1}}{\partial u_n} du_n - \frac{\partial M_{y,n+1}}{\partial \kappa_{x,n+1}} \frac{\partial \kappa_{x,n+1}}{\partial u_{n+2}} du_{n+2} \\
& - \frac{\partial M_{y,n+1}}{\partial \kappa_{y,n+1}} \frac{\partial \kappa_{y,n+1}}{\partial v_n} dv_n - \frac{\partial M_{y,n+1}}{\partial \kappa_{y,n+1}} \frac{\partial \kappa_{y,n+1}}{\partial v_{n+2}} dv_{n+2}
\end{aligned}
\tag{4.74}
$$

Summary

This section described a numerical procedure for calculating the complete biaxial load-deflection response of braced columns subjected to either monotonic increasing axial or lateral load. The method provides full flexibility in terms the column's cross-sectional dimensions and spatial variations in the stress-strain characteristics of the materials. Two FORTRAN programs have been developed based on the theoretical approach. The first program is used to generate a biaxial interaction diagram, and the second to carry out a load-deflection analysis. Listings of the computer programs are given in Appendix B.

4.3 Validation of Numerical Models

This section validates the developed numerical models in terms of predicting the structural response of pin-ended reinforced concrete columns subjected to eccentric compression. For this purpose, the results from 122 full-scale column tests, taken from seven different experimental research programmes, were reviewed. The validation process also provided a basis for a general assessment of the influence of column slenderness, load eccentricity and concrete grade on the structural response of reinforced concrete columns. Furthermore, the beneficial effect of confinement, as well as the counterbalancing effect of the cover concrete, is discussed.

4.3.1 Concrete Columns Failing in Uniaxial Bending

Most of the published experimental data on eccentrically loaded concrete columns are on columns failing in uniaxial bending. Details from five of the more recent experimental investigations of such columns are given in the references (Saatcioglu, 1995), (Lloyd, 1996), (Foster, 1997), (Claeson, 1998) and (Kim, 1995). These investigations, reviewed in the following, represent a large variation in geometric and physical column properties: geometric slenderness ratio, L/d, between 3.0 and 30.0; load eccentricity to depth ratio, e_y/d, between 0.05 and 0.37; volumetric ratio of longitudinal reinforcement, ρ_g, between 1.47% and 4.02%; tie spacings, s, between 30 mm and 240 mm; volumetric ratio of lateral reinforcement, ρ_s, between 0.52% and 3.04%; and compressive cylinder strength, $f_{c,cyl}$, between 26 MPa and 97 MPa.

The analytical results were all obtained under the assumption that the unconfined concrete strength of a full-scale column could be set equal to 81% of the mean value of the 100×200 mm cylinder strengths, and to 85% of the mean value of the 150×300 mm cylinder

strengths. The other essential material properties, i.e. the modulus of elasticity, the strain at peak stress, and the softening parameter were estimated from the unconfined concrete strength employing equations 3.3, 3.5 and 3.13 respectively.

The maximum effective confining stress, $\sigma_{1,eff}$, was determined by the modified arching action method described in section 3.4.2, and the stress-strain curve for both confined and unconfined concrete by the computational model described in section 3.4.3. The stress-strain behaviour of the core concrete in 66 out of the 111 test columns was predicted to have benefited from passive confinement. When generating the stress-strain curve for passively confined concrete, the yield strain of the transverse steel reinforcement bars was determined from the yield stress, f_{sy}, by assuming a modulus of elasticity of 205 GPa.

The cross-section of each test column was modelled as a composite section consisting of a concrete cover, a nominal concrete core and a number of longitudinal steel reinforcement bars (see figure 4.6). The cover concrete was assumed to follow the stress-strain curve for unconfined concrete, and the core concrete, depending on the tie arrangement, that of confined or unconfined concrete. The longitudinal reinforcement steel was assumed to behave as an elastic perfectly plastic material.

Whenever the core concrete was estimated to have benefited from confinement, an additional analysis in which the confinement effects were ignored was carried out. The additional analysis established a benchmark for assessing the structural effect of the provided confinement. Furthermore, in order to ensure that the computed peak loads constituted the global maxima of the load-deflection curves, the confined columns were also analysed under the assumption that the concrete cover on the most compressed side of the columns spalled off at the onset of loading. The assumption of premature cover spalling

always resulted in a reduction in the load capacity, which for all except two of the test columns was reduced below the capacity of the corresponding unconfined column.

As is customary when analysing structural concrete members, the tensile strength of concrete was not taken into account. In this context, it should be mentioned that due to the higher tensile strength, the risk of high strength concrete members exhibiting brittle failure upon the formation of the first tensile crack is increased when compared to normal strength concrete members (Collins, 1993). This phenomenon, though not investigated in this thesis, raises some interesting questions regarding the code provisions for minimum reinforcement.

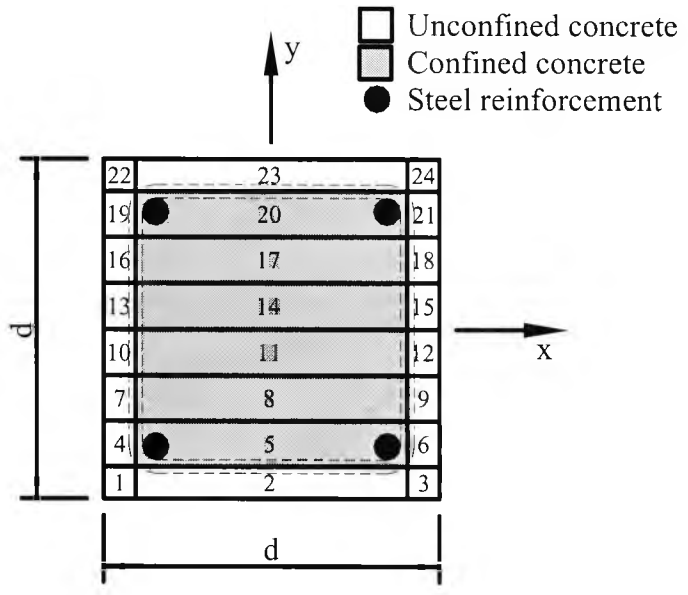

Figure 4.6
Modelling of cross-sections of uniaxially bent columns

The accuracy with which the internal forces are calculated will, in general, improve with an increase in the number of quadrilateral elements, as well as with the number of numerical integration points within these elements. By comparing the interaction diagrams calculated for various mesh densities and integration orders, it was concluded that 8

elements in the direction of bending combined with a 3×3 integration rule produced sufficiently accurate results. The accuracy to which the displaced column configuration is calculated will further depend on the number of stations along the length of the column. The more stations used, the more accurate is the calculated curvature distribution and equilibrium configuration. The preliminary study showed that sufficiently accurate results could be obtained by dividing the test columns into 16 segments.

Saatcioglu, Salamat and Razvi (1995)

Saatcioglu *et al* examined the behaviour of confined concrete columns under eccentric loading by testing twelve 210×210×1640 mm columns. For half the test columns, the axial load was applied at an eccentricity to depth ratio of 0.28, and for the other half at an eccentricity to depth ratio of 0.36. For a given eccentricity, both columns with 50 mm and 100 mm tie spacings were tested for each of the three tie configurations shown in figure 4.7. The concrete in the test columns with the closer tie spacings had a compressive cylinder strength of 26 MPa, and in those with the larger tie spacings a compressive cylinder strength of 35 MPa. The test parameters for the individual columns are given in table 4.1a.

Figure 4.8 shows the calculated stress-strain behaviour of the two concrete grades at the confining pressures relevant to the experimental investigation. For the columns made from concrete with a cylinder strength of 35 MPa, the confining reinforcement was calculated to raise the strength and the peak strain of the core concrete by a maximum of 55% and 155% respectively. Similarly, for the columns made from concrete with a cylinder strength of 26 MPa, the confining reinforcement was calculated to raise the strength and the peak strain of the core concrete by a maximum of 25% and 84% respectively. In the case of the columns transversely reinforced with the least efficient tie configuration, i.e. configuration

(1), the strength and the peak strain of the core concrete in the columns made from the 35 MPa concrete was raised by 14% and 84% respectively, and in the columns made from the 26 MPa concrete by 4% and 25% respectively. It should be emphasised that the four longitudinal reinforcement bars positioned at the mid-point of the tie legs were ignored when calculating the effective confining pressure associated with the type (1) tie configuration.

Table 4.1b compares the experimental failure load, P_c , and the corresponding mid-height deflection, v_{max} , for the individual test columns to their analytical counterparts. It can be noted that the inclusion of confinement effects has a rather limited, though improving, influence on the correlation between the analytical and the experimental results. When including confinement effects, the average ratio of the test failure load to the calculated failure load was 1.16, with a standard deviation of 0.04. The table also shows that the mid-height deflection at failure was predicted with less accuracy than the failure load itself. Both were consistently underestimated by the numerical model.

Figure 4.9 illustrates the analytical load-deflection curves for the six test columns which were transversely reinforced with a tie pitch of 50 mm. When comparing these curves to the similar curves for unconfined columns, it appears that only the behaviour of the columns C3-1 and C6-2 were significantly influenced by confinement, and that the most noticeable influence was the development of a nearly flat yield plateau. In this context, it should be mentioned that Saatcioglu *et al* reported that the columns C3-1 and C6-2 exhibited extremely ductile post-peak behaviour when compared to the other columns tested.

The provided confinement was calculated to raise the axial load capacity of the columns by a maximum of 7%, despite the strength of the core concrete being raised by up to 55% above the unconfined concrete strength. The modest increase in the axial load capacity can be explained by means of the three interaction diagrams shown in figure 4.10. For the first diagram, the stress-strain curve for the unconfined concrete was applied to both the core and the cover of the cross-section. For the second diagram, the stress-strain curve for the confined concrete was applied to the core and the stress-strain curve for the unconfined concrete to the cover, and finally for the third diagram, the stress-strain curve for the confined concrete was applied to both the core and the cover. By comparing the diagrams, it can be concluded that the strength properties of the confined test columns were significantly influenced by the unconfined concrete cover. Thus, if the benefits of passive confinement in general are to be efficiently explored, it is essential that the thickness of the concrete cover is reduced to an absolute minimum. In the columns tested by Saatcioglu *et al*, the concrete cover constituted a considerable 23% of their total volume.

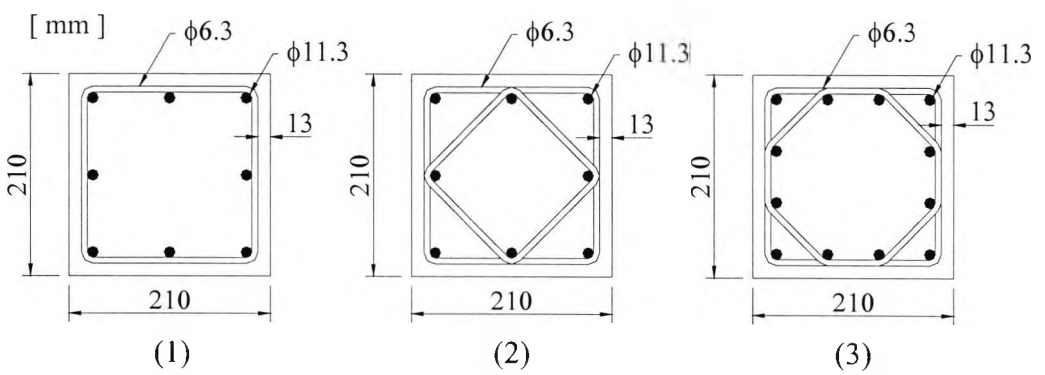

Figure 4.7
Cross-sections of columns tested by Saatcioglu *et al*

Table 4.1a
Details of columns tested by Saatcioglu *et al*

Column		Slend.	Eccen.	Conc.	Longitudinal reinforcement		Transverse reinforcement		
ID	Sec.	L/d (-)	e_y/d (-)	$f_{c,cyl}$ (MPa)	ρ_g (%)	f_{sy} (MPa)	s (mm)	ρ_s (%)	f_{sy} (MPa)
C1-1	1	7.8	0.28	35	1.82	517	50	1.40	410
C2-1	2	7.8	0.28	35	1.82	517	50	2.38	410
C3-1	3	7.8	0.28	35	2.73	517	50	2.52	410
C4-2	1	7.8	0.36	35	1.82	517	50	1.40	410
C5-2	2	7.8	0.36	35	1.82	517	50	2.38	410
C6-2	3	7.8	0.36	35	2.73	517	50	2.52	410
C7-1	1	7.8	0.28	26	1.82	517	100	0.70	410
C8-1	2	7.8	0.28	26	1.82	517	100	1.19	410
C9-1	3	7.8	0.28	26	2.73	517	100	1.26	410
C10-2	1	7.8	0.36	26	1.82	517	100	0.70	410
C11-2	2	7.8	0.36	26	1.82	517	100	1.19	410
C12-2	3	7.8	0.36	26	2.73	517	100	1.26	410

$f_{c,cyl}$: compressive strength of 150×300 mm cylinders.

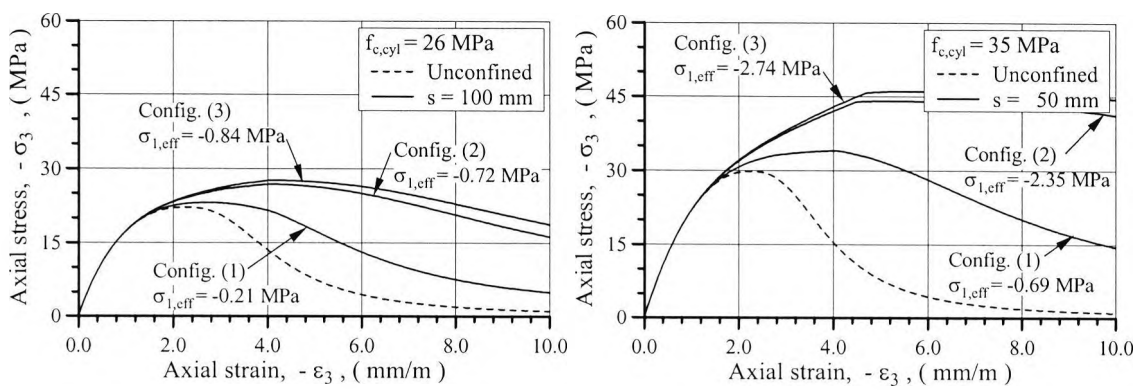

Figure 4.8
Assumed stress-strain behaviour of concretes

Table 4.1b
Comparison of experimental and analytical results

Column		Experimental		Analytical excl. confinement			Analytical incl. confinement		
ID	Sec.	$P_{c,e}$ (kN)	$v_{max,e}$ (mm)	$P_{c,a}$ (kN)	$v_{max,a}$ (mm)	$P_{c,e}/P_{c,a}$ (-)	$P_{c,a}$ (kN)	$v_{max,a}$ (mm)	$P_{c,e}/P_{c,a}$ (-)
C1-1	1	959	9.3	756	7.2	1.27	773	7.4	1.24
C2-1	2	938	13.4	756	7.2	1.24	793	7.9	1.18
C3-1	3	1061	15.4	849	7.0	1.25	908	14.6	1.17
C4-2	1	734	17.1	627	8.6	1.17	640	8.8	1.15
C5-2	2	745	16.5	627	8.6	1.19	655	11.0	1.14
C6-2	3	877	16.9	711	8.2	1.23	760	12.8	1.15
C7-1	1	755	7.8	628	7.1	1.20	635	7.3	1.19
C8-1	2	755	10.6	628	7.1	1.20	648	7.7	1.17
C9-1	3	816	14.0	720	7.1	1.13	746	8.2	1.09
C10-2	1	612	22.9	527	8.4	1.16	533	8.6	1.15
C11-2	2	622	16.3	527	8.4	1.18	543	9.1	1.15
C12-2	3	704	21.6	609	8.2	1.16	634	12.9	1.11
				Mean		1.20			1.16
				Standard deviation		0.04			0.04

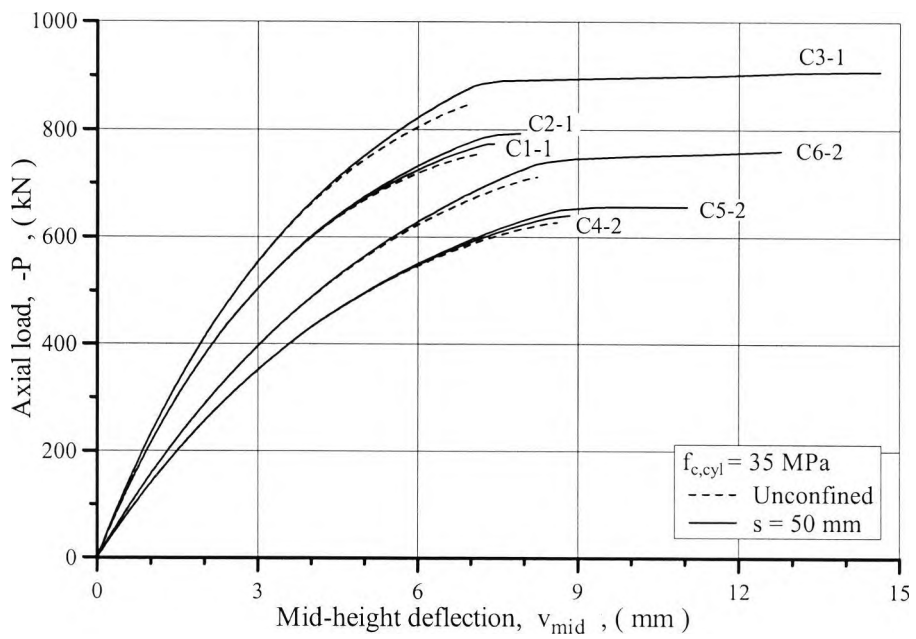

Figure 4.9
Computed influence of confinement on load-deflection diagrams

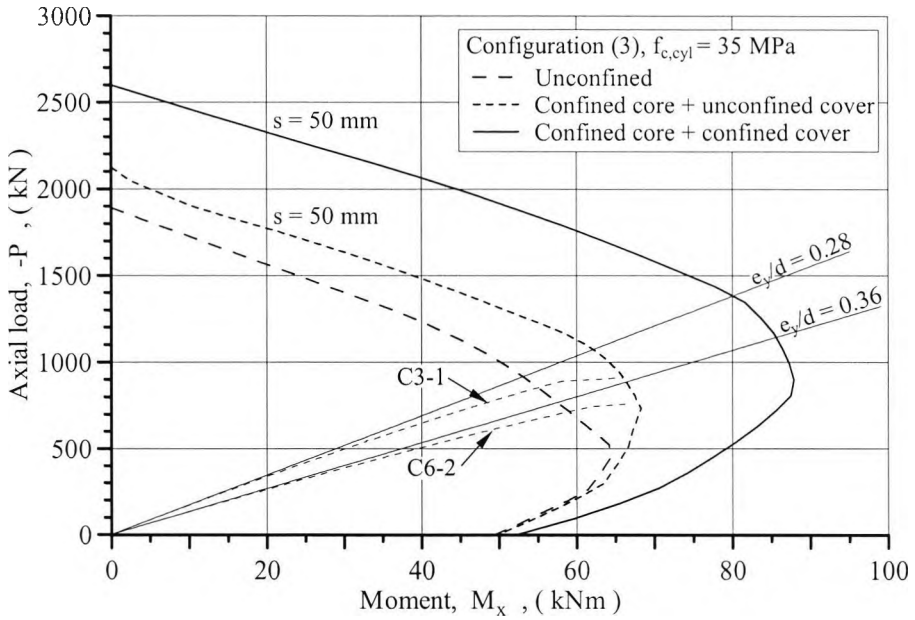

Figure 4.10
Computed influence of confinement on interaction diagrams

Lloyd and Rangan (1996)

Figure 4.11 together with table 4.2a give the details of eighteen 175×175×1680 mm concrete columns tested by Lloyd and Rangan. The test parameters included the load eccentricity, the concrete strength and the number of longitudinal reinforcement bars. The columns were tested under an eccentricity to depth ratio of either 0.09, 0.29 or 0.37 had a compressive concrete cylinder strength of either 58 MPa, 92 MPa or 97 MPa and were longitudinally reinforced by either four or six 12 mm high yield steel bars. Since all of the columns contained the same amount of lateral reinforcement, the influence of passive confinement was not explicitly addressed in the experimental investigation.

Figure 4.12 shows the estimated effect of the provided transverse reinforcement on the stress-strain behaviour of the core concrete, and table 4.2b shows that this had virtually no influence on the computed column behaviour. In both cases, the average ratio of test failure load to calculated failure load was 1.05, with a standard deviation of 0.07.

The test observations given in table 4.2b show, with two exceptions, that an increase in

both the grade of concrete and a decrease in the load eccentricity had the effect of increasing the axial load capacity. Figure 4.13 shows the relationship between the axial load capacity and the eccentricity ratio for the test columns which were manufactured from concrete with a cylinder strength of either 58 MPa or 97 MPa. It can be seen from the figure that the reduction in the axial load capacity with increasing eccentricity was larger for the columns manufactured from the stronger concrete, but also that the difference in the rate of reduction decreased with an increasing eccentricity. These trends were accurately captured by the analytical model.

Figures 4.14a and 4.14b compare the observed load-deflection curves for the columns belonging to test series I and XI to their analytical counterparts. Clearly the numerical model is capable of capturing the ascending part of the load-deflection curves satisfactorily. It is interesting that the mid-height deflection at failure appeared to be almost independent of the grade of concrete.

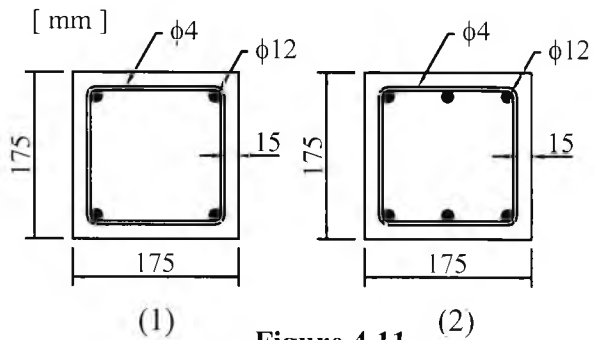

Figure 4.11
Cross-sections of columns tested by Lloyd and Rangan

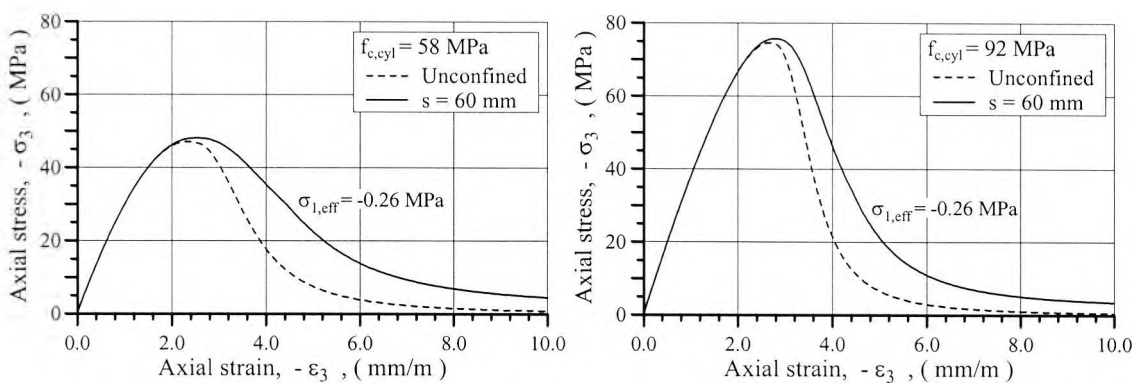

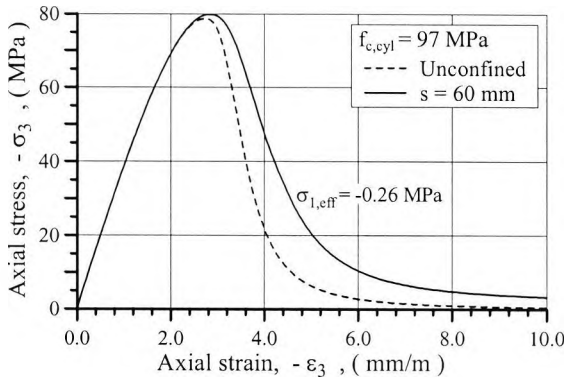

Figure 4.12
Assumed stress-strain behaviour of concretes

Table 4.2a
Details of columns tested by Lloyd and Rangan

Column		Slend.	Eccen.	Conc.	Longitudinal reinforcement		Transverse reinforcement		
ID	Sec.	L/d (-)	e_y/d (-)	$f_{c,cyl}$ (MPa)	ρ_g (%)	f_{sy} (MPa)	s (mm)	ρ_s (%)	f_{sy} (MPa)
IA	2	9.6	0.09	58	2.22	430	60	0.59	450
IB	2	9.6	0.29	58	2.22	430	60	0.59	450
IC	2	9.6	0.37	58	2.22	430	60	0.59	450
IIIA	1	9.6	0.09	58	1.47	430	60	0.59	450
IIIB	1	9.6	0.29	58	1.47	430	60	0.59	450
IIIC	1	9.6	0.37	58	1.47	430	60	0.59	450
VA	2	9.6	0.09	92	2.22	430	60	0.59	450
VB	2	9.6	0.29	92	2.22	430	60	0.59	450
VC	2	9.6	0.37	92	2.22	430	60	0.59	450
VIIA	1	9.6	0.09	92	1.47	430	60	0.59	450
VIIB	1	9.6	0.29	92	1.47	430	60	0.59	450
VIIC	1	9.6	0.37	92	1.47	430	60	0.59	450
IXA	2	9.6	0.09	97	2.22	430	60	0.59	450
IXB	2	9.6	0.29	97	2.22	430	60	0.59	450
IXC	2	9.6	0.37	97	2.22	430	60	0.59	450
XIA	1	9.6	0.09	97	1.47	430	60	0.59	450
XIB	1	9.6	0.29	97	1.47	430	60	0.59	450
XIC	1	9.6	0.37	97	1.47	430	60	0.59	450

$f_{c,cyl}$: compressive strength of 100×200 mm cylinders.

Table 4.2b
Comparison of experimental and analytical results

Column		Experimental		Analytical excl. confinement			Analytical incl. confinement		
ID	Sec.	$P_{c,e}$ (kN)	$v_{max,e}$ (mm)	$P_{c,a}$ (kN)	$v_{max,a}$ (mm)	$P_{c,e}/P_{c,a}$ (-)	$P_{c,a}$ (kN)	$v_{max,a}$ (mm)	$P_{c,e}/P_{c,a}$ (-)
IA	2	1476	8.3	1231	4.7	1.20	1237	4.8	1.19
IB	2	830	12.5	710	8.6	1.17	712	8.6	1.17
IC	2	660	13.2	581	10.3	1.14	583	10.4	1.13
IIIA	1	1140	8.8	1161	4.9	0.98	1167	4.9	0.98
IIIB	1	723	12.9	643	9.1	1.12	644	9.0	1.12
IIIC	1	511	11.7	516	11.2	0.99	515	11.1	0.99
VA	2	1704	6.2	1763	5.1	0.97	1767	5.2	0.96
VB	2	1018	9.7	964	9.5	1.06	965	9.5	1.05
VC	2	795	12.3	770	11.5	1.03	772	11.6	1.03
VIIA	1	1745	7.6	1698	5.2	1.03	1702	5.2	1.03
VIIB	1	908	11.1	888	9.8	1.02	890	9.9	1.02
VIIC	1	663	15.4	661	11.5	1.00	662	11.0	1.00
IXA	2	1975	6.4	1840	5.2	1.07	1844	5.2	1.07
IXB	2	1002	10.9	997	9.5	1.00	998	9.4	1.00
IXC	2	746	14.2	795	11.5	0.94	795	11.5	0.94
XIA	1	1932	5.6	1776	5.3	1.09	1779	5.3	1.09
XIB	1	970	10.7	925	10.0	1.05	921	10.0	1.05
XIC	1	747	13.9	679	11.8	1.10	680	11.8	1.10
				Mean		1.05			1.05
				Standard deviation		0.07			0.07

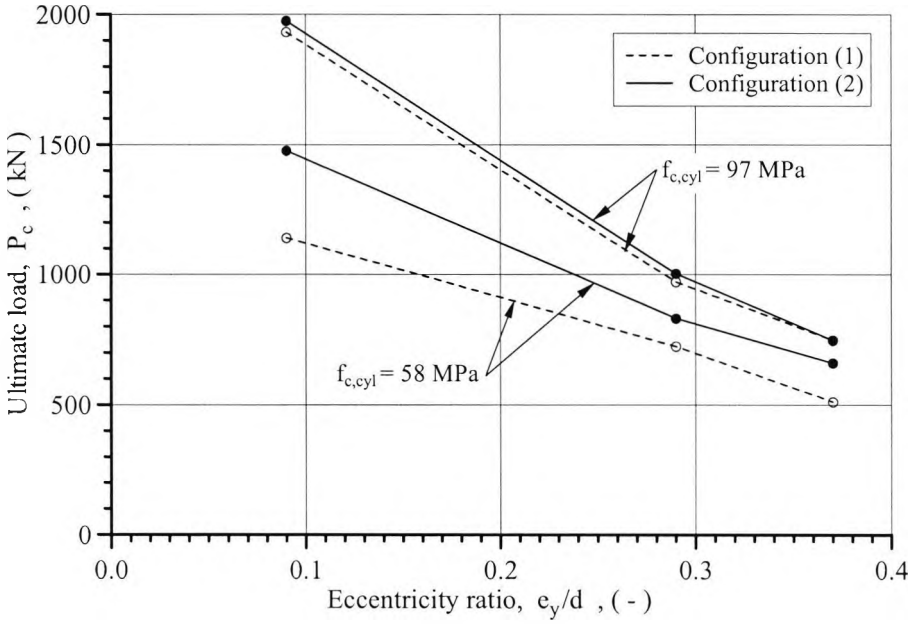

Figure 4.13
Observed effect of eccentricity on ultimate load capacity of columns in test series I, III, IX and XI

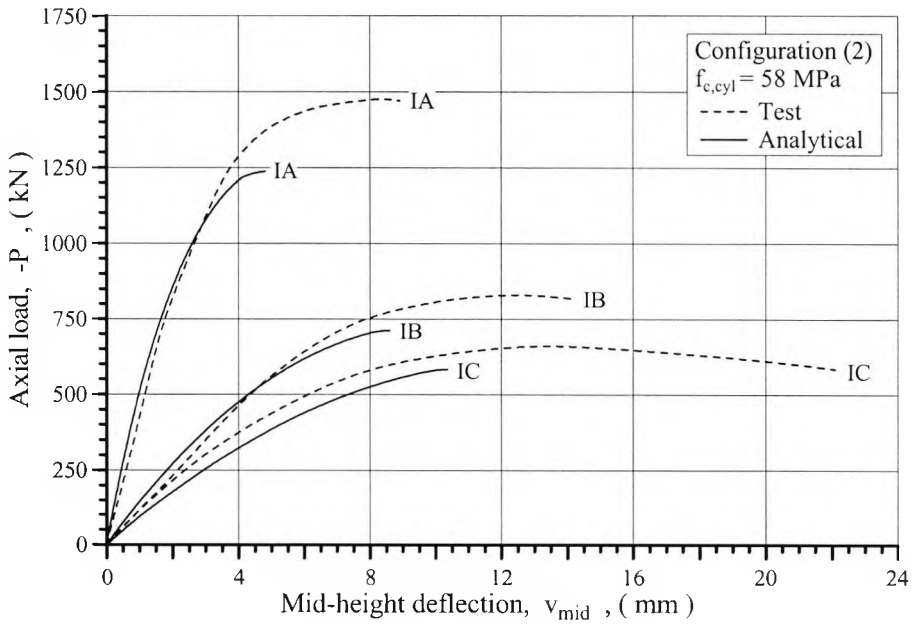

Figure 4.14a
Load-deflection curves for columns in test series I

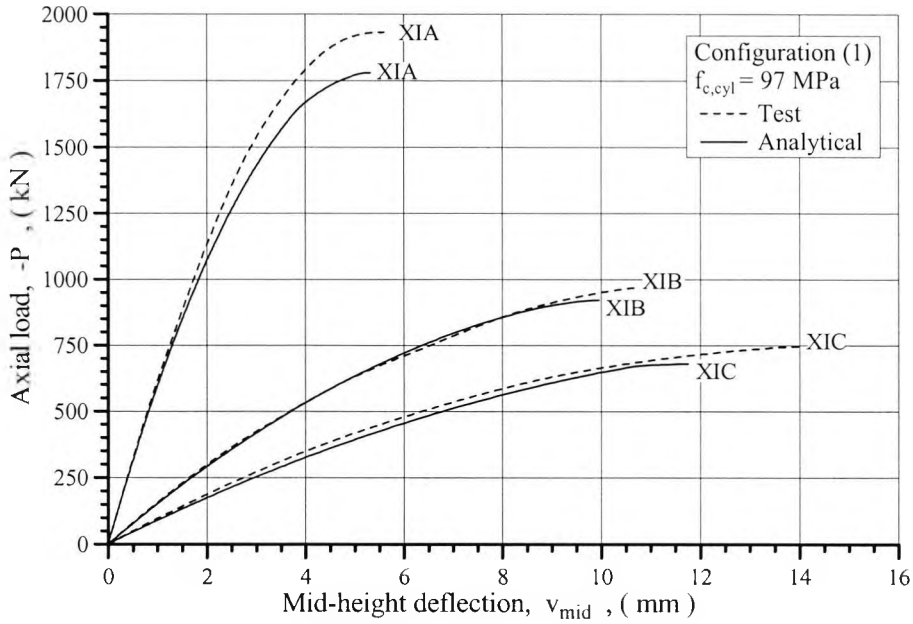

Figure 4.14b
Load-deflection curves for columns in test series XI

Foster and Attard (1997)

Figure 4.15 together with table 4.3a provide the details of fifty-four 150×150×1500 mm concrete columns tested by Foster and Attard. The test columns had a compressive cylinder strength of either 42 MPa, 74 MPa or 91 MPa; were longitudinally reinforced by either four or eight 12 mm high yield steel bars; were laterally reinforced by square hoops with spacings of either 30 mm, 60 mm or 120 mm; and were subjected to an axial load acting at an eccentricity to depth ratio of either 0.05, 0.13 or 0.33.

Figure 4.16 shows the confined and unconfined stress-strain curves generated for the three different concrete grades employed in the test programme. For the columns transversely reinforced with a tie pitch of 30 mm, the strength and peak strain of the core concrete was estimated to be raised by 9 - 10 MPa and 0.9 - 1.2 mm/m respectively. By contrast, the stress-strain behaviour of the concrete in the columns with a tie pitch of 120 mm was estimated not to be influenced by confinement.

The experimental results (see table 4.3b) show that a reduction in the tie spacings in general did not enhance the axial load capacity of the columns. For only one out of the eighteen columns manufactured from the strongest concrete, i.e. the H-series, did a reduction in the tie spacings from 120 mm to either 60 mm or 30 mm lead to a higher failure load. In the L-series four out of the twelve columns, and in the M-series five out of the twelve columns, with closer tie spacings than 120 mm, failed prematurely.

An explanation for the premature column failure frequently observed can be given by means of figure 4.17. The figure illustrates the estimated effect of the provided confinement on the interaction diagrams for the test columns transversely reinforced with tie configuration type (1). Since the confinement had an insignificant influence on the interaction diagrams, it is likely that the occurrence of premature cover spalling often reduced the load capacity of a column with a dense reinforcement cage below the capacity of a similar unconfined column. In this context, it can also be noted that the experimental results given in table 4.3b, in general, support the hypothesis stated in section 3.4.1, of both an increase in the concrete strength and in the density of the reinforcement cage having an adverse effect on the stability of the cover shell.

The experiments also show that the mid-height deflections at peak load in general increased with increasing load eccentricity, but the deflections did not appear to correlate with either the concrete strength or the tie spacings. However, a reduction in the tie spacings was reported to have the effect of increasing the post-peak ductility of the columns, and more so for the columns manufactured from the lesser grade of concrete.

Although the analytical model does not incorporate stability failure of the cover shell, it conforms well with the overall test results. The average ratio of the test failure load to

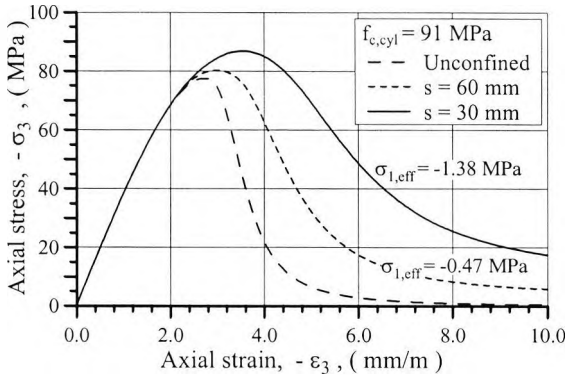

Figure 4.16
Assumed stress-strain behaviour of concretes

Table 4.3a
Details of columns tested by Foster and Attard

Column		Slend.	Eccen	Conc.	Longitudinal reinforcement		Transverse reinforcement		
ID	Sec.	L/d (-)	e_y/d (-)	$f_{c,cyl}$ (MPa)	ρ_g (%)	f_{sy} (MPa)	s (mm)	ρ_s (%)	f_{sy} (MPa)
2L8-30	1	10.0	0.05	42	2.01	480	30	3.04	360
2L8-60	1	10.0	0.05	42	2.01	480	60	1.52	360
2L8-120	1	10.0	0.05	42	2.01	480	120	0.76	360
2L20-30	1	10.0	0.13	42	2.01	480	30	3.04	360
2L20-60	1	10.0	0.13	42	2.01	480	60	1.52	360
2L20-120	1	10.0	0.13	42	2.01	480	120	0.76	360
2L50-30	1	10.0	0.33	42	2.01	480	30	3.04	360
2L50-60	1	10.0	0.33	42	2.01	480	60	1.52	360
2L50-120	1	10.0	0.33	42	2.01	480	120	0.76	360
4L8-30	2	10.0	0.05	42	4.02	480	30	3.04	360
4L8-60	2	10.0	0.05	42	4.02	480	60	1.52	360
4L8-120	2	10.0	0.05	42	4.02	480	120	0.76	360
4L20-30	2	10.0	0.13	42	4.02	480	30	3.04	360
4L20-60	2	10.0	0.13	42	4.02	480	60	1.52	360
4L20-120	2	10.0	0.13	42	4.02	480	120	0.76	360
4L50-30	2	10.0	0.33	42	4.02	480	30	3.04	360
4L50-60	2	10.0	0.33	42	4.02	480	60	1.52	360
4L50-120	2	10.0	0.33	42	4.02	480	120	0.76	360

Column		Slend.	Eccen	Conc.	Longitudinal reinforcement		Transverse reinforcement		
ID	Sec.	L/d (-)	e_y/d (-)	$f_{c,cyl}$ (MPa)	ρ_g (%)	f_{sy} (MPa)	s (mm)	ρ_s (%)	f_{sy} (MPa)
2M8-30	1	10.0	0.05	74	2.01	480	30	3.04	360
2M8-60	1	10.0	0.05	74	2.01	480	60	1.52	360
2M8-120	1	10.0	0.05	74	2.01	480	120	0.76	360
2M20-30	1	10.0	0.13	74	2.01	480	30	3.04	360
2M20-60	1	10.0	0.13	74	2.01	480	60	1.52	360
2M20-120	1	10.0	0.13	74	2.01	480	120	0.76	360
2M50-30	1	10.0	0.33	74	2.01	480	30	3.04	360
2M50-60	1	10.0	0.33	74	2.01	480	60	1.52	360
2M50-120	1	10.0	0.33	74	2.01	480	120	0.76	360
4M8-30	2	10.0	0.05	74	4.02	480	30	3.04	360
4M8-60	2	10.0	0.05	74	4.02	480	60	1.52	360
4M8-120	2	10.0	0.05	74	4.02	480	120	0.76	360
4M20-30	2	10.0	0.13	74	4.02	480	30	3.04	360
4M20-60	2	10.0	0.13	74	4.02	480	60	1.52	360
4M20-120	2	10.0	0.13	74	4.02	480	120	0.76	360
4M50-30	2	10.0	0.33	74	4.02	480	30	3.04	360
4M50-60	2	10.0	0.33	74	4.02	480	60	1.52	360
4M50-120	2	10.0	0.33	74	4.02	480	120	0.76	360
2H8-30	1	10.0	0.05	91	2.01	480	30	3.04	360
2H8-60	1	10.0	0.05	91	2.01	480	60	1.52	360
2H8-120	1	10.0	0.05	91	2.01	480	120	0.76	360
2H20-30	1	10.0	0.13	91	2.01	480	30	3.04	360
2H20-60	1	10.0	0.13	91	2.01	480	60	1.52	360
2H20-120	1	10.0	0.13	91	2.01	480	120	0.76	360
2H50-30	1	10.0	0.33	91	2.01	480	30	3.04	360
2H50-60	1	10.0	0.33	91	2.01	480	60	1.52	360
2H50-120	1	10.0	0.33	91	2.01	480	120	0.76	360
4H8-30	2	10.0	0.05	91	4.02	480	30	3.04	360
4H8-60	2	10.0	0.05	91	4.02	480	60	1.52	360
4H8-120	2	10.0	0.05	91	4.02	480	120	0.76	360

analytical failure load was 1.10, with a standard deviation of 0.11.

Figure 4.18 shows the computed enhancement in ultimate load due to confinement for the test columns with 30 mm spaced ties of configuration type (1). It can be seen that the difference between the load capacity of a confined and a similar unconfined column is reduced with increasing eccentricity, and that the efficiency of the given tie arrangement is reduced with increasing concrete strength. However, as illustrated by figure 4.19, the latter trend is not a general column feature. If the same columns are analysed under the assumption of having no concrete cover whatsoever, the columns manufactured from the stronger concrete gain more strength at low levels of eccentricity than the columns manufactured from the less strong concrete.

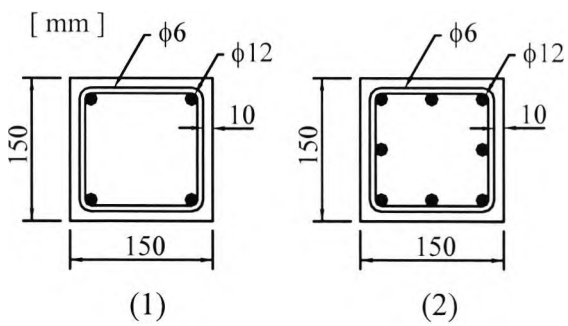

Figure 4.15
Cross-sections of columns tested by Foster and Attard

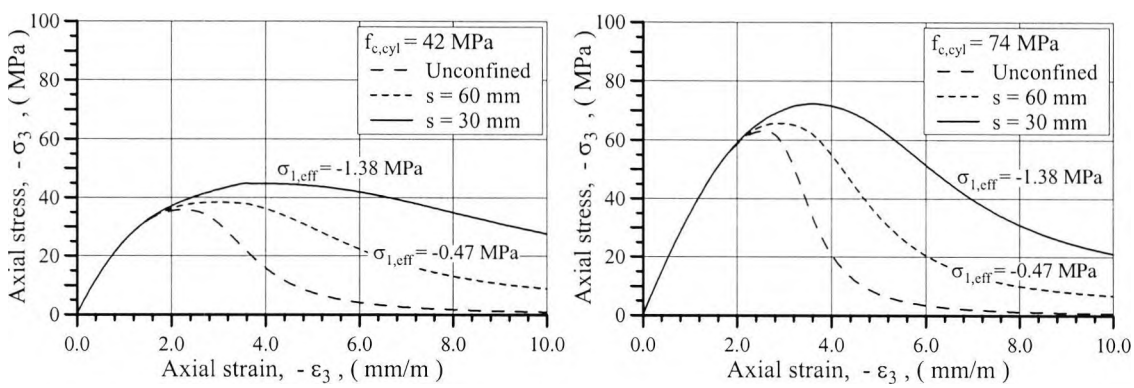

Column		Slend.	Eccen	Conc.	Longitudinal reinforcement		Transverse reinforcement		
ID	Sec.	L/d (-)	e_y/d (-)	$f_{c,cyl}$ (MPa)	ρ_g (%)	f_{sy} (MPa)	s (mm)	ρ_s (%)	f_{sy} (MPa)
4H20-30	2	10.0	0.13	91	4.02	480	30	3.04	360
4H20-60	2	10.0	0.13	91	4.02	480	60	1.52	360
4H20-120	2	10.0	0.13	91	4.02	480	120	0.76	360
4H50-30	2	10.0	0.33	91	4.02	480	30	3.04	360
4H50-60	2	10.0	0.33	91	4.02	480	60	1.52	360
4H50-120	2	10.0	0.33	91	4.02	480	120	0.76	360

$f_{c,cyl}$: compressive strength of 150×300 mm cylinders.

Table 4.3b
Comparison of experimental and analytical results

Column		Experimental		Analytical excl. confinement			Analytical incl. confinement		
ID	Sec.	$P_{c,e}$ (kN)	$v_{max,e}$ (mm)	$P_{c,a}$ (kN)	$v_{max,a}$ (mm)	$P_{c,e}/P_{c,a}$ (-)	$P_{c,a}$ (kN)	$v_{max,a}$ (mm)	$P_{c,e}/P_{c,a}$ (-)
2L8-30	1	960	6.5	821	3.6	1.17	850	3.8	1.13
2L8-60	1	857	4.0	821	3.6	1.04	835	3.7	1.03
2L8-120	1	912	6.0	821	3.6	1.11	821	3.6	1.11
2L20-30	1	750	4.8	657	5.3	1.14	676	5.6	1.11
2L20-60	1	700	6.2	657	5.3	1.07	666	5.4	1.05
2L20-120	1	782	5.5	657	5.3	1.19	657	5.3	1.19
2L50-30	1	440	9.0	389	9.2	1.13	398	9.4	1.11
2L50-60	1	472	8.5	389	9.2	1.21	393	9.3	1.20
2L50-120	1	440	9.0	389	9.2	1.13	389	9.2	1.13
4L8-30	2	1100	9.0	963	3.6	1.14	993	3.9	1.11
4L8-60	2	1150	6.0	963	3.6	1.19	977	3.7	1.18
4L8-120	2	975	5.7	963	3.6	1.01	963	3.6	1.01
4L20-30	2	1020	7.0	760	5.4	1.34	781	5.7	1.31
4L20-60	2	968	3.5	760	5.4	1.27	770	5.6	1.26
4L20-120	2	900	4.0	760	5.4	1.18	760	5.4	1.18
4L50-30	2	517	18.5	456	8.9	1.13	466	9.3	1.11
4L50-60	2	550	8.0	456	8.9	1.21	461	9.0	1.19
4L50-120	2	525	8.0	456	8.9	1.15	456	8.9	1.15

Column		Experimental		Analytical excl. confinement			Analytical incl. confinement		
ID	Sec.	$P_{c,e}$ (kN)	$v_{max,e}$ (mm)	$P_{c,a}$ (kN)	$v_{max,a}$ (mm)	$P_{c,e}/P_{c,a}$ (-)	$P_{c,a}$ (kN)	$v_{max,a}$ (mm)	$P_{c,e}/P_{c,a}$ (-)
2M8-30	1	1348	5.0	1286	3.6	1.05	1309	3.8	1.03
2M8-60	1	1432	5.0	1286	3.6	1.11	1296	3.7	1.10
2M8-120	1	1239	4.0	1286	3.6	0.96	1286	3.6	0.96
2M20-30	1	1160	6.0	1004	5.4	1.16	1018	5.7	1.14
2M20-60	1	1231	6.0	1004	5.4	1.23	1011	5.6	1.22
2M20-120	1	1067	5.0	1004	5.4	1.06	1004	5.4	1.06
2M50-30	1	630	9.5	553	9.9	1.14	557	10.0	1.13
2M50-60	1	747	11.5	553	9.9	1.35	555	9.9	1.35
2M50-120	1	652	11.5	553	9.9	1.18	553	9.9	1.18
4M8-30	2	1102	3.0	1423	3.6	0.77	1446	3.8	0.76
4M8-60	2	1404	4.0	1423	3.6	0.99	1434	3.7	0.98
4M8-120	2	1404	3.5	1423	3.6	0.99	1423	3.6	0.99
4M20-30	2	1052	4.0	1103	5.5	0.95	1117	5.7	0.94
4M20-60	2	1004	5.0	1103	5.5	0.91	1110	5.6	0.90
4M20-120	2	1226	5.0	1103	5.5	1.11	1103	5.5	1.11
4M50-30	2	656	9.5	625	9.5	1.05	630	9.5	1.04
4M50-60	2	686	9.5	625	9.5	1.10	627	9.5	1.09
4M50-120	2	677	9.5	625	9.5	1.08	625	9.5	1.08
2H8-30	1	1576	3.5	1524	3.7	1.03	1544	3.8	1.02
2H8-60	1	1647	4.5	1524	3.7	1.08	1533	3.8	1.07
2H8-120	1	1806	3.6	1524	3.7	1.19	1524	3.7	1.19
2H20-30	1	1207	6.5	1177	5.6	1.03	1189	5.7	1.02
2H20-60	1	1247	5.3	1177	5.6	1.06	1183	5.7	1.05
2H20-120	1	1473	5.6	1177	5.6	1.25	1177	5.6	1.25
2H50-30	1	749	9.7	631	10.3	1.19	635	10.6	1.18
2H50-60	1	685	10.0	631	10.3	1.09	631	10.2	1.09
2H50-120	1	851	8.3	631	10.3	1.35	631	10.3	1.35
4H8-30	2	1601	4.8	1659	3.8	0.97	1679	3.9	0.95
4H8-60	2	1702	5.5	1659	3.8	1.03	1668	3.8	1.02
4H8-120	2	1654	4.2	1659	3.8	1.00	1659	3.8	1.00

Column		Experimental		Analytical excl. confinement			Analytical incl. confinement		
ID	Sec.	$P_{c,e}$ (kN)	$v_{max,e}$ (mm)	$P_{c,a}$ (kN)	$v_{max,a}$ (mm)	$P_{c,e}/P_{c,a}$ (-)	$P_{c,a}$ (kN)	$v_{max,a}$ (mm)	$P_{c,e}/P_{c,a}$ (-)
4H20-30	2	1352	7.0	1274	5.7	1.06	1285	5.8	1.05
4H20-60	2	1358	7.5	1274	5.7	1.07	1279	5.7	1.06
4H20-120	2	1374	7.0	1274	5.7	1.08	1274	5.7	1.08
4H50-30	2	780	10.5	706	9.8	1.10	709	9.8	1.10
4H50-60	2	790	9.5	706	9.8	1.12	707	9.8	1.12
4H50-120	2	818	9.5	706	9.8	1.16	706	9.8	1.16
				Mean		1.11			1.10
				Standard deviation		0.11			0.11

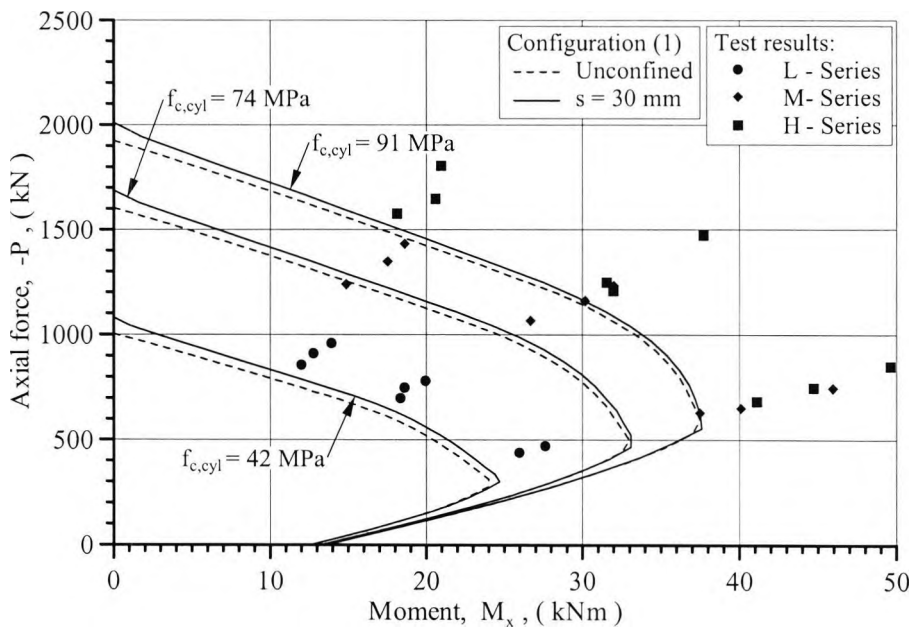

Figure 4.17
Computed influence of confinement on interaction diagrams

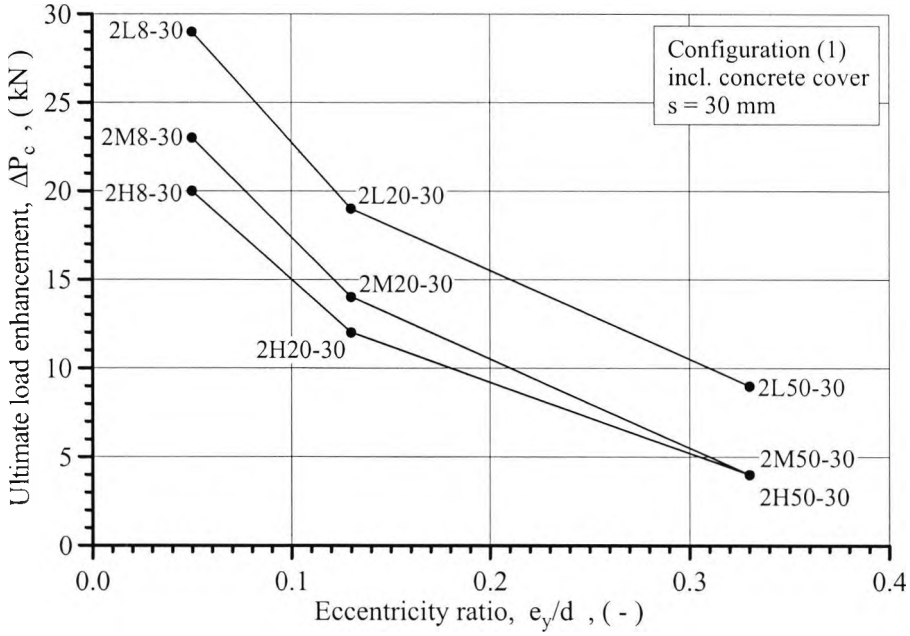

Figure 4.18
Computed increase in axial load capacity due to confinement

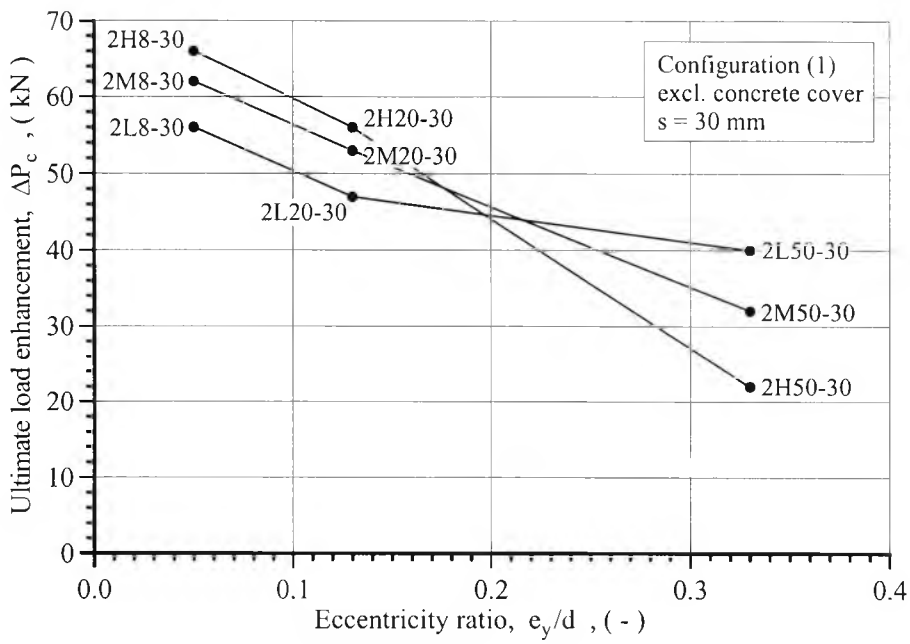

Figure 4.19
Computed increase in axial load capacity due to confinement when ignoring the presence of the concrete cover

Claeson and Gylltoft (1998)

Claeson and Gylltoft tested four columns of each of the three dimensions 120×120×2400 mm, 200×200×3000 mm and 200×200×4000 mm. For each dimension, two of the columns were manufactured from concrete with a cylinder strength of about 38 MPa, and two from concrete with a cylinder strength of about 90 MPa. The columns with the smaller cross-section were transversely reinforced with tie spacings of either 100 mm or 180 mm, and the columns with the larger cross-section with tie spacings of either 130 mm or 240 mm. The eccentricity of the applied axial load was a constant 20 mm throughout the experimental programme. The further details of the test columns are given in figure 4.20 and table 4.4a.

Figure 4.21 shows that only in the case of the test columns 27, 29, 31 and 33 was the transverse reinforcement estimated to have an effect on the stress-strain behaviour of the core concrete. However, as illustrated by figure 4.22, the provided reinforcement was insufficient to significantly affect the ascending part of the load-deflection diagram of the columns. In contrast, the descending part of the load-deflection diagrams was in general observed to become more ductile with increased confinement, and this being most noticeable for the columns manufactured from the lower concrete grade.

As expected, an increase in the column's geometric slenderness ratio from 15 to 20 reduced the failure load, and increased the mid-height deflection at failure. Figure 4.23 shows both the experimental and calculated relationships between the slenderness ratio and the axial load capacity for the test columns with the larger cross-section. It can be seen that the high strength concrete columns always failed at a significantly higher load than the normal strength concrete columns, but also that the difference in the failure loads reduced with increasing slenderness. The average ratio of the test failure load to the calculated failure load was 1.07, with a standard deviation of 0.10.

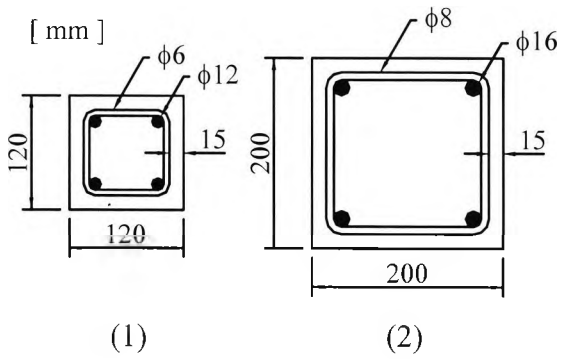

Figure 4.20
Cross-sections of columns tested by Claeson and Gylltoft

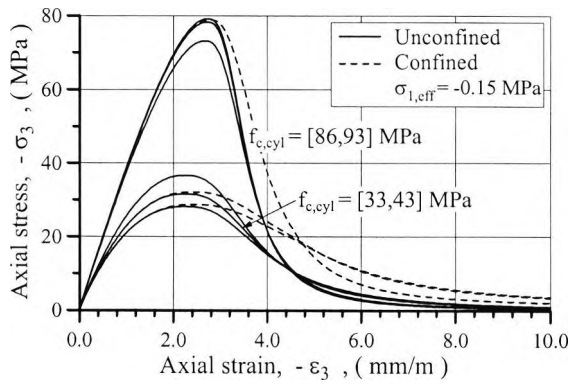

Figure 4.21
Assumed stress-strain behaviour of concretes

Table 4.4a
Details of columns tested by Claeson and Gylltoft

Column		Slend.	Eccen.	Conc.	Longitudinal reinforcement		Transverse reinforcement		
ID	Sec.	L/d (-)	e_y/d (-)	$f_{c,cyl}$ (MPa)	ρ_g (%)	f_{sy} (MPa)	s (mm)	ρ_s (%)	f_{sy} (MPa)
23	1	20.0	0.17	43	3.14	684	100	1.35	512
24	1	20.0	0.17	43	3.14	684	180	0.75	512
25	1	20.0	0.17	86	3.14	684	100	1.35	512
26	1	20.0	0.17	86	3.14	684	180	0.75	512
27	2	15.0	0.10	33	2.01	636	130	0.95	466
28	2	15.0	0.10	33	2.01	636	240	0.52	466

Column		Slend.	Eccen.	Conc.	Longitudinal reinforcement		Transverse reinforcement		
ID	Sec.	L/d (-)	e_y/d (-)	$f_{c,cyl}$ (MPa)	ρ_g (%)	f_{sy} (MPa)	s (mm)	ρ_s (%)	f_{sy} (MPa)
29	2	15.0	0.10	92	2.01	636	130	0.95	466
30	2	15.0	0.10	92	2.01	636	240	0.52	466
31	2	20.0	0.10	37	2.01	636	130	0.95	466
32	2	20.0	0.10	37	2.01	636	240	0.52	466
33	2	20.0	0.10	93	2.01	636	130	0.95	466
34	2	20.0	0.10	93	2.01	636	240	0.52	466

$f_{c,cyl}$: compressive strength of 150×300 mm cylinders.

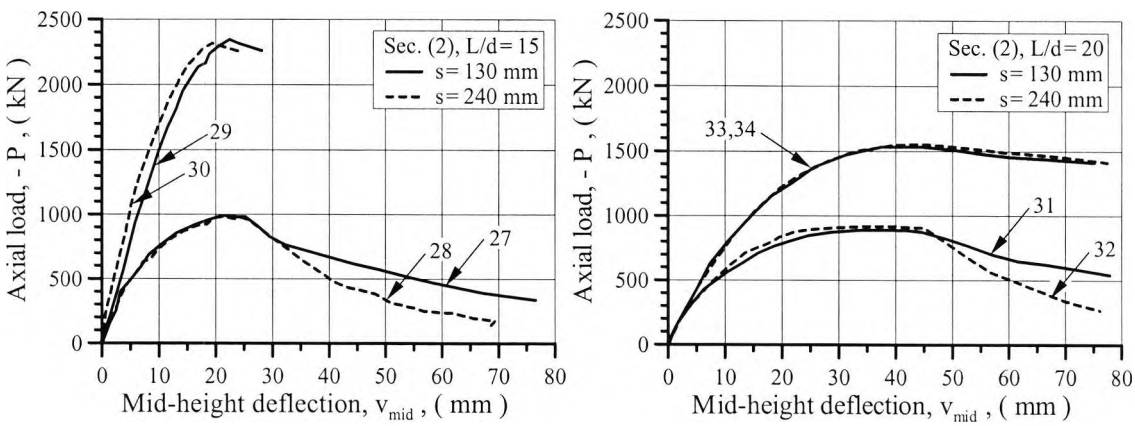

Figure 4.22
Observed load-deflection curves for columns with type 2 cross-section

Table 4.4b
Comparison of experimental and analytical results

Column		Experimental		Analytical excl. confinement			Analytical incl. confinement		
ID	Sec.	$P_{c,e}$ (kN)	$v_{max,e}$ (mm)	$P_{c,a}$ (kN)	$v_{max,a}$ (mm)	$P_{c,e}/P_{c,a}$ (-)	$P_{c,a}$ (kN)	$v_{max,a}$ (mm)	$P_{c,e}/P_{c,a}$ (-)
23	1	320	26.0	258	19.7	1.24	-	-	-
24	1	280	24.0	258	19.7	1.09	-	-	-
25	1	370	36.0	385	21.3	0.96	-	-	-
26	1	330	47.0	385	21.3	0.86	-	-	-
27	2	990	22.0	924	17.3	1.07	929	17.7	1.07
28	2	990	21.0	924	17.3	1.07	-	-	-

Column		Experimental		Analytical excl. confinement			Analytical incl. confinement		
ID	Sec.	$P_{c,e}$ (kN)	$v_{max,e}$ (mm)	$P_{c,a}$ (kN)	$v_{max,a}$ (mm)	$P_{c,e}/P_{c,a}$ (-)	$P_{c,a}$ (kN)	$v_{max,a}$ (mm)	$P_{c,e}/P_{c,a}$ (-)
29	2	2310	23.0	1995	16.9	1.16	1997	16.8	1.16
30	2	2350	20.0	1995	16.9	1.18	-	-	-
31	2	900	40.0	829	26.7	1.09	830	26.5	1.08
32	2	920	36.0	829	26.7	1.11	-	-	-
33	2	1530	39.0	1565	29.4	0.98	1565	28.9	0.98
34	2	1560	41.0	1565	29.4	1.00	-	-	-
				Mean		1.07			-
				Standard deviation		0.10			-

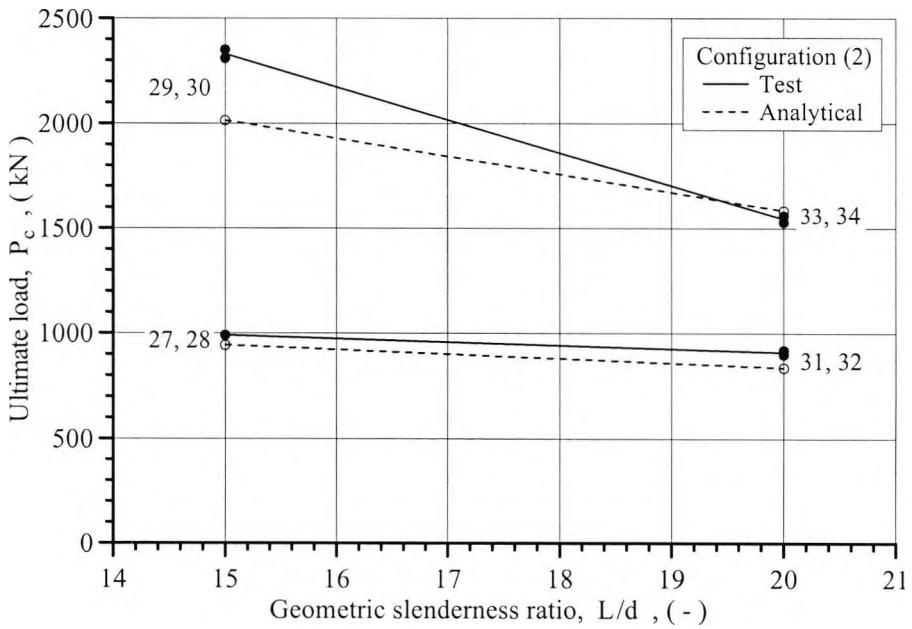

Figure 4.23
Influence of slenderness on ultimate load

Kim and Yang (1995)

Kim and Yang investigated the effects of slenderness, concrete strength and longitudinal steel ratio on the structural behaviour of reinforced concrete columns. The tested columns had a geometric slenderness ratio of either 3.0, 18.0 or 30.0; a concrete cylinder strength of either 26 MPa, 64 MPa or 86 MPa; and a longitudinal steel ratio of either 1.98% or 3.96%. The columns were all subjected to an axial load acting at a constant eccentricity of 24 mm. The further details of the tested columns are given in figure 4.24 and table 4.5a.

Because of the relatively large tie spacings, none of the tested columns was estimated to have benefited from passive confinement. Thus the analytical results listed in table 4.5b were all based on the stress-strain curves for unconfined concrete shown in figure 4.25.

The test results confirm that the axial load capacity of a column is reduced, and its lateral deflections increased, with an increase in the geometric slenderness ratio. Furthermore, as illustrated by figure 4.26, the reduction in load capacity with increasing slenderness is larger for the high strength concrete columns than for the normal strength concrete columns, so that for a geometric slenderness ratio of 30, the axial load capacity becomes almost independent of the concrete strength. Thus, the structural benefits of high strength concrete are significant in the short but not in the very slender columns. The average ratio of the test failure load to the calculated failure load was determined to be 1.07 with a standard deviation of 0.12.

Figure 4.27 plots the calculated combinations of axial load and bending moment at failure for the test columns with four longitudinal reinforcement bars. When compared to the interaction diagrams it can be seen that material strength rather than stability governed the failure mode of these test columns.

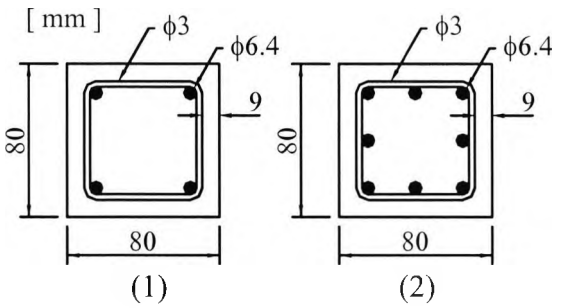

Figure 4.24
Cross-sections of columns tested by Kim and Yang

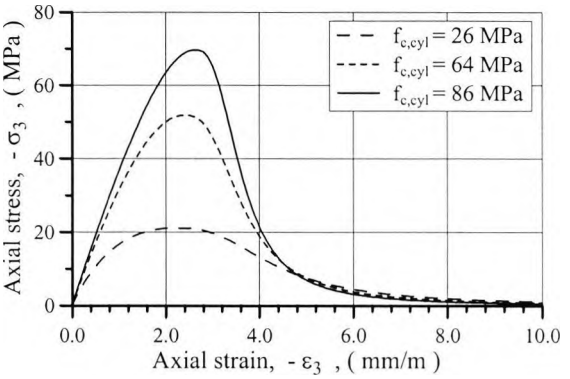

Figure 4.25
Assumed stress-strain behaviour of concretes

Table 4.5a
Details of columns tested by Kim and Yang

Column		Slend.	Eccen.	Conc.	Longitudinal reinforcement		Transverse reinforcement		
ID	Sec.	L/d (-)	e_y/d (-)	$f_{c,cyl}$ (MPa)	ρ_g (%)	f_{sy} (MPa)	s (mm)	ρ_s (%)	f_{sy} (MPa)
10L2	1	3.0	0.30	26	1.98	387	60	0.80	250
10L4	2	3.0	0.30	26	3.96	387	60	0.80	250
60L2	1	18.0	0.30	26	1.98	387	60	0.80	250
100L2	1	30.0	0.30	26	1.98	387	60	0.80	250
100L4	2	30.0	0.30	26	3.96	387	60	0.80	250
10M2	1	3.0	0.30	64	1.98	387	60	0.80	250
10M4	2	3.0	0.30	64	3.96	387	60	0.80	250
60M2	1	18.0	0.30	64	1.98	387	60	0.80	250
100M2	1	30.0	0.30	64	1.98	387	60	0.80	250
100M4	2	30.0	0.30	64	3.96	387	60	0.80	250

Column		Slend.	Eccen.	Conc.	Longitudinal reinforcement		Transverse reinforcement		
ID	Sec.	L/d (-)	e_y/d (-)	$f_{c,cyl}$ (MPa)	ρ_g (%)	f_{sy} (MPa)	s (mm)	ρ_s (%)	f_{sy} (MPa)
10H2	1	3.0	0.30	86	1.98	387	60	0.80	250
10H4	2	3.0	0.30	86	3.96	387	60	0.80	250
60H2	1	18.0	0.30	86	1.98	387	60	0.80	250
100H2	1	30.0	0.30	86	1.98	387	60	0.80	250
100H4	2	30.0	0.30	86	3.96	387	60	0.80	250

$f_{c,cyl}$: compressive strength of 100×200 mm cylinders.

Table 4.5b
Comparison of experimental and analytical results

Column		Experimental		Analytical excl. confinement			Analytical incl. confinement		
ID	Sec.	$P_{c,e}$ (kN)	$v_{max,e}$ (mm)	$P_{c,a}$ (kN)	$v_{max,a}$ (mm)	$P_{c,e}/P_{c,a}$ (-)	$P_{c,a}$ (kN)	$v_{max,a}$ (mm)	$P_{c,e}/P_{c,a}$ (-)
10L2	1	83	0.4	85	0.4	0.98	-	-	-
10L4	2	109	0.4	102	0.4	1.07	-	-	-
60L2	1	65	15.5	60	15.3	1.08	-	-	-
100L2	1	37	31.3	35	37.5	1.06	-	-	-
100L4	2	48	37.2	44	42.4	1.09	-	-	-
10M2	1	181	0.4	158	0.4	1.15	-	-	-
10M4	2	206	0.4	175	0.4	1.18	-	-	-
60M2	1	108	19.2	95	15.2	1.14	-	-	-
100M2	1	46	26.7	47	32.7	0.98	-	-	-
100M4	2	60	32.7	74	59.0	0.81	-	-	-
10H2	1	238	0.5	200	0.4	1.19	-	-	-
10H4	2	257	0.5	215	0.4	1.20	-	-	-
60H2	1	123	16.1	108	15.0	1.14	-	-	-
100H2	1	55	24.0	51	31.8	1.08	-	-	-
100H4	2	66	32.9	80	51.2	0.83	-	-	-
				Mean		1.07			-
				Standard deviation		0.12			-

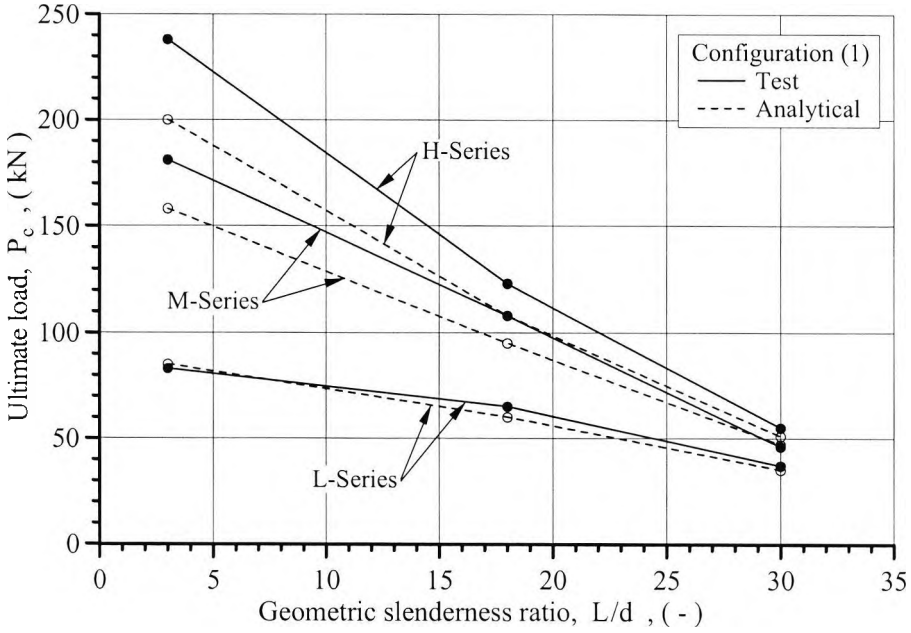

Figure 4.26
Influence of slenderness ratio on ultimate load

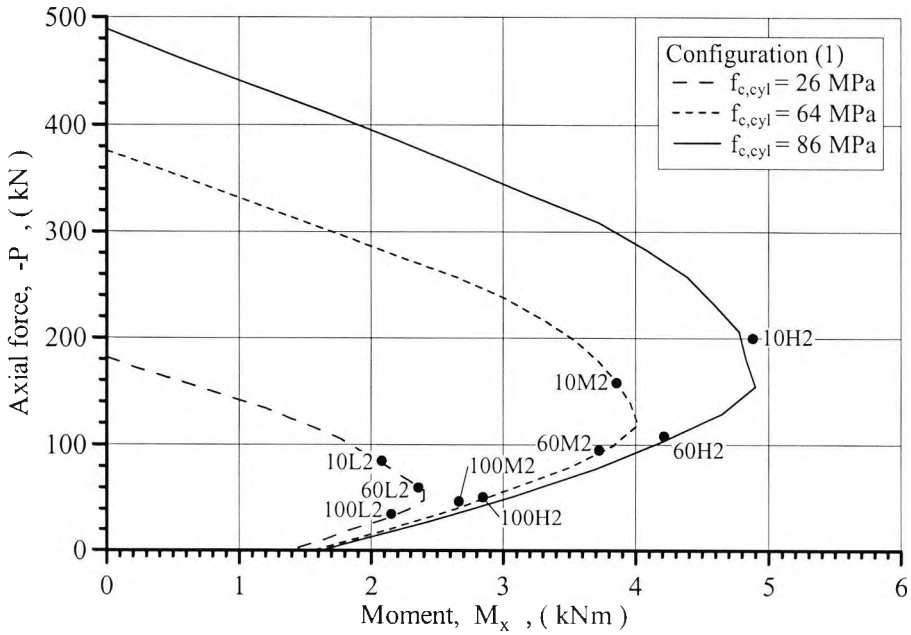

Figure 4.27
Computed interaction diagrams and failure combinations

4.3.2 Concrete Columns Failing in biaxial Bending

Test data on reinforced concrete columns failing in biaxial bending are in general very scarce, and none of the data is produced with the objective of systematically exploring the structural effect of confining reinforcement.

The ability of the numerical model to simulate the biaxial load-deflection response of eccentrically loaded concrete columns was validated against the test results reported by Cranston and Sturrock (1971) and Wang and Hsu (1992). Since none of the reviewed test columns were estimated to have benefited from passive confinement, the cover concrete did not require separate modelling. The cross-section of each test column was represented by a 6×6 mesh of equal sized rectangular elements together with a number of embedded point elements (see figure 4.28). Numerical convergence in the deflections was obtained by dividing each column into 16 segments along its length.

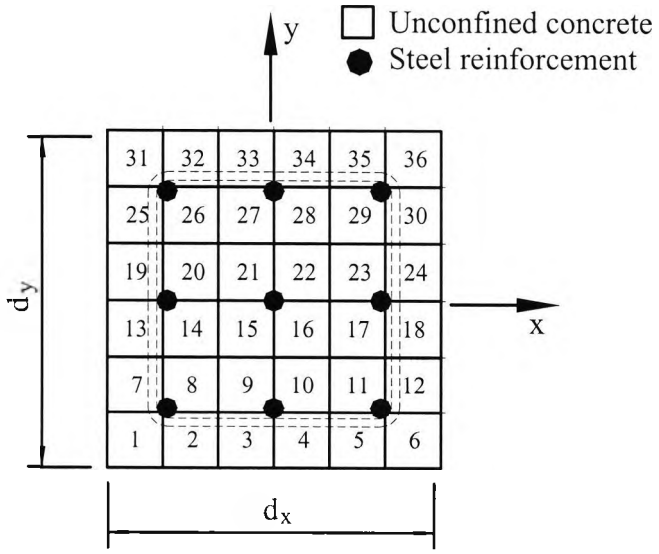

Figure 4.28
Modelling of cross-sections of biaxially bent columns

Cranston and Sturrock (1971)

Cranston and Sturrock investigated the possible interaction between major and minor axis buckling of slender columns having a narrow rectangular cross-section. The details of the five test columns are given by figure 4.29 together with table 4.6a. Even though the columns were subjected to eccentric loading about the major axis only, they all eventually failed by buckling about the minor axis.

Figure 4.30 shows the computed stress-strain curves for the various concrete grades employed in the test programme.

It can be seen from table 4.6b that the ensuing analytical results for the columns, though always somewhat conservative, correlate reasonably well with the test results. In order to numerically trigger buckling about the minor axis, the columns were all assumed to have a small mid-height imperfection of 1 mm.

Figure 4.31 compares the calculated and the observed biaxial load-deflection response at mid-height of test column 3. The response is characterised by an almost linear increase in the major axis deflections, and an accelerating increase in the minor axis deflections. In this context, it can be noticed that in the vicinity of failure the minor axis deflections are computed to exceed the major axis deflections. Furthermore, the loss of stiffness associated with major axis bending caused the column's failure load to be reduced far below the failure loads calculated under the condition of the column being restrained so as to deflect in a single direction only.

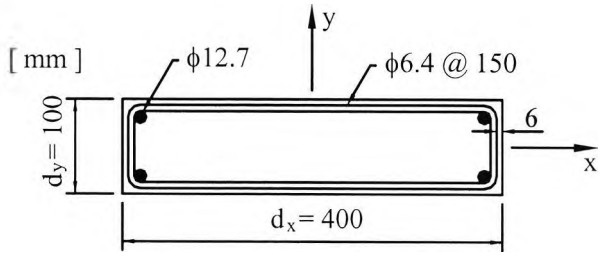

Figure 4.29
Cross-section of columns tested by Cranston and Sturrock

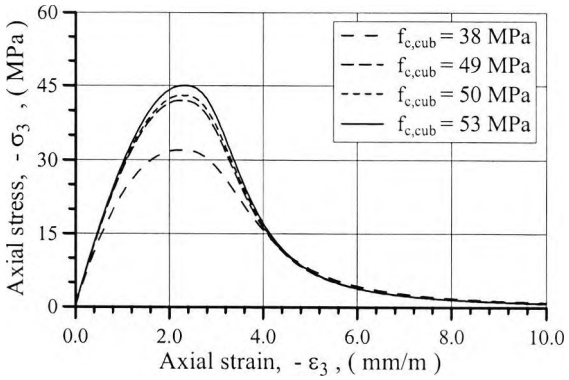

Figure 4.30
Assumed stress-strain behaviour of concretes

Table 4.6a
Details of columns tested by Cranston and Sturrock

Column	Slend.		Eccen.	Conc.	Longitudinal reinforcement		Transverse reinforcement		
ID	L/d_x (-)	L/d_y (-)	e_x/d_x (-)	$f_{c,cyl}$ (MPa)	ρ_g (%)	f_{sy} (MPa)	s (mm)	ρ_s (%)	f_{sy} (MPa)
3	12.5	50.0	0.39	49	1.27	296	150	0.64	296
4	12.5	50.0	0.25	50	1.27	437	150	0.64	437
5	12.5	50.0	0.30	49	1.27	437	150	0.64	437
6	12.5	50.0	0.39	38	1.27	437	150	0.64	437
7	12.5	50.0	0.34	53	1.27	437	150	0.64	437

$f_{c,cub}$: compressive strength of 150 mm cubes.

Table 4.6b
Comparison of experimental and analytical results

Column	Experimental			Analytical excl. confinement			
ID	$P_{c,e}$ (kN)	$u_{max,e}$* (mm)	$v_{max,e}$* (mm)	$P_{c,a}$ (kN)	$u_{max,a}$ (mm)	$v_{max,a}$ (mm)	$P_{c,e}/P_{c,a}$ (-)
3	276	9.4	5.0	233	9.6	14.0	1.18
4	456	8.4	4.9	327	6.5	9.6	1.39
5	344	7.8	6.8	281	7.6	11.8	1.22
6	320	12.1	1.9	209	9.3	13.0	1.53
7	376	9.6	4.7	263	8.5	13.2	1.43
					Mean		1.35
					Standard deviation		0.15

* last recording taken at approximately 90% of the ultimate load

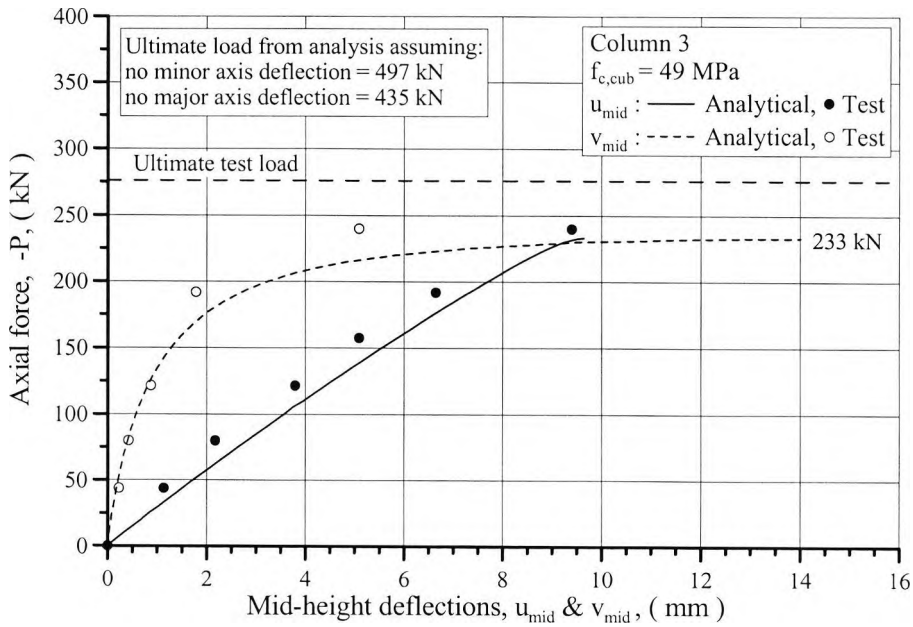

Figure 4.31
Load-deflection curves for test column 3

Wang and Hsu (1992)

Figure 4.32 and table 4.7a provide the details, taken after (Wang, 1992), of six reinforced concrete columns tested under various biaxial loading conditions by Hsu (1974).

When assuming that the stress-strain behaviour of the concrete can be represented by the curve given in figure 4.33, the strength data calculated for the columns are in good agreement with the experimental results (see table 4.7b).

Figures 4.34a and 4.34b compare the computed and observed biaxial moment-curvature relationships for column U-5. For reasons of clarity, the experimental results are plotted as discrete points in the figures. It should be emphasised that the numerical model is unable to predict post-peak behaviour.

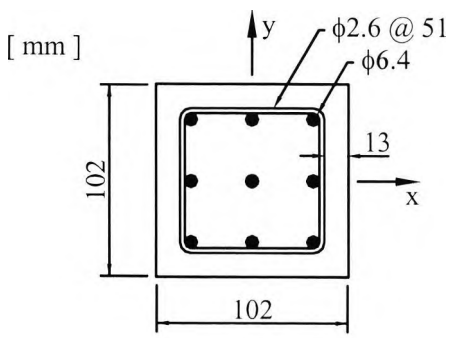

Figure 4.32
Cross-section of columns tested by Hsu

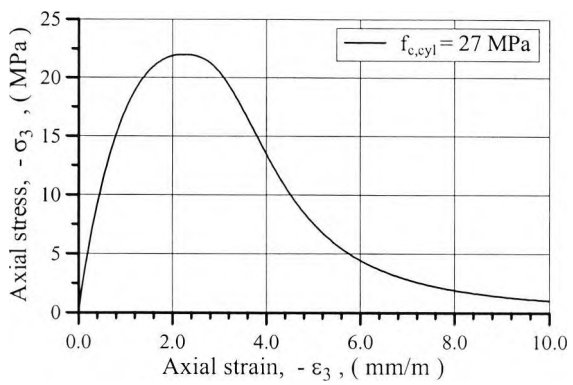

Figure 4.33
Assumed stress-strain behaviour of concrete

Table 4.7a
Details of columns tested by Hsu

Column	Slend.	Eccen.		Conc.	Longitudinal reinforcement		Transverse reinforcement		
ID	L/d (-)	e_x/d (-)	e_y/d (-)	$f_{c,cyl}$ (MPa)	ρ_g (%)	f_{sy} (MPa)	s (mm)	ρ_s (%)	f_{sy} (MPa)
U-1	10.0	0.63	0.88	27	2.78	503	51	0.57	-
U-2	10.0	0.75	0.88	27	2.78	503	51	0.57	-
U-3	10.0	0.88	0.88	27	2.78	503	51	0.57	-
U-4	10.0	0.50	0.50	27	2.78	503	51	0.57	-
U-5	10.0	0.13	1.00	27	2.78	503	51	0.57	-
U-6	10.0	0.13	1.75	27	2.78	503	51	0.57	-

$f_{c,cyl}$: compressive strength of 76×150 mm cylinders.

Table 4.7b
Comparison of experimental and analytical results

Column	Experimental			Analytical excl. confinement			
ID	$P_{c,e}$ (kN)	$u_{max,e}$ (mm)	$v_{max,e}$ (mm)	$P_{c,a}$ (kN)	$u_{max,a}$ (mm)	$v_{max,a}$ (mm)	$P_{c,e}/P_{c,a}$ (-)
U-1	43	-	-	40	5.3	7.0	1.08
U-2	39	-	-	37	5.8	6.6	1.05
U-3	36	8.1	8.1	35	6.3	6.3	1.03
U-4	64	8.4	8.4	58	4.9	4.9	1.10
U-5	48	1.8	13.9	47	1.6	9.3	1.02
U-6	28	1.3	16.2	27	1.0	11.6	1.04
					Mean		1.05
					Standard deviation		0.03

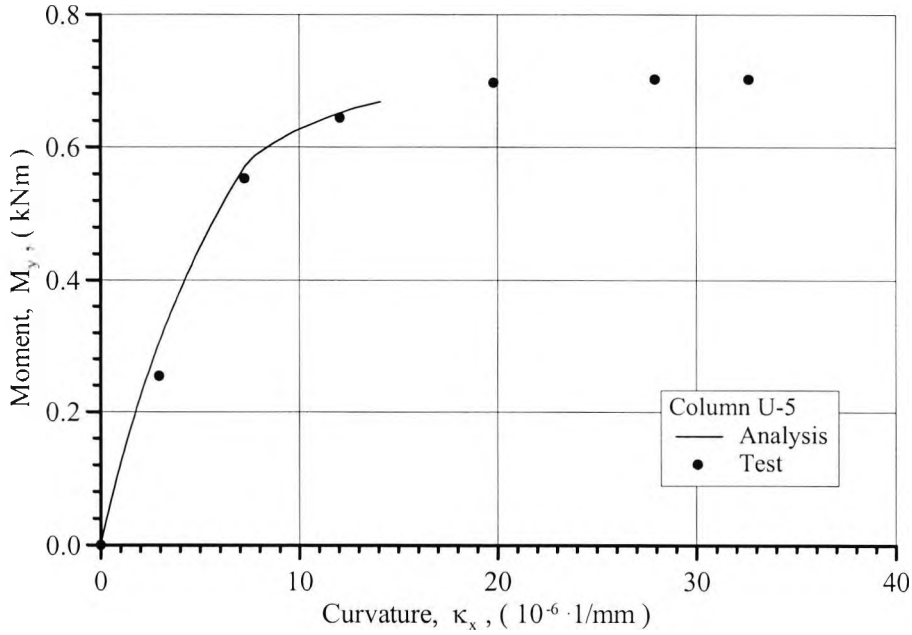

Figure 4.34a
Biaxial moment curvature relations for column U-5

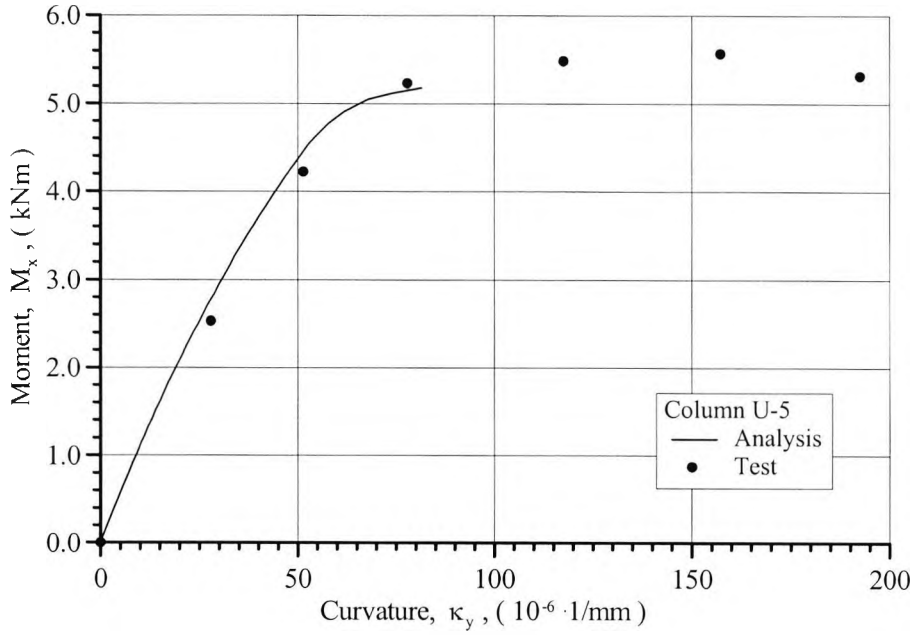

Figure 4.34b
Biaxial moment curvature relations for column U-5

4.3.3 Summary

Section 4.3.2. demonstrated the ability of the numerical model to accurately calculate the ascending branch of the load-deflection diagram for an eccentrically loaded reinforced concrete column. The average of the ratios of test failure load to predicted failure load for the seven reviewed tests series was 1.12. This is regarded as a good correlation considering the variability of concrete as a material. Like the axial load capacity, also the mid-height deflection at peak load was in general underestimated somewhat by the numerical model.

Although the transverse reinforcement was often estimated to have significantly influenced the stress-strain characteristics of the core concrete, for none of the reviewed test columns did it significantly enhance the strength or pre-peak ductility of the column. The reason for this can, at least partly, be ascribed to the presence of an unconfined concrete cover. The purpose of a concrete cover is to provide the necessary bond between the reinforcement and the concrete, and to protect the reinforcement from corrosion, weathering and fire. Yet, the concrete cover often contributes significantly to a column's load carrying capacity.

In summary, the validation process high-lighted the following characteristics regarding the structural response of reinforced concrete columns:

- The load capacity decreases with increasing load eccentricity, and more so with higher concrete strength.
- The load capacity decreases with increasing slenderness, and more so with higher concrete strength.
- The mid-height deflection at strength failure increases both with increasing load eccentricity and increasing column slenderness, but appear to be fairly independent of the concrete strength.

- The mid-height deflection at strength failure is often largely unaffected by passive confinement, despite the post-peak ductility being significantly enhanced.
- The presence of an unconfined concrete cover counteracts the beneficial effects of passive confinement.
- Due to the increased instability of the cover shell the use of closely spaced ties may result in a defacto reduction in a column's load capacity.

Chapter 5: Full-Scale Tests of High Strength Concrete Columns

5.1 Experimental Programme

This section provides a detailed description of the 12 full-scale high strength concrete columns manufactured and tested in the laboratories of the Civil Engineering Department at City University as a part of the present investigation. The range of test parameters to be varied was determined in consultation with the British Cement Association during the preliminary phase of the project. The parameters included the column slenderness, the eccentricity of the applied axial loading, the concrete strength and the spacing of the lateral reinforcement hoops.

5.1.1 Test Columns

Of the 12 test columns six were manufactured to a length of 3250 mm and six to a length of 7250 mm. When taking account of the practical arrangement providing the pinned end conditions, the corresponding effective lengths of the test columns were 3975 mm and 7975 mm respectively. Since all the columns had a 250×250 mm cross-section their geometrical slenderness ratio was either 15.9 or 31.9, and they were as such classified as slender according to BS 8110 (1985).

The columns were to be tested under conditions of either uniaxial or biaxial eccentric compression. The nominal load eccentricity for all of the shorter columns was 50 mm with respect to bending about the first principal axis. For the shorter columns which were designed for biaxial bending, the load eccentricity was 25 mm with respect to bending about the second principal axis. For the longer columns the eccentricities were halved for

both directions. The load eccentricities were built into the columns during the manufacturing process by shifting the centre of the tilt caps relative to the centroid of the concrete section. Control measurements taken prior to testing showed that the prescribed eccentricities could be achieved to within an accuracy of about 3 mm.

Half the test columns were manufactured using the grade C100 concrete, and the other half using the grade C120 concrete. The concrete strengths were assessed from testing 100×200 mm cylinders which had been cured under similar conditions as the columns. At the time of testing the columns manufactured from the grade C100 concrete were associated with average cylinder strengths, $f_{c,cyl}$, ranging from 95 MPa to 110 MPa, and the columns manufactured from the grade C120 concrete with average cylinder strengths ranging from 120 MPa to 129 MPa. The utilised concrete materials are described in detail in section 2.1.

The columns were longitudinally reinforced by 4 ribbed steel bars of grade 460 with a diameter of either 10 mm or 12 mm. Thus, the test columns had a volumetric ratio of longitudinal reinforcement, ρ_g, of either 0.50% or 0.72%. This compares to the minimum ratio of 0.40% specified in BS 8110 (1985). The reason for stipulating a minimum requirement is to ensure that a concrete column can always resist a small amount of bending, as well as prevent brittle failure on the formation of the first tensile crack. Furthermore, as the self-equilibrating effects of creep and shrinkage of concrete shed compressive load to the reinforcement bars, the minimum reinforcement ratio ensures that these effects in themselves do not cause the bars to be severely stressed. Since the reinforcement bars were delivered in lengths of 6000 mm, it was necessary to splice the bars in the longer test columns. With a provided lap length of 450 mm, according to BS 8110 (1985) the splice can be assumed to be of full strength.

The columns had a constant concrete cover of 20 mm, and were transversely reinforced by square perimeter hoops fabricated from either 8 mm or 10 mm plain steel bars of grade 250. The tie pitch was either 200 mm, 150 mm, 100 mm or 50 mm. Thus, the test columns had a volumetric ratio of transverse reinforcement, ρ_s, as determined with respect to the nominal concrete core, of between 0.50% and 3.14%. It should be noted that for six of the columns the tie pitch exceeded the maximum specified in BS 8110. The code of practice specifies a maximum pitch of 12 times the diameter of the compression bar in order to warrant against premature stability failure of the compression bars (BS 8110, 1985). The reason for choosing a higher pitch was to virtually eliminate any confining effects in these columns, although a risk of buckling of longitudinal bars was introduced.

In order to prevent premature failure occurring in the end regions of the columns during testing, these were locally strengthened by three closely spaced welded reinforcement grids.

Transport of the columns was facilitated by welding either two or four T16 lifting loops to the reinforcement cage. The number and distribution of lifting loops ensured that the maximum tensile stress developing in the concrete during the lifting and haulage process remained sufficiently low so as not to cause damage to the columns. It was estimated that a maximum tensile stress of 0.4 MPa developed during the lifting and haulage process, i.e. the stress remained less than 1/10 of the tensile strength of the concrete.

In the case of the test columns SH20U, SL15U, SH10U and SL05U, full strength anchorage of the reinforcement hoops was ensured by means of metal-arc welding. In the remaining eight columns, full strength anchorage was provided in accordance with BS 8110 (1985) by passing the bars round the main reinforcement bars through an angle of 90°, and continuing beyond for a length of 90 mm.

Table 5.1 lists the test parameters for the individual columns, as well as a reference to the relevant construction drawing.

Table 5.1
Details of columns included in the experimental investigation

Column		Length	Eccentricity		Concrete	Longitudinal reinforcement		Transverse reinforcement		
Label	Dwg ref	L (mm)	e_y (mm)	e_x (mm)	$f_{c,cyl}$ (MPa)	ρ_g (%)	f_{sy} (MPa)	s (mm)	ρ_s (%)	f_{sy} (MPa)
SH20U	5.1	3975	50	0	129	0.50	535	200	0.79	369
SL15U	5.1	3975	50	0	95	0.50	535	150	1.05	369
SH10U	5.1	3975	50	0	129	0.50	535	100	1.57	369
SL05U	5.1	3975	50	0	95	0.50	535	50	3.14	369
SH20B	5.2	3975	50	25	128	0.72	539	200	0.50	316
SL15B	5.2	3975	50	25	110	0.72	539	150	0.66	316
LL20U	5.3	7975	25	0	101	0.72	539	200	0.50	316
LH15U	5.3	7975	25	0	129*	0.72	539	150	0.66	316
LL10U	5.3	7975	25	0	102	0.72	539	100	1.00	316
LH05U	5.3	7975	25	0	123	0.72	539	50	1.99	316
LH10B	5.3	7975	25	13	120	0.72	539	100	1.00	316
LL05B	5.3	7975	25	13	98	0.72	539	50	1.99	316

$f_{c,cyl}$: compressive strength of 100×200 mm cylinders.
* cylinder strength estimated from 100 mm cube strength.

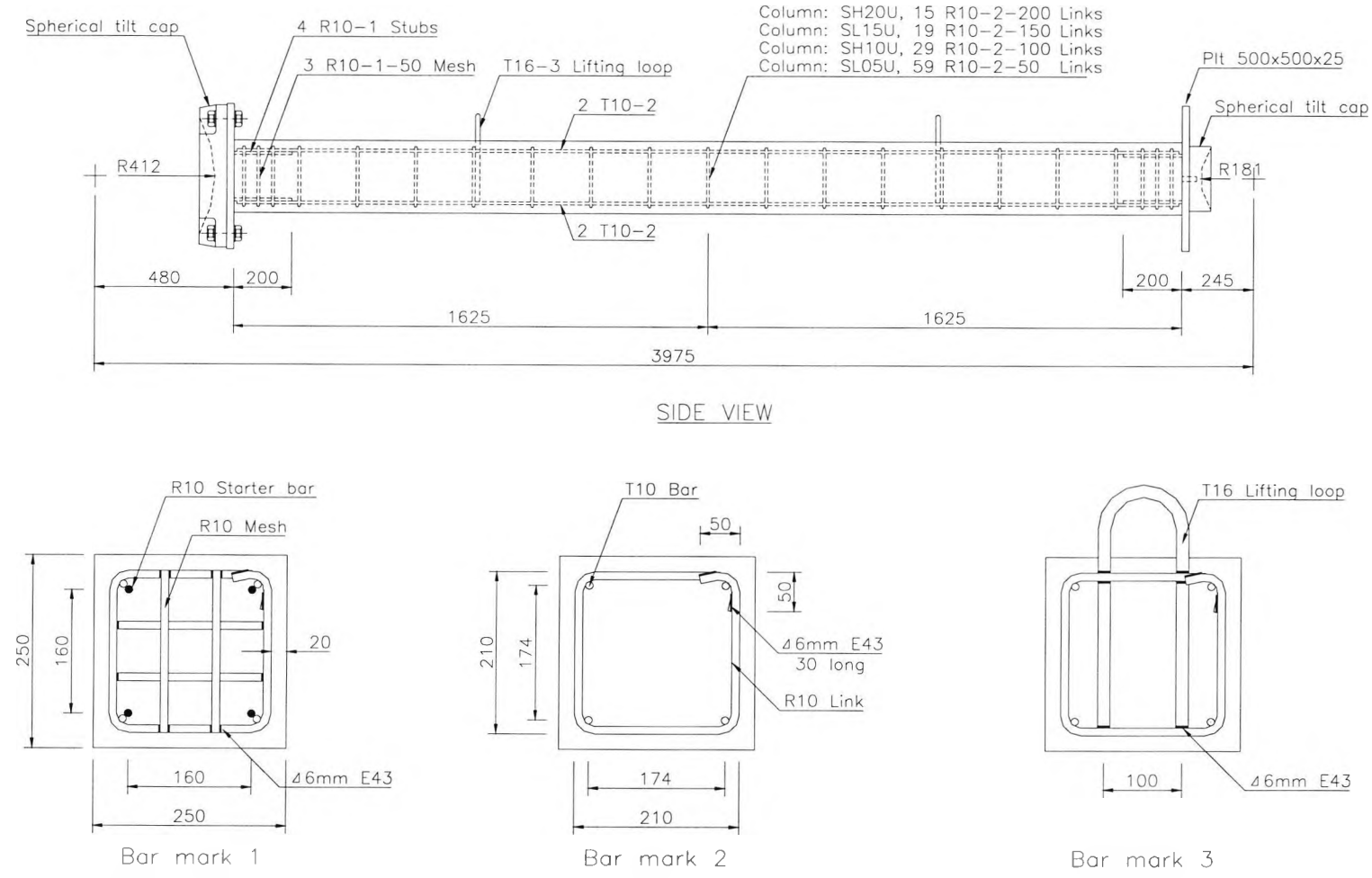

Figure 5.1
Test columns SH20U, SL15U, SH10U and SL05U

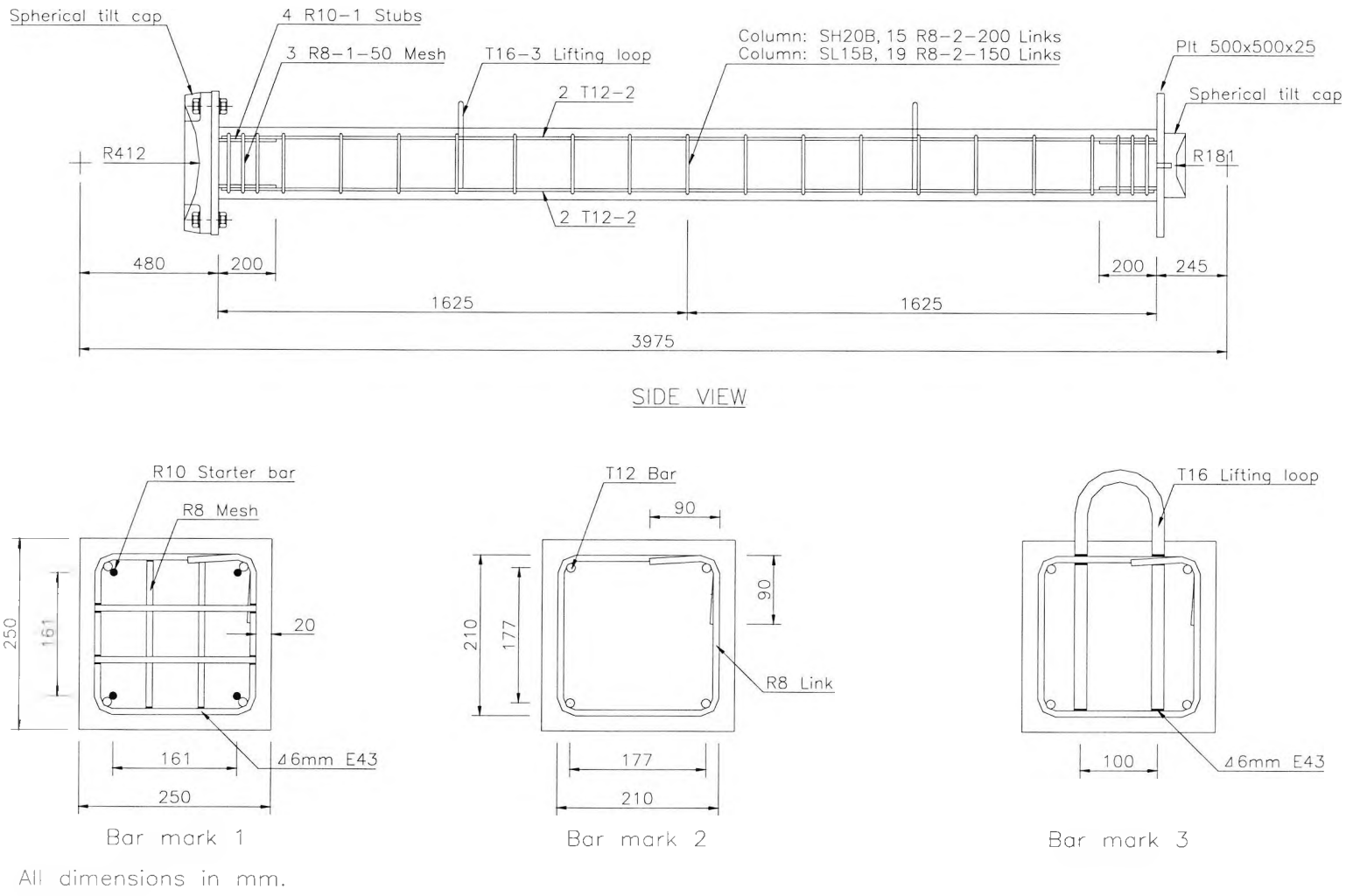

Figure 5.2
Test columns SH20B and SL15B

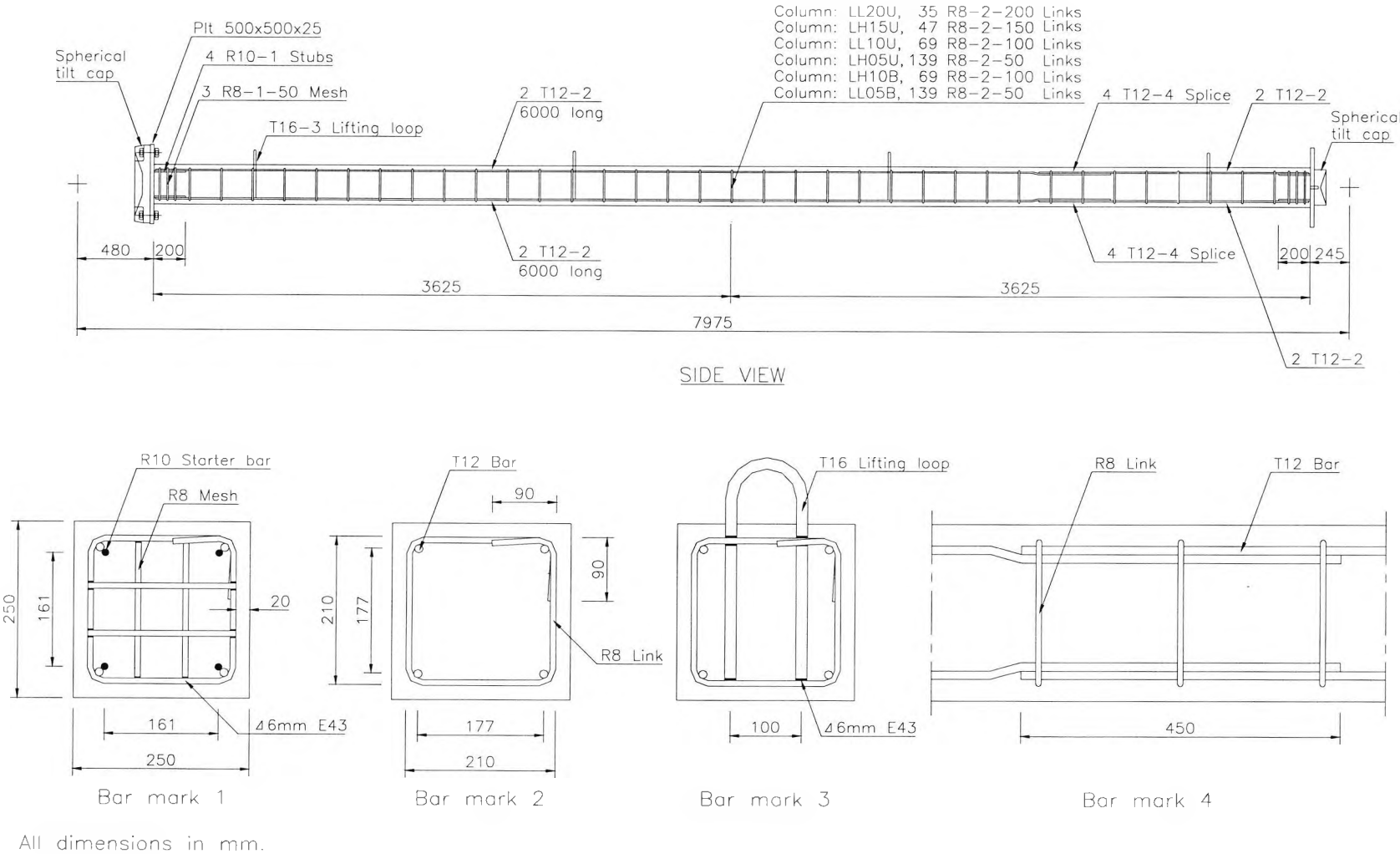

Figure 5.3
Test columns LL20U, LH15U, LL10U, LH05U, LH10B and LL05B

5.1.2 Testing Rig

In view of the large dimensions of the columns and the explosive failure mode of high strength concrete, for safety reasons it was decided to test the columns in a horizontal rather than a vertical position. Besides reducing the risk to the operating personnel, the horizontal position has the advantage of simplifying the monitoring of the possible development and propagation of cracks in the column during testing. Horizontal column testing was also employed in an earlier investigation at City University (Brant, 1984), and parts of the loading rig was available for the current investigation. Nevertheless, a considerable amount of work had to be put into the design and fabrication of a rig for testing the high strength concrete columns.

Figure 5.4 illustrates the loading rig as it was assembled for the testing of the 4 m long columns. The columns were tested in between two large reaction blocks approximately 1 m above the floor of the laboratory. The reaction blocks were bolted to the floor, and connected by high yield MacAlloy tie bars. The tie bars not only enhanced the capacity of the testing rig, but also counteracted the tilt of the reaction blocks during the tests. Before testing the 8 m long columns, the loading rig was modified and rearranged so as to accommodate the extra length.

The load capacity of the rig configuration for the testing of the shorter and the longer columns, following the recommendations given in BS 5910 (1990), was calculated to be 3500 kN and 3000 kN respectively. The relative little difference between the load capacity of the two configurations is explained by changes in the critical design check. Whereas web buckling in the front beam constituted the critical design check for the first rig configuration, strength failure of the MacAlloy bars constituted the critical design check for the second rig configuration. The calculation of the load capacities was based on a

testing procedure in which the tie bars were tightened when the applied axial load reached 600 kN. It was estimated, and indeed experimentally confirmed, that after tightening the bars 66% of all additional loading was sustained by these. The axial load was applied by means of a hydraulic jack with a capacity of 500 tonnes.

A PTFE-coated bridge bearing of the type Glacier GZ450 with a maximum load capacity of 4500 kN, was employed to provide the pinned end condition at the end of the column where the axial load was applied. The pinned end condition at the opposite end of the column was provided by the polished steel cap of a 500 tonnes load cell of the type Transducers 02-1810. Both the Glazier GZ450 bearing and the polished steel cap of the load cell had spherical tilt capability.

The testing of the columns in a horizontal position necessitated the construction of a new suspension rig to counter the self-weight of the test column. Figure 5.5 illustrates the suspension rig as assembled for the testing of the 4 m long columns. The columns were suspended from a portal frame using a system of carriers so as to be evenly supported at four points along their length. A Dartec M1000 servo-hydraulic actuator, with a capacity of 250 kN, and a Dartec M9500 controller was employed to automatically counterbalance the self-weight of the column during testing.

Figure 5.6 shows a general view of the experimental setup for the testing of the 8 m long columns. It can be seen that the testing of the longer columns incorporated the insertion of an additional layer of carrier beams in the suspension rig so as to obtain eight bearing points along the length of the column.

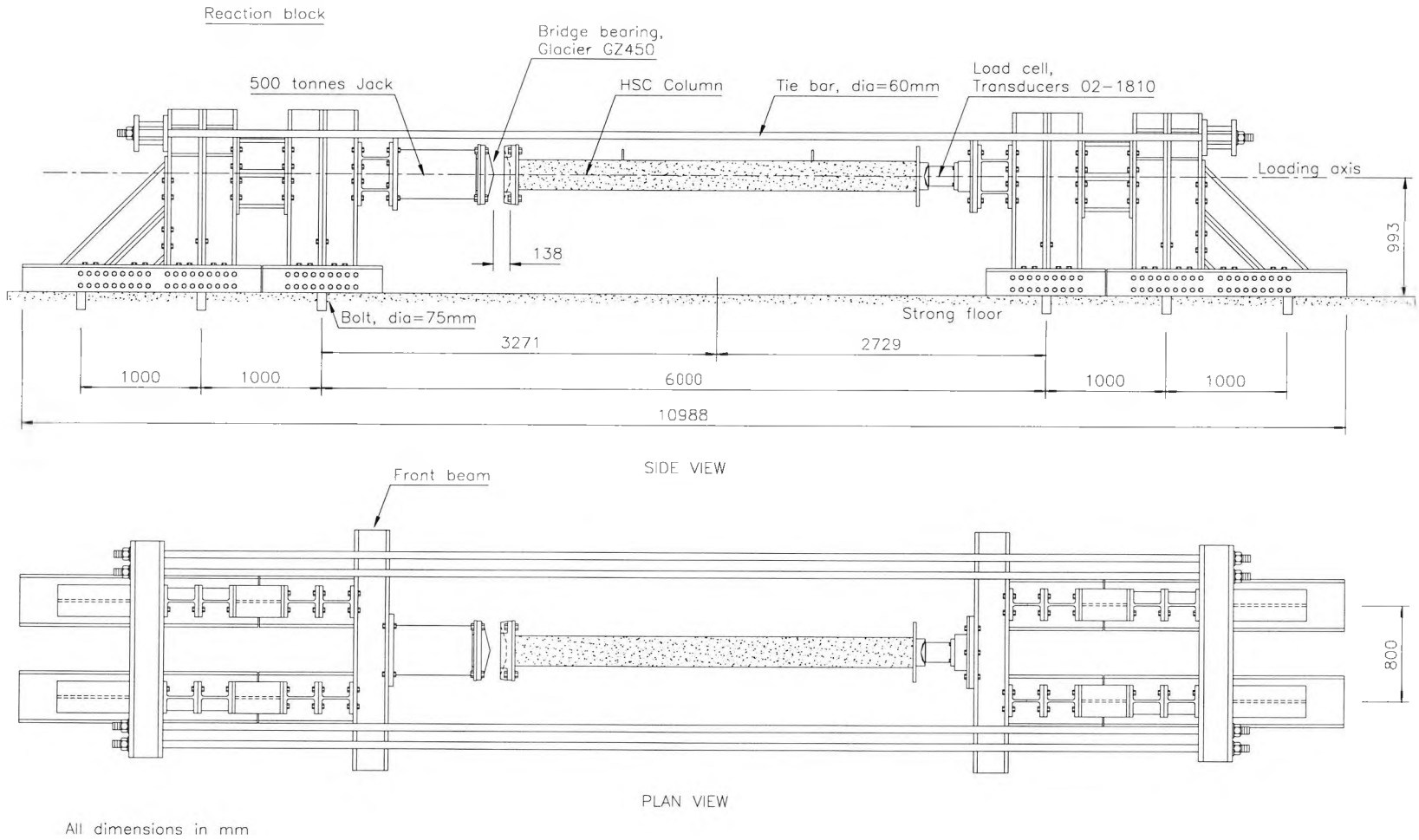

Figure 5.4
Loading rig for the testing of the 4 m long columns

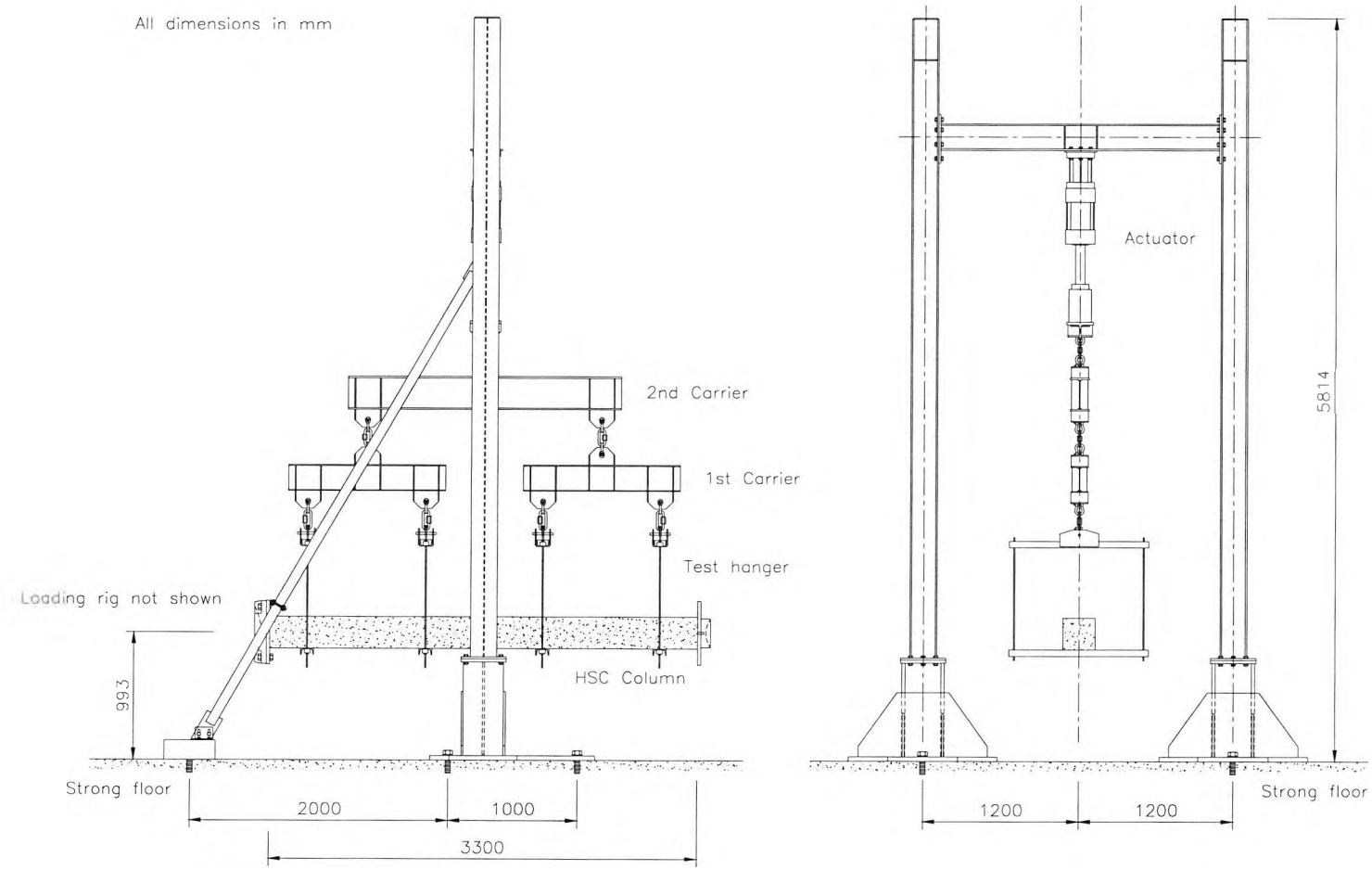

Figure 5.5
Suspension rig for the testing of the 4 m long columns



Figure 5.6
Experimental setup for the testing of the 8 m long columns

5.1.3 Instrumentation and Testing Procedure

The applied axial load was measured by a 500 tonnes load cell, which, like all the other electronic instrumentation used in the experiments, was linked up to an Intercole data acquisition system.

The deflections of the test columns were measured by LVDTs. It was originally planned to be the standard procedure to measure both the horizontal and vertical deflections at seven evenly spaced stations along the length of the columns. However, during the testing of the first column, SL05U, four of the transducers were damaged, and as a consequence the horizontal deflections were only measured at three stations during the testing of the remainder of the shorter columns. At the time of testing the longer columns, two additional transducers became available. Thus, the horizontal deflections of the longer columns were measured at five points along their length. Figure 5.7 together with table 5.2 show the position of the displacement transducers. The LVDTs, similar to the load cell, were calibrated once and for all prior to commencing the experimental programme.

The concrete strains were recorded by 40 electrical strain gauges of the type PL-60-11, which were pasted onto the hardened column a few days before testing. As the PL-60-11 gauge measures the apparent strain over a gauge length of 60 mm, it is well suited for measuring strains in a heterogenous material such as concrete. The surface strains were recorded at three sections located within the middle fifth of the column's effective length, i.e. in the expected failure region, and at one section located at about the 1/4 division point of the column's effective length. At each section, five gauges were positioned on either side of the column, so as to provide particularly detailed information about the strain distribution in the vertical, i.e. primary, bending plane. The five gauges were uniformly distributed along the vertical, with the outer gauges positioned 25 mm from the edges. The

specific details regarding the positioning of the PL-60-11 gauges can be read from figure 5.8 in conjunction with table 5.2. It should be noted that the gauges numbered 45 - 64 were pasted onto what will be referred to as the front face of the column, and the gauges numbered 65 - 80 onto what will be referred to as the rear face of the column.

Since spalling of the concrete cover and the development of tensile cracks was anticipated to render surface mounted gauges redundant during the later stages of testing, a total of 20 supplementary strain measurements were made on the longitudinal steel reinforcement bars. The strains were recorded in the four reinforcement bars at five sections, of which four were located within the middle fifth of the column's effective length. The gauges mounted on the longitudinal reinforcement bars, numbered 25 - 44, were always positioned mid-way between adjacent links.

All the test columns had strain gauges pasted onto three of the ties located within the middle fifth of the column's effective length, and onto one tie located near the 1/4 division point of the column's effective length. The strain gauges were always positioned at opposite ends of the bar diameters in order to allow for a separation of bending strains and axial strains. As described in section 3.4.2, it is the axial strains, and not the bending strains, which give rise to confinement. The strain gauges pasted onto the ties, numbered 1 - 24, were like the gauges pasted onto the longitudinal reinforcement bars of the type FLA-6-11. All internal gauges were covered by a thick layer of epoxy resin in order to protect them against environmental and mechanical damage. Figure 5.9 together with table 5.2 provide the specific details for the strain gauging of the longitudinal and transverse reinforcement bars.

In all tests, a laboratory overhead crane was used to lift the test column into the loading rig, where it was temporarily supported by four props. The hangers of the suspension rig were

assembled, and the actuator operating in a displacement controlled mode was employed for the final alignment of the column in the loading rig. After the column was aligned, a small nominal axial force of 10 kN was applied in order to ensure that the column remained in position. The actuator was switched to a force controlled mode, and the force was adjusted so as to be 1 kN less than the self-weight of the test column. The LVDTs were positioned, and all the electronic measurement devices were linked up to the data acquisition system and initialised. During testing of the columns the drift of the actuator was observed to be about ±1 kN.

The test columns were loaded to failure at a rate of about 25 kN/min, which was achieved by manually adjusting the hydraulic flow to the 500 tonnes ram. After each load increment of approximately 50 kN, a scan of all the data channels was performed. On reaching an applied axial load of approximately 600 kN, the testing was temporarily paused in order to tighten the MacAlloy bars.

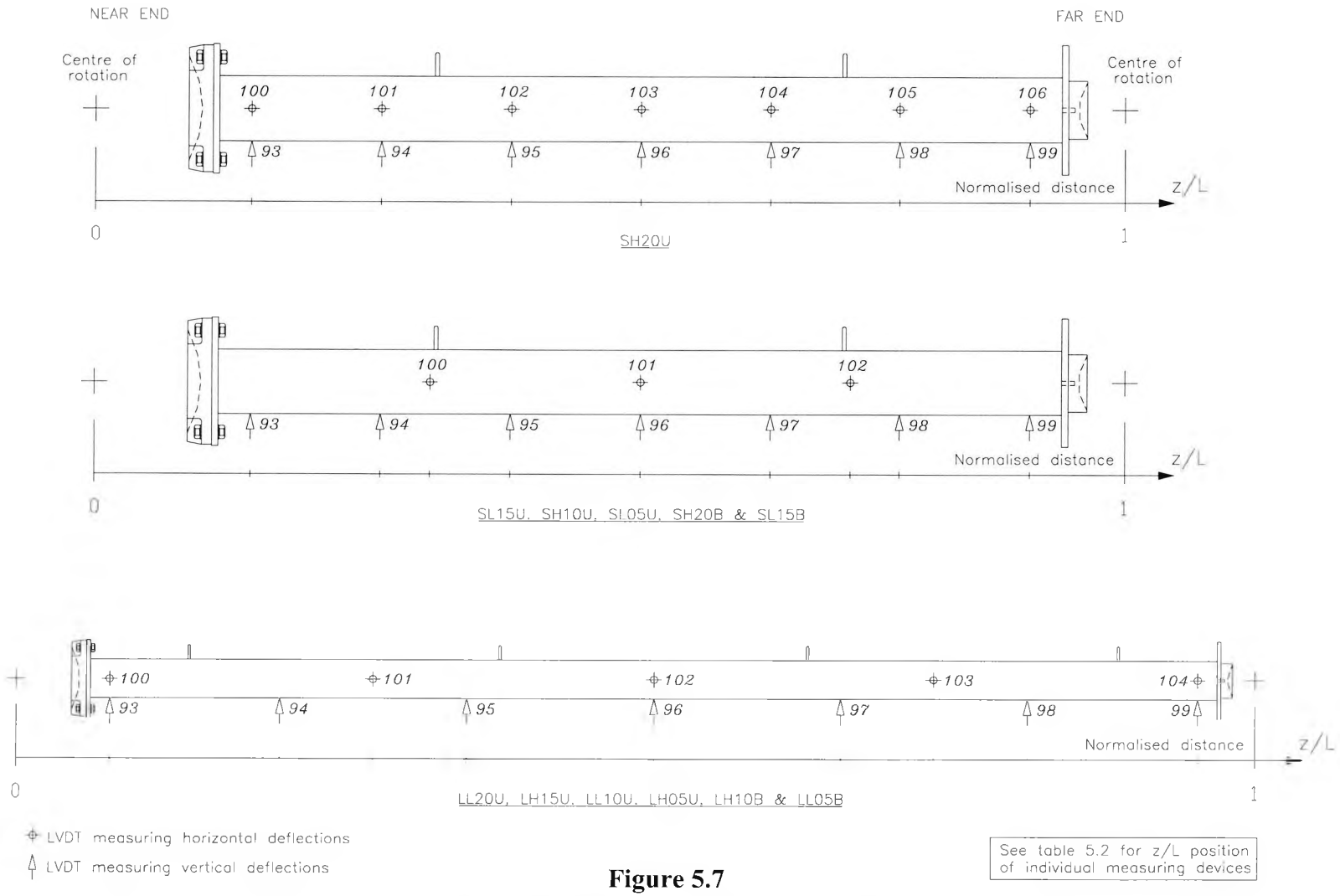

Figure 5.7
Positioning of displacement transducers

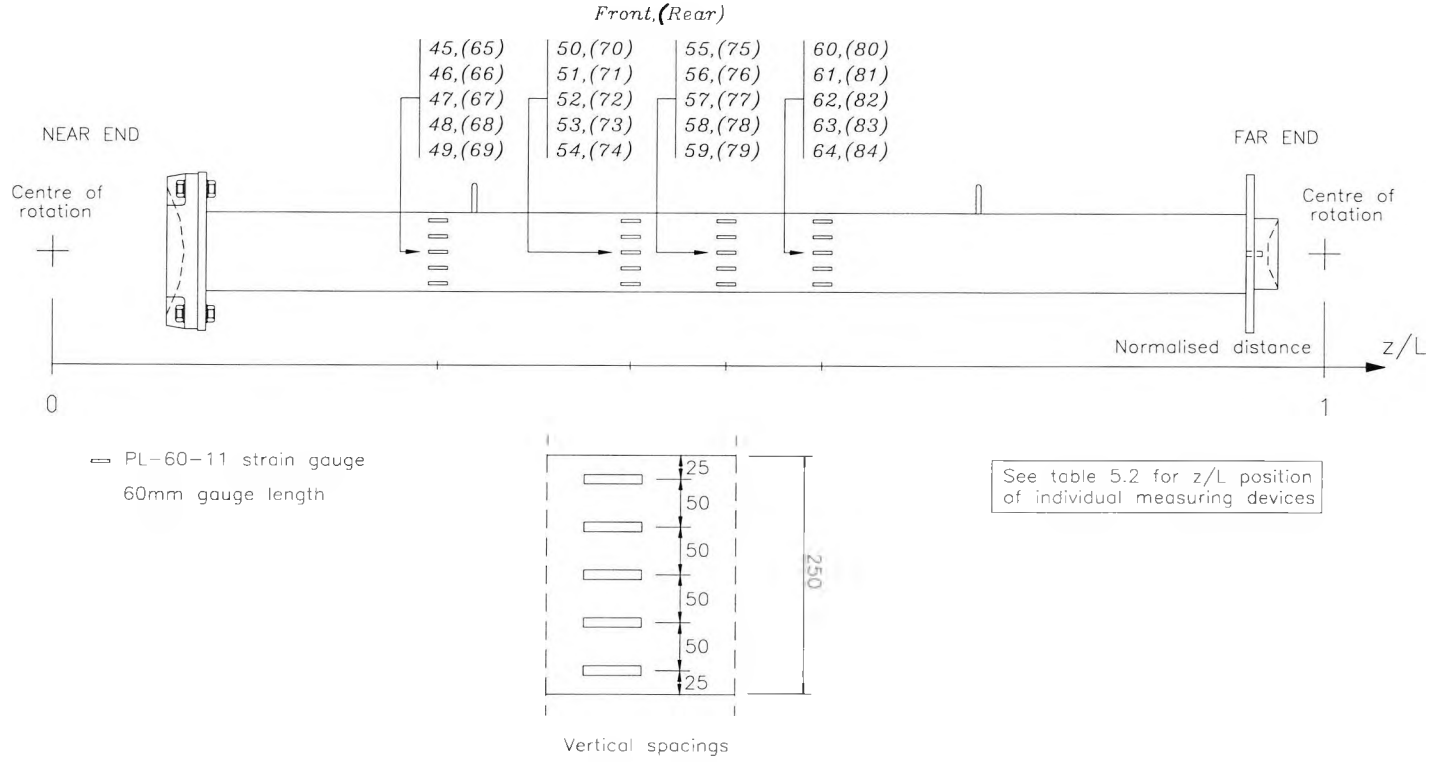

Figure 5.8
Positioning of external strain gauges

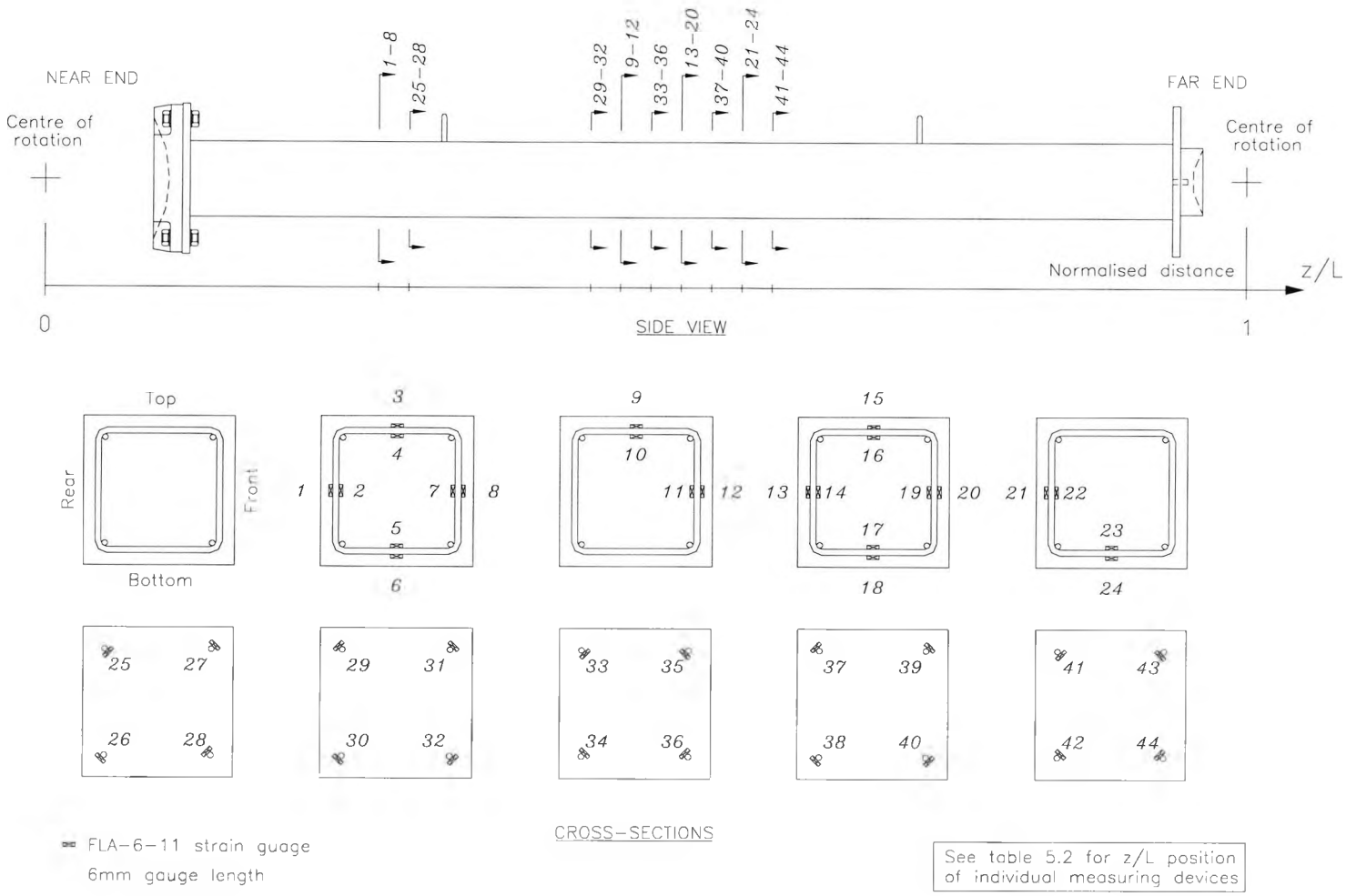

Figure 5.9
Positioning of internal strain gauges

Table 5.2
Normalised position, z/L, of gauges and transducers

	Channel	SH20U	SL15U	SH10U	SL05U	SH20B	SL15B	LL20U	LH15U	LL10U	LH05U	LH10B	LL05B
Strains Ties	1-8	0.278	0.265	0.278	0.278	0.278	0.265	0.239	0.233	0.239	0.213	0.239	0.239
	9-12	0.479	0.492	0.479	0.492	0.479	0.492	0.439	0.458	0.452	0.446	0.452	0.446
	13-20	0.530	0.530	0.530	0.530	0.530	0.530	0.515	0.515	0.515	0.515	0.515	0.515
	21-24	0.580	0.567	0.580	0.567	0.580	0.567	0.590	0.571	0.577	0.584	0.577	0.586
Strains Rebar	25-28	0.303	0.247	0.291	0.284	0.303	0.284	0.251	0.242	0.245	0.242	0.245	0.242
	29-32	0.454	0.473	0.416	0.473	0.454	0.473	0.472	0.430	0.433	0.436	0.433	0.430
	33-36	0.504	0.511	0.467	0.511	0.504	0.511	0.477	0.487	0.483	0.487	0.483	0.480
	37-40	0.555	0.548	0.517	0.548	0.555	0.548	0.552	0.543	0.546	0.543	0.546	0.549
	41-44	0.605	0.586	0.567	0.586	0.605	0.586	0.603	0.599	0.596	0.593	0.596	0.599
Strains Concrete	45-49, 65-69	0.303	0.284	0.316	0.309	0.303	0.284	0.251	0.242	0.245	0.242	0.245	0.242
	50-54, 70-74	0.454	0.473	0.467	0.460	0.454	0.473	0.427	0.430	0.433	0.430	0.433	0.430
	55-59, 75-79	0.530	0.530	0.530	0.530	0.530	0.530	0.515	0.515	0.515	0.515	0.515	0.515
	60-64, 80-84	0.605	0.586	0.592	0.599	0.605	0.586	0.603	0.599	0.596	0.599	0.596	0.599
Deflections Vertical	93	0.152	0.152	0.152	0.152	0.152	0.152	0.076	0.076	0.076	0.076	0.076	0.076
	94	0.278	0.278	0.278	0.278	0.278	0.278	0.214	0.214	0.214	0.214	0.214	0.214
	95	0.404	0.404	0.404	0.404	0.404	0.404	0.364	0.364	0.364	0.364	0.364	0.364
	96	0.530	0.530	0.530	0.530	0.530	0.530	0.515	0.515	0.515	0.515	0.515	0.515
	97	0.655	0.655	0.655	0.655	0.655	0.655	0.665	0.665	0.665	0.665	0.665	0.665
	98	0.781	0.781	0.781	0.781	0.781	0.781	0.816	0.816	0.816	0.816	0.816	0.816
	99	0.907	0.907	0.907	0.907	0.907	0.907	0.954	0.954	0.954	0.954	0.954	0.954
Deflections Horizontal	100	0.326	0.326	0.326	0.152	0.326	0.326	0.076	0.076	0.076	0.076	0.076	0.076
	101	0.530	0.530	0.530	0.278	0.530	0.530	0.289	0.289	0.289	0.289	0.289	0.289
	102	0.733	0.733	0.733	0.404	0.733	0.733	0.515	0.515	0.515	0.515	0.515	0.515
	103	-	-	-	0.530	-	-	0.740	0.740	0.740	0.740	0.740	0.740
	104	-	-	-	0.655	-	-	0.954	0.954	0.954	0.954	0.954	0.954
	105	-	-	-	0.781	-	-	-	-	-	-	-	-
	106	-	-	-	0.907	-	-	-	-	-	-	-	-

5.2 Test Observations

This section provides a summary of the results obtained from testing 11 of the 12 full-scale high strength concrete columns included in the experimental programme. No test data was recorded for test column SL15U, as this column was severely damaged through accidental overloading prior to commencing the instrumented test.

5.2.1 Test Loads and Failure Modes

Table 5.3 lists the observed failure loads for the test columns. The failure loads ranged from 1829 kN to 2796 kN, or when expressing these as percentages of the unconfined squash loads from 28% to 57%. The squash loads were calculated from equation 3.33, in which the 150×300 mm cylinder strength was taken as 0.95 times the mean strength of the 100×200 mm cylinders. The test results indicate that a reduction in the tie spacing enhanced the load capacity of the shorter columns, but had no such effect on the load capacity of the longer columns.

All the test columns failed explosively upon reaching their ultimate load. The failure manifested itself in a dense cloud of finely crushed concrete and a shower of larger concrete debris. Except for column SH20B, none of the columns developed tensile cracking or cover spalling so as to provide visual warning of imminent failure. In the case of test column SH20B, parts of the concrete cover spalled off upon reaching an axial load corresponding to about 96% of the column's load capacity. The spalling occurred at a section located approximately 1/3 along the column's effective length when measured from the rotational centre of the bridge bearing. When the applied load reached about 99% of the column's load capacity, parts of the concrete cover at mid-length of the column also spalled off. However, the column eventually failed at the end-section where cover failure had initiated.

Test column SL05U, like test column SH20B, failed at a section located approximately 1/3 along the column's effective length. The remaining test columns all failed in accordance with the symmetric nature of the test arrangement within the heavily instrumented region at mid-length.

Table 5.3
Failure loads for columns tested

Column	Failure load	Concrete	Longitudinal reinforcement		Squash load	
Name	$P_{c,e}$ (kN)	$f_{c,cyl}$ (MPa)	ρ_g (%)	f_{sy} (MPa)	$P_{c,a}$ (kN)	$P_{c,e}/P_{c,a}$ (-)
SH20U	2347	129	0.50	535	6666	0.35
SL15U	-	95	0.50	535	4953	-
SH10U	2436	129	0.50	535	6666	0.37
SL05U	2796	95	0.50	535	4953	0.57
SH20B	1892	128	0.72	539	6677	0.28
SL15B	1899	110	0.72	539	5772	0.33
LL20U	1834	101	0.72	539	5320	0.35
LH15U	2485	129*	0.72	539	6727	0.40
LL10U	1937	102	0.72	539	5370	0.36
LH05U	1828	123	0.72	539	6426	0.28
LH10B	2125	120	0.72	539	6275	0.32
LL05B	2049	98	0.72	539	5169	0.40

$f_{c,cyl}$: compressive strength of 100×200 mm cylinders.
* Estimated from 100 mm cube strength.

From carefully studying the video footage recorded during the tests, a marked difference between the failure mode of the shorter and the longer columns could be noted. Whereas failure of the shorter columns appeared to be directly triggered by cover spalling on the concave side of the bent columns, the failure of the longer columns appeared to take place due to the loss of overall stability. With the exception of column SH20B, cover spalling always occurred within a second prior to the complete disintegration of the section, and no

changes in deflections or loading could be registered after the occurrence of cover spalling. When the longer columns reached their ultimate load, they suddenly began to deflect continuously until they failed in a clearly bent configuration. In this case the break-up of the critical section exhibited no distinct phases, but like the shorter columns no changes in deflections or loading could be registered in the short time elapsing between failure initiation and the complete break-up of the section.

The overall effect of decreasing the tie spacings was to reduce the volume of crushed core concrete, as well as to increase the inclination of the failure plane to the column axis. For the test columns with the smallest tie spacings of 50 mm, i.e. column SL05U, LH05U and LL05B, only a small amount of core concrete was lost due to crushing, and the failure plane was predominantly perpendicular to the column axis. Thus, the failure mechanism for these columns consisted primarily of rotations about the pinned ends of the column segments on either side of the failed section. These end rotations were sufficiently large to cause the two longitudinal reinforcement bars positioned at the top face of the column to snap during testing. Except for column SH20B and SL15B, i.e. the shorter columns tested with a biaxial load eccentricity, all the columns with tie spacings in excess of 50 mm developed a failure plane, or shear crack plane, inclined between 30° and 60° to the column axis. The inclined failure plane permitted the two column segments on either side of the failed section to slide over one another. Evidence of the sliding motion was apparent in the deformation of the two longitudinal reinforcement bars positioned at the convex face of the bent column, as well as in the extensive spalling of the concrete cover from this face of the column. In the special case of columns SH20B and SL15B, the failure plane was predominantly perpendicular to the column axis. However, in contrast to the three columns with tie spacings of 50 mm, failure of both of these columns was characterised by extensive crushing of core concrete. For all the tested columns the failure plane was noted to pass through mortar and coarse aggregates without bias.

Figure 5.10 shows the failed section of column SH20U. The failure plane developed at an angle of approximately 45° to the column axis, and was bridged by a single reinforcement link. The longitudinal reinforcement bars had buckled, and much of the concrete cover had spalled off on all four faces of the column. Furthermore, a large volume of the column's core concrete had been lost due to crushing.

The failure plane in column SH10U, see figure 5.11, formed at an angle of about 60° to the column axis, and was entirely confined to the space between two adjacent reinforcement ties. The extensive damage caused to the concrete cover on the top face of the column indicated the occurrence of the previously described failure mechanism of two column segments sliding over one another. However, the relative sliding had not progressed sufficiently to buckle the two longitudinal reinforcement bars positioned at the top face of the column. In contrast, both the reinforcement bars at the bottom face of the column, where a significant volume of core concrete had been lost due to crushing, had buckled.

The failure zone of column SL05U, see figure 5.12, was located at the instrumented section nearest to the bridge bearing, i.e. at $z/L = 0.31$. Almost none of the core concrete was lost due to crushing, and the failure plane was predominantly perpendicular to the column axis. A large area of the concrete cover on the lower half of the column had spalled off, and both the longitudinal reinforcement bars exposed had buckled. The reinforcement bars positioned at the top face of the column had been pulled over during failure. This, together with the absence of cover spalling on the top face of the column, indicates that the underlying failure mechanism was of the previously described rotational type.

Like for column SL05U, post-failure inspection of column SH20B, see figure 5.13, showed that failure had involved the propagation of a vertical crack at the instrumented section

nearest the bridge bearing. A large volume of core concrete had been crushed, and both of the longitudinal reinforcement bars located within the crushing zone had buckled. On all column faces, except the top face, extensive cover spalling was noted.

Column SL15B, see figure 5.14, was similar to column SH20B in nominally being subjected to biaxial loading conditions, and in failing along a plane which was predominantly perpendicular to the column axis. Failure of both the columns SH20B and SL15B involved a substantial loss of core concrete due to crushing. However, in contrast to column SH20B, the cover spalling was limited to the rear and bottom face of the column, and one of the reinforcement bars had snapped.

The fracture plane of column LL20U, see figure 5.15, was inclined about 30° to the column axis, and was bridged by a single transverse reinforcement link. Loss of the concrete cover could be observed on all four faces of the column, but was particularly pronounced on the top and bottom face of the column. The main reinforcement bars had all buckled as a consequence of the sliding motion of the two column wedges.

In the case of column LH15U, see figure 5.16, the angle between the failure plane and the column axis was about 30°. The crack was bridged by two transverse reinforcement links, one of which had opened up during the failure process. All the longitudinal reinforcement bars had buckled, and a substantial amount of the concrete cover on the top and bottom face of the column had spalled off.

The shear crack in column LL10U (see figure 5.17) had an inclination of about 45° to the horizontal, and crossed a single reinforcement tie. The parts of the concrete cover that spalled off during the test came almost exclusively from the top and bottom face of the column. Both of the longitudinal reinforcement bars located at the bottom face of the

column had buckled.

The failure zone of column LH05U, see figure 5.18, was characterised by a crack which was predominantly perpendicular to the column axis. Spalling of the concrete cover was almost exclusively isolated to the bottom face of the column. Both the longitudinal reinforcement bars located at the top face of the column had snapped. Of the 11 columns tested, LH05U was the only column for which neither of the two longitudinal bars located at the bottom face displayed signs of buckling.

The failure plane in column LH10B, see figure 5.19, was inclined at about 45° to the horizontal, but did not display the skewness expected from the biaxial loading conditions. A large area of concrete cover had spalled from the top and bottom face of the column, and all the longitudinal reinforcement bars had buckled. A single reinforcement link within the failure zone had been severed.

Column LL05B (see figure 5.20) failed along a plane which was principally perpendicular to the column axis. Both of the longitudinal reinforcement bars located at the top face of the column had been pulled over during testing. As expected from the biaxial loading conditions, the spalling of the concrete cover was primarily isolated to the bottom and front face of the column, and the longitudinal bar positioned at this edge had buckled. Similar to the other columns with 50 mm tie spacings, but in contrast to the columns with larger tie spacings, only a minor volume of the core concrete of column LL05B was lost due to crushing.

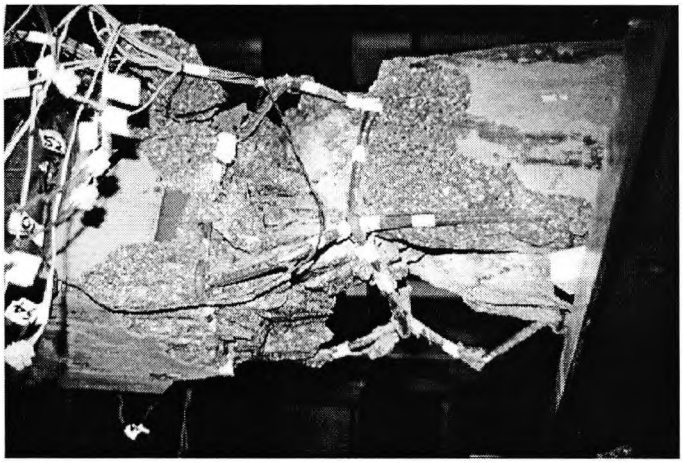

Figure 5.10
Failed section of column SH20U



Figure 5.11
Failed section of column SH10U

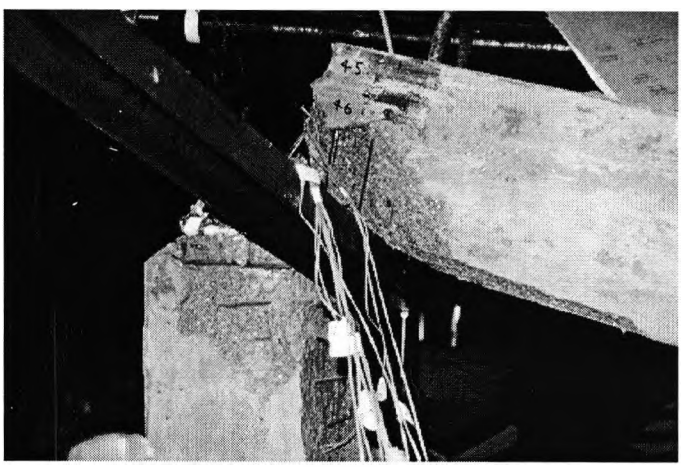

Figure 5.12
Failed section of column SL05U

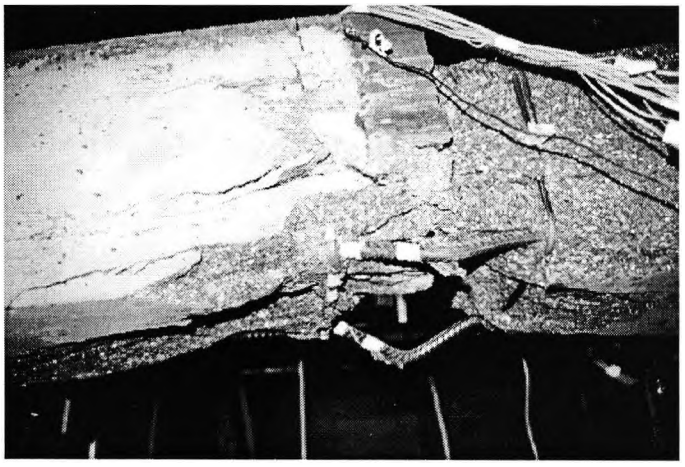

Figure 5.13
Failed section of column SH20B

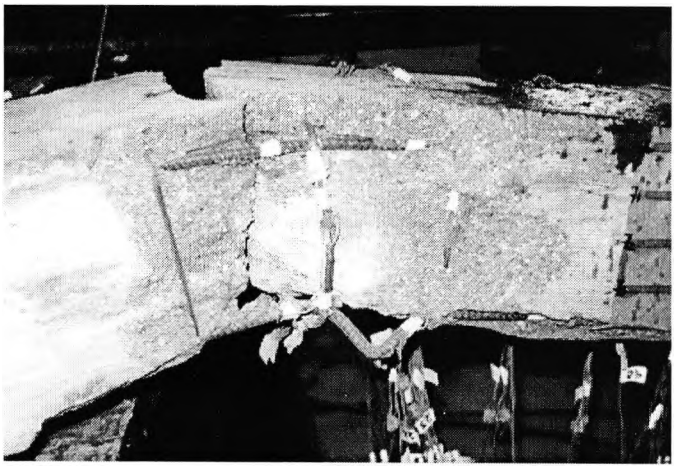

Figure 5.14
Failed section of column SL15B

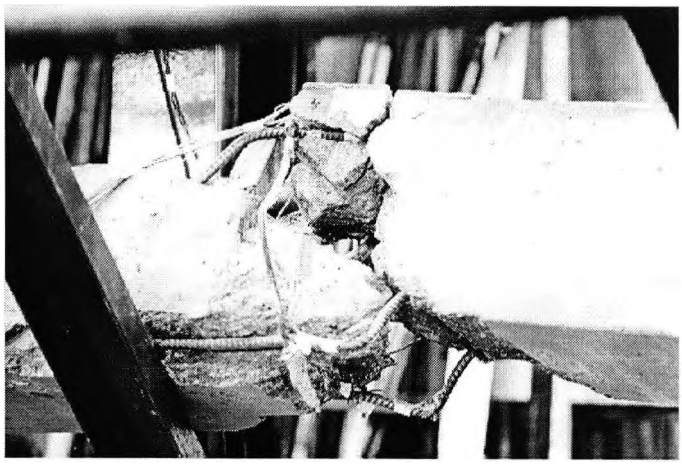

Figure 5.15
Failed section of column LL20U

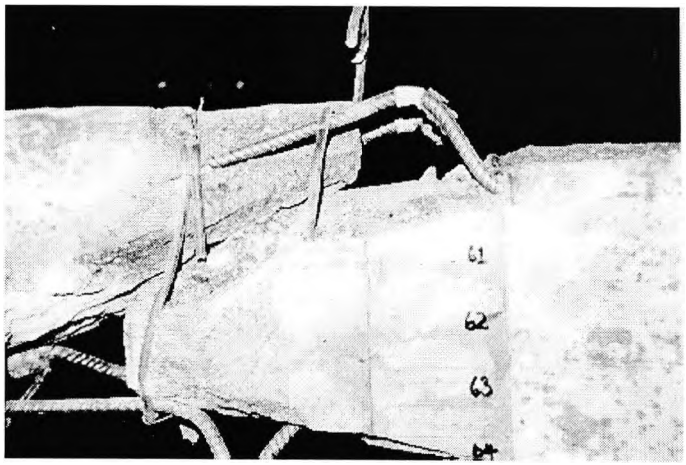

Figure 5.16
Failed section of column LH15U

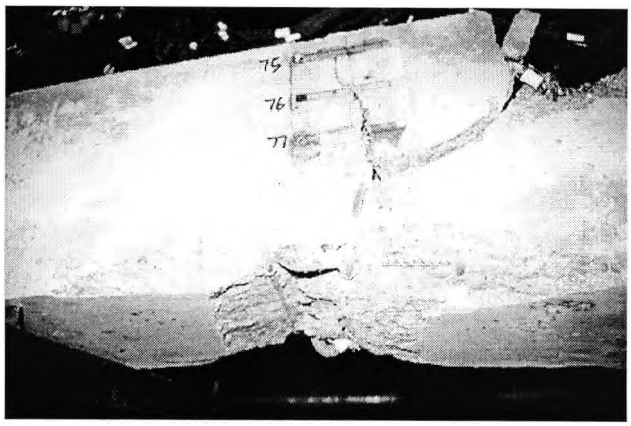

Figure 5.17
Failed section of column LL10U

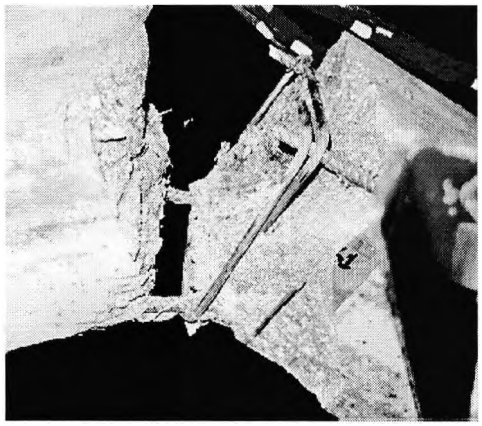

Figure 5.18
Failed section of column LH05U

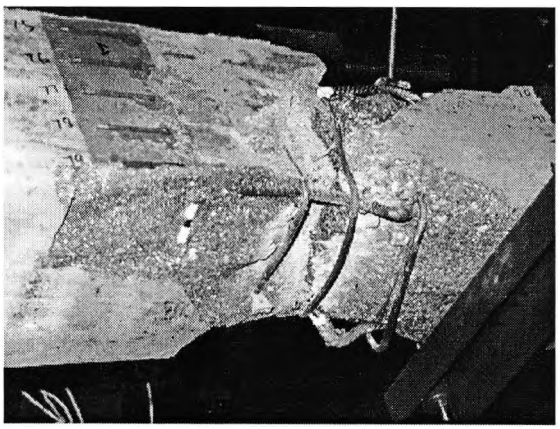

Figure 5.19
Failed section of column LH10B

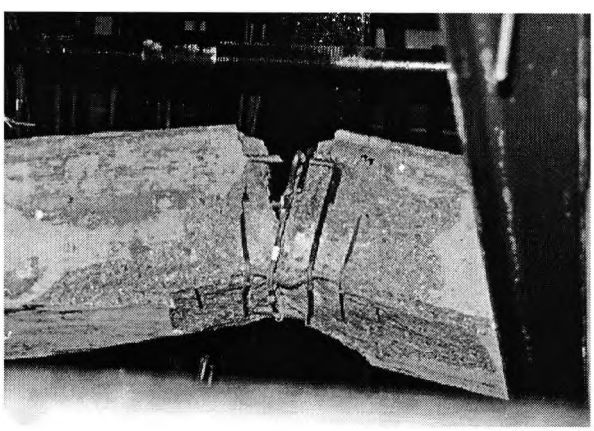

Figure 5.20
Failed section of column LL05B

5.2.2 Load-Strain Behaviour

The following summarises the observed load-strain behaviour of the 11 full-scale columns tested during the experimental investigation.

Strain profiles

The figures 5.21 to 5.30 show the development in the strains measured on both the front and the rear face of the test columns at, or in the immediate vicinity of, the section where failure occurred. Except for the columns SL05U and SH20B, which both failed at the instrumented section nearest the bridge-bearing, all columns failed at a section near mid-length. The strain profiles are plotted at regular intervals for axial loads up to and including the maximum loads recorded during the tests.

The figures also show the linear strain distributions obtained by least square fitting of the experimental data. For each set of strain data, the unknowns in equation 5.1, i.e. the centroidal strain, ε_o , and the curvature, κ_y , were found by solving equation 5.2. The summation required in equation 5.2 was taken over the number of reliable strain readings on each of the two sides of the column. Usually the readings from all five gauges were reliable, but in a few cases one of the strain gauges had malfunctioned, reducing the number of reliable strain readings to four.

$$\varepsilon = \varepsilon_o + \kappa_y(y - y_o) \tag{5.1}$$

$$\begin{bmatrix} n & \sum_{i=1}^{n}(y_i - y_o) \\ \sum_{i=1}^{n}(y_i - y_o) & \sum_{i=1}^{n}(y_i - y_o)^2 \end{bmatrix} \begin{Bmatrix} \varepsilon_o \\ \kappa_y \end{Bmatrix} = \begin{Bmatrix} \sum_{i=1}^{n}\varepsilon_i \\ \sum_{i=1}^{n}\varepsilon_i(y_i - y_o) \end{Bmatrix} \tag{5.2}$$

It can be seen that the measured surface strains in general agree very well with the assumption of plane sections remaining plane. However, for each of the columns SH20B,

LH15U, LL10U and LH05U one or more of the strain gauges, despite appearing to have functioned perfectly well, recorded compressive strains significantly out of line with the strains recorded by the remaining gauges in the set. The compressive strains recorded by the gauges 49 and 69 on column SH20B (figure 5.24), and gauge 64 on column LH05U (figure 5.29), are smaller than expected. Likewise, the compressive strains recorded by gauge 76 on column LH15U (figure 5.27) and gauge 57 on column LL10U (figure 5.28) are larger than expected. However, the effect on the calculated strain distributions of including these outliers was negligible.

The strain data also show that strain reversal occurred in all but one of the columns, and that only during the testing of the columns SL05U, SH20B, SL15B, LL10U and LH05U were tensile strains recorded. It was noted that the tensile strains agreed with a linear strain distribution for tensile strains up to about 0.5 mm/m, a value which incidentally is two to four times larger than the expected cracking strains. Only for column SL15B (figure 5.25), and only during the very final phase of testing, did the measured tensile strains clearly disagree with a linear strain distribution.

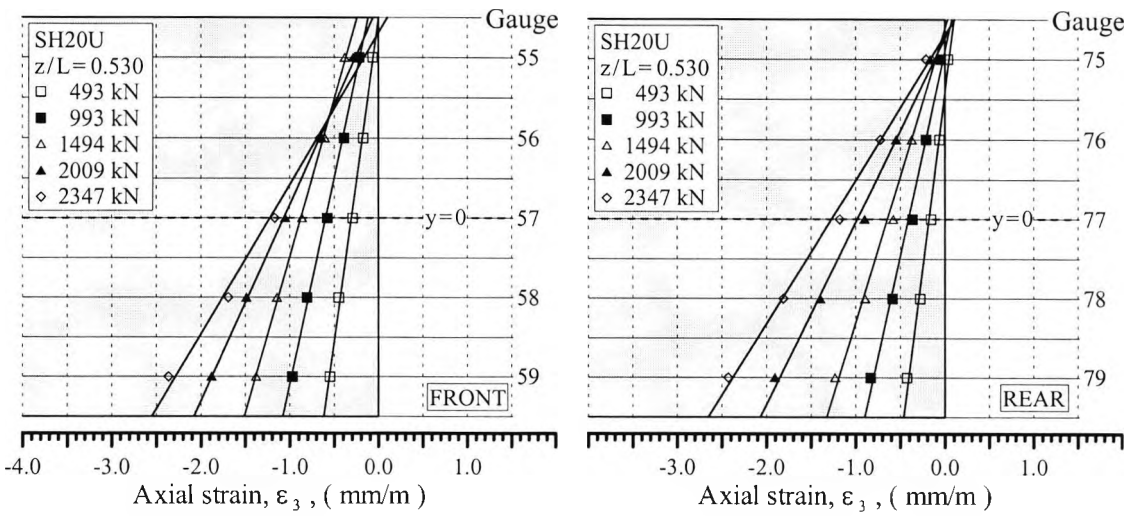

Figure 5.21
Strain profiles for test column SH20U

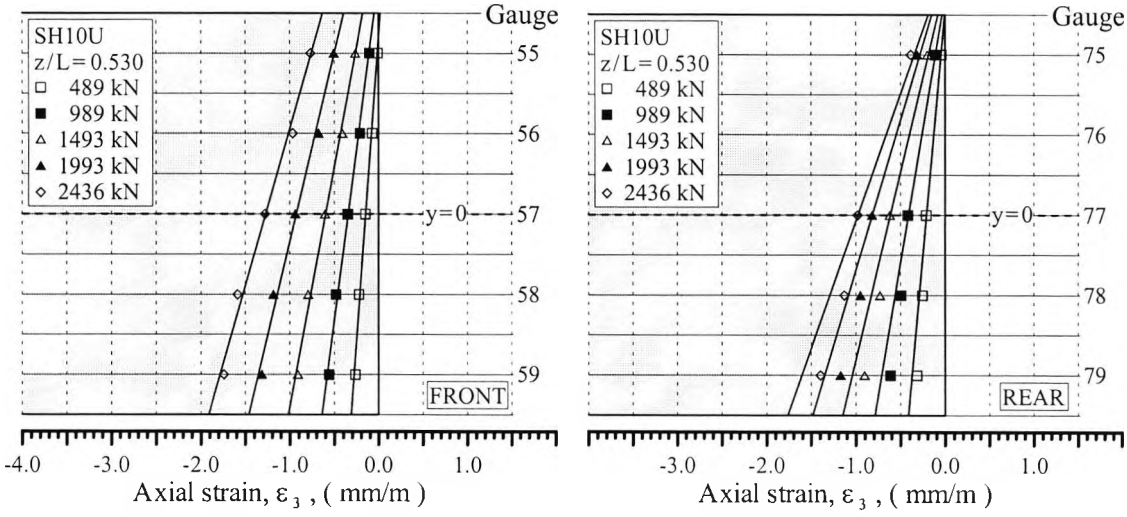

Figure 5.22
Strain profiles for test column SH10U

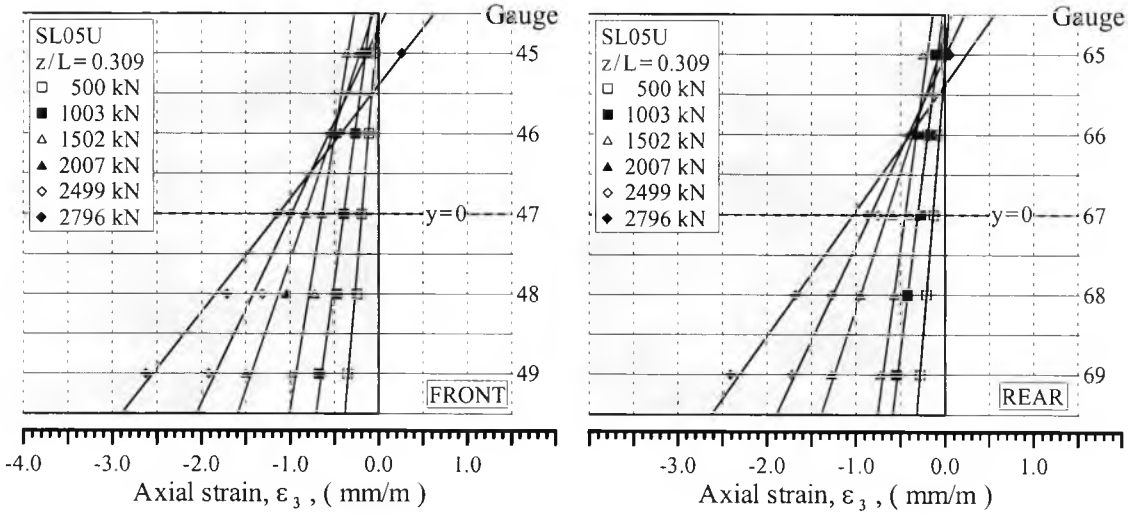

Figure 5.23
Strain profiles for test column SL05U

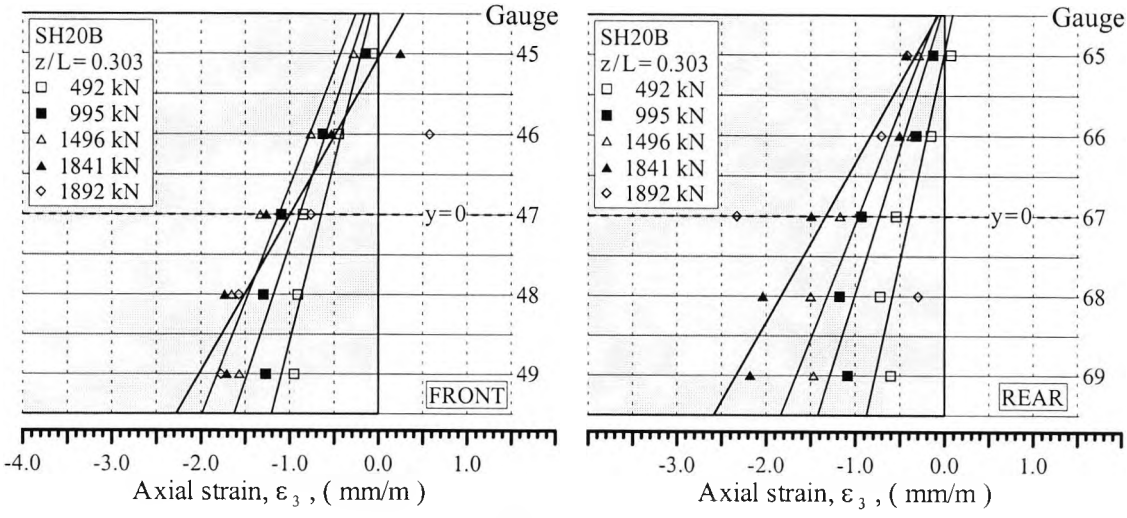

Figure 5.24
Strain profiles for test column SH20B

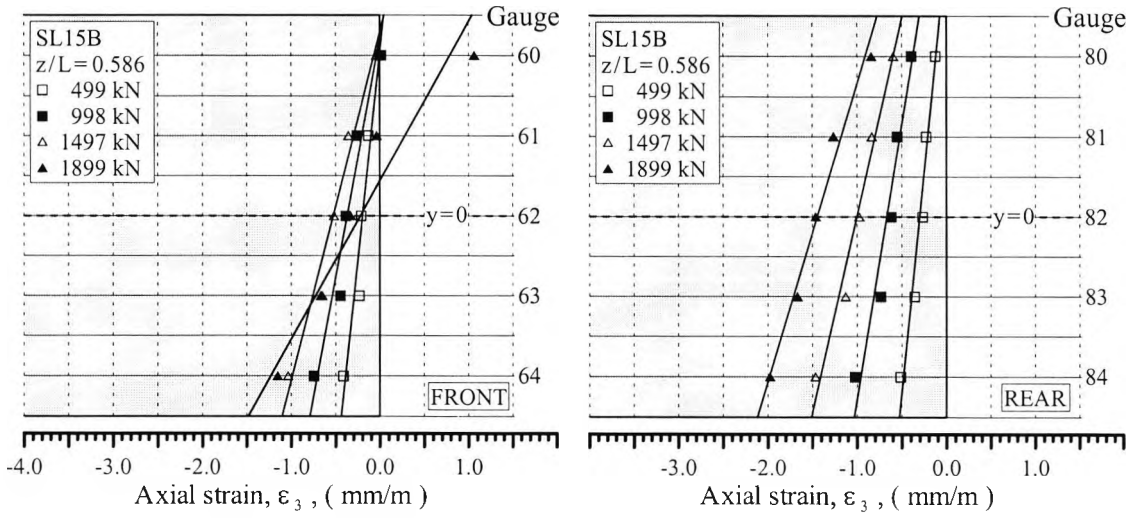

Figure 5.25
Strain profiles for test column SL15B

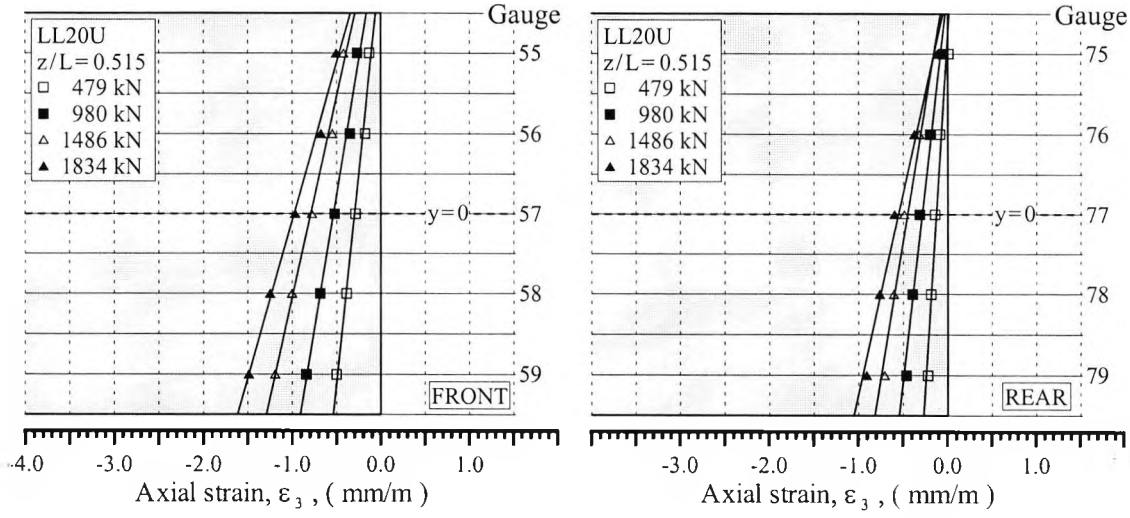

Figure 5.26
Strain profiles for test column LL20U

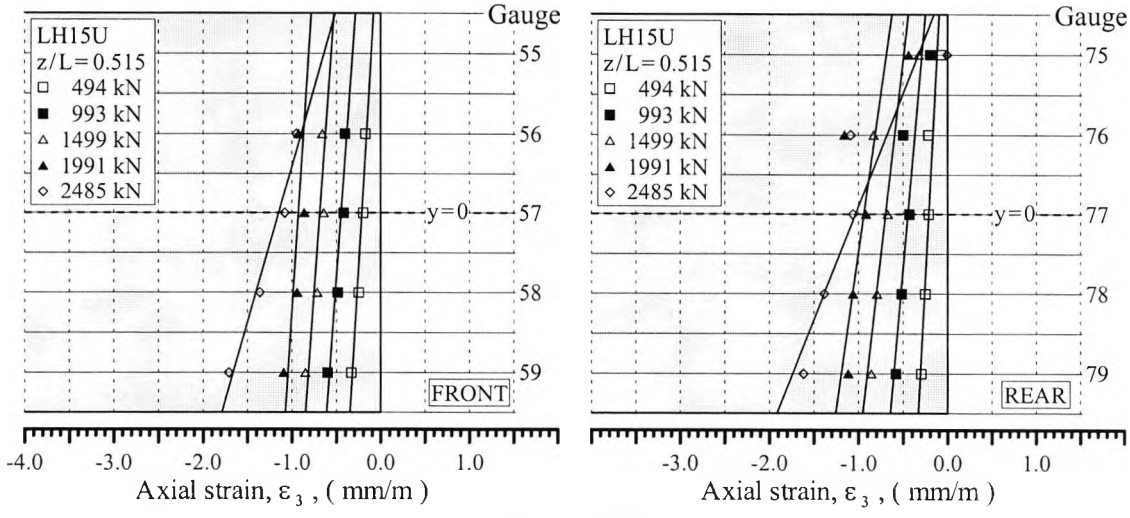

Figure 5.27
Strain profiles for test column LH15U

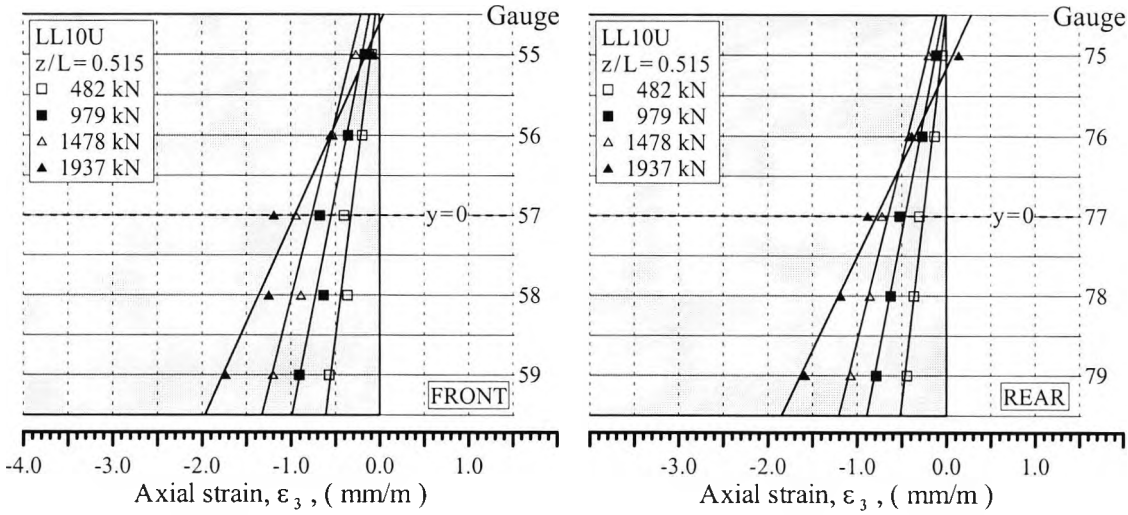

Figure 5.28
Strain profiles for test column LL10U

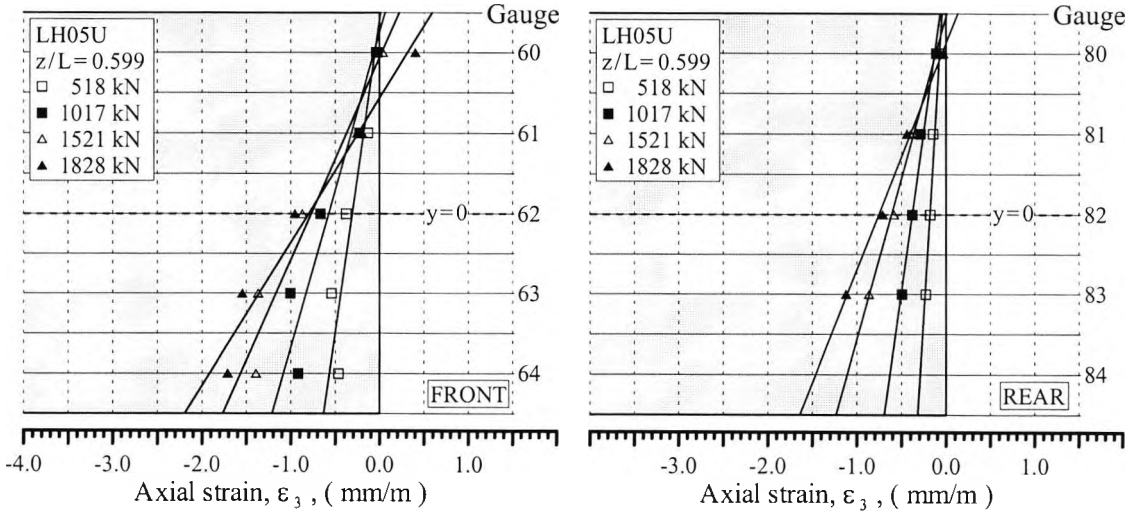

Figure 5.29
Strain profiles for test column LH05U

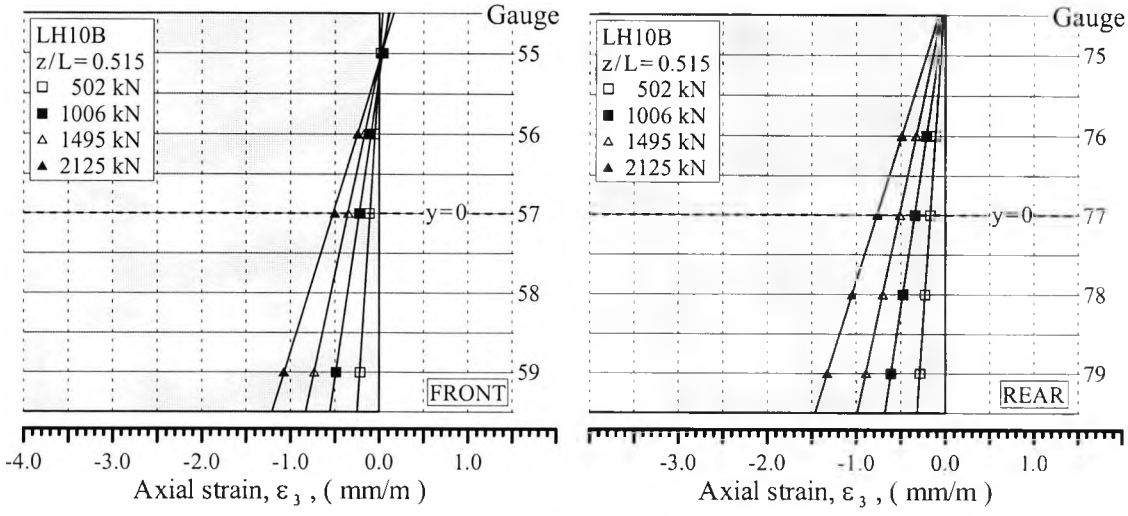

Figure 5.30
Strain profiles for test column LH10B

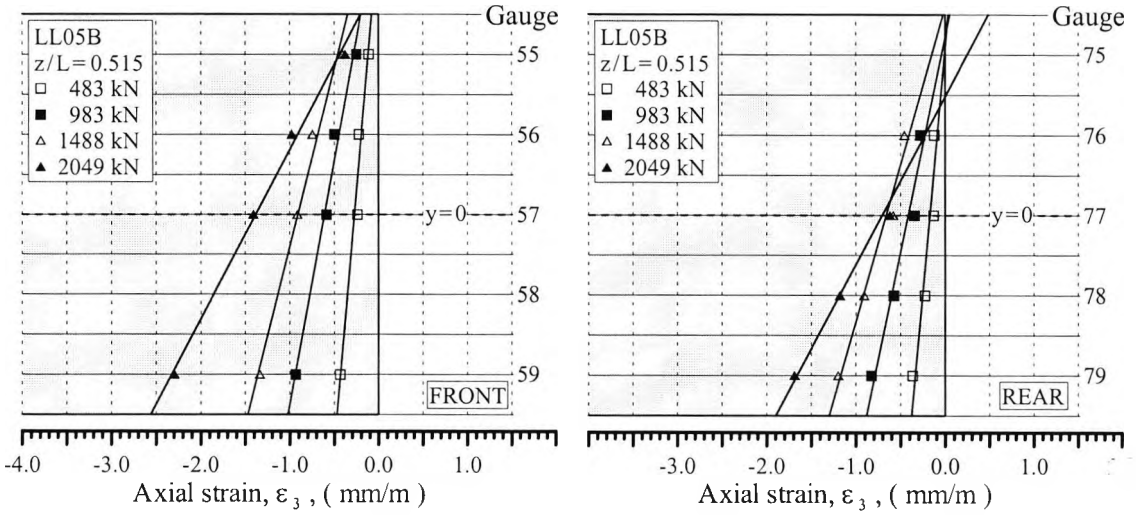

Figure 5.31
Strain profiles for test column LL05B

Extreme fibre strains

Figures 5.32 - 5.42 show the extreme fibre strains near mid-length as a function of the applied axial load for each test column. Both load-strain diagrams derived from the data recorded by the external concrete strain gauges and from the data recorded by the internal steel strain gauges are shown in the figures. The four vertices of the cross-section, i.e. the extreme fibres, are identified by the labels BF (Bottom Front), BR (Bottom Rear), TF (Top Front) and TR (Top Rear) on the diagrams (see figures 5.6 and 5.9 for further details).

The extreme fibre strains were calculated for each load step by extrapolating the plane, given by equation 5.3, best fitting the strain data recorded at the cross-section in question.

$$\varepsilon = \varepsilon_o + \kappa_x(x - x_o) + \kappa_y(y - y_o) \tag{5.3}$$

Thus, the strain parameters, ε_o , κ_x and κ_y , were found by solving the following linear equations:

$$\begin{bmatrix} n & \sum_{i=1}^{n}(x_i - x_o) & \sum_{i=1}^{n}(y_i - y_o) \\ \sum_{i=1}^{n}(x_i - x_o) & \sum_{i=1}^{n}(x_i - x_o)^2 & \sum_{i=1}^{n}(x_i - x_o)(y_i - y_o) \\ \sum_{i=1}^{n}(y_i - y_o) & \sum_{i=1}^{n}(x_i - x_o)(y_i - y_o) & \sum_{i=1}^{n}(y_i - y_o)^2 \end{bmatrix} \begin{Bmatrix} \varepsilon_o \\ \kappa_x \\ \kappa_y \end{Bmatrix} = \begin{Bmatrix} \sum_{i=1}^{n}\varepsilon_i \\ \sum_{i=1}^{n}\varepsilon_i(x_i - x_o) \\ \sum_{i=1}^{n}\varepsilon_i(y_i - y_o) \end{Bmatrix} \quad (5.4)$$

In general, the load-strain diagrams derived from the data recorded by the external strain gauges agree well with those derived from the data recorded by the internal strain gauges. The differences can at least partially be ascribed to the fact that the two sets of strain data often did not originate from the exact same column section, though it is likely that the extreme fibre strains derived from the strain data recorded by the external gauges, in general, are the more accurate. The obvious reason is the larger sample size, combined with the fact that the proper working of the external gauges was not impaired by the occurrence of tensile cracking or cover spalling.

It is interesting that some of the test columns which were subjected to nominally identical loading conditions resulted in rather different load-strain diagrams.

The load-strain curves for column SH20U (figure 5.32) were observed to consist of three distinct phases. In the first phase the extreme fibre strains developed almost linearly with the applied axial load. This phase terminated upon reaching an axial load corresponding to about 77% of the column's failure load, at which point the column suddenly began to yield. Soon after, the column regained a resistance to incremental loading comparable to that of the linear phase. During the final phase the strains developed at an increasing rate. The load-strain diagrams also show that the front of the column in general was more compressed than the rear.

In the case of column SH10U (figure 5.33) the load-strain response remained nearly linear until the occurrence of failure. Throughout the test the column was subjected to an increasing amount of flexure in the horizontal plane, and at the time of failure a difference of up to about 0.5 mm/m existed between the extreme fibre strains observed on the front and rear side of the column.

Like for column SH20U, the load-strain diagrams for column SL05U (figure 5.34) display three distinct phases. The transition from nearly linear to yielding behaviour occurred at an axial load corresponding to about 58% of the column's load capacity. At the time of failure the maximum compressive strain at the rear of the column exceeded the same strain at the front by approximately 0.6 mm/m.

In accordance with the biaxial loading conditions, the rear of column SH20B (figure 5.35) was observed to experience more compression than the front. However, with a maximum of about 0.5 mm/m, the difference between the strains observed on the two sides was comparable to that for the shorter columns expected to deflect in the vertical plane only. The load-strain diagrams for column SH20B display temporary yielding at an axial load to failure load ratio of approximately 0.85.

The load-strain response for column SL15B (figure 5.36) was, as expected, quite similar to that of column SH20B, though the strains associated with bending in the horizontal plane are somewhat more pronounced. For both columns, the strain distribution determined on the basis of the data recorded by the internal steel gauges has a larger maximum compressive strain than the distribution determined on the basis of the data recorded by the external concrete gauges.

Although expected to deflect in the vertical plane only, the front of column LL20U (figure 5.37) was found to pick up significantly more compression than the rear. At failure, the maximum compressive strain at the front of the column was approximately 0.4 mm/m larger than the same strain at the rear. It can also be noted that the load-strain curves determined for column LL20U are nearly linear until the occurrence of failure.

The response of column LH15U (figure 5.38) displayed the three distinct phases, with the linear phase terminating upon reaching an axial load corresponding to about 93% of the column's failure load. As it was the case for the majority of the longer columns, the straining associated with bending in the horizontal plane was relatively insignificant.

In the case of test column LL10U (figure 5.39), the sudden deviation from nearly linear load-strain behaviour took place upon reaching an axial load corresponding to about 88% of the column's failure load.

The diagrams for column LH05U (Figure5.40) show that the load-strain response of this column softened somewhat upon reaching an axial load corresponding to approximately 71% the column's failure load. In contrast to the response of the columns LH15U and LL10U, the intermediate phase where the strains grow rapidly under a condition of little or no increase in the applied load was absent.

The load-strain response of column LH10B (figure 5.41) was nearly linear up to the occurrence of failure. The column was nominally subjected to biaxial eccentric loading, but the strain gradient associated with bending in the horizontal plane was observed to be significantly smaller than the similar gradient for column LL20U, though the latter column was expected to deflect in the vertical plane only.

When based on the data recorded by the external strain gauges the extreme fibre strains at the opposite sides of column LL05B (figure 5.42) differed by up to 0.7 mm/m. In contrast, the same calculations based on the data recorded by the internal gauges indicated that the bending in the horizontal plane was negligible. Column LL05B, unlike the three other columns tested for biaxial compression, had a built-in eccentricity so as to be expected to experience more compression at its front than its rear side.

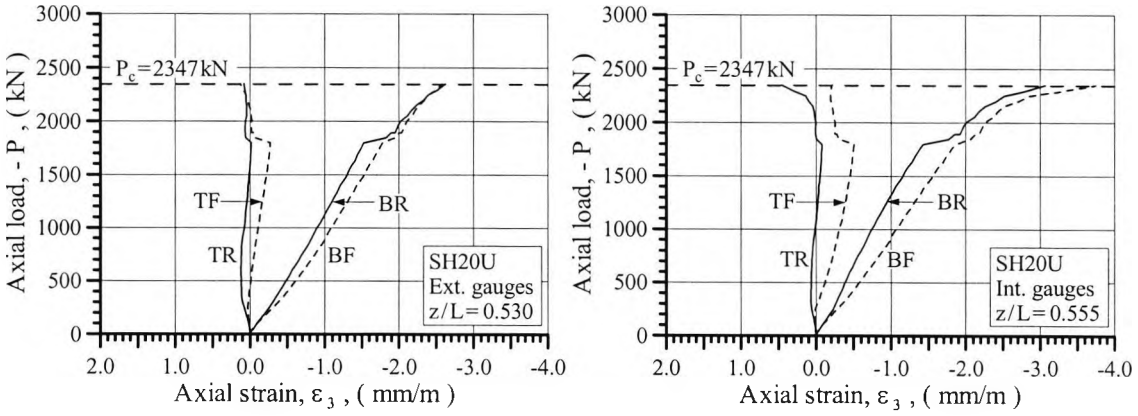

Figure 5.32
Extreme fibre strains for column SH20U

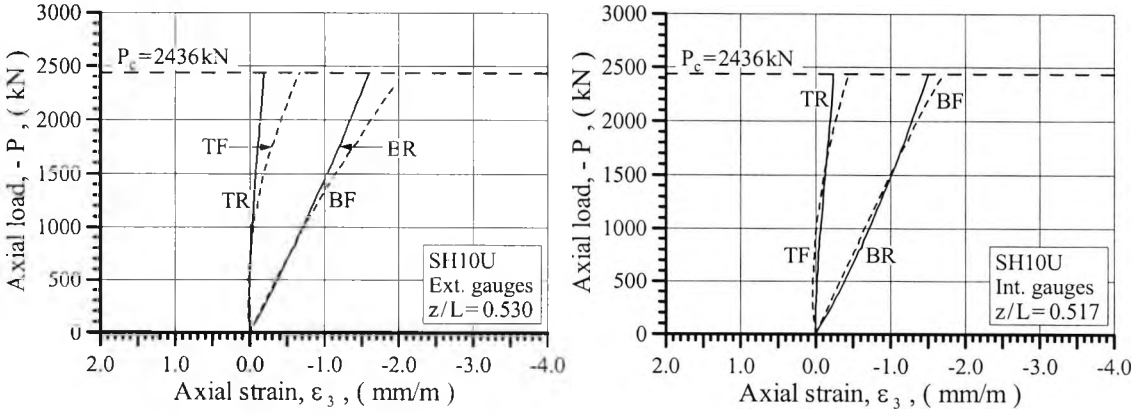

Figure 5.33
Extreme fibre strains for column SH10U

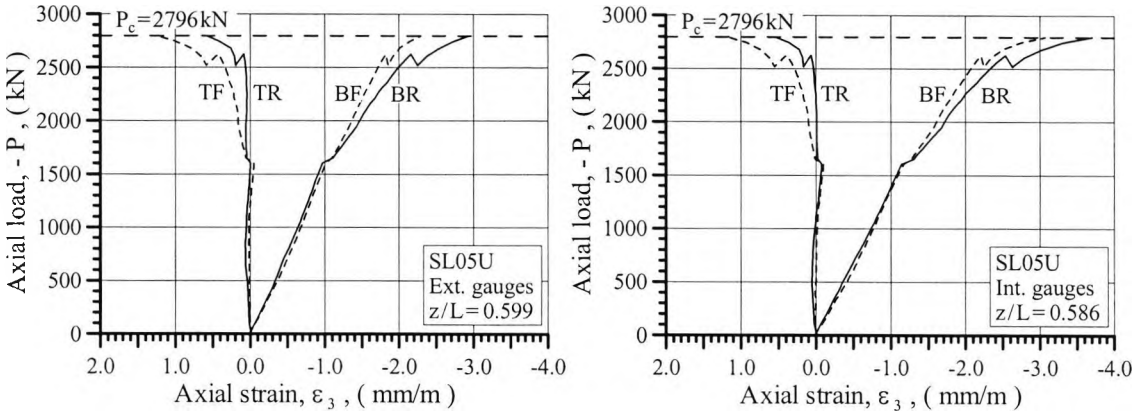

Figure 5.34
Extreme fibre strains for column SL05U

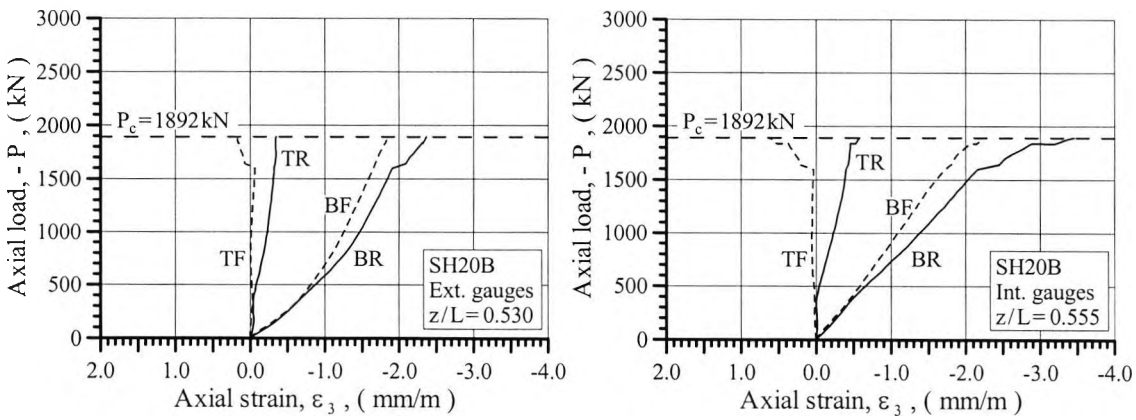

Figure 5.35
Extreme fibre strains for column SH20B

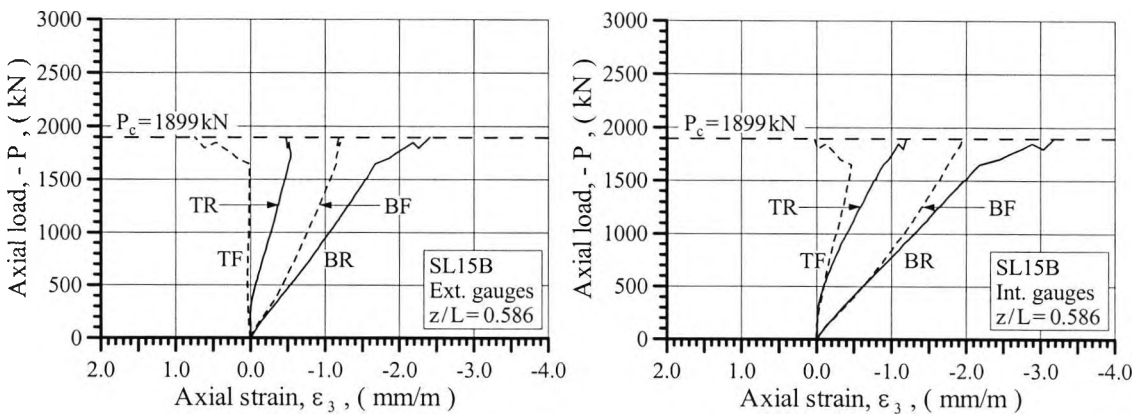

Figure 5.36
Extreme fibre strains for column SL15B

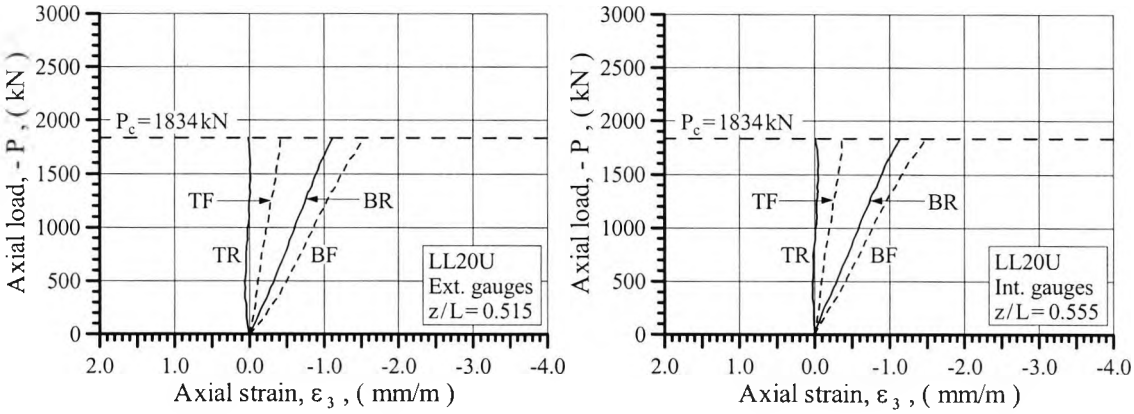

Figure 5.37
Extreme fibre strains for column LL20U

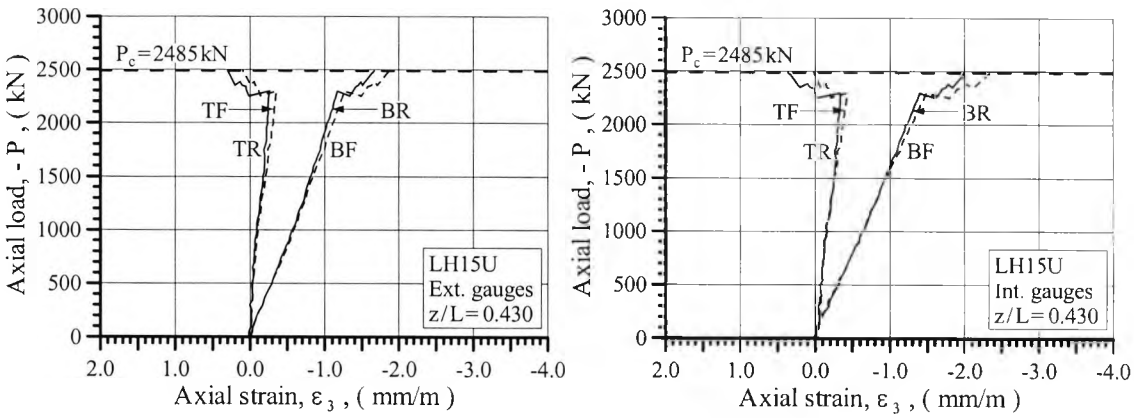

Figure 5.38
Extreme fibre strains for column LH15U

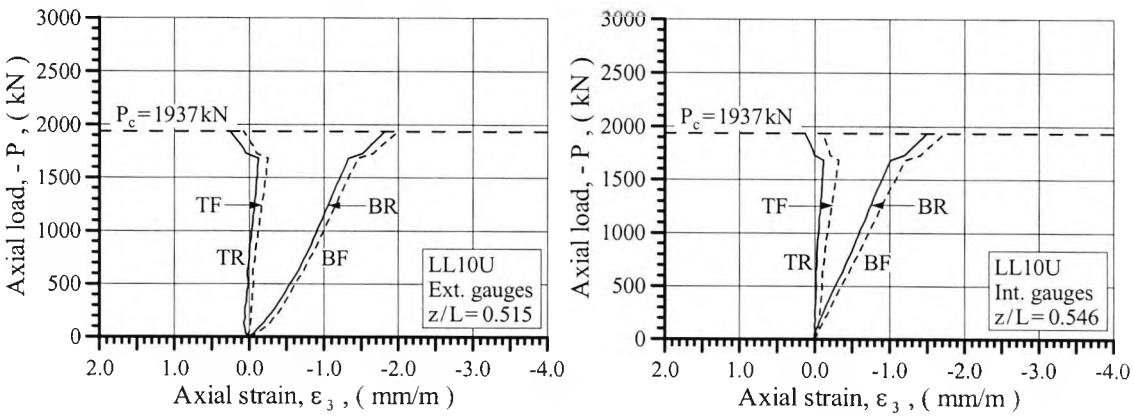

Figure 5.39
Extreme fibre strains for column LL10U

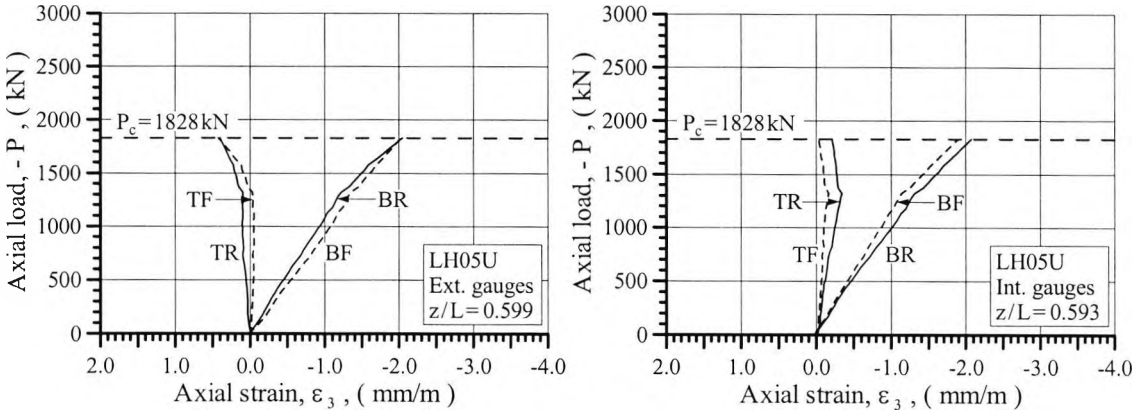

Figure 5.40
Extreme fibre strains for column LH05U

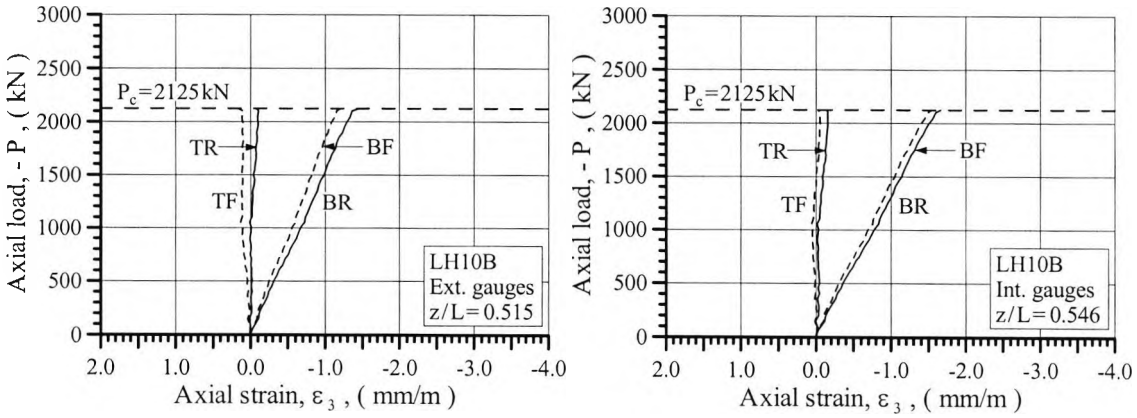

Figure 5.41
Extreme fibre strains for column LH10B

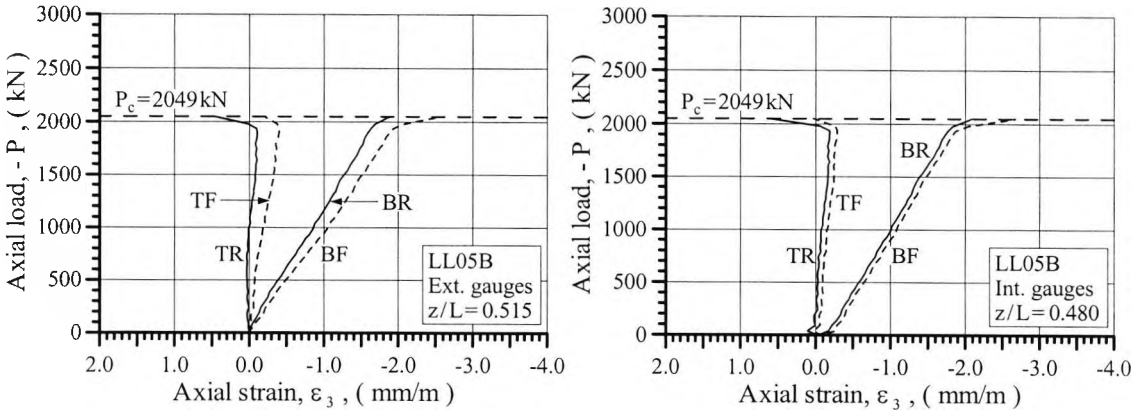

Figure 5.42
Extreme fibre strains for column LL05B

Table 5.4 lists the maximum and minimum value of strain at peak load for each of the tested columns. When determined on the basis of data recorded by the external strain gauges, the minimum strain was between -1.5 mm/m and -2.9 mm/m, and the maximum strain between -0.2 mm/m and 1.2 mm/m. Thus, for none of the tested high-strength concrete columns did the maximum compressive strain reach the limiting value of 3.5 mm/m adopted in BS8110 (1985). Indeed all columns, except column SL05U, failed at a maximum compressive strain which was less than the peak strain, ε_c , predicted by equation 3.5 when assuming the concrete strength, f_c , to be equal to 81% of the average strength of the 100×200 mm cylinders.

The maximum compressive strain determined on the basis of the data recorded by the strain gauges mounted on the longitudinal steel bars was larger for most of the columns than the maximum compressive strain determined on the basis of the data recorded by the strain gauges mounted on the surface of the column. Nevertheless, only for three of the test columns did the maximum compressive strain equal or exceed 3.5 mm/m, and of the remaining columns six failed at a maximum compressive strain which was less than the peak strain predicted by equation 3.5.

Table 5.4 also shows that the compressive strain at failure in general was less for the longer columns than for the shorter columns. According to the calculations based on data recorded by the concrete strain gauges, the shorter columns failed at an average maximum compressive strain of 2.5 mm/m, and the longer columns at an average maximum compressive strain of 1.9 mm/m. For the calculations based on data recorded by the steel strain gauges, the similar average strains were 3.2 mm/m and 2.0 mm/m respectively. Furthermore, the results indicate that an increase in the density of the steel reinforcement

cage had the effect of increasing the ductility of the columns. The increased ductility manifested itself in a small increase in the absolute values of the maximum and minimum strains at column failure.

Table 5.4
Summary of extreme fibre strains at column failure

Column	Failure load	Concrete		External strain gauges		Internal strain gauges	
Name	P_c (kN)	f_c (MPa)	ε_c (mm/m)	$\varepsilon_{3,min}$ (mm/m)	$\varepsilon_{3,max}$ (mm/m)	$\varepsilon_{3,min}$ (mm/m)	$\varepsilon_{3,max}$ (mm/m)
SH20U	2347	104.5	3.0	-2.6	0.1	-3.7	0.5
SL15U	-	-	-	-	-	-	-
SH10U	2436	104.5	3.0	-2.1	-0.2	-1.7	-0.2
SL05U	2796	77.0	2.7	-2.9	1.2	-3.7	1.2
SH20B	1892	103.7	3.0	-2.4	0.2	-3.5	0.6
SL15B	1899	89.1	2.8	-2.4	0.7	-3.2	0.0
LL20U	1834	81.8	2.7	-1.5	0.0	-1.5	0.0
LH15U	2485	104.5	3.0	-1.9	0.3	-2.3	0.4
LL10U	1937	82.6	2.8	-2.0	0.3	-1.7	0.1
LH05U	1828	99.6	2.9	-2.0	0.4	-2.1	0.0
LH10B	2125	97.2	2.9	-1.5	0.2	-1.7	0.0
LL05B	2049	79.4	2.7	-2.6	0.5	-2.7	0.6

Longitudinal reinforcement

The strain gauges mounted on the longitudinal reinforcement bars showed that for all of the shorter columns, except for column SH10U, at least one of the bars yielded in compression during testing. In the special case of column SH10U, the maximum compressive strain observed in the longitudinal reinforcement bars was 2.1 mm/m, which is 0.6 mm/m less than the average yield strain measured for the bars. For the longer columns, the maximum compressive strain lay between 1.5 mm/m, observed during the testing of column LL10U,

and 2.5 mm/m, observed during the testing of column LH15U. Thus, the test observations indicate that for none of the longer columns had the main reinforcement reached its yield strength at the time of column failure.

As mentioned in section 5.1.3, the bar strains in each column were recorded mid-way between adjacent links at four evenly spaced sections within the middle fifth of the column's effective length. Thus, the gradual development of buckling failure of a given bar would cause one of the strain gauges on the bar to measure strains deviating significantly from those measured by the adjacent gauges. Only in the case of column SH20U did the recorded bar strains suggest that buckling of the longitudinal reinforcement bars could have initiated column failure. Figure 5.43 show the strains recorded by a group of gauges during the testing of the columns SH20U and SL05U. On reaching an axial load corresponding to about 92% of the column's failure load, the strains recorded by gauge 40 of column SH20U began to deviate significantly from the strains recorded by the other gauges in the group. As illustrated by the diagram for column SL05U, such a deviation from the general trend was not observed during the testing of any of the other columns.

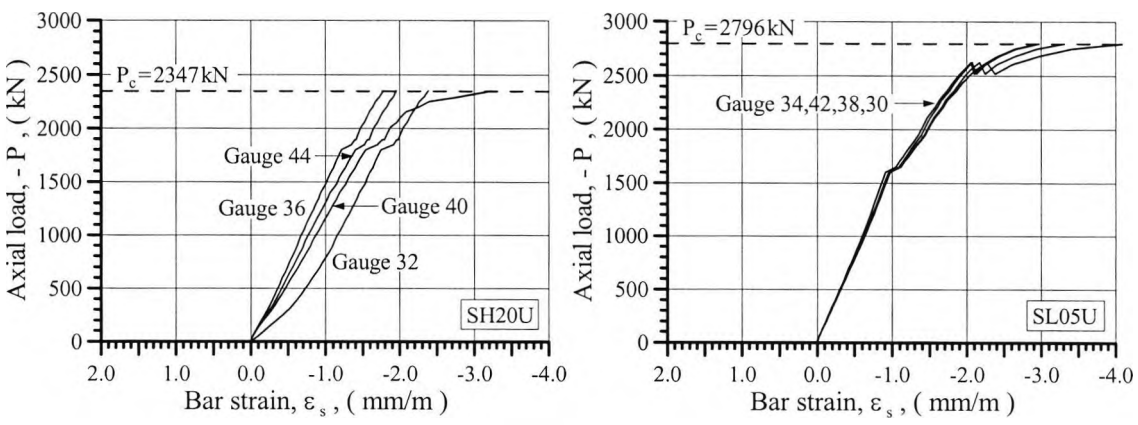

Figure 5.43
Straining of main reinforcement bars

Transverse reinforcement

Figure 5.44 shows the relationship between the tensile strains and the axial load for one of the instrumented ties of column SL15B. The tensile strain in a given tie leg was calculated as the mean value of the strains recorded by a pair of gauges. The figure confirms that the tensile strain is largest in the lower tie leg parallel with the bottom face of the column, and that the strain achieves its maximum at the time of failure. The figure is at least qualitatively representative for all of the tested columns.

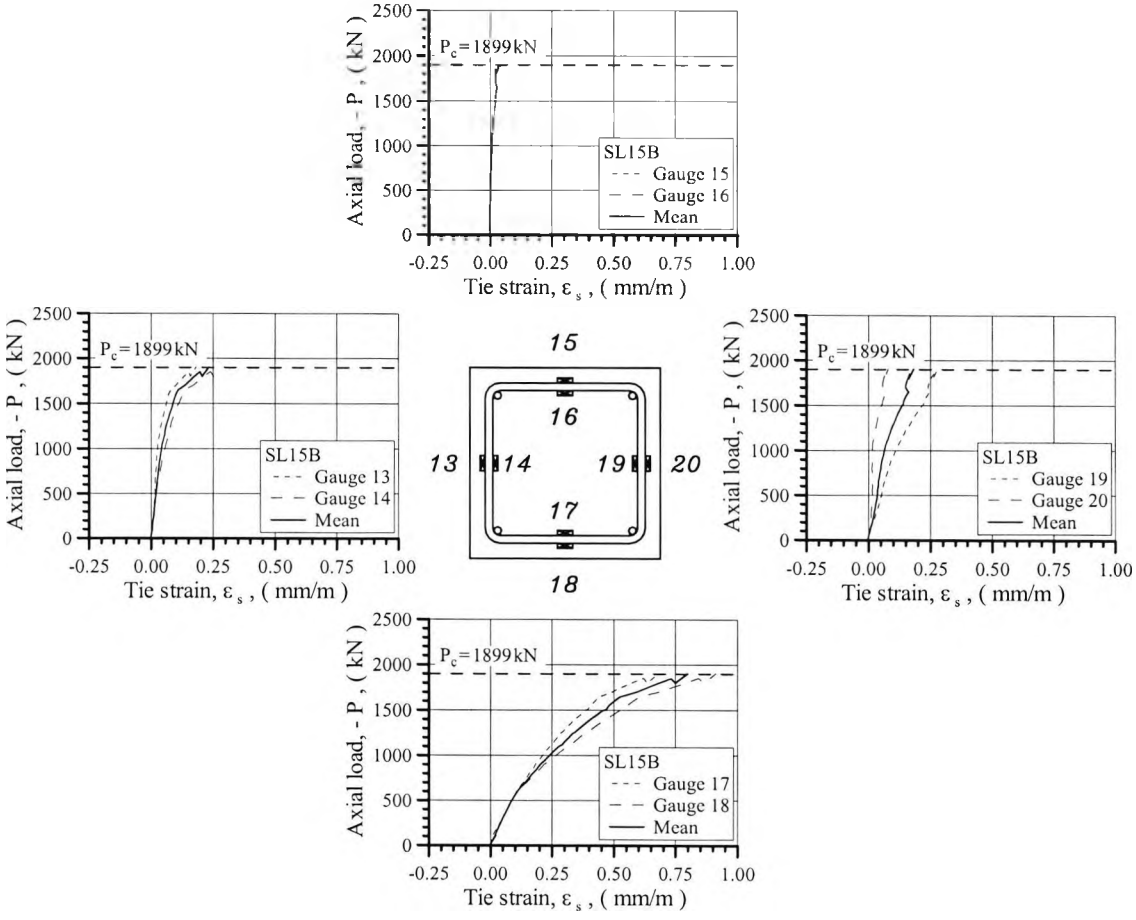

Figure 5.44
Typical straining of transverse reinforcement

For the columns SH20B, SL15B, LL20U, LL10U and SL05U, the maximum tensile strain was observed to develop in the instrumented tie located nearest to the bridge bearing. Otherwise, the maximum tensile strain was always detected in one of the instrumented ties located within the central region of the column. However, a comparison of the tensile

strains measured at similar points on the three ties located within the central region of a column revealed that the straining of neighbouring ties could be quite different. For the shorter columns a strain variation up to 1.2 mm/m, and for the longer columns a strain variation up to 0.5 mm/m, was observed.

The maximum tensile strain, $\varepsilon_{s,max}$, measured in the transverse reinforcement of each test column can be read in table 5.5. It is interesting that for none of the test columns did the transverse reinforcement reach its yield strain prior to column failure. The ratio between the maximum tensile strain and the yield strain varied from 0.20 to 0.90, with an average value of 0.60. A weak tendency of the strain ratio to increase with decreasing column length, and with increasing concrete grade, could be noted. In contrast, the tie spacings did not appear to affect the ratio between the observed maximum tensile strain and the yield strain.

Table 5.5
Maximum tensile strain in links

Column	Failure load	Concrete	Transverse reinforcement		
Name	P_c (kN)	$f_{c,cyl}$ (MPa)	ε_{sy} (mm/m)	$\varepsilon_{s,max}$ (mm/m)	$\varepsilon_{s,max}/\varepsilon_{sy}$ (-)
SH20U	2347	129	1.8	1.5	0.84
SL15U	-	95	1.8	-	-
SH10U	2436	129	1.8	1.6	0.90
SL05U	2796	95	1.8	0.7	0.41
SH20B	1892	128	1.5	1.2	0.77
SL15B	1899	110	1.5	1.0	0.69
LL20U	1834	101	1.5	0.3	0.20
LH15U	2485	129*	1.5	1.3	0.85
LL10U	1937	102	1.5	0.4	0.25
LH05U	1828	123	1.5	1.2	0.77
LH10B	2125	120	1.5	0.4	0.29
LL05B	2049	98	1.5	1.0	0.67

$f_{c,cyl}$: compressive strength of 100×200 mm cylinders.
* Estimated from 100 mm cube strength.

5.2.3 Load-Deflection Behaviour

The following summarises the load-deflection behaviour of the 11 full-scale columns tested during the experimental investigation.

Mid-height deflections

Figures 5.45 and 5.46 show the graphs for the mid-height deflections recorded for the shorter and longer columns respectively. The vertical deflections are assumed to be positive in the direction pointing from the bottom towards the top of the column, and the horizontal deflections in the direction pointing from the rear towards the front (see figure 5.6 for details).

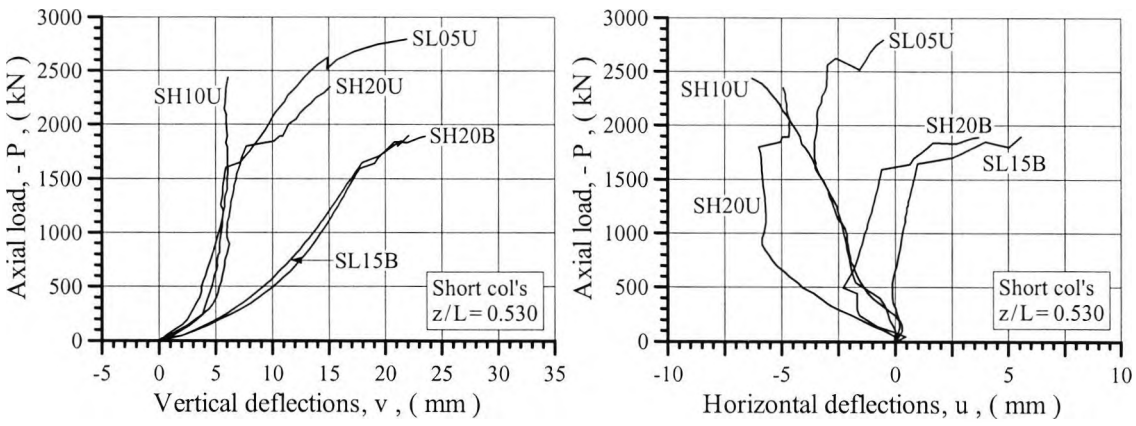

Figure 5.45
Mid-height deflections of shorter columns

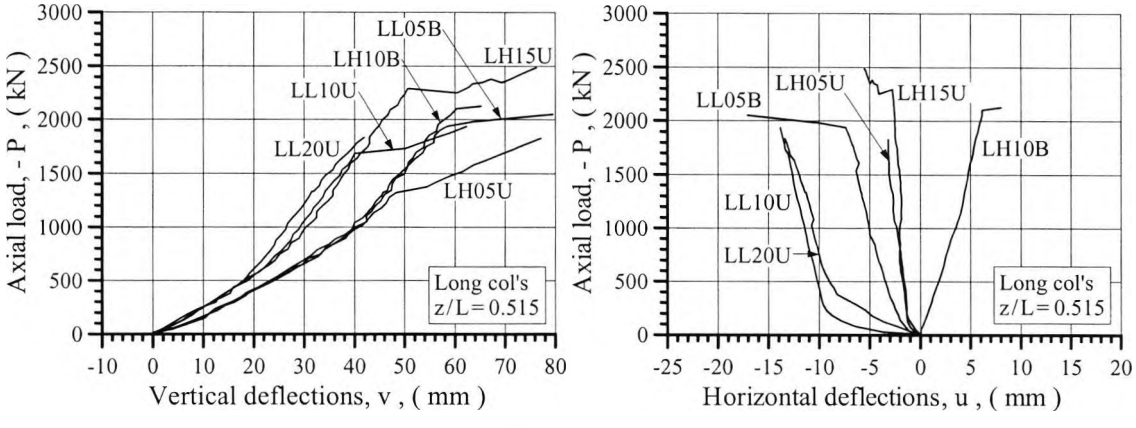

Figure 5.46
Mid-height deflections of longer columns

The curves for the vertical mid-height deflections indicate that, the columns initially responded in a stiffening fashion to the applied axial load. Furthermore, with the exception of the columns SH10U and LL20U, the response suddenly softened significantly at a point within the second half of the loading process. It can be seen that the overall load-deflection response of the columns manufactured with biaxial end-eccentricities was much softer than the response of the similar columns manufactured with uniaxial end-eccentricities.

In the case of the shorter columns, the vertical mid-height deflection at failure of column SH10U was a very modest 6 mm, whereas the remaining of the shorter columns failed at deflections between 15 mm and 24 mm. In the case of the longer columns, the mid-height deflection at failure of column LL20U was 42 mm, and as such, was significantly less than the deflections recorded for the remaining of the longer columns. The vertical mid-height deflection at failure of these ranged from 62 mm to 80 mm.

It is suspected that both the experimental setup for the shorter and the longer columns promoted a bias towards horizontal deflections in the negative direction. Indeed, the horizontal mid-height deflections recorded for two of the three shorter columns nominally tested under a condition of uniaxial eccentric compression were larger than those recorded for the two columns nominally tested under a condition of biaxial eccentric compression. Likewise, the horizontal mid-height deflections registered during the testing of the longer columns LL20U and LL10U were larger than those registered during the testing of the column LH10B. However, the quantifiable manifestation of the bias appeared to be rather erratic. For example, only during the very final stage of loading were the deflections recorded for column LL05B larger than those recorded for the columns LL20U and LL10U, and this despite the fact that column LL05B inadvertently had been manufactured with

inverted eccentricities so as to promote horizontal deflections in the negative rather than the positive direction.

By comparing the recorded mid-height deflections (figures 5.45 and 5.46) with the extreme fibre strains (figures 5.32 to 5.42), or rather with the curvatures associated with the extreme fibre strains (figures 5.47 and 5.48), a few apparent conflicts between the test observations could be identified. For example, the soft load-deflection response observed for column SL15B when compared to the remaining of the shorter columns is not reflected in the curvature diagrams. The vertical mid-height deflections of the columns SH20U, SH10U and SL05U were for axial loads between 500 kN and 1500 kN almost stationary, yet the recorded strains indicate continuing bending in the vertical plane. The horizontal deflections recorded for column SL05U, and to a large extent also those recorded for column SH20B, were negative. Nevertheless the measured strains suggest that these columns primarily deflected in the positive direction. Finally, the horizontal mid-height deflection curves for column LL20U and column LL10U were almost identical, yet the measured strains suggest that column LL10U experienced significantly less bending in the horizontal plane than column LL20U.

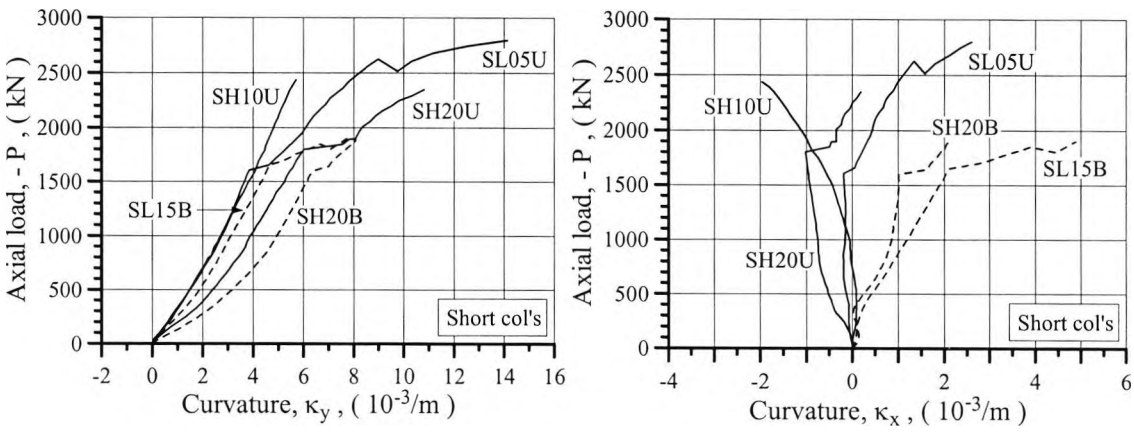

Figure 5.47
Mid-height curvatures of shorter columns

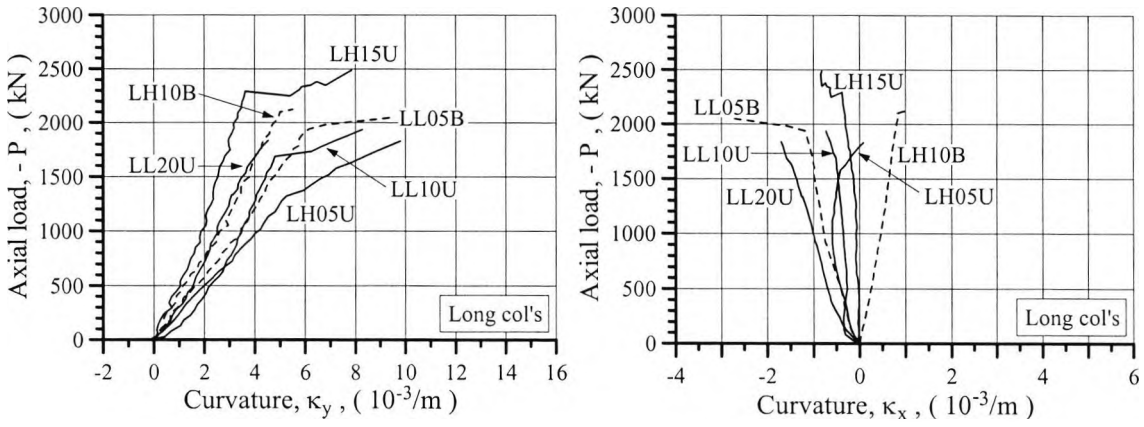

Figure 5.48
Mid-height curvatures of longer columns

Modified mid-height deflections

Control measurements taken directly on the loading rig during the testing of the longer columns showed the rig to undergo significant movements. However, since the experimental programme at the time of taking the control measurements was halfway to completion, and since it was subjected to a combination of tight financial and time constraints, it was decided not to introduce major alteration to the test arrangement or to redo any of the tests. Instead, the extensive displacement data collected during the tests were to be used in an attempt to filter out rigid body displacements.

As seen from figures 5.49 - 5.59, the deflections measured along the length of the test columns indicate that the boundary condition of zero displacements at the normalised locations of $z/L = 0$ and $z/L = 1$ was often violated during testing. It can also be seen from the figures that the maximum horizontal deflection was often measured away from the mid-point of the column.

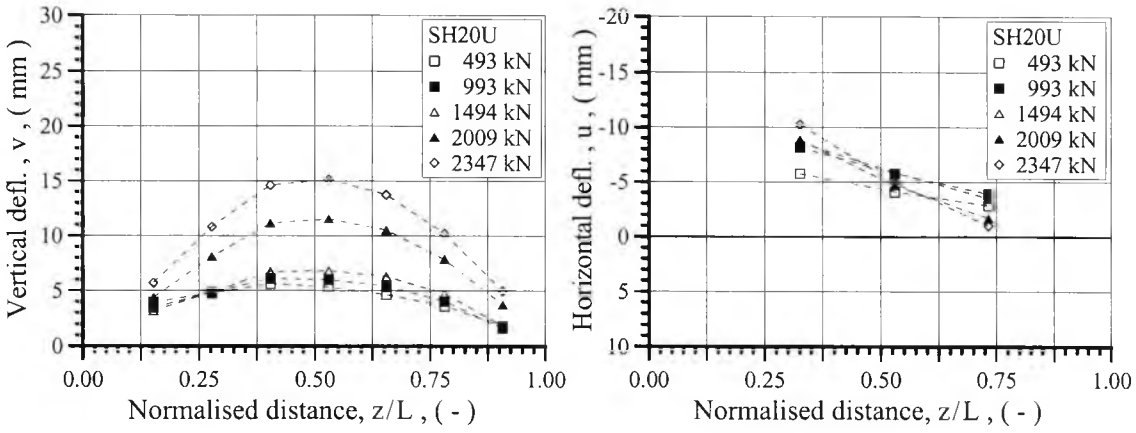

Figure 5.49
Deflected shape of column SH20U

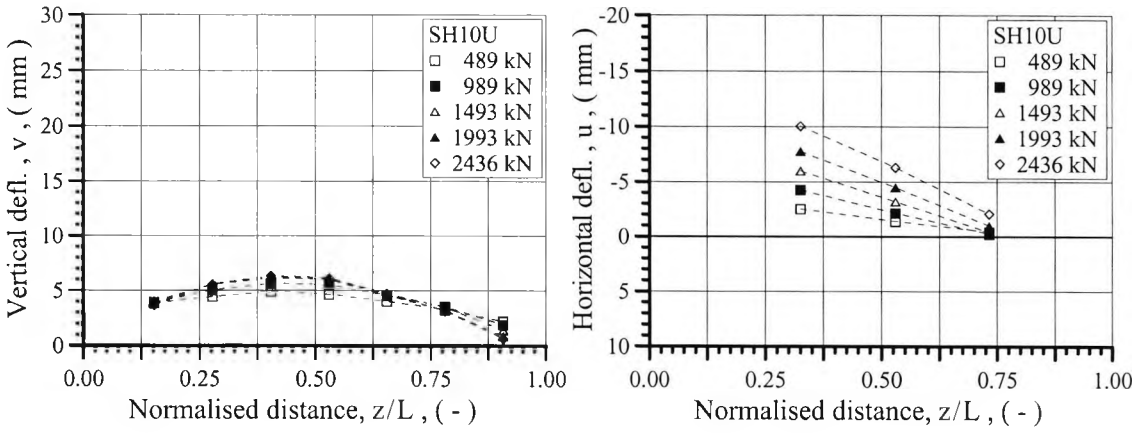

Figure 5.50
Deflected shape of column SH10U

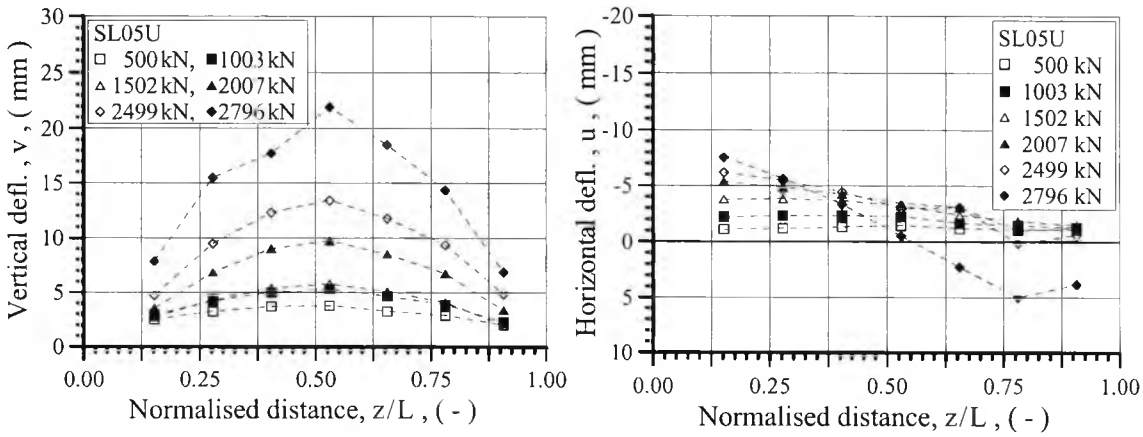

Figure 5.51
Deflected shape of column SL05U

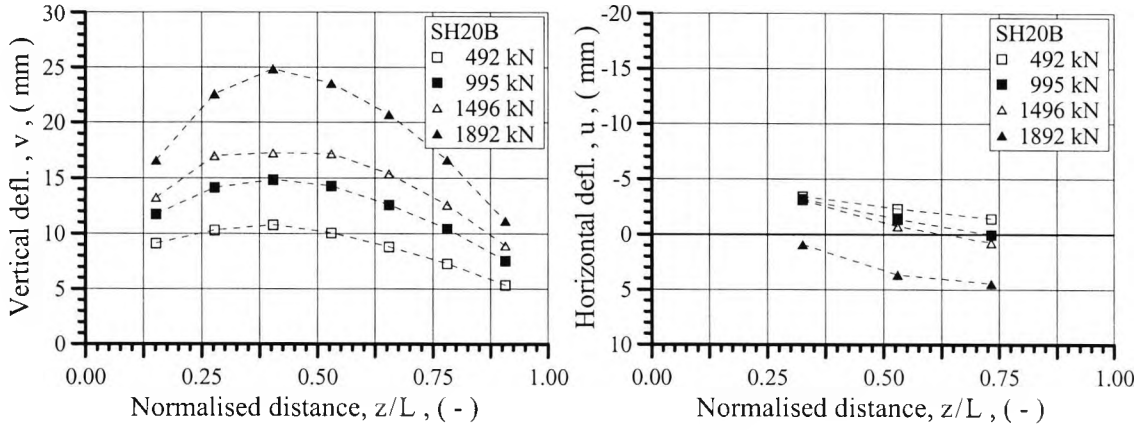

Figure 5.52
Deflected shape of column SH20B

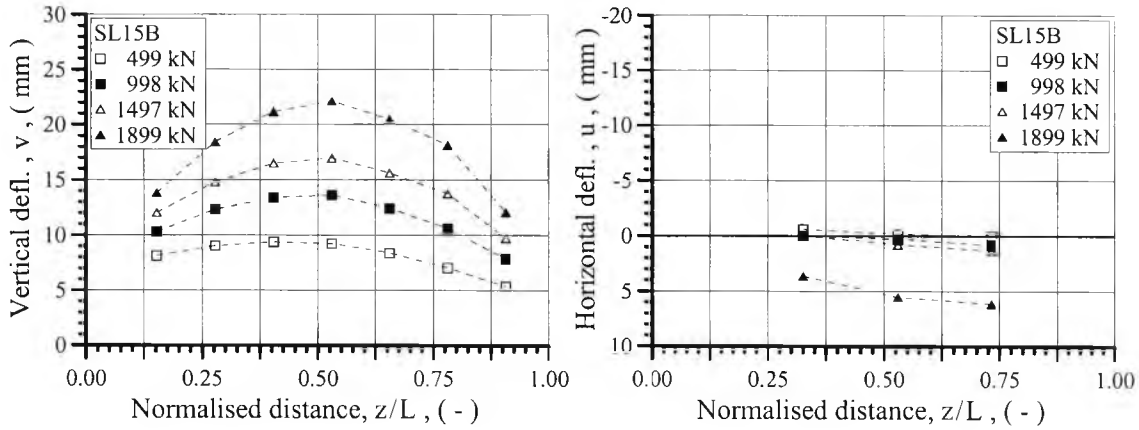

Figure 5.53
Deflected shape of column SL15B

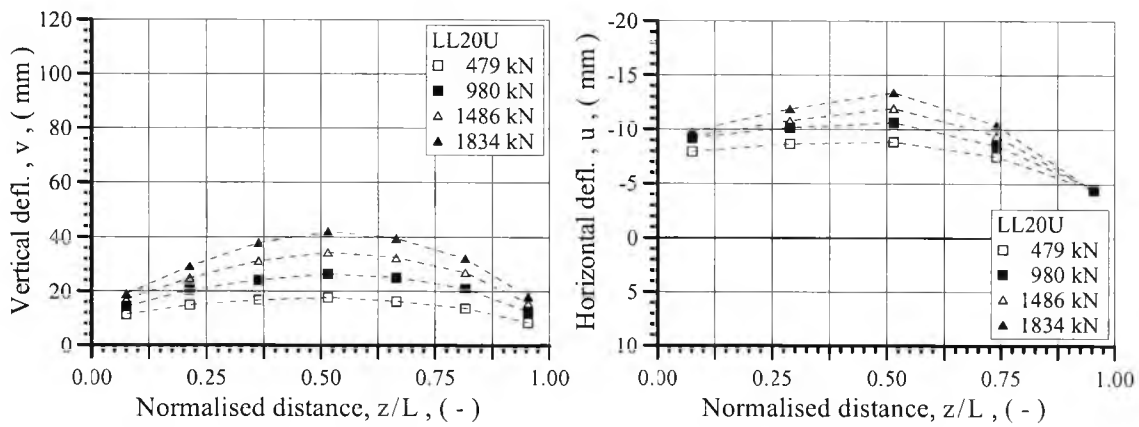

Figure 5.54
Deflected shape of column LL20U

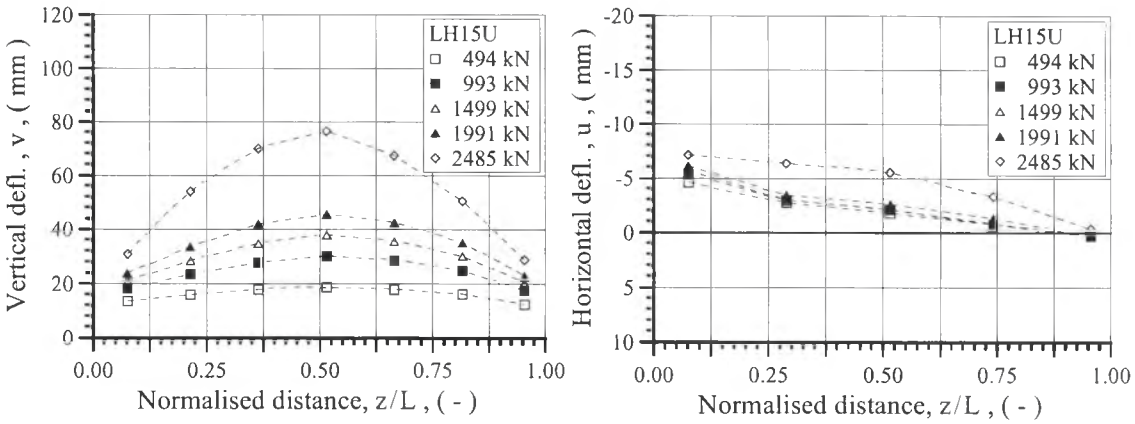

Figure 5.55
Deflected shape of column LH15U

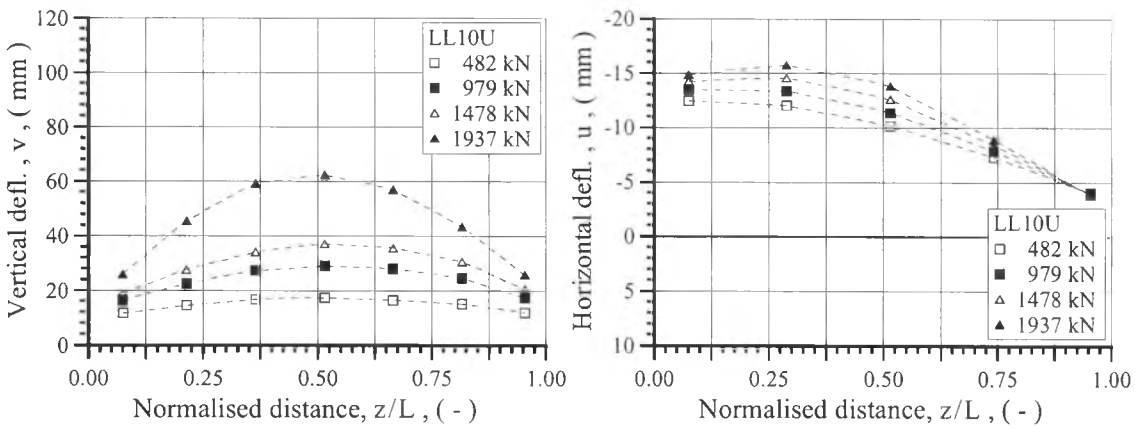

Figure 5.56
Deflected shape of column LL10U

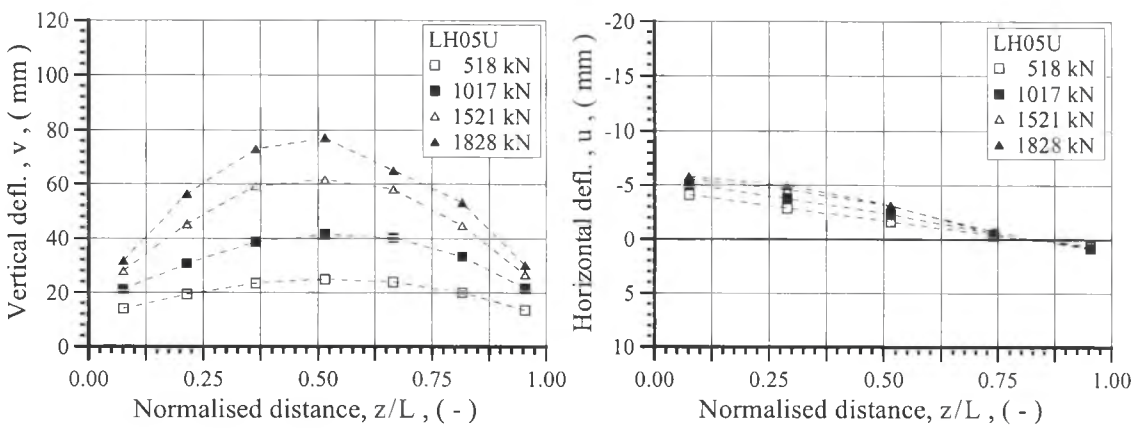

Figure 5.57
Deflected shape of column LH05U

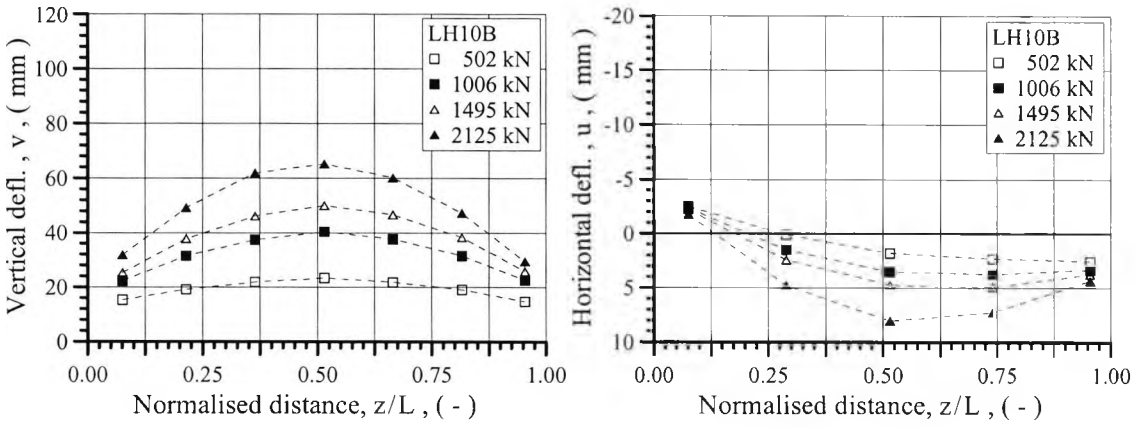

Figure 5.58
Deflected shape of column LH10B

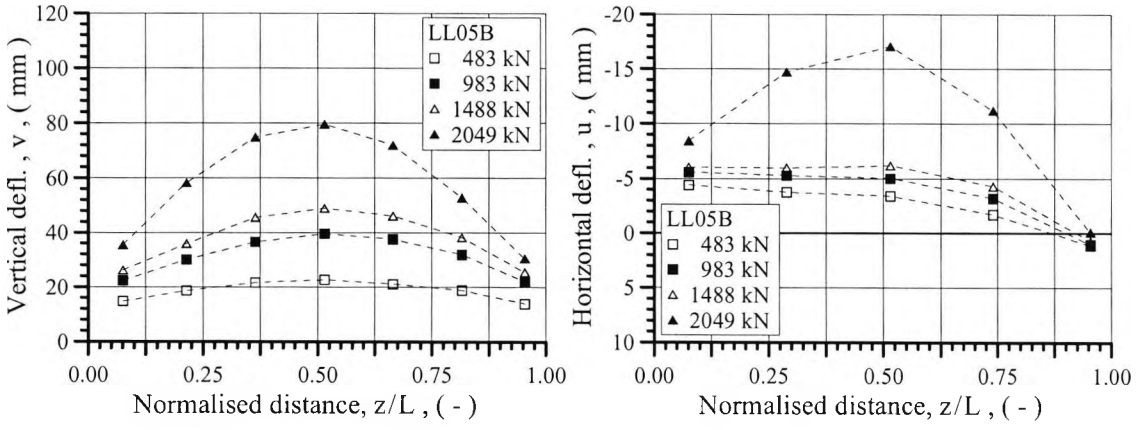

Figure 5.59
Deflected shape of column LL05B

The least square method was employed to fit equations 5.5 and 5.6 to the recorded deflection data. Thus, for each load step, the deformed shape of a test column was approximated by a simple sinusoidal function in each of the two bending planes.

$$v = a_1 + b_1 \frac{z}{L} + c_1 \sin(\pi \frac{z}{L}) \tag{5.5}$$

$$u = a_2 + b_2 \frac{z}{L} + c_2 \sin(\pi \frac{z}{L}) \tag{5.6}$$

Using this procedure for filtering out rigid body displacements, it was estimated that the pinned ends moved upwards by up to 11 mm during testing of column SH20B, and by up

to 9 mm during testing of column SL15B. For the remainder of the shorter columns, the pinned ends were estimated to have moved upwards by less than 4 mm. In the case of the longer columns, the pinned ends were estimated to have moved upwards by between 11 mm and 24 mm, with an average of 18 mm at the end of the bridge bearing and of 21 mm at the end of the load cell.

Figures 5.60 and 5.61 illustrate the mid-height deflections of the test columns after modifying the results for rigid body displacements. It can be noted that the modified deflection diagrams go some way in eradicating the previously described discrepancies existing between deflections and strains. Furthermore, the initial stiffening in the load-deflection response observed for all of the columns has almost entirely disappeared.

Table 5.6 lists the measured mid-height deflections at failure for each of the test columns, and compares these to their modified counterparts. It can be noted that for the shorter columns the mid-height deflections modified for rigid body displacements are up to about 8 mm less, and for the longer columns up to about 23 mm less, than those measured in the tests. Despite the modifications, the vertical deflections for the longer columns remained significantly larger than those for the shorter columns. Furthermore, the deflection data suggest that a reduction in the tie spacing, in general, had the effect of enhancing the pre-peak ductility of the columns.

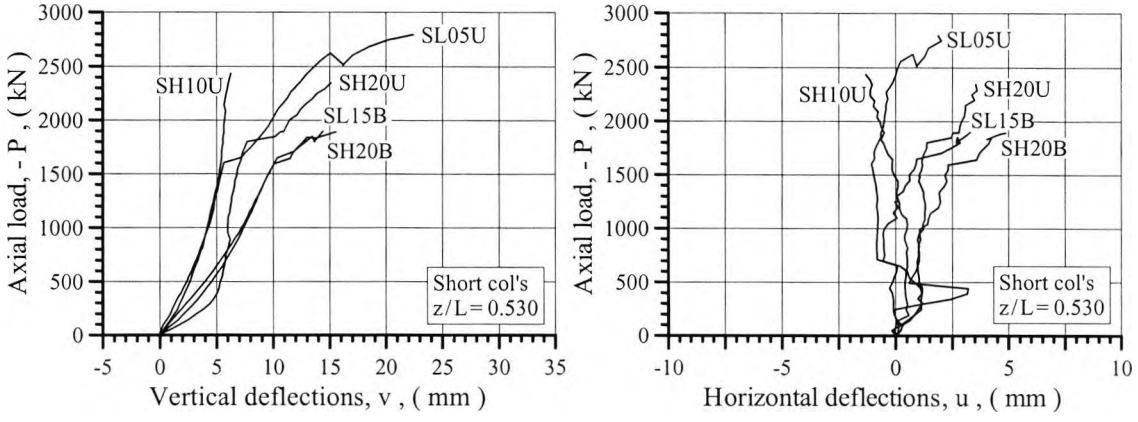

Figure 5.60
Modified mid-height deflections of shorter columns

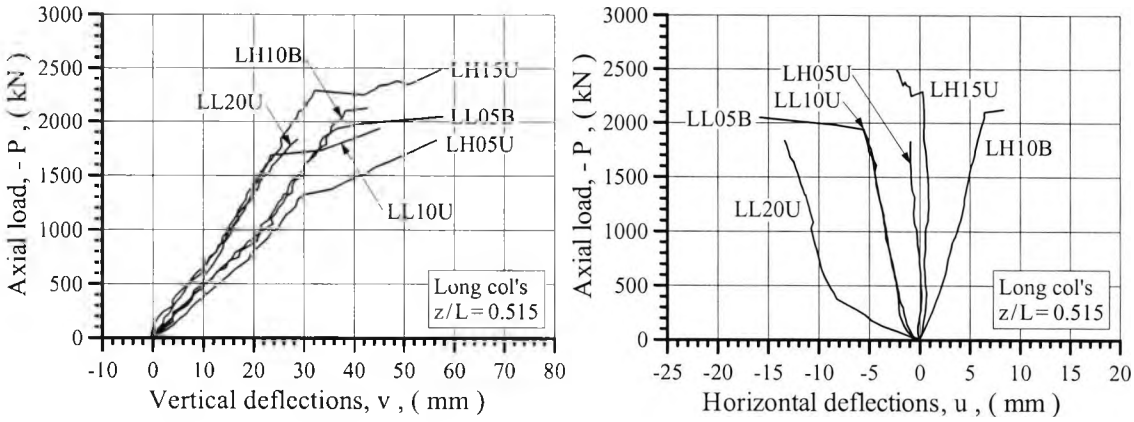

Figure 5.61
Modified mid-height deflections of longer columns

Table 5.6
Mid-height deflections at column failure - measured and modified

Column	Failure load	Measured deflections		Modified deflections	
Name	P_c (kN)	v_{mid} (mm)	u_{mid} (mm)	v_{mid} (mm)	u_{mid} (mm)
SH20U	2347	15.1	-4.9	15.8	3.5
SL15U	-	-	-	-	-
SH10U	2436	6.1	-6.3	6.3	-1.1
SL05U	2796	21.9	-0.5	22.4	1.9
SH20B	1892	23.5	3.7	15.5	4.9
SL15B	1899	22.1	5.6	14.4	3.3
LL20U	1834	41.9	-13.4	28.7	-5.8
LH15U	2485	76.3	-5.5	57.3	-2.2
LL10U	1937	62.3	-13.8	45.1	-5.6
LH05U	1828	77.2	-3.2	56.4	-0.9
LH10B	2125	65.2	8.0	42.7	8.4
LL05B	2049	79.6	-17.1	57.7	-15.8

Deflections taken at position $z/L = 0.530$ for shorter columns, and at $z/L = 0.515$ for longer columns.

5.3 Analysis of Test Results

This section describes the numerical analysis of the full-scale columns. The numerical results are compared with the test results, and possible explanations for differences are investigated.

5.3.1 Expected Behaviour of Test Columns

The structural behaviour of the test columns was computed using the numerical method described in section 4.2.2. The columns were divided into 16 segments along their length, and their cross-sections were modelled by an 8×8 mesh of quadrilateral concrete elements, into which four point elements representing the longitudinal steel reinforcement bars were embedded. Figure 5.62 illustrates the adopted meshing. Three material models were employed in defining the cross-sections. The first material model described the stress-strain behaviour of the unconfined cover concrete, the second the stress-strain behaviour of the confined core concrete, and the third the stress-strain behaviour of the steel reinforcement. The essential material properties of the two concrete components of each test column are listed in table 5.7.

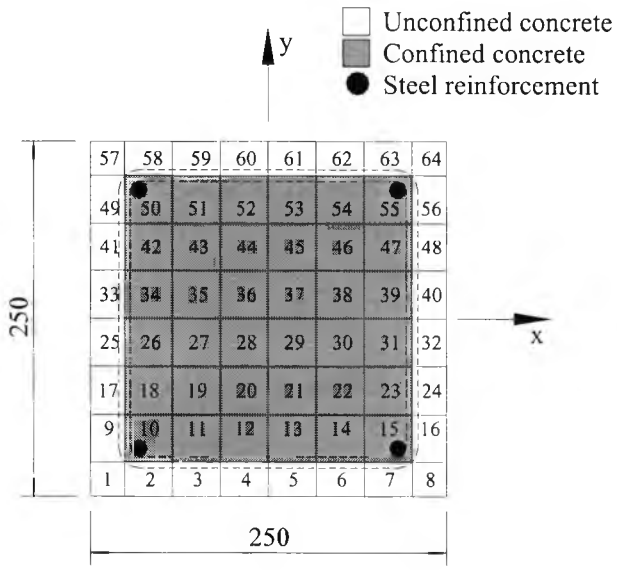

Figure 5.62
Modelling of cross-sections

Table 5.7
Material properties of concrete components

Column	Cover concrete				Core concrete				
Name	f_c (MPa)	E_c (GPa)	ε_c (mm/m)	β (-)	$-\sigma_{1,eff}$ (MPa)	f_{cc} (MPa)	f_{cc}/f_c (-)	ε_{cc} (mm/m)	$\varepsilon_{cc}/\varepsilon_c$ (-)
SH20U	104.5	44.5	3.0	130.1	0.0	104.5	1.00	3.0	1.00
SL15U	77.0	40.6	2.7	32.9	0.2	77.9	1.01	2.8	1.02
SH10U	104.5	44.5	3.0	130.1	0.5	107.5	1.03	3.1	1.04
SL05U	77.0	40.6	2.7	32.9	1.5	86.9	1.13	3.3	1.22
SH20B	103.7	44.4	3.0	125.0	0.0	103.7	1.00	3.0	1.00
SL15B	89.1	42.4	2.8	60.2	0.1	89.7	1.01	2.8	1.01
LL20U	81.8	41.3	2.7	41.8	0.0	81.8	1.00	2.7	1.00
LH15U	104.5	44.5	3.0	130.1	0.1	105.1	1.01	3.0	1.01
LL10U	82.6	41.4	2.8	43.5	0.3	84.4	1.02	2.9	1.04
LH05U	99.6	43.8	2.9	101.8	0.8	105.3	1.06	3.1	1.08
LH10B	97.2	43.5	2.9	90.3	0.3	99.1	1.02	3.0	1.03
LL05B	79.4	41.0	2.7	37.1	0.8	85.0	1.07	3.0	1.12

The unconfined concrete strength, f_c , was taken as 81% of the mean strength of the 100×200 mm cylinders, and the values for the modulus of elasticity, E_c , the peak strain, ε_c , and the softening parameter, β , were determined using equation 3.3, 3.5 and 3.13 respectively. The maximum effective confining pressure, $-\sigma_{1,eff}$, was calculated in accordance with the method described in section 3.4.2, and the stress-strain curves were generated by the computational model described in section 3.4.3. In the case of column SH05U, the compressive strength of the confined core concrete, f_{cc} , was estimated to exceed the unconfined concrete strength by 13%. For the remaining columns, the effect of the provided confinement on the strength and peak strain of the core concrete was estimated to be either small or, in the case of the columns SH20U, SH20B and LL20U, non-existent. The stress-strain behaviour of the longitudinal reinforcement bars was idealised employing an elastic perfectly plastic material model.

Table 5.8 gives a comparison of the experimental and computed results for failure loads and corresponding vertical mid-height deflections. It can be noted that the columns, in general, failed at a significantly higher load than expected. The ratio of test failure load to computed failure load varied from 1.11 to 2.22, with an average of 1.30 for the shorter columns, and an average of 1.96 for the longer columns. These results should be seen in the light of section 4.3, in which it was demonstrated that it is reasonable to expect the numerical model to predict the failure loads to within an accuracy of 10%. The mid-height deflections at failure were significantly overestimated for the shorter columns and, with the exception of column LL20U, underestimated for the longer columns.

Table 5.8
Comparison of experimental and computed results - failure loads and corresponding vertical mid-height deflections

Column	Experimental		Analytical excl. confinement		Analytical incl. confinement			
Name	$P_{c,e}$ (kN)	$v_{max,e}$* (mm)	$P_{c,a}$ (kN)	$v_{max,a}$ (mm)	$P_{c,a}$ (kN)	$v_{max,a}$ (mm)	$P_{c,e}/P_{c,a}$ (-)	$v_{max,e}/v_{max,a}$ (-)
SH20U	2347	15.8	1950	31.8	1950	31.8	1.20	0.50
SL15U	-	-	1617	30.3	1617	30.4	-	-
SH10U	2436	6.3	1950	31.8	1950	32.8	1.25	0.19
SL05U	2796	22.4	1617	30.3	1617	30.0	1.73	0.75
SH20B	1892	15.5	1710	29.4	1710	29.4	1.11	0.53
SL15B	1899	14.4	1559	27.4	1559	27.3	1.22	0.53
LL20U	1834	28.7	1048	41.4	1048	41.4	1.75	0.69
LH15U	2485	57.3	1151	43.1	1151	43.1	2.16	1.33
LL10U	1937	45.1	1052	41.8	1052	41.6	1.84	1.08
LH05U	1828	56.4	1130	41.8	1131	43.1	1.62	1.31
LH10B	2125	42.7	995	38.2	995	36.3	2.14	1.18
LL05B	2049	57.7	921	36.0	921	36.3	2.22	1.59
					Mean		1.66	0.88
					Standard deviation		0.41	0.44

* Deflections modified for rigid body displacements.

Interestingly, the results from the numerical analysis suggest that the benefits of passive confinement do not carry through to the structural level. This can partly be explained by the structural influence of the unconfined concrete cover outweighing the beneficial effect that the confinement has on the stress-strain behaviour of the core concrete.

Figures 5.63 and 5.64 show the relationships between the mid-height deflections and the axial load for the shorter and longer columns respectively. It can be noted that the shape of the computed deflection curves is quite different from the shape of the curves obtained from the tests (figures 5.60 and 5.61). Whereas all the computed deflection curves are of the classical concave shape, i.e. the deflections develop at an increasing rate throughout loading, the test curves are in general characterised by distinct phases.

Furthermore, the figures show that the deflections in the vertical plane calculated for the columns subjected to biaxial eccentric compression, i.e. columns SH20B, SL15B, LH10B and LL05B, are not much different from the deflections calculated for the similar columns subjected to uniaxial eccentric compression. In this context, it should be recalled that the experimental load-deflection curves not modified for rigid body displacements (figures 5.45 and 5.46), suggest that the biaxial load eccentricity had the effect of significantly reducing the initial stiffness of the columns. However, as described in section 5.2.3, this behavioural difference was almost eliminated by the adopted procedure for filtering out rigid body displacements.

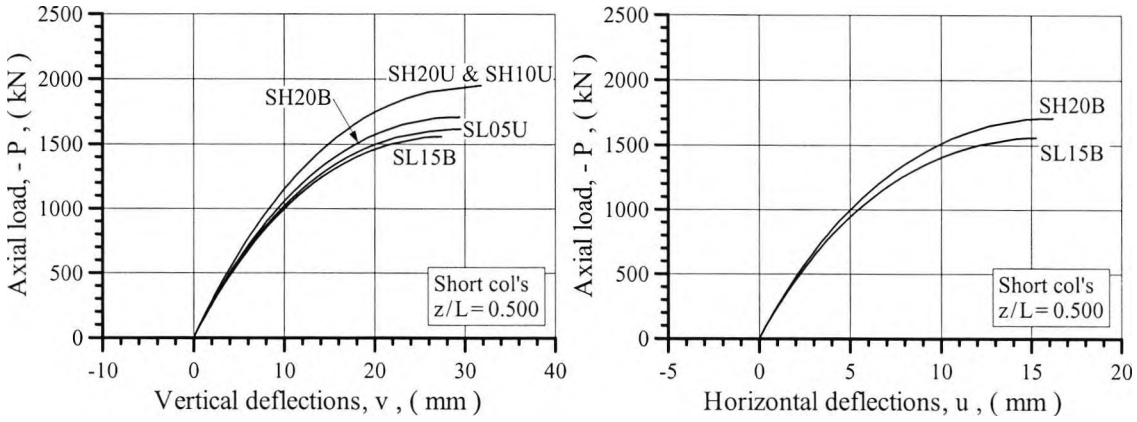

Figure 5.63
Computed mid-height deflections for shorter columns

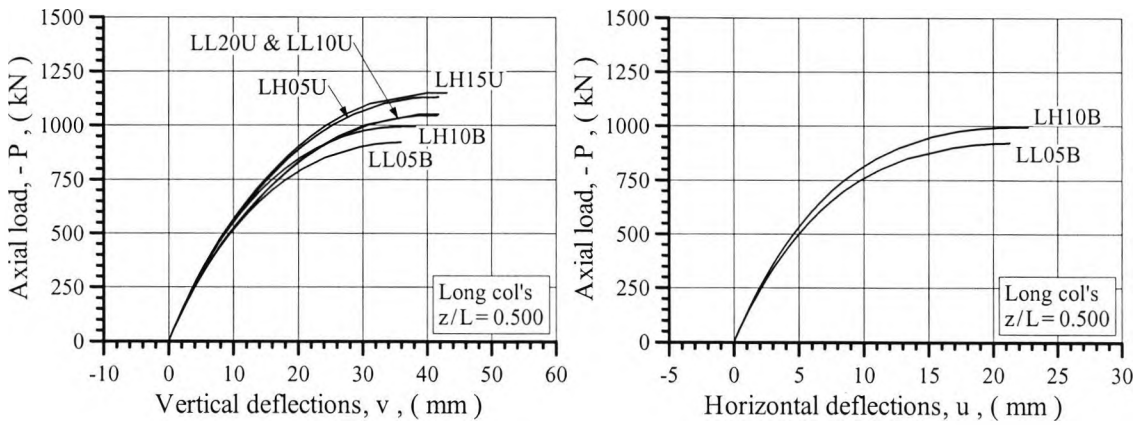

Figure 5.64
Computed mid-height deflections for longer columns

Figures 5.65 and 5.66 show the computed relationship between the extreme fibre strains and the applied axial load for four of the test columns made from the grade C120 concrete. The illustrated load-strain diagrams cover all the column lengths and nominal loading conditions employed in the experimental programme. The diagrams for the remaining test columns can be approximated by load scaling. In contrast to the load-strain curves determined on the basis of the experimental data, see figures 5.32 - 5.42, the computed curves are smoothly curved, and contain no sudden or reversed changes in the rate of straining.

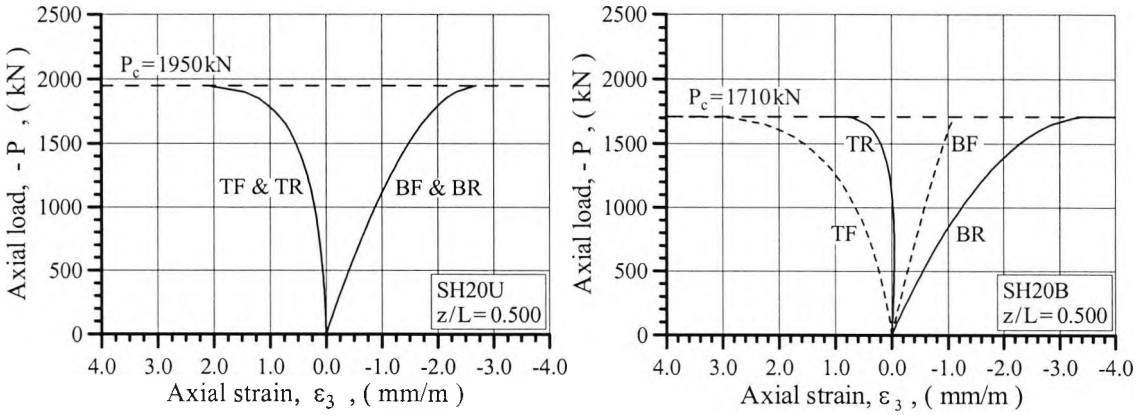

Figure 5.65
Computed extreme fibre strains for shorter columns

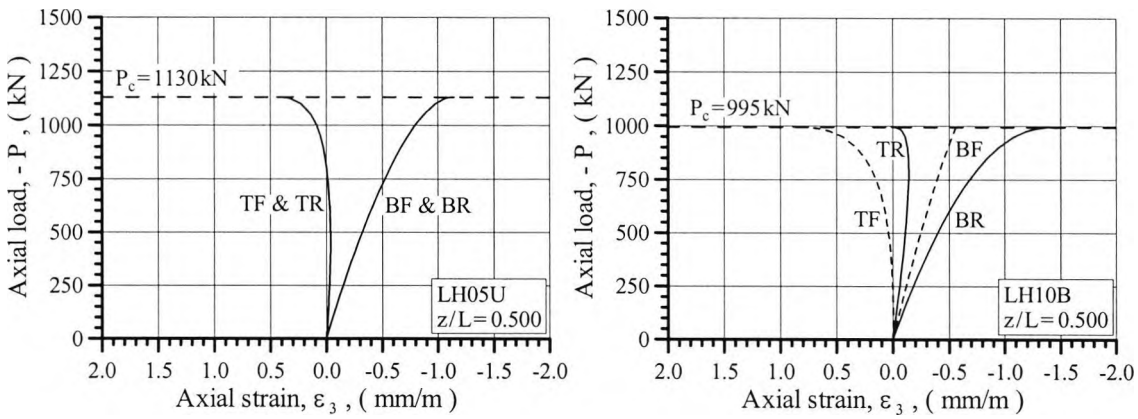

Figure 5.66
Computed extreme fibre strains for longer columns

The extreme fibre strains at column failure, as determined from the numerical analysis and from the test data recorded by the external concrete strain gauges, can be read from table 5.9. It can be noted that, for the shorter columns nominally subjected to uniaxial eccentric compression the maximum compressive strains predicted by the numerical analysis are in good agreement with the test results. However, according to the numerical analysis the neutral axis was located near the centre of the cross-section at failure, whereas, except for column SL05U, the test results indicate that the neutral axis was located near the edge of the cross-section. For the shorter columns customised for biaxial eccentric

compression testing the computed extreme fibre strains are much larger than those derived from the test data. In the case of the longer test columns the numerical analysis consistently underestimated the maximum compressive strain, and somewhat overestimated the maximum tensile strain. As a consequence, the location of the neutral axis was computed to be nearer the centre of the cross-section at failure than indicated by the test results. As was the case for the shorter columns, the numerical results for the columns which were nominally tested under a condition of biaxial eccentric compression showed least agreement with the experimental results for the longer columns as well.

Table 5.9
Comparison of experimental and computed results - extreme fibre strains at column failure

Column	Experimental*			Analytical		
Name	P_c (kN)	$\varepsilon_{3,min}$ (mm/m)	$\varepsilon_{3,max}$ (mm/m)	P_c (kN)	$\varepsilon_{3,min}$ (mm/m)	$\varepsilon_{3,max}$ (mm/m)
SH20U	2347	-2.6	0.1	1950	-2.7	2.1
SL15U	-	-	-	1617	-2.6	2.0
SH10U	2436	-2.1	-0.2	1950	-2.7	2.1
SL05U	2796	-2.9	1.2	1617	-2.6	2.0
SH20B	1892	-2.4	0.2	1710	-3.9	3.8
SL15B	1899	-2.4	0.7	1559	-3.4	3.1
LL20U	1834	-1.5	0.0	1048	-1.1	0.4
LH15U	2485	-1.9	0.3	1151	-1.2	0.5
LL10U	1937	-2.0	0.3	1052	-1.1	0.4
LH05U	1828	-2.0	0.4	1130	-1.1	0.4
LH10B	2125	-1.5	0.2	995	-1.4	0.9
LL05B	2049	-2.6	0.5	921	-1.4	0.8

* Based on data from external strain gauges

5.3.2 Supplementary Investigation

A number of possible explanations for the rather poor correlation between the computed and observed results were considered. The influence on the computed results of ignoring the tensile strength of concrete and possible frictional forces developing in the spherical tilt joints at the column supports, and of underestimating the compressive strength of concrete was insufficient to explain the rather poor correlation. It is believed that the single most important reason for the poor correlation was that the eccentricity by which the axial load was applied reduced during testing.

Tensile strength of concrete

The influence of a non-zero tensile strength of concrete on the structural response was computed for test columns SH20U and LL20U. The direct tensile strengths were, in accordance with the CEB Model Code 90 (1990), estimated to 90% of the split cylinder strengths. Thus, the grade C120 concrete was assumed to have a tensile strength of 6.6 MPa, a corresponding peak strain of 0.15 mm/m, and an ultimate tensile strain of 0.20 mm/m. The grade C100 concrete was assumed to have a tensile strength of 5.5 MPa. Figure 5.67 illustrates the stress-strain curves for concrete employed in the numerical analysis.

As seen from table 5.10, the inclusion of the tensile strength of concrete raised the computed axial load capacity of columns SH20U and LL20U by a modest 26 kN and 49 kN respectively. Thus, the potential influence of the tensile concrete strength is far from being sufficient to explain the differences of 397 kN and 786 kN existing between the test failure loads and computed failure loads. Furthermore, figure 5.68 shows that the inclusion of the tensile strength has no effect in improving the resemblance of the computed load-strain curves with those obtained from the tests. The test curves represent the average

strains on the top and bottom faces of the columns at mid-height, and were determined on the basis of the readings from the externally mounted strain gauges.

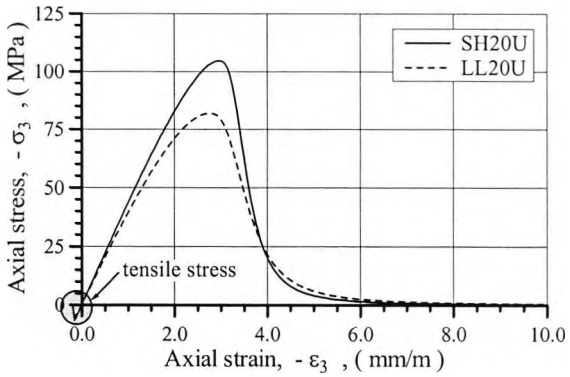

Figure 5.67
Assumed stress-strain behaviour of concretes

Table 5.10
Computed effect of non-zero tensile concrete strength on failure loads and deflections

Column	Experimental		Analytical excl. tension		Analytical incl. tension			
Name	$P_{c,e}$ (kN)	$v_{max,e}$* (mm)	$P_{c,a}$ (kN)	$v_{max,a}$ (mm)	$P_{c,a}$ (kN)	$v_{max,a}$ (mm)	$P_{c,e}/P_{c,a}$ (-)	$v_{max,e}/v_{max,a}$ (-)
SH20U	2347	15.8	1950	31.8	1976	32.1	1.19	0.49
LL20U	1834	28.7	1048	41.4	1197	43.0	1.53	0.67

* Deflections modified for rigid body displacements.

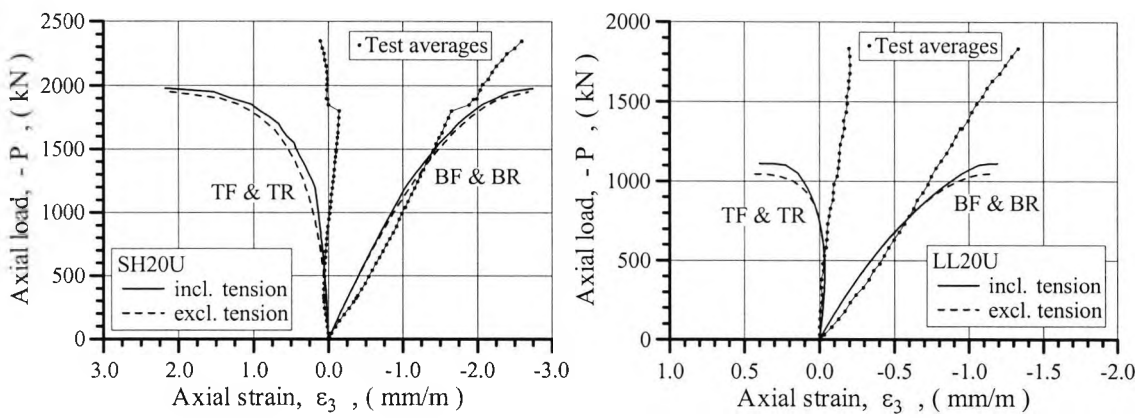

Figure 5.68
Computed effect of non-zero tensile strength on extreme strains

Friction forces developing at the pinned ends

The manufacturer's data sheet states that the GZ450 bridge bearing has a coefficient of friction of 0.005. Thus, as the centre of rotation was 412 mm away from the PTFE coated contact faces of the bearing, the resisting moment caused by the friction forces can be estimated to have an effect equivalent to a 2 mm ($0.005 \cdot P \cdot 412\,mm / P$) reduction in the load eccentricity. The spherical radius of the tilt components of the load cell had been measured to 181 mm, but no data existed regarding the coefficient of friction for the polished high strength steel. However, it is reasonable to assume that a 5 mm reduction in the load eccentricity would provide an upper limit for the possible effect that the friction forces could have played on the structural response of the test columns.

As seen from table 5.11, a 5 mm reduction in the load eccentricity raised the axial load capacity of column SH20U by 284 kN, and the axial load capacity of column LL20U by 149 kN. While these increases are significant, it seems unlikely that friction alone could have been responsible for the test loads being much larger than expected. Figure 5.69 illustrates the effect of the friction forces on the computed load-strain behaviour of the two test columns. It is noticeable that while including the friction forces had the effect of improving the overall correlation of the computed strains with the test strains, it had little effect on the ability of the numerical model to accurately predict the tensile strains.

Table 5.11
Computed effect of friction forces on failure loads and deflections

Column	Experimental		Analytical excl. friction		Analytical incl. friction			
Name	$P_{c,e}$ (kN)	$v_{max,e}$* (mm)	$P_{c,a}$ (kN)	$v_{max,a}$ (mm)	$P_{c,a}$ (kN)	$v_{max,a}$ (mm)	$P_{c,e}/P_{c,a}$ (-)	$v_{max,e}/v_{max,a}$ (-)
SH20U	2347	15.8	1950	31.8	2234	30.2	1.05	0.52
LL20U	1834	28.7	1048	41.4	1197	43.0	1.53	0.67

* Deflections modified for rigid body displacements.

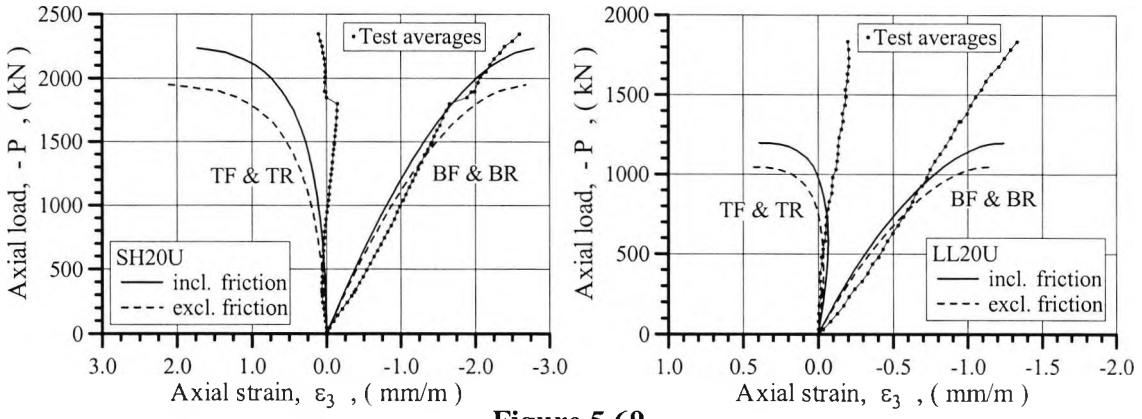

Figure 5.69
Computed effect of friction forces on extreme strains

Underestimated concrete strength

All the numerical work carried out so far has been based on the assumption that the unconfined concrete strength of the full-scale columns could be set equal to 0.85 times the strength of 150×300 mm cylinders. This conversion coefficient was not experimentally verified in the present investigation, and as mentioned in section 3.1.2 it is often larger for high strength concrete than for normal strength concrete. In order to further investigate the consequences of underestimating the compressive concrete strength on the structural behaviour of the columns, the columns SH20U and LL20U were re-analysed employing the stress-strain curves given in figure 5.70. These stress-strain curves were generated on the basis of the compressive concrete strength being equal to 0.95 times the average of the measured 100×200 mm cylinders strengths, and as such they represent a situation where environmental factors, such as the concrete compaction, curing conditions and the slower rate of loading, have negligible influence on the strength of the full scale columns.

As seen from table 5.12, the increased concrete strength raised the computed axial load capacity of the short and the long column by a modest 171 kN and 68 kN respectively. Furthermore, the analysis based on the higher concrete strengths failed to improve capturing the observed development in the tensile strains, see figure 5.71. Thus, it appears that, the

large discrepancy between the observed and expected column behaviour could only partly be explained by the concrete strength being higher than originally estimated.

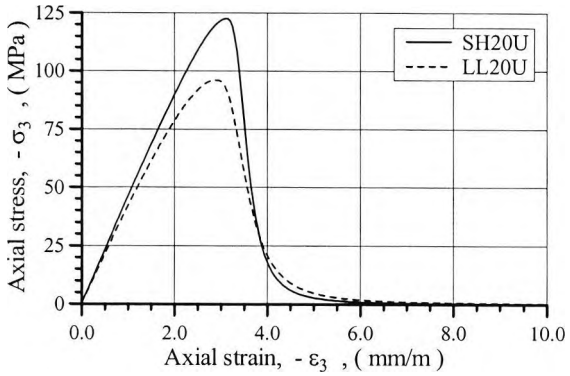

Figure 5.70
Assumed stress-strain behaviour of concrete

Table 5.12
Computed effect of underestimated concrete strength on failure loads and deflections

Column	Experimental		Analytical incl. reduction		Analytical excl. reduction			
Name	$P_{c,e}$ (kN)	$v_{max,e}$* (mm)	$P_{c,a}$ (kN)	$v_{max,a}$ (mm)	$P_{c,a}$ (kN)	$v_{max,a}$ (mm)	$P_{c,e}/P_{c,a}$ (-)	$v_{max,e}/v_{max,a}$ (-)
SH20U	2347	15.8	1950	31.8	2121	42.2	1.11	0.37
LL20U	1834	28.7	1048	41.4	1116	41.8	1.64	0.69

* Deflections modified for rigid body displacements.

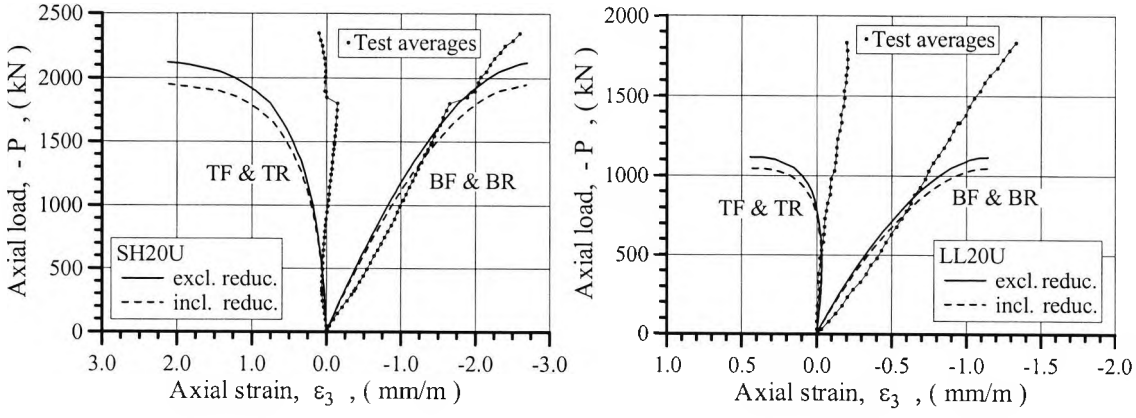

Figure 5.71
Computed effect of underestimated concrete strength on extreme strains

Reduced end-eccentricities

It is believed that the large difference between the observed and the expected behaviour of the test columns was caused primarily by non-stationary boundary conditions, which had the effect of reducing the load eccentricity during testing. Whether this was caused by crude end details or insufficient stiffness, or anchorage, of the loading rig remains unknown. However, a similar testing arrangement was apparently employed successfully in an earlier investigation of normal strength concrete columns carried out at City University by Brant (1984).

Figure 5.72 illustrates the numerically obtained load-strain behaviour of the columns SH20U and LL20U for different load eccentricities. The graphs suggest that the actual load eccentricity at failure of column SH20U may have been about 10 mm less than the nominal eccentricity, and that the actual load eccentricity at failure of column LL20U may have been about 20 mm less than the nominal eccentricity.

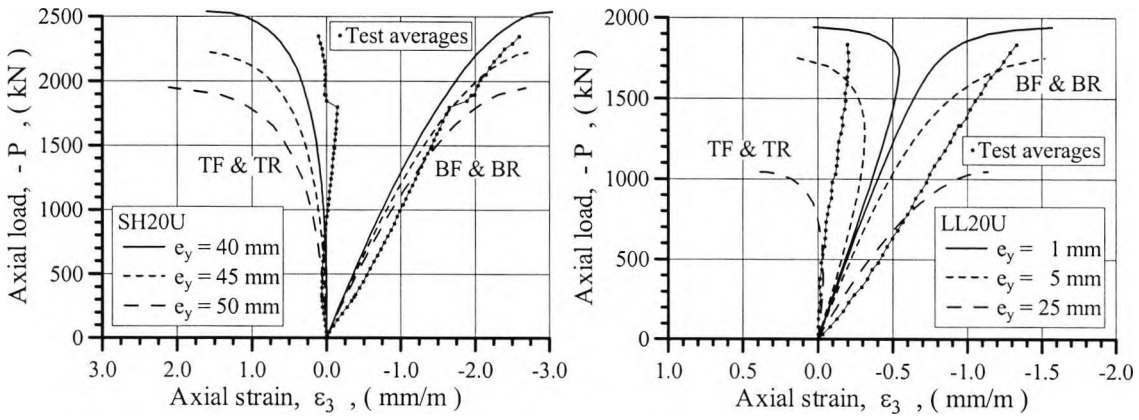

Figure 5.72
Computed effect of load eccentricity on extreme strains

5.4 Summary

This chapter described an experimental investigation, carried out at City University, into the structural performance of slender high strength concrete columns subjected to eccentric compression. Special attention was given to the effect of the distribution of the hoop reinforcement.

The columns were tested in a horizontal position in a rig built for the purpose, and with the exception of column SH20B all failed explosively without visible signs of warning. From studying the video footage, it was concluded that failure of the 4 m long columns was initiated by spalling of the concrete cover, and failure of the 8 m long columns by a sudden loss of overall stability.

Post failure inspections revealed that a reduction in the tie spacings had the effect of increasing the inclination of the failure plane to the column axis as well as reducing the volume of crushed core concrete. The columns with tie spacings of 50 mm failed along a plane which was nearly perpendicular to the column axis, and the columns with the larger tie spacings of 100 - 200 mm along a plane inclined 30° - 60° to the column axis. Thus, the failure mechanism for the columns with the larger tie spacings was characterised by the two column segments on either side of the failed section sliding over each other, and the failure mechanism for the columns with the smallest tie spacings by a rotation about the pinned ends of these. The end-rotations were sufficiently large to cause both of the longitudinal reinforcement bars located at the convex side of the bent columns to snap.

The test loads ranged from 1829 kN to 2796 kN, and indicate that a reduction in the tie spacings had some effect on increasing the load capacity of the shorter columns. This was not the case for the longer columns. The ratio between the measured failure load and the

failure load computed on the basis of the numerical model varied from 1.11 to 2.22, with an average 1.30 for the shorter columns and 1.96 for the longer columns.

A total of 60 strain gauges, a combination of 60 mm gauges mounted on the concrete surface and 5 mm gauges mounted on the steel reinforcement bars, was employed to acquire information about the longitudinal strains at various sections of the columns. The strains measured by the two types of gauges were in good agreement with each other, and confirmed that the standard assumption of plane sections remaining plane applied to the high strength concrete columns.

For most of the columns the relationship between the extreme fibre strains and the applied axial load was observed to display three distinct phases. In the first phase the extreme fibre strains developed almost linearly with the applied load. The linear phase terminated at a point well within the second half of the loading regime, when the strains suddenly began to develop under a condition of little, or no, increase in the applied load. However, after a short while the column regained a resistance to incremental loading comparable to that of the linear phase. In the special case of the columns SH10U, LL20U, LH10B and LL05B the load-strain curves displayed no distinct phases, as the extreme fibre strains developed almost linearly with the applied axial load until the occurrence of failure.

The maximum compressive strains at mid-height of the columns ranged from 2.1 mm/m to 2.9 mm/m, with an average of 2.5 mm/m, in the case of the shorter columns, and from 1.5 mm/m to 2.6 mm/m, with an average of 1.9 mm/m, in the case of the longer columns. These strains, determined on the basis of the strains measured by the external concrete gauges, suggest that the maximum compressive strain at failure is less than the 3.5 mm/m adopted in BS 8110. Furthermore, an increase in the density of the steel reinforcement cage

was observed to have some effect in improving the ductility of the columns.

The transverse strains measured during the tests indicate that for none of the columns did the tie steel yield prior to failure. The maximum ratio between the tensile strains measured in the tie legs and the yield strain varied from 0.20 to 0.90, with an average of 0.60. The tie strains did not appear to be correlated to the tie spacings.

Deflections in both the vertical and horizontal directions were measured by LVDT's positioned at regular intervals along the length of the columns. From examining the distributed deflection data it was concluded that the pinned ends of the test columns often moved substantially during testing. Supporting evidence for this was provided by the displacement measurements taken directly on the loading rig during the final stages of the experimental programme. A modification of the experimental results for rigid body displacements was shown to improve the degree of compatibility between the strain and the displacement data. At column failure the vertical mid-height deflections for the shorter columns ranged from 6 mm to 24 mm, and for the longer columns from 42 mm to 80 mm.

In general, rather large discrepancies existed between the extreme fibre strains predicted by the numerical model and those determined on the basis of the test data. For the shorter columns the maximum compressive strain was in average overestimated by 0.6 mm/m and the tensile strain by 2.2 mm/m. The maximum compressive strain in the longer columns was on average underestimated by 0.7 mm/m, and the tensile strain was on average overestimated by 0.3 mm/m. For both column lengths the results for the columns nominally subjected to biaxial eccentric compression were the least accurate.

Various possibilities for the rather large differences between the numerical and the experimental results were investigated. It was shown, that the likely impact of experimental

uncertainties, such as those associated with the development of frictional forces at the pinned ends of the columns, the tensile concrete stresses and the actual compressive strength of concrete, was insufficient to explain these discrepancies. It appears that the principal reason for the somewhat erratic test results is that the testing arrangement failed to ensure stationary boundary conditions, allowing a continuous, though unsystematic, reduction in the load eccentricity to take place during testing.

According to the numerical analysis the provided confinement was insufficient to have more than a negligible effect on the column behaviour, and it did as such not confirm the test observations.

Chapter 6: Parametric Study of the Behaviour of Confined Concrete Columns

6.1 Parametric Study

This chapter describes a numerical investigation of reinforced concrete columns subjected to uniaxial eccentric compression. In particular, the structural effects of variations in key parameters such as the concrete strength, the level of passive confinement, the column slenderness, the load eccentricity and the size of the longitudinal reinforcement bars are studied. In addition, the structural benefits of confining the columns by means of internal ties are compared to the benefits obtained had the confining pressure been applied to the surface of the columns.

6.1.1 Influence of Concrete Strength

The numerical investigation was limited to pinned columns having cross-sectional dimensions identical to the columns tested in the experimental investigation. Thus, as illustrated in figure 6.1, the cross-sections measured 250×250 mm, had a concrete cover with a thickness of 20 mm, and was longitudinally reinforced by four bars positioned with a centre-to-centre distance of 182 mm.

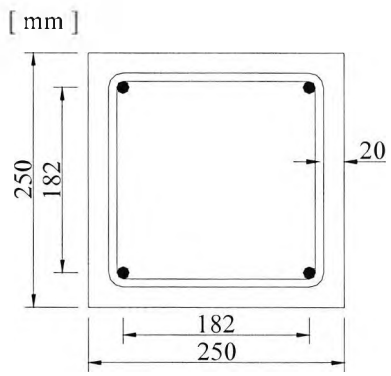

Figure 6.1
Cross-sections of analysed columns

The analysed columns had lengths of 2 m, 4 m and 8 m, i.e. geometric slenderness ratios, L/d , of 8, 16 and 32. In this context it should be recalled that the columns included in the experimental investigation had lengths of approximately 4 m and 8 m. The longitudinal reinforcement bars were assumed to have a diameter of 12 mm, which also was the bar size used in 8 of the 12 columns included in the experimental investigation.

Figure 6.2 illustrates the unconfined stress-strain curves for the three grades of concrete included in the parametric study. The modulus of elasticity, E_c , and the peak strain, ε_c , were calculated from the compressive strength, f_c , using the CEB recommended expressions given by equation 3.3 and 3.5 respectively. The softening parameter, β , governing the steepness of the descending branch of the stress-strain curve, was determined from the compressive strength by equation 3.13 proposed herein. The essential material properties for the three grades of concrete are listed in table 6.1.

The stress-strain behaviour of the longitudinal steel reinforcement bars was idealised as being linear elastic perfectly plastic. The yield strength, f_{sy} , of 539 MPa was chosen so as to be similar to the yield strength of the bars employed in the experimental investigation.

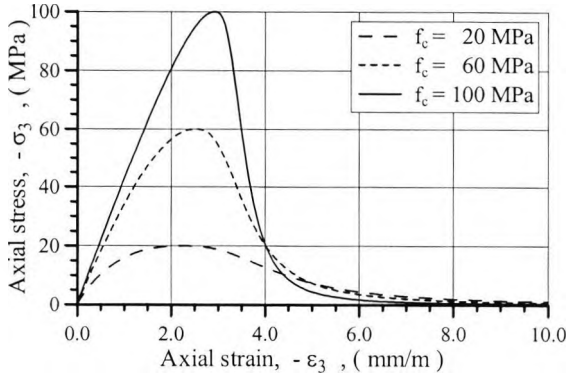

Figure 6.2
Stress-strain behaviour of unconfined concretes

Table 6.1
Material properties of concretes

Grade	f_c (MPa)	E_c (GPa)	ε_c (mm/m)	β (-)
C20	20.0	27.1	2.20	1.9
C60	60.0	37.7	2.49	14.1
C100	100.0	43.9	2.92	103.9

Figure 6.3 shows the computed relationship between load eccentricity and axial load capacity for the unconfined C20 columns having a slenderness ratio of 8, 16 and 32 respectively. For the column having a slenderness ratio of 8, an increase in the load eccentricity to depth ratio, e_y/d , from 0.004 to 0.8, reduced the column's failure load from 1426 kN (corresponding to 97% of the squash load) to 193 kN (13%). For the column having a slenderness ratio of 32, the same increase in load eccentricity reduced the failure load from 754 kN (51%) to 99 kN (7%). In the special case of a load eccentricity to depth ratio of 0.05, i.e. the minimum eccentricity allowed in a design situation according to BS 8110, the C20 column having a slenderness ratio of 8 failed at an axial load of 1219 kN (83%), and the C20 column having a slenderness ratio of 32 failed at an axial load of 604 kN (41%).

In figure 6.4, the load capacities calculated for the unconfined columns made from the grade C60 and C100 concrete are plotted relative to the capacities for the columns made from the C20 concrete. At an eccentricity to depth ratio of 0.05 the load capacity of the C60 and C100 column having a slenderness ratio of 8 was respectively 2.62 and 4.15 times larger than the load capacity of the similar C20 column. When increasing the slenderness ratio to 32, the relative load capacity of the C60 and C100 column was reduced to 2.04 and

2.62 respectively. As with the increase in the slenderness ratio, an increase in the load eccentricity diminished the advantage of employing the higher concrete strengths. When subjected to an axial load acting at the maximum eccentricity to depth ratio of 0.8, the C60 and C100 columns having a slenderness ratio of 8 were determined to fail at a relative axial load of 1.16 and 1.21 respectively. For the larger slenderness ratio of 32, these capacities were reduced to 1.13 and 1.16 respectively.

In summary, the numerical results for the unconfined concrete columns demonstrated that the relative increase in load capacity obtained by employing a higher grade of concrete is reduced with both an increase in column length and load eccentricity. Thus, from an economical point of view, the use of high strength concrete was found to be most cost effective in short columns subjected to nearly concentric loading.

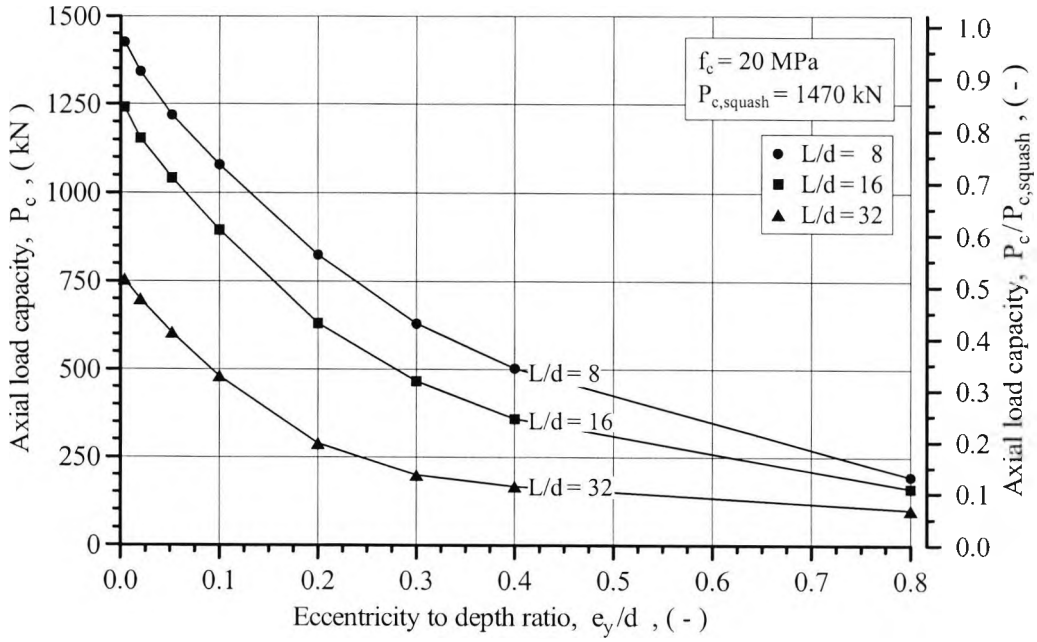

Figure 6.3
Eccentric load capacities for unconfined C20 columns

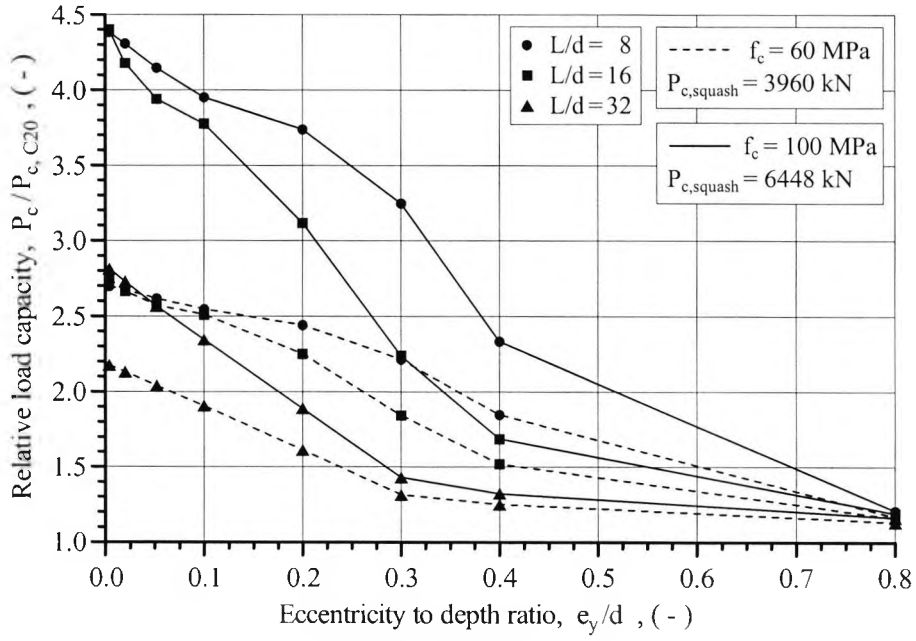

Figure 6.4
Eccentric load capacities for unconfined C60 and C100 columns

6.1.2 Influence of Confinement

The structural effects of passive confinement were assessed by analysing each column under the conditions of the concrete core being subjected to an effective confining pressure of either 2 MPa, 5 MPa, 10 MPa or 20 MPa. The effect of confinement on the stress-strain curves is shown in figure 6.5. The stress-strain curves were generated using the computational model described in section 4.4.3 when subjected to the assumption that the full confining pressure was mobilised at a transverse strain of 1.54 mm/m. This value of strain is approximately equal to the yield strain determined for the R8 bars employed in the experimental investigation.

A confining pressure of 2 MPa was calculated to raise the compressive strength of the C20, C60 and C100 concrete by 59%, 22% and 14% respectively. Likewise, a confining pressure of 20 MPa was calculated to raise their compressive strength by 346%, 154% and 103% respectively. It should be noted that an effective confining pressure of 20 MPa is

approximately equal to the maximum achieved in tests on transversely reinforced concrete columns (see appendix A for a compilation of test results).

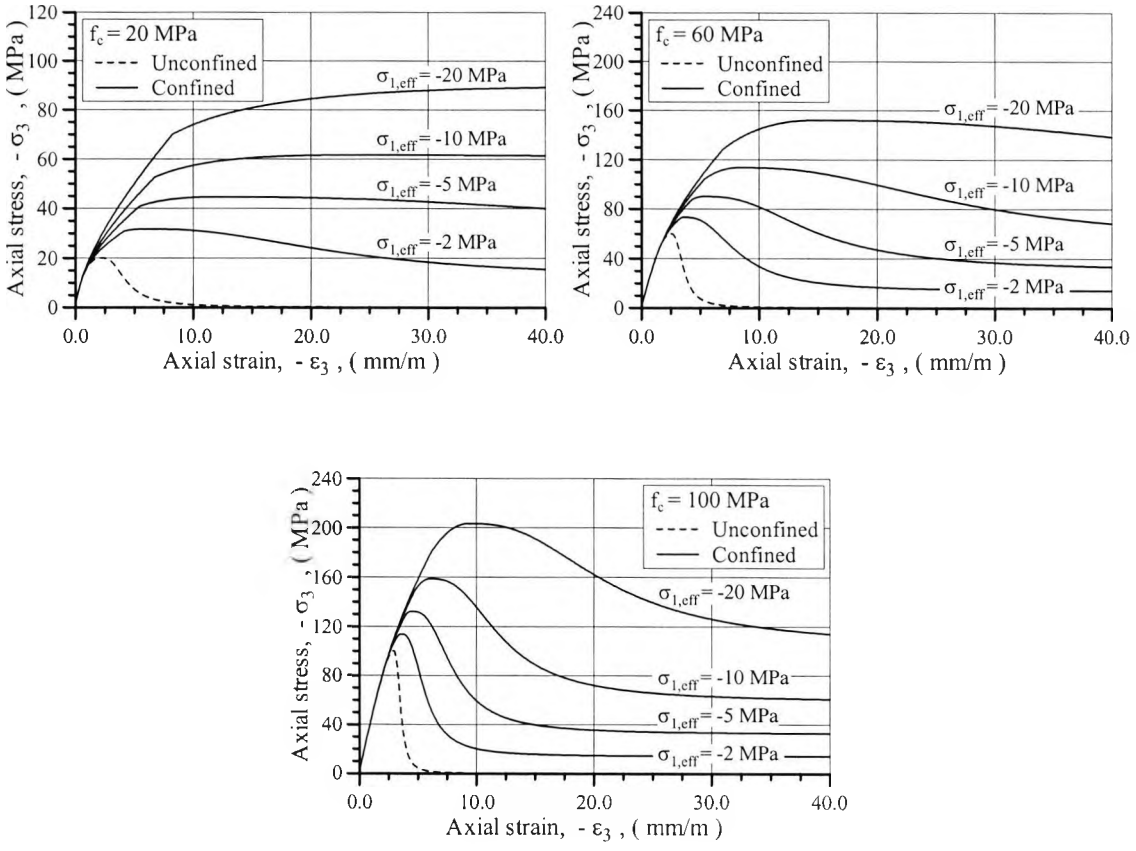

Figure 6.5
Stress-strain behaviour of confined concretes

Figure 6.6 illustrates the influence of passive confinement on the squash load of the columns as determined under displacement controlled conditions. For confining pressures of 10 MPa and 20 MPa the load versus axial displacement curves computed for both the C60 and the C100 columns displayed two distinct peaks. Furthermore, as illustrated in the figure, with the exception of the curve for the C100 columns subjected to a confining pressure of 10 MPa, the second peak always occurred at a higher axial load than the first peak.

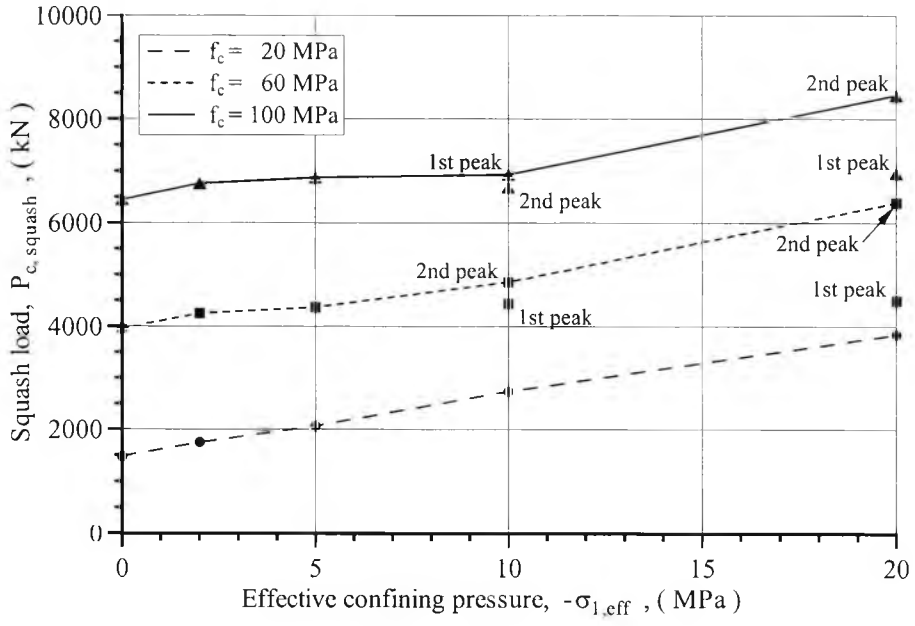

Figure 6.6
Effect of confinement on the squash loads

The effect of confinement on the eccentric load capacity of the C20 columns having a slenderness ratio of 8, 16 and 32 are illustrated in figure 6.7a, 6.7b and 6.7c respectively. For the column having a slenderness ratio of 8 the confining pressure of 2 MPa produced a 118 kN (10%) increase, and the confining pressure of 20 MPa a 647 kN (53%) increase in the load capacity at an eccentricity to depth ratio of 0.05. The similar enhancements for the column having a slenderness ratio of 16 were reduced to 70 kN (7%) and 203 kN (19%) respectively, and for the column having a slenderness ratio of 32 to 2 kN (0.3%) and 16 kN (3%) respectively.

Figures 6.8a-c show the influence of confinement on the eccentric load capacity of the columns made from the grade C60 concrete. For the column having a slenderness ratio of 8 and subjected to an axial load acting at an eccentricity to depth ratio of 0.05, the confining pressure of 2 MPa produced a 89 kN (3%) increase, and the confining pressure of 20 MPa

a 260 kN (8%) increase, in the load capacity of the column. When increasing the slenderness ratio to 16 the strength gains produced by these confining pressures were reduced to 42 kN (2%) and 78 kN (3%) respectively, and when further increasing the slenderness ratio to 32 they became negligible.

The influence of passive confinement on the strength of the C100 columns can be read from figures 6.9a-c. When loaded at an eccentricity to depth ratio of 0.05, the confining pressure of 2 MPa produced a 65 kN (1%) increase, and the confining pressure of 20 MPa produced a 110 kN (2%) increase, in the load capacity of the column having a slenderness ratio of 8. For the C100 column having the larger slenderness ratio of 16, the similar capacity gains were 24 kN (1%) and 35 kN (1%) respectively. In many of the figures the curves corresponding to the different levels of confinement are not discernible.

Besides an increase in slenderness, an increase in the eccentricity also had the effect of rapidly reducing the beneficial effects of confinement. Furthermore, for eccentricity to depth ratios ranging from 0.004 to 0.8, the difference between the confined and unconfined load capacity was found to reduce with an increase in the strength of concrete. Since the utilised confinement model predicts the higher strength concrete to gain more strength than the lower strength concrete at a given confining pressure, this behaviour must be a consequence of the shape of the stress-strain curves, where, irrespective of the confining pressure, the stress-strain curve becomes more pointed with increasing concrete strength. Finally, it should be emphasised that the numerical results given in this chapter were all obtained under the assumption of the integrity of the columns being maintained throughout the loading process, i.e. the effects of possible cover spalling were ignored.

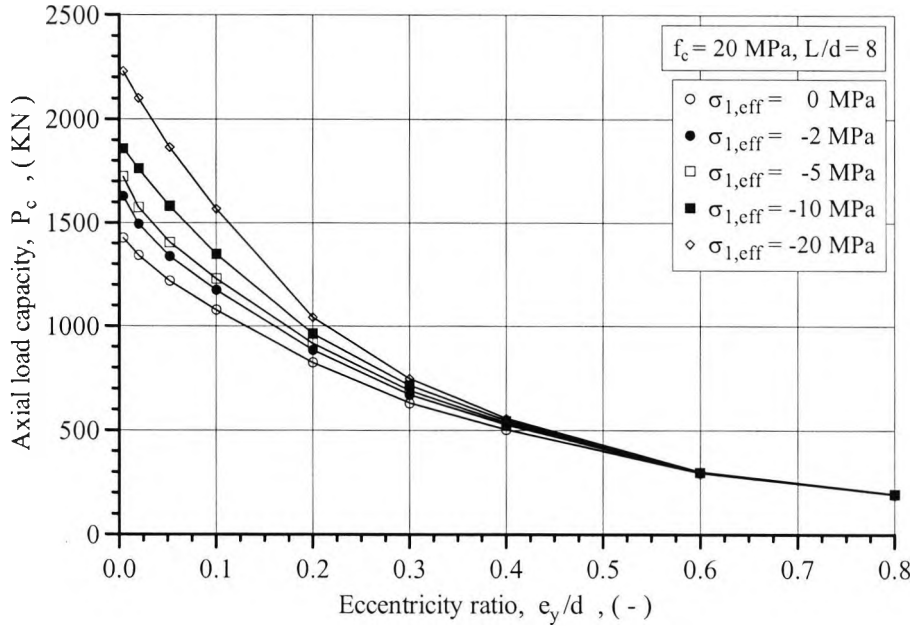

Figure 6.7a
Effect of confinement on eccentric load capacity of the C20 column having a slenderness ratio of 8

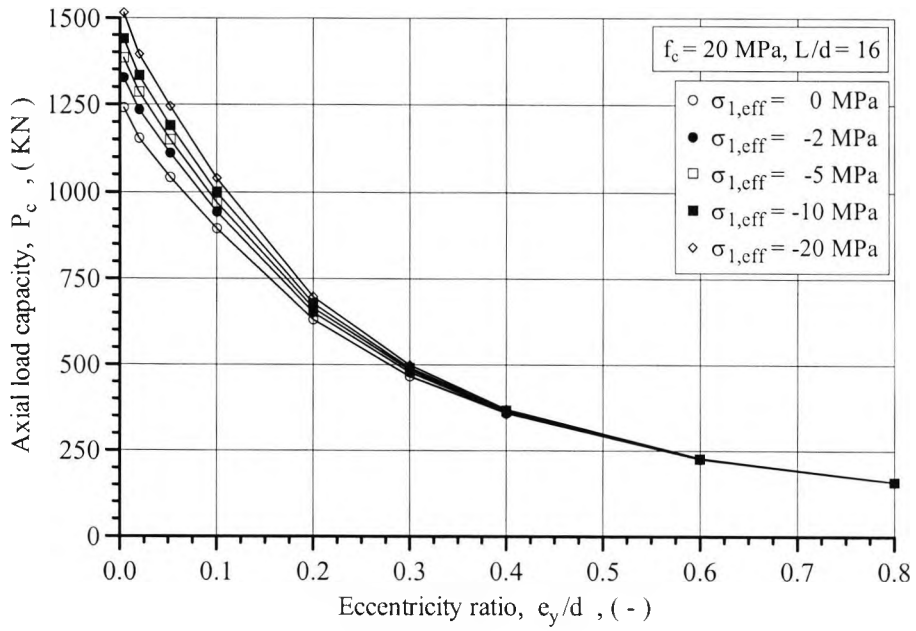

Figure 6.7b
Effect of confinement on eccentric load capacity of the C20 column having a slenderness ratio of 16

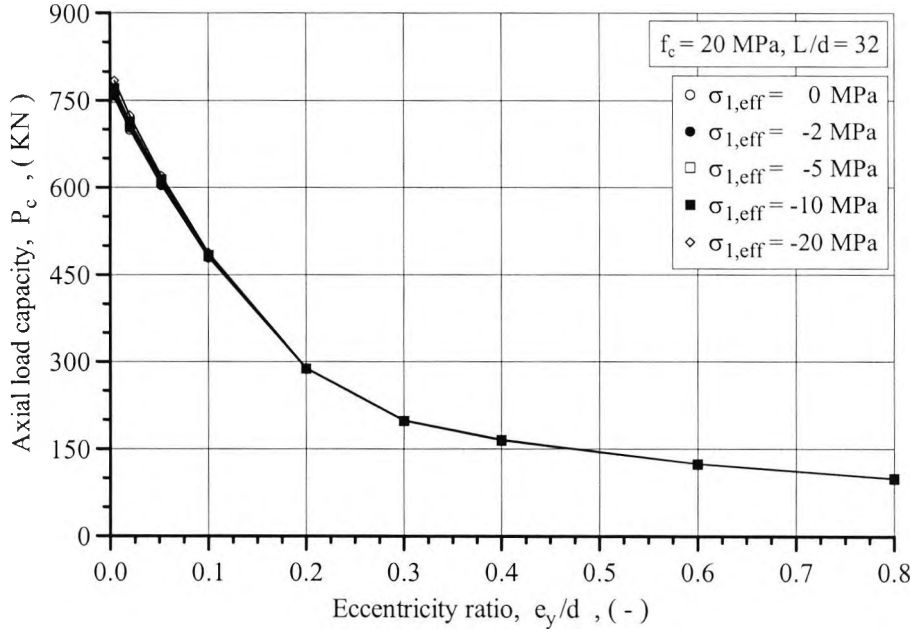

Figure 6.7c
Effect of confinement on eccentric load capacity of the C20 column having a slenderness ratio of 32

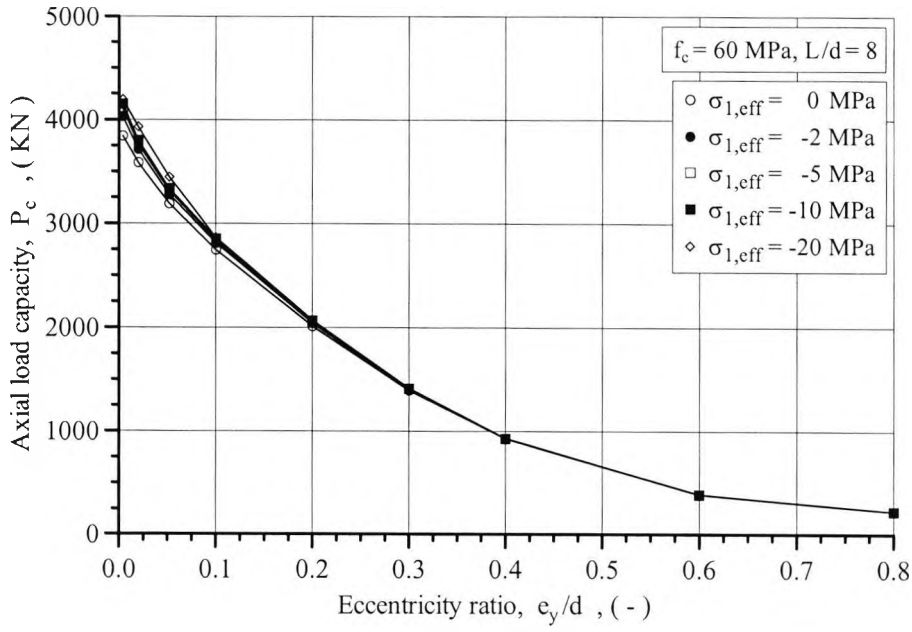

Figure 6.8a
Effect of confinement on eccentric load capacity of the C60 column having a slenderness ratio of 8

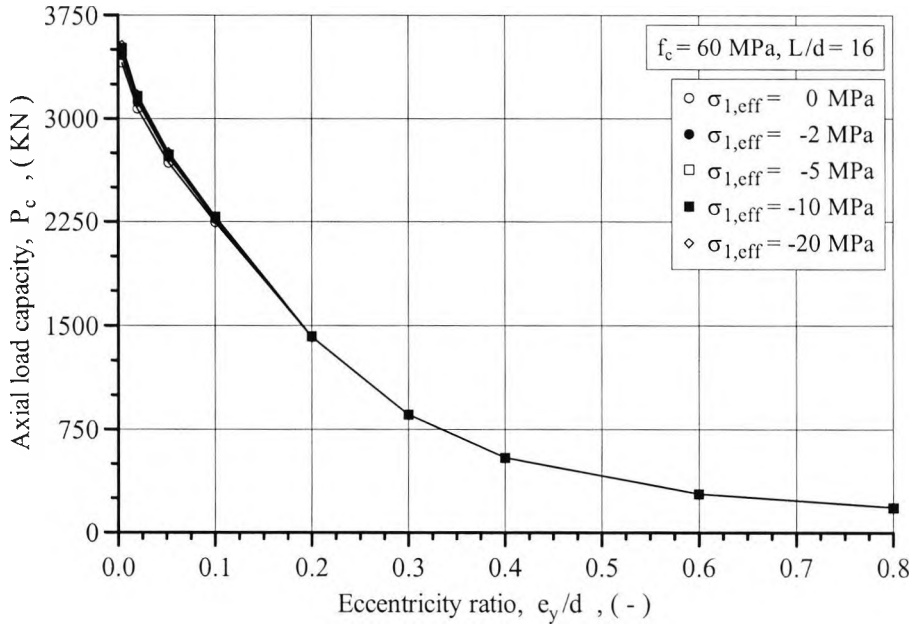

Figure 6.8b
Effect of confinement on eccentric load capacity of the C60 column having a slenderness ratio of 16

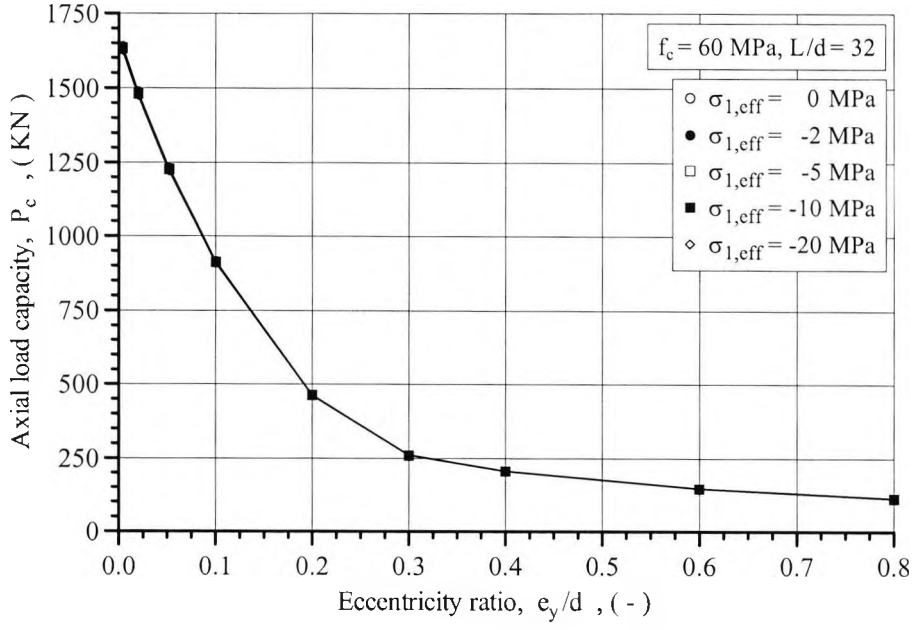

Figure 6.8c
Effect of confinement on eccentric load capacity of the C60 column having a slenderness ratio of 32

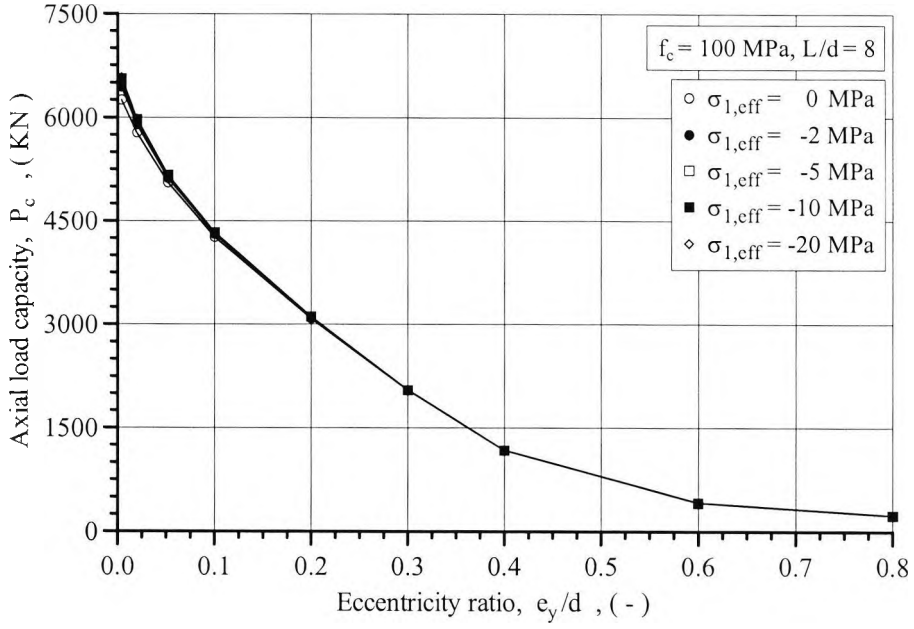

Figure 6.9a
Effect of confinement on eccentric load capacity of the C100 column having a slenderness ratio of 8

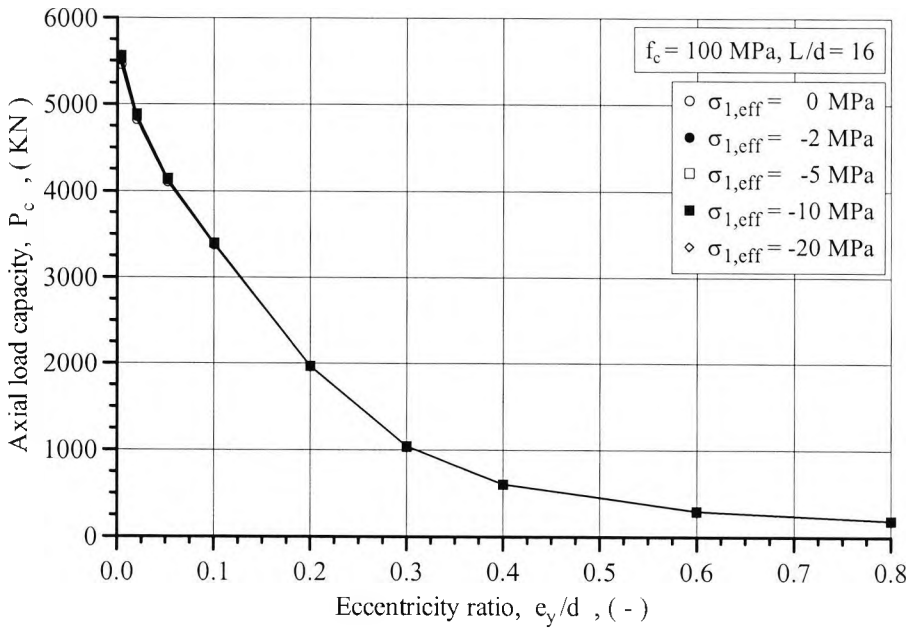

Figure 6.9b
Effect of confinement on eccentric load capacity of the C100 column having a slenderness ratio of 16

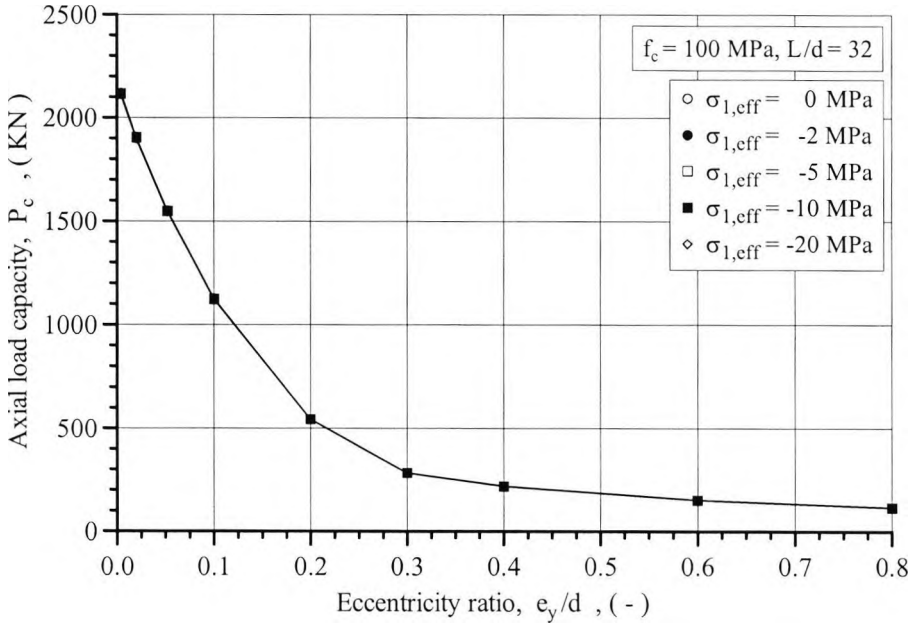

Figure 6.9c
Effect of confinement on eccentric load capacity of the C100 column having a slenderness ratio of 32

In general, the considered levels of confinement were determined to have little or no effect on the pre peak ductility of the columns. Only for the shortest of the C20 columns, and only for relatively small eccentricities, did even the largest confining pressure of 20 MPa significantly increase the column's mid-height deflection at failure. Figures 6.10a-c and 6.11a-c show the load-deflection curves determined for some of the columns made from the C20 concrete and C100 concrete respectively. It should be emphasised that, since the columns were isolated and subjected to eccentric monotonic compression, the plotted load-deflection diagrams convey no information about the post-critical state. Information regarding the load-deflection response beyond the point of strength failure, though outside the scope of the present investigation, is of paramount importance when performing a thorough analysis of a structural assembly for which load redistribution between its various components can take place. Experimental investigations carried out under displacement controlled conditions have shown that amounts of transverse reinforcement which have little or no effect on the peak load can significantly enhance the ductility after the peak load

has been reached (Saatcioglu, 1995; Foster, 1997; Claeson, 1998).

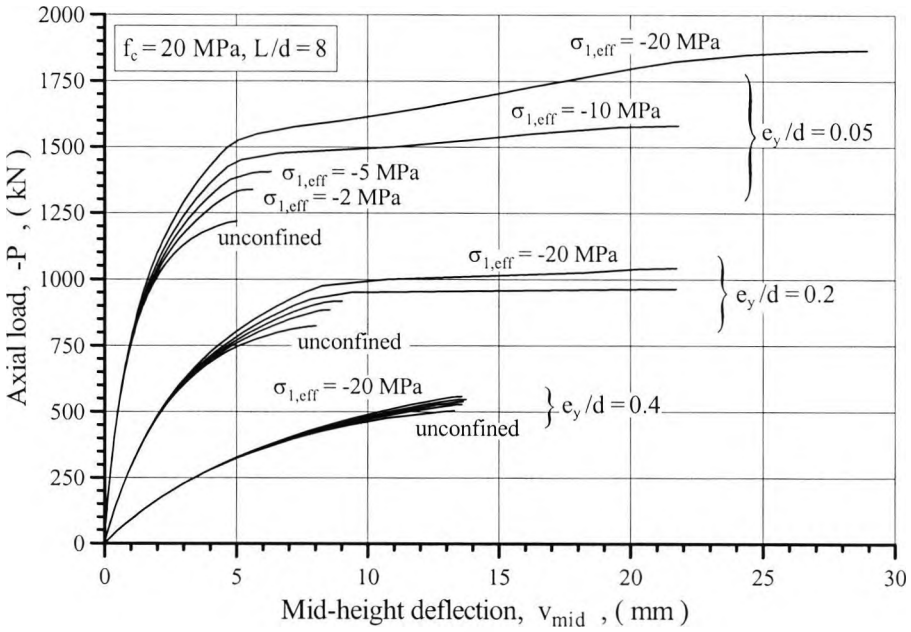

Figure 6.10a
Effect of confinement on load-deflection diagrams for the C20 column having a slenderness ratio of 8

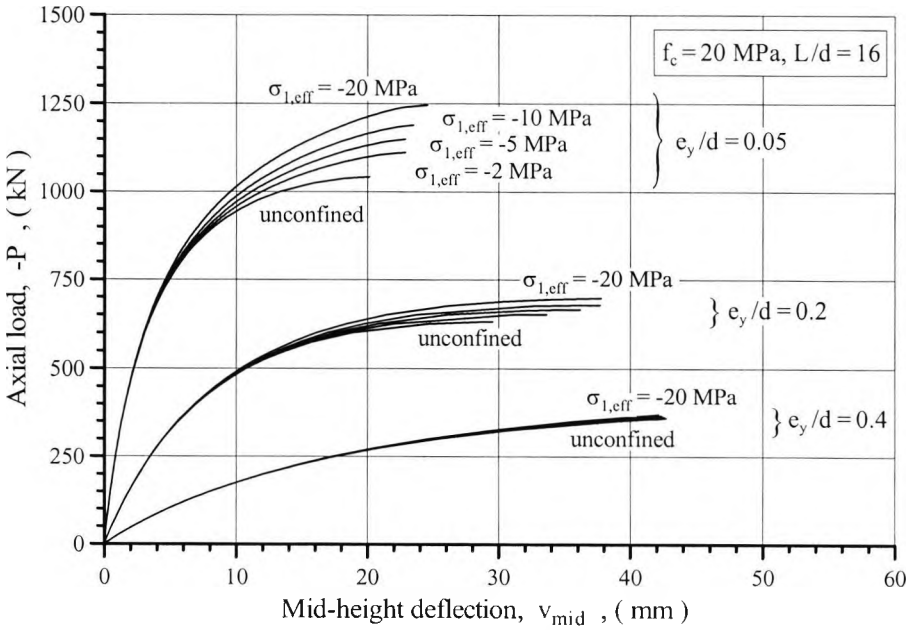

Figure 6.10b
Effect of confinement on load-deflection diagrams for the C20 column having a slenderness ratio of 16

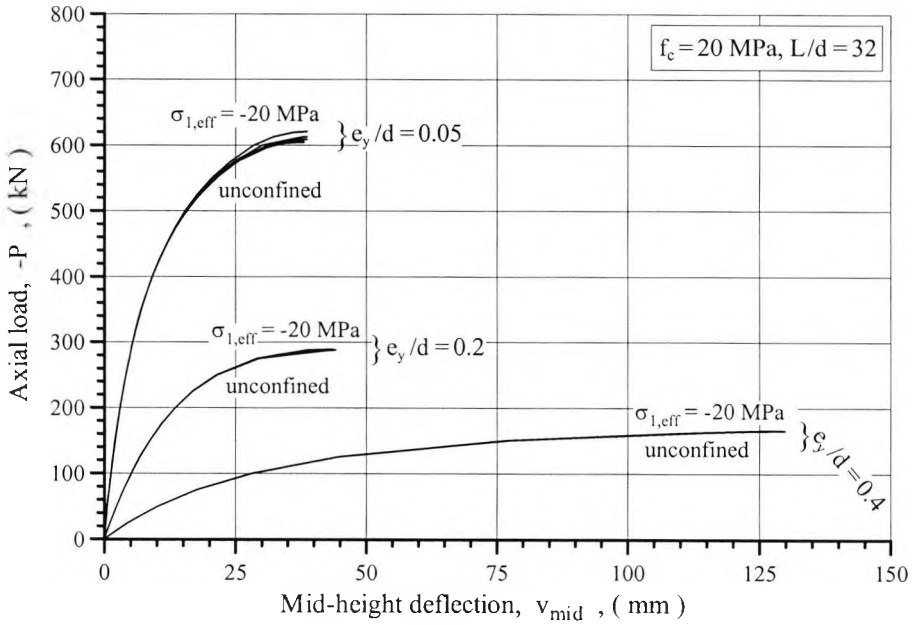

Figure 6.10c
Effect of confinement on load-deflection diagrams for the C20 column having a slenderness ratio of 32

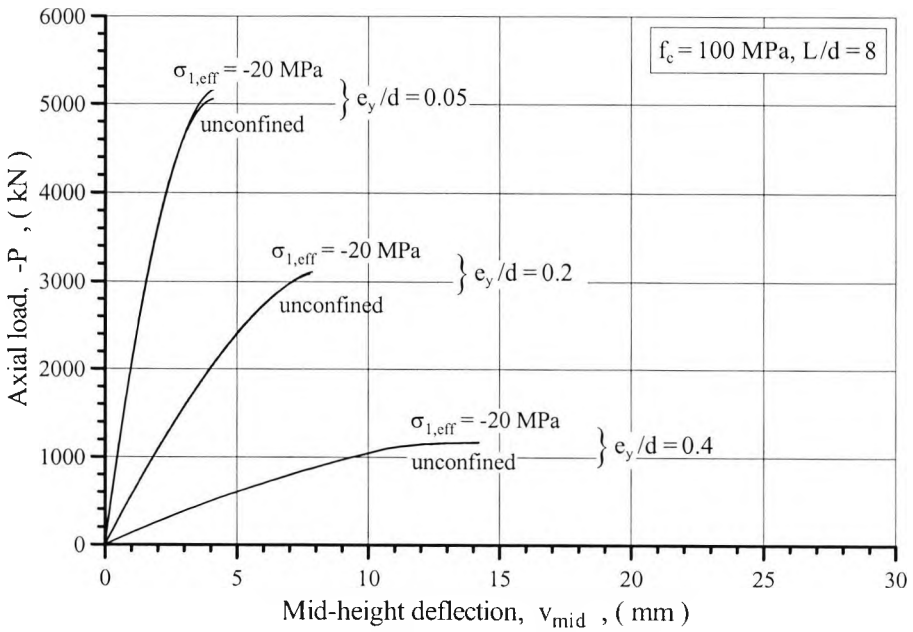

Figure 6.11a
Effect of confinement on load-deflection diagrams for the C100 column having a slenderness ratio of 8

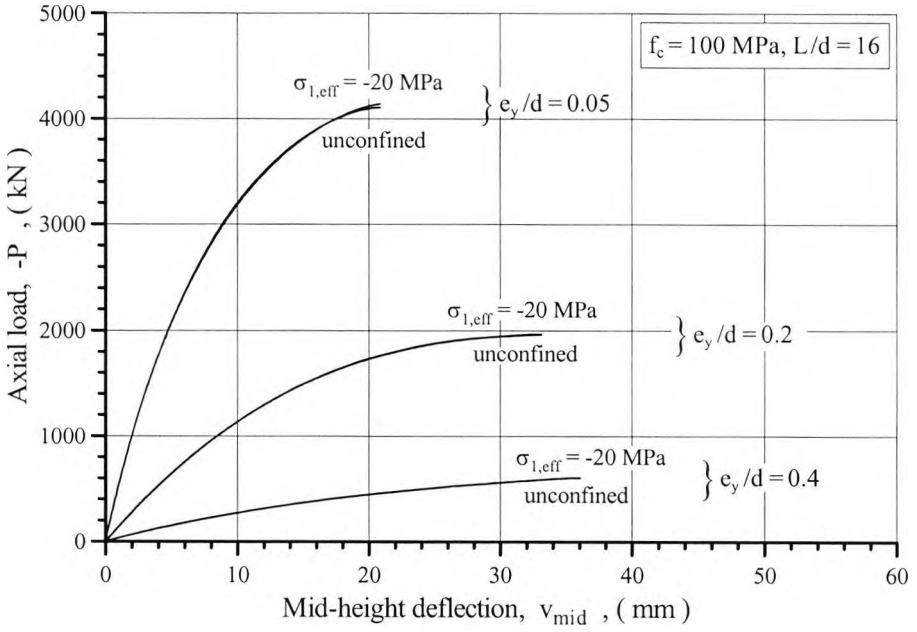

Figure 6.11b
Effect of confinement on load-deflection diagrams for the C100 column having a slenderness ratio of 16

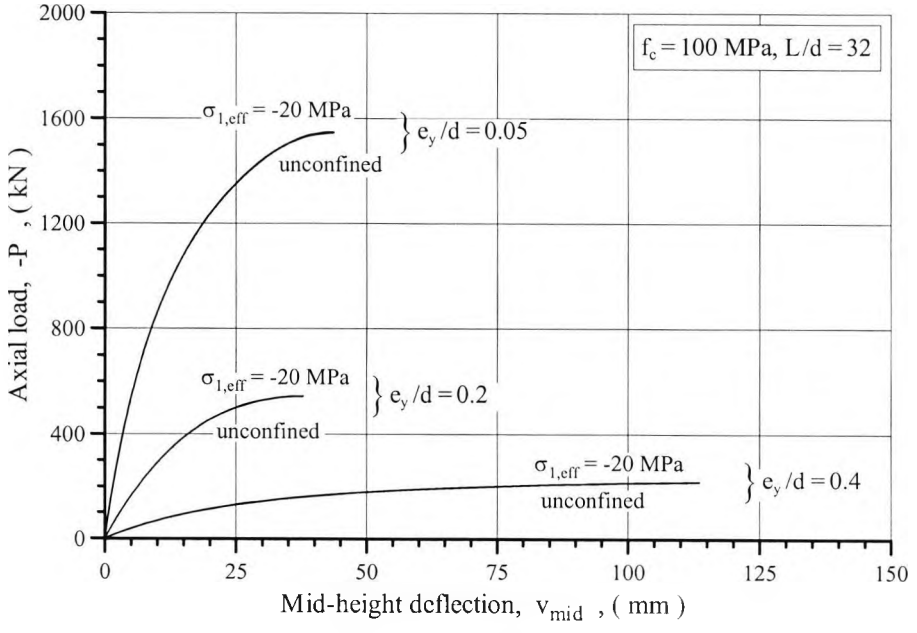

Figure 6.11c
Effect of confinement on load-deflection diagrams for the C100 column having a slenderness ratio of 32

6.1.3 Influence of Longitudinal Reinforcement

Figures 6.12a-c and 6.13a-c show the effect that an increase in the size of the longitudinal reinforcement bars has on the load capacity of the unconfined C20 and C100 columns respectively. For an axial load acting at an eccentricity to depth ratio of 0.05 the replacement of the T12 bars with T20 bars was determined to enhance the capacity of the C20 columns having a slenderness ratio of 8, 16 and 32 by 362 kN (30%), 312 kN (30%) and 129 kN (21%) respectively. For the C100 columns the similar enhancements were determined to 323 kN (6%), 301 kN (7%) and 138 kN (9%). In a similar manner a replacement of the T12 bars with T32 bars raised the strengths calculated for the three C20 columns by 1247 kN (102%), 1105 kN (106%) and 479 kN (79%), and the strengths calculated for the three C100 columns by 1097 kN (22%), 1027 kN (25%) and 480 kN (31%).

When loaded at the maximum eccentricity to depth ratio of 0.8, the replacement of the T12 bars with T20 bars increased the axial load capacities determined for the C20 columns by 245 kN (126%), 196 kN (123%) and 119 kN (120%), and the axial load capacities determined for the C100 columns by 337 kN (145%), 264 kN (140%) and 158 kN (137%). Likewise, the replacement of the T12 bars with T32 bars raised the load capacities calculated for the C20 columns by 598 kN (310%), 540 kN (340%) and 369 kN (373%), and the load capacities calculated for the C100 columns by 1023 kN (439%), 807 kN (426%) and 473 kN (411%).

It is interesting that the replacement of the T12 bars with the larger reinforcement bars had relatively more effect on the strength of the columns made from the C20 concrete at low levels of eccentricity, and relatively more effect on the strength of the columns made from the C100 concrete at high levels of eccentricity.

By comparing the figures it can be seen that from an eccentricity to depth ratio of about 0.2 for the columns having a slenderness ratio of 8, and from an eccentricity to depth ratio of about 0.1 for the columns having a slenderness ratio of either 16 or 32, the replacement of the T12 bars with larger bars raised the strength of the C100 columns more than the strength of the C20 columns. The curves for the load capacity gains for the C100 column having a slenderness ratio of 8 (see figure 6.13a) achieved a maximum at an eccentricity to depth ratio of approximately 0.5. In the case of the more slender of the C100 columns, similar curves shown in figures 6.13b and 6.13c achieved their maximum at an eccentricity to depth ratio of approximately 0.3.

The figures also show that only in the case of the C20 column having a slenderness ratio of 8, and only when loaded at an eccentricity to depth ratio less than approximately 0.2, did the maximum confining pressure of 20 MPa result in an axial load capacity which was above the capacity obtained by simply replacing the T12 bars in an unconfined column with T20 bars. According to BS8110 (1985), the links should have a diameter of at least one-quarter of the diameter of the largest longitudinal bar, and a maximum link spacing no larger than 12 times the diameter of the smallest longitudinal bar. Thus, the minimum allowed volumetric ratio of steel in the unconfined columns longitudinally reinforced by the T12, T20 and T32 bars is 0.8%, 2.1% and 5.3% respectively. It follows from equation 3.35 that a 5% volume ratio transverse reinforcement with a yield strength of about 500 MPa can generate a nominal confining pressure of approximately 13 MPa. Thus, raising the load capacity of the columns by means of large amounts of transverse reinforcement is not economical when compared to the alternative of increasing the volumetric ratio of the longitudinal reinforcement. In this context, it should also be pointed out that the fabrication of a dense reinforcement cage is a rather labour intensive affair.

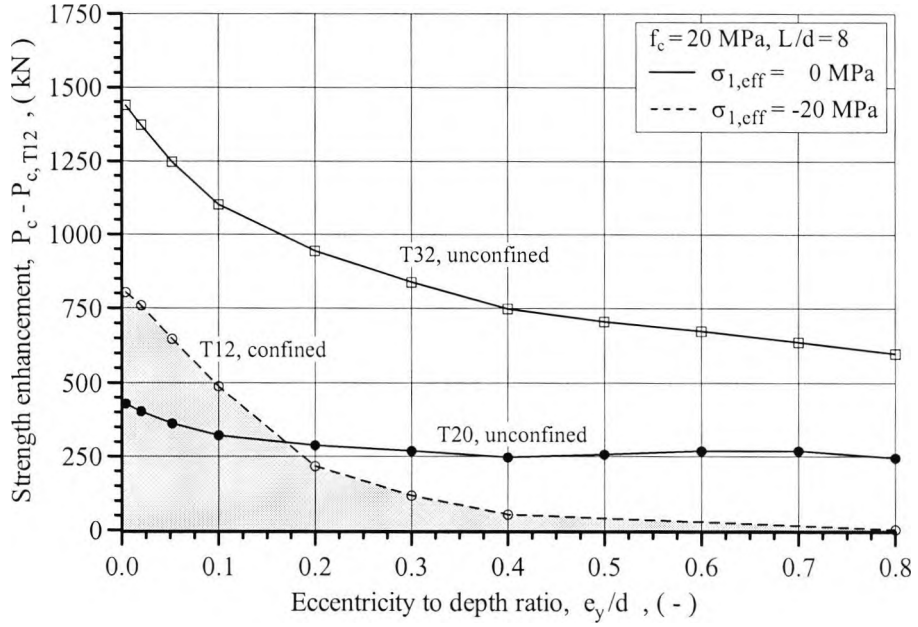

Figure 6.12a
Effect of increased bar size on eccentric load capacity of the C20 column having a slenderness ratio of 8

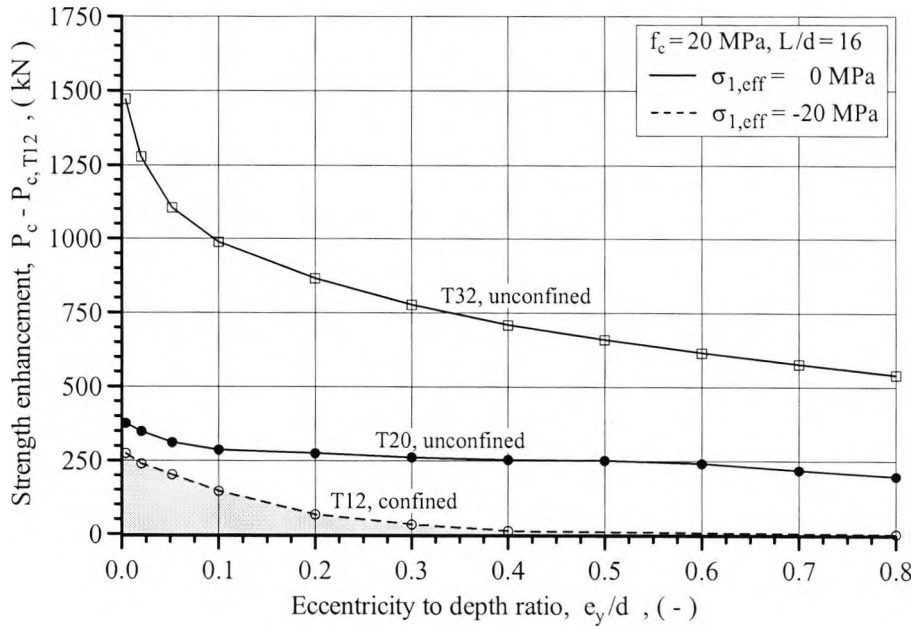

Figure 6.12b
Effect of increased bar size on eccentric load capacity of the C20 column having a slenderness ratio of 16

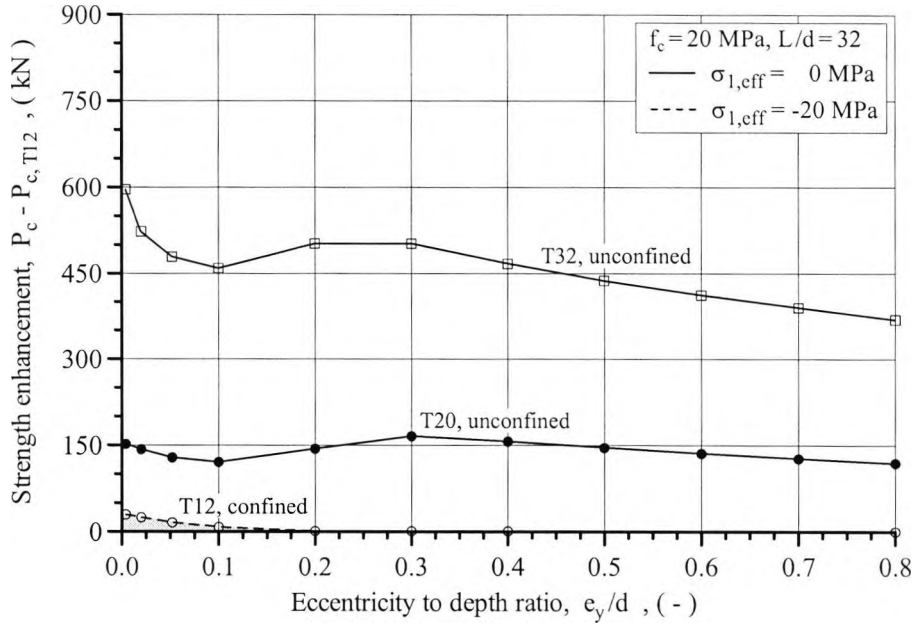

Figure 6.12c
Effect of increased bar size on eccentric load capacity of the C20 column having a slenderness ratio of 32

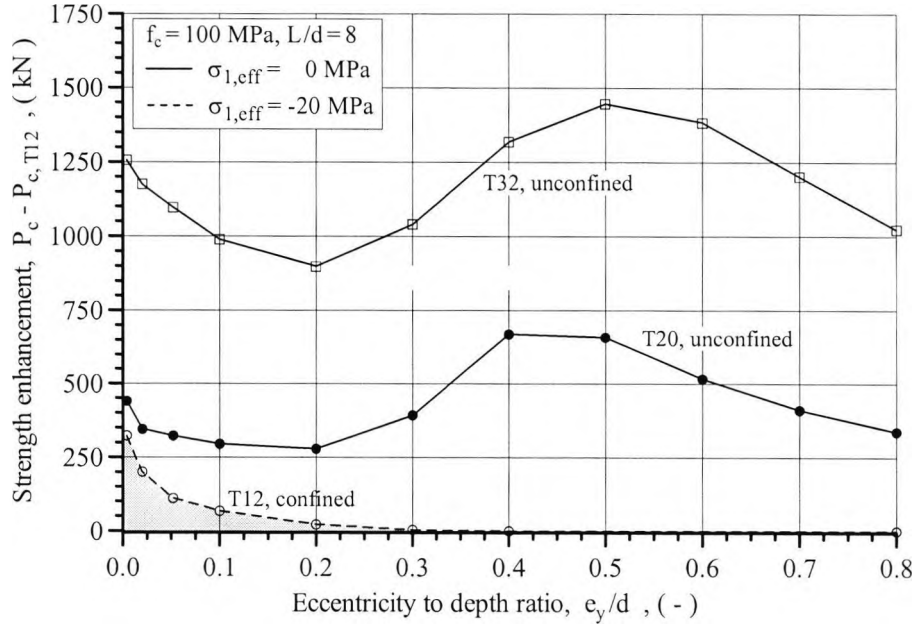

Figure 6.13a
Effect of increased bar size on eccentric load capacity of the C100 column having a slenderness ratio of 8

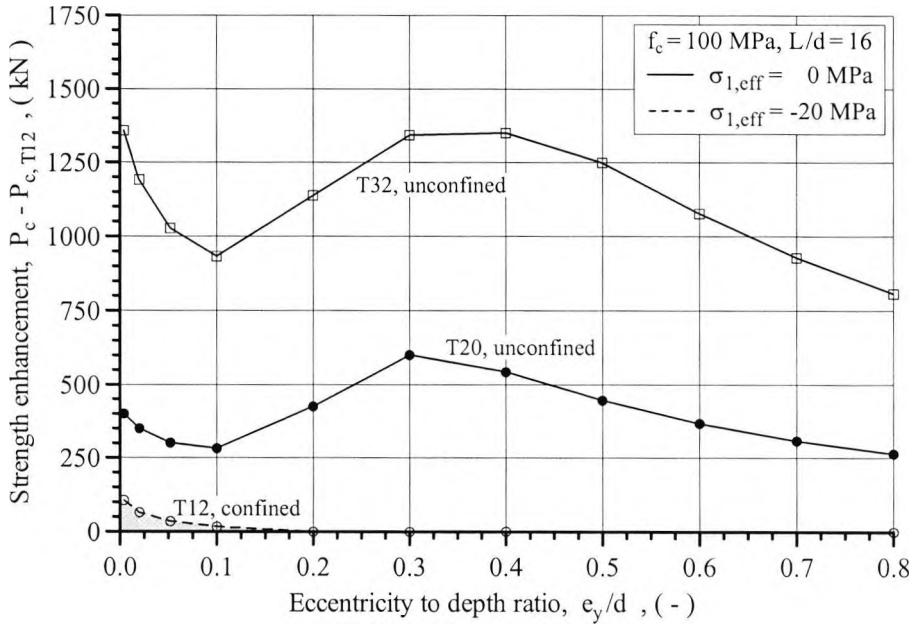

Figure 6.13b
Effect of increased bar size on eccentric load capacity of the C100 column having a slenderness ratio of 16

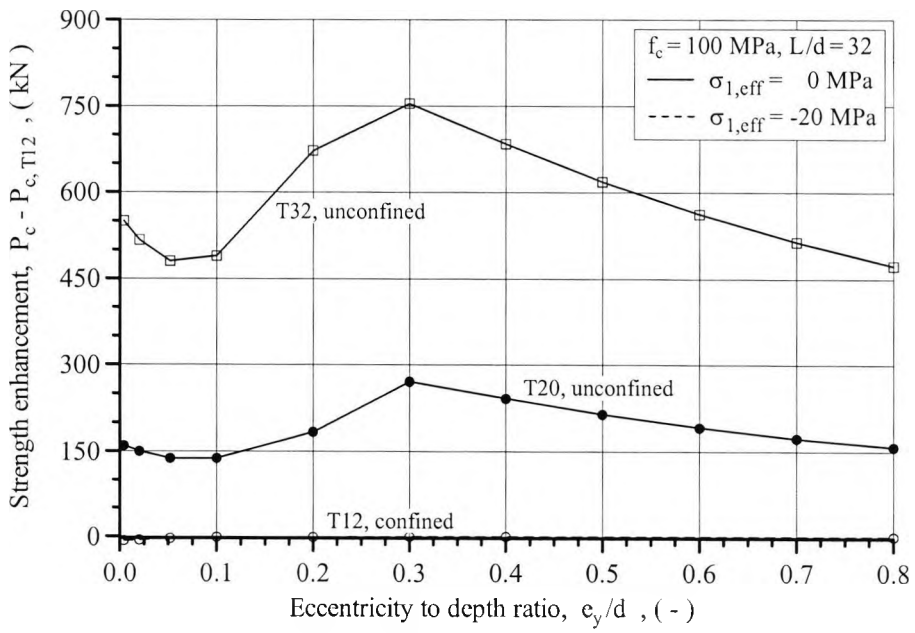

Figure 6.13c
Effect of increased bar size on eccentric load capacity of the C100 column having a slenderness ratio of 32

Figures 6.14a-c and 6.15a-c show the effect that the size of the longitudinal reinforcement bars has on the load-deflection response of the unconfined columns made from the C20 and C100 concrete respectively. For the C20 column having a slenderness ratio of 8 an increase in the size of the bars resulted in reduced mid-height deflections at strength failure. However, when increasing the slenderness ratio to 32 the situation was reversed, as the columns reinforced by the larger bars failed at larger mid-height deflections than the column reinforced by the T12 bars. By comparing the load-deflection diagrams for the C20 columns with the similar diagrams for the C100 columns it can be seen that the deflections at failure predicted by the computer programme were only marginally influenced by the strength of concrete.

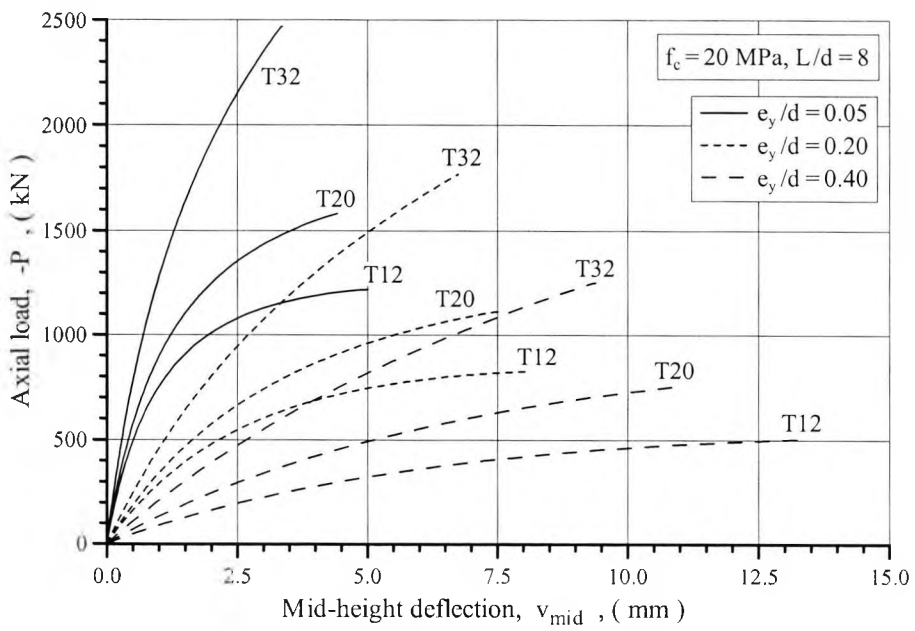

Figure 6.14a
Effect of increased bar size on load-deflection diagrams for the C20 column having a slenderness ratio of 8

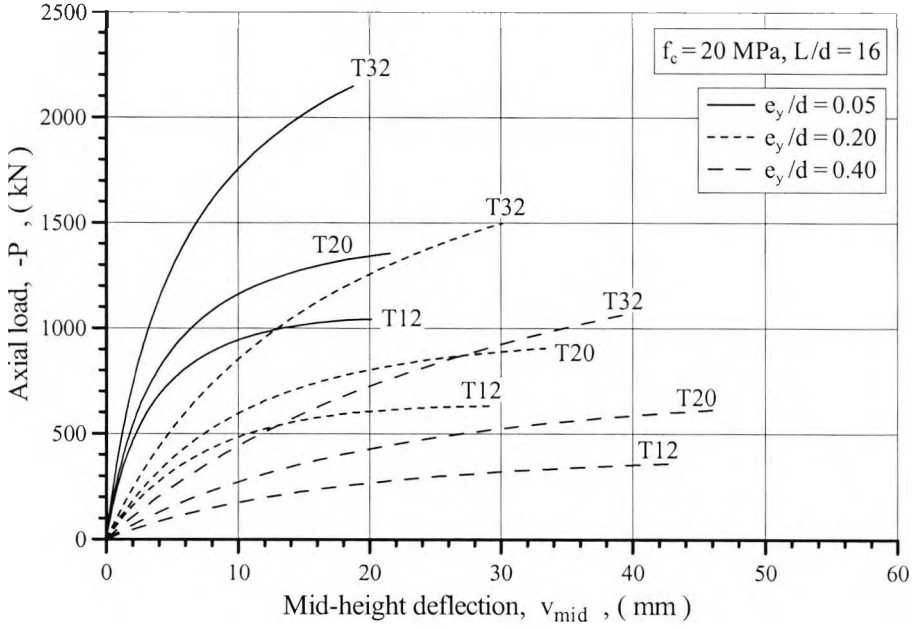

Figure 6.14b
Effect of increased bar size on load-deflection diagrams for the C20 column having a slenderness ratio of 16

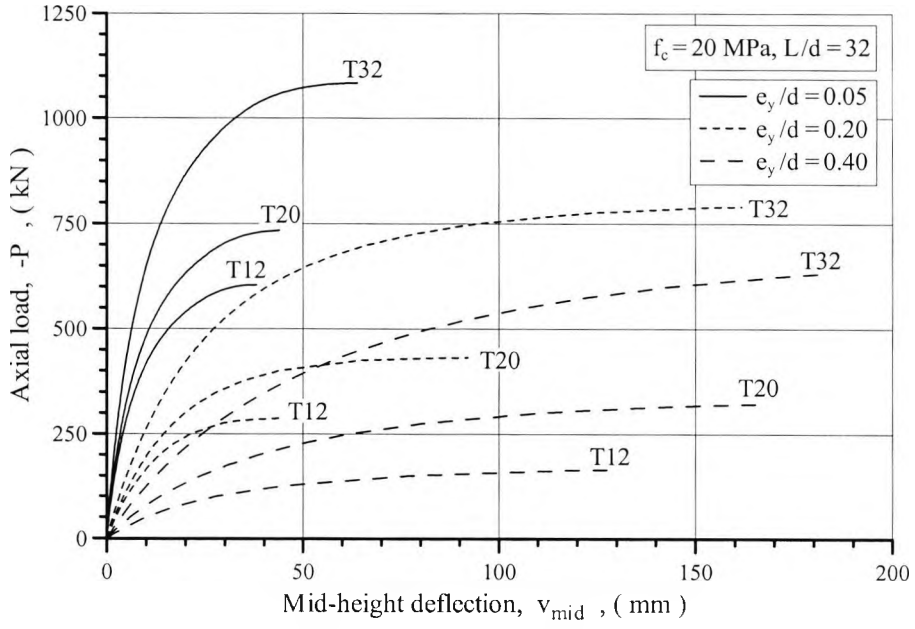

Figure 6.14c
Effect of increased bar size on load-deflection diagrams for the C20 column having a slenderness ratio of 32

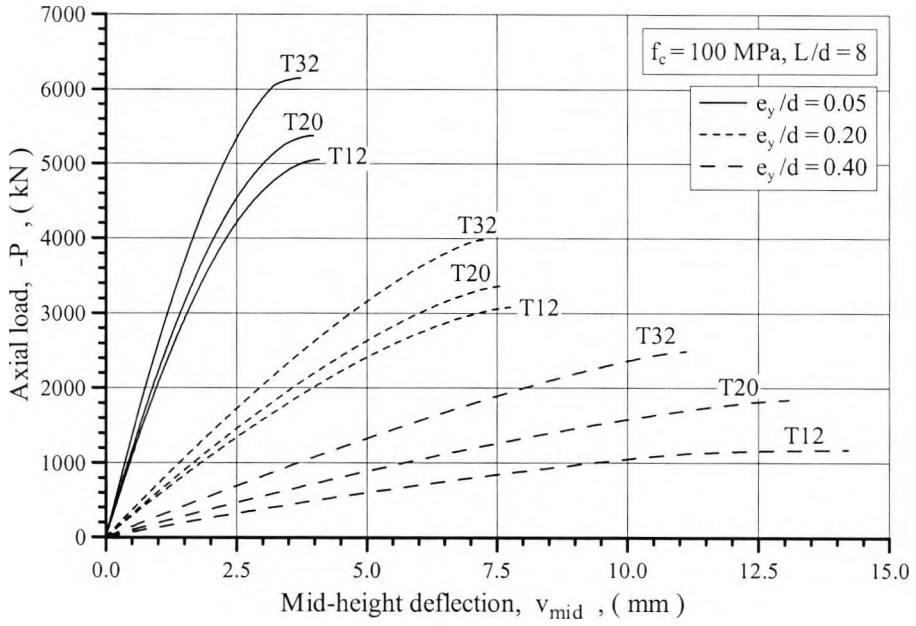

Figure 6.15a
Effect of increased bar size on load-deflection diagrams for the C100 column having a slenderness ratio of 8

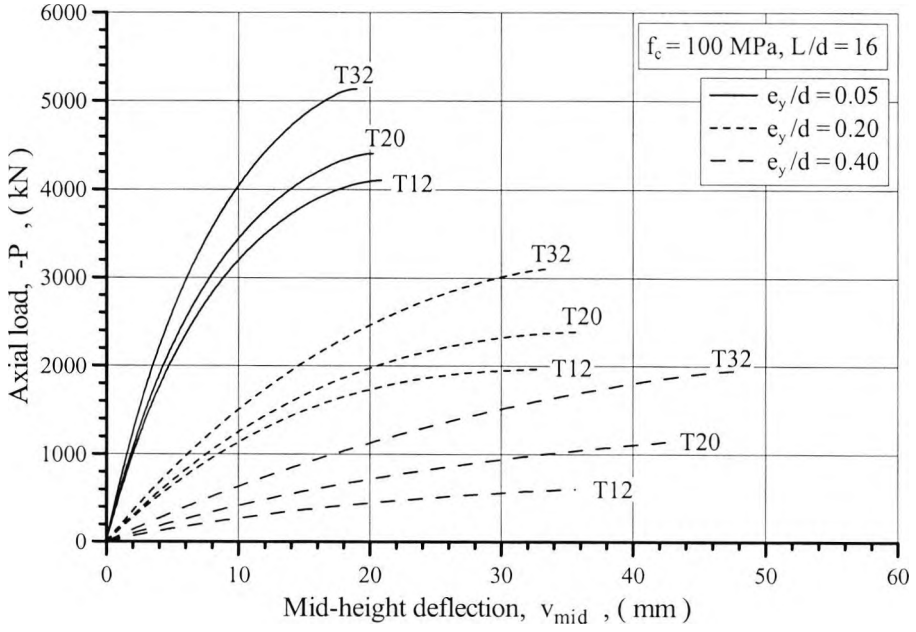

Figure 6.15b
Effect of increased bar size on load-deflection diagrams for the C100 column having a slenderness ratio of 16

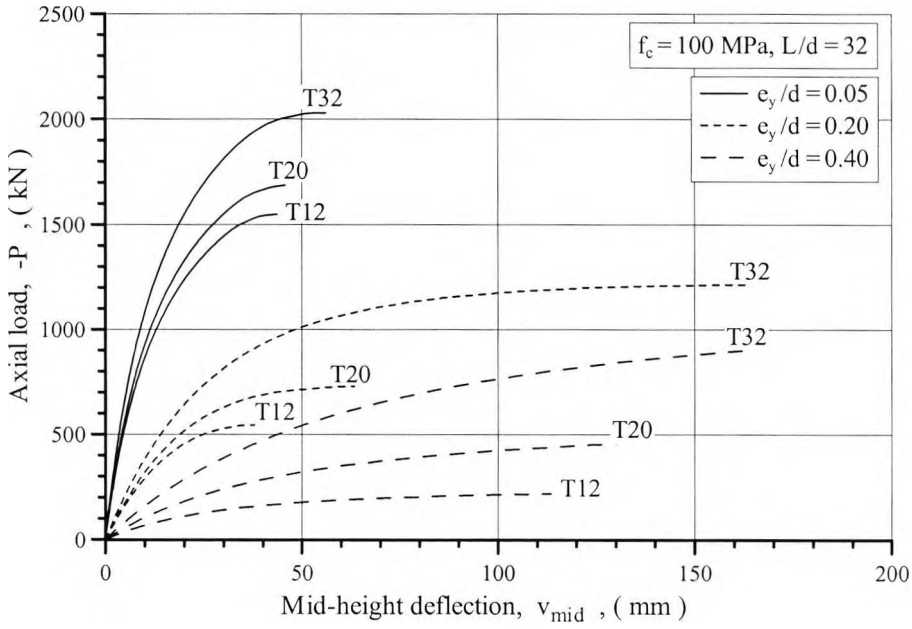

Figure 6.15c
Effect of increased bar size on load-deflection diagrams for the C100 column having a slenderness ratio of 32

6.1.4 Influence of Concrete Cover

By comparing the results obtained when assuming that both the cover and core concrete are confined to those obtained when assuming only the core concrete is confined, it is possible to assess to what extent the presence of the unconfined concrete cover influences the structural behaviour of the confined columns. Figures 6.16a and 6.16b illustrate the effect of the unconfined concrete cover on the load capacity of the C20 columns having a slenderness ratio of 8 and 16 respectively, and figures 6.17a-b illustrate the effect of the unconfined concrete cover on the load capacity of the C100 columns.

When loaded at a load eccentricity to depth ratio of 0.05 an externally applied confining pressure of 2 MPa, 5 MPa, 10 MPa and 20 MPa was found to raise the load-carrying capacity of the shortest of the C20 columns by 38% (469 kN), 73% (894 kN), 111% (1356 kN) and 163% (1987 kN) respectively. This compares to the much more

modest increases of 10% (118 kN), 15% (186 kN), 30% (362 kN) and 53% (647 kN) obtained when only the stress-strain characteristics of the core concrete benefited from confinement. For the longer column having a slenderness ratio of 16 the load capacity at the same eccentricity was found to be raised by 18% (192 kN), 29% (303 kN), 40% (416 kN) and 54% (563 kN) when applying the confining pressure externally, and by 7% (70 kN), 10% (108 kN), 14% (148 kN) and 19% (203 kN) when applying the confining pressure internally. The figures also show that at large eccentricity to depth ratios neither method of confinement had much influence on the load capacity.

Compared to the C20 columns, the C100 columns benefited relatively less from confinement. When loaded at an eccentricity to depth ratio of 0.05 the capacity of the C100 column having a slenderness ratio of 8 was raised by 13% (649 kN), 28% (1422 kN), 48% (2419 kN) and 75% (3795 kN) when subjecting the surface of the column to a confining pressure of 2 MPa, 5 MPa, 10 MPa and 20 MPa respectively. The similar enhancements in the load capacity of the column for which the confinement only affected the stress-strain behaviour of the core concrete were 1% (65 kN), 2% (95 kN), 2% (110 kN) and 2% (110 kN). An increase in the column's slenderness ratio to 16 reduced the load capacity gains of the C100 column to 6% (264 kN), 11% (469 kN), 14% (583 kN) and 16% (643 kN) assuming that both the core and cover concrete benefited from confinement, and to less than 1% (24 kN - 40 kN) assuming that only the core concrete benefited from confinement.

Figures 6.18a-b and 6.19a-b show load-deflection diagrams for the C20 and C100 columns which were confined by means of an external agent. Compared to the corresponding columns having an unconfined concrete cover (see figures 6.10a-b and 6.11a-b), the

confinement in general was found to have a significant effect in raising both the strength and pre-peak ductility of the columns. Thus it is the presence of the unconfined concrete cover which is responsible for the rather disappointing pre-peak performance of the columns passively confined by means of tie reinforcement. However, it should be pointed out that the enhancing effects of confinement were reduced with an increase in concrete strength, slenderness ratio and load eccentricity.

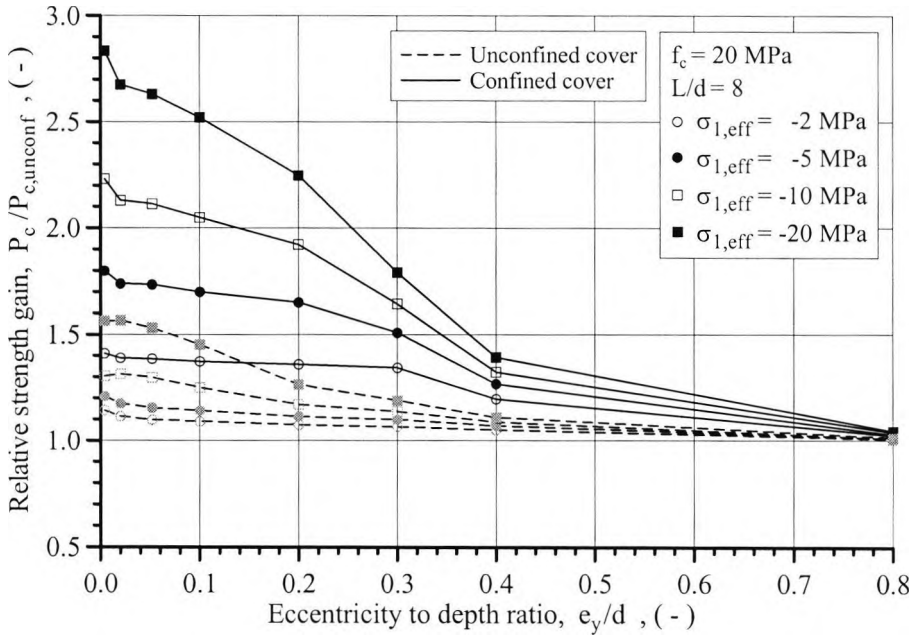

Figure 6.16a
Influence of concrete cover on eccentric load capacity of confined C20 columns having a slenderness ratio of 8

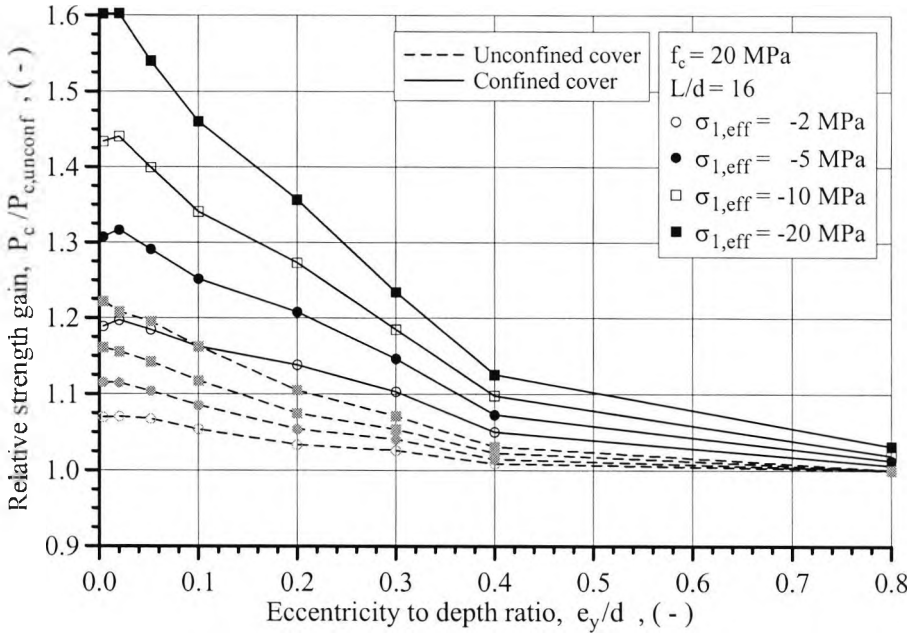

Figure 6.16b
Influence of concrete cover on eccentric load capacity of confined C20 columns having a slenderness ratio of 16

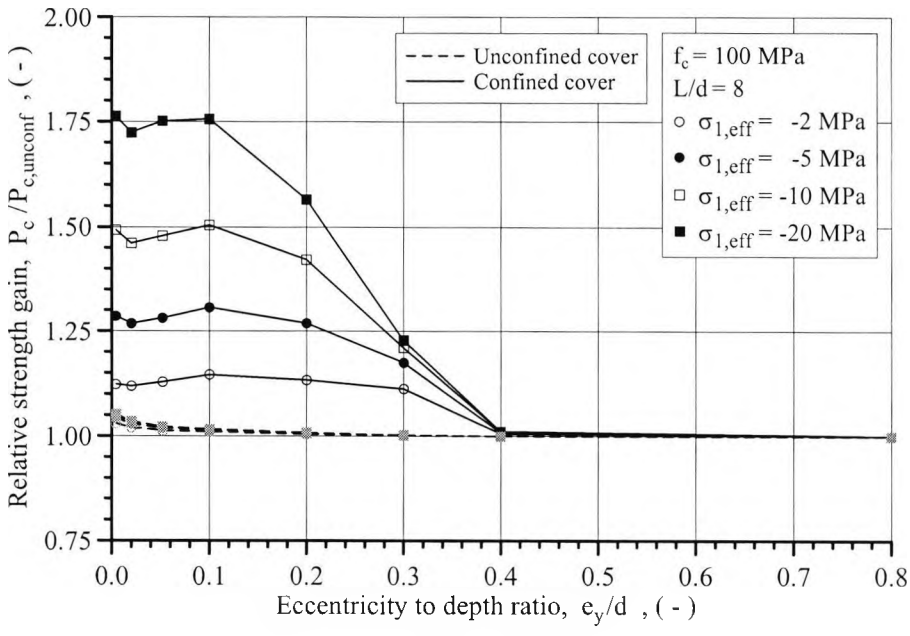

Figure 6.17a
Influence of concrete cover on eccentric load capacity of confined C100 columns having a slenderness ratio of 8

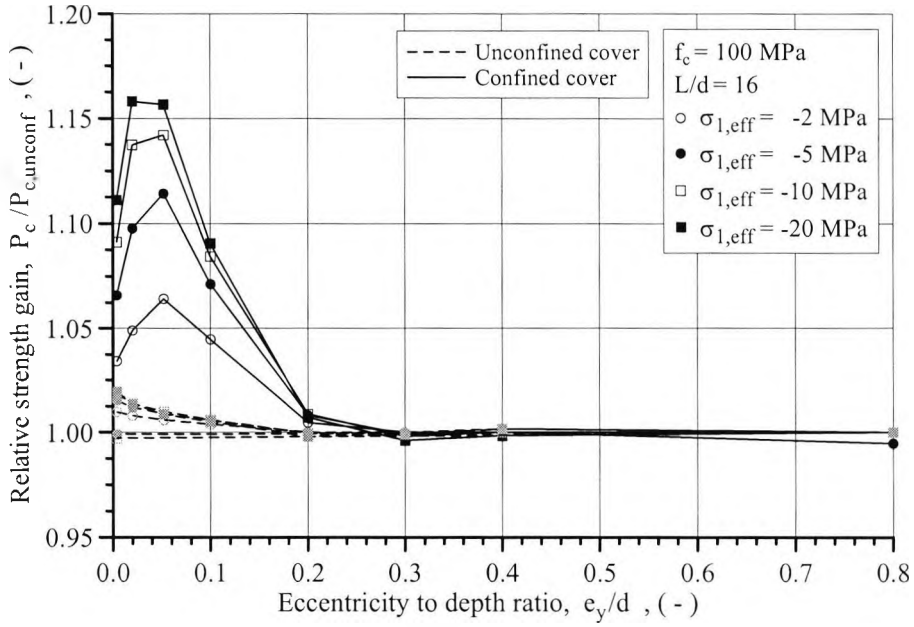

Figure 6.17b
Influence of concrete cover on eccentric load capacity of confined C100 columns having a slenderness ratio of 16

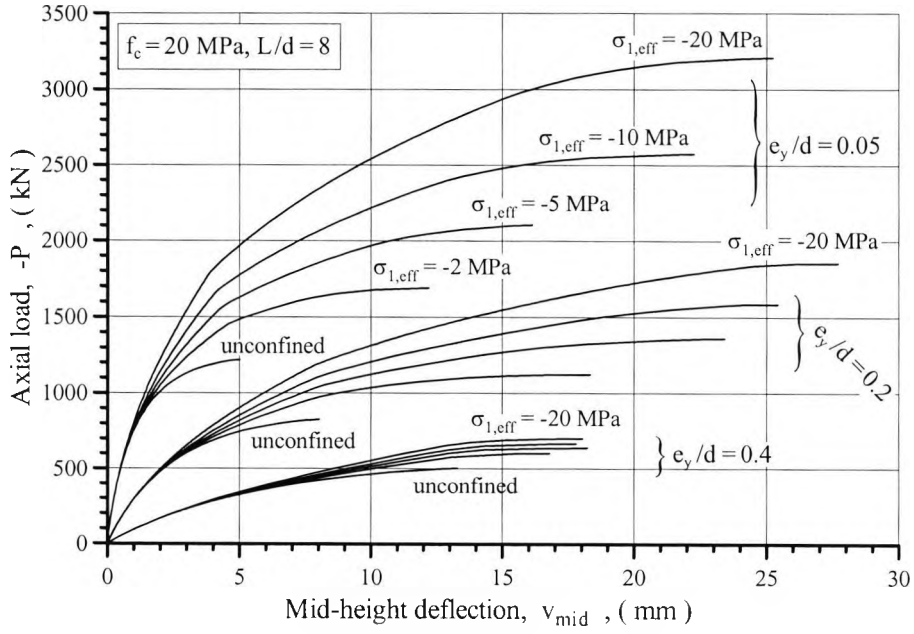

Figure 6.18a
Load-deflection diagrams for externally confined C20 columns having a slenderness ratio of 8

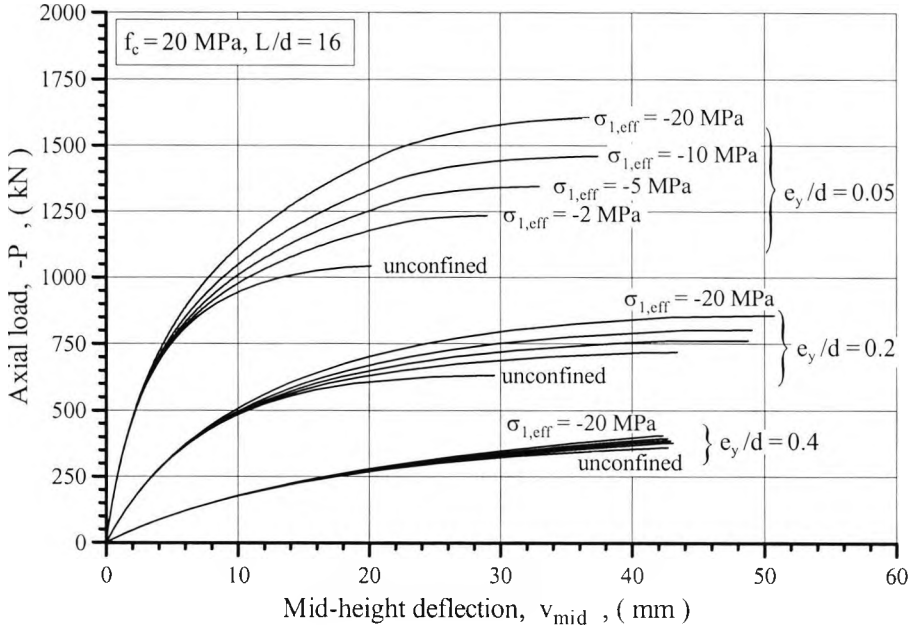

Figure 6.18b
Load-deflection diagrams for externally confined C20 columns having a slenderness ratio of 16

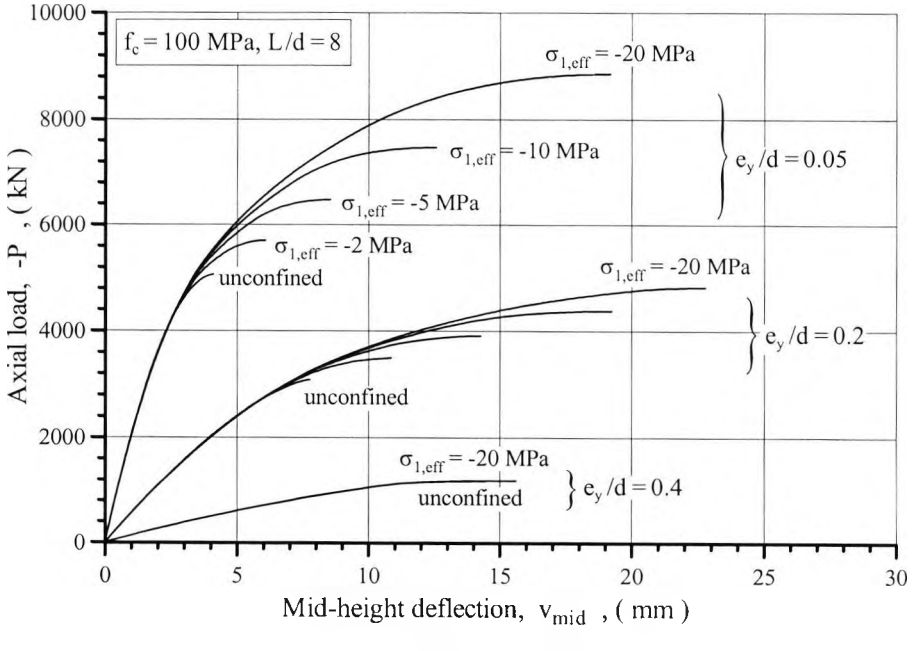

Figure 6.19a
Load-deflection diagrams for externally confined C100 columns having a slenderness ratio of 8

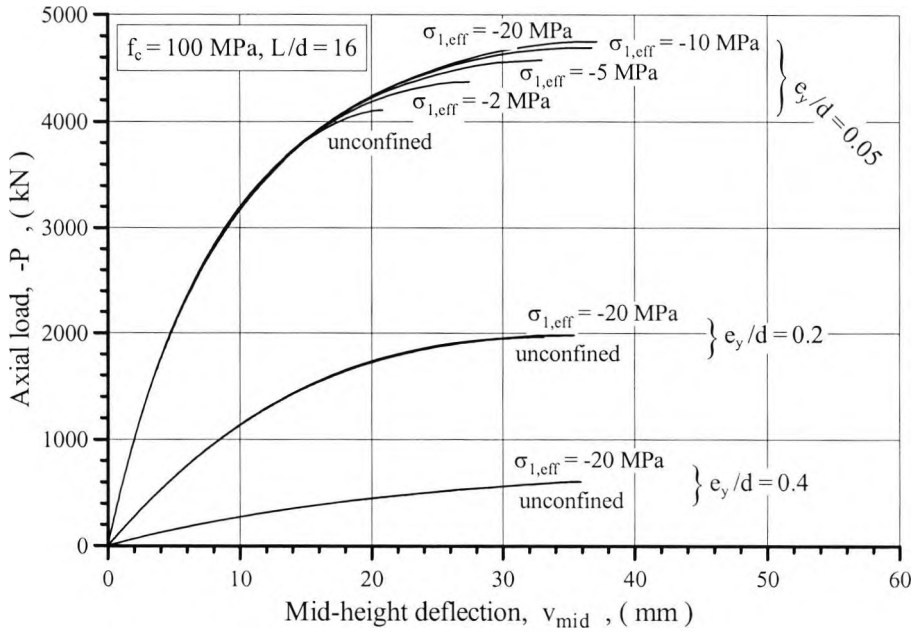

Figure 6.19b
Load-deflection diagrams for externally confined C100 columns having a slenderness ratio of 16

6.1.5 Summary

In this chapter the effect of passive confinement on the load-deflection characteristics of reinforced concrete columns subjected to eccentric compression was numerically investigated. The confined columns all had a 250×250 mm cross-section, a 20 mm thick concrete cover and were longitudinally reinforced by 4 T12 bars positioned with a centre-to-centre distance of 182 mm. The columns were analysed for effective confining pressures up to 20 MPa, slenderness ratios ranging from 8 to 32, concrete strengths ranging from 20 MPa to 100 MPa and eccentricity to depth ratios ranging from 0.004 to 0.8. The numerical analysis was based on the assumption that the integrity of the columns was maintained throughout the loading process. Since premature cover spalling has often been observed to occur in experimental tests on confined concrete columns (see chapter 3), the

numerical results can be considered to represent upper bound values. Based on the results of the numerical investigation it could be concluded that:

- For the unconfined columns, the additional load capacity gained by simply increasing the strength of the concrete was reduced with both an increase in the slenderness and the load eccentricity. In other words, the use of high strength concrete was found to be most cost effective in short columns subjected to nearly concentric compression.
- Passive confinement had in general a limited effect on the load-deflection characteristics of the columns, and the effect reduced with an increase in concrete strength. Only for the columns having a slenderness ratio of 8 and made from the C20 concrete did even the largest confining pressure of 20 MPa significantly enhance the pre-peak ductility of the column, and this only for load eccentricities less than approximately 0.3. The pre-peak ductility, as measured by the mid-height deflection at the peak load, appeared in general to be less affected by confinement than the peak load itself.
- As an alternative to passive confinement, the use of T20 bars in place of the T12 bars as longitudinal reinforcement was judged to be a more cost efficient method of enhancing the strength of the columns. When loaded at an eccentricity to depth ratio in excess of about 0.2 the larger bar size enhanced the strength of the high strength concrete columns more than the strength of the normal strength concrete columns. In general, the use of a larger size of longitudinal reinforcement bars had little bearing on the mid-height deflections at failure, but the trend was for the deflections to be reduced for the columns having a slenderness ratio of 8 and to be increased for the columns having a slenderness ratio of 32. The deflections appeared to be largely independent of the concrete strength.

- By analysing the columns under the assumption of both the cover and core concrete being confined, it could be concluded that it was largely the presence of the unconfined concrete cover that was responsible for the disappointing performance of the passively confined columns. Had it not been because of the unconfined cover, even a confining pressure of 2 MPa was sufficient to significantly improve both the strength and the pre-peak ductility of the columns. Furthermore, in sharp contrast to the experience drawn from analysing the columns having an unconfined concrete cover, the high strength concrete columns having a slenderness ratio of 8 did for small load eccentricities gain more strength from being subjected to an external confining pressure than the similar columns made from the normal strength concrete.

Chapter 7: Conclusions and Future Research

7.1 General Comments

The conclusions are divided into two groups. The first relates to the basic material characteristics of high strength concrete and the other to the structural performance of slender high strength concrete columns. In both cases particular attention has been given to the effects of confinement.

The conclusions in section 7.2 relate in part to the material characteristics of the two high strength concrete mixes employed in the experimental investigation, and the conclusions in section 7.3 relate to the structural response of full-scale concrete columns.

Section 7.4 lists a few suggestions for future research topics.

7.2 Mechanical Behaviour of High Strength Concrete

The average conversion factor between the compressive strengths of 100×200 mm cylinders and 100 mm cubes made from the grade C100 and C120 concrete was determined to be 0.87 and 0.92 respectively. These coefficients, which are supported by the findings of similar experimental investigations, indicate that the conversion coefficients typically used for normal strength concrete are conservative for high strength concrete, and that the use of microsilica has the effect of increasing the conversion factor.

The average critical stress to strength ratio determined for the grade C100 and C120 concrete was 0.82 and 0.87 respectively. These ratios are significantly higher than the ratios of 0.70 to 0.75 reported for normal strength concrete. These ratios reflect a more linear stress-strain response, and a delay in the beginning of the unstable break-up of the internal

micro-structure, when compared to normal strength concrete.

The empirical expressions recommended in CEB (1995) for predicting the modulus of elasticity, the peak strain and the tensile strength as a function of the compressive strength were in agreement with the test results for the employed high strength concretes. The CEB expressions predicted the modulus of elasticity to within 5%, the peak strain to within 6% and the tensile strength to within 11% of the test results. By including experimental data from other sources, it was demonstrated that the CEB expressions are often significantly less accurate, and that the accuracy by which the modulus of elasticity and the peak strain are predicted appears to be independent of the concrete strength.

The lateral expansion observed during testing of the high strength concrete specimens was larger than expected. At a stress to strength ratio of 0.8, the apparent Poisson's ratios determined for the C100 and C120 concrete were approximately 40% larger than the ratio predicted by the expression given in the CEB Model Code 90.

As a basis for the further investigation into the behaviour of confined high strength concrete, a new model was proposed to describe the stress-strain behaviour of normal weight concrete subjected to short term uniaxial compression. The model, which incorporates a distinct material parameter to control the steepness of the descending branch of the stress-strain curve, was demonstrated to provide a good fit to experimental data on concrete having compressive strengths ranging from 20 MPa to 110 MPa. The proposed stress-strain model may be considered to be a generalisation of a similar model recommended in the CEB Model Code 90.

The investigation into the effects of confinement showed that the relative increase in concrete strength solely depends on the confinement ratio, and that the rate of the strength

increase is reduced with increasing confining pressure. Furthermore, the experimental data showed that, when subjected to the same amount of confinement, a specimen made from high strength concrete tends to gain somewhat more strength than a specimen made from normal strength concrete. The expression for the compressive meridian in Ottosen's failure criterion was found to accurately describe the effect of confinement on the strength of concrete.

Confinement was seen to have the effect of increasing the peak strain, as well as reducing the steepness of the descending branch of the stress-strain curve. The effect is reduced with an increase in the grade of concrete, and a given confining pressure will always improve the peak strain relatively more than the strength.

By introducing a new method for calculating the maximum effective confining pressure associated with a given tie configuration and distribution, it was possible to develop an incremental stress-strain model which is equally capable of representing test results obtained under active and passive confinement conditions. The proposed model was validated against experimental data representing all practical concrete qualities and confinement levels, i.e. unconfined compressive concrete strengths up to about 120 MPa and confining pressures up to about 20 MPa. Under the non-uniform confinement conditions existing in concentric compression tests on transversely reinforced stub columns, the model describes the relationship between the strain and the average stress in the core concrete, and accounts for the stiffness of the restraining reinforcement ties.

The proposed confinement model was compared to existing closed form models when applied to the core concrete of two of the high strength concrete columns tested in the experimental programme. It was shown that the models produced quite similar stress-strain

curves in the pre peak region, but vastly different curves in the post peak region. The new model predicted a less ductile response than most of the existing confinement models.

7.3 Slender High Strength Concrete Columns

The conclusions in this section are grouped into those relating to the experimental investigation and those relating to the numerical investigation.

7.3.1 Experimental Investigation

Failure of the test columns was explosive and occurred, except in one case, without warning. In the shorter of the columns failure appeared to be initiated by cover spalling, and in the longer of the columns by a sudden loss of stability. A reduction in the tie spacings was observed to increase the inclination of the failure plane, and to reduce the volume of crushed core concrete. In the case of the columns with the closest tie spacings of 50 mm the failure plane was almost perpendicular to the longitudinal axis, and only a small volume of core concrete was lost due to crushing. As a consequence, failure of these columns was of a very kinetic nature, and caused two of the longitudinal bars to be pulled over.

When taken as a percentage of the squash load, the observed test loads indicated that a reduction in the tie spacings had the effect of increasing the load capacity of the shorter of the test columns. For the longer of the test columns, the load capacity appeared to be independent of the tie spacings.

The strain measurements taken during the testing of the slender high strength concrete columns confirmed that plane sections remained plane. According to the strains measured directly on the surface of the columns, the shorter of the test columns failed at an average maximum compressive strain of 2.5 mm/m, and the longer at an average maximum

compressive strain of 1.9 mm/m. Thus, the value of 3.5 mm/m adopted in BS 8110 significantly overestimates the maximum compressive strain at failure, although it is recognised that the stress blocks used in the code are idealised. The test results revealed a weak tendency of the failure strain to increase with a reduction in the tie spacings.

The mid-height deflections measured at failure were found to increase significantly with an increase in the column length. Likewise, a reduction in the tie pitch appeared to have some effect in improving the pre-peak ductility of the columns.

For none of the high strength concrete columns was the transverse reinforcement observed to yield at the time of failure. The maximum tensile strain measured in the tie legs varied from 20% to 90% of the yield strain, and appeared to be independent of the tie spacings. In addition, the large variations observed in the straining of the ties in any given column give rise to concern, regarding the detailing required in order to confidently include confinement effects in structural design calculations.

During much, or all, of the loading process the experimental curves for the vertical mid-height deflections and extreme fibre strains displayed less softening than expected. Furthermore, two of the test columns failed at a section located outside the middle fifth of the column length, and significant horizontal deflections could be noted where none were expected. After having investigated a number of possible explanations, it was concluded that the principal reason for these discrepancies between the experimental and the analytical results, and at times also between the measured strains and measured deflections, was caused by unexpected movements of the rig. In effect, the test observations were influenced by a combination of rigid body displacements and continuous reductions in the eccentricity by which the axial load was applied. Corrections to the observed deformations accounting for the movements of the rig improved the apparent load-deflection response.

7.3.2 Numerical Investigation

A computer program, which incorporates the effect of the transverse reinforcement on the longitudinal stress-strain characteristics of the core concrete, was developed for calculating the structural response of slender high strength concrete columns. The program was validated against 122 column tests representing a large range of geometric and physical properties.

Although the material characteristics of the core concrete of many of the eccentrically loaded test columns were estimated to have benefited significantly from confinement, their load-deflection response appeared only to be marginally affected by confinement. It was concluded that the concrete cover played a major role in counteracting the benefits of passive confinement, and that instability of the cover shell at times may have been responsible for premature column failure.

For the slender high strength concrete columns tested in the experimental investigation the average experimental to predicted failure load was 1.30 for the shorter columns. For the longer columns the average ratio was 1.96. The latter value is significantly higher than the ratios, ranging from 1.15 to 1.35, determined for the seven test programmes from published literature. The numerical calculations indicated that, for none of the columns, the provided transverse reinforcement was sufficient to influence the overall column behaviour. In all numerical calculations the material properties of unconfined concrete were estimated on the basis of the compressive strength, where the compressive strength was taken as 81% of the mean strength of tested 100×200 mm cylinders, or alternatively as 85% of the mean strength of tested 150×300 mm cylinders.

A number of general conclusions could be drawn on the basis of the parametric study on columns having cross-sectional dimensions similar to those of the columns tested in the

experimental investigation. All conclusions were drawn under the assumption of a stable cover shell.

The extra load capacity obtained by replacing normal strength concrete with high strength concrete in an unconfined concrete column is reduced with an increase in both column slenderness and load eccentricity. The deflections at strength failure are increased with both an increase in column slenderness and load eccentricity, but appear to be largely independent of the concrete strength. Thus, the use of high strength concrete is most cost effective in short columns subjected to nearly concentric compression.

The enhancing effect of confinement on both strength and ductility of isolated columns having practically detailed reinforcement reduces rapidly with an increase in column slenderness, load eccentricity and concrete strength. For load eccentricity to depth ratios in excess of 0.05, a slender column made from normal strength concrete may benefit somewhat from passive confinement, but a high strength concrete column of medium slenderness is unlikely to do so.

The presence of an unconfined concrete cover counteracts the benefits of confinement, and this being more so for high strength concrete columns than for normal strength concrete columns. From analysing eccentrically loaded columns under the assumption of being subjected to an externally applied pressure, it appears that even a relatively small effective confining pressure of 2 MPa may significantly enhance both the ultimate load capacity and the pre-peak ductility of high strength concrete columns. Once again the benefits of confinement reduce rapidly with an increase in column slenderness, load eccentricity and concrete strength. Nevertheless, at a load eccentricity to depth ratio of 0.05, the benefits of confinement on the structural response of a high strength concrete column of medium to slender length may well be more pronounced than the benefits on a similar column made from normal strength concrete.

7.2 Suggestions for Future Research

Although the tested columns displayed some ductility towards the end, the level was not sufficiently high. It is suggested that the level of ductility may be enhanced by the use of fibres in the concrete mix.

Since confinement is most efficient when applied to the entire concrete section, it is considered that column wraps in general may be more suited than conventional shear reinforcement in enhancing the strength and ductility of high strength concrete columns. However, there are aspects related to the use of column wraps, such as fire protection and concrete shrinkage, that may negate their usefulness.

The problem of premature cover spalling sometimes associated with high strength concrete needs to be quantified through targeted experimental research.

The computer program developed in this work could be modified so as to calculate the post-peak descending branch of the load-deflection curve. This is required when performing a rigorous analysis of a structural frames for which load redistribution may interact with the behaviour of a given column to trigger collapse.

Finally, it is recommended to use the available computational tool to examine the applicability of the design rules to columns made from high strength concrete, and determine any changes if so required.

References

ACI Committee 363 (1984) - *State-of-the-art report on high strength concrete - ACI Journal: Jul.-Aug. 1984, pp. 364-411*

ACI-ASCE Committee 441 (1997) - *High strength concrete columns: State of the art - ACI Structural Journal: May-Jun. 1997, pp. 323-335*

Ahmad, S.H. and Shah, S.P. (1982) - *Stress-strain curves of concrete confined by spiral reinforcement - ACI Journal: Nov.-Dec. 1982, pp. 484-490*

Ammann, W., Mühlmatter, M. and Bachmann, H. (1982) - *Stress-strain behaviour of non-prestressed and prestressed reinforcing steel at high strain rates - Bundesanstalt für Materialprüfung, RILEM-CEB-IABSE-IASS Interassociation Symposium, Berlin, Jun. 2-4, 1982*

Assa, B., Nishiyama, M. and Watanabe, F. (2001) - *New approach for modelling confined concrete. Circular columns - ASCE Journal of Structural Engineering: Vol. 127, No. 7, Jul. 2001, pp. 743-750*

Attard, M.M. and Setunge, S. (1996) - *Stress-strain relationship of confined and unconfined concrete - ACI Materials Journal: Sep.-Oct. 1996, pp. 432-442*

Baalbaki, W., Benmokrane, B., Chaallal, O. and Aitcin, P. (1991) - *Influence of coarse aggregate on elastic properties of high performance concrete - ACI Materials Journal: Sep.-Oct. 1991, pp. 499-503*

Baalbaki, W., Aitcin, P. and Ballivy, G. (1992) - *On predicting modulus of elasticity in high strength concrete - ACI Materials Journal: Sep.-Oct. 1992, pp. 517-520*

Bazant, Z.P., Cedolin, L. and Tabbara, M. (1991) - *New method of analysis for slender columns - ACI Structural Journal: Jul.-Aug. 1991, pp. 391-401*

Bjerkeli, L., Tomaszewicz, A. and Jensen, J.J. (1993) - *Deformation properties and ductility of high strength concrete - ACI Special Publication SP 121-12, pp. 215-238*

Brant, N.F.A. - *Reinforced concrete columns of variable cross-section - PhD thesis, City University, London, 1984*

BS 1881: Part 102 (1983) - *Testing concrete - Methods for determination of slump*

BS 1881: Part 105 (1984) - *Testing concrete - Methods for determination of flow*

BS 1881: Part 110 (1983) - *Testing concrete - Method for making test cylinders from fresh concrete*

BS 1881: Part 111 (1983) - *Testing concrete - Method for normal curing of test specimens (20 °C method)*

BS 1881: Part 116 (1983) - *Testing concrete - Method for determination of the compressive strength of concrete cubes*

BS 1881: Part 117 (1983) - *Testing concrete - Method for determination of tensile splitting strength*

BS 1881: Part 120 (1983) - *Testing concrete - Method for determination of the compressive strength of concrete cores*

BS 1881: Part 121 (1983) - *Testing concrete - Method for determination of the static modulus of elasticity in compression*

BS 4449 (1988) - *Carbon steel bars for the reinforcement of concrete*

BS 5950: Part 1 (1990) - *Structural use of steelwork in building - Code of practice for design in simple and continuous construction: hot rolled sections*

BS 8110: Part 1 (1985, 1997) - *Structural use of concrete - Code of practice for design and construction*

BS 8110: Part 2 (1985) - *Structural use of concrete - Code of practice for special circumstances*

BS 8110: Part 3 (1985) - *Structural use of concrete - Design charts for singly reinforced beams, doubly reinforced beams and rectangular columns*

BS 812: Section 103.1 (1985) - *Testing aggregates - Methods for determination of particle size distribution*

BS 812: Part 2 (1995) - *Testing aggregates - Methods for determination of density*

Carrasquillo, R.L., Slate, F.O. and Nilson, A.H. (1981a) - *Microcracking and behaviour of high strength concrete subject to short term loading - ACI Journal: May-Jun. 1981, pp. 179-186*

Carrasquillo, R.L., Nilson, A.H. and Slate, F.O. (1981b) - *Properties of high strength concrete subject to short term loads - ACI Journal: May-Jun. 1981, pp. 171-178*

CEB, (1990) - *CEB-FIP Model Code 90 (Guidelines for HSC)*

CEB, (1994) - *Application of high performance concrete - Bulletin d'Information: No. 222, Nov. 1994.*

CEB, (1995) - *High performance concrete, Recommended extensions to the model code 90 - Bulletin d'Information: No. 228, Jul. 1995.*

Chen, W.F. and Atsuta, T. (1977) - *Theory of beam columns. Volume 2: Space behaviour and design - McGraw-Hill, 1977*

Chen, W.F. (1982) - *Plasticity in reinforced concrete - McGraw-Hill, 1982*

Cheong, H.K. and Perry, S.H.. (1993) - *Cyclic loading of laterally confined concrete columns - Materials and Structures: Vol. 26, 1993, pp. 557-562*

Choi, S., Thienel, K. and Shah, S.P. (1996) - *Strain softening of concrete in compression under different constraints - Magazine of Concrete Research: Vol. 48, No. 175, Jun. 1996, pp. 103-115*

Chuang, P.H. and Kong, S.K. (1995) - *Failure loads of slender reinforced concrete columns - Proceedings Institution of Civil Engineers, Structures & Buildings: Vol. 110, Nov. 1995, pp. 339-350*

Chuang, P.H. and Kong, S.K. (1997) - *Large-scale tests on slender reinforced concrete columns - The Structural Engineer: Vol. 75, No.23 & 24, Dec. 1997, pp. 410-415*

Chuang, P.H. and Kong, S.K. (1998) - *Strength of slender reinforced concrete columns - ASCE Journal of Structural Engineering: Vol. 124, No. 9, Sep. 1998, pp. 992-998*

Claeson, C. and Gylltoft, K. (1998) - *Slender high-strength concrete columns subjected to eccentric loading - ASCE, Journal of Structural Engineering, Vol. 124, No. 3, Mar. 1998, pp. 233-240*

Collins, M.P., Mitchell, D. and McGregor, J.G. (1993) - *Structural design considerations for high-strength concrete - Cancer International Structural, May 1993, pp. 27-34*

Cranston, W.B. and Sturrock, R.D. (1971) - *Lateral instability of slender reinforced concrete columns - RILEM international symposium, Buenos Aires, 1971, pp. 117-141*

Cranston, W.B. (1972) - *Analysis and design of reinforced concrete columns - Cement and Concrete Association, Research report No 20, 1972*

Cusson, D. and Paultre, P. (1994) - *High strength concrete columns confined by rectangular ties - ASCE Journal of Structural Engineering: Vol. 120, No. 3, Mar. 1994, pp. 783-804*

Cusson, D. and Paultre, P. (1995) - *Stress-strain model for confined high strength concrete - ASCE Journal of Structural Engineering: Vol. 121, No. 3, Mar. 1995, pp. 468-477*

Cusson, D., Larrard, F., Boulay, C. and Paultre, P. (1996) - *Strain localisation in confined high strength concrete columns - ASCE Journal of Structural Engineering: Vol. 122, No. 9, Sep. 1996, pp. 1055-1061*

Dahl, K.K.B. (1992a) - *Uniaxial stress-strain curves for normal and high strength concrete - Technical University of Denmark, Department of Structural Engineering: Report R282, 1992*

Dahl, K.K.B. (1992b) - *A constitutive model for normal and high strength strength concrete - Technical University of Denmark, Department of Structural Engineering: Report R287, 1992*

Dahl, K.K.B. (1992c) - *A failure criterion for normal and high strength concrete - Technical University of Denmark, Department of Structural Engineering: Report R286, 1992*

Diniz, S.M. and Frangopol, D.M. (1997) - *Strength and ductility simulation of high-strength concrete columns - ASCE Journal of Structural Engineering: Vol. 123, No. 10, Oct. 1997, pp. 1365-1374*

DS 411 (1984) - *Betonkonstruktioner, Teknisk forlag Publikation NP-169-N*

El-Dash, K.M. and Ahmad, S.H. (1994) - *A model for the stress-strain relationship of rectangular confined normal and high strength concrete columns - Materials and Structures: Vol. 27, 1994, pp. 572-579*

Foster, S.J. and Attard, M.M. (1997) - *Experimental tests on eccentrically loaded high strength concrete columns - ACI Structural Journal: May-Jun. 1997, pp. 295-303*

Foster, S.J., Liu, J. and Sheikh, S.A. (1998) - *Cover spalling in HSC columns loaded in concentric compression - ASCE Journal of Structural Engineering: Vol. 124, No. 12, Dec. 1998, pp. 1431-1437*

Hansen, E. and Tomaszewicz, A. (1993) - *Effect of confinement on the ductility of structural members with high strength concrete - Utilisation of high strength concrete, Proceedings: Symposium in Lillehammer, Norway, Jun. 20-23, 1993, pp. 184-191*

Held, M., König, G. and Simsch, G. (1993) - *Ductility of large high strength concrete columns in high rise buildings - Utilisation of high strength concrete, Proceedings: Symposium in Lillehammer, Norway, June 20-23, 1993, pp. 200-208*

Hognestad, E., Hanson, N.W. and McHenry, D. (1955) - *Concrete stress distribution in ultimate strength design - ACI Journal: Dec. 1955, pp. 455-479*

Hong, H.P (2001) - *Strength of slender reinforced concrete columns under biaxial bending - ASCE Journal of Structural Engineering: Vol. 127, No. 7, Jul. 2001, pp. 758-762*

Hoshikuma, J., Kawashima, K., Nagaya, K. and Taylor A.W. (1997) - *Stress-strain model for confined reinforced concrete in bridge piers - ASCE Journal of Structural Engineering: Vol. 123, No. 7, May 1997, pp. 624-633*

Hsu, T.C., Slate, F.O., Sturman,G.M. and Winter, G. (1963) - *Microcracking of plain concrete and the shape of the stress-strain curve - ACI Journal: Feb. 1963, pp. 209-223*

Hsu, C.T. (1974) - *Behaviour of structural concrete subjected to biaxial flexure and axial compression - PhD thesis, McGill University, Montreal, 1974*

Hsu, L.S. and Hsu, C.T. (1994) - *Complete stress-strain behaviour of high strength concrete under compression - Magazine of Concrete Research: Vol. 46, No. 169, Dec. 1994, pp.301-312*

Ibrahim, H.H. and MacGregor, J.G. (1996a) - *Tests of eccentrically loaded high strength concrete columns - ACI Structural Journal: Sep.-Oct. 1996, pp. 585-594*

Ibrahim, H.H. and MacGregor, J.G. (1996b) - *Flexural behaviour of laterally reinforced high-strength concrete sections - ACI Structural Journal: Nov.-Dec. 1996, pp. 674-684*

Imam, M., Vandewalle, L. and Mortelmans, F. (1995) - *Are current concrete strength tests suitable for high strength concrete ? - Materials and Structures: Vol. 28, pp. 384-391*

Iravani S. (1996) - *Mechanical properties of high performance concrete - ACI Materials Journal: Sep.-Oct. 1996, pp. 416-426*

Issa, M.A. and Tobaa, H. (1994) - *Strength and ductility enhancement in high strength confined concrete - Magazine of Concrete Research: Vol. 46, No. 168, Sep. 1994, pp. 177-189*

Iyengar, K.T., Desayi, P. and Reddy, K.N. (1970) - *Stress-strain characteristics of concrete confined in steel binders - Magazine of Concrete Research: Vol. 22, No. 72, Sep. 1970, pp. 173-184*

Jeyarupaligham, N. (1996) - *Steel, concrete and steel/concrete composite beams and columns exposed to fire - PhD thesis, City University, London, 1996*

Karsan, D. and Jirsa, J.O. (1970) - *Behaviour of concrete under varying strain gradients - ASCE Journal of the Structural Division: Aug. 1970, pp. 1675-1696*

Kim, J.K. and Yang. J.K. (1995) - *Buckling behaviour of slender high-strength concrete columns - Engineering and Structures, Vol. 17, No. 1, 1995, pp. 39-51*

Kotsovos, M. (1974) - *Failure criteria for concrete under generalised stress states - PhD thesis, Imperial College of Technology, London, 1974*

Kotsovos, M.D. (1983) - *Effect of testing techniques on the post-ultimate behaviour of concrete in compression - Materials and Structures: Vol. 16, pp. 3-12*

Kotsovos, M.D. and Pavlovic, M.N. (1995) - *Structural concrete, Finite element analysis for limit state design - Thomas Telford, 1995*

Kupfer, H. (1973) - *Das verhalten des betons unter mehrachsiger kurzzeitbelastung unter besonderer berücksichtung der zweiachsigen beanspruchung - Deutsher Ausschuss für stahlbeton: Heft 229, 1973*

Larrard, F.D., Belloc, A. Renwez, S. and Boulay, C. (1994) - *Is the cube test suitable for high performance concrete - Materials and Structures: Vol. 27, 1994, pp. 580-583*

Legeron, F., Mongeau, D. and Paultre, P. (1997) - *Behaviour of high-strength concrete columns under combined flexure and axial loads - Proceedings Annual Conference, Canadian Society for Civil Engineers, Vol. 7, 1997, pp. 163-172*

Lessard, M.., Chaallal, O. and Aitcin, P. (1993) - *Testing high strength concrete compressive strength - ACI Materials Journal: Jul.-Aug. 1993, pp. 303-308*

Limsuwan, E. (1993) - *Strengths of high strength concrete columns -Utilisation of high strength concrete, Proceedings: Symposium in Lillehammer, Norway, June 20-23, 1993, pp. 277-284*

Liu, J. and Foster, S.J. (1998) - *Finite element model for confined concrete columns - ASCE Journal of Structural Engineering: Vol. 124, No. 9, Sep. 1998, pp. 1011-1017*

Liu, J. and Foster, S.J. (2000) - *A three-dimensional finite element model for confined concrete structures - Computers & Structures: Vol. 77, 2000, pp. 441-451*

Loo, Y.H. (1995) - *Propagation of microcracks in concrete under uniaxial compression - Magazine of Concrete Research: Vol. 47, No. 170, Mar. 1995, pp. 83-91*

Lloyd, N. and Rangan, B.V. (1996) - *Studies on high-strength concrete columns under eccentric compression - ACI Structural Journal: Nov.-Dec. 1996, pp. 631-638*

Mander, J.B., Priestley, M.J.N. and Park, R. (1988a) - *Theoretical stress-strain model for confined concrete - ASCE Journal of Structural Engineering: Vol. 114, No. 8, Aug. 1988, pp. 1804-1826*

Mander, J.B., Priestley, M.J.N. and Park, R. (1988b) - *Observed stress-strain behaviour of confined concrete - ASCE Journal of Structural Engineering: Vol. 114, No. 8, Aug. 1988, pp. 1827-1849*

Martinez, S., Nilson, A.H. and Slate, F.O. (1984) - *Spirally reinforced high strength concrete columns - ACI Journal: Sep.-Oct. 1984, pp. 431-442*

Metwally, S.E., El-Shahhat, A.M.and Chen, W.F. (1990) - *3-D nonlinear analysis of RC slender columns - Computers & Structures: Vol. 37, No. 5, 1990, pp. 863-872*

Neville, A.M. (1959) - *The relation between standard deviation and mean strength of concrete test cubes - Magazine of Concrete Research: Vol. 11, No. 32, Jul. 1959, pp. 75-84*

Neville, A.M. (1997) - *Aggregate bond and modulus of elasticity of concrete - ACI Materials Journal: Jan.-Feb. 1997, pp. 71-74*

Newman, J.B. (1973) - *Deformational behaviour, failure mechanisms, and design criteria for concretes under combinations of stress - PhD thesis, Imperial College of Technology, London, 1973*

Ngab, A.S., Slate, F.O. and Nilson, A.H.(1981) - *Microcracking and time-dependent strains in high strength concrete - ACI Journal: Jul.-Aug. 1981, pp. 262-268*

Nishiyama, M., Fukoshima, I., Watanabe, F. and Muguruma, H. (1993) - *Axial loading tests on high strength concrete prisms confined by ordinary and high strength steel - Utilisation of high strength concrete, Proceedings: Symposium in Lillehammer, Norway, Jun. 20-23, 1993, pp. 322-329*

Ottosen, N.S. (1977) - *A failure criterion for concrete - ASCE Journal of the Engineering Mechanics Division: Vol. 103, No. EM4, Aug. 1977, pp. 527-535*

Ottesen, N.S. (1979) - *Constitutive model for short-time loading of concrete - ASCE Journal of the Engineering Mechanics Division: Vol. 101, No. EM1, Feb. 1979, pp. 127-141*

Pessiki, S. and Pieroni, A. (1997) - *Axial load behaviour of large-scale spirally-reinforced high-strength concrete columns - ACI Structural Journal , May-Jun. 1997, pp. 304-309*

Press, W.H., Flannery, B.P., Teukolsky, S.A. and Vetterling, W.T (1989) - *Numerical recipies, The art of scientific computing - Cambridge University Press, 1989*

Priestley, M.J.N., Park, R. and Potangora, R.T. (1981) - *Ductility of spirally confined concrete columns - ASCE Journal of Structural Engineering, Vol. 107, No. ST1, Jan. 1981, pp. 181-202*

Ragupathy, P. (1994) - *Nonlinear behaviour of precast concrete frames - PhD thesis, City University, London, 1994*

Razvi, S. and Saatcioglu, M. (1989) - *Confinement of reinforced concrete columns with welded wire fabric - ACI Structural Journal , Sep.-Oct. 1989, pp. 615-623*

Razvi, S.R. and Saatcioglu, M. (1994) - *Strength and deformability of confined high strength concrete - ACI Structural Journal: Nov.-Dec. 1994, pp. 678-687*

Razvi, S. and Saatcioglu, M. (1998) - *High-strength concrete columns with square sections under concentric compressions - ASCE Journal of Structural Engineering, Vol. 124, No. 12, Dec. 1998, pp. 1438-1447*

Razvi, S. and Saatcioglu, M. (1999) - *Confinement model for high-strength concrete - ASCE Journal of Structural Engineering, Vol. 125 No. 3, Mar. 1999, pp. 281-289*

Richart, F.E., Brandtzaeg, A. and Brown, R.L. (1928) - *A study of the failure of concrete under combined compressive stresses - Engineering Experiment Station, University of Illinois, Bulletin No. 185, 1928.*

Richart, F.E., Brandtzaeg, A. and Brown, R.L. (1929) - *The failure of plain and spirally reinforced concrete in compression - Engineering Experiment Station, University of Illinois, Bulletin No. 190, 1929.*

Rodriguez, J.A. and Aristizabal-Ochoa, J.D. (1999) - *Biaxial interaction diagrams for short RC columns of any cross-section - ASCE, Journal of Structural Engineering, Vol. 125, No. 6, Jun. 1999, pp. 672-683*

Saatcioglu, M. and Razvi, S.R. (1992) - *Strength and ductility of confined concrete - ASCE Journal of Structural Engineering, Vol. 118, No. 6, Jun. 1992, pp. 1590-1607*

Saatcioglu, M., Salamat, A.H. and Razvi, S.R. (1995) - *Confined concrete columns under eccentric loading - ASCE Journal of Structural Engineering, Vol. 121, No. 11, Nov. 1995, pp. 1547-1556*

Saatcioglu, M. and Razvi, S.R. (1998) - *High-strength concrete columns with square sections under concentric compression - ASCE Journal of Structural Engineering, Vol. 124, No. 12, Dec. 1998, pp. 1438-1447*

Saenz, L.P. (1964) - *Equation for the stress-strain curve of concrete - ACI Journal: Sep. 1964, pp. 1229-1235*

Sangha, C.M. and Dhir, R.K. (1972) - *Strength and complete stress-strain relationships for concrete tested in uniaxial compression under different test conditions - Materials and Structures: Vol. 5, 1972, pp. 361-370*

Sargin, M. (1971) - *Stress-strain relationship for concrete and the analysis of structural concrete sections - Study No. 4, Solid Mechanics Division, University of Waterloo, Ontario, 1971, 167 pp.*

Schickert, G. and Winkler, H.(1977) - *Results of tests concerning strength and strain of concrete subjected to multiaxial compressive stresses - Deutscher Ausschuss für Stahlbeton, heft 277, 1977.*

Scott, B.D., Park, R. and Priestley, J.N. (1982) - *Stress-strain behaviour of concrete confined by overlapping hoops at low and high strain rates - ACI Journal: Jan.-Feb. 1982, pp. 13-27*

Setunge, S., Attard, M.M. and Darvall, P. (1993) - *Ultimate strength of confined very high strength concretes - ACI Structural Journal: Nov.-Dec. 1993, pp. 632-641*

Sfer, D., Carol, I., Gettu, R. and Etse, G. (2002) - *Study of the behaviour of concrete under triaxial compression - ASCE Journal of Engineering Mechanics: Vol. 128, No. 2, Feb. 2002, pp. 156-163*

Shah, S.P. and Chandra, S. (1968) - *Critical stress, volume change and microcracking of concrete - ACI Journal: Sept. 1968, pp. 770-781*

Shah, S.P., Fafitis, A. and Arnold, R. (1983) - *Cyclic loading of spirally reinforced concrete - ASCE Journal of Structural Engineering, Vol. 109, No. 7, Jul. 1983, pp. 1695-1710*

Sheikh. S.A. and Uzumeri, S.M. (1980) - *Strength and ductility of tied concrete columns - ASCE Journal of the Structural Division: Vol. 106, No. ST5, May 1980, pp. 1079-1102*

Sheikh. S.A. and Uzumeri, S.M. (1982) - *Analytical model for concrete confinement in tied columns - ASCE Journal of the Structural Division: Vol. 108, No. ST12, Dec. 1982, pp. 2703- 2722*

Sheikh. S.A. and Yeh, C.C. (1986) - *Flexural behaviour of confined concrete columns - ACI Journal, May-Jun. 1986, pp. 389-404*

Sheikh. S.A. and Yeh, C.C. (1990) - *Tied concrete columns under axial load and flexure - ASCE Journal of Structural Engineering: Vol. 116, No. 10, Oct. 1990, pp. 2780-2800*

Sheikh. S.A. and Yeh, C.C. (1992) - *Analytical moment-curvature relations for tied concrete members - ASCE Journal of Structural Engineering: Vol. 118, No. 2, Feb. 1992, pp. 529-544*

Sheikh, S.A., Shah, D. and Khoury, S.S. (1994) - *Confinment of high strength concrete columns - ACI Structural Journal: Jan.-Feb. 1994, pp. 100-111*

Smadi, M.M., Slate, F.O. and Nilson, A.H. (1985) - *High-, medium-, and low-strength concretes subject to sustained overloads - strains, strengths, and failure mechanisms - ACI Journal, Sep.-Oct. 1985, pp. 657-664*

Smadi, M.M. and Slate, F.O. (1989) - *Microcracking of high and normal strength concretes under short- and long-term loadings - ACI Materials Journal: Mar.-Apr. 1989, pp. 117-127*

Somes, N.F. (1970) - *Compression tests on hoop reinforced concrete - ASCE Journal of the Structural Division, Vol. 96, No. ST7, Jul. 1970, pp. 1495-1509*

Sturman, G.M., Shah, S.P. and Winter, G. (1965) - *Effects of flexural strain gradients on microcracking and stress-strain behaviour of concrete - ACI Journal, Jul. 1965, pp. 805-822*

Sudo, E., Masuda, Y., Abe, M. and Yasuda, M. (1993) - *Mechanical properties of confined high strength concrete - Utilisation of high strength concrete, Proceedings: Symposium in Lillehammer, Norway, Jun. 20-23, 1993, pp. 369-376*

Thomson, J.H. and Wallace, J.W. (1994) - *Lateral load behaviour of reinforced concrete columns constructed using high strength materials - ACI Structural Journal: Sep.-Oct. 1994, pp. 605-615*

Torrenti, J.M., Benaija, E.H. and Boulay, C. (1993) - *Influence of boundary conditions of strain softening in concrete compression test - ASCE Journal of Engineering Mechanics: Vol. 119, No. 12, Dec. 1993, pp. 2369-2384*

Van Mier, J.G.M (1986) - *Fracture of concrete under complex stress - Heron: Vol 31, No. 3, 1986*

Virdi , K.S. (1980) - *Variable cross-section columns loaded up to failure - Numerical methods for non-linear problems, Proceedings of the international conference held at University College Swansea, 2nd-5th Sep. 1980*

Virdi, K.S. (1981) - *Biaxially loaded slender reinforced concrete columns - IABSE Collequium, Delft 1981. Advanced mechanics of reinforced concrete: Vol. 34, 1981*

Wang, G.G. and Hsu, C.T. (1992) - *Complete biaxial load-deformation behaviour of RC columns - ASCE, Journal of Structural Engineering, Vol. 118, No. 9, Sep. 1992, pp. 2590-2609*

Willam, K.J. and Warnke, E.P. (1974) - *Constitutive model for the triaxial behaviour of concrete - IABSE-AIPC-IVBH Seminar on concrete structures subjected to triaxial stresses - Bergamo (Italy), May 17-19, 1974*

Xie, J., Elwi, A.E. and McGregor, J.G. (1995) - *Mechanical properties of three high strength concretes containing silica fume - ACI Materials Journal: Mar.-Apr. 1995, pp. 135-145*

Xie, J., McGregor, J.G. and Elwi, A.E. (1996) - *Numerical investigation of eccentrically loaded high strength concrete tied columns - ACI Structural Journal: Jul.-Aug. 1996, pp. 449-461*

Xie, J., Elwi, A.E. and McGregor, J.G. (1997) - *Performance of high strength concrete tied columns - A parametric study - ACI Structural Journal: Mar.-Apr. 1997, pp. 91-102*

Xue, H. (1997) - *Structural behaviour of high strength concrete columns - PhD thesis, University of Westminster, London, 1997*

Yong, Y-K., Nour, M.G. and Nawy, E.G. (1988) - *Behaviour of laterally confined high strength concrete under axial loads - ASCE Journal of Structural Engineering, Vol. 114, No. 2, Feb. 1988, pp. 332-351*

Zienkiewicz, O.C and Taylor, R.L (1989) - *The finite element method. Volume 1: Basic formulation and linear problems - MCGraw-Hill Book Company, 1989*

Appendix A: Test Results on Passively Confined Concrete Columns

This appendix contains a compilation of tables, which summarise the strength properties and test parameters for a number of transversely reinforced concrete columns tested under concentric compression. For each test column, the effective confining pressure at peak load, $-\sigma_{l,eff}$, was calculated under the assumption of the stress in the ties being at yield. However, whenever the data permitted it, the effective confining pressures calculated on the basis of the actual tie strains are also given in the tables. In both cases the effective confining pressure was calculated employing the modified arching action method described in section 3.4.

Table A1
Details of circular columns tested by Nagi, taken after (Iyengar, 1970)

Column	Concrete core*				Transverse reinforcement					
Label	f_c (MPa)	f_{cc}/f_c (-)	ε_c (mm/m)	$\varepsilon_{cc}/\varepsilon_c$ (-)	Tie	d_c (mm)	s (mm)	ρ_s (%)	f_{sy} (MPa)	$-\sigma_{l,eff}$ (MPa)
1:2:4,120	15.4	1.24	2.1	2.16	A-spi	144	120	0.77	319	0.2
1:2:4,60	15.4	1.60	2.1	2.76	A-spi	144	60	1.54	319	1.4
1:2:4,45	15.4	2.15	2.1	9.61	A-spi	144	45	2.06	319	2.3
1:2:4,30	15.4	2.86	2.1	11.00	A-spi	144	30	3.08	319	3.9
1:1:1.5:3,120	25.3	1.03	2.3	1.15	A-spi	144	120	0.77	319	0.2
1:1:1.5:3,90	25.3	1.18	2.3	1.43	A-spi	144	90	1.03	319	0.6
1:1:1.5:3,60	25.3	1.41	2.3	1.88	A-spi	144	60	1.54	319	1.4
1:1:2:120	33.3	1.02	1.8	1.09	A-spi	144	120	0.77	319	0.2
1:1:2:90	33.3	1.06	1.8	1.41	A-spi	144	90	1.02	319	0.6
1:1:2:60	33.3	1.17	1.8	2.75	A-spi	144	60	1.54	319	1.4
1:1:2:45	33.3	1.44	1.8	4.22	A-spi	144	45	2.06	319	2.3

Specimens tested: 150×300 mm cylinders without longitudinal reinforcement.
* All material properties extracted from the stress-strain curves given in source.

Table A2
Details of square columns tested by Nagi, taken after (Iyengar, 1970)

Column	Concrete core*				Transverse reinforcement					
Label	f_c (MPa)	f_{cc}/f_c (-)	ε_c (mm/m)	$\varepsilon_{cc}/\varepsilon_c$ (-)	Tie	d_c (mm)	s (mm)	ρ_s (%)	f_{sy} (MPa)	$-\sigma_{l,eff}$ (MPa)
1:2:4,60	26.6	1.04	2.7	1.60	B-spi	95	60	1.38	627	0.5
1:2:4,45	26.6	1.23	2.7	1.82	B-spi	95	45	1.83	627	1.0
1:2:4,30	26.6	1.31	2.7	4.89	B-spi	95	30	2.36	627	1.6
1:1:1.5:3,60	31.6	1.06	2.6	1.47	B-spi	95	60	1.38	627	0.5
1:1:1.5:3,45	31.6	1.15	2.6	1.67	B-spi	95	45	1.83	627	1.0
1:1:1.5:3,30	31.6	1.26	2.6	1.86	B-spi	95	30	2.36	627	1.6
1:1:2:60	36.2	1.05	2.5	1.14	B-spi	95	60	1.38	627	0.5
1:1:2:45	36.2	1.05	2.5	1.43	B-spi	95	45	1.83	627	1.0
1:1:2:30	36.2	1.16	2.5	2.62	B-spi	95	30	2.36	627	1.6

Specimens tested: 100×200 mm prisms without longitudinal reinforcement.

* All material properties extracted from the stress-strain curves given in source.

Table A3
Details of columns tested by Somes (1970)

Column	Concrete core				Transverse reinforcement*					
Label	f_c (MPa)	f_{cc}/f_c (-)	ε_c (mm/m)	$\varepsilon_{cc}/\varepsilon_c$ (-)	Tie	d_c (mm)	s (mm)	ρ_s (%)	f_{sy} (MPa)	$-\sigma_{l,eff}$ (MPa)
A1-0.75	30.2	2.09	-	-	B	96	19	8.97	324	3.9
A1-1.00	30.2	1.83	-	-	B	96	25	6.73	324	2.7
A1-1.25	30.2	1.73	-	-	B	96	32	5.38	324	1.9
A1-1.50	30.2	1.66	-	-	B	96	38	4.48	324	1.5
A1-1.75	30.2	1.48	-	-	B	96	44	3.84	324	1.1
A1-2.00	30.2	1.51	-	-	B	96	51	3.36	324	0.9
A1-2.25	30.2	1.52	-	-	B	96	57	2.99	324	0.7
A2-2.50	31.7	1.32	-	-	B	96	64	2.69	324	0.5
A2-3.00	31.7	1.26	-	-	B	96	76	2.24	324	0.2
A2-3.50	31.7	1.18	-	-	B	96	89	1.92	324	0.1
A2-4.00	31.7	1.19	-	-	B	96	102	1.68	324	0.0
A2-4.50	31.7	1.17	-	-	B	96	114	1.49	324	0.0
A2-5.50	31.7	1.11	-	-	B	96	140	1.22	324	0.0
A2-6.00	31.7	1.03	-	-	B	96	152	1.12	324	0.0

Column	Concrete core				Transverse reinforcement*					
Label	f_c (MPa)	f_{cc}/f_c (-)	ε_c (mm/m)	$\varepsilon_{cc}/\varepsilon_c$ (-)	Tie	d_c (mm)	s (mm)	ρ_s (%)	f_{sy} (MPa)	$-\sigma_{l,eff}$ (MPa)
B1-0.75	28.5	1.88	-	-	B	97	19	6.49	324	2.8
B1-1.00	28.5	1.64	-	-	B	97	25	4.87	324	1.9
B1-1.25	28.5	1.47	-	-	B	97	32	3.90	324	1.4
B1-1.50	28.5	1.40	-	-	B	97	38	3.25	324	1.1
B1-1.75	28.5	1.34	-	-	B	97	44	2.78	324	0.8
B1-2.00	28.5	1.26	-	-	B	97	51	2.44	324	0.6
B1-2.25	28.5	1.28	-	-	B	97	57	2.16	324	0.5
B2-2.50	30.3	1.30	-	-	B	97	64	1.95	324	0.4
B2-3.00	30.3	1.24	-	-	B	97	76	1.62	324	0.2
B2-3.50	30.3	1.18	-	-	B	97	89	1.39	324	0.1
B2-4.00	30.3	1.13	-	-	B	97	102	1.22	324	0.0
B2-4.50	30.3	1.11	-	-	B	97	114	1.08	324	0.0
B2-5.50	30.3	1.04	-	-	B	97	140	0.89	324	0.0
B2-6.00	30.3	1.00	-	-	B	97	152	0.81	324	0.0
C1-0.75	30.9	1.47	-	-	B	98	19	5.74	324	2.5
C1-1.00	30.9	1.39	-	-	B	98	25	4.31	324	1.7
C1-1.25	30.9	1.31	-	-	B	98	32	3.45	324	1.3
C1-1.50	30.9	1.29	-	-	B	98	38	2.87	324	0.9
C1-1.75	30.9	1.25	-	-	B	98	44	2.46	324	0.7
C1-2.00	30.9	1.20	-	-	B	98	51	2.15	324	0.6
C1-2.25	30.9	1.17	-	-	B	98	57	1.91	324	0.4
C2-2.50	32.5	1.15	-	-	B	98	64	1.72	324	0.3
C2-3.00	32.5	1.14	-	-	B	98	76	1.44	324	0.2
C2-3.50	32.5	1.24	-	-	B	98	89	1.23	324	0.1
C2-4.00	32.5	1.08	-	-	B	98	102	1.08	324	0.0
C2-4.50	32.5	1.09	-	-	B	98	114	0.96	324	0.0
C2-5.50	32.5	1.06	-	-	B	98	140	0.78	324	0.0
C2-6.00	32.5	1.04	-	-	B	98	152	7.18	324	0.0

Specimens tested: 102×305 mm prisms without longitudinal reinforcement.

* Hoops were 6.4 mm slices machined from hot-rolled structural steel tubing.

Table A4
Details of columns tested by Sheikh and Uzumeri (1980)

Col.	Concrete core				Longitudinal reinforcement		Transverse reinforcement					
Lab.	f_c** (MPa)	f_{cc}/f_c (-)	ε_c (mm/m)	$\varepsilon_{cc}/\varepsilon_c$ (-)	ρ_g (%)	f_{sy} (MPa)	Tie	d_c (mm)	s (mm)	ρ_s (%)	σ_s*** (MPa)	$-\sigma_{l,eff}$* (MPa)
1	31.9	1.18	2.2	2.00	1.72	372	C	267	57	0.80	455	0.9
2	31.4	1.26	2.2	2.50	1.72	372	C	267	57	0.80	252	0.5
3	30.9	1.21	2.2	2.05	3.44	372	D'	267	51	0.75	489	1.0
4	31.2	1.20	2.2	-	3.44	372	D'	267	51	0.75	282	0.6
5	29.7	1.64	2.2	6.82	3.44	372	D'	267	38	2.25	500	3.4
6	29.2	1.53	2.2	3.64	3.44	372	D'	267	38	2.25	255	1.7
7	34.7	1.28	2.2	2.09	3.33	385	C	267	76	1.66	475	1.9
8	34.7	1.36	2.2	2.59	3.33	385	C	267	29	1.59	420	2.0
9	34.4	1.23	2.2	2.27	3.33	385	C	267	76	2.39	345	2.0
10	34.6	1.31	2.2	4.55	3.33	385	C	267	35	2.31	455	3.0
11	34.6	1.27	2.2	2.32	3.44	407	D'	267	95	1.60	358	1.3
12	34.7	1.46	2.2	4.09	3.44	407	D'	267	25	1.50	469	2.2
13	26.6	1.30	2.2	2.05	3.33	439	C	267	57	0.90	475	1.0
14	26.8	1.38	2.2	3.18	1.72	403	C	267	76	2.39	427	2.4
15	26.9	1.47	2.2	3.64	1.72	403	C	267	35	2.31	413	2.8
16	27.6	1.36	2.2	2.55	2.22	414	C'	267	51	0.75	589	1.3
17	27.9	1.36	2.2	3.23	2.22	414	D'	267	102	2.34	347	1.8
18	28.1	1.70	2.2	11.36	2.22	414	D'	267	38	2.25	551	3.7
19	28.4	1.43	2.2	2.77	3.67	392	D	267	102	1.64	400	1.4
20	29.5	1.52	2.2	3.64	3.67	392	D	267	38	1.58	544	2.5
21	30.2	1.54	2.2	6.36	3.67	392	D	267	48	2.24	489	3.1
22	30.2	1.44	2.2	2.50	3.67	392	E	267	83	1.62	386	1.6
23	30.5	1.54	2.2	3.45	3.67	392	E	267	29	1.68	531	2.9
24	30.5	1.63	2.2	3.64	3.67	392	E	267	38	2.25	475	3.4

Specimens tested: 300×2000 mm prisms (tapered).

D' is a tie configuration with 16 longitudinal steel bars.

*** Average stress in tie steel at confined strength.

** 0.85 times 150×300 mm cylinder strength.

* Effective confining pressure determined on the basis of measured hoop strains.

Table A5
Details of columns tested by Ahmad and Shah (1982)

Test	Concrete core				Transverse reinforcement					
Series	f_c (MPa)	f_{cc}/f_c (-)	ε_c (mm/m)	$\varepsilon_{cc}/\varepsilon_c$ (-)	Tie	d_c (mm)	s (mm)	ρ_s (%)	f_{sy} (MPa)	$-\sigma_{1,eff}$ (MPa)
I-1	20.7	1.04	2.1	1.05	A-spi	73	95	0.43	413	0.0
I-2	20.7	1.03	2.1	1.00	A-spi	73	102	0.40	413	0.0
I-3	20.7	1.10	2.1	1.10	A-spi	73	76	0.53	413	0.0
II-1	26.2	1.21	2.1	1.52	A-spi	73	25	1.60	413	2.1
II-2	26.2	1.49	2.1	4.86	A-spi	73	13	3.19	413	5.4
III-1	37.9	1.05	2.2	1.14	A-spi	73	38	1.06	413	1.1
III-2	37.9	1.11	2.2	1.41	A-spi	73	25	1.60	413	2.1
III-3	37.9	1.25	2.2	2.27	A-spi	73	13	3.19	413	5.4
IV-1	51.7	1.03	2.5	1.20	A-spi	73	38	1.06	413	1.1
IV-2	51.7	1.07	2.5	1.56	A-spi	73	25	1.60	413	2.1
V-1*	65.5	1.05	3.0	1.17	A-spi	73	25	1.60	413	2.1
V-2*	65.5	1.12	3.0	1.33	A-spi	73	13	3.19	413	5.4

The test results are the average values from testing 4 specimens.

Specimens tested: In general 76×152 mm cylinders without longitudinal reinforcement.

* 76×304 mm cylinders without longitudinal reinforcement.

Table A6
Details of columns tested by Martinez *et al* (1984)

Column	Concrete core				Transverse reinforcement						
Label.	f_c (MPa)	f_{cc}/f_c (-)	ε_c** (mm/m)	$\varepsilon_{cc}/\varepsilon_c$ (-)	Tie	d_c (mm)	s (mm)	ρ_s (%)	f_{sy} (MPa)	$-\sigma_{1,eff}$* (MPa)	$-\sigma_{1,eff}$ (MPa)
NC161-1	22.1	1.27	2.4	3.96	A-spi	100	100	1.05	380	1.7	1.8
NC161-2	22.1	1.25	2.4	3.30	A-spi	100	100	1.05	380	1.7	1.8
NC161-3	22.1	1.29	2.4	3.74	A-spi	100	100	1.05	380	1.7	1.8
NC162-1	23.5	1.59	2.4	5.99	A-spi	100	100	2.09	380	3.6	3.7
NC162-2	23.5	1.57	2.4	6.25	A-spi	100	100	2.09	380	3.6	3.7
NC162-3	23.5	1.57	2.4	6.04	A-spi	100	100	2.09	380	3.6	3.7
NC163-1	20.8	2.12	2.4	10.03	A-spi	100	100	3.14	380	5.5	5.7
NC163-2	20.8	2.14	2.4	11.69	A-spi	100	100	3.14	380	5.5	5.7
NC163-3	20.8	2.16	2.4	11.89	A-spi	100	100	3.14	380	5.5	5.7

Column	Concrete core				Transverse reinforcement						
Label.	f_c (MPa)	f_{cc}/f_c (-)	ε_c** (mm/m)	$\varepsilon_{cc}/\varepsilon_c$ (-)	Tie	d_c (mm)	s (mm)	ρ_s (%)	f_{sy} (MPa)	$-\sigma_{1,eff}$* (MPa)	$-\sigma_{1,eff}$ (MPa)
NC164-1	50.2	1.31	2.7	2.62	A-spi	100	100	3.57	380	3.9	4.1
NC164-2	50.2	1.26	2.7	2.60	A-spi	100	100	3.57	380	3.9	4.1
NC164-3	50.2	1.27	2.7	2.42	A-spi	100	100	3.57	380	3.9	4.1
NC165-1	46.1	4.63	2.7	4.09	A-spi	100	100	4.48	414	8.2	8.9
NC165-2	46.1	1.64	2.7	3.80	A-spi	100	100	4.48	414	8.6	8.9
NC165-3	46.1	1.63	2.7	4.19	A-spi	100	100	4.48	414	8.6	8.9
NC166-1	50.2	1.92	2.7	5.64	A-spi	99	98	7.17	414	14.0	13.9
NC166-2	50.2	1.89	2.7	5.95	A-spi	98	98	7.17	414	14.0	13.9
NC166-3	50.2	1.88	2.7	5.73	A-spi	98	98	7.17	414	13.9	13.9
NC167-1	67.4	1.42	3.0	1.66	A-spi	100	100	3.49	380	6.1	6.4
NC167-2	67.4	1.41	3.0	1.72	A-spi	100	100	3.49	380	6.1	6.4
NC167-3	67.4	1.31	3.0	1.50	A-spi	100	100	3.49	380	3.6	6.4
NC168-1	68.6	1.66	3.0	2.82	A-spi	98	98	7.29	414	12.1	14.2
NC168-2	68.6	1.76	3.0	2.91	A-spi	98	98	7.29	414	12.9	14.2
NC168-3	68.6	1.74	3.0	2.94	A-spi	98	98	7.29	414	14.3	14.2
NC169-1	68.1	2.03	3.0	3.00	A-spi	97	97	11.55	414	16.6	22.0
NC169-2	68.1	2.12	3.0	3.17	A-spi	97	97	11.55	414	20.9	22.0
NC169-3	68.1	1.93	3.0	2.53	A-spi	97	97	11.55	414	14.2	22.0

Specimens tested: 102×457 mm cylinders without longitudinal reinforcement.

** Estimated from graph given in source.

* Effective confining pressure determined on the basis of measured hoop strains.

Table A7
Details of columns tested by Mander *et al* (1988b)

Col.	Concrete core				Longitudinal reinforcement		Transverse reinforcement					
Label	f_c (MPa)	f_{cc}/f_c (-)	ε_c (mm/m)	$\varepsilon_{cc}/\varepsilon_c$ (-)	ρ_g (%)	f_{sy} (MPa)	Tie	d_c (mm)	s (mm)	ρ_s (%)	f_{sy} (MPa)	$-\sigma_{l,eff}$ (MPa)
S1-1	29.0	1.76	1.5	4.87	1.23	295	A-spi	438	41	2.52	340	3.9
S1-2	29.0	1.59	1.5	3.33	1.23	295	A-spi	438	69	1.50	340	2.1
S1-3	29.0	1.38	1.5	2.67	1.23	295	A-spi	438	103	1.00	340	1.3
S1-4	29.0	1.24	1.5	2.20	1.23	295	A-spi	440	119	0.60	320	0.7
S1-5	29.0	1.62	1.5	4.33	1.23	295	A-spi	440	36	1.98	320	2.9
S1-6	29.0	1.59	1.5	3.87	1.23	295	A-spi	434	93	1.99	307	2.4
S2-7	32.0	1.63	1.4	4.07	2.51	296	A-spi	438	52	1.99	340	3.0
S2-8	30.0	1.63	1.4	4.14	2.53	260	A-spi	438	52	1.99	340	3.0
S2-9	32.0	1.63	1.4	3.86	2.56	286	A-spi	438	52	1.99	340	3.0
S2-10	30.0	1.67	1.4	4.57	2.46	295	A-spi	438	52	1.99	340	3.0
S2-11	30.0	1.80	1.4	3.21	3.69	295	A-spi	438	52	1.99	340	3.0
S2-12	32.0	1.63	1.8	4.00	2.46	360	A-spi	438	52	1.99	340	3.0

Specimens tested: 500×1500 mm cylinders.

Table A8
Details of columns tested by Yong *et al* (1988)

Test.	Concrete core				Longitudinal reinforcement		Transverse reinforcement					
Series	f_c (MPa)	f_{cc}/f_c (-)	ε_c (mm/m)	$\varepsilon_{cc}/\varepsilon_c$ (-)	ρ_g (%)	f_{sy} (MPa)	Tie	d_c (mm)	s (mm)	ρ_s (%)	f_{sy} (MPa)	$-\sigma_{l,eff}$ (MPa)
A	80.9	1.22	2.4	2.13	1.70	424	C	130	25	2.48	496	3.3
B	84.1	1.21	2.8	1.76	1.70	424	C	130	51	1.24	469	1.2
C	80.5	1.13	2.2	1.56	1.70	424	C	130	76	0.83	496	0.6
D	81.5	1.02	2.3	1.30	1.70	424	C	130	152	0.41	496	0.0
N*	78.6	1.16	2.3	1.84	1.70	424	C	130	51	1.24	496	1.2
L**	86.7	1.03	2.7	1.23	0.85	424	C	130	76	0.83	496	0.6

The test results are the average values from testing 3 specimens.

Specimens tested: 152×457 mm prisms.

* Column tested without a concrete cover.

** 4 instead of 8 longitudinal steel bars.

Table A9
Details of columns tested by Razvi and Saatcioglu (1989)

Col.	Concrete core				Longitudinal reinforcement		Transverse reinforcement					
Label	f_c* (MPa)	f_{cc}/f_c (-)	ε_c (mm/m)	$\varepsilon_{cc}/\varepsilon_c$ (-)	ρ_g (%)	f_{sy} (MPa)	Tie	d_c (mm)	s (mm)	ρ_s (%)	f_{sy} (MPa)	$-\sigma_{l,eff}$ (MPa)
3	31.9	1.22	-	-	3.14	470	B	143	35	2.68	470	1.6
4	31.9	1.04	-	-	3.14	470	B	143	70	1.34	470	0.5
6	39.0	1.32	-	-	1.57	480	B	138	35	2.77	480	1.7
7	39.0	1.18	-	-	1.57	480	B	138	70	1.39	480	0.5
15	28.9	1.15	-	-	3.14	470	B	143	70	1.34	470	0.5
16	28.9	1.31	-	-	3.14	470	B	143	35	2.68	470	1.6

Specimens tested: 160×460 mm prisms.

* 150×300 mm cylinder strength.

Table A10
Details of circular columns tested by Bjerkeli and Tomaszewicz (1993)

Col.	Concrete core*				Transverse reinforcement					
Label	f_c (MPa)	f_{cc}/f_c (-)	ε_c (mm/m)	$\varepsilon_{cc}/\varepsilon_c$ (-)	Tie	d_c (mm)	s (mm)	ρ_s (%)	f_{sy} (MPa)	$-\sigma_{l,eff}$ (MPa)
1	48	1.80	-	-	A-spi	144	25	3.1	613	8.0
2	66	0.88	-	-	A-spi	144	70	1.1	613	1.8
3	66	1.51	-	-	A-spi	144	25	3.1	613	8.0
4	66	1.54	-	-	A-spi	144	25	3.1	613	8.0
5	94	1.23	-	-	A-spi	144	25	3.1	613	8.0

Specimens tested: 150×500 mm cylinders without longitudinal reinforcement.

* All material properties extracted from stress-strain curves given in source.

Table A11
Details of columns tested by Nishiyama *et al* (1993)

Col.	Concrete core*				Longitudinal reinforcement		Transverse reinforcement					
Label	f_c** (MPa)	f_{cc}/f_c (-)	ε_c (mm/m)	$\varepsilon_{cc}/\varepsilon_c$ (-)	ρ_g (%)	f_{sy} (MPa)	Tie	d_c (mm)	s (mm)	ρ_s (%)	f_{sy} (MPa)	$-\sigma_{l,eff}$ (MPa)
H6-31	88.3	1.64	3.2	2.48	2.44	351	D	214	31	3.84	813	9.2
H6-60	88.3	1.39	3.2	1.55	2.44	351	D	214	60	1.98	813	4.0
L6-31	91.5	1.47	3.4	1.79	2.44	351	D	214	31	3.84	462	5.2
L6-60	91.5	1.26	3.4	1.43	2.44	351	D	214	60	1.98	462	2.3

Specimens tested: 250×750 mm longitudinally reinforced prisms.

* Material properties for confined concrete extracted from stress-strain curves given in source.

** 0.81 times 100×200 mm cylinder strength.

Table A12
Details of columns tested by Sudo *et al* (1993)

Col.	Concrete core**				Transverse reinforcement						
Label	f_c (MPa)	f_{cc}/f_c (-)	ε_c (mm/m)	$\varepsilon_{cc}/\varepsilon_c$ (-)	Tie	d_c (mm)	s (mm)	ρ_s (%)	f_{sy} (MPa)	$-\sigma_{l,eff}$* (MPa)	$-\sigma_{l,eff}$ (MPa)
O65%-48	37.7	1.42	-	3.50	A-spi	144	48	1.63	571	3.1	3.1
O65%-24	37.7	2.15	-	-	A-spi	144	24	3.26	571	8.0	7.8
O65%-12	37.7	3.08	-	-	A-spi	144	12	6.53	571	17.3	17.1
O45%-48	69.6	1.14	3.1	1.63	A-spi	144	48	1.63	571	2.4	3.1
O45%-24	69.6	1.29	3.1	2.67	A-spi	144	24	3.26	571	7.6	7.8
O45%-12	69.6	2.11	3.1	4.74	A-spi	144	12	6.53	571	17.0	17.1
O35%-48	84.1	1.03	-	1.39	A-spi	144	48	1.63	571	2.0	3.1
O35%-24	84.1	1.21	-	2.46	A-spi	144	24	3.26	571	7.5	7.8
O35%-12	84.1	1.90	-	2.93	A-spi	144	12	6.53	571	14.9	17.1
O25%-48	101.4	1.18	3.5	1.15	A-spi	144	48	1.63	571	1.4	3.1
O25%-24	101.4	1.54	3.5	1.65	A-spi	144	24	3.26	571	3.4	7.8
O25%-12	101.4	1.71	3.5	2.49	A-spi	144	12	6.53	571	14.7	17.1
O22%-48	113.0	1.13	-	1.28	A-spi	144	48	1.63	571	1.2	3.1
O22%-24	113.0	1.33	-	1.51	A-spi	144	24	3.26	571	5.2	7.8
O22%-12	113.0	-	-	2.34	A-spi	144	12	6.53	571	-	17.1
T65%-48	43.5	1.33	-	2.89	A-spi	144	48	1.63	571	2.5	3.1
T65%-24	43.5	1.87	-	-	A-spi	144	24	3.26	571	7.5	7.8
T65%-12	43.5	2.60	-	-	A-spi	144	12	6.53	571	16.9	17.1

Col.	Concrete core**				Transverse reinforcement						
Label	f_c (MPa)	f_{cc}/f_c (-)	ε_c (mm/m)	$\varepsilon_{cc}/\varepsilon_c$ (-)	Tie	d_c (mm)	s (mm)	ρ_s (%)	f_{sy} (MPa)	$-\sigma_{l,eff}$* (MPa)	$-\sigma_{l,eff}$ (MPa)
T45%-48	68.4	1.14	-	1.91	A-spi	144	48	1.63	571	2.9	3.1
T45%-24	68.4	1.61	-	3.25	A-spi	144	24	3.26	571	7.7	7.8
T45%-12	68.4	2.20	-	-	A-spi	144	12	6.53	571	17.0	17.1
T35%-48	84.1	1.03	-	-	A-spi	144	48	1.63	571	2.5	3.1
T35%-24	84.1	1.41	-	1.51	A-spi	144	24	3.26	571	7.2	7.8
T35%-12	84.1	-	-	2.38	A-spi	144	12	6.53	571	-	17.1
T25%-48	92.8	1.31	-	1.16	A-spi	144	48	1.63	571	1.2	3.1
T25%-24	92.8	1.51	-	1.68	A-spi	144	24	3.26	571	5.3	7.8
T25%-12	92.8	1.63	-	2.28	A-spi	144	12	6.53	571	12.9	17.1
T22%-48	106.1	0.89	-	1.10	A-spi	144	48	1.63	571	1.5	3.1
T22%-24	106.1	1.17	-	1.74	A-spi	144	24	3.26	571	4.6	7.8
T22%-12	106.1	1.78	-	2.46	A-spi	144	12	6.53	571	14.1	17.1

Specimens tested: 150×300 mm cylinders without longitudinal reinforcement.

** All material properties extracted from graphical information given in source.

* Effective confining pressure determined on the basis of measured hoop strains.

Table A13
Details of square columns tested by Cusson and Paultre (1994)

Col	Concrete core				Longitudinal reinforcement		Transverse reinforcement						
	f_c** (MPa)	f_{cc}/f_c (-)	ε_c (mm/m)	$\varepsilon_{cc}/\varepsilon_c$ (-)	ρ_g (%)	f_{sy} (MPa)	Tie	d_c (mm)	s (mm)	ρ_s (%)	f_{sy} (MPa)	$-\sigma_{l,eff}$* (MPa)	$-\sigma_{l,eff}$ (MPa)
1A	81.1	1.23	2.9	1.13	2.28	406	B	195	50	2.91	410	1.5	1.5
2A	81.9	1.12	3.0	1.14	2.28	406	B	195	50	2.01	392	0.8	1.0
3A	83.4	0.98	3.1	1.10	2.28	406	B	195	100	1.45	410	0.3	0.5
4A	79.1	1.22	2.9	1.14	3.56	420	B	195	50	2.91	410	0.6	1.5
5A	84.9	1.17	3.0	1.15	3.56	420	B	195	50	2.91	705	0.7	2.5
1B	81.1	1.3	3.0	1.62	1.85	450	C	195	50	3.43	392	3.3	3.3
2B	81.9	1.12	3.0	1.17	1.85	450	C	195	50	2.25	414	2.3	2.3
3B	83.4	1.03	3.0	1.13	1.85	450	C	195	100	2.48	410	1.4	1.7
4B	79.1	1.30	2.9	1.62	3.56	450	C	195	50	3.43	392	3.3	3.3
5B	84.9	1.23	3.0	1.57	3.56	450	C	195	50	3.43	770	3.4	6..6
6B	98.5	1.24	3.3	2.95	3.56	482	C	195	50	4.96	715	8.5	8.8

Col	Concrete core				Longitudinal reinforcement		Transverse reinforcement						
	f_c** (MPa)	f_{cc}/f_c (-)	ε_c (mm/m)	$\varepsilon_{cc}/\varepsilon_c$ (-)	ρ_g (%)	f_{sy} (MPa)	Tie	d_c (mm)	s (mm)	ρ_s (%)	f_{sy} (MPa)	$-\sigma_{l,eff}$* (MPa)	$-\sigma_{l,eff}$ (MPa)
7B	64.5	1.66	2.7	5.71	3.56	482	C	195	50	4.96	715	8.1	8.8
8B	44.7	2.00	2.3	13.73	3.56	482	C	195	50	4.96	715	9.3	8.8
1C	81.1	1.25	2.9	1.60	1.71	450	C	195	50	3.63	392	3.9	3.9
2C	81.9	1.21	3.0	1.20	1.71	450	E	195	50	2.38	414	1.6	2.7
3C	83.4	1.08	3.0	1.16	1.71	450	E	195	100	2.62	410	1.5	1.9
4C	79.1	1.34	2.9	1.62	3.41	450	E	195	50	3.63	392	3.0	3.9
5C	84.9	1.30	3.0	2.27	3.41	450	E	195	50	3.63	770	6.6	7.6
1D	85.3	1.32	3.0	1.89	1.71	450	D	195	50	4.52	392	4.6	4.6
1D1	85.3	1.46	3.0	1.99	2.36	450	D	195	50	4.52	392	4.3	4.6
2D	81.9	1.20	2.9	1.36	1.71	450	D	195	50	2.97	414	2.6	3.2
3D	83.4	1.12	3.0	1.52	1.71	450	D	195	100	3.27	410	2.0	2.3
4D	79.1	1.41	2.9	2.20	3.41	450	D	195	50	4.52	392	4.6	4.6
5D	84.9	1.51	3.0	3.23	3.41	450	D	195	50	4.52	770	8.1	9.0
6D	96.6	1.31	3.3	2.71	3.41	482	D	195	50	4.52	680	6.9	7.9
7D	57.7	1.74	2.6	5.95	3.41	482	D	195	50	4.52	680	8.0	7.9
8D	47.3	1.92	2.3	12.68	3.41	482	D	195	50	4.52	680	8.5	7.9

Specimens tested: 235×1400 mm tapered prisms.

** 0.85 times 150×300 mm cylinder strength.

* Effective confining pressure determined on the basis of measured hoop strains.

Table A14
Details of circular columns tested by Hsu and Hsu (1994)

Col.	Concrete core				Transverse reinforcement					
Label	f_c (MPa)	f_{cc}/f_c (-)	ε_c (mm/m)	$\varepsilon_{cc}/\varepsilon_c$ (-)	Tie	d_c (mm)	s (mm)	ρ_s (%)	f_{sy} (MPa)	$-\sigma_{l,eff}$ (MPa)
S31	80.8	1.03	3.2	1.19	A-cir	74	76	0.40	456	0.0
S32	80.8	1.06	3.2	1.22	A-cir	74	76	0.40	456	0.0
S33	80.8	1.03	3.2	1.21	A-cir	74	76	0.40	456	0.0
S21	80.8	1.11	3.2	1.44	A-cir	74	51	0.60	456	0.4
S22	80.8	1.09	3.2	1.45	A-cir	74	51	0.60	456	0.4
S23	80.8	1.10	3.2	1.45	A-cir	74	51	0.60	456	0.4
S24	80.8	1.14	3.2	1.43	A-cir	74	51	0.60	456	0.4

Col.	Concrete core				Transverse reinforcement					
Label	f_c (MPa)	f_{cc}/f_c (-)	ε_c (mm/m)	$\varepsilon_{cc}/\varepsilon_c$ (-)	Tie	d_c (mm)	s (mm)	ρ_s (%)	f_{sy} (MPa)	$-\sigma_{l,eff}$ (MPa)
S11	80.8	1.20	3.2	1.65	A-cir	74	25	1.20	456	1.8
S12	80.8	1.19	3.2	1.63	A-cir	74	25	1.20	456	1.8
S13	80.8	1.22	3.2	1.68	A-cir	74	25	1.20	456	1.8
S14	80.8	1.21	3.2	1.64	A-cir	74	25	1.20	456	1.8
S15	80.8	1.21	3.2	1.65	A-cir	74	25	1.20	456	1.8

Specimens tested: 76×152 mm cylinders without longitudinal reinforcement.

Table A15
Details of columns with circular ties tested by Issa (1994)

Col.	Concrete core				Transverse reinforcement					
Label	f_c (MPa)	f_{cc}/f_c (-)	ε_c (mm/m)	$\varepsilon_{cc}/\varepsilon_c$ (-)	Tie	d_c (mm)	s (mm)	ρ_s (%)	f_{sy} (MPa)	$-\sigma_{l,eff}$ (MPa)
B-1	68.7	1.50	2.2	2.64	A-spi	104	25	3.81	586	8.4
B-2	68.7	1.29	2.2	2.50	A-spi	104	38	2.54	586	4.7
B-3	68.7	1.23	2.2	1.97	A-spi	104	51	1.91	586	2.9
B-4	68.7	1.17	2.2	1.40	A-spi	104	64	1.52	586	1.7
C-1	49.0	1.98	1.8	2.34	A-spi	104	25	3.68	372	5.2
C-2	49.0	1.65	1.8	1.97	A-spi	104	38	2.45	372	2.9
C-3	49.0	1.52	1.8	1.57	A-spi	104	51	1.84	372	1.7
C-4	49.0	1.48	1.8	1.80	A-spi	104	64	1.47	372	1.1
D-1	53.0	1.82	2.0	2.00	A-spi	104	25	3.68	372	5.2
D-2	53.0	1.81	2.0	2.00	A-spi	104	38	2.45	372	2.9
D-3	53.0	1.59	2.0	1.99	A-spi	104	51	1.84	372	1.7
D-4	53.0	1.37	2.0	1.90	A-spi	104	64	1.47	372	1.1
E-1	35.9	2.13	1.6	2.50	A-spi	104	25	3.68	372	5.2
E-2	35.9	1.86	1.6	1.95	A-spi	104	38	2.45	372	2.9
E-3	35.9	1.48	1.6	1.73	A-spi	104	51	1.84	372	1.7
E-4	35.9	1.44	1.6	1.64	A-spi	104	64	1.47	372	1.1

Specimens tested: 125×400 mm prisms without longitudinal reinforcement.

Table A16
Details of columns with square ties tested by Issa (1994)

Col.	Concrete core				Transverse reinforcement					
Label	f_c (MPa)	f_{cc}/f_c (-)	ε_c (mm/m)	$\varepsilon_{cc}/\varepsilon_c$ (-)	Tie	d_c (mm)	s (mm)	ρ_s (%)	f_{sy} (MPa)	$-\sigma_{1,eff}$ (MPa)
A-1	48.3	1.56	2.1	1.57	B-spi	111	25	3.08	290	1.1
A-2	48.3	1.56	2.1	1.86	B-spi	104	38	2.45	372	0.9
A-3	48.3	1.27	2.1	1.24	B-spi	111	51	1.54	290	0.4
A-4	48.3	1.50	2.1	1.57	B-spi	104	64	1.47	372	0.3

Specimens tested: 125×400 mm prisms without longitudinal reinforcement.

Table A17
Details of circular columns tested by Cusson *et al* (1996)

Col.	Concrete core				Longitudinal reinforcement		Transverse reinforcement					
Label	f_c (MPa)	f_{cc}/f_c (-)	ε_c (mm/m)	$\varepsilon_{cc}/\varepsilon_c$ (-)	ρ_g (%)	f_{sy} (MPa)	Tie	d_c (mm)	s (mm)	ρ_s (%)	f_{sy} (MPa)	$-\sigma_{1,eff}$ (MPa)
II2	66.0	1.42	-	-	0.00	-	A-spi	144	36	2.18	580	4.7
I1A	112.0	1.13	-	-	0.00	-	A-spi	144	36	2.18	580	4.7
I1B	112.0	1.13	-	-	0.00	-	A-spi	144	36	2.18	580	4.7
III3	92.0	1.23	-	-	0.00	-	A-spi	144	36	2.18	580	4.7
III4	92.0	1.22	-	-	0.00	-	A-spi	145	51	1.06	588	2.0
I7*	112.0	1.17	-	-	0.00	-	A-spi	144	36	2.18	580	4.7
I8*	112.0	1.08	-	-	0.00	-	A-spi	144	36	2.18	580	4.7
I10	112.0	1.25	-	-	0.00	-	A-spi	144	18	4.36	580	11.1
I11	112.0	1.13	-	-	0.00	-	A-spi	145	51	1.06	588	2.0
I12	112.0	1.12	-	-	2.28	627	A-spi	144	36	2.18	580	4.7
I13	112.0	1.13	-	-	4.53	534	A-spi	144	36	2.18	580	4.7

Specimens tested: In general 160×500 mm cylinders.

* Column I7 was a 160×320 and column I8 a 160×1000 mm cylinder.

Table A18
Details of cylinder columns Hoshikuma *et al* (1997)

Col.	Concrete core				Longitudinal reinforcement		Transverse reinforcement					
Label	f_c (MPa)	f_{cc}/f_c (-)	ε_c (mm/m)	$\varepsilon_{cc}/\varepsilon_c$ (-)	ρ_g (%)	f_{sy} (MPa)	Tie	d_c (mm)	s (mm)	ρ_s (%)	f_{sy} (MPa)	$-\sigma_{l,eff}$ (MPa)
SC1	18.5	1.23	2.2	1.59	0.00	-	A-cir	194	150	0.39	235	0.1
SC2	18.5	1.32	2.2	2.18	0.00	-	A-cir	194	100	0.58	235	0.3
SC3	18.5	1.67	22	2.55	0.00	-	A-cir	194	50	1.17	235	1.0
SC4	18.5	2.20	2.2	6.41	0.00	-	A-cir	194	25	2.33	235	2.4
SC5	18.5	3.24	2.2	9.91	0.00	-	A-cir	194	13	4.66	235	5.1
LC1	28.8	1.12	2.2	1.77	1.01	295	A-cir	490	300	0.21	295	0.1
LC2	28.8	1.29	2.2	1.95	1.01	295	A-cir	490	150	0.43	295	0.4
LC3	28.8	1.41	2.2	2.05	1.01	295	A-cir	490	100	0.64	295	0.8
LC4	28.8	1.55	2.2	2.50	1.01	295	A-cir	490	50	1.28	295	1.7

Specimens tested: Series SC 200×600 mm cylinders without longitudinal reinforcement
Series LC 500×1500 mm cylinders.

* Material properties for confined concrete extracted from stress-strain curves given in source.

Table A19
Details of square columns Hoshikuma *et al* (1997)

Col.	Concrete core				Longitudinal reinforcement		Transverse reinforcement					
Label	f_c (MPa)	f_{cc}/f_c (-)	ε_c (mm/m)	$\varepsilon_{cc}/\varepsilon_c$ (-)	ρ_g (%)	f_{sy} (MPa)	Tie	d_c (mm)	s (mm)	ρ_s (%)	f_{sy} (MPa)	$-\sigma_{l,eff}$ (MPa)
SS1	23.2	1.06	2.5	1.36	0.00	-	B	194	150	0.39	235	0.0
SS2	23.2	1.09	2.5	1.64	0.00	-	B	194	100	0.58	235	0.1
SS3	23.2	1.14	2.5	1.92	0.00	-	B	194	50	1.17	235	0.3
SS4	23.2	1.33	2.5	2.08	0.00	-	B	194	25	2.33	235	0.8
SS5	23.2	1.46	2.5	3.72	0.00	-	B	194	13	4.66	235	1.7
LS1	24.3	1.09	2.5	1.92	0.95	295	B	490	60	1.81	295	0.8
LS2	24.3	1.23	2.5	1.80	0.95	295	B	490	75	2.19	295	0.9
LS3	24.3	1.21	2.5	2.00	0.95	295	B	490	40	2.71	295	1.2
LS4	24.3	1.27	2.5	3.64	0.95	295	B	490	40	4.10	295	1.9

Specimens tested: Series SS 200×600 mm prisms without longitudinal reinforcement.
Series LS 500×1500 mm prisms.

* Material properties for confined concrete extracted from stress-strain curves given in source.

Table A20
Details of square columns tested by Razvi and Saatcioglu (1998)

Col.	Concrete core				Longitudinal reinforcement		Transverse reinforcement					
Label	f_c* (MPa)	f_{cc}/f_c (-)	ε_c (mm/m)	$\varepsilon_{cc}/\varepsilon_c$ (-)	ρ_g (%)	f_{sy} (MPa)	Tie	d_c (mm)	s (mm)	ρ_s (%)	f_{sy} (MPa)	$-\sigma_{1,eff}$ (MPa)
CS-1	105.4	1.15	-	-	1.29	470	B	219	55	3.34	400	1.7
CS-2	105.4	1.15	-	-	2.57	470	C'	224	55	1.62	570	2.3
CS-3	105.4	1.22	-	-	3.86	470	D	224	55	2.43	570	3.6
CS-4	105.4	1.17	-	-	2.57	470	C'	223	55	2.17	1000	5.4
CS-5	105.4	1.16	-	-	3.86	470	D	223	120	1.49	1000	2.4
CS-6	105.4	1.10	-	-	2.57	470	C'	224	85	1.05	400	0.9
CS-7	105.4	1.09	-	-	3.86	470	D	224	120	1.11	400	0.7
CS-8	105.4	1.12	-	-	2.57	470	C'	219	85	3.24	400	2.6
CS-9	105.4	1.27	-	-	3.86	470	D	219	120	3.44	400	2.1
CS-11	68.9	1.36	-	-	1.29	470	B	219	40	4.59	400	2.5
CS-12	68.9	1.19	-	-	1.29	470	B	219	55	3.34	400	1.7
CS-13	78.2	1.10	-	-	2.57	470	C'	224	55	1.62	570	2.3
CS-14	78.2	1.21	-	-	3.86	470	D	224	55	2.43	570	3.6
CS-15	68.9	1.39	-	-	2.57	470	C'	223	55	2.17	1000	5.4
CS-16	68.9	1.38	-	-	3.86	470	D	223	85	2.10	1000	4.5
CS-17	68.9	1.09	-	-	2.57	470	C'	224	85	1.05	400	0.9
CS-18	68.9	1.11	-	-	3.86	470	D	224	85	1.57	400	1.3
CS-19	78.2	1.33	-	-	2.57	470	C'	219	85	3.24	400	2.6
CS-20	78.2	1.36	-	-	3.86	470	D	219	85	4.86	400	4.1
CS-22	51.0	1.33	-	-	2.57	470	C'	223	85	1.40	1000	2.9
CS-23	51.0	1.40	-	-	3.86	470	D	223	120	1.49	1000	2.4
CS-24	51.0	1.42	-	-	2.57	470	C'	219	85	3.24	400	2.6
CS-25	51.0	1.37	-	-	3.86	470	D	219	120	3.44	400	2.1
CS-26	51.0	1.50	-	-	3.86	470	D	224	55	2.43	570	3.6

Specimens tested: 250×900 mm prisms.

C' is a 6 legged tie configuration with 8 longitudinal steel bars.

* 0.85 times 150×300 mm cylinder strength.

Table A21
Details of circular columns tested by Li, taken after (Razvi, 1999)

Col.	Concrete core				Transverse reinforcement					
Label	f_c (MPa)	f_{cc}/f_c (-)	ε_c (mm/m)	$\varepsilon_{cc}/\varepsilon_c$ (-)	Tie	d_c (mm)	s (mm)	ρ_s (%)	f_{sy} (MPa)	$-\sigma_{1,eff}$ (MPa)
3A	63.0	1.48	-	-	A-cir	204	20	2.77	445	5.6
6A	63.0	1.24	-	-	A-cir	204	35	1.58	445	2.9
9A	63.0	1.19	-	-	A-cir	204	50	1.11	445	1.9
12A	63.0	1.12	-	-	A-cir	204	65	0.85	445	1.3
3B	72.3	1.50	-	-	A-cir	204	20	2.77	445	5.6
6B	72.3	1.28	-	-	A-cir	204	35	1.58	445	2.9
9B	72.3	1.18	-	-	A-cir	204	50	1.11	445	1.9
12B	72.3	1.02	-	-	A-cir	204	65	0.85	445	1.3
2HB	52.0	2.42	-	-	A-cir	204	20	3.16	1318	18.8
4HB1	52.0	1.68	-	-	A-cir	204	35	1.71	1318	9.9
6HB	52.0	1.32	-	-	A-cir	204	50	1.26	1318	6.3
2HC1	82.5	1.78	-	-	A-cir	204	20	3.16	1318	18.8
4HC	82.5	1.29	-	-	A-cir	204	35	1.81	1318	9.9
6HC	82.5	1.12	-	-	A-cir	204	50	1.26	1318	6.3

Table A22
Details of square columns tested by Nagashima *et al*, taken after (Razvi, 1999)

Col.	Concrete core				Transverse reinforcement					
Lab.	f_c (MPa)	f_{cc}/f_c (-)	ε_c (mm/m)	$\varepsilon_{cc}/\varepsilon_c$ (-)	Tie	d_c (mm)	s (mm)	ρ_s (%)	f_{sy} (MPa)	$-\sigma_{1,eff}$ (MPa)
1	92.4	1.57	-	-	D	214	31	3.84	813	9.2
2	92.4	1.48	-	-	D	214	31	3.84	813	9.2
3	92.4	1.57	-	-	D	214	31	3.84	813	9.2
4	92.4	1.32	-	-	D	214	45	2.64	813	5.9
5	92.4	1.30	-	-	D	214	60	1.98	813	4.0
6	92.4	1.19	-	-	D	214	60	1.98	813	4.0
7	92.4	1.30	-	-	D	214	60	1.98	813	4.0
8	92.4	1.30	-	-	D	216	31	1.69	840	4.2

Col.	Concrete core				Transverse reinforcement					
Lab.	f_c (MPa)	f_{cc}/f_c (-)	ε_c (mm/m)	$\varepsilon_{cc}/\varepsilon_c$ (-)	Tie	d_c (mm)	s (mm)	ρ_s (%)	f_{sy} (MPa)	$-\sigma_{1,eff}$ (MPa)
9	96.2	1.39	-	-	D	214	31	3.84	462	5.2
10	96.2	1.38	-	-	D	214	31	3.84	462	5.2
11	96.2	1.22	-	-	D	214	45	2.64	462	3.3
12	96.2	1.25	-	-	D	214	60	1.98	462	2.3
13	96.2	1.20	-	-	D	214	60	1.98	462	2.3
14	96.2	1.20	-	-	D	216	31	1.69	481	2.4

* Effective confining pressure determined on the basis of measured hoop strains.

Table A23
Details of circular columns tested by Razvi and Saatcioglu (1999)

Col.	Concrete core				Transverse reinforcement					
Label	f_c (MPa)	f_{cc}/f_c (-)	ε_c (mm/m)	$\varepsilon_{cc}/\varepsilon_c$ (-)	Tie	d_c (mm)	s (mm)	ρ_s (%)	f_{sy} (MPa)	$-\sigma_{1,eff}$ (MPa)
CC-1	51.0	1.17	-	-	A-spi	224	135	0.41	660	0.5
CC-2	51.0	1.22	-	-	A-spi	219	135	1.36	400	1.0
CC-3	51.0	1.34	-	-	A-spi	224	70	0.80	660	1.8
CC-4	51.0	1.32	-	-	A-spi	224	70	0.80	660	1.8
CC-8	105.4	1.17	-	-	A-spi	224	70	0.80	660	1.8
CC-9	105.4	1.28	-	-	A-spi	219	135	1.36	400	1.0
CC-10	105.4	1.28	-	-	A-spi	219	60	3.06	400	4.4
CC-11	105.4	1.18	-	-	A-spi	224	60	0.93	660	2.2
CC-12	105.4	1.21	-	-	A-spi	223	60	1.32	1000	4.8
CC-14	78.2	1.31	-	-	A-spi	223	60	1.32	1000	4.8
CC-15	78.2	1.35	-	-	A-spi	219	60	3.06	400	4.4
CC-16	78.2	1.22	-	-	A-spi	223	100	0.79	1000	2.2
CC-19	78.2	1.21	-	-	A-spi	219	100	1.83	400	2.0
CC-20	78.2	1.13	-	-	A-spi	224	100	0.56	660	1.0
CC-21	78.2	1.19	-	-	A-spi	224	70	0.80	660	1.8
CC-22	78.2	1.14	-	-	A-spi	219	135	1.36	400	1.0

Table A24
Details of square columns tested by Nagashima *et al*, taken after (Cusson, 1995) and (Razvi, 1999)

Col.	Concrete core				Transverse reinforcement						
Label	f_c (MPa)	f_{cc}/f_c (-)	ε_c** (mm/m)	$\varepsilon_{cc}/\varepsilon_c$ (-)	Tie	d_c (mm)	s (mm)	ρ_s (%)	f_{sy} (MPa)	$-\sigma_{1,eff}$* (MPa)	$-\sigma_{1,eff}$ (MPa)
HH08LA	98.8	1.24	2.9	1.51	D	200	55	1.67	1387	1.4	5.8
HH10LA	98.8	1.24	2.9	1.82	D	200	45	2.04	1387	3.0	7.6
HH13LA	98.8	1.33	2.9	1.89	D	200	35	2.63	1387	3.8	10.4
HH15LA	98.8	1.29	2.9	3.06	D	200	45	3.24	1368	6.4	11.9
HH20LA	100.4	1.47	2.9	5.85	D	200	35	4.17	1368	15.7	16.2
HL06LA	100.4	1.17	2.9	1.47	D	200	45	1.96	807	2.5	4.3
HL08LA	100.4	1.33	2.9	1.78	D	200	35	2.52	807	4.4	5.8
LL05LA	51.3	1.34	2.4	1.52	D	200	55	1.61	807	2.2	3.3
LL08LA	51.3	1.55	2.4	3.20	D	200	35	2.52	807	5.1	5.8
LH08LA	51.3	1.38	2.4	2.40	D	200	55	1.67	1387	3.2	5.8
LH13LA	51.3	1.67	2.4	4.89	D	200	35	2.63	1387	9.5	10.4
HH13MA	100.4	1.31	2.9	1.64	D	200	35	2.63	1387	3.6	10.4
HH13HA	100.4	1.29	2.9	2.12	D	200	35	2.63	1387	4.7	10.4
LL08MA	51.03	1.55	2.4	3.79	D	200	35	2.52	807	5.2	5.8
LL08HA	51.3	1.52	2.4	4.17	D	200	35	2.52	807	5.1	5.8
LH15LA	52.4	1.69	2.4	9.34	D	200	45	3.24	1368	11.9	11.9
HH13LB	100.4	1.31	2.9	2.19	D	200	27	3.41	1387	4.9	14.1
HH13LD	100.4	1.28	2.9	1.75	C'	200	25	2.45	1387	2.9	9.9
LL08LB	52.4	1.57	2.4	2.93	D	200	27	3.27	807	6.0	7.9
LL08LD	52.4	1.48	2.4	4.06	C'	200	25	2.36	807	4.7	5.5
HH13MSA	100.4	1.29	2.9	-	D	200	35	2.63	1387	-	10.4
HH13HSA	100.4	1.34	2.9	-	D	200	35	2.63	1387	-	10.4
LL08MSA	52.4	1.51	2.4	-	D	200	35	2.52	807	-	5.8
LL08HSA	52.4	1.54	2.4	-	D	200	35	2.52	807	-	5.8

C' is a 6 legged tie configuration with 8 longitudinal steel bars.

* Effective confining pressure determined on the basis of measured hoop strains.

** Estimated using equation 3.5.

Table A25
Details of columns tested by Assa *et al* (Assa, 2001)

Col.	Concrete core				Transverse reinforcement						
Label	f_c (MPa)	f_{cc}/f_c (-)	ε_c (mm/m)	$\varepsilon_{cc}/\varepsilon_c$ (-)	Tie	d_c (mm)	s (mm)	ρ_s (%)	f_{sy} (MPa)	$-\sigma_{l,eff}$* (MPa)	$-\sigma_{l,eff}$ (MPa)
20M25	25.0	3.83	3.3	16.52	A-spi	145	28	3.05	1296	16.1	16.0
20M38	25.0	2.31	3.3	10.06	A-spi	145	44	1.92	1296	8.7	8.6
30M19	34.1	3.78	2.4	20.25	A-spi	145	20	4.15	1296	24.3	23.1
30M25	34.1	2.93	2.4	16.69	A-spi	145	28	3.04	1296	15.2	15.9
30M38	34.1	1.84	2.4	8.93	A-spi	145	47	1.80	1296	6.8	7.9
30M50	34.1	1.71	2.4	5.45	A-cir	145	50	1.69	909	5.0	5.0
30M75	34.1	1.24	2.4	2.44	A-cir	145	75	1.13	909	1.6	2.5
40M25	41.4	2.44	2.5	10.08	A-spi	145	28	3.05	1296	16.3	16.0
40M38	41.4	1.85	2.5	5.28	A-spi	145	44	1.92	1296	7.8	8.6
50M25	49.8	2.53	2.2	9.40	A-spi	145	28	3.05	1296	16.2	16.0
50M38	49.8	1.74	2.2	5.64	A-spi	145	44	1.92	1296	7.2	8.6
60M25	64.4	2.09	2.3	7.26	A-spi	145	28	3.02	1296	15.7	15.8
60M25R	64.4	2.03	2.3	5.09	A-spi	145	28	3.05	1296	14.4	16.0
60M38	64.4	1.50	2.3	3.46	A-spi	145	44	1.92	1296	6.8	8.6
70M25	70.1	1.85	2.0	5.95	A-spi	145	28	3.02	1296	13.9	15.8
70M38	70.1	1.30	2.0	2.35	A-spi	145	44	1.92	1296	3.4	8.6
80M19	83.0	1.96	2.3	8.51	A-spi	145	20	4.15	1296	23.4	23.1
80M25	83.0	1.56	2.3	4.30	A-spi	145	28	3.01	1296	13.0	15.7
80M38	85.0	1.24	2.3	2.54	A-spi	145	47	1.82	1296	3.5	8.0
80M50	83.0	1.20	2.3	2.06	A-cir	145	50	1.69	909	2.8	5.0
80M75	83.0	1.00	2.3	1.49	A-cir	145	75	1.13	909	1.2	2.5
90M25	75.0	1.79	2.0	4.60	A-spi	145	28	3.02	1296	12.6	15.8
90M38	75.0	1.40	2.0	2.08	A-spi	145	45	1.88	1296	2.9	8.4
90M25T	74.5	1.97	1.9	5.76	A-spi	145	28	3.05	1296	11.6	16.0

C' is a 6 legged tie configuration with 8 longitudinal steel bars.

* Effective confining pressure determined on the basis of measured hoop strains.

Appendix B: Programs for Numerical Analysis of Concrete Columns

The following provides the source code for the two major computer programs developed as part of this investigation into the behaviour of confined high strength concrete columns. The first program, MNCALC, calculates all supportable combinations of axial load and biaxial bending moments for a given cross-section, and the second program, COLS, calculates the load-deflection response for a slender column. The generic input files assist in the understanding of the working of the computer programs.

B.1 MNCALC - Program for Generating Interaction Diagrams

Input file

```
*=========================================================================
*  MN-DIAGRAM : Title: Saatcioglu, config (3)
*=========================================================================
*  PROBLEM SIZE
*  nmt   = Number of material specifications
*  maxmd = Maximum data points defining a single stress-strain curve
*  nqc   = Number of quadrilateral elements in cross-section
*  npc   = Number of point elements in cross-section
*  ngaus = Order of numerical integration
*-------------------------------------------------------------------------
*  nmt  maxmd  nqc  npc  ngaus
SZ=======================================================================
    3    301    24   12    3
*=========================================================================
*  CONTROL PARAMETERS FOR ANALYSIS
*  daPz0   (KN), Initial axial load increment
*  naPz        , Axial load resolution
*  eraPz   (KN), Accuracy of axial load capacity
*  erPres  (KN), Convergence criteria for axial load residuals
*  daM0   (KNm), Initial increment of bending moments
*  phi    (deg), Biaxial moment relation, dMx= cos(phi)*daM,
*                                         dMy= sin(phi)*daM
*  eraM    (KN), Accuracy of moment capacity
*  erMres (KNm), convergence criteria for residual moments
*-------------------------------------------------------------------------
*   daPz0  naPz  eraPz  erPres  daM0  phi  eraM  erMres
CP=======================================================================
    -1.0    30    .1     .001     1.  .0   .01    .005
*=========================================================================
*  ELEMENTS DEFINING CROSS-SECTION
*  Description of each quadrilateral element within the cross-section in terms
*  of material number and nodal coordinates. This followed by a description of
*  each point element in terms of material number, coordinate, lumped area, and
```

```
*  the material number of the replaced material.
*-------------------------------------------------------------------------------
*  material coord.node1 coord.node2 coord.node3 coord.node4
*  number      X     Y     X     Y     X     Y     X     Y
*  ( - )      (mm)  (mm)  (mm)  (mm)  (mm)  (mm)  (mm)  (mm)
*  material coord.node   area  replaced
*  number      X     Y          material
*  ( - )      (mm)  (mm) (mm^2) ( - )
DC===============================================================================
 5 -105.0  -105.0  -88.8  -105.0  -88.8  -88.8  -105.0  -88.8
 5  -88.8  -105.0   88.8  -105.0   88.8  -88.8   -88.8  -88.8
 5   88.8  -105.0  105.0  -105.0  105.0  -88.8    88.8  -88.8
 5 -105.0   -88.8  -88.8   -88.8  -88.8  -59.2  -105.0  -59.2
 8  -88.8   -88.8   88.8   -88.8   88.8  -59.2   -88.8  -59.2
 5   88.8   -88.8  105.0   -88.8  105.0  -59.2    88.8  -59.2
 5 -105.0   -59.2  -88.8   -59.2  -88.8  -29.6  -105.0  -29.6
 8  -88.8   -59.2   88.8   -59.2   88.8  -29.6   -88.8  -29.6
 5   88.8   -59.2  105.0   -59.2  105.0  -29.6    88.8  -29.6
 5 -105.0   -29.6  -88.8   -29.6  -88.8    0.0  -105.0    0.0
 8  -88.8   -29.6   88.8   -29.6   88.8    0.0   -88.8    0.0
 5   88.8   -29.6  105.0   -29.6  105.0    0.0    88.8    0.0
 5 -105.0     0.0  -88.8     0.0  -88.8   29.6  -105.0   29.6
 8  -88.8     0.0   88.8     0.0   88.8   29.6   -88.8   29.6
 5   88.8     0.0  105.0     0.0  105.0   29.6    88.8   29.6
 5 -105.0    29.6  -88.8    29.6  -88.8   59.2  -105.0   59.2
 8  -88.8    29.6   88.8    29.6   88.8   59.2   -88.8   59.2
 5   88.8    29.6  105.0    29.6  105.0   59.2    88.8   59.2
 5 -105.0    59.2  -88.8    59.2  -88.8   88.8  -105.0   88.8
 8  -88.8    59.2   88.8    59.2   88.8   88.8   -88.8   88.8
 5   88.8    59.2  105.0    59.2  105.0   88.8    88.8   88.8
 5 -105.0    88.8  -88.8    88.8  -88.8  105.0  -105.0  105.0
 5  -88.8    88.8   88.8    88.8   88.8  105.0   -88.8  105.0
 5   88.8    88.8  105.0    88.8  105.0  105.0    88.8  105.0
 9 -80.0  -80.0  100.3  8
 9 -27.0  -80.0  100.3  8
 9  27.0  -80.0  100.3  8
 9  80.0  -80.0  100.3  8
 9 -80.0  -27.0  100.3  8
 9  80.0  -27.0  100.3  8
 9 -80.0   27.0  100.3  8
 9  80.0   27.0  100.3  8
 9 -80.0   80.0  100.3  8
 9 -27.0   80.0  100.3  8
 9  27.0   80.0  100.3  8
 9  80.0   80.0  100.3  8
*===============================================================================
*  MATERIAL PROPERTIES
*  Material number, number of data points defining stress-strain curve,
*  strain corresponding to initial stress data, strain corresponding to
*  final stress data. This followed by the stress values corresponding to
*  the equidistant strain values.
*  Repeat for the definition of other materials.
*  5 = C35 unconfined
*  8 = C35 confined (3)
*  9 = reinforcement bars
*-------------------------------------------------------------------------------
*  material   number of    initial  final
*  number     data points  strain   strain
*  ( - )      ( - )        (mm/m)   (mm/m)
*  stress ...
*  (MPa)
MP===============================================================================
 5  301  0.0  -15.0
   0.00   -1.50   -2.96   -4.36   -5.72   -7.04   -8.31   -9.54  -10.72
 -11.87  -12.97  -14.03  -15.05  -16.03  -16.97  -17.88  -18.74  -19.57
 -20.37  -21.12  -21.84  -22.53  -23.18  -23.80  -24.39  -24.94  -25.46
```

```
-25.95  -26.40  -26.83  -27.23  -27.59  -27.93  -28.23  -28.51  -28.76
-28.98  -29.18  -29.35  -29.49  -29.60  -29.69  -29.75  -29.79  -29.80
-29.80  -29.79  -29.77  -29.74  -29.68  -29.60  -29.48  -29.34  -29.16
-28.94  -28.69  -28.40  -28.07  -27.70  -27.30  -26.86  -26.39  -25.89
-25.37  -24.82  -24.26  -23.67  -23.08  -22.47  -21.86  -21.24  -20.63
-20.01  -19.40  -18.80  -18.20  -17.61  -17.04  -16.48  -15.93  -15.39
-14.88  -14.37  -13.88  -13.41  -12.95  -12.51  -12.08  -11.67  -11.28
-10.89  -10.53  -10.17   -9.84   -9.51   -9.20   -8.90   -8.61   -8.33
 -8.06   -7.81   -7.56   -7.32   -7.10   -6.88   -6.67   -6.47   -6.27
 -6.09   -5.91   -5.74   -5.57   -5.41   -5.26   -5.11   -4.97   -4.84
 -4.70   -4.58   -4.46   -4.34   -4.23   -4.12   -4.01   -3.91   -3.81
 -3.72   -3.62   -3.54   -3.45   -3.37   -3.29   -3.21   -3.14   -3.06
 -2.99   -2.93   -2.86   -2.80   -2.74   -2.68   -2.62   -2.56   -2.51
 -2.45   -2.40   -2.35   -2.31   -2.26   -2.21   -2.17   -2.13   -2.08
 -2.04   -2.01   -1.97   -1.93   -1.89   -1.86   -1.82   -1.79   -1.76
 -1.73   -1.70   -1.67   -1.64   -1.61   -1.58   -1.55   -1.53   -1.50
 -1.47   -1.45   -1.43   -1.40   -1.38   -1.36   -1.34   -1.31   -1.29
 -1.27   -1.25   -1.23   -1.21   -1.20   -1.18   -1.16   -1.14   -1.13
 -1.11   -1.09   -1.08   -1.06   -1.05   -1.03   -1.02   -1.00   -0.99
 -0.97   -0.96   -0.95   -0.94   -0.92   -0.91   -0.90   -0.89   -0.87
 -0.86   -0.85   -0.84   -0.83   -0.82   -0.81   -0.80   -0.79   -0.78
 -0.77   -0.76   -0.75   -0.74   -0.73   -0.72   -0.71   -0.71   -0.70
 -0.69   -0.68   -0.67   -0.67   -0.66   -0.65   -0.64   -0.64   -0.63
 -0.62   -0.61   -0.61   -0.60   -0.59   -0.59   -0.58   -0.58   -0.57
 -0.56   -0.56   -0.55   -0.55   -0.54   -0.53   -0.53   -0.52   -0.52
 -0.51   -0.51   -0.50   -0.50   -0.49   -0.49   -0.48   -0.48   -0.47
 -0.47   -0.46   -0.46   -0.45   -0.45   -0.45   -0.44   -0.44   -0.43
 -0.43   -0.43   -0.42   -0.42   -0.41   -0.41   -0.41   -0.40   -0.40
 -0.40   -0.39   -0.39   -0.38   -0.38   -0.38   -0.37   -0.37   -0.37
 -0.36   -0.36   -0.36   -0.36   -0.35   -0.35   -0.35   -0.34   -0.34
 -0.34   -0.34   -0.33   -0.33
8  301   0.0  -15.0
  0.00   -1.50   -2.96   -4.36   -5.72   -7.04   -8.31   -9.53  -10.72
-11.86  -12.96  -14.02  -15.03  -16.01  -16.96  -17.86  -18.73  -19.56
-20.36  -21.13  -21.86  -22.56  -23.23  -23.87  -24.49  -25.08  -25.65
-26.19  -26.71  -27.21  -27.70  -28.16  -28.61  -29.04  -29.45  -29.86
-30.25  -30.62  -30.99  -31.35  -31.69  -32.03  -32.35  -32.67  -32.98
-33.29  -33.59  -33.88  -34.16  -34.44  -34.71  -34.98  -35.24  -35.50
-35.76  -36.01  -36.25  -36.49  -36.73  -36.97  -37.20  -37.43  -37.66
-37.88  -38.10  -38.32  -38.53  -38.75  -38.96  -39.16  -39.37  -39.58
-39.78  -39.98  -40.18  -40.37  -40.57  -40.76  -40.96  -41.15  -41.34
-41.52  -41.71  -41.89  -42.08  -42.26  -42.44  -42.60  -42.62  -42.64
-42.65  -42.66  -42.67  -42.67  -42.67  -42.67  -42.67  -42.67  -42.67
-42.66  -42.66  -42.66  -42.66  -42.66  -42.66  -42.65  -42.65  -42.64
-42.64  -42.63  -42.63  -42.62  -42.62  -42.61  -42.60  -42.59  -42.58
-42.57  -42.56  -42.55  -42.53  -42.52  -42.50  -42.49  -42.47  -42.45
-42.44  -42.42  -42.40  -42.38  -42.35  -42.33  -42.31  -42.28  -42.26
-42.23  -42.20  -42.17  -42.14  -42.11  -42.08  -42.05  -42.02  -41.98
-41.95  -41.91  -41.87  -41.83  -41.79  -41.75  -41.71  -41.67  -41.63
-41.58  -41.54  -41.49  -41.44  -41.39  -41.34  -41.29  -41.24  -41.19
-41.14  -41.08  -41.03  -40.97  -40.91  -40.86  -40.80  -40.74  -40.68
-40.61  -40.55  -40.49  -40.43  -40.36  -40.29  -40.23  -40.16  -40.09
-40.02  -39.95  -39.88  -39.81  -39.74  -39.67  -39.60  -39.52  -39.45
-39.37  -39.30  -39.22  -39.14  -39.06  -38.99  -38.91  -38.83  -38.75
-38.67  -38.58  -38.50  -38.42  -38.34  -38.25  -38.17  -38.09  -38.00
-37.92  -37.83  -37.74  -37.66  -37.57  -37.48  -37.40  -37.31  -37.22
-37.13  -37.04  -36.95  -36.86  -36.78  -36.69  -36.59  -36.50  -36.41
-36.32  -36.23  -36.14  -36.05  -35.96  -35.87  -35.77  -35.68  -35.59
-35.50  -35.41  -35.31  -35.22  -35.13  -35.04  -34.94  -34.85  -34.76
-34.67  -34.57  -34.48  -34.39  -34.30  -34.20  -34.11  -34.02  -33.93
-33.83  -33.74  -33.65  -33.56  -33.47  -33.37  -33.28  -33.19  -33.10
-33.01  -32.92  -32.83  -32.73  -32.64  -32.55  -32.46  -32.37  -32.28
-32.19  -32.10  -32.01  -31.92  -31.84  -31.75  -31.66  -31.57  -31.48
-31.39  -31.31  -31.22  -31.13  -31.05  -30.96  -30.87  -30.79  -30.70
-30.62  -30.53  -30.45  -30.36  -30.28  -30.19  -30.11  -30.03  -29.94
-29.86  -29.78  -29.70  -29.61
```

```
 9  2  -2.52  2.52
  -517.  517.
*==============================================================================
```

Program MNCALC

```
*********************************************************************
*                Automatic generation of MN-diagrams                *
*                         MNCALC Version 1.1                        *
*                               2001                                *
*********************************************************************
*                       Main Program                                *
*   nmt   = Number of material specifications.                      *
*   maxmd = Max number of data defining a stress-strain curve.      *
*   nqc   = Number of quadrilateral elements in cross-section.      *
*   npc   = Number of point elements in cross-section.             *
*   ngaus = Order of numerical integration.                         *
*********************************************************************
      program mncalc
      integer nmt_,maxmd_,nqc_,npc_,ngaus_
      parameter ( nmt_  = 25,
     +            maxmd_=500,
     +            nqc_  =100,
     +            npc_  =100,
     +            ngaus_=  5)
      character*60 datfil,resfil
      character key*1
      logical fextn,ffile
      integer nmt,maxmd,nqc,npc,ngaus,gpdim,naPz
      integer lmatr(nmt_),nmds(nmt_),melq(nqc_),melp(2*npc_),
     +        gpm(nqc_*ngaus_**2+2*npc_)
      real cenx,ceny,daPz0,eraPz,erPres,daM0,phi,eraM,erMres
      real xelp(npc_),yelp(npc_),aelp(npc_),shape(4*ngaus_**2),
     +     dNdxie(4*ngaus_**2),dNdeta(4*ngaus_**2),
     +     eweigp(ngaus_**2),posgpl(ngaus_),weigpl(ngaus_)
      real stnmd(2,nmt_),strmd(maxmd_,nmt_),xelq(4,nqc_),
     +     yelq(4,nqc_),gpx(nqc_*ngaus_**2+2*npc_),
     +     gpy(nqc_*ngaus_**2+2*npc_),gpa(nqc_*ngaus_**2+2*npc_)
      integer k,kk
      write(6,*)
      write(6,*)'*************************************************'
      write(6,*)'*                                               *'
      write(6,*)'*     Automatic generation of MN-diagrams       *'
      write(6,*)'*                                               *'
      write(6,*)'*              MNCALC Version 1.1               *'
      write(6,*)'*                     2001                      *'
      write(6,*)'*                                               *'
      write(6,*)'*************************************************'
      write(6,*)
 5    write(6,*)'Input name of data file'
      write(6,*)
      read(6,810) datfil
      fextn=.false.
      do 10 k=60,4,-1
       if(datfil(k-3:k).eq.'.dat') then
        fextn=.true.
        goto 20
       endif
 10   continue
 20   if (.not.fextn) then
       write(6,*)'Data file does not contain .dat extension'
       write(6,*)
       goto 5
      endif
```

```
      inquire(file=datfil,exist=ffile)
      if (.not.ffile) then
       write(6,*) 'Data file not found'
       write(6,*) 'Try again yes/no'
       read(6,815) key
       if (key.eq.'y') then
        goto 5
       else
        goto 1000
       endif
      endif
      kk=index(datfil,'.dat')-1
      resfil=datfil(1:kk)//'.res'
      call storeq(datfil,nmt,maxmd,nqc,npc,ngaus)
      write(6,*)
      write(6,*)
      write(6,*)   'Size of problem:'
      write(6,820) 'Number of material specifications ',' =',nmt
      write(6,820) 'Max number of material data points',' =',maxmd
      write(6,820) 'Number of q-elems in section      ',' =',nqc
      write(6,820) 'Number of p-elems in section      ',' =',npc
      write(6,820) 'Order of numerical integration    ',' =',ngaus
      write(6,*)
      if (nmt.gt.nmt_) then
       goto 930
      else if (maxmd.gt.maxmd_) then
       goto 930
      else if (nqc.gt.nqc_) then
       goto 930
      else if (npc.gt.npc_) then
       goto 930
      else if (ngaus.gt.ngaus_) then
       goto 930
      endif
      call input(datfil,nmt,maxmd,lmatr,stnmd,nmds,strmd,nqc,
     +           melq,xelq,yelq,npc,melp,xelp,yelp,aelp,
     +           daPz0,naPz,eraPz,erPres,daM0,phi,eraM,
     +           erMres)
      gpdim=nqc*ngaus**2+2*npc
      call numint(nqc,npc,ngaus,shape,dNdxie,dNdeta,eweigp,
     +            melq,xelq,yelq,melp,xelp,yelp,aelp,gpdim,
     +            gpx,gpy,gpa,gpm,posgpl,weigpl)
      call cenoid(cenx,ceny,nqc,npc,ngaus,gpx,gpy,gpa)
      write(6,*) 'Origin of reference system'
      write(6,825)'cenx=',cenx,'mm','ceny=',ceny,'mm'
      call Sect(resfil,nmt,nmds,stnmd,maxmd,strmd,gpdim,gpx,
     +          gpy,gpa,gpm,cenx,ceny,daPz0,naPz,eraPz,erPres,
     +          daM0,phi,eraM,erMres)
 810  format(a60)
 815  format(a1)
 820  format(2x,a34,a2,i4)
 825  format(2x,a5,f8.1,a2,2x,a5,f8.1,a2)
      stop
 930  write(6,*)'Problem too large'
      goto 1000
 1000 write(6,*)'Program terminated'
      stop
      end
c=====================================================================
c                Subroutine storeq( )
c     Reads key parameters governing the computer storage, and checks
c     the presence of required field identifiers.
c=====================================================================
      subroutine storeq(datfil,nmt,maxmd,nqc,npc,ngaus)
      character*60 datfil
      integer nmt,maxmd,nqc,npc,ngaus
```

```
      open(12,file=datfil,status='old')
      rewind(12)
      call detect('SZ')
      read(12,*,err=910) nmt,maxmd,nqc,npc,ngaus
      call detect('CP')
      call detect('DC')
      call detect('MP')
      close(12)
      return
 910  write(6,*) 'Format error reading SZ field'
      goto 1000
 1000 write(6,*) 'Program terminated'
      stop
      end
c=======================================================================
c                Subroutine detect( )
c     Search for a named data field.
c=======================================================================
      subroutine detect(obj)
      character*2 obj,text
      rewind(12)
 121  read(12,'(a2)',end=900) text
      if (text.ne.obj) then
        goto 121
      endif
      return
 900  write(6,*) 'Numerical field identifier ',obj,' missing'
      write(6,*) 'Program terminated'
      stop
      end
c=======================================================================
c                Subroutine input( )
c     Reads and checks format of the data file.
c=======================================================================
      subroutine input(datfil,nmt,maxmd,lmatr,stnmd,nmds,strmd,nqc,
     +                 melq,xelq,yelq,npc,melp,xelp,yelp,aelp,
     +                 daPz0,naPz,eraPz,erPres,daM0,phi,eraM,
     +                 erMres)
      character*60 datfil
      integer nmt,maxmd,nqc,npc,naPz
      integer lmatr(nmt),nmds(nmt),melq(nqc),melp(2*npc)
      real daPz0,eraPz,erPres,daM0,phi,eraM,erMres,pi
      real xelp(npc),yelp(npc),aelp(npc)
      real stnmd(2,nmt),strmd(maxmd,nmt),xelq(4,nqc),yelq(4,nqc)
      integer matr,nmd
      integer i,j,k
      open(12,file=datfil,status='old')
      rewind(12)
      do 101 i=1,nqc
       melq(i)=0
 101  continue
      do 102 i=1,2*npc
       melp(i)=0
 102  continue
      do 104 j=1,nmt
       do 103 i=1,maxmd
        strmd(i,j)=0.
 103   continue
 104  continue
      call detect('CP')
      read(12,*,err=900) daPz0,naPz,eraPz,erPres,daM0,phi,eraM,
     +                   erMres
      daPz0=1000.*daPz0
      eraPz=abs(1000.*eraPz)
      erPres=abs(1000.*erPres)
      daM0=1.E6*daM0
```

```
      pi=acos(-1.)
      phi=phi*pi/180.
      eraM=abs(1.E6*eraM)
      erMres=abs(1.E6*erMres)
      call detect('MP')
      do 10 i=1,nmt
       read(12,*,err=910) matr,nmd
       backspace(12)
       read(12,*,err=910) lmatr(i),nmds(i),(stnmd(j,i),j=1,2),
     +                    (strmd(j,i),j=1,nmd)
 10   continue
      do 11 j=1,nmt
       stnmd(1,j)=stnmd(1,j)/1000.
       stnmd(2,j)=stnmd(2,j)/1000.
 11   continue
      do 13 i=1,nmt
       matr=lmatr(i)
       do 12 j=i+1,nmt
        if (matr.eq.lmatr(j)) then
         goto 912
        endif
 12     continue
 13   continue
      call detect('DC')
      read(12,*,err=920) (melq(j),(xelq(i,j),yelq(i,j),i=1,4),
     +                    j=1,nqc)
      read(12,*,err=920) (melp(j),xelp(j),yelp(j),aelp(j),
     +                    melp(npc+j),j=1,npc)
      do 24 i=1,nqc
       matr=melq(i)
       do 23 k=1,nmt
        if (matr.eq.lmatr(k)) then
         melq(i)=k
         goto 24
        endif
 23     continue
       goto 924
 24   continue
      do 27 i=1,2*npc
       matr=melp(i)
       do 26 k=1,nmt
        if (matr.eq.lmatr(k)) then
         melp(i)=k
         goto 27
        endif
 26     continue
       goto 927
 27   continue
      close(12)
      return
 900  write(6,*) 'Format error reading CP field'
      goto 1000
 910  write(6,*) 'Format error reading line ',i,' of MP field'
      goto 1000
 912  write(6,*) 'Material number ',matr,' not unique'
      goto 1000
 920  write(6,*) 'Format error reading DC field'
      goto 1000
 924  write(6,*) 'Material number ',matr,' not defined'
      goto 1000
 927  write(6,*) 'Material number ',matr,' not defined'
      goto 1000
 1000 write(6,*) 'program terminated'
      stop
      end
C=======================================================================
```

```
c                Subroutine numint( )
c     Evaluates the coordinates of the numerical integration points,
c     the associated integration areas and material numbers. Replaced
c     material is assigned a negative area.
c=====================================================================
      subroutine numint(nqc,npc,ngaus,shape,dNdxie,dNdeta,eweigp,
     +                  melq,xelq,yelq,melp,xelp,yelp,aelp,gpdim,
     +                  gpx,gpy,gpa,gpm,posgpl,weigpl)
      integer nqc,npc,ngaus,gpdim
      integer melq(nqc),melp(2*npc),gpm(gpdim)
      real shape(4*ngaus**2),dNdxie(4*ngaus**2),dNdeta(4*ngaus**2),
     +     eweigp(ngaus**2),xelp(npc),gpx(gpdim),yelp(npc),
     +     gpy(gpdim),aelp(npc),gpa(gpdim),
     +     posgpl(ngaus),weigpl(ngaus)
      real xelq(4,nqc),yelq(4,nqc)
      integer matr,elem
      real xie,eta,mulvec,J11,J12,J21,J22,detJ
      integer i,ii,ii1,j,jj,nn,kk
      call gaussl(ngaus,posgpl,weigpl)
      nn=0
      kk=0
      do 15 i=1,ngaus
       do 10 j=1,ngaus
        xie=posgpl(i)
        eta=posgpl(j)
        shape(kk+1)= 0.25*(1-xie)*(1-eta)
        shape(kk+2)= 0.25*(1+xie)*(1-eta)
        shape(kk+3)= 0.25*(1+xie)*(1+eta)
        shape(kk+4)= 0.25*(1-xie)*(1+eta)
        dNdxie(kk+1)=-0.25*(1-eta)
        dNdxie(kk+2)= 0.25*(1-eta)
        dNdxie(kk+3)= 0.25*(1+eta)
        dNdxie(kk+4)=-0.25*(1+eta)
        dNdeta(kk+1)=-0.25*(1-xie)
        dNdeta(kk+2)=-0.25*(1+xie)
        dNdeta(kk+3)= 0.25*(1-xie)
        dNdeta(kk+4)= 0.25*(1+xie)
        kk=kk+4
        eweigp(nn+1)=weigpl(i)*weigpl(j)
        nn=nn+1
10     continue
15    continue
      elem=0
      do 35 j=1,nqc
       elem=elem+1
       matr=melq(j)
       jj=ngaus**2*(j-1)
       do 30 i=1,ngaus**2
        ii=4*(i-1)
        ii1=ii+1
        gpx(jj+i)=mulvec(shape(ii1),xelq(1,j),4)
        gpy(jj+i)=mulvec(shape(ii1),yelq(1,j),4)
        J11=mulvec(dNdxie(ii1),xelq(1,j),4)
        J12=mulvec(dNdxie(ii1),yelq(1,j),4)
        J21=mulvec(dNdeta(ii1),xelq(1,j),4)
        J22=mulvec(dNdeta(ii1),yelq(1,j),4)
        detJ= J11*J22-J12*J21
        if (detJ.le.0.0) goto 910
        gpa(jj+i)=detJ*eweigp(i)
        gpm(jj+i)=matr
30     continue
35    continue
      jj=nqc*ngaus**2
      do 25 j=1,npc
       gpx(jj+j)=xelp(j)
       gpy(jj+j)=yelp(j)
```

```
       gpa(jj+j)=aelp(j)
       gpm(jj+j)=melp(j)
       gpx(jj+npc+j)=xelp(j)
       gpy(jj+npc+j)=yelp(j)
       gpa(jj+npc+j)=-aelp(j)
       gpm(jj+npc+j)=melp(npc+j)
 25    continue
       return
 910   write(6,*) 'Incorrect geometry of quadrilateral element',elem
       goto 1000
 1000  write(6,*) 'program terminated'
       stop
       end
c=======================================================================
c                Subroutine gaussl( )
c     Sets numerical integration constants for exact integration of a
c     polynomium of degree 2*ngaus-1 over an interval -1 to 1.
c=======================================================================
       subroutine gaussl(ngaus,posgpl,weigpl)
       integer ngaus,kk
       real  posgpl(ngaus),weigpl(ngaus)
       kk=0
       if (ngaus.eq.1) then
        posgpl(kk+1)=0.0
        weigpl(kk+1)=2.0
       else if (ngaus.eq.2) then
        posgpl(kk+1)=-0.5773502692
        posgpl(kk+2)=0.5773502692
        weigpl(kk+1)=1.0
        weigpl(kk+2)=1.0
       else if (ngaus.eq.3) then
        posgpl(kk+1)=-0.7745966692
        posgpl(kk+2)=0.0
        posgpl(kk+3)=0.7745966692
        weigpl(kk+1)=0.5555555556
        weigpl(kk+2)=0.8888888889
        weigpl(kk+3)=0.5555555556
       else if (ngaus.eq.4) then
        posgpl(kk+1)=-0.8611363116
        posgpl(kk+2)=-0.3399810436
        posgpl(kk+3)=0.3399810436
        posgpl(kk+4)=0.8611363116
        weigpl(kk+1)=0.3478548451
        weigpl(kk+2)=0.6521451549
        weigpl(kk+3)=0.6521451549
        weigpl(kk+4)=0.3478548451
       else if (ngaus.eq.5) then
        posgpl(kk+1)=-0.9061798459
        posgpl(kk+2)=-0.5384693101
        posgpl(kk+3)=0.0
        posgpl(kk+4)=0.5384693101
        posgpl(kk+5)=0.9061798459
        weigpl(kk+1)=0.2369268851
        weigpl(kk+2)=0.4786286705
        weigpl(kk+3)=0.5688888889
        weigpl(kk+4)=0.4786286705
        weigpl(kk+5)=0.2369268851
       else
        goto 900
       endif
       return
 900   write(6,*)'Specified number of gauss points outside range'
       goto 1000
 1000  write(6,*)'Program terminated'
       stop
       end
```

```
c=======================================================================
c                Function mulvec( )
c     Calculates the dot product of two vectors.
c=======================================================================
      function mulvec(vec1,vec2,ndim)
      integer ndim
      real mulvec
      real vec1(ndim),vec2(ndim)
      integer i
      mulvec=0.0
      do 10 i=1,ndim
       mulvec=mulvec+vec1(i)*vec2(i)
 10   continue
      end
c=======================================================================
c                Subroutine cenoid( )
c     Evaluates the cartesian coordinate set for the centroid of the
c     cross-section as defined by quadrilateral elements.
c=======================================================================
      subroutine cenoid(cenx,ceny,nqc,npc,ngaus,gpx,gpy,gpa)
      integer nqc,npc,ngaus
      real cenx,ceny
      real gpx(nqc*ngaus**2+2*npc),gpy(nqc*ngaus**2+2*npc),
     +     gpa(nqc*ngaus**2+2*npc)
      real areax,areay,area
      integer i
      areax=0.
      areay=0.
      area=0.
      do 10 i=1,nqc*ngaus**2
       areax=areax+gpx(i)*gpa(i)
       areay=areay+gpy(i)*gpa(i)
       area=area+gpa(i)
 10   continue
      cenx=areax/area
      ceny=areay/area
      end
c=======================================================================
c                Subroutine Sect( )
c     Calculates the sections squash load, aPzmax, to within an
c     accuracy of eraPz. For gradually reduced applied axial loads,
c     the biaxial moment capacity, Mx and My, is calculated. The
c     moment capacity is determined to within an error of eraM.
c     Within the iterative procedure the axial load is bound by an
c     error of erPres, and the biaxial residual moment by erMres.
c     Locally defined parameters:
c      dastn = Initial increment for the evaluation of the axial
c              strain at the centroid
c      dkapx = Fixed curvature increment for evaluation of
c              partial derivatives of moments
c      dkapy = Fixed curvature increment for evaluation of
c              partial derivatives of moments
c      tiny  = Numeric zero
c      nimax = Max iterations for detecting strain distribution
c              causing force and moment equilibrium
c=======================================================================
      subroutine Sect(resfil,nmt,nmds,stnmd,maxmd,strmd,gpdim,gpx,
     +               gpy,gpa,gpm,cenx,ceny,daPz0,naPz,eraPz,erPres,
     +               daM0,phi,eraM,erMres)

      character*60 resfil
      integer nmt,maxmd,gpdim,naPz
      integer nmds(nmt),gpm(gpdim)
      real cenx,ceny,daPz0,erPres,daM0,phi,eraM,erMres
      real stnmd(2,nmt),strmd(maxmd,nmt),gpx(gpdim),
     +     gpy(gpdim),gpa(gpdim)
```

```
      logical fsol
      integer ni,nimax
      real astn,astn0,astnj,dastn,kapx,kapx0,kapxj,dkapx,kapy,
     +     kapy0,kapyj,dkapy,daPz,aPz,aPzmax,daM,aMx,aMy,Mx,My,
     +     Mxres,Myres,Mres,MxdxB,MydxB,MxdyB,MydyB,MxdxA,MydxA,
     +     MxdyA,MydyA,dMydx,dMydy,dMxdx,dMxdy,Det,tiny
      integer i
      parameter (dastn= -0.1e-3,
     +           dkapx=  1.e-12,
     +           dkapy=  1.e-12,
     +           tiny =  1.e-50,
     +           nimax=    500)
      write(6,*)
      write(6,*) 'Evaluation of MN-diagram'
      write(6,*)
      fsol=.true.
      astn=0.
      astn0=0.
      kapx=0.
      kapy=0.
      daPz=daPz0
      aPz=0.0
3     if (eraPz.lt.abs(daPz)) then
       call censtn(nmt,nmds,stnmd,maxmd,strmd,gpdim,gpx,gpy,
     +             gpa,gpm,cenx,ceny,aPz,erPres,kapx,kapy,
     +             dastn,astn,fsol)
       if (.not.fsol) then
        daPz=daPz/2.
        aPz=aPz-daPz
        astn=astn0
       else
        astn0=astn
        aPzmax=aPz
        aPz=aPz+daPz
        write(6,820) 'aPzmax=',aPzmax/1.e3,'KN',
     +               'astn=',astn*1.e3,'mm/m'
       endif
       goto 3
      endif
      open(12,file=resfil)
      rewind(12)
      write(12,871) 'aPzmax=',aPzmax/1.e3,'KN'
      write(12,872) 'astn=',astn*1.e3,'mm/m'
      write(12,*)
      call Pforce(nmt,nmds,stnmd,maxmd,strmd,gpdim,gpx,gpy,
     +            gpa,gpm,cenx,ceny,astn,kapx,kapy,Pz)
      call Mforce(nmt,nmds,stnmd,maxmd,strmd,gpdim,gpx,gpy,
     +            gpa,gpm,cenx,ceny,astn,kapx,kapy,Mx,My)
      write(12,873) 'astn','kapx','kapy','aPz','aMx','aMy'
      write(12,874) 'mm/m','1/mm','1/mm','KN','KNm','KNm'
      write(12,875) astn*1.e3,kapx,kapy,Pz/1.e3,
     +              Mx/1.e6,My/1.e6
      do 100 i=1,naPz-1
       astn=0.
       kapx=0.
       kapy=0.
       aPz=aPzmax-real(i)*aPzmax/real(naPz-1)
       if (abs(aPz).lt.erPres) then
        aPz=sign(erPres,aPzmax)
       endif
       call censtn(nmt,nmds,stnmd,maxmd,strmd,gpdim,gpx,gpy,
     +             gpa,gpm,cenx,ceny,aPz,erPres,kapx,kapy,
     +             dastn,astn,fsol)
       if (.not.fsol) then
        goto 1000
       endif
```

```
      astn0=astn
      kapx0=0.
      kapy0=0.
      daM=daM0
      aMx=cos(phi)*daM
      aMy=sin(phi)*daM
      Mxres=aMx
      Myres=aMy
      Mres=abs(daM)
      write(6,*)
5     if (eraM.lt.abs(daM)) then
       ni=0
       if (.not.fsol) then
        fsol=.true.
        astn=astn0
        kapx=kapx0
        kapy=kapy0
        daM=daM/2.
        aMx=aMx-cos(phi)*daM
        aMy=aMy-sin(phi)*daM
        Mxres=cos(phi)*daM
        Myres=sin(phi)*daM
        Mres=abs(daM)
       endif
       write(6,*)
7      if (erMres.lt.Mres) then
        ni=ni+1
        write(6,830) 'aPz=',aPz/1.e3,'KN',
     +               'aMx=',aMx/1.e6,'KNm',
     +               'aMy=',aMy/1.e6,'KNm',
     +               'ni=',ni,
     +               'Mres=',Mres/1.e6,'KNm'
        astnj=astn
        kapxj=kapx+dkapx
        kapyj=kapy
        call censtn(nmt,nmds,stnmd,maxmd,strmd,gpdim,gpx,gpy,
     +              gpa,gpm,cenx,ceny,aPz,erPres,kapxj,kapyj,
     +              dastn,astnj,fsol)
        if (.not.fsol) then
         write(6,*) 'No equilibrium state for incremented x-curvature'
         goto 5
        endif
        call Mforce(nmt,nmds,stnmd,maxmd,strmd,gpdim,gpx,gpy,
     +              gpa,gpm,cenx,ceny,astnj,kapxj,kapyj,
     +              MxdxB,MydxB)
        astnj=astn
        kapxj=kapx-dkapx
        kapyj=kapy
        call censtn(nmt,nmds,stnmd,maxmd,strmd,gpdim,gpx,gpy,
     +              gpa,gpm,cenx,ceny,aPz,erPres,kapxj,kapyj,
     +              dastn,astnj,fsol)
        if (.not.fsol) then
         write(6,*) 'No equilibrium state for decremented x-curvature'
         goto 5
        endif
        call Mforce(nmt,nmds,stnmd,maxmd,strmd,gpdim,gpx,gpy,
     +              gpa,gpm,cenx,ceny,astnj,kapxj,kapyj,
     +              MxdxA,MydxA)
        astnj=astn
        kapxj=kapx
        kapyj=kapy+dkapy
        call censtn(nmt,nmds,stnmd,maxmd,strmd,gpdim,gpx,gpy,
     +              gpa,gpm,cenx,ceny,aPz,erPres,kapxj,kapyj,
     +              dastn,astnj,fsol)
        if (.not.fsol) then
         write(6,*) 'No equilibrium state for incremented y-curvature'
```

```
      goto 5
     endif
     call Mforce(nmt,nmds,stnmd,maxmd,strmd,gpdim,gpx,gpy,
+              gpa,gpm,cenx,ceny,astnj,kapxj,kapyj,
+              MxdyB,MydyB)
     astnj=astn
     kapxj=kapx
     kapyj=kapy-dkapy
     call censtn(nmt,nmds,stnmd,maxmd,strmd,gpdim,gpx,gpy,
+              gpa,gpm,cenx,ceny,aPz,erPres,kapxj,kapyj,
+              dastn,astnj,fsol)
     if (.not.fsol) then
      write(6,*) 'No equilibrium state for decremented y-curvature'
      goto 5
     endif
     call Mforce(nmt,nmds,stnmd,maxmd,strmd,gpdim,gpx,gpy,
+              gpa,gpm,cenx,ceny,astnj,kapxj,kapyj,
+              MxdyA,MydyA)
     dMydx=(MydxB-MydxA)/(2.*dkapx)
     dMydy=(MydyB-MydyA)/(2.*dkapy)
     dMxdx=(MxdxB-MxdxA)/(2.*dkapx)
     dMxdy=(MxdyB-MxdyA)/(2.*dkapy)
     Det=dMydx*dMxdy-dMydy*dMxdx
     If (abs(Det).gt.tiny) then
      kapx=kapx+( dMxdy*Myres-dMydy*Mxres)/Det
      kapy=kapy+(-dMxdx*Myres+dMydx*Mxres)/Det
     else
      fsol=.false.
      write(6,*) 'Stiffness matrix singular'
      goto 5
     endif
     if (ni.gt.nimax) then
      fsol=.false.
      write(6,*) 'Not converged'
      goto 5
     endif
     call censtn(nmt,nmds,stnmd,maxmd,strmd,gpdim,gpx,gpy,
+              gpa,gpm,cenx,ceny,aPz,erPres,kapx,kapy,
+              dastn,astn,fsol)
     if (.not.fsol) then
      write(6,*) 'Load capacity exhausted'
      goto 5
     endif
     call Mforce(nmt,nmds,stnmd,maxmd,strmd,gpdim,gpx,gpy,
+              gpa,gpm,cenx,ceny,astn,kapx,kapy,Mx,My)
     Mxres=aMx-Mx
     Myres=aMy-My
     Mres=sqrt(Mxres**2+Myres**2)
     goto 7
    endif
    astn0=astn
    kapx0=kapx
    kapy0=kapy
    aMy=aMy+sin(phi)*daM
    aMx=aMx+cos(phi)*daM
    Mxres=cos(phi)*daM
    Myres=sin(phi)*daM
    Mres=abs(daM)
    goto 5
   endif
   astn=astn0
   kapx=kapx0
   kapy=kapy0
   call Pforce(nmt,nmds,stnmd,maxmd,strmd,gpdim,gpx,gpy,
+             gpa,gpm,cenx,ceny,astn,kapx,kapy,Pz)
   call Mforce(nmt,nmds,stnmd,maxmd,strmd,gpdim,gpx,gpy,
```

```
     +             gpa,gpm,cenx,ceny,astn,kapx,kapy,Mx,My)
       write(12,875) astn*1.e3,kapx,kapy,Pz/1.e3,
     +               Mx/1.e6,My/1.e6
 100   continue
       close(12)
       return

 820   format(2x,a7,f8.1,a2,2x,a5,f8.3,a4)
 830   format(2x,a4,f8.1,a2,2x,a4,f8.1,a3,2x,a4,f8.1,a3,2x,a3,i4,
     +       2x,a5,f8.3,a3)
 871   format(a7,f10.3,1x,a2)
 872   format(a7,f10.3,1x,a4)
 873   format(5x,a4,5x,a4,7x,a4,8x,a3,7x,a3,8x,a3)
 874   format(5x,a4,5x,a4,7x,a4,9x,a2,7x,a3,8x,a3)
 875   format(f10.3,1x,e10.3,1x,e10.3,1x,f10.3,1x,e10.3,1x,e10.3)
 1000  write(6,*) 'Unexpected program termination'
       stop
       end
c=======================================================================
c                Subroutine censtn( )
c     For a given combination of applied axial load and curvatures,
c     aPz, kapx and kapy, the axial strain at the centre, astn, is
c     iterated until the internal axial load, Pz, equals aPz to
c     within an error of erPres. That is abs(aPz-Pz).lt.erPres.
c     If the solution is non-existent or in-accurate this is flagged
c     by 'fsol' being '.false.'.
c
c     Locally defined parameters:
c      goldm  = Golden ratio for calculating minimum
c      maxstn = Search range limit for bracketing
c      nimax  = Allowed limit for number of iterations
c=======================================================================
       subroutine censtn(nmt,nmds,stnmd,maxmd,strmd,gpdim,gpx,gpy,
     +                   gpa,gpm,cenx,ceny,aPz,erPres,kapx,kapy,
     +                   dastn,astn,fsol)
       logical fsol
       integer nmt,maxmd,gpdim
       integer nmds(nmt),gpm(gpdim)
       real kapx,kapy,cenx,ceny,astn,dastn,aPz,erPres,
     +      astn_a,astn_b,astn_c
       real gpx(gpdim),gpy(gpdim),gpa(gpdim)
       real stnmd(2,nmt),strmd(maxmd,nmt)
       integer ni,nimax
       real maxstn,astn_u,Pz_a,Pz_b,Pz_c,Pz_u,fa,fb,fc,fu,astn_0,
     +      astn_1,astn_2,astn_3,Pz_1,Pz_2,f1,f2,goldm
       real dum
       parameter ( goldm=0.61803399,
     +             maxstn=1.,
     +             nimax= 100)
       astn_a=astn
       astn_b=astn+dastn
       fsol=.true.
       call Pforce(nmt,nmds,stnmd,maxmd,strmd,gpdim,gpx,gpy,
     +             gpa,gpm,cenx,ceny,astn_a,kapx,kapy,Pz_a)
       fa=abs(aPz-Pz_a)
       call Pforce(nmt,nmds,stnmd,maxmd,strmd,gpdim,gpx,gpy,
     +             gpa,gpm,cenx,ceny,astn_b,kapx,kapy,Pz_b)
       fb=abs(aPz-Pz_b)
       if (fb.gt.fa) then
        dum=astn_a
        astn_a=astn_b
        astn_b=dum
        dum=fb
        fb=fa
        fa=dum
        dum=Pz_b
```

```
      Pz_b=Pz_a
      Pz_a=dum
     endif
     astn_c=2.*astn_b-astn_a
     call Pforce(nmt,nmds,stnmd,maxmd,strmd,gpdim,gpx,gpy,
    +            gpa,gpm,cenx,ceny,astn_c,kapx,kapy,Pz_c)
     fc=abs(aPz-Pz_c)
111  if (fb.ge.fc) then
      astn_u=2.*astn_c-astn_b
      if (abs(astn_u).gt.maxstn) then
       write(6,*) 'Strain bracketing failed'
       fsol=.false.
       return
      endif
      call Pforce(nmt,nmds,stnmd,maxmd,strmd,gpdim,gpx,gpy,
    +             gpa,gpm,cenx,ceny,astn_u,kapx,kapy,Pz_u)
      fu=abs(aPz-Pz_u)
      astn_a=astn_b
      astn_b=astn_c
      astn_c=astn_u
      Pz_a=Pz_b
      Pz_b=Pz_c
      Pz_c=Pz_u
      fa=fb
      fb=fc
      fc=fu
      goto 111
     endif
     astn_0=astn_a
     astn_1=astn_b-(1.-goldm)*(astn_b-astn_a)
     astn_2=astn_b
     astn_3=astn_c
     call Pforce(nmt,nmds,stnmd,maxmd,strmd,gpdim,gpx,gpy,
    +            gpa,gpm,cenx,ceny,astn_1,kapx,kapy,Pz_1)
     f1=abs(aPz-Pz_1)
     call Pforce(nmt,nmds,stnmd,maxmd,strmd,gpdim,gpx,gpy,
    +            gpa,gpm,cenx,ceny,astn_2,kapx,kapy,Pz_2)
     f2=abs(aPz-Pz_2)
     ni=0
222  if ((f1.gt.erPres).and.(ni.lt.nimax)) then
      ni=ni+1
      if (f2.lt.f1) then
       astn_0=astn_1
       astn_1=astn_2
       astn_2=goldm*astn_1+(1.-goldm)*astn_3
       Pz_1=Pz_2
       f1=f2
       call Pforce(nmt,nmds,stnmd,maxmd,strmd,gpdim,gpx,gpy,
    +              gpa,gpm,cenx,ceny,astn_2,kapx,kapy,Pz_2)
       f2=abs(aPz-Pz_2)
      else
       astn_3=astn_2
       astn_2=astn_1
       astn_1=goldm*astn_2+(1.-goldm)*astn_0
       Pz_2=Pz_1
       f2=f1
       call Pforce(nmt,nmds,stnmd,maxmd,strmd,gpdim,gpx,gpy,
    +              gpa,gpm,cenx,ceny,astn_1,kapx,kapy,Pz_1)
       f1=abs(aPz-Pz_1)
      endif
      goto 222
     endif
     if (ni.eq.nimax) then
      write(6,*) 'Convergence criteria, erPres, not satisfied'
      fsol=.false.
      return
```

```
      endif
      astn=astn_1
      end
c=======================================================================
c                Subroutine Pforce( )
c     Evaluates the axial force, Pz, corresponding to a strain
c     distribution given by astn, kapx and kapy.
c=======================================================================
      subroutine Pforce(nmt,nmds,stnmd,maxmd,strmd,gpdim,gpx,gpy,
     +                  gpa,gpm,cenx,ceny,astn,kapx,kapy,Pz)
      integer nmt,maxmd,gpdim
      integer nmds(nmt),gpm(gpdim)
      real kapx,kapy,cenx,ceny,astn,Pz
      real gpx(gpdim),gpy(gpdim),gpa(gpdim)
      real stnmd(2,nmt),strmd(maxmd,nmt)
      real stn,str
      integer nmd,matr
      integer i
      Pz=0.
      do 100 i=1,gpdim
       matr=gpm(i)
       nmd=nmds(matr)
       stn=astn+kapx*(gpx(i)-cenx)+kapy*(gpy(i)-ceny)
       call strstn(stn,str,nmd,strmd(1,matr),stnmd(1,matr))
       Pz=Pz+str*gpa(i)
 100  continue
      end
c=======================================================================
c                Subroutine Mforce( )
c     Evaluates the biaxial moments, Mx and My, corresponding to a
c     strain distribution given by astn, kapx and kapy.
c=======================================================================
      subroutine Mforce(nmt,nmds,stnmd,maxmd,strmd,gpdim,gpx,gpy,
     +                  gpa,gpm,cenx,ceny,astn,kapx,kapy,Mx,My)
      integer nmt,maxmd,gpdim
      integer nmds(nmt),gpm(gpdim)
      real cenx,ceny,astn,kapx,kapy,Mx,My
      real gpx(gpdim),gpy(gpdim),gpa(gpdim)
      real stnmd(2,nmt),strmd(maxmd,nmt)
      integer matr,nmd
      real stn,str
      integer i
      Mx=0.
      My=0.
      do 100 i=1,gpdim
       matr=gpm(i)
       nmd=nmds(matr)
       stn=astn+kapx*(gpx(i)-cenx)+kapy*(gpy(i)-ceny)
       call strstn(stn,str,nmd,strmd(1,matr),stnmd(1,matr))
       My=My+str*gpa(i)*(gpx(i)-cenx)
       Mx=Mx+str*gpa(i)*(gpy(i)-ceny)
 100  continue
      end
c=======================================================================
c                Subroutine strstn( )
c     Calculates the stress corresponding to a given value of strain
c     using the look-up table for materials stress-strain behaviour.
c=======================================================================
      subroutine strstn(stn,str,nmd,strmd,stnmd)
      integer nmd
      real stn,str
      real strmd(nmd),stnmd(2)
      real stnA,stnB,dstn,stn1,str1,str2
      integer n1,n2
      stnA=stnmd(1)
      stnB=stnmd(2)
```

```
      if (stnB.gt.stnA) then
       if (stn.le.stnA) then
        str=strmd(1)
        return
       else if (stn.ge.stnB) then
        str=strmd(nmd)
        return
       endif
       dstn=(stnB-stnA)/(nmd-1)
       n1=int((stn-stnA)/dstn)+1
       n2=n1+1
       str1=strmd(n1)
       str2=strmd(n2)
       stn1=stnA+(n1-1)*dstn
       str=str1+(stn-stn1)*(str2-str1)/dstn
      else
       if (stn.ge.stnA) then
        str=strmd(1)
        return
       else if (stn.le.stnB) then
        str=strmd(nmd)
        return
       endif
       dstn=(stnB-stnA)/(nmd-1)
       n1=int((stn-stnA)/dstn)+1
       n2=n1+1
       str1=strmd(n1)
       str2=strmd(n2)
       stn1=stnA+(n1-1)*dstn
       str=str1+(stn-stn1)*(str2-str1)/dstn
      endif
      end
C=======================================================================
```

B.2 COLS - Program for Analysing Slender Columns

Input file

```
*=========================================================================
* SLENDER COLUMN : Title: Saatcioglu, config (3)
*=========================================================================
*  TYPE OF ANALYSIS
*  atype = 1, Ultimate axial load capacity (constant lateral load)
*  atype = 2, Ultimate lateral load factor (constant axial load)
*-------------------------------------------------------------------------
*  atype
AN=======================================================================
     1
*=========================================================================
*  CONTROL PARAMETERS FOR ANALYSIS
*  required data:
*   atype = 1 : lf, daPz0, eraPz, erPz, erdw, select
*   atype = 2 : (aPz, dlf0, erlf, erPz, erdw, select)
*  where:
*   aPz    (KN), Applied axial load
*   daPz0  (KN), Initial axial load increment
*   eraPz  (KN), Accuracy of axial load capacity
*   lf         , Applied load factor for lateral load
*   dlf0       , Initial load factor increment
*   erlf       , Accuracy in lateral load factor
*   erPz   (KN), Convergence criteria for axial load
*   erdw   (mm), Convergence criteria for deflections
*   select     , Station number for which to provide a summary report
*-------------------------------------------------------------------------
*   lf  daPz0  eraPz  erPz  erdw  select
* (aPz   dlf0  erlf   erPz  erdw  select)
CP=======================================================================
   1.0    -5.  .1     .001  .01     9
*=========================================================================
*  PROBLEM SIZE
*  nseg  = Number of column segments
*  nmt   = Number of defined materials
*  maxmd = Max number of data points defining a stress-strain curve
*  ncr   = Number of different cross-sections
*  maxq  = Max number of quadrilateral elements per cross-section
*  maxp  = Max number of point elements per cross-section
*  nPx   = Number of point loads after X-axis
*  nPy   = Number of point loads after Y-axis
*  ngaus = Order of numerical integration
*-------------------------------------------------------------------------
*  nseg  nmt  maxmd  ncr  maxq  maxp  nPx  nPy  ngaus
SZ=======================================================================
    16    4    301    1    24    12     0    0    3
*=========================================================================
*  MATERIAL PROPERTIES
*  Material number, number of data points defining stress-strain curve,
*  strain corresponding to initial stress data, strain corresponding to
*  final stress data. This followed by the stress values corresponding to
*  the equidistant strain values.
*  Repeat for the definition of other materials.
*   5 = C35 unconfined
*   8 = C35 confined (3)
*   9 = reinforcement bars
*  10 = spalled off concrete
*-------------------------------------------------------------------------
*  material   number of    initial  final
*  number     data points  strain   strain
*  ( - )      ( - )        (mm/m)   (mm/m)
```

```
*  stress ...
*  (MPa)
MP==========================================================================
 5  301   0.0  -15.0
   0.00   -1.50   -2.96   -4.36   -5.72   -7.04   -8.31   -9.54  -10.72
 -11.87  -12.97  -14.03  -15.05  -16.03  -16.97  -17.88  -18.74  -19.57
 -20.37  -21.12  -21.84  -22.53  -23.18  -23.80  -24.39  -24.94  -25.46
 -25.95  -26.40  -26.83  -27.23  -27.59  -27.93  -28.23  -28.51  -28.76
 -28.98  -29.18  -29.35  -29.49  -29.60  -29.69  -29.75  -29.79  -29.80
 -29.80  -29.79  -29.77  -29.74  -29.68  -29.60  -29.48  -29.34  -29.16
 -28.94  -28.69  -28.40  -28.07  -27.70  -27.30  -26.86  -26.39  -25.89
 -25.37  -24.82  -24.26  -23.67  -23.08  -22.47  -21.86  -21.24  -20.63
 -20.01  -19.40  -18.80  -18.20  -17.61  -17.04  -16.48  -15.93  -15.39
 -14.88  -14.37  -13.88  -13.41  -12.95  -12.51  -12.08  -11.67  -11.28
 -10.89  -10.53  -10.17   -9.84   -9.51   -9.20   -8.90   -8.61   -8.33
  -8.06   -7.81   -7.56   -7.32   -7.10   -6.88   -6.67   -6.47   -6.27
  -6.09   -5.91   -5.74   -5.57   -5.41   -5.26   -5.11   -4.97   -4.84
  -4.70   -4.58   -4.46   -4.34   -4.23   -4.12   -4.01   -3.91   -3.81
  -3.72   -3.62   -3.54   -3.45   -3.37   -3.29   -3.21   -3.14   -3.06
  -2.99   -2.93   -2.86   -2.80   -2.74   -2.68   -2.62   -2.56   -2.51
  -2.45   -2.40   -2.35   -2.31   -2.26   -2.21   -2.17   -2.13   -2.08
  -2.04   -2.01   -1.97   -1.93   -1.89   -1.86   -1.82   -1.79   -1.76
  -1.73   -1.70   -1.67   -1.64   -1.61   -1.58   -1.55   -1.53   -1.50
  -1.47   -1.45   -1.43   -1.40   -1.38   -1.36   -1.34   -1.31   -1.29
  -1.27   -1.25   -1.23   -1.21   -1.20   -1.18   -1.16   -1.14   -1.13
  -1.11   -1.09   -1.08   -1.06   -1.05   -1.03   -1.02   -1.00   -0.99
  -0.97   -0.96   -0.95   -0.94   -0.92   -0.91   -0.90   -0.89   -0.87
  -0.86   -0.85   -0.84   -0.83   -0.82   -0.81   -0.80   -0.79   -0.78
  -0.77   -0.76   -0.75   -0.74   -0.73   -0.72   -0.71   -0.71   -0.70
  -0.69   -0.68   -0.67   -0.67   -0.66   -0.65   -0.64   -0.64   -0.63
  -0.62   -0.61   -0.61   -0.60   -0.59   -0.59   -0.58   -0.58   -0.57
  -0.56   -0.56   -0.55   -0.55   -0.54   -0.53   -0.53   -0.52   -0.52
  -0.51   -0.51   -0.50   -0.50   -0.49   -0.49   -0.48   -0.48   -0.47
  -0.47   -0.46   -0.46   -0.45   -0.45   -0.45   -0.44   -0.44   -0.43
  -0.43   -0.43   -0.42   -0.42   -0.41   -0.41   -0.41   -0.40   -0.40
  -0.40   -0.39   -0.39   -0.38   -0.38   -0.38   -0.37   -0.37   -0.37
  -0.36   -0.36   -0.36   -0.36   -0.35   -0.35   -0.35   -0.34   -0.34
  -0.34   -0.34   -0.33   -0.33
 8  301   0.0  -15.0
   0.00   -1.50   -2.96   -4.36   -5.72   -7.04   -8.31   -9.53  -10.72
 -11.86  -12.96  -14.02  -15.03  -16.01  -16.96  -17.86  -18.73  -19.56
 -20.36  -21.13  -21.86  -22.56  -23.23  -23.87  -24.49  -25.08  -25.65
 -26.19  -26.71  -27.21  -27.70  -28.16  -28.61  -29.04  -29.45  -29.86
 -30.25  -30.62  -30.99  -31.35  -31.69  -32.03  -32.35  -32.67  -32.98
 -33.29  -33.59  -33.88  -34.16  -34.44  -34.71  -34.98  -35.24  -35.50
 -35.76  -36.01  -36.25  -36.49  -36.73  -36.97  -37.20  -37.43  -37.66
 -37.88  -38.10  -38.32  -38.53  -38.75  -38.96  -39.16  -39.37  -39.58
 -39.78  -39.98  -40.18  -40.37  -40.57  -40.76  -40.96  -41.15  -41.34
 -41.52  -41.71  -41.89  -42.08  -42.26  -42.44  -42.60  -42.62  -42.64
 -42.65  -42.66  -42.67  -42.67  -42.67  -42.67  -42.67  -42.67  -42.67
 -42.66  -42.66  -42.66  -42.66  -42.66  -42.66  -42.65  -42.65  -42.64
 -42.64  -42.63  -42.63  -42.62  -42.62  -42.61  -42.60  -42.59  -42.58
 -42.57  -42.56  -42.55  -42.53  -42.52  -42.50  -42.49  -42.47  -42.45
 -42.44  -42.42  -42.40  -42.38  -42.35  -42.33  -42.31  -42.28  -42.26
 -42.23  -42.20  -42.17  -42.14  -42.11  -42.08  -42.05  -42.02  -41.98
 -41.95  -41.91  -41.87  -41.83  -41.79  -41.75  -41.71  -41.67  -41.63
 -41.58  -41.54  -41.49  -41.44  -41.39  -41.34  -41.29  -41.24  -41.19
 -41.14  -41.08  -41.03  -40.97  -40.91  -40.86  -40.80  -40.74  -40.68
 -40.61  -40.55  -40.49  -40.43  -40.36  -40.29  -40.23  -40.16  -40.09
 -40.02  -39.95  -39.88  -39.81  -39.74  -39.67  -39.60  -39.52  -39.45
 -39.37  -39.30  -39.22  -39.14  -39.06  -38.99  -38.91  -38.83  -38.75
 -38.67  -38.58  -38.50  -38.42  -38.34  -38.25  -38.17  -38.09  -38.00
 -37.92  -37.83  -37.74  -37.66  -37.57  -37.48  -37.40  -37.31  -37.22
 -37.13  -37.04  -36.95  -36.86  -36.78  -36.69  -36.59  -36.50  -36.41
 -36.32  -36.23  -36.14  -36.05  -35.96  -35.87  -35.77  -35.68  -35.59
 -35.50  -35.41  -35.31  -35.22  -35.13  -35.04  -34.94  -34.85  -34.76
```

```
 -34.67  -34.57  -34.48  -34.39  -34.30  -34.20  -34.11  -34.02  -33.93
 -33.83  -33.74  -33.65  -33.56  -33.47  -33.37  -33.28  -33.19  -33.10
 -33.01  -32.92  -32.83  -32.73  -32.64  -32.55  -32.46  -32.37  -32.28
 -32.19  -32.10  -32.01  -31.92  -31.84  -31.75  -31.66  -31.57  -31.48
 -31.39  -31.31  -31.22  -31.13  -31.05  -30.96  -30.87  -30.79  -30.70
 -30.62  -30.53  -30.45  -30.36  -30.28  -30.19  -30.11  -30.03  -29.94
 -29.86  -29.78  -29.70  -29.61
 9  2  -2.52  2.52
   -517.  517.
10  2  -1.  1.
  -0.00  0.00
*===========================================================================
*  ELEMENTS DEFINING CROSS-SECTIONS
*  First line:
*   Cross-section number, number of quadrilateral elements and point elements
*   included in cross-section.
*  Following lines:
*   Description of each quadrilateral element in terms of material number and
*   nodal coordinates. This followed by a description of each point element in
*   terms of material number, coordinate, lumped area, and the material number
*   of the replaced material.
*  Repeat for each cross-section defined.
*---------------------------------------------------------------------------
*  cross  number of  number of
*   sec.   q-elems    p-elems
*  ( - )    ( - )      ( - )
*  material coord.node1 coord.node2 coord.node3 coord.node4
*  number      X     Y     X     Y     X     Y     X     Y
*  ( - )      (mm)  (mm)  (mm)  (mm)  (mm)  (mm)  (mm)  (mm)
*  material coord.node   area  replaced
*  number      X     Y          material
*  ( - )      (mm)  (mm) (mm^2) ( - )
DC===========================================================================
     1        24        12
 5 -105.0  -105.0  -88.8  -105.0  -88.8  -88.8  -105.0  -88.8
 5  -88.8  -105.0   88.8  -105.0   88.8  -88.8   -88.8  -88.8
 5   88.8  -105.0  105.0  -105.0  105.0  -88.8    88.8  -88.8
 5 -105.0   -88.8  -88.8   -88.8  -88.8  -59.2  -105.0  -59.2
 8  -88.8   -88.8   88.8   -88.8   88.8  -59.2   -88.8  -59.2
 5   88.8   -88.8  105.0   -88.8  105.0  -59.2    88.8  -59.2
 5 -105.0   -59.2  -88.8   -59.2  -88.8  -29.6  -105.0  -29.6
 8  -88.8   -59.2   88.8   -59.2   88.8  -29.6   -88.8  -29.6
 5   88.8   -59.2  105.0   -59.2  105.0  -29.6    88.8  -29.6
 5 -105.0   -29.6  -88.8   -29.6  -88.8    0.0  -105.0    0.0
 8  -88.8   -29.6   88.8   -29.6   88.8    0.0   -88.8    0.0
 5   88.8   -29.6  105.0   -29.6  105.0    0.0    88.8    0.0
 5 -105.0     0.0  -88.8     0.0  -88.8   29.6  -105.0   29.6
 8  -88.8     0.0   88.8     0.0   88.8   29.6   -88.8   29.6
 5   88.8     0.0  105.0     0.0  105.0   29.6    88.8   29.6
 5 -105.0    29.6  -88.8    29.6  -88.8   59.2  -105.0   59.2
 8  -88.8    29.6   88.8    29.6   88.8   59.2   -88.8   59.2
 5   88.8    29.6  105.0    29.6  105.0   59.2    88.8   59.2
 5 -105.0    59.2  -88.8    59.2  -88.8   88.8  -105.0   88.8
 8  -88.8    59.2   88.8    59.2   88.8   88.8   -88.8   88.8
 5   88.8    59.2  105.0    59.2  105.0   88.8    88.8   88.8
 5 -105.0    88.8  -88.8    88.8  -88.8  105.0  -105.0  105.0
 5  -88.8    88.8   88.8    88.8   88.8  105.0   -88.8  105.0
 5   88.8    88.8  105.0    88.8  105.0  105.0    88.8  105.0
 9 -80.0  -80.0  100.3  8
 9 -27.0  -80.0  100.3  8
 9  27.0  -80.0  100.3  8
 9  80.0  -80.0  100.3  8
 9 -80.0  -27.0  100.3  8
 9  80.0  -27.0  100.3  8
 9 -80.0   27.0  100.3  8
 9  80.0   27.0  100.3  8
```

```
 9 -80.0   80.0  100.3  8
 9 -27.0   80.0  100.3  8
 9  27.0   80.0  100.3  8
 9  80.0   80.0  100.3  8
*=============================================================================
*  VARIATION OF CROSS SECTION GEOMETRY
*  Cross section number associated with the discrete stations along the member
*  length. If only a single cross-section is defined no data is required in
*  this field as all sections are assumed to be equal. Otherwise, the list
*  must contain all cross-section numbers corresponding to the nseg+1
*  stations, beginning at end1 (Z=0 mm).
*-----------------------------------------------------------------------------
*         cross-section numbers
*   end1             ...            end2
CR=============================================================================
*=============================================================================
*  GEOMETRIC DATA
*  Length of column, and imperfections at mid-length after the X- and Y-axis
*  respectively.
*-----------------------------------------------------------------------------
*  length       imperfections
*   (mm)      X-axis       Y-axis
*              (mm)         (mm)
GD=============================================================================
    1640.        0.           0.
*=============================================================================
*  BOUNDARY CONDITIONS
*  Restraining conditions at column ends for rotation about the X-axis and
*  Y-axis respectively.
*  code = 1  , free to rotate.
*  code = 2  , fully fixed.
*  code = 3  , semi rigid (rotational spring)
*-----------------------------------------------------------------------------
*          end1               end2
*     Y-axis  X-axis     Y-axis  X-axis
BC=============================================================================
        1       1          1       1
*=============================================================================
*  ROTATIONALLY SPRING CONSTANTS
*  Spring constants at column ends for rotation about the X-axis and Y-axis
*  respectively.
*-----------------------------------------------------------------------------
*           end1                 end2
*     Y-axis     X-axis     Y-axis     X-axis
*   (KNm/rad) (KNm/rad) (KNm/rad) (KNm/rad)
KC=============================================================================
*=============================================================================
*  ECCENTRICITY
*  Eccentricity after the X-axis and Y-axis at column ends.
*-----------------------------------------------------------------------------
*       end1            end2
*    ex       ey      ex       ey
*   (mm)     (mm)    (mm)     (mm)
EC=============================================================================
      0.     -75.       0.     -75.
*=============================================================================
*  APPLIED END-MOMENTS
*  Applied moments about the X-axis and Y-axis at column ends.
*-----------------------------------------------------------------------------
*       end1             end2
*    My       Mx      My       Mx
*   (KNm)    (KNm)   (KNm)    (KNm)
AM=============================================================================
     0.0      0.0      0.0      0.0
*=============================================================================
*  POINT LOADS AFTER X-AXIS
```

```
*  Size and position of point loads.
*-------------------------------------------------------------------------------
*    Px        Z
*   (KN)     (mm)
PX=============================================================================
*=============================================================================
*  POINT LOADS AFTER Y-AXIS
*  Size and position of point loads.
*-------------------------------------------------------------------------------
*    Py       Z
*   (KN)     (mm)
PY=============================================================================
*=============================================================================
*  UNIFORMLY DISTRIBUTED LOADS
*  Uniformly distributed loads after the X- and Y-axis respectively.
*-------------------------------------------------------------------------------
*    upx        upy
*   (KN/m)     (KN/m)
PU=============================================================================
     0.0        0.0
*=============================================================================
```

Program COLS

```
************************************************************************
*         Inelastic analysis of columns in biaxial bending.            *
*                          COLS Version 4.2                            *
*                                2001                                  *
************************************************************************
*                        Main Program                                  *
*   nseg  = Number of column segments.                                 *
*   nmt   = Number of material specifiactions.                         *
*   maxmd = Max number of data defining a stress-strain curve.         *
*   ncr   = Number of different cross-sections.                        *
*   maxq  = Max number of quadrilateral elements per cross-section.    *
*   maxp  = Max number of point elements per cross-section.            *
*   nPx   = Number of point loads after X-axis.                        *
*   nPy   = Number of point loads after Y-axis.                        *
*   ngaus = Order of numerical integration.                            *
************************************************************************
      program cols
      integer nseg_,nmt_,maxmd_,ncr_,maxq_,maxp_,nPx_,nPy_,ngaus_
      parameter ( nseg_ = 50,
     +            nmt_  = 25,
     +            maxmd_=500,
     +            ncr_  = 50,
     +            maxq_ =100,
     +            maxp_ =100,
     +            nPx_  = 51,
     +            nPy_  = 51,
     +            ngaus_=  5)
      character*60 datfil,resfil,selfil
      character key*1
      logical fextn,ffile
      integer atype,nseg,nmt,maxmd,ncr,maxq,maxp,nPx,nPy,ngaus,
     +        bcxA,bcyA,bcxB,bcyB,select
      integer lmatr(nmt_),nmds(nmt_),lcrse(ncr_),
     +        nqcs(ncr_),npcs(ncr_),crses(nseg_+1)
      integer melq(maxq_,ncr_),melp(2*maxp_,ncr_),
     +        gpm(maxq_*ngaus_**2+2*maxp_,ncr_)
      real aPz,daPz0,eraPz,lf,dlf0,erlf,erPz,erdw,
     +     lngth,midxi,midyi,exA,eyA,exB,eyB,
     +     aMxA,aMyA,aMxB,aMyB,upx,upy,
     +     kcxA,kcyA,kcxB,kcyB
```

```
      real Px(nPx_),zPx(nPx_),Py(nPy_),zPy(nPy_),
     +     xi(nseg_+1),yi(nseg_+1),fMx(nseg_+1),fMy(nseg_+1),
     +     shape(4*ngaus_**2),dNdxie(4*ngaus_**2),
     +     dNdeta(4*ngaus_**2),eweigp(ngaus_**2),
     +     cenx(nseg_+1),ceny(nseg_+1),
     +     u(nseg_+1),v(nseg_+1),u0(nseg_+1),v0(nseg_+1),
     +     dw(2*nseg_+2),
     +     astn(nseg_+1),astn0(nseg_+1),
     +     kapx(nseg_+1),kapy(nseg_+1),
     +     Mx(nseg_+1),My(nseg_+1),
     +     Mxres(nseg_+1),Myres(nseg_+1),
     +     MxdxB(nseg_+1),MydxB(nseg_+1),
     +     MxdyB(nseg_+1),MydyB(nseg_+1),
     +     MxdxA(nseg_+1),MydxA(nseg_+1),
     +     MxdyA(nseg_+1),MydyA(nseg_+1),
     +     posgpl(ngaus_),weigpl(ngaus_)
      real stnmd(2,nmt_),strmd(maxmd_,nmt_),
     +     xelp(maxp_,ncr_),yelp(maxp_,ncr_),aelp(maxp_,ncr_),
     +     gpx(maxq_*ngaus_**2+2*maxp_,ncr_),
     +     gpy(maxq_*ngaus_**2+2*maxp_,ncr_),
     +     gpa(maxq_*ngaus_**2+2*maxp_,ncr_),
     +     dMdw(2*nseg_+2,2*nseg_+2)
      real xelq(4,maxq_,ncr_),yelq(4,maxq_,ncr_)
      integer k,kk
      write(6,*)
      write(6,*)'************************************************'
      write(6,*)'*                                              *'
      write(6,*)'*   Inelastic analysis of columns in biaxial   *'
      write(6,*)'*                    bending                   *'
      write(6,*)'*                                              *'
      write(6,*)'*              Cols Version 4.2                *'
      write(6,*)'*                    2001                      *'
      write(6,*)'*                                              *'
      write(6,*)'************************************************'
      write(6,*)
5     write(6,*)'Input name of data file'
      write(6,*)
      read(6,810) datfil
      fextn=.false.
      do 10 k=60,4,-1
       if(datfil(k-3:k).eq.'.dat') then
        fextn=.true.
        goto 20
       endif
10    continue
20    if (.not.fextn) then
       write(6,*)'Data file does not contain .dat extension'
       write(6,*)
       goto 5
      endif
      inquire(file=datfil,exist=ffile)
      if (.not.ffile) then
       write(6,*) 'Data file not found'
       write(6,*) 'Retry Yes/No'
       read(6,815) key
       if (key.eq.'Y') then
        goto 5
       else
        goto 1000
       endif
      endif
      kk=index(datfil,'.dat')-1
      resfil=datfil(1:kk)//'.res'
      selfil=datfil(1:kk)//'.sel'
      call storeq(datfil,atype,nseg,nmt,maxmd,ncr,maxq,maxp,
     +            nPx,nPy,ngaus)
```

```
      write(6,*)
      if (atype.eq.1) then
       write(6,*) 'Type of analysis :'
     +          //' Ultimate axial load capacity'
      else if (atype.eq.2) then
       write(6,*) 'Type of analysis :'
     +          //' Ultimate lateral load factor'
      else
       write(6,*) 'Type of analysis :'
     +          //' Unknown'
       goto 1000
      endif
      write(6,*)
      write(6,*)   'Size of problem:'
      write(6,820) 'Number of column segments         ',' =',nseg
      write(6,820) 'Number of defined materials       ',' =',nmt
      write(6,820) 'Max number of material data points',' =',maxmd
      write(6,820) 'Number of cross-section geometries',' =',ncr
      write(6,820) 'Max number of q-elems per section ',' =',maxq
      write(6,820) 'Max number of p-elems per section ',' =',maxp
      write(6,820) 'Number of point loads after X-axis',' =',nPx
      write(6,820) 'Number of point loads after Y-axis',' =',nPy
      write(6,820) 'Order of numerical integration    ',' =',ngaus
      write(6,*)
      if (nseg.gt.nseg_) then
       goto 930
      else if (nmt.gt.nmt_) then
       goto 930
      else if (maxmd.gt.maxmd_) then
       goto 930
      else if (ncr.gt.ncr_) then
       goto 930
      else if (maxq.gt.maxq_) then
       goto 930
      else if (maxp.gt.maxp_) then
       goto 930
      else if (nPx.gt.nPx_) then
       goto 930
      else if (nPy.gt.nPy_) then
       goto 930
      else if (ngaus.gt.ngaus_) then
       goto 930
      endif
      call input(datfil,atype,aPz,daPz0,eraPz,lf,dlf0,erlf,
     +           erPz,erdw,nmt,lmatr,nmds,stnmd,maxmd,strmd,
     +           ncr,lcrse,nqcs,npcs,maxq,melq,xelq,yelq,maxp,
     +           melp,xelp,yelp,aelp,nseg,crses,lngth,midxi,
     +           midyi,bcxA,bcyA,bcxB,bcyB,exA,eyA,exB,eyB,
     +           aMxA,aMyA,aMxB,aMyB,nPx,Px,zPx,nPy,Py,zPy,
     +           upx,upy,xi,yi,fMx,fMy,kcxA,kcyA,kcxB,kcyB,
     +           select)
      call numint(ncr,nqcs,npcs,ngaus,shape,dNdxie,dNdeta,
     +            eweigp,maxq,melq,xelq,yelq,maxp,melp,xelp,
     +            yelp,aelp,gpx,gpy,gpa,gpm,posgpl,weigpl)
      call cenoid(nseg,crses,ncr,nqcs,cenx,ceny,ngaus,maxq,
     +            maxp,gpx,gpy,gpa)
      call outdat(resfil,atype,aPz,daPz0,eraPz,lf,dlf0,erlf,
     +            erPz,erdw,nmt,lmatr,nmds,stnmd,maxmd,
     +            strmd,ncr,lcrse,nqcs,npcs,maxq,melq,xelq,
     +            yelq,maxp,melp,xelp,yelp,aelp,nseg,crses,
     +            lngth,bcxA,bcyA,bcxB,bcyB,exA,eyA,exB,eyB,
     +            aMxA,aMyA,aMxB,aMyB,nPx,Px,zPx,nPy,Py,zPy,
     +            upx,upy,xi,yi,fMx,fMy,ngaus,cenx,ceny,
     +            kcxA,kcyA,kcxB,kcyB,selfil)
      call struct(resfil,atype,bcxA,bcxB,bcyA,bcyB,nmt,nmds,
     +            stnmd,maxmd,strmd,lngth,aPz,daPz0,eraPz,lf,
```

```
     +            dlf0,erlf,erPz,erdw,exA,exB,eyA,eyB,aMxA,
     +            aMxB,aMyA,aMyB,ncr,nqcs,npcs,nseg,crses,xi,
     +            yi,cenx,ceny,fMx,fMy,u,u0,v,v0,dw,astn,
     +            astn0,kapx,kapy,Mx,My,Mxres,Myres,MxdxB,
     +            MydxB,MxdyB,MydyB,MxdxA,MydxA,MxdyA,MydyA,
     +            dMdw,ngaus,maxq,maxp,gpx,gpy,gpa,gpm,kcxA,
     +            kcyA,kcxB,kcyB,select,selfil)
 810  format(a60)
 815  format(a1)
 820  format(2x,a34,a2,i4)
      stop
 930  write(6,*)'Problem too large'
      goto 1000
 1000 write(6,*)'Program terminated'
      stop
      end
c=====================================================================
c                Subroutine storeq( )
c     Reads key parameters governing the computer storage, and checks
c     the presence of required field identifiers.
c=====================================================================
      subroutine storeq(datfil,atype,nseg,nmt,maxmd,ncr,maxq,maxp,
     +                  nPx,nPy,ngaus)
      character*60 datfil
      integer atype,nseg,nmt,maxmd,ncr,maxq,maxp,nPx,nPy,ngaus
      open(12,file=datfil,status='old')
      rewind(12)
      call detect('AN')
      read(12,*,err=900) atype
      call detect('SZ')
      read(12,*,err=910) nseg,nmt,maxmd,ncr,maxq,maxp,nPx,nPy,ngaus
      if (nseg.lt.2) goto 911
      call detect('CP')
      call detect('MP')
      call detect('DC')
      call detect('CR')
      call detect('GD')
      call detect('BC')
      call detect('KC')
      call detect('EC')
      call detect('AM')
      call detect('PX')
      call detect('PY')
      call detect('PU')
      close(12)
      return
 900  write(6,*) 'Format error reading AN field'
      goto 1000
 910  write(6,*) 'Format error reading SZ field'
      goto 1000
 911  write(6,*) 'Error reading AN field, specified nseg invalid'
      goto 1000
 1000 write(6,*) 'Program terminated'
      stop
      end
c=====================================================================
c                Subroutine detect( )
c     Search for a named data field.
c=====================================================================
      subroutine detect(obj)
      character*2 obj,text
      rewind(12)
 121  read(12,'(a2)',end=900) text
      if (text.ne.obj) then
        goto 121
      endif
```

```
      return
  900 write(6,*) 'Numerical field identifier ',obj,' missing'
      write(6,*) 'Program terminated'
      stop
      end
c=======================================================================
c                Subroutine input( )
c     Reads and checks the format of the data file.
c=======================================================================
      subroutine input(datfil,atype,aPz,daPz0,eraPz,lf,dlf0,erlf,
     +                 erPz,erdw,nmt,lmatr,nmds,stnmd,maxmd,strmd,
     +                 ncr,lcrse,nqcs,npcs,maxq,melq,xelq,yelq,maxp,
     +                 melp,xelp,yelp,aelp,nseg,crses,lngth,midxi,
     +                 midyi,bcxA,bcyA,bcxB,bcyB,exA,eyA,exB,eyB,
     +                 aMxA,aMyA,aMxB,aMyB,nPx,Px,zPx,nPy,Py,zPy,
     +                 upx,upy,xi,yi,fMx,fMy,kcxA,kcyA,kcxB,kcyB,
     +                 select)
      character*60 datfil
      integer atype,nmt,maxmd,ncr,maxq,maxp,nseg,
     +        bcxA,bcyA,bcxB,bcyB,nPx,nPy,select
      integer lmatr(nmt),nmds(nmt),lcrse(ncr),
     +        nqcs(ncr),npcs(ncr),crses(nseg+1)
      integer melq(maxq,ncr),melp(2*maxp,ncr)
      real aPz,daPz0,eraPz,lf,dlf0,erlf,erPz,erdw,lngth,
     +     midxi,midyi,exA,eyA,exB,eyB,aMxA,
     +     aMyA,aMxB,aMyB,upx,upy,
     +     kcxA,kcyA,kcxB,kcyB
      real Px(nPx),zPx(nPx),Py(nPy),zPy(nPy),
     +     xi(nseg+1),yi(nseg+1),
     +     fMx(nseg+1),fMy(nseg+1)
      real stnmd(2,nmt),strmd(maxmd,nmt),
     +     xelp(maxp,ncr),yelp(maxp,ncr),aelp(maxp,ncr)
      real xelq(4,maxq,ncr),yelq(4,maxq,ncr)
      integer matr,nmd,crse,nqc,npc
      real pi,FxA,FyA,z
      integer i,j,k
      open(12,file=datfil,status='old')
      rewind(12)
      pi=acos(-1.0)
      do 103 j=1,ncr
       do 102 i=1,maxq
        melq(i,j)=0
  102  continue
       do 101 i=1,2*maxp
        melp(i,j)=0
  101   continue
  103 continue
      do 104 i=1,nseg+1
       crses(i)=1
  104 continue
      call detect('CP')
      if (atype.eq.1) then
       read(12,*,err=905) lf,daPz0,eraPz,erPz,erdw,select
       daPz0=1000.*daPz0
       eraPz=1000.*eraPz
       eraPz=abs(eraPz)
       erPz=1000.*erPz
       erPz=abs(erPz)
       erdw=abs(erdw)
      else if (atype.eq.2) then
       read(12,*,err=905) aPz,dlf0,erlf,erPz,erdw,select
       aPz=1000.*aPz
       erlf=abs(erlf)
       erPz=1000.*erPz
       erPz=abs(erPz)
       erdw=abs(erdw)
```

```
      endif
      call detect('MP')
      do 10 j=1,nmt
       read(12,*,err=910) matr,nmd
       backspace(12)
       read(12,*,err=910) lmatr(j),nmds(j),(stnmd(i,j),i=1,2),
     +                    (strmd(i,j),i=1,nmd)
10    continue
      do 11 j=1,nmt
       stnmd(1,j)=stnmd(1,j)/1000.
       stnmd(2,j)=stnmd(2,j)/1000.
11    continue
      do 13 i=1,nmt
       matr=lmatr(i)
       do 12 j=i+1,nmt
        if (matr.eq.lmatr(j)) then
         goto 912
        endif
12     continue
13    continue
      call detect('DC')
      do 20 k=1,ncr
       read(12,*,err=920) crse,nqc,npc
       lcrse(k)=crse
       nqcs(k)=nqc
       npcs(k)=npc
       read(12,*,err=920) (melq(j,k),(xelq(i,j,k),yelq(i,j,k),i=1,4),
     +                     j=1,nqc)
       read(12,*,err=920) (melp(j,k),xelp(j,k),yelp(j,k),aelp(j,k),
     +                     melp(npc+j,k),j=1,npc)
20    continue
      do 22 i=1,ncr
       crse=lcrse(i)
       do 21 j=i+1,ncr
        if (crse.eq.lcrse(j)) then
         goto 922
        endif
21     continue
22    continue
      do 29 j=1,ncr
       nqc=nqcs(j)
       npc=npcs(j)
       do 24 i=1,nqc
        matr=melq(i,j)
        do 23 k=1,nmt
         if (matr.eq.lmatr(k)) then
          melq(i,j)=k
          goto 24
         endif
23      continue
        goto 924
24     continue
       do 27 i=1,2*npc
        matr=melp(i,j)
        do 26 k=1,nmt
         if (matr.eq.lmatr(k)) then
          melp(i,j)=k
          goto 27
         endif
26      continue
        goto 927
27     continue
29    continue
      call detect('CR')
      if (ncr.gt.1) then
       read(12,*,err=930) (crses(i),i=1,nseg+1)
```

```
      do 32 i=1,nseg+1
       crse=crses(i)
       do 31 j=1,ncr
        if (crse.eq.lcrse(j)) then
         crses(i)=j
         goto 32
        endif
31     continue
       goto 932
32    continue
     endif
     call detect('GD')
     read(12,*,err=935) lngth,midxi,midyi
     xi(1)=0.
     yi(1)=0.
     xi(nseg+1)=0.
     yi(nseg+1)=0.
     do 200 i=2,nseg
      xi(i)=midxi*sin(pi*real(i-1)/real(nseg))
      yi(i)=midyi*sin(pi*real(i-1)/real(nseg))
200  continue
     call detect('BC')
     read(12,*,err=940) bcyA,bcxA,bcyB,bcxB
     if ((bcyA.ne.1).and.(bcyA.ne.2).and.(bcyA.ne.3)) then
      goto 941
     endif
     if ((bcxA.ne.1).and.(bcxA.ne.2).and.(bcxA.ne.3)) then
      goto 941
     endif
     if ((bcyB.ne.1).and.(bcyB.ne.2).and.(bcyB.ne.3)) then
      goto 941
     endif
     if ((bcxB.ne.1).and.(bcxB.ne.2).and.(bcxB.ne.3)) then
      goto 941
     endif
     call detect('KC')
     if ((bcyA.eq.3).or.(bcxA.eq.3).or.
    +    (bcyB.eq.3).or.(bcxB.eq.3)) then
      read(12,*,err=942) kcyA,kcxA,kcyB,kcxB
      kcyA=1.e6*kcyA
      kcxA=1.e6*kcxA
      kcyB=1.e6*kcyB
      kcxB=1.e6*kcxB
     endif
     call detect('EC')
     read(12,*,err=945) exA,eyA,exB,eyB
     call detect('AM')
     read(12,*,err=950) aMyA,aMxA,aMyB,aMxB
     aMxA=1.e6*aMxA
     aMyA=1.e6*aMyA
     aMxB=1.e6*aMxB
     aMyB=1.e6*aMyB
     call detect('PX')
     do 55 i=1,nPx
      read(12,*,err=955) Px(i),zPx(i)
      Px(i)=1000.*Px(i)
55   continue
     do 56 i=1,nPx
      if ((zPx(i).lt.0.0).or.(zPx(i).gt.lngth)) then
       goto 956
      endif
56   continue
     call detect('PY')
     do 60 i=1,nPy
      read(12,*,err=960) Py(i),zPy(i)
      Py(i)=1000.*Py(i)
```

```
60    continue
      do 61 i=1,nPy
       if ((zPy(i).lt.0.0).or.(zPy(i).gt.lngth)) then
        goto 961
       endif
61    continue
      call detect('PU')
      read(12,*,err=965) upx,upy
      FxA=0.
      fMy(1)=0.
      fMy(nseg+1)=0.
      do 220 i=1,nPx
       FxA=FxA+Px(i)*(1.-zPx(i)/lngth)
220   continue
      FxA=FxA+upx*lngth/2.
      do 222 i=2,nseg
       z=lngth*real(i-1)/real(nseg)
       fMy(i)=FxA*z-0.5*upx*z**2
       do 221 j=1,nPx
        if (z.gt.zPx(j)) then
         fMy(i)=fMy(i)-Px(j)*(z-zPx(j))
        endif
221    continue
222   continue
      FyA=0.
      fMx(1)=0.
      fMx(nseg+1)=0.
      do 230 i=1,nPy
       FyA=FyA+Py(i)*(1.-zPy(i)/lngth)
230   continue
      FyA=FyA+upy*lngth/2.
      do 232 i=2,nseg
       z=lngth*real(i-1)/real(nseg)
       fMx(i)=FyA*z-0.5*upy*z**2
       do 231 j=1,nPy
        if (z.gt.zPy(j)) then
         fMx(i)=fMx(i)-Py(j)*(z-zPy(j))
        endif
231    continue
232   continue
      return
905   write(6,*) 'Format error reading AT field'
      goto 1000
910   write(6,*) 'Format error reading line ',i,' of MP field'
      goto 1000
912   write(6,*) 'Material number ',matr,' not unique'
      goto 1000
920   write(6,*) 'Format error reading section ',crse,' of DC field'
      goto 1000
922   write(6,*) 'Cross-section number ',crse,' not unique'
      goto 1000
924   write(6,*) 'Material number ',matr,' not defined'
      goto 1000
927   write(6,*) 'Material number ',matr,' not defined'
      goto 1000
930   write(6,*) 'Format error reading CR field'
      goto 1000
932   write(6,*) 'Cross-section number ',crse,' not defined'
      goto 1000
935   write(6,*) 'Format error reading GD field'
      goto 1000
940   write(6,*) 'Format error reading BC field'
      goto 1000
941   write(6,*) 'Boundary condition not recognised'
      goto 1000
942   write(6,*) 'Format error reading KC field'
```

```
      goto 1000
 945  write(6,*) 'Format error reading EC field'
      goto 1000
 950  write(6,*) 'Format error reading AM field'
      goto 1000
 955  write(6,*) 'Format error reading line ',i,' of PX field'
      goto 1000
 956  write(6,*) 'Load position exceeds columns geometric limits'
      goto 1000
 960  write(6,*) 'Format error reading line ',i,' of PY field'
      goto 1000
 961  write(6,*) 'Load position exceeds columns geometric limits'
      goto 1000
 965  write(6,*) 'Format error reading PU field'
      goto 1000
 1000 write(6,*) 'program terminated'
      stop
      end
c=====================================================================
c                Subroutine numint( )
c     For all the defined cross-sections, evaluates the coordinates
c     of the numerical integration points,the associated integration
c     areas and material numbers. Replaced material is assigned a
c     negative area.
c=====================================================================
      subroutine numint(ncr,nqcs,npcs,ngaus,shape,dNdxie,dNdeta,
     +                  eweigp,maxq,melq,xelq,yelq,maxp,melp,xelp,
     +                  yelp,aelp,gpx,gpy,gpa,gpm,posgpl,weigpl)
      integer ncr,ngaus,maxq,maxp
      integer nqcs(ncr),npcs(ncr)
      integer melq(maxq,ncr),melp(2*maxp,ncr),
     +        gpm(maxq*ngaus**2+2*maxp,ncr)
      real shape(4*ngaus**2),dNdxie(4*ngaus**2),dNdeta(4*ngaus**2),
     +     eweigp(ngaus**2),posgpl(ngaus),weigpl(ngaus)
      real xelp(maxp,ncr),gpx(maxq*ngaus**2+2*maxp,ncr),
     +     yelp(maxp,ncr),gpy(maxq*ngaus**2+2*maxp,ncr),
     +     aelp(maxp,ncr),gpa(maxq*ngaus**2+2*maxp,ncr)
      real xelq(4,maxq,ncr),yelq(4,maxq,ncr)
      integer nqc,npc,matr,elem
      real xie,eta,mulvec,J11,J12,J21,J22,detJ
      integer i,ii,ii1,j,jj,nn,k,kk
      call gaussl(ngaus,posgpl,weigpl)
      nn=0
      kk=0
      do 15 i=1,ngaus
       do 10 j=1,ngaus
        xie=posgpl(i)
        eta=posgpl(j)
        shape(kk+1)= 0.25*(1-xie)*(1-eta)
        shape(kk+2)= 0.25*(1+xie)*(1-eta)
        shape(kk+3)= 0.25*(1+xie)*(1+eta)
        shape(kk+4)= 0.25*(1-xie)*(1+eta)
        dNdxie(kk+1)=-0.25*(1-eta)
        dNdxie(kk+2)= 0.25*(1-eta)
        dNdxie(kk+3)= 0.25*(1+eta)
        dNdxie(kk+4)=-0.25*(1+eta)
        dNdeta(kk+1)=-0.25*(1-xie)
        dNdeta(kk+2)=-0.25*(1+xie)
        dNdeta(kk+3)= 0.25*(1-xie)
        dNdeta(kk+4)= 0.25*(1+xie)
        kk=kk+4
        eweigp(nn+1)=weigpl(i)*weigpl(j)
        nn=nn+1
 10    continue
 15   continue
      elem=0
```

```
      do 40 k=1,ncr
       nqc=nqcs(k)
       npc=npcs(k)
       do 35 j=1,nqc
        elem=elem+1
        matr=melq(j,k)
        jj=ngaus**2*(j-1)
        do 30 i=1,ngaus**2
         ii=4*(i-1)
         ii1=ii+1
         gpx(jj+i,k)=mulvec(shape(ii1),xelq(1,j,k),4)
         gpy(jj+i,k)=mulvec(shape(ii1),yelq(1,j,k),4)
         J11=mulvec(dNdxie(ii1),xelq(1,j,k),4)
         J12=mulvec(dNdxie(ii1),yelq(1,j,k),4)
         J21=mulvec(dNdeta(ii1),xelq(1,j,k),4)
         J22=mulvec(dNdeta(ii1),yelq(1,j,k),4)
         detJ= J11*J22-J12*J21
         if (detJ.le.0.0) goto 910
         gpa(jj+i,k)=detJ*eweigp(i)
         gpm(jj+i,k)=matr
 30     continue
 35    continue
       jj=nqc*ngaus**2
       do 25 j=1,npc
        gpx(jj+j,k)=xelp(j,k)
        gpy(jj+j,k)=yelp(j,k)
        gpa(jj+j,k)=aelp(j,k)
        gpm(jj+j,k)=melp(j,k)
        gpx(jj+npc+j,k)=xelp(j,k)
        gpy(jj+npc+j,k)=yelp(j,k)
        gpa(jj+npc+j,k)=-aelp(j,k)
        gpm(jj+npc+j,k)=melp(npc+j,k)
 25    continue
 40   continue
      return
 910  write(6,*) 'Incorrect geometry of quadrilateral element',elem
      goto 1000
 1000 write(6,*) 'program terminated'
      stop
      end
c=====================================================================
c                Subroutine gaussl( )
c     Sets numerical integration constants for exact integration of a
c     polynomium of degree 2*ngaus-1 over an interval -1 to 1.
c=====================================================================
      subroutine gaussl(ngaus,posgpl,weigpl)
      integer ngaus,kk
      real  posgpl(ngaus),weigpl(ngaus)
      kk=0
      if (ngaus.eq.1) then
       posgpl(kk+1)=0.0
       weigpl(kk+1)=2.0
      else if (ngaus.eq.2) then
       posgpl(kk+1)=-0.5773502692
       posgpl(kk+2)=0.5773502692
       weigpl(kk+1)=1.0
       weigpl(kk+2)=1.0
      else if (ngaus.eq.3) then
       posgpl(kk+1)=-0.7745966692
       posgpl(kk+2)=0.0
       posgpl(kk+3)=0.7745966692
       weigpl(kk+1)=0.5555555556
       weigpl(kk+2)=0.8888888889
       weigpl(kk+3)=0.5555555556
      else if (ngaus.eq.4) then
       posgpl(kk+1)=-0.8611363116
```

```
       posgpl(kk+2)=-0.3399810436
       posgpl(kk+3)=0.3399810436
       posgpl(kk+4)=0.8611363116
       weigpl(kk+1)=0.3478548451
       weigpl(kk+2)=0.6521451549
       weigpl(kk+3)=0.6521451549
       weigpl(kk+4)=0.3478548451
      else if (ngaus.eq.5) then
       posgpl(kk+1)=-0.9061798459
       posgpl(kk+2)=-0.5384693101
       posgpl(kk+3)=0.0
       posgpl(kk+4)=0.5384693101
       posgpl(kk+5)=0.9061798459
       weigpl(kk+1)=0.2369268851
       weigpl(kk+2)=0.4786286705
       weigpl(kk+3)=0.5688888889
       weigpl(kk+4)=0.4786286705
       weigpl(kk+5)=0.2369268851
      else
       goto 900
      endif
      return
 900  write(6,*)'Specified number of gauss points outside range'
      goto 1000
 1000 write(6,*)'Program terminated'
      stop
      end
c=======================================================================
c                Function mulvec( )
c     Calculates the dot product of two vectors.
c=======================================================================
      function mulvec(vec1,vec2,ndim)
      integer ndim
      real mulvec
      real vec1(ndim),vec2(ndim)
      integer i
      mulvec=0.0
      do 10 i=1,ndim
       mulvec=mulvec+vec1(i)*vec2(i)
 10   continue
      end
c=======================================================================
c                Subroutine cenoid( )
c     Evaluates the cartesian coordinates x and y of the gravitational
c     centre at the nseg+1 stations along the member length.
c=======================================================================
      subroutine cenoid(nseg,crses,ncr,nqcs,cenx,ceny,ngaus,maxq,
     +                  maxp,gpx,gpy,gpa)
      integer nseg,ncr,ngaus,maxq,maxp
      integer crses(nseg+1),nqcs(ncr)
      real cenx(nseg+1),ceny(nseg+1)
      real gpx(maxq*ngaus**2+2*maxp,ncr),
     +     gpy(maxq*ngaus**2+2*maxp,ncr),
     +     gpa(maxq*ngaus**2+2*maxp,ncr)
      integer nqc
      real areax,areay,area
      integer j,i
      do 20 j=1,ncr
       nqc=nqcs(j)
       areax=0.
       areay=0.
       area=0.
       do 10 i=1,nqc*ngaus**2
        areax=areax+gpx(i,j)*gpa(i,j)
        areay=areay+gpy(i,j)*gpa(i,j)
        area=area+gpa(i,j)
```

```
10    continue
      do 15 i=1,nseg+1
       if (j.eq.crses(i)) then
        cenx(i)=areax/area
        ceny(i)=areay/area
       endif
15    continue
20    continue
      end
c=====================================================================
c                Subroutine outdat( )
c     Writes the pre-analysis data to the output file.
c=====================================================================
      subroutine outdat(resfil,atype,aPz,daPz0,eraPz,lf,dlf0,erlf,
     +                  erPz,erdw,nmt,lmatr,nmds,stnmd,maxmd,
     +                  strmd,ncr,lcrse,nqcs,npcs,maxq,melq,xelq,
     +                  yelq,maxp,melp,xelp,yelp,aelp,nseg,crses,
     +                  lngth,bcxA,bcyA,bcxB,bcyB,exA,eyA,exB,eyB,
     +                  aMxA,aMyA,aMxB,aMyB,nPx,Px,zPx,nPy,Py,zPy,
     +                  upx,upy,xi,yi,fMx,fMy,ngaus,cenx,ceny,
     +                  kcxA,kcyA,kcxB,kcyB,selfil)
      character*60 resfil,selfil
      integer atype,nmt,maxmd,ncr,maxq,maxp,nseg,
     +        bcxA,bcyA,bcxB,bcyB,nPx,nPy,ngaus
      integer lmatr(nmt),nmds(nmt),lcrse(ncr),nqcs(ncr),npcs(ncr),
     +        crses(nseg+1),melq(maxq,ncr),melp(2*maxp,ncr)
      real aPz,daPz0,eraPz,lf,dlf0,erlf,erPz,erdw,lngth,
     +     exA,eyA,exB,eyB,aMxA,aMyA,aMxB,aMyB,upx,upy,
     +     kcxA,kcyA,kcxB,kcyB
      real Px(nPx),zPx(nPx),Py(nPy),zPy(nPy),xi(nseg+1),yi(nseg+1),
     +     fMx(nseg+1),fMy(nseg+1),cenx(nseg+1),ceny(nseg+1)
      real stnmd(2,nmt),strmd(maxmd,nmt),xelp(maxp,ncr),
     +     yelp(maxp,ncr),aelp(maxp,ncr)
      real xelq(4,maxq,ncr),yelq(4,maxq,ncr)
      integer matr,nmd,matr1,matr2,crse,nqc,npc
      real z,stnA,stnB,stn,dstn,str
      integer i,j,k,kk
      open(12,file=resfil)
      rewind(12)
      write(12,*)
      write(12,805)'*****************************************************'
      write(12,805)'*                                                   *'
      write(12,805)'*   Inelastic analysis of columns in biaxial        *'
      write(12,805)'*                    bending                        *'
      write(12,805)'*                                                   *'
      write(12,805)'*              Cols Version 4.2                     *'
      write(12,805)'*                    2001                           *'
      write(12,805)'*                                                   *'
      write(12,805)'*****************************************************'
      write(12,*)
      write(12,*)
      if (atype.eq.1) then
       write(12,*) 'ANALYSIS OF ULTIMATE AXIAL LOAD CAPACITY'
      else if (atype.eq.2) then
       write(12,*) 'ANALYSIS OF ULTIMATE LATERAL LOAD FACTOR'
      endif
      write(12,810) 'FILE :',resfil
      write(12,*)
      write(12,*)
      write(12,*) '=================='
      write(12,*) 'CONTROL PARAMETERS'
      write(12,*) '=================='
      write(12,*)
      write(12,815) 'Number of column segments             =',
     +              nseg
      write(12,815) 'Order of numerical integration        =',
```

```
     +               ngaus
      if (atype.eq.1) then
       write(12,816) 'Lateral load factor                    =',
     +               lf,'  '
       write(12,816) 'Largest axial load increment          =',
     +               daPz0/1000.,'KN'
       write(12,817) 'Accuracy of axial load capacity       =',
     +               eraPz/1000.,'KN'
       write(12,817) 'Convergence criteria for axial load   =',
     +               erPz/1000.,'KN'
       write(12,817) 'Convergence criteria for deflections  =',
     +               erdw,'mm'
      else if (atype.eq.2) then
       write(12,816) 'Applied axial load                    =',
     +               aPz/1000.,'KN'
       write(12,816) 'Largest lateral load factor increment =',
     +               dlf0,'  '
       write(12,817) 'Accuaracy for lateral load factor     =',
     +               erlf,'  '
       write(12,817) 'Convergence criteria for axial load   =',
     +               erPz/1000.,'KN'
       write(12,817) 'Convergence criteria for deflections  =',
     +               erdw,'mm'
      endif
      write(12,*)
      write(12,*)
      write(12,*)'===================='
      write(12,*)'MATERIAL PROPERTIES'
      write(12,*)'===================='
      do 20 j=1,nmt
       matr=lmatr(j)
       nmd=nmds(j)
       stnA=stnmd(1,j)*1000.
       stnB=stnmd(2,j)*1000.
       dstn=(stnB-stnA)/(nmd-1)
       write(12,*)
       write(12,820)'MATERIAL No.=',matr
       write(12,*)
       write(12,821)'STRAIN (mm/m)','STRESS (MPa)'
       do 22 i=1,nmd
        stn=stnA+(i-1)*dstn
        str=strmd(i,j)
        write(12,822) stn,str
22    continue
20    continue
      write(12,*)
      write(12,*)
      write(12,*)'=================='
      write(12,*)'CROSS SECTION DATA'
      write(12,*)'=================='
      write(12,*)
      do 30 k=1,ncr
       crse=lcrse(k)
       nqc=nqcs(k)
       npc=npcs(k)
       write(12,830)'CROSS SECTION No.=',crse
       write(12,*)
       do 32 j=1,nqc
        kk=melq(j,k)
        matr=lmatr(kk)
        write(12,831)'ELEMENT No.=',j,'MATERIAL No.=',matr
        write(12,*)
        write(12,832)'NODE','X (mm)','Y (mm)'
        write(12,833)(i,xelq(i,j,k),yelq(i,j,k),i=1,4)
        write(12,*)
32     continue
```

```
      if (npc.gt.0) then
       write(12,834)'POINT ELEMENTS'
       write(12,835) 'MATERIAL'
       write(12,836)'No.','X (mm)','Y (mm)','AREA (mm^2)','PRO',
     +              'ANTI'
       do 34 j=1,npc
        kk=melp(j,k)
        matr1=lmatr(kk)
        kk=melp(npc+j,k)
        matr2=lmatr(kk)
        write(12,837)j,xelp(j,k),yelp(j,k),aelp(j,k),matr1,
     +               matr2
34     continue
      endif
      write(12,*)
30    continue
      write(12,*)
      write(12,*)'=============='
      write(12,*)'GEOMETRIC DATA'
      write(12,*)'=============='
      write(12,*)
      write(12,840) 'LENGTH OF COLUMN =',lngth,'mm'
      write(12,*)
      write(12,841) 'STATION','POSITON','CROSS','CENTRE',
     +              'IMPERFECTIONS'
      write(12,842) 'Z (mm)','SECTION','X (mm)','Y (mm)',
     +              'dX (mm)','dY (mm)'
      do 40 i=1,nseg+1
       z=lngth*real(i-1)/real(nseg)
       kk=crses(i)
       crse=lcrse(kk)
       write(12,843) i,z,crse,cenx(i),ceny(i),xi(i),yi(i)
40    continue
      write(12,*)
      write(12,*)
      write(12,*)'==================='
      write(12,*)'BOUNDARY CONDITIONS'
      write(12,*)'==================='
      write(12,*)
      if (bcyA.eq.1) then
       write(12,*) 'END 1 : FREE TO ROTATE ABOUT Y-AXIS'
      else if (bcyA.eq.2) then
       write(12,*) 'END 1 : FIXED AGAINST ROTATION ABOUT Y-AXIS'
      else if (bcyA.eq.3) then
       write(12,*) 'END 1 : FLEXIBLE AGAINST ROTATION ABOUT Y-AXIS'
       write(12,847) '        SPRING CONSTANT =',kcyA/1.e6,'KNm/rad'
      endif
      if (bcxA.eq.1) then
       write(12,*) 'END 1 : FREE TO ROTATE ABOUT X-AXIS'
      else if (bcxA.eq.2) then
       write(12,*) 'END 1 : FIXED AGAINST ROTATION ABOUT X-AXIS'
      else if (bcxA.eq.3) then
       write(12,*) 'END 1 : FLEXIBLE AGAINST ROTATION ABOUT X-AXIS'
       write(12,847) '        SPRING CONSTANT =',kcxA/1.e6,'KNm/rad'
      endif
      if (bcyB.eq.1) then
       write(12,*) 'END 2 : FREE TO ROTATE ABOUT Y-AXIS'
      else if (bcyB.eq.2) then
       write(12,*) 'END 2 : FIXED AGAINST ROTATION ABOUT Y-AXIS'
      else if (bcyB.eq.3) then
       write(12,*) 'END 2 : FLEXIBLE AGAINST ROTATION ABOUT Y-AXIS'
       write(12,847) '        SPRING CONSTANT =',kcyB/1.e6,'KNm/rad'
      endif
      if (bcxB.eq.1) then
       write(12,*) 'END 2 : FREE TO ROTATE ABOUT X-AXIS'
      else if (bcxB.eq.2) then
```

```
      write(12,*) 'END 2 : FIXED AGAINST ROTATION ABOUT X-AXIS'
     else if (bcxB.eq.3) then
      write(12,*) 'END 2 : FLEXIBLE AGAINST ROTATION ABOUT X-AXIS'
      write(12,847) '        SPRING CONSTANT =',kcxB/1.e6,'KNm/rad'
     endif
     write(12,*)
     write(12,*)
     write(12,*)'============'
     write(12,*)'LOADING DATA'
     write(12,*)'============'
     write(12,*)
     write(12,850) 'AXIAL LOAD                                '
     write(12,850) 'END 1 : ECCENTRICITY AFTER X-AXIS      =',
    +              exA,'mm'
     write(12,850) 'END 1 : ECCENTRICITY AFTER Y-AXIS      =',
    +              eyA,'mm'
     write(12,850) 'END 2 : ECCENTRICITY AFTER X-AXIS      =',
    +              exB,'mm'
     write(12,850) 'END 2 : ECCENTRICITY AFTER Y-AXIS      =',
    +              eyB,'mm'
     write(12,*)
     write(12,851) 'END 1 : APPLIED MOMENT ABOUT Y-AXIS    =',
    +              aMyA/1.e6,'KNm'
     write(12,851) 'END 1 : APPLIED MOMENT ABOUT X-AXIS    =',
    +              aMxA/1.e6,'KNm'
     write(12,851) 'END 2 : APPLIED MOMENT ABOUT Y-AXIS    =',
    +              aMyB/1.e6,'KNm'
     write(12,851) 'END 2 : APPLIED MOMENT ABOUT X-AXIS    =',
    +              aMxB/1.e6,'KNm'
     write(12,*)
     write(12,*) 'LATERAL LOADING AFTER X-AXIS'
     write(12,860) 'UNIFORMLY DISTRIBUTED LOAD            =',
    +              upx,'KN/m'
     if (nPx.gt.0) then
      write(12,861) 'POINT LOADS : ','LOAD (KN)','Z (mm)'
      write(12,862) (Px(i)/1000.,zPx(i),i=1,nPx)
     endif
     write(12,*)
     write(12,*) 'LATERAL LOADING AFTER Y-AXIS'
     write(12,860) 'UNIFORMLY DISTRIBUTED LOAD            =',
    +              upy,'KN/m'
     if (nPy.gt.0) then
      write(12,861) 'POINT LOADS : ','LOAD (KN)','Z (mm)'
      write(12,862) (Py(i)/1000.,zPy(i),i=1,nPy)
     endif
     write(12,*)
     write(12,*) 'FREE BENDING MOMENTS DUE TO LATERAL LOADING'
     write(12,863) 'STATION','POSITON','CROSS','MOMENTS'
     write(12,864) 'Z (mm)','SECTION','MY (KNm)','MX (KNm)'
     do 60 i=1,nseg+1
      z=lngth*real(i-1)/real(nseg)
      kk=crses(i)
      crse=lcrse(kk)
      write(12,865) i,z,crse,fMy(i)/1.e6,fMx(i)/1.e6
60   continue
     close(12)
     open(13,file=selfil)
     rewind(13)
     write(13,901)'STA','aPz',' u',' v',' My','Myres',' Mx','Mxres',
    +             'astn','kapx','kapy'
     write(13,901)' * ',' KN','mm','mm','KNm',' KNm ','KNm',' KNm ',
    +             'mm/m',' *  ',' *  '
     write(13,*)
     close(13)
805  format(10x,a48)
810  format(1x,a6,1x,a60)
```

```
 815  format(1x,a40,1x,i6)
 816  format(1x,a40,1x,f10.3,1x,a2)
 817  format(1x,a40,1x,e10.3,1x,a2)
 820  format(1x,a13,1x,i2)
 821  format(2x,a13,2x,a12)
 822  format(1x,f10.2,5x,f10.2)
 830  format(1x,a18,1x,i3)
 831  format(2x,a12,1x,i3,5x,a13,1x,i3)
 832  format(3x,a4,5x,a6,6x,a6)
 833  format(4x,i1,2x,f10.3,2x,f10.3)
 834  format(2x,a14)
 836  format(3x,a3,6x,a6,6x,a6,2x,a11,3x,a3,2x,a4)
 835  format(46x,a8)
 837  format(3x,i2,2x,f10.3,2x,f10.3,1x,f10.3,4x,i4,2x,i4)
 840  format(1x,a18,1x,f10.0,1x,a2)
 841  format(1x,a7,1x,a7,3x,a5,8x,a6,11x,a14)
 842  format(10x,a6,2x,a7,2x,a6,5x,a6,4x,a7,4x,a7)
 843  format(2x,i3,1x,f10.0,3x,i3,1x,f10.3,1x,f10.3,
     +       1x,f10.3,1x,f10.3)
 847  format(1x,a25,1x,f10.3,1x,a7)
 850  format(1x,a40,1x,f10.3,1x,a2)
 851  format(1x,a40,1x,f10.3,1x,a3)
 860  format(2x,a39,1x,f10.3,1x,a4)
 861  format(2x,a13,1x,a9,5x,a6)
 862  format(14x,f10.3,2x,f10.3)
 863  format(2x,a7,3x,a7,3x,a5,9x,a8)
 864  format(13x,a6,2x,a7,3x,a8,4x,a8)
 865  format(3x,i3,3x,f10.0,3x,i3,3x,f10.3,2x,f10.3)
 901  format(1x,a3,6x,a3,10x,a2,10x,a2,8x,a3,9x,a5,
     +       7x,a3,8x,a5,11x,a4,6x,a4,8x,a4)
      end
c=======================================================================
c                Subroutine outres( )
c     Streams data during the analysis to the output file.
c=======================================================================
      subroutine outres(resfil,aPz,lf,ashort,bshort,nseg,u,v,My,Mx,
     +                  Myres,Mxres,kapx,kapy,astn,select,selfil)
      character*60 resfil,selfil
      integer nseg,select
      real aPz,lf,ashort,bshort
      real u(nseg+1),v(nseg+1),My(nseg+1),Mx(nseg+1),Myres(nseg+1),
     +     Mxres(nseg+1),kapx(nseg+1),kapy(nseg+1),astn(nseg+1)
      integer i
      open(12,file=resfil,status='append')
      write(12,*)
      write(12,*)'================================================='//
     +           '==================='
      write(12,*)
      write(12,810)'Axial load','=',aPz/1000.,'KN'
      write(12,811)'Load factor','=',lf
      write(12,812)'Axial displacement','=',ashort,'mm'
      write(12,813)'Relative displacement of ends','=',bshort,'mm'
      write(12,*)
      write(12,815)'STATION','u (mm)','My (KNm)','Myres (KNm)',
     +             'astn (mm/m)','kapx (1/mm)'
      write(12,820) 1,0.,My(1)/1.e6,Myres(1)/1.e6,1000.*astn(1),
     +              kapx(1)
      write(12,820)(i,u(i),My(i)/1.e6,Myres(i)/1.e6,1000.*astn(i),
     +              kapx(i),i=2,nseg)
      write(12,820) nseg+1,0.,My(nseg+1)/1.e6,Myres(nseg+1)/1.e6,
     +              1000.*astn(nseg+1),kapx(nseg+1)
      write(12,*)
      write(12,815)'STATION','v (mm)','Mx (KNm)','Mxres (KNm)',
     +             'astn (mm/m)','kapy (1/mm)'
      write(12,820) 1,0.,Mx(1)/1.e6,Mxres(1)/1.e6,1000.*astn(1),
     +              kapy(1)
```

```
      write(12,820)(i,v(i),Mx(i)/1.e6,Mxres(i)/1.e6,1000.*astn(i),
     +             kapy(i),i=2,nseg)
      write(12,820) nseg+1,0.,Mx(nseg+1)/1.e6,Mxres(nseg+1)/1.e6,
     +             1000.*astn(nseg+1),kapy(nseg+1)
      close(12)
      open(13,file=selfil,status='append')
      if ((select.gt.1).and.(select.lt.(nseg+1))) then
       write(13,901) select,aPz/1000.,u(select),v(select),
     +               My(select)/1.e6,Myres(select)/1.e6,Mx(select)/1.e6,
     +               Mxres(select)/1.e6,1000.*astn(select),
     +               kapx(select),kapy(select)
      else if ((select.eq.1).or.(select.eq.(nseg+1))) then
       write(13,901) select,aPz/1000.,0.0,0.0,
     +               My(select)/1.e6,Myres(select)/1.e6,Mx(select)/1.e6,
     +               Mxres(select)/1.e6,1000.*astn(select),
     +               kapx(select),kapy(select)
      endif
      close(13)
 810  format(1x,a10,20x,a1,1x,f10.3,1x,a2)
 811  format(1x,a11,19x,a1,1x,f10.3)
 812  format(1x,a18,12x,a1,1x,f10.3,1x,a2)
 813  format(1x,a29,1x,a1,1x,f10.3,1x,a2)
 815  format(1x,a7,5x,a6,3x,a8,2x,a11,2x,a11,2x,a11)
 820  format(2x,i3,3x,f10.3,2x,e10.3,2x,e10.3,1x,f10.3,5x,e10.3)
 901  format(i3,2x,f10.3,2x,f10.3,2x,f10.3,4x,e10.3,2x,e10.3,2x,
     +       e10.3,2x,e10.3,2x,f10.3,2x,e10.3,2x,e10.3)
      end
c=======================================================================
c               Subroutine struct( )
c     Controls incrementation of the external load. If an equilibrium
c     state corresponding to the current external load cannot be
c     established (flagged by 'fsol') the increment is halved and
c     the procedure is repeated. The procedure terminates when the
c     load increment is reduced to a user specified tolerance 'eraPz'
c     or 'erlf', depending on the type of analysis.
c=======================================================================
      subroutine struct(resfil,atype,bcxA,bcxB,bcyA,bcyB,nmt,nmds,
     +                  stnmd,maxmd,strmd,lngth,aPz,daPz0,eraPz,lf,
     +                  dlf0,erlf,erPz,erdw,exA,exB,eyA,eyB,aMxA,
     +                  aMxB,aMyA,aMyB,ncr,nqcs,npcs,nseg,crses,xi,
     +                  yi,cenx,ceny,fMx,fMy,u,u0,v,v0,dw,astn,
     +                  astn0,kapx,kapy,Mx,My,Mxres,Myres,MxdxB,
     +                  MydxB,MxdyB,MydyB,MxdxA,MydxA,MxdyA,MydyA,
     +                  dMdw,ngaus,maxq,maxp,gpx,gpy,gpa,gpm,kcxA,
     +                  kcyA,kcxB,kcyB,select,selfil)
      character*60 resfil,selfil
      integer atype,bcxA,bcxB,bcyA,bcyB,nmt,maxmd,ncr,nseg,
     +        ngaus,maxq,maxp,select
      integer nmds(nmt),nqcs(ncr),npcs(ncr),crses(nseg+1)
      integer gpm(maxq*ngaus**2+2*maxp,ncr)
      real lngth,aPz,daPz0,eraPz,lf,dlf0,erlf,erPz,erdw,exA,exB,
     +     eyA,eyB,aMxA,aMxB,aMyA,aMyB,kcxA,kcyA,kcxB,kcyB
      real stnmd(2,nmt),strmd(maxmd,nmt),xi(nseg+1),yi(nseg+1),
     +     cenx(nseg+1),ceny(nseg+1),fMx(nseg+1),fMy(nseg+1),
     +     u(nseg+1),u0(nseg+1),v(nseg+1),v0(nseg+1),dw(2*nseg+2),
     +     astn(nseg+1),astn0(nseg+1),kapx(nseg+1),kapy(nseg+1),
     +     Mx(nseg+1),My(nseg+1),Mxres(nseg+1),Myres(nseg+1),
     +     MxdxB(nseg+1),MydxB(nseg+1),
     +     MxdyB(nseg+1),MydyB(nseg+1),
     +     MxdxA(nseg+1),MydxA(nseg+1),
     +     MxdyA(nseg+1),MydyA(nseg+1),
     +     gpx(maxq*ngaus**2+2*maxp,ncr),
     +     gpy(maxq*ngaus**2+2*maxp,ncr),
     +     gpa(maxq*ngaus**2+2*maxp,ncr),
     +     dMdw(2*nseg+2,2*nseg+2)
      logical fsol
```

```
      real daPz,dlf,dz,sqrdz,ashort,bshort
      integer i
      daPz=daPz0
      dlf=dlf0
      do 10 i=1,nseg+1
       u(i)=0.0
       v(i)=0.0
       astn(i)=0.0
10    continue
      dz=lngth/real(nseg)
      sqrdz=dz**2
      if (atype.eq.1) then
       aPz=0.
3      if (eraPz.lt.abs(daPz)) then
        write(6,*)
        write(6,810) 'aPz=',aPz/1.e3,'KN'
        fsol=.true.
        call profil(bcxA,bcxB,bcyA,bcyB,nmt,nmds,stnmd,maxmd,
     +              strmd,lngth,aPz,erPz,erdw,exA,exB,eyA,eyB,
     +              lf,aMxA,aMxB,aMyA,aMyB,ncr,nqcs,npcs,nseg,
     +              crses,xi,yi,cenx,ceny,fMx,fMy,u,v,dw,astn,
     +              kapx,kapy,Mx,My,Mxres,Myres,MxdxB,MydxB,
     +              MxdyB,MydyB,MxdxA,MydxA,MxdyA,MydyA,dMdw,
     +              ngaus,maxq,maxp,gpx,gpy,gpa,gpm,fsol,
     +              kcxA,kcyA,kcxB,kcyB)
        if (.not.fsol) then
         do 110 i=1,nseg+1
          u(i)=u0(i)
          v(i)=v0(i)
          astn(i)=astn0(i)
110      continue
         daPz=daPz/2.
         aPz=aPz-daPz
         goto 3
        endif
        ashort=(astn(1)+astn(nseg+1))/2.
        do 120 i=2,nseg
         ashort=ashort+astn(i)
120     continue
        ashort=ashort*dz
        bshort= sqrt(sqrdz+xi(2)**2+yi(2)**2)
     +         -sqrt(sqrdz+(xi(2)+u(2))**2
     +                    +(yi(2)+v(2))**2)
     +         +sqrt(sqrdz+xi(nseg)**2+yi(nseg)**2)
     +         -sqrt(sqrdz+(xi(nseg)+u(nseg))**2
     +                    +(yi(nseg)+v(nseg))**2)
        do 130 i=3,nseg
         bshort= bshort+sqrt(sqrdz+(xi(i)-xi(i-1))**2
     +                             +(yi(i)-yi(i-1))**2)
     +                 -sqrt(sqrdz+((xi(i)+u(i))-(xi(i-1)+u(i-1)))**2
     +                             +((yi(i)+v(i))-(yi(i-1)+v(i-1)))**2)
130     continue
        bshort=bshort+ashort
        call outres(resfil,aPz,lf,ashort,bshort,nseg,u,v,
     +              My,Mx,Myres,Mxres,kapx,kapy,astn,
     +              select,selfil)
        do 140 i=1,nseg+1
         u0(i)=u(i)
         v0(i)=v(i)
         astn0(i)=astn(i)
140     continue
        aPz=aPz+daPz
        goto 3
       endif
      else if (atype.eq.2) then
       lf=0.
```

```
5     if (erlf.lt.abs(dlf)) then
       write(6,*)
       write(6,820) 'lf=',lf
       fsol=.true.
       call profil(bcxA,bcxB,bcyA,bcyB,nmt,nmds,stnmd,maxmd,
     +             strmd,lngth,aPz,erPz,erdw,exA,exB,eyA,eyB,
     +             lf,aMxA,aMxB,aMyA,aMyB,ncr,nqcs,npcs,nseg,
     +             crses,xi,yi,cenx,ceny,fMx,fMy,u,v,dw,astn,
     +             kapx,kapy,Mx,My,Mxres,Myres,MxdxB,MydxB,
     +             MxdyB,MydyB,MxdxA,MydxA,MxdyA,MydyA,dMdw,
     +             ngaus,maxq,maxp,gpx,gpy,gpa,gpm,fsol,
     +             kcxA,kcyA,kcxB,kcyB)
       if (.not.fsol) then
        do 210 i=1,nseg+1
         u(i)=u0(i)
         v(i)=v0(i)
         astn(i)=astn0(i)
210     continue
        dlf=dlf/2.
        lf=lf-dlf
        goto 5
       endif
       ashort=(astn(1)+astn(nseg+1))/2.
       do 220 i=2,nseg
        ashort=ashort+astn(i)
220    continue
       ashort=ashort*dz
       bshort= sqrt(sqrdz+xi(2)**2+yi(2)**2)
     +         -sqrt(sqrdz+(xi(2)+u(2))**2
     +                    +(yi(2)+v(2))**2)
     +         +sqrt(sqrdz+xi(nseg)**2+yi(nseg)**2)
     +         -sqrt(sqrdz+(xi(nseg)+u(nseg))**2
     +                    +(yi(nseg)+v(nseg))**2)
       do 230 i=3,nseg
        bshort= bshort+sqrt(sqrdz+(xi(i)-xi(i-1))**2
     +                           +(yi(i)-yi(i-1))**2)
     +                -sqrt(sqrdz+((xi(i)+u(i))-(xi(i-1)+u(i-1)))**2
     +                           +((yi(i)+v(i))-(yi(i-1)+v(i-1)))**2)
230    continue
       bshort=bshort+ashort
       call outres(resfil,aPz,lf,ashort,bshort,nseg,u,v,
     +             My,Mx,Myres,Mxres,kapx,kapy,astn,
     +             select,selfil)
       do 240 i=1,nseg+1
        u0(i)=u(i)
        v0(i)=v(i)
        astn0(i)=astn(i)
240    continue
       lf=lf+dlf
       goto 5
      endif
     endif
810  format(a3,1x,f10.3,1x,a2)
820  format(a3,1x,f10.3)
     end
c=====================================================================
c               Subroutine profil( )
c     For given external load employs the Newton-Raphson (NR) procedure
c     to evaluate the discrete deflections, u and v, and centroidal
c     strains, astn, such as to establish force and moment equilibrium
c     in the sections. Convergence is assumed when the largest absolute
c     increment in any deflection is less than erdw. If the equilibrium
c     at any station cannot be established this is flagged by fsol.
c     Locally defined Parameters:
c      dastn = Initial increment for the centroidal strain iteration.
c      dkapx = Incremental curvature after x-axis for calculation of
```

```
c              partial derivatives of moments.
c      dkapy = Incremental curvature after y-axis for calculation of
c              partial derivatives of moments.
c      nimax = Maximum allowed number of NR iterations.
c=====================================================================
      subroutine profil(bcxA,bcxB,bcyA,bcyB,nmt,nmds,stnmd,maxmd,
     +                  strmd,lngth,aPz,erPz,erdw,exA,exB,eyA,eyB,
     +                  lf,aMxA,aMxB,aMyA,aMyB,ncr,nqcs,npcs,nseg,
     +                  crses,xi,yi,cenx,ceny,fMx,fMy,u,v,dw,astn,
     +                  kapx,kapy,Mx,My,Mxres,Myres,MxdxB,MydxB,
     +                  MxdyB,MydyB,MxdxA,MydxA,MxdyA,MydyA,dMdw,
     +                  ngaus,maxq,maxp,gpx,gpy,gpa,gpm,fsol,
     +                  kcxA,kcyA,kcxB,kcyB)
      logical fsol
      integer bcxA,bcxB,bcyA,bcyB,nmt,maxmd,ncr,nseg,ngaus,
     +        maxq,maxp
      integer nmds(nmt),nqcs(ncr),npcs(ncr),crses(nseg+1)
      integer gpm(maxq*ngaus**2+2*maxp,ncr)
      real lngth,aPz,erPz,erdw,exA,exB,eyA,eyB,lf,aMxA,aMxB,aMyA,
     +     aMyB,kcxA,kcyA,kcxB,kcyB
      real xi(nseg+1),yi(nseg+1),cenx(nseg+1),ceny(nseg+1),
     +     fMx(nseg+1),fMy(nseg+1),u(nseg+1),v(nseg+1),
     +     dw(2*nseg+2),astn(nseg+1),kapx(nseg+1),kapy(nseg+1),
     +     Mx(nseg+1),My(nseg+1),Mxres(nseg+1),Myres(nseg+1),
     +     MxdxB(nseg+1),MydxB(nseg+1),MxdyB(nseg+1),
     +     MydyB(nseg+1),MxdxA(nseg+1),MydxA(nseg+1),
     +     MxdyA(nseg+1),MydyA(nseg+1)
      real stnmd(2,nmt),strmd(maxmd,nmt),
     +     gpx(maxq*ngaus**2+2*maxp,ncr),
     +     gpy(maxq*ngaus**2+2*maxp,ncr),
     +     gpa(maxq*ngaus**2+2*maxp,ncr),
     +     dMdw(2*nseg+2,2*nseg+2)
      integer nqc,npc,gpdim,crse
      real dastn,dkapx,dkapy,astnj,kapxj,kapyj,maxdw
      integer nimax,ni,i,j
      parameter (dastn=-0.1e-3,
     +           dkapx= 1.e-12,
     +           dkapy= 1.e-12,
     +           nimax=    100)
      fsol=.true.
      ni=0
 5    ni=ni+1
      call curv(bcxA,bcxB,bcyA,bcyB,lngth,nseg,u,v,kapx,kapy)
      do 110 j=1,nseg+1
       crse=crses(j)
       nqc=nqcs(crse)
       npc=npcs(crse)
       gpdim=nqc*ngaus**2+2*npc
       if (fsol) then
        call censtn(nmt,nmds,stnmd,maxmd,strmd,gpdim,gpx(1,crse),
     +              gpy(1,crse),gpa(1,crse),gpm(1,crse),cenx(j),
     +              ceny(j),aPz,erPz,kapx(j),kapy(j),dastn,
     +              astn(j),fsol)
        call Mforce(nmt,nmds,stnmd,maxmd,strmd,gpdim,gpx(1,crse),
     +              gpy(1,crse),gpa(1,crse),gpm(1,crse),cenx(j),
     +              ceny(j),astn(j),kapx(j),kapy(j),Mx(j),My(j))
       endif
 110  continue
      if (.not.fsol) then
       write(6,*) 'Load capacity exhausted'
       return
      endif
      call residu(bcxA,bcxB,bcyA,bcyB,lf,aMxA,aMxB,aMyA,aMyB,
     +            aPz,exA,exB,eyA,eyB,nseg,fMx,fMy,cenx,ceny,
     +            xi,yi,u,v,Mx,My,Mxres,Myres,lngth,kcxA,kcxB,
     +            kcyA,kcyB)
```

```
      do 120 j=1,nseg+1
       crse=crses(j)
       nqc=nqcs(crse)
       npc=npcs(crse)
       gpdim=nqc*ngaus**2+2*npc
       if (fsol) then
        astnj=astn(j)
        kapxj=kapx(j)+dkapx
        kapyj=kapy(j)
        call censtn(nmt,nmds,stnmd,maxmd,strmd,gpdim,gpx(1,crse),
     +              gpy(1,crse),gpa(1,crse),gpm(1,crse),cenx(j),
     +              ceny(j),aPz,erPz,kapxj,kapyj,dastn,
     +              astnj,fsol)
        call Mforce(nmt,nmds,stnmd,maxmd,strmd,gpdim,gpx(1,crse),
     +              gpy(1,crse),gpa(1,crse),gpm(1,crse),cenx(j),
     +              ceny(j),astnj,kapxj,kapyj,MxdxB(j),MydxB(j))
       endif
  120  continue
      if (.not.fsol) then
       write(6,*) 'No equilibrium state for incremented x-curvature'
       return
      endif
      do 125 j=1,nseg+1
       crse=crses(j)
       nqc=nqcs(crse)
       npc=npcs(crse)
       gpdim=nqc*ngaus**2+2*npc
       if (fsol) then
        astnj=astn(j)
        kapxj=kapx(j)-dkapx
        kapyj=kapy(j)
        call censtn(nmt,nmds,stnmd,maxmd,strmd,gpdim,gpx(1,crse),
     +              gpy(1,crse),gpa(1,crse),gpm(1,crse),cenx(j),
     +              ceny(j),aPz,erPz,kapxj,kapyj,dastn,
     +              astnj,fsol)
        call Mforce(nmt,nmds,stnmd,maxmd,strmd,gpdim,gpx(1,crse),
     +              gpy(1,crse),gpa(1,crse),gpm(1,crse),cenx(j),
     +              ceny(j),astnj,kapxj,kapyj,MxdxA(j),MydxA(j))
       endif
  125  continue
      if (.not.fsol) then
       write(6,*) 'No equilibrium state for decremented x-curvature'
       return
      endif
      do 130 j=1,nseg+1
       crse=crses(j)
       nqc=nqcs(crse)
       npc=npcs(crse)
       gpdim=nqc*ngaus**2+2*npc
       if (fsol) then
        astnj=astn(j)
        kapxj=kapx(j)
        kapyj=kapy(j)+dkapy
        call censtn(nmt,nmds,stnmd,maxmd,strmd,gpdim,gpx(1,crse),
     +              gpy(1,crse),gpa(1,crse),gpm(1,crse),cenx(j),
     +              ceny(j),aPz,erPz,kapxj,kapyj,dastn,
     +              astnj,fsol)
        call Mforce(nmt,nmds,stnmd,maxmd,strmd,gpdim,gpx(1,crse),
     +              gpy(1,crse),gpa(1,crse),gpm(1,crse),cenx(j),
     +              ceny(j),astnj,kapxj,kapyj,MxdyB(j),MydyB(j))
       endif
  130  continue
      if (.not.fsol) then
       write(6,*) 'No equilibrium state for incremented y-curvature'
       return
      endif
```

```
      do 135 j=1,nseg+1
       crse=crses(j)
       nqc=nqcs(crse)
       npc=npcs(crse)
       gpdim=nqc*ngaus**2+2*npc
       if (fsol) then
        astnj=astn(j)
        kapxj=kapx(j)
        kapyj=kapy(j)-dkapy
        call censtn(nmt,nmds,stnmd,maxmd,strmd,gpdim,gpx(1,crse),
     +              gpy(1,crse),gpa(1,crse),gpm(1,crse),cenx(j),
     +              ceny(j),aPz,erPz,kapxj,kapyj,dastn,
     +              astnj,fsol)
        call Mforce(nmt,nmds,stnmd,maxmd,strmd,gpdim,gpx(1,crse),
     +              gpy(1,crse),gpa(1,crse),gpm(1,crse),cenx(j),
     +              ceny(j),astnj,kapxj,kapyj,MxdyA(j),MydyA(j))
       endif
  135  continue
       if (.not.fsol) then
        write(6,*) 'No equilibrium state for decremented y-curvature'
        return
       endif
       call stiff(bcxA,bcxB,bcyA,bcyB,lngth,aPz,dkapx,dkapy,
     +            nseg,Mx,My,MxdxB,MxdyB,MydxB,MydyB,MxdxA,
     +            MxdyA,MydxA,MydyA,dMdw,kcxA,kcxB,kcyA,kcyB)
       do 140 i=1,nseg+1
        dw(i)=-Myres(i)
        dw(nseg+1+i)=-Mxres(i)
  140  continue
       call lusol(dMdw,dw,2*nseg+2,fsol)
       if (.not.fsol) then
        write(6,*) 'Instantaneous stiffness matrix singular'
        return
       endif
       do 145 i=1,nseg+1
        u(i)=u(i)+dw(i)
        v(i)=v(i)+dw(nseg+1+i)
  145  continue
       maxdw=abs(dw(1))
       do 150 i=2,2*nseg+2
        if (abs(dw(i)).gt.maxdw) then
         maxdw=abs(dw(i))
        endif
  150  continue
       write(6,'(a4,i3,a8,e9.3)') 'ni= ',ni,' maxdw= ',maxdw
       if (maxdw.gt.erdw) then
        if (ni.lt.nimax) then
         goto 5
        else
         fsol=.false.
         write(6,*) 'Convergence in displacements failed'
         return
        endif
       endif
       end
c=======================================================================
c                Subroutine curv( )
c     Evaluates the curvature of the deflected column using the
c     central difference method. The curvature is calculated in
c     the x and y direction respectively. Note the calculation
c     at the ends reflects the no sway assumption, and that the
c     first and last entry in the deflection arrays are for the
c     auxillary stations outside the length of the column.
c=======================================================================
       subroutine curv(bcxA,bcxB,bcyA,bcyB,lngth,nseg,u,v,kapx,kapy)
       integer bcxA,bcxB,bcyA,bcyB,nseg
```

```
      real lngth
      real u(nseg+1),v(nseg+1),kapx(nseg+1),kapy(nseg+1)
      real sqrdz
      integer i
      sqrdz=(lngth/real(nseg))**2
      if(bcyA.eq.2) then
       kapx(1)=-2.*u(2)/sqrdz
      else
       kapx(1)=(-u(1)-u(2))/sqrdz
      endif
      if(bcxA.eq.2) then
       kapy(1)=-2.*v(2)/sqrdz
      else
       kapy(1)=(-v(1)-v(2))/sqrdz
      endif
      kapx(2)=(2.*u(2)-u(3))/sqrdz
      kapy(2)=(2.*v(2)-v(3))/sqrdz
      do 100 i=3,nseg-1
       kapx(i)=(-u(i-1)+2.*u(i)-u(i+1))/sqrdz
       kapy(i)=(-v(i-1)+2.*v(i)-v(i+1))/sqrdz
  100 continue
      kapx(nseg)=(-u(nseg-1)+2.*u(nseg))/sqrdz
      kapy(nseg)=(-v(nseg-1)+2.*v(nseg))/sqrdz
      if(bcyB.eq.2) then
       kapx(nseg+1)=-2.*u(nseg)/sqrdz
      else
       kapx(nseg+1)=(-u(nseg)-u(nseg+1))/sqrdz
      endif
      if(bcxB.eq.2) then
       kapy(nseg+1)=-2.*v(nseg)/sqrdz
      else
       kapy(nseg+1)=(-v(nseg)-v(nseg+1))/sqrdz
      endif
      end
c=======================================================================
c                Subroutine censtn( )
c     For a given combination of applied axial load and curvatures,
c     aPz, kapx and kapy, the axial strain at the centre, astn, is
c     iterated until the internal axial load, Pz, equals aPz to
c     within an error of erPres. That is abs(aPz-Pz).lt.erPres.
c     If the solution is non-existent or in-accurate this is flagged
c     by 'fsol' being '.false.'.
c     Locally defined parameters:
c      goldm  = Golden ratio for calculating minimum
c      maxstn = Search range limit for bracketing
c      nimax  = Allowed limit for number of iterations
c=======================================================================
      subroutine censtn(nmt,nmds,stnmd,maxmd,strmd,gpdim,gpx,gpy,
     +                  gpa,gpm,cenx,ceny,aPz,erPz,kapx,kapy,
     +                  dastn,astn,fsol)
      logical fsol
      integer nmt,maxmd,gpdim
      integer nmds(nmt),gpm(gpdim)
      real kapx,kapy,cenx,ceny,astn,dastn,aPz,erPz,
     +     astn_a,astn_b,astn_c
      real gpx(gpdim),gpy(gpdim),gpa(gpdim)
      real stnmd(2,nmt),strmd(maxmd,nmt)
      integer ni,nimax
      real maxstn,astn_u,Pz_a,Pz_b,Pz_c,Pz_u,fa,fb,fc,fu,astn_0,
     +     astn_1,astn_2,astn_3,Pz_1,Pz_2,f1,f2,goldm
      real dum
      parameter ( goldm=0.61803399,
     +            maxstn=1.,
     +            nimax= 100)
      astn_a=astn
      astn_b=astn+dastn
```

```
      fsol=.true.
      call Pforce(nmt,nmds,stnmd,maxmd,strmd,gpdim,gpx,gpy,
     +            gpa,gpm,cenx,ceny,astn_a,kapx,kapy,Pz_a)
      fa=abs(aPz-Pz_a)
      call Pforce(nmt,nmds,stnmd,maxmd,strmd,gpdim,gpx,gpy,
     +            gpa,gpm,cenx,ceny,astn_b,kapx,kapy,Pz_b)
      fb=abs(aPz-Pz_b)
      if (fb.gt.fa) then
       dum=astn_a
       astn_a=astn_b
       astn_b=dum
       dum=fb
       fb=fa
       fa=dum
       dum=Pz_b
       Pz_b=Pz_a
       Pz_a=dum
      endif
      astn_c=2.*astn_b-astn_a
      call Pforce(nmt,nmds,stnmd,maxmd,strmd,gpdim,gpx,gpy,
     +            gpa,gpm,cenx,ceny,astn_c,kapx,kapy,Pz_c)
      fc=abs(aPz-Pz_c)
111   if (fb.ge.fc) then
       astn_u=2.*astn_c-astn_b
       if (abs(astn_u).gt.maxstn) then
        write(6,*) 'Strain bracketing failed'
        fsol=.false.
        return
       endif
       call Pforce(nmt,nmds,stnmd,maxmd,strmd,gpdim,gpx,gpy,
     +             gpa,gpm,cenx,ceny,astn_u,kapx,kapy,Pz_u)
       fu=abs(aPz-Pz_u)
       astn_a=astn_b
       astn_b=astn_c
       astn_c=astn_u
       Pz_a=Pz_b
       Pz_b=Pz_c
       Pz_c=Pz_u
       fa=fb
       fb=fc
       fc=fu
       goto 111
      endif
      astn_0=astn_a
      astn_1=astn_b-(1.-goldm)*(astn_b-astn_a)
      astn_2=astn_b
      astn_3=astn_c
      call Pforce(nmt,nmds,stnmd,maxmd,strmd,gpdim,gpx,gpy,
     +            gpa,gpm,cenx,ceny,astn_1,kapx,kapy,Pz_1)
      f1=abs(aPz-Pz_1)
      call Pforce(nmt,nmds,stnmd,maxmd,strmd,gpdim,gpx,gpy,
     +            gpa,gpm,cenx,ceny,astn_2,kapx,kapy,Pz_2)
      f2=abs(aPz-Pz_2)
      ni=0
222   if ((f1.gt.erPz).and.(ni.lt.nimax)) then
       ni=ni+1
       if (f2.lt.f1) then
        astn_0=astn_1
        astn_1=astn_2
        astn_2=goldm*astn_1+(1.-goldm)*astn_3
        Pz_1=Pz_2
        f1=f2
        call Pforce(nmt,nmds,stnmd,maxmd,strmd,gpdim,gpx,gpy,
     +              gpa,gpm,cenx,ceny,astn_2,kapx,kapy,Pz_2)
        f2=abs(aPz-Pz_2)
       else
```

```
        astn_3=astn_2
        astn_2=astn_1
        astn_1=goldm*astn_2+(1.-goldm)*astn_0
        Pz_2=Pz_1
        f2=f1
        call Pforce(nmt,nmds,stnmd,maxmd,strmd,gpdim,gpx,gpy,
     +              gpa,gpm,cenx,ceny,astn_1,kapx,kapy,Pz_1)
        f1=abs(aPz-Pz_1)
       endif
       goto 222
      endif
      if (ni.eq.nimax) then
       write(6,*) 'Convergence criteria, erPz, not satisfied'
       fsol=.false.
       return
      endif
      astn=astn_1
      end
c=======================================================================
c                Subroutine Pforce( )
c     Evaluates the axial force, Pz, corresponding to a strain
c     distribution given by astn, kapx and kapy.
c=======================================================================
      subroutine Pforce(nmt,nmds,stnmd,maxmd,strmd,gpdim,gpx,gpy,
     +                  gpa,gpm,cenx,ceny,astn,kapx,kapy,Pz)
      integer nmt,maxmd,gpdim
      integer nmds(nmt),gpm(gpdim)
      real kapx,kapy,cenx,ceny,astn,Pz
      real gpx(gpdim),gpy(gpdim),gpa(gpdim)
      real stnmd(2,nmt),strmd(maxmd,nmt)
      real stn,str
      integer nmd,matr
      integer i
      Pz=0.
      do 100 i=1,gpdim
       matr=gpm(i)
       nmd=nmds(matr)
       stn=astn+kapx*(gpx(i)-cenx)+kapy*(gpy(i)-ceny)
       call strstn(stn,str,nmd,strmd(1,matr),stnmd(1,matr))
       Pz=Pz+str*gpa(i)
 100  continue
      end
c=======================================================================
c                Subroutine Mforce( )
c     Evaluates the biaxial moments, Mx and My, corresponding to a
c     strain distribution given by astn, kapx and kapy. The moments
c     are taken about cartesian axes with origin at the sections
c     centroid.
c=======================================================================
      subroutine Mforce(nmt,nmds,stnmd,maxmd,strmd,gpdim,gpx,gpy,
     +                  gpa,gpm,cenx,ceny,astn,kapx,kapy,Mx,My)
      integer nmt,maxmd,gpdim
      integer nmds(nmt),gpm(gpdim)
      real cenx,ceny,astn,kapx,kapy,Mx,My
      real gpx(gpdim),gpy(gpdim),gpa(gpdim)
      real stnmd(2,nmt),strmd(maxmd,nmt)
      integer matr,nmd
      real stn,str
      integer i
      Mx=0.
      My=0.
      do 100 i=1,gpdim
       matr=gpm(i)
       nmd=nmds(matr)
       stn=astn+kapx*(gpx(i)-cenx)+kapy*(gpy(i)-ceny)
       call strstn(stn,str,nmd,strmd(1,matr),stnmd(1,matr))
```

```
       My=My+str*gpa(i)*(gpx(i)-cenx)
       Mx=Mx+str*gpa(i)*(gpy(i)-ceny)
 100   continue
       end
c=======================================================================
c                Subroutine strstn( )
c     Calculates the stress corresponding to a given value of strain
c     using the look-up table for materials stress-strain behaviour.
c=======================================================================
       subroutine strstn(stn,str,nmd,strmd,stnmd)
       integer nmd
       real stn,str
       real strmd(nmd),stnmd(2)
       real stnA,stnB,dstn,stn1,str1,str2
       integer n1,n2
       stnA=stnmd(1)
       stnB=stnmd(2)
       if (stnB.gt.stnA) then
        if (stn.le.stnA) then
         str=strmd(1)
         return
        else if (stn.ge.stnB) then
         str=strmd(nmd)
         return
        endif
        dstn=(stnB-stnA)/(nmd-1)
        n1=int((stn-stnA)/dstn)+1
        n2=n1+1
        str1=strmd(n1)
        str2=strmd(n2)
        stn1=stnA+(n1-1)*dstn
        str=str1+(stn-stn1)*(str2-str1)/dstn
       else
        if (stn.ge.stnA) then
         str=strmd(1)
         return
        else if (stn.le.stnB) then
         str=strmd(nmd)
         return
        endif
        dstn=(stnB-stnA)/(nmd-1)
        n1=int((stn-stnA)/dstn)+1
        n2=n1+1
        str1=strmd(n1)
        str2=strmd(n2)
        stn1=stnA+(n1-1)*dstn
        str=str1+(stn-stn1)*(str2-str1)/dstn
       endif
       end
c=======================================================================
c                Subroutine residu( )
c     Evaluates the moment residuals at the stations.
c=======================================================================
       subroutine residu(bcxA,bcxB,bcyA,bcyB,lf,aMxA,aMxB,aMyA,aMyB,
      +                  aPz,exA,exB,eyA,eyB,nseg,fMx,fMy,cenx,ceny,
      +                  xi,yi,u,v,Mx,My,Mxres,Myres,lngth,kcxA,kcxB,
      +                  kcyA,kcyB)
       integer nseg,bcxA,bcxB,bcyA,bcyB
       real lf,aMxA,aMxB,aMyA,aMyB,aPz,exA,exB,eyA,eyB,lngth,
      +     kcxA,kcxB,kcyA,kcyB
       real fMx(nseg+1),fMy(nseg+1),cenx(nseg+1),ceny(nseg+1),
      +     xi(nseg+1),yi(nseg+1),u(nseg+1),v(nseg+1),Mx(nseg+1),
      +     My(nseg+1),Mxres(nseg+1),Myres(nseg+1)
       real rMxA,rMxB,rMyA,rMyB,dz
       integer i
       dz=lngth/real(nseg)
```

```
      if (bcyA.eq.1) then
       rMyA=aMyA
      elseif (bcyA.eq.2) then
       rMyA=My(1)-aPz*(exA-cenx(1))
      elseif (bcyA.eq.3) then
       rMyA=kcyA*(u(2)-u(1))/(2.*dz)+aMyA
      endif
      if (bcyB.eq.1) then
       rMyB=aMyB
      elseif (bcyB.eq.2) then
       rMyB=My(nseg+1)-aPz*(exB-cenx(nseg+1))
      elseif (bcyB.eq.3) then
       rMyB=kcyB*(u(nseg)-u(nseg+1))/(2.*dz)+aMyB
      endif
      if (bcxA.eq.1) then
       rMxA=aMxA
      elseif (bcxA.eq.2) then
       rMxA=Mx(1)-aPz*(eyA-ceny(1))
      elseif (bcxA.eq.3) then
       rMxA=kcxA*(v(2)-v(1))/(2.*dz)+aMxA
      endif
      if (bcxB.eq.1) then
       rMxB=aMxB
      elseif (bcxB.eq.2) then
       rMxB=Mx(nseg+1)-aPz*(eyB-ceny(nseg+1))
      elseif (bcxB.eq.3) then
       rMxB=kcxB*(v(nseg)-v(nseg+1))/(2.*dz)+aMxB
      endif
      Myres(1)=rMyA+aPz*exA-aPz*cenx(1)-My(1)
      Mxres(1)=rMxA+aPz*eyA-aPz*ceny(1)-Mx(1)
      do 100 i=2,nseg
       Myres(i)= lf*fMy(i)
     +          +(rMyA+aPz*exA)*(1.-real(i-1)/real(nseg))
     +          +(rMyB+aPz*exB)*(real(i-1)/real(nseg))-aPz*u(i)
     +          -aPz*(xi(i)+cenx(i))-My(i)
       Mxres(i)= lf*fMx(i)
     +          +(rMxA+aPz*eyA)*(1.-real(i-1)/real(nseg))
     +          +(rMxB+aPz*eyB)*(real(i-1)/real(nseg))-aPz*v(i)
     +          -aPz*(yi(i)+ceny(i))-Mx(i)
 100  continue
      Myres(nseg+1)=rMyB+aPz*exB-aPz*cenx(nseg+1)-My(nseg+1)
      Mxres(nseg+1)=rMxB+aPz*eyB-aPz*ceny(nseg+1)-Mx(nseg+1)
      end
c=====================================================================
c                Subroutine stiff( )
c     Constructs the matrix containing the instantaneous partial deri-
c     vatives of the residual moments with respect to the deflections.
c     The derivatives are calculated at each station after both axes,
c     but the first and last deflection in each direction refers to
c     the auxillary points. The deflections of end-points implicit
c     given as zero.
c=====================================================================
      subroutine stiff(bcxA,bcxB,bcyA,bcyB,lngth,aPz,dkapx,dkapy,
     +                 nseg,Mx,My,MxdxB,MxdyB,MydxB,MydyB,MxdxA,
     +                 MxdyA,MydxA,MydyA,dMdw,kcxA,kcxB,kcyA,kcyB)
      integer bcxA,bcxB,bcyA,bcyB,nseg
      real lngth,aPz,dkapx,dkapy,kcxA,kcxB,kcyA,kcyB
      real Mx(nseg+1),My(nseg+1),MxdxB(nseg+1),MxdyB(nseg+1),
     +     MydxB(nseg+1),MydyB(nseg+1),MxdxA(nseg+1),MxdyA(nseg+1),
     +     MydxA(nseg+1),MydyA(nseg+1),dMdw(2*nseg+2,2*nseg+2)
      real dMxdxi,dMxdyi,dMydxi,dMydyi,dz,sqrdz,fract
      integer i,j
      dz=lngth/real(nseg)
      sqrdz=dz**2
      do 20 i=1,2*nseg+2
       do 10 j=1,2*nseg+2
```

```
        dMdw(i,j)=0.0
10     continue
20    continue
      do 100 i=2,nseg
       dMdw(i,i)=-aPz
       dMdw(i+nseg+1,i+nseg+1)=-aPz
100   continue
      do 110 i=2,nseg
       dMydxi=(MydxB(i)-MydxA(i))/(2.*dkapx)
       dMydyi=(MydyB(i)-MydyA(i))/(2.*dkapy)
       dMxdyi=(MxdyB(i)-MxdyA(i))/(2.*dkapy)
       dMxdxi=(MxdxB(i)-MxdxA(i))/(2.*dkapx)
       dMdw(i,i-1)=-dMydxi*(-1./sqrdz)
       dMdw(i,i)  =dMdw(i,i)-dMydxi*(2./sqrdz)
       dMdw(i,i+1)=-dMydxi*(-1./sqrdz)
       dMdw(i,nseg+i)  =-dMydyi*(-1./sqrdz)
       dMdw(i,nseg+1+i)=-dMydyi*(2./sqrdz)
       dMdw(i,nseg+2+i)=-dMydyi*(-1./sqrdz)
       dMdw(nseg+1+i,i-1)=-dMxdxi*(-1./sqrdz)
       dMdw(nseg+1+i,i)  =-dMxdxi*(2./sqrdz)
       dMdw(nseg+1+i,i+1)=-dMxdxi*(-1./sqrdz)
       dMdw(nseg+1+i,nseg+i)  =-dMxdyi*(-1./sqrdz)
       dMdw(nseg+1+i,nseg+1+i)= dMdw(nseg+1+i,nseg+1+i)
     +                          -dMxdyi*(2./sqrdz)
       dMdw(nseg+1+i,nseg+2+i)=-dMxdyi*(-1./sqrdz)
110   continue
      dMdw(2,1)=0.0
      dMdw(2,nseg+2)=0.0
      dMdw(nseg,nseg+1)=0.0
      dMdw(nseg,2*nseg+2)=0.0
      dMdw(nseg+3,1)=0.0
      dMdw(nseg+3,nseg+2)=0.0
      dMdw(2*nseg+1,nseg+1)=0.0
      dMdw(2*nseg+1,2*nseg+2)=0.0
      dMydxi=(MydxB(1)-MydxA(1))/(2.*dkapx)
      dMydyi=(MydyB(1)-MydyA(1))/(2.*dkapy)
      if (bcyA.eq.1) then
       dMdw(1,1)=-dMydxi*(-1./sqrdz)
       dMdw(1,2)=-dMydxi*(-1./sqrdz)
       if (bcxA.eq.1) then
        dMdw(1,nseg+2)=-dMydyi*(-1./sqrdz)
        dMdw(1,nseg+3)=-dMydyi*(-1./sqrdz)
       elseif (bcxA.eq.2) then
        dMdw(1,nseg+3)=-dMydyi*(-2./sqrdz)
       elseif (bcxA.eq.3) then
        dMdw(1,nseg+2)=-dMydyi*(-1./sqrdz)
        dMdw(1,nseg+3)=-dMydyi*(-1./sqrdz)
       endif
      elseif (bcyA.eq.2) then
       dMdw(1,1)=1.0
       do 120 i=2,nseg
        fract=(1.-real(i-1)/real(nseg))
        dMdw(i,2)=dMdw(i,2)+dMydxi*(-2./sqrdz)*fract
120    continue
       if (bcxA.eq.1) then
        do 122 i=2,nseg
         fract=(1.-real(i-1)/real(nseg))
         dMdw(i,nseg+2)=dMdw(i,nseg+2)+dMydyi*(-1./sqrdz)*fract
         dMdw(i,nseg+3)=dMdw(i,nseg+3)+dMydyi*(-1./sqrdz)*fract
122     continue
       elseif (bcxA.eq.2) then
        do 124 i=2,nseg
         fract=(1.-real(i-1)/real(nseg))
         dMdw(i,nseg+3)=dMdw(i,nseg+3)+dMydyi*(-2./sqrdz)*fract
124     continue
       elseif (bcxA.eq.3) then
```

```
       do 126 i=2,nseg
        fract=(1.-real(i-1)/real(nseg))
        dMdw(i,nseg+2)=dMdw(i,nseg+2)+dMydyi*(-1./sqrdz)*fract
        dMdw(i,nseg+3)=dMdw(i,nseg+3)+dMydyi*(-1./sqrdz)*fract
126    continue
      endif
     elseif (bcyA.eq.3) then
      dMdw(1,1)=-dMydxi*(-1./sqrdz)
      dMdw(1,2)=-dMydxi*(-1./sqrdz)
      do 130 i=1,nseg
       fract=(1.-real(i-1)/real(nseg))
       dMdw(i,1)=dMdw(i,1)-kcyA*fract/(2*dz)
       dMdw(i,2)=dMdw(i,2)+kcyA*fract/(2*dz)
130    continue
      if (bcxA.eq.1) then
       dMdw(1,nseg+2)=-dMydyi*(-1./sqrdz)
       dMdw(1,nseg+3)=-dMydyi*(-1./sqrdz)
      elseif (bcxA.eq.2) then
       dMdw(1,nseg+3)=-dMydyi*(-2./sqrdz)
      elseif (bcxA.eq.3) then
       dMdw(1,nseg+2)=-dMydyi*(-1./sqrdz)
       dMdw(1,nseg+3)=-dMydyi*(-1./sqrdz)
      endif
     endif
     dMydxi=(MydxB(nseg+1)-MydxA(nseg+1))/(2.*dkapx)
     dMydyi=(MydyB(nseg+1)-MydyA(nseg+1))/(2.*dkapy)
     if (bcyB.eq.1) then
      dMdw(nseg+1,nseg)=-dMydxi*(-1./sqrdz)
      dMdw(nseg+1,nseg+1)=-dMydxi*(-1./sqrdz)
      if (bcxB.eq.1) then
       dMdw(nseg+1,2*nseg+1)=-dMydyi*(-1./sqrdz)
       dMdw(nseg+1,2*nseg+2)=-dMydyi*(-1./sqrdz)
      elseif (bcxB.eq.2) then
       dMdw(nseg+1,2*nseg+1)=-dMydyi*(-2./sqrdz)
      elseif (bcxB.eq.3) then
       dMdw(nseg+1,2*nseg+1)=-dMydyi*(-1./sqrdz)
       dMdw(nseg+1,2*nseg+2)=-dMydyi*(-1./sqrdz)
      endif
     elseif (bcyB.eq.2) then
      dMdw(nseg+1,nseg+1)=1.0
      do 220 i=2,nseg
       fract=real(i-1)/real(nseg)
       dMdw(i,nseg)=dMdw(i,nseg)+dMydxi*(-2./sqrdz)*fract
220    continue
      if (bcxB.eq.1) then
       do 222 i=2,nseg
        fract=real(i-1)/real(nseg)
        dMdw(i,2*nseg+1)=dMdw(i,2*nseg+1)+dMydyi*(-1./sqrdz)*fract
        dMdw(i,2*nseg+2)=dMdw(i,2*nseg+2)+dMydyi*(-1./sqrdz)*fract
222    continue
      elseif (bcxB.eq.2) then
       do 224 i=2,nseg
        fract=real(i-1)/real(nseg)
        dMdw(i,2*nseg+1)=dMdw(i,2*nseg+1)+dMydyi*(-2./sqrdz)*fract
224    continue
      elseif (bcxB.eq.3) then
       do 226 i=2,nseg
        fract=real(i-1)/real(nseg)
        dMdw(i,2*nseg+1)=dMdw(i,2*nseg+1)+dMydyi*(-1./sqrdz)*fract
        dMdw(i,2*nseg+2)=dMdw(i,2*nseg+2)+dMydyi*(-1./sqrdz)*fract
226    continue
      endif
     elseif (bcyB.eq.3) then
      dMdw(nseg+1,nseg)=-dMydxi*(-1./sqrdz)
      dMdw(nseg+1,nseg+1)=-dMydxi*(-1./sqrdz)
      do 230 i=2,nseg+1
```

```
       fract=real(i-1)/real(nseg)
       dMdw(i,nseg)=dMdw(i,nseg)+kcyB*fract/(2*dz)
       dMdw(i,nseg+1)=dMdw(i,nseg+1)-kcyB*fract/(2*dz)
230    continue
       if (bcxB.eq.1) then
        dMdw(nseg+1,2*nseg+1)=-dMydyi*(-1./sqrdz)
        dMdw(nseg+1,2*nseg+2)=-dMydyi*(-1./sqrdz)
       elseif (bcxB.eq.2) then
        dMdw(nseg+1,2*nseg+1)=-dMydyi*(-2./sqrdz)
       elseif (bcxB.eq.3) then
        dMdw(nseg+1,2*nseg+1)=-dMydyi*(-1./sqrdz)
        dMdw(nseg+1,2*nseg+2)=-dMydyi*(-1./sqrdz)
       endif
      endif
      dMxdxi=(MxdxB(1)-MxdxA(1))/(2.*dkapx)
      dMxdyi=(MxdyB(1)-MxdyA(1))/(2.*dkapy)
      if (bcxA.eq.1) then
       dMdw(nseg+2,nseg+2)=-dMxdyi*(-1./sqrdz)
       dMdw(nseg+2,nseg+3)=-dMxdyi*(-1./sqrdz)
       if (bcyA.eq.1) then
        dMdw(nseg+2,1)=-dMxdxi*(-1./sqrdz)
        dMdw(nseg+2,2)=-dMxdxi*(-1./sqrdz)
       elseif (bcyA.eq.2) then
        dMdw(nseg+2,2)=-dMxdxi*(-2./sqrdz)
       elseif (bcyA.eq.3) then
        dMdw(nseg+2,1)=-dMxdxi*(-1./sqrdz)
        dMdw(nseg+2,2)=-dMxdxi*(-1./sqrdz)
       endif
      elseif (bcxA.eq.2) then
       dMdw(nseg+2,nseg+2)=1.0
       do 320 i=2,nseg
        fract=(1.-real(i-1)/real(nseg))
        dMdw(nseg+1+i,nseg+3)= dMdw(nseg+1+i,nseg+3)
     +                         +dMxdyi*(-2./sqrdz)*fract
320    continue
       if (bcyA.eq.1) then
        do 322 i=2,nseg
         fract=(1.-real(i-1)/real(nseg))
         dMdw(nseg+1+i,1)= dMdw(nseg+1+i,1)+dMxdxi*(-1./sqrdz)*fract
         dMdw(nseg+1+i,2)= dMdw(nseg+1+i,2)+dMxdxi*(-1./sqrdz)*fract
322     continue
       elseif (bcyA.eq.2) then
        do 324 i=2,nseg
         fract=(1.-real(i-1)/real(nseg))
         dMdw(nseg+1+i,2)=dMdw(nseg+1+i,2)+dMxdxi*(-2./sqrdz)*fract
324     continue
       elseif (bcyA.eq.3) then
        do 326 i=2,nseg
         fract=(1.-real(i-1)/real(nseg))
         dMdw(nseg+1+i,1)=dMdw(nseg+1+i,1)+dMxdxi*(-1./sqrdz)*fract
         dMdw(nseg+1+i,2)=dMdw(nseg+1+i,2)+dMxdxi*(-1./sqrdz)*fract
326     continue
       endif
      elseif (bcxA.eq.3) then
       dMdw(nseg+2,nseg+2)=-dMxdyi*(-1./sqrdz)
       dMdw(nseg+2,nseg+3)=-dMxdyi*(-1./sqrdz)
       do 330 i=1,nseg
        fract=(1.-real(i-1)/real(nseg))
        dMdw(nseg+1+i,nseg+2)=dMdw(nseg+1+i,nseg+2)-kcxA*fract/(2*dz)
        dMdw(nseg+1+i,nseg+3)=dMdw(nseg+1+i,nseg+3)+kcxA*fract/(2*dz)
330    continue
       if (bcyA.eq.1) then
        dMdw(nseg+2,1)=-dMxdxi*(-1./sqrdz)
        dMdw(nseg+2,2)=-dMxdxi*(-1./sqrdz)
       elseif (bcyA.eq.2) then
        dMdw(nseg+2,2)=-dMxdxi*(-2./sqrdz)
```

```
      elseif (bcyA.eq.3) then
       dMdw(nseg+2,1)=-dMxdxi*(-1./sqrdz)
       dMdw(nseg+2,2)=-dMxdxi*(-1./sqrdz)
      endif
     endif
     dMxdxi=(MxdxB(nseg+1)-MxdxA(nseg+1))/(2.*dkapx)
     dMxdyi=(MxdyB(nseg+1)-MxdyA(nseg+1))/(2.*dkapy)
     if (bcxB.eq.1) then
      dMdw(2*nseg+2,2*nseg+1)=-dMxdyi*(-1./sqrdz)
      dMdw(2*nseg+2,2*nseg+2)=-dMxdyi*(-1./sqrdz)
      if (bcyB.eq.1) then
       dMdw(2*nseg+2,nseg)=-dMxdxi*(-1./sqrdz)
       dMdw(2*nseg+2,nseg+1)=-dMxdxi*(-1./sqrdz)
      elseif (bcyB.eq.2) then
       dMdw(2*nseg+2,nseg)=-dMxdxi*(-2./sqrdz)
      elseif (bcyB.eq.3) then
       dMdw(2*nseg+2,nseg)=-dMxdxi*(-1./sqrdz)
       dMdw(2*nseg+2,nseg+1)=-dMxdxi*(-1./sqrdz)
      endif
     elseif (bcxB.eq.2) then
      dMdw(2*nseg+2,2*nseg+2)=1.0
      do 420 i=2,nseg
       fract=real(i-1)/real(nseg)
       dMdw(nseg+1+i,2*nseg+1)= dMdw(nseg+1+i,2*nseg+1)
     +                          +dMxdyi*(-2./sqrdz)*fract
420   continue
      if (bcyB.eq.1) then
       do 422 i=2,nseg
        fract=real(i-1)/real(nseg)
        dMdw(nseg+1+i,nseg)= dMdw(nseg+1+i,nseg)
     +                       +dMxdxi*(-1./sqrdz)*fract
        dMdw(nseg+1+i,nseg+1)= dMdw(nseg+1+i,nseg+1)
     +                         +dMxdxi*(-1./sqrdz)*fract
422    continue
      elseif (bcyB.eq.2) then
       do 424 i=2,nseg
        fract=real(i-1)/real(nseg)
        dMdw(nseg+1+i,nseg)= dMdw(nseg+1+i,nseg)
     +                       +dMxdxi*(-2./sqrdz)*fract
424    continue
      elseif (bcyB.eq.3) then
       do 426 i=2,nseg
        fract=real(i-1)/real(nseg)
        dMdw(nseg+1+i,nseg)= dMdw(nseg+1+i,nseg)
     +                       +dMxdxi*(-1./sqrdz)*fract
        dMdw(nseg+1+i,nseg+1)= dMdw(nseg+1+i,nseg+1)
     +                         +dMxdxi*(-1./sqrdz)*fract
426    continue
      endif
     elseif (bcxB.eq.3) then
      dMdw(2*nseg+2,2*nseg+1)=-dMxdyi*(-1./sqrdz)
      dMdw(2*nseg+2,2*nseg+2)=-dMxdyi*(-1./sqrdz)
      do 430 i=2,nseg+1
       fract=real(i-1)/real(nseg)
       dMdw(nseg+1+i,2*nseg+1)= dMdw(nseg+1+i,2*nseg+1)
     +                          +kcxB*fract/(2*dz)
       dMdw(nseg+1+i,2*nseg+2)= dMdw(nseg+1+i,2*nseg+2)
     +                          -kcxB*fract/(2*dz)
430   continue
      if (bcyB.eq.1) then
       dMdw(2*nseg+2,nseg)=-dMxdxi*(-1./sqrdz)
       dMdw(2*nseg+2,nseg+1)=-dMxdxi*(-1./sqrdz)
      elseif (bcyB.eq.2) then
       dMdw(2*nseg+2,nseg)=-dMxdxi*(-2./sqrdz)
      elseif (bcyB.eq.3) then
       dMdw(2*nseg+2,nseg)=-dMxdxi*(-1./sqrdz)
```

```
        dMdw(2*nseg+2,nseg+1)=-dMxdxi*(-1./sqrdz)
       endif
      endif
      end
c=======================================================================
c                Subroutine lusol( )
c     Solves linear algebraic equations using Crout's algorithm.
c     The matrix A(Adim,Adim) is overwritten by the results from the
c     LU decomposition, and the vector b(Adim) is overwritten by the
c     solution.
c     [A]{x} = [L][U]{x} = {b}
c     |A11 A12 A13|    |U11 U12 U13|   |b1|    |x1|
c     |A21 A22 A23| => |L21 U22 U33| , |b2| => |x2|
c     |A31 A32 A33|    |L31 L32 U33|   |b3|    |x3|
c     Diagonal elements of lower triangular matrix are all unity,
c     hence implicit understood.
c=======================================================================
      subroutine lusol(A,b,Adim,fsol)
      logical fsol
      integer Adim
      real b(Adim)
      real A(Adim,Adim)
      integer i,j,k
      real tiny,sum
      parameter (tiny=1.e-20)
      do 150 j=1,Adim
       do 120 i=1,j
        sum=0.0
        do 110 k=1,i-1
         sum=sum+A(i,k)*A(k,j)
 110    continue
        A(i,j)=A(i,j)-sum
 120   continue
       do 140 i=j+1,Adim
        sum=0.0
        do 130 k=1,j-1
         sum=sum+A(i,k)*A(k,j)
 130    continue
        if (abs(A(j,j)).lt.tiny) then
         fsol=.false.
         return
        endif
        A(i,j)=(A(i,j)-sum)/A(j,j)
 140   continue
 150  continue
      do 170 i=1,Adim
       sum=0.0
       do 160 j=1,i-1
        sum=sum+A(i,j)*b(j)
 160   continue
       b(i)=b(i)-sum
 170  continue
      do 190 i=Adim,1,-1
       sum=0.0
       do 180 j=i+1,Adim
        sum=sum+A(i,j)*b(j)
180    continue
       if (abs(A(i,i)).lt.tiny) then
        fsol=.false.
        return
       endif
       b(i)=(b(i)-sum)/A(i,i)
190   continue
      end
c=======================================================================
```